



UNIVERSITY  
OF  
JOHANNESBURG

## COPYRIGHT AND CITATION CONSIDERATIONS FOR THIS THESIS/ DISSERTATION



- o Attribution of you will give appropriate credit to the original author(s) and the source, provide a link to the Creative Commons licence, and indicate if changes were made. The images or other third party material in this document are included in the article's Creative Commons licence, unless indicated otherwise in a credit line to the material. If material is not included in the article's Creative Commons licence and your intended use is not permitted by statutory regulation or exceeds the permitted use, you will need to obtain permission directly from the copyright holder. To view a copy of this licence, visit <http://creativecommons.org/licenses/by-nc-sa/4.0/>.
- o You are not to use the material for commercial purposes.
- o Where possible, you should allow others to copy, distribute and remix your work under the same or similar licence as the original.

### How to cite this thesis

Surname, Initial(s). (2012). Title of the thesis or dissertation (Doctoral Thesis / Master's Dissertation). Johannesburg: University of Johannesburg. Available from: <http://hdl.handle.net/102000/0002> (Accessed: 22 August 2017).



**THEORETICAL PREDICTION OF SOLUBILITY, REACTIVITY AND  
DEGRADATION PATHWAYS OF SELECTED AZO DISPERSE DYES**

---

**By**

**WAHAB OLAIDE OLALEKAN**

**Student number: 201602083**

**Thesis in fulfilment of the requirement for the degree**

**PHILOSOPHIAE DOCTOR**

**In**

**CHEMISTRY**

**UNIVERSITY  
OF  
JOHANNESBURG**

**In the**

**FACULTY OF SCIENCE**

**Of the**

**UNIVERSITY OF JOHANNESBURG**

**Supervisor : PROF PP GOVENDER  
Co-supervisors : DR KK KRISHNA  
: DR LO OLASUNKANMI**

**JULY, 2019**

## DEDICATION.

---

I dedicate this work to almighty Allah without whom this project would not have been a success, to my wife and kids for their endurance, patience and understanding, and to my late father, Mr. Abdulwahab Abdussalam Bamigboye for fostering in me the positive attitudes needed to overcome challenges. *May Allah forgive his shortcomings and admit him into the paradise on the day of resurrection!!!*



## PUBLICATIONS AND PRESENTATIONS:

---

The work presented in this thesis has been presented at national and international conferences. Furthermore, results emanating from this study have also been either published or submitted to peer-reviewed journals.

### Peer-reviewed Publications

- ❖ **O. O. Wahab**, L. O. Olasunkanmi, K. K. Govender and P. P. Govender. DMol<sup>3</sup>/COSMO-RS prediction of aqueous solubility and reactivity of selected Azo dyes: Effect of global orbital cut-off and COSMO segment variation. *Journal of Molecular Liquids* **249** (2018) 346-360.
- ❖ **O. O. Wahab**, L. O. Olasunkanmi, K. K. Govender and P. P. Govender. Synergistic effect of opposite polar substituents on selected properties of disperse yellow 119 dye. *Chemical Physics Letters* **704** (2018) 55-61.
- ❖ **O. O. Wahab**, L. O. Olasunkanmi, K. K. Govender and P. P. Govender. A DFT study of disperse yellow 119 degradation mechanism by hydroxyl radical attack. *ChemistrySelect* **2000** (2018) 1-11.
- ❖ **O. O. Wahab**, L. O. Olasunkanmi, K. K. Govender and P. P. Govender. Tuning the aqueous solubility, chemical reactivity and absorption wavelength of disperse red 73 through systematic adjustment of molecular charge density: A theoretical study. *Molecular Physics* (2019) 1-21. <https://doi.org/10.1080/00268976.2019.1626508>.
- ❖ **O. O. Wahab**, L. O. Olasunkanmi, K. K. Govender and P. P. Govender. Prediction of aqueous solubility of azo dyes by treatment of COSMO-RS data with known

empirical solubility equations: The roles of global orbital cut-off and COSMO solvent radius. *Theoretical Chemistry Account* **138** (2019) 80(1)-80(13).

### Conference Presentations

- ❖ **O. O. Wahab**, L. O. Olasunkanmi, K. K. Govender and P. P. Govender. Theoretical modelling of effects of substituent groups on solubility and reactivity of C.I. disperse yellow 119 dye (**Oral presentation**). International Conference on Pure and Applied Chemistry (ICPAC-2018), Mauritius, 2 - 6 July, 2018.
- ❖ **O. O. Wahab**, L. O. Olasunkanmi, K. K. Govender and P. P. Govender. DMol<sup>3</sup>/COSMO-RS prediction of aqueous solubility and chemical reactivity of selected azo dyes: Effect of global orbital cut-off and COSMO segment variation (**Poster**). University of Johannesburg UJ-ESKOM Workshop – Johannesburg, South Africa, 11 – 12 September, 2018.
- ❖ **O. O. Wahab**, L. O. Olasunkanmi, K. K. Govender and P. P. Govender. DMol<sup>3</sup>/COSMO-RS prediction of aqueous solubility and chemical reactivity of selected azo dyes: Effect of global orbital cut-off and COSMO segment variation (**Oral presentation**). Centre for High Performance Computing (CHPC) National Meeting and Conference, Velmore Hotel, Pretoria, South Africa, 3 – 7 December, 2017.
- ❖ **O. O. Wahab**, L. O. Olasunkanmi, K. K. Govender and P. P. Govender. A DMol<sup>3</sup>/COSMO-RS prediction of aqueous solubility and chemical reactivity of selected azo dyes: Effect of global orbital cut-off and COSMO segment variation (**Oral presentation**). 9<sup>th</sup> International Conference on Research in Chemical,

Agricultural, Biological and Environmental Sciences (RCABES-2017), Parys, South Africa, 27 – 28 November, 2017.

- ❖ **O. O. Wahab**, L. O. Olasunkanmi, K. K. Govender and P. P. Govender. Qualitative DMol<sup>3</sup> Assessment of Aqueous Solubility, Reactivity and Gibb's Free Energies of Disperse Yellow 119 and its Selected Derivatives (**Oral presentation**). Annual Inter-Faculty Postgraduate Symposium, University of Johannesburg, Johannesburg, Auckland Park Bunting (APB) Campus, School of Tourism and Hospitality, 27th October, 2017.
- ❖ **O. O. Wahab**, L. O. Olasunkanmi, K. K. Govender and P. P. Govender. Theoretical prediction of the aqueous solubility of selected azo dyes: Effects of real space cut-off and COSMO segment variation (**Oral presentation**). University of Johannesburg UJ-ESKOM Workshop – Johannesburg, South Africa, 13 – 14 July, 2017.



## ACKNOWLEDGEMENTS

---

My profound gratitude goes to Allah, the creator and sustainer of the universe for the gift of life, inspiration, intellectual capacity and strength without which this project would not have been a success.

My sincere appreciation goes to a woman of outstanding personality, a role model, a leader per excellence, my supervisor, Prof. Penny Govender for giving me the opportunity to undertake this project under her supervision and for providing a conducive atmosphere for it. Your timely supports, swift response to issues, words of motivation, guidance and counselling, and invaluable suggestions, have contributed immensely to the successful completion of this study. Thank you ma.

My heartfelt gratitude goes to my co-supervisors, Dr. Krishna Govender and Dr. Lukman Olasunkanmi for providing useful guidance, suggestions, contributions, comments, and constructive criticisms that have made this work a success. Your painstaking perusal of this work since the time of proposal preparation to thesis compilation, is highly appreciated. Your unwavering love, support, advice, encouragement, and contributions towards the success of this project will forever be remembered. Thank you. More grease to your elbow.

All members of my research group including Dr. Anku William, Dr. Adeniyi Osikoya, Dr. Samuel Opong, Dr. Martin Magu, Mr. Francis Opoku, Mr. Ephraim Muriithi Kiarri, Mr. Ephraim Maronedze, Mr. Chijioke Peter, Mr. Seiso Tsoeu, Mr. Sechaba Manyedi, Miss Renu Kumari, and Miss Nokuthula Ndaba, have been exceptionally supportive throughout this program. I thank you all for your valuable contributions and wish you success in your various endeavors.

I extend my gratitude to the administrative and technical staff of the Department of Applied Chemistry, University of Johannesburg (UJ), for their assistance and cooperation. Thank you all.

I specially thank Mr. Sifiso, Ms. Leah, Ms. Dorcas, and Ms. Dereshni for their assistance. Many thanks you for the love and understanding we have enjoyed together.

Special appreciation goes to the Faculty of Science, Department of Applied Chemistry, UJ, for the financial support, and the Center for High Performance Computing (CHPC), South Africa for providing necessary facilities for this study. Thank you.

To my mother, sisters, children and my lovely wife, I thank you for your love, patience, endurance, mutual understanding and prayers without which it would have been difficult to complete this project. May you all reap the fruits of your labor.

Finally, I thank all my friends and well-wishers for their useful advice and encouragement. May you all be successful in your life endeavors.





## ABSTRACT

---

Azo disperse dyes are the most successful group of disperse dyes used for coloring hydrophobic substrates such as polyesters, nylons, acrylics and cellulose acetate fibers. However, poor aqueous solubility of these dyes serves as a major hindrance to the use of ordinary water as the dissolution medium. Consequently, when dyeing is being carried out in water, carrier and dispersing agents containing toxic chemical components such as o-phenylphenol, biphenyls, and phenyl chloride are usually added to obtain a finely dispersed solution for better interaction with the substrates. This leads to increase in production costs and an endangerment to life and the natural environment.

Azo disperse dyes themselves are potential causes of environmental pollution and human conditions such as bladder cancer, allergy, eczema, contact dermatitis and genetic disorder. Their relatively low degradation tendency in natural environments has been attributed to the stiffness of the azo ( $N=N$ ) chromophore, which acts as an intramolecular charge transfer bridge, and confers high stability on the dyes. Photocatalytic degradation has been considered as an efficient method of treating dye pollutants because it ensures complete transformation of dyes into harmless degradation products at relatively low cost. However, the reaction between photo-generated hydroxyl radicals and azo dyes during photocatalytic degradation is identified with arguable mechanistic routes due to a number of factors such as molecular symmetry, tautomeric forms of the dyes and hydrogen bonding. Understanding the mechanisms, energetics and factors affecting this process is therefore necessary for proper prediction of photodegradation products of different azo dyes.

As a step towards addressing the highlighted problems, the current study is designed to investigate the effect of selected polar substituent groups on the aqueous solubility and chemical reactivity of azopyridone dye; Disperse yellow 119 (DY119) and aminoazobenzene dye; Disperse red 73 (DR73). The aim is to theoretically design a set of new azo disperse dyes with improved aqueous solubility and reactivity, predict suitable photocatalyst(s) for their degradation, identify prospective sites for the attack of photo-generated hydroxyl ( $\bullet\text{OH}$ ) radicals and hence, predict their photodegradation mechanisms. The selected polar functional groups are electron withdrawing  $-\text{CN}$  and  $\text{NO}_2$ , and electron donating  $-\text{NH}_2$ ,  $-\text{NHCH}_3$  and  $-\text{N}(\text{CH}_3)_2$  groups, while the photocatalysts considered include Si, CdSe, CdS,  $\text{TiO}_2$ , ZnO and ZnS. The photodegradation mechanisms of the selected dyes were also investigated to predict their photodegradation products and also account for the roles of symmetry, hydrogen bonding and tautomerism. All calculations were carried out using Density functional theory (DFT) with the aid of DMol<sup>3</sup> module embedded in the Material studio (version 2016) modelling software. The conductor-like screening model for realistic solvation (COSMO-RS) implemented in the DMol<sup>3</sup> program was employed for the solvent phase calculations, and for determining essential thermodynamic properties. Aqueous solubility calculation was accomplished with Cramer *et al.* solubility model while chemical reactivity was predicted based on calculated global and local reactivity indices. Photocatalyst suitability was assessed in terms of the energy gap between appropriate frontier molecular orbitals of the dyes and the band edges of the catalysts while photodegradation mechanism was investigated through potential energy scans and transition state optimization.

This study resulted in numerous derivatives of DY119 and DR73 dyes with striking improvement in solubility and reactivity properties. Of interest are the variations observed in the performances of the substituent groups, where electron withdrawing -CN substituent was found to enhance the solubility of the dyes better than -NO<sub>2</sub> group, while -NH<sub>2</sub> substituent showed the greatest effect on solubility among the electron donating groups (EDG) considered. Highest solubility value was obtained with a combination of -CN and -NH<sub>2</sub>, and predicted properties showed appreciable dependency on substituent group positions in the parent dye structures. Nearly all the derivatives were predicted to be more thermodynamically and thermally stable (i.e. more resistant to sublimation) than the parent dyes. Most of dyes were predicted to be more reactive in water, and among the selected photocatalysts, TiO<sub>2</sub> and ZnO were found to have the highest catalytic affinity for the dyes, though with different modes of interaction. DY119 was predicted to be amenable to photodegradation via a C-N bond cleavage mechanism, while the degradation of its derivatives appeared to be more feasible via N-N bond cleavage pathway. In the case of DR73, 85% of the studied derivatives and the unsubstituted dye were predicted to be susceptible to photodegradation through an N-N bond cleavage pathway, about 7% of them favored a C-N bond cleavage pathway while the remaining derivatives showed evidence of competing C-N and N-N bond cleavage photodegradation pathways.

The reaction profile obtained for DY119 degradation confirmed that the C–N bond cleavage mechanism is the preferred photodegradation pathway for this dye. In the case of DR73, kinetic evidence showed that initial addition of •OH radical through one of the azo (N=N) nitrogen atoms (i.e. radical attack on N) will occur more rapidly compared to

its addition through a ring carbon attached to the azo group (i.e. radical attack on C), which is in accord with the local reactivity prediction. However, the overall activation energy for the N-N bond cleavage mechanism of this dye was found to be higher than that of the C-N bond. Removal of intramolecular hydrogen bond in DY119 resulted in a significant increase in the rate of both mechanisms, but with prevalence of the C-N bond. Mineralisation of the bond cleavage products through deamination and nitrogen evolution reactions was found to be kinetically and thermodynamically feasible.

Finally, the study revealed that molecular symmetry does not play a significant role in the choice of photodegradation mechanism of azo dyes. However, the existence of an azo dye in different tautomeric forms could significantly influence the choice of photodegradation pathway. We conclude that the findings of this work could be useful in developing new azo disperse dyes with interesting physicochemical properties for more economic, eco-friendly and wider range of application.

## TABLE OF CONTENTS

---

<b><u>Section</u></b>	<b><u>Page</u></b>
Declaration .....	iii
Dedication .....	iv
Publications and Presentations.....	v
Acknowledgements.....	viii
Abstract.....	x
Table of Contents.....	xiv
List of Figures.....	xxiii
List of Tables.....	xxviii
List of Schemes.....	xxx
List of Abbreviations.....	xxxi
List of Equations.....	xxxv
<b>CHAPTER 1.....</b>	<b>1</b>
<b>INTRODUCTION.....</b>	<b>1</b>
1.1 BACKGROUND.....	1
1.2 PROBLEM STATEMENTS.....	5
1.3 JUSTIFICATION.....	8
1.4 AIM AND OBJECTIVES OF THE STUDY.....	12
1.4.1 AIM.....	12
1.4.2 OBJECTIVES.....	12
1.5 OUTLINE OF THE THESIS.....	13

1.6	REFERENCES .....	15
<b>CHAPTER 2</b>	<b>.....</b>	<b>22</b>
<b>LITERATURE REVIEW</b>	<b>.....</b>	<b>22</b>
2.1	INTRODUCTION .....	22
2.2	DISPERSE DYES.....	22
2.3	DISPERSE DYE CLASSIFICATIONS .....	23
2.4	AZO CLASS.....	24
2.5	WHY FOCUS ON AZO DISPERSE DYES .....	26
2.6	ENVIRONMENTAL AND HEALTH IMPACTS OF AZO DISPERSE DYES .....	28
2.7	PHOTOCATALYTIC DEGRADATION .....	30
2.8	POLLUTANT – PHOTOCATALYST INTERACTION .....	32
2.9	INTRINSIC PROPERTIES AFFECTING DISPERSE DYE APPLICATION .....	34
2.10	AQUEOUS SOLUBILITY .....	35
2.11	LEVELLING AND FASTNESS.....	35
2.11.1	LIGHT FASTNESS .....	36
2.11.2	WASH FASTNESS .....	37
2.11.3	SUBLIMATION FASTNESS.....	38
2.11.4	PERSPIRATION FASTNESS .....	38
2.12	CHALLENGES OF AZO DISPERSE DYE APPLICATION .....	39
2.13	PREVIOUS WORKS ON IMPROVING AZO DISPERSE DYE APPLICATION ..	40
2.14	PREVIOUS THEORETICAL STUDIES ON AZO DYES .....	45
2.15	THE CURRENT STUDY .....	46
2.15.1	AQUEOUS SOLUBILITY STUDY .....	48
2.15.2	CHEMICAL REACTIVITY STUDY .....	49
2.15.3	PHOTOCATALYTIC DEGRADATION PATHWAYS .....	50
2.16	REFERENCE.....	52
<b>CHAPTER 3</b>	<b>.....</b>	<b>67</b>
<b>THEORETICAL CHEMISTRY</b>	<b>.....</b>	<b>67</b>
3.1	INTRODUCTION .....	67
3.2	DENSITY FUNCTIONAL THEORY (DFT) .....	67

3.3	WAVEFUNCTION-BASED ELECTRONIC STRUCTURE CALCULATION .....	68
3.4	ELECTRON DENSITY-BASED ELECTRONIC STRUCTURE CALCULATION .	73
3.5	DENSITY FUNCTIONALS .....	77
3.5.1	LOCAL DENSITY APPROXIMATION (LDA).....	77
3.5.2	GENERALIZED-GRADIENT APPROXIMATION (GGA).....	78
3.5.3	HYBRID DENSITY FUNCTIONALS.....	80
3.5.4	VAN DER WAAL DENSITY FUNCTIONALS (vdW-DF).....	81
3.6	BASIS SETS.....	81
3.6.1	SLATER-TYPE ORBITALS (STOs) .....	82
3.6.2	GAUSSIAN TYPE ORBITALS (GTOs) .....	83
3.6.3	MINIMAL BASIS SET (MBS) .....	85
3.6.4	SPLIT-VALENCE BASIS SET (SVBS).....	86
3.6.5	POLARIZATION BASIS SET (PBS).....	86
3.6.6	DIFFUSE BASIS SET (DBS) .....	87
3.6.7	THE DUNNING BASIS SETS (DNBS) .....	88
3.6.8	NUMERICAL BASIS SETS (NBS) .....	88
3.6.9	GENERATION OF NUMERICAL BASIS SETS .....	889
3.7	SOLUBILITY PREDICTION MODELS.....	91
3.7.1	INFORMATICS .....	92
3.7.2	GENERAL SOLUBILITY EQUATION (GSE).....	93
3.7.3	EXPLICIT SOLVATION MODELS (ESM) .....	94
3.7.4	IMPLICIT SOLVATION MODELS (ISM) .....	95
3.7.5	POLARIZABLE CONTINUUM MODELS (PCM) .....	95
3.7.6	POISSON-BOLTZMANN (PB) MODELS .....	97
3.7.7	GENERALIZED BORN (GB) MODEL.....	98
3.7.8	INTEGRAL EQUATION FORMALISM POLARIZABLE CONTINUUM MODELS (IEFPCM).....	98
3.7.9	CONDUCTOR-LIKE SCREENING MODEL (COSMO) .....	99
3.7.10	COSMO-RS .....	101
3.7.11	SOLUBILITY AND SOLVATION FREE ENERGY RELATIONSHIP .	103
3.8	CHEMICAL REACTIVITY INDICES (CRI) .....	105

3.8.1	GLOBAL REACTIVITY DESCRIPTORS (GRD) .....	105
3.8.2	LOCAL REACTIVITY DESCRIPTORS (LRD).....	107
3.8.3	FUKUI FUNCTION.....	108
3.9	POTENTIAL ENERGY SURFACES (PES).....	110
3.9.1	POTENTIAL ENERGY SURFACE AND KINETICS.....	110
3.9.2	POTENTIAL ENERGY SURFACE AND THERMODYNAMICS .....	112
3.9.3	KINETIC AND THERMODYNAMIC CONTROLLED REACTIONS ....	113
3.9.4	REACTIONS WITHOUT ENERGY BARRIER .....	114
3.10	REFERENCE.....	114
<b>CHAPTER 4.....</b>		<b>123</b>
<b>COMPUTATIONAL RESOURCES .....</b>		<b>123</b>
4.1	INTRODUCTION .....	123
4.2	BIOVIA MATERIAL STUDIO .....	123
4.3	MATERIALS STUDIO DMOL <sup>3</sup> .....	125
4.3.1	USES OF DMOL <sup>3</sup> .....	125
4.3.2	ADVANTAGES OF DMOL <sup>3</sup> .....	126
4.3.3	PERFORMANCE OF DMOL <sup>3</sup> .....	126
4.3.4	FEATURES OF MSDMOL <sup>3</sup> .....	128
4.3.5	CALCULATION TASKS .....	128
4.3.6	FUNCTIONALS.....	128
4.3.7	BASIS SETS.....	129
4.3.8	PREDICTABLE PROPERTIES .....	129
4.4	PROPERTIES OF THE CHPC LENGAU CLUSTER .....	129
4.5	REFERENCES .....	130
<b>CHAPTER 5.....</b>		<b>133</b>
<b>DMOL<sup>3</sup>/COSMO-RS PREDICTION OF AQUEOUS SOLUBILITY AND REACTIVITY OF SELECTED AZO DYES: EFFECT OF GLOBAL ORBITAL CUT-OFF AND COSMO SEGMENT VARIATION.....</b>		<b>133</b>
PREAMBLE.....		133



5.1	INTRODUCTION .....	133
5.2	COMPUTATIONAL DETAILS .....	137
5.3	RESULTS AND DISCUSSIONS .....	141
5.3.1	AQUEOUS SOLUBILITY STUDY .....	141
5.3.2	EFFECT OF ORBITAL CUT-OFF VARIATION.....	143
5.3.3	EFFECT OF NSPA (COSMO SEGMENT) VARIATION .....	149
5.3.4	CHEMICAL REACTIVITY STUDY .....	155
5.3.5	EFFECTS OF NO <sub>2</sub> <sup>-</sup> AND Cl <sup>-</sup> SUBSTITUENTS ON SOLUBILITY AND REACTIVITY OF D1-D4 .....	163
5.4	CONCLUSION.....	166
5.5	REFERENCES .....	166
<b>CHAPTER 6.....</b>		<b>174</b>
<b>PREDICTION OF AQUEOUS SOLUBILITY BY TREATMENT OF COSMO-RS DATA WITH EMPIRICAL SOLUBILITY EQUATIONS: THE ROLES OF GLOBAL ORBITAL CUT-OFF AND COSMO SOLVENT RADIUS.....</b>		<b>174</b>
PREAMBLE.....		174
6.1	INTRODUCTION .....	174
6.2	COMPUTATIONAL DETAILS .....	178
6.3	RESULTS AND DISCUSSION .....	181
6.3.1	AQUEOUS SOLUBILITY STUDY .....	181
6.3.2	EFFECT OF CUT-OFF ON CSE PREDICTED SOLUBILITY (S <sub>CSE</sub> )..	183
6.3.3	EFFECT OF CUT-OFF ON GSE PREDICTED SOLUBILITY (S <sub>GSE</sub> ) .	185
6.3.4	EFFECT OF COSMO SOLVENT RADIUS ON CSE PREDICTED SOLUBILITY (S <sub>CSE</sub> ) .....	187
6.3.4	EFFECT OF CSR ON GSE PREDICTED SOLUBILITY (S <sub>GSE</sub> ) .....	192
6.4	CONCLUSION.....	194
6.5	REFERENCES .....	195
<b>CHAPTER 7.....</b>		<b>201</b>

**COMPUTATIONAL STUDY OF THE EFFECTS OF SUBSTITUENT GROUPS ON SOLUBILITY AND REACTIVITY OF DISPERSE YELLOW 119 DYE ..... 201**

PREAMBLE.....	201
7.1 INTRODUCTION .....	201
7.2 COMPUTATIONAL DETAILS.....	204
7.3 RESULTS AND DISCUSSIONS.....	207
7.3.1 AQUEOUS SOLUBILITY STUDY .....	207
7.3.2 CORRELATION OF AQUEOUS SOLUBILITY WITH DIPOLE MOMENT ( $\mu$ ), POLARIZABILITY ( $\alpha$ ) AND SCREENING CHARGES ( $q$ ).....	219
7.3.3 CHEMICAL REACTIVITY STUDY .....	221
7.3.4 PREDICTION OF SUITABLE CATALYST FOR PHOTOCATALYTIC DEGRADATION OF THE DYES.....	229
7.3.5 SITE EVALUATION FOR RADICAL ATTACK AND PREDICTION OF DEGRADATION PATHWAY.....	232
7.4 CONCLUSION.....	235
7.5 REFERENCES.....	237
<b>CHAPTER 8.....</b>	<b>244</b>

**SYNERGISTIC EFFECT OF OPPOSITE POLAR SUBSTITUENTS ON SELECTED PROPERTIES OF DISPERSE YELLOW 119 DYE ..... 244**

PREAMBLE.....	244
8.1 INTRODUCTION .....	244
8.2 COMPUTATIONAL DETAILS.....	246
8.2.1 PROCEDURE FOR CALCULATING THE AQUEOUS SOLUBILITY AND GIBB'S FREE ENERGIES.....	247
8.2.2 PROCEDURE FOR PREDICTING THE CHEMICAL REACTIVITY...	248
8.3 RESULTS AND DISCUSSIONS.....	249
8.3.1 AQUEOUS SOLUBILITY STUDY .....	249
8.3.2 GLOBAL REACTIVITY STUDY .....	260
8.3.3 LOCAL REACTIVITY STUDY.....	260
8.3.4 CATALYTIC SELECTIVITY .....	266

8.4	CONCLUSION.....	267
8.5	REFERENCES .....	268
<b>CHAPTER 9.....</b>		<b>275</b>
<b>THEORETICAL MODELLING OF SUBSTITUENT EFFECTS ON AQUEOUS SOLUBILITY, CHEMICAL REACTIVITY AND ABSORPTION WAVELENGTH OF DISPERSE RED 73.....</b>		<b>275</b>
PREAMBLE.....		275
9.1	INTRODUCTION .....	275
9.2	COMPUTATIONAL DETAILS.....	280
9.3	RESULTS AND DISCUSSIONS.....	284
9.3.1	AQUEOUS SOLUBILITY STUDY .....	284
9.3.2	EFFECTS OF X <sup>-</sup> GROUPS ON SOLUBILITY.....	287
9.3.3	EFFECTS OF X <sup>+</sup> GROUPS ON SOLUBILITY .....	291
9.3.4	EFFECTS OF X <sup>-</sup> AND X <sup>+</sup> GROUPS ON SOLUBILITY.....	296
9.3.5	PREDICTION OF HEAT RESISTANCE CAPACITY AND THERMODYNAMIC STABILITY OF THE DYES.....	297
9.3.6	CHEMICAL REACTIVITY STUDY .....	298
9.3.7	EFFECTS OF X <sup>-</sup> SUBSTITUTION ON REACTIVITY .....	298
9.3.8	EFFECTS OF X <sup>+</sup> SUBSTITUTION ON REACTIVITY .....	303
9.3.9	EFFECTS OF X <sup>-</sup> AND X <sup>+</sup> ON REACTIVITY.....	305
9.3.10	PREDICTION OF SUITABLE CATALYSTS FOR PHOTOCATALYTIC DEGRADATION OF THE DYES.....	308
9.3.11	SITE SELECTIVITY STUDY FOR RADICAL ATTACK AND PREDICTION OF PHOTODEGRADATION PATHWAY .....	311
9.3.12	PREDICTION OF THE ABSORPTION WAVELENGTHS OF SOME AZO DISPERSE DYES.....	315
9.3.13	EFFECTS OF SUBSTITUTION ON THE ABSORPTION WAVELENGTH OF DR73 .....	316
9.4	CONCLUSION.....	320
9.5	REFERENCES .....	321

<b>CHAPTER 10.....</b>	<b>333</b>
<b>A COMPUTATIONAL MECHANISTIC STUDY OF HYDROXYL RADICAL INITIATED DEGRADATION OF DISPERSE YELLOW 119 .....</b>	<b>333</b>
PREAMBLE.....	333
10.1 INTRODUCTION .....	333
10.2 COMPUTATIONAL DETAILS.....	337
10.2.1 COMPUTATIONAL SOFTWARE.....	337
10.2.2 CALCULATION PROCEDURE .....	338
10.3 RESULTS AND DISCUSSIONS.....	339
10.3.1 DETERMINATION OF SITE PROPENSITY TO RADICAL ATTACK.....	339
10.3.2 C-N BOND RUPTURE DEGRADATION MECHANISM.....	340
10.3.3 EFFECT OF WATER ON C-N BOND RUPTURE DEGRADATION MECHANISM.....	342
10.3.4 N-N BOND RUPTURE DEGRADATION MECHANISM.....	343
10.3.5 EFFECT OF WATER ON N-N BOND RUPTURE DEGRADATION MECHANISM.....	345
10.3.6 COMPARISON BETWEEN THE C-N AND THE N-N BOND RUPTURE DEGRADATION MECHANISMS .....	346
10.3.7 EFFECT OF HYDROGEN BONDING.....	347
10.3.8 EVOLUTION OF NITROGEN MOLECULE.....	350
10.4 CONCLUSION.....	351
10.5 REFERENCES .....	352
<b>CHAPTER 11.....</b>	<b>358</b>
<b>A DFT STUDY OF HYDROXYL RADICAL DEGRADATION OF DISPERSE RED 73 (DR73).....</b>	<b>358</b>
PREAMBLE.....	358
11.1 INTRODUCTION .....	358
11.2 COMPUTATIONAL DETAILS.....	361
11.2.1 COMPUTATIONAL SOFTWARE.....	362

11.2.2	CALCULATION PROCEDURE .....	362
11.3	RESULTS AND DISCUSSIONS .....	364
11.3.1	ASSESSMENT OF SITE SUSCEPTIBILITY TO RADICAL ATTACK .....	364
11.3.2	N-N BOND RUPTURE DEGRADATION MECHANISM.....	365
11.3.3	EFFECT OF WATER ON N–N BOND RUPTURE DEGRADATION MECHANISM.....	367
11.3.4	C-N BOND RUPTURE DEGRADATION MECHANISM.....	368
11.3.5	EFFECT OF WATER ON C–N BOND RUPTURE DEGRADATION MECHANISM.....	370
11.3.6	COMPARISON BETWEEN THE N–N AND THE C–N BOND RUPTURE DEGRADATION MECHANISMS .....	371
11.3.7	DEAMINATION.....	373
11.3.8	LOSS OF MOLECULAR NITROGEN.....	378
11.3.9	IMPLICATIONS OF DEAMINATION AND NITROGEN EVOLUTION PROCESSES .....	379
11.4	CONCLUSION.....	380
11.5	REFERENCES .....	381
<b>CHAPTER 12</b>	.....	<b>387</b>
<b>CONCLUSIONS AND RECOMMENDATIONS</b>	.....	<b>387</b>
12.1	CONCLUSIONS .....	387
12.1.1	AQUEOUS SOLUBILITY STUDY .....	387
12.1.2	CHEMICAL REACTIVITY STUDY .....	388
12.1.3	PHOTODEGRADATION PATHWAY STUDY.....	389
12.2	RECOMMENDATIONS .....	390
<b>APPENDIX</b>	.....	<b>392</b>

## LIST OF FIGURES

<u>Figure</u>	<u>Description</u>	<u>Page</u>
Figure 1.1:	The general molecular structures of aminoazobenzene and azopyridone disperse dyes.....	4
Figure 1.2:	The molecular structures of DY119 and DR73.....	11
Figure 2.1:	General molecular structure of aminoazobenzene dyes..	25
Figure 2.2:	Molecular structure of azopyridone, azothiophene and azobenzothiazole dyes. ....	26
Figure 2.3:	A schematic diagram showing the band gap ( $E_g$ ) of a photocatalyst.....	31
Figure 2.4:	C–N and N–N bond cleavage degradation mechanisms of azo dyes. ....	51
Figure 3.1:	Negative poles of water molecules oriented around a solvated charged solute, $Q^+$ .....	96
Figure 3.2:	A schematic diagram showing an ideally screened and solvated solute in a perfect conductor. ....	100
Figure 3.3:	A typical sigma profile of a four component mixture .....	102
Figure 3.4:	A one step reaction PES of reactant R occurring via pathways A and B with activation energies $E_A$ and $E_B$ respectively to form products $P_A$ and $P_B$ .. .....	111
Figure 3.5:	A multi-step reaction PES of reactant R where $E_1$ , $E_2$ and $E_3$ are the activation energies for the three steps. ....	112
Figure 4.1:	The Material Studio Interface .....	124
Figure 5.1:	Base ten logarithm of the aqueous solubility values for D1, D2, D3 and D4 as a function of orbital cut-off.....	144
Figure 5.2:	Log $S_{GSE}$ and Log P for D1, D2, D3 and D4 as a function of orbital cut-off.....	145
Figure 5.3:	Solvation free energy, vapour pressure and Log $S_{CSE}$ for D1, D2, D3 and D4 as a function of orbital cut-off.....	146
Figure 5.4:	Best log $S_{CSE}$ and log $S_{GSE}$ values obtained for D1, D2, D3 and D4 as functions of NSPA. ....	150

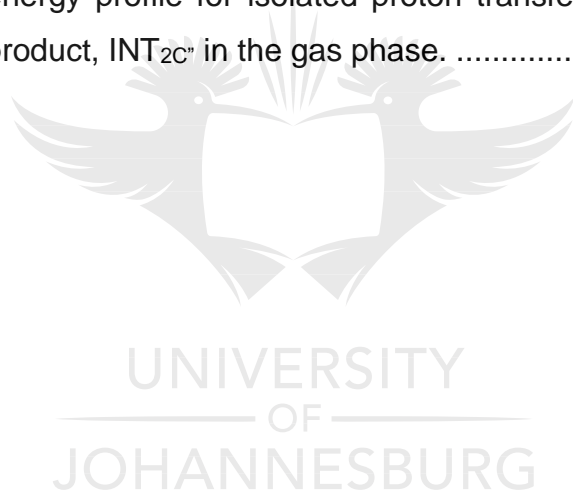
Figure 5.5: COSMO screening charges for D1, D2, D3 and D4 as a function of NSPA.....	152
Figure 5.6: Dipole moments for D1, D2, D3 and D4 as a function of Orbital cut-off. ...	153
Figure 5.7: Calculated polarizability values for D1, D2, D3 and D4 as a function of NSPA. .....	154
Figure 5.8: HOMO energy as a function of orbital cut-off. ....	157
Figure 5.9: LUMO energy as a function of orbital cut-off. ....	158
Figure 5.10: HOMO-LUMO energy gap as a function of orbital cut-off.....	159
Figure 5.11: Isosurfaces of the HOMOs of D1, D2, D3 and D4 in gas and water.....	160
Figure 5.12: Isosurfaces of the LUMOs of D1, D2, D3 and D4 in gas and water. ....	161
Figure 5.13: Aqueous phase frontier molecular orbitals of the dyes as a function of NSPA at a cut-off value of 4.5 Å. ....	163
Figure 6.1: Base ten logarithm of average CSE and GSE predicted solubility values for B1, B2, B3 and B4 at 298 K. ....	182
Figure 6.2: Variation of log $S_{CSE}$ values of B1, B2, B3 and B4 with orbital cut-off. ....	184
Figure 6.3: Log $S_{GSE}$ for B1, B2, B3 and B4 as a function of orbital cut-off. ....	186
Figure 6.4: Log $S_{CSE}$ for B1, B2, B3 and B4 as a function of COSMO solvent radius..	188
Figure 6.5: COSMO screening charges for B1, B2, B3 and B4 as a function of COSMO solvent radius.....	189
Figure 6.6: Dipole moments for B1, B2, B3 and B4 as a function of COSMO solvent radius. .....	190
Figure 6.7: Molecular structures of B1, B2, B3 and B4 with their respective Molecular weights.....	192
Figure 6.8: Log $S_{GSE}$ for B1, B2, B3 and B4 as a function of COSMO solvent radius.	194
Figure 7.1: General molecular structures of the azo and hydrazone forms of the studied dyes. ....	204
Figure 7.2: Optimized structures of E21, E25 and E29 showing the torsion angles of $NH_2$ , $NHCH_3$ and $N(CH_3)_2$ substituents respectively at positions $R_4$ and $R_5$ ...	211
Figure 7.3: Optimized structures of E21, E25 and E29 showing the lengths of the C – N and N – N bond formed at positions $R_4$ and $R_5$ respectively, by $NH_2$ , $NHCH_3$ and $N(CH_3)_2$ substituents. ....	212

Figure 7.4: Optimized structures of E21, E25 and E29 showing the available sites for hydrogen bonding. ....	214
Figure 7.5: Equilibrium geometries of azo and hydrazone tautomeric forms of of DY119 dye showing the direction of dipole moment vectors. ....	214
Figure 7.6: VWN-BP/DNP optimized geometries of the azo and hydrazone forms of DY119.....	215
Figure 7.7: Optimized geometries of NH <sub>2</sub> , NHCH <sub>3</sub> and N(CH <sub>3</sub> ) <sub>2</sub> showing their respective dipole moment vectors. ....	218
Figure 7.8: Dependence of solubility of the EWG substituted derivatives on screening charge, dipole moment and polarizability.....	220
Figure 7.9: Dependence of solubility of some EDG substituted derivatives on screening charge, dipole moment and polarizability.....	220
Figure 7.10: Optimized model of DY119 showing the showing the prospectives sites for radical attack.....	233
Figure 8.1: General molecular structure of DY 119 (R <sub>1</sub> = R <sub>3</sub> = H, R <sub>4</sub> = CH <sub>3</sub> and R <sub>5</sub> = C <sub>2</sub> H <sub>5</sub> ) and its studied derivatives.....	246
Figure 8.2: Comparison of aqueous solubility values of Group A (I) and Group B (II) (derivatives of DY119) .....	251
Figure 8.3: Comparison of the screening charges of Group A (I) and Group B (II) derivatives.....	253
Figure 8.4: Comparison of the dipole moments of Group A (I) and Group B (II) derivatives. ....	254
Figure 8.5: Some optimized NH <sub>2</sub> , NHCH <sub>3</sub> and N(CH <sub>3</sub> ) <sub>2</sub> substituted derivatives for which the substituents occupy positions R <sub>4</sub> and R <sub>5</sub> in the dye structures.. .....	257
Figure 8.6: Some optimized geometries of NH <sub>2</sub> , NHCH <sub>3</sub> and N(CH <sub>3</sub> ) <sub>2</sub> substituted derivatives showing the lengths of the bonds formed between the substituents and the donor unit at substitution positions R <sub>4</sub> and R <sub>5</sub> in the dye structures.....	258
Figure 8.7: HOMO (I) and LUMO (II) energies of Group C derivatives.....	261
Figure 8.8: HOMO (I) and LUMO (II) energies of Group D derivatives.....	262



Figure 8.9: An optimized geometry of DY119 showing the probable sites C <sub>4</sub> , N <sub>7</sub> , N <sub>8</sub> and C <sub>9</sub> for radical attack.....	265
Figure 9.1: General molecular structure of the studied DR73 dyes.....	280
Figure 9.2: Isosurfaces of the HOMO (I) and LUMO (II) of DR73 showing electron density distribution between the acceptor and donator units of the molecule. ...	287
Figure 9.3: Models of some X <sup>+</sup> substituted DR73 showing different torsion angles between the planes of the ring and the amine substituents due to varying magnitude of steric effect at positions R <sub>4</sub> and R <sub>5</sub> .....	293
Figure 9.4: Models of some X <sup>+</sup> substituted DR73 showing the lengths of the C – N bonds formed by the X <sup>+</sup> substituents at positions R <sub>4</sub> and R <sub>5</sub> . ....	295
Figure 9.5: Optimized model of DR73 showing the prospective sites for attack of radicals..	312
Figure 10.1: Molecular structure of disperse yellow 119 (DY119). ....	347
Figure 10.2: Optimized geometry of DY119 showing the prospective reaction sites for •OH radical.....	339
Figure 10.3: Potential energy profile for •OH radical initiated degradation of DY119 via a C–N bond cleavage mechanism. ....	341
Figure 10.4: Potential energy profile for •OH radical initiated degradation of DY119 via an N–N bond cleavage mechanism. ....	344
Figure 10.5: Molecular structure of disperse yellow 119 conformer (DYIS).....	347
Figure 10.6: Potential energy profile for •OH radical initiated degradation of DYIS via a C–N bond cleavage mechanism. ....	348
Figure 10.7: Potential energy profile for •OH radical initiated degradation of DYIS via an N–N bond cleavage mechanism. ....	348
Figure 10.8: Potential energy profile for •OH radical initiated loss of nitrogen molecule. ....	351
Figure 11.1: Molecular structure of Disperse red 73 (DR73). ....	361
Figure 11.2: Optimized geometry of DR73 showing the prospective reaction sites for •OH radical. ....	364
Figure 11.3: Potential energy profile for •OH radical initiated degradation of DR73 via an N–N bond cleavage mechanism. ....	367

Figure 11.4: Potential energy profile for •OH radical initiated degradation of DR73 via a C–N bond rupture mechanism. ....	370
Figure 11.5: Potential energy profile for •OH radical initiated deamination of P <sub>N2</sub> . ....	376
Figure 11.6: Potential energy profile for •OH radical initiated deamination of P <sub>C2</sub> . ....	376
Figure 11.7: Potential energy profile for •OH radical initiated loss of nitrogen molecule from the C–N bond cleavage product, P <sub>C1</sub> . ....	379
Figure A.1: Equilibrium geometry of DR73 dye showing the direction of dipole moment vectors. ....	418
Figure A.2: Molecular structures of the test azo disperse dyes. ....	418
Figure A.3: Geometry of the cyclic transition state structure, TS <sub>2N</sub> . ....	419
Figure A.4: Comparison of selected dihedral angles between INT <sub>1N</sub> and INT <sub>2N</sub> . ....	419
Figure A.5: Potential energy profile for isolated proton transfer reaction of the radical addition product, INT <sub>2C</sub> * in the gas phase. ....	420



## LIST OF TABLES

<u>Table</u>	<u>Description</u>	<u>Page</u>
Table 3.1:	Generation of Numerical basis set for Carbon.....	91
Table 3.2:	Some elemental atomic radii used for construction of COSMO molecular cavity. .....	100
Table 5.1:	Molecular structures of studied dyes and their physicochemical properties. .....	136
Table 5.2:	Comparison of the best $S_{CSE}$ and $S_{GSE}$ results obtained for D1, D2, D3 and D4 with their respective experimental solubility ( $S_{Expt.}$ ) at 25 °C. ....	141
Table 5.3:	Calculated solubility ( $S_{CSE}$ and $S_{GSE}$ ), screening charge, $q$ , dipole moment, $\mu$ , polarizability, $\alpha$ , solvation free energy (SFE), HOMO and LUMO energies for D1, D2, D3 and D4 at 25 °C.....	164
Table 6.1:	Molecular structures of studied dyes and their physicochemical properties. .....	178
Table 7.1:	Aqueous solubility ( $S_{aq}$ ), SFE ( $\Delta G_{sol}$ ), vapour pressure ( $p$ ) and the Gibb's free energies ( $G_{gas}$ ) obtained for DY119 and its studied derivatives at 25 °C. .....	208
Table 7.2:	Screening charges, $q$ , polarizability, $\alpha$ , and dipole moment, $\mu$ of DY119 and its studied derivatives at 25 °C. ....	209
Table 7.3:	HOMO energies ( $E_{HOMO}$ ), LUMO energies ( $E_{LUMO}$ ), HOMO-LUMO energy gap ( $E_g$ ) and hardness ( $\eta$ ) of DY119 and its studied derivatives.....	222
Table 7.4:	Softness, $\sigma$ , electronegativity, $\chi$ , chemical potential, $\Phi$ , and electrophilicity indices, $\omega$ , of DY119 and its studied derivatives.....	226
Table 7.5:	Calculated energy gaps between the FMO (i.e. HOMO and LUMO) of the studied dyes and the band edges of the catalysts. ....	230
Table 7.6:	Radical attack Fukui functions, $f^0$ for the most active sites in the studied dyes. .....	233
Table 8.1:	Predicted solubility values of members of groups A and B derivatives of DY119 at 25 °C.....	252

Table 9.1: Aqueous solubility ( $S_{aq}$ ), SFE ( $\Delta G_{sol}$ ), vapour pressure ( $p$ ) and the Gibb's free energies ( $\Delta G_{gas}$ ) obtained for DR73 and its studied derivatives at 25 °C. .....	285
Table 9.2: Screening charges, $q$ , polarizability, $\alpha$ , and dipole moment, $\mu$ of DR73 and its studied derivatives at 25 °C. ....	288
Table 9.3: HOMO energies ( $E_{HOMO}$ ), LUMO energies ( $E_{LUMO}$ ), HOMO-LUMO energy gap ( $E_g$ ) and hardness ( $\eta$ ) of DR73 and its studied derivatives. ....	301
Table 9.4: Calculated energy gaps between the FMO (i.e. HOMO and LUMO) of the studied dyes and the band edges of the catalysts. ....	310
Table 9.5: Fukui functions, $f^0$ for prospective sites for radical attack in the studied dyes. .....	313
Table 9.6: Comparison of predicted and experimental absorption wavelengths of some test azo disperse dyes. ....	316
Table 9.7: Predicted dipole moment ( $\mu$ ), HOMO-LUMO energy gap (H-L gap) and absorption wavelength ( $\lambda_{cis}$ and $\lambda_{H-L}$ ) of DR73 and its studied analogues. .....	317
Table 10.1: Mulliken radical attack Fukui functions, $f_0$ for the prospective reaction sites in DY119.....	340
Table 10.2: Energetic parameters for the C-N and the N-N bond cleavage degradation mechanisms.....	347
Table 11.1: Mulliken radical attack Fukui functions, $f^0$ for the prospective reaction sites in DR73.....	364
Table 11.2: Energetic parameters for the C-N and the N-N bond rupture degradation mechanisms.....	372
Table 11.3: Activation parameters for the deamination of $P_{N2}$ and $P_{C2}$ by $\bullet OH$ radical. .....	377

## LIST OF SCHEMES

<u>Scheme</u>	<u>Description</u>	<u>Page</u>
Scheme 1.1:	Azo – hydrazone tautomerism in 2-methyl-4-(4'-sulfophenylazo) phenol, Acid Orange 7 and Alizarin Yellow R. ....	8
Scheme 1.2:	Azo – hydrazone tautomerism involving the azo and the hydrazone tautomers of Disperse Yellow 119 dye.....	11
Scheme 2.1:	Synthesis of azo pyridone disperse dye from pyridone (coupling agent) and benzenediazonium ion (diazotization agent).....	28
Scheme 2.2:	Photocatalytic degradation of a pollutant initiated by photo-generated holes and electrons. ....	32
Scheme 3.1:	A tri-phasic equilibrium system of a pure solute S, its vapor and its aqueous solution. ....	110
Scheme 3.2:	An overall bi-phasic equilibrium equation involving the solute vapor and its aqueous solution.....	110
Scheme 10.1:	Photocatalytic production of •OH radical. ....	334
Scheme 10.2:	C–N bond rupture degradation mechanism.....	342
Scheme 10.3:	N–N bond rupture degradation mechanism.....	345
Scheme 11.1:	Photochemical production of •OH radical during a photocatalytic degradation process. ....	359
Scheme 11.2:	N–N bond rupture degradation mechanism.....	366
Scheme 11.3:	C–N bond rupture degradation mechanism.....	369
Scheme 11.4:	•OH radical initiated deamination of P <sub>N2</sub> .....	374
Scheme 11.5:	•OH radical initiated deamination of P <sub>C2</sub> .....	375
Scheme 11.6:	•OH radical initiated removal of molecular nitrogen from the C-N bond cleavage product, P <sub>C1</sub> .....	378

## LIST OF ABBREVIATIONS

---

3D-RISM	3-Dimensional Reference Interaction Site Models
CB	Conduction Band
CBE	Conduction Band Edge
COD/BOD	Chemical/Biochemical oxygen demand
COSMO	Conductor-Like Screening Model
COSMO-RS	Conductor-Like Screening Model for Realistic Solvation
COSMO-SAC	Conductor-Like Screening Model – Segment Activity Coefficient
CRI	Chemical Reactivity Indices
CSE	Cramer et al. Solubility Equation
CSR	Cosmo Solvent Radius
DBS	Diffused Basis Set
DFT	Density Functional Theory
DNBS	Dunning Basis Sets
DR73	Disperse Red 73
DY119	Disperse Yellow 119

DYIS	Disperse Yellow 119 Conformer
EDG	Electron Donating Group
EDS	Electron Donating Substituent
ESM	Explicit Solvation Models
EWG	Electron Withdrawing Group
EWS	Electron Withdrawing Substituent
FMO	Frontier Molecular Orbital
GB	Generalized Born
GGA	Generalized-Gradient Approximation
GRD	Global Reactivity Descriptors
GSE	General Solubility Equation
GTOs	Gaussian Type Orbitals
HF	Hartree-Fock
HOMO	Highest Occupied Molecular Orbital
HTHP	High Temperature High Pressure
ICI	Imperial Chemical Industries
IEFPCM	Integral Equation Formalism Polarizable Continuum Models

ISM	Implicit Solvation Models
LDA	Local Density Approximation
LRD	Local Reactivity Descriptors
LUMO	Lowest Unoccupied Molecular Orbital
MBS	Minimal Basis Set
MSDMol <sup>3</sup>	Materials Studio DMol <sup>3</sup>
NBS	Numerical Basis Sets
NSPA	Number of Surface Segment per Atom
PB	Poisson-Boltzmann
PBS	Polarization Basis Set
PCM	Polarizable Continuum Models
PES	Potential Energy Surfaces
SCD	Supercritical Carbon Dioxide
S <sub>CSE</sub>	CSE Predicted Solubility
SFE	Solvation Free Energy
S <sub>GSE</sub>	GSE Predicted Solubility
SM	Solvation Models



STOs	Slater-Type Orbitals
SVBS	Split-Valence Basis Set
TDDFT	Time Dependent Density Functional Theory
VB	Valence Band
VBE	Valence Band Edge
vdW-DF	Van der Waal Density Functionals
VWN-BP	Becke and Perdew Version of Vosko Wilsk Nusair Functional



## LIST OF EQUATIONS

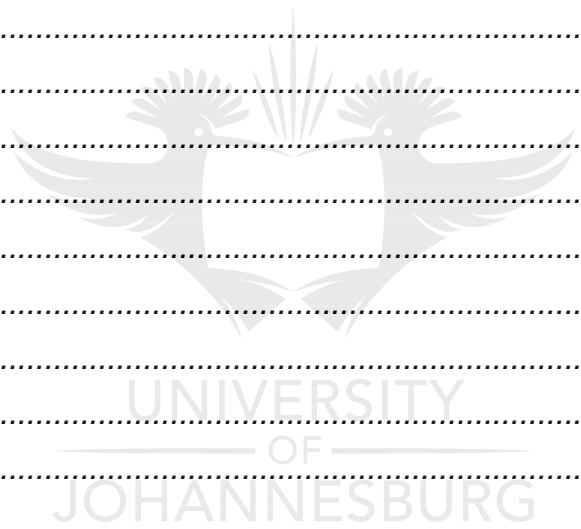
---

<u>Equation</u>	<u>Page</u>
Equation 2. 1 .....	49
Equation 2. 2 .....	49
Equation 3. 1 .....	69
Equation 3. 2 .....	69
Equation 3. 3 .....	70
Equation 3. 4 .....	70
Equation 3. 5 .....	70
Equation 3. 6 .....	71
Equation 3. 7 .....	71
Equation 3. 8 .....	72
Equation 3. 9 .....	72
Equation 3. 10 .....	72
Equation 3. 11 .....	73
Equation 3. 12 .....	73
Equation 3. 13 .....	73
Equation 3. 14 .....	74
Equation 3. 15 .....	75
Equation 3. 16 .....	75
Equation 3. 17 .....	75
Equation 3. 18 .....	75
Equation 3. 19 .....	75
Equation 3. 20 .....	75
Equation 3. 21 .....	75
Equation 3. 22 .....	75
Equation 3. 23 .....	75
Equation 3. 24 .....	76
Equation 3. 25 .....	76
Equation 3. 26 .....	76

Equation 3. 27.....	78
Equation 3. 28.....	78
Equation 3. 29.....	78
Equation 3. 30.....	78
Equation 3. 31.....	79
Equation 3. 32.....	80
Equation 3. 33.....	80
Equation 3. 34.....	81
Equation 3. 35.....	81
Equation 3. 36.....	83
Equation 3. 37.....	83
Equation 3. 38.....	84
Equation 3. 39.....	84
Equation 3. 40.....	84
Equation 3. 41.....	93
Equation 3. 42.....	93
Equation 3. 43.....	94
Equation 3. 44.....	94
Equation 3. 45.....	94
Equation 3. 46.....	96
Equation 3. 47.....	96
Equation 3. 48.....	97
Equation 3. 49.....	97
Equation 3. 50.....	97
Equation 3. 51.....	98
Equation 3. 52.....	100
Equation 3. 53.....	101
Equation 3. 54.....	103
Equation 3. 55.....	104
Equation 3. 56.....	104
Equation 3. 57.....	104



Equation 3. 58.....	104
Equation 3. 59.....	105
Equation 3. 60.....	106
Equation 3. 61.....	106
Equation 3. 62.....	107
Equation 3. 63.....	107
Equation 3. 64.....	107
Equation 3. 65.....	108
Equation 3. 66.....	108
Equation 3. 67.....	108
Equation 3. 68.....	109
Equation 3. 69.....	109
Equation 3. 70.....	109
Equation 3. 71.....	109
Equation 3. 72.....	109
Equation 3. 73.....	109
Equation 3. 74.....	111
Equation 3. 75.....	111
Equation 3. 76.....	112
Equation 3. 77.....	113
Equation 3. 78.....	113
Equation 5. 1.....	138
Equation 5. 2.....	139
Equation 5. 3.....	139
Equation 5. 4.....	139
Equation 5. 5.....	140
Equation 5. 6.....	140
Equation 5. 7.....	140
Equation 5. 8.....	140
Equation 5. 9.....	140
Equation 5. 10.....	140



Equation 6.1.....	180
Equation 6.2.....	180
Equation 6.3.....	180
Equation 6.4.....	181
Equation 7.1.....	205
Equation 7.2.....	205
Equation 7.3.....	205
Equation 7.4.....	206
Equation 7.5.....	206
Equation 7.6.....	206
Equation 7.7.....	206
Equation 7.8.....	206
Equation 7.9.....	206
Equation 7.10.....	206
Equation 7.11.....	207
Equation 7.12.....	219
Equation 7.13.....	220
Equation 7.14.....	220
Equation 8.1.....	247
Equation 8.2.....	247
Equation 8.3.....	247
Equation 8.4.....	247
Equation 8.5.....	248
Equation 8.6.....	248
Equation 8.7.....	248
Equation 8.8.....	248
Equation 8.9.....	248
Equation 8.10.....	248
Equation 8.11.....	249
Equation 9.1.....	281
Equation 9.2.....	281



<i>Equation 9. 3</i> .....	281
<i>Equation 9. 4</i> .....	282
<i>Equation 9. 5</i> .....	282
<i>Equation 9. 6</i> .....	282
<i>Equation 9. 7</i> .....	282
<i>Equation 9. 8</i> .....	282
<i>Equation 9. 9</i> .....	282
<i>Equation 9. 10</i> .....	283
<i>Equation 9. 11</i> .....	283
<i>Equation 9. 12</i> .....	284
<i>Equation 10. 1</i> .....	338
<i>Equation 11. 1</i> .....	363



UNIVERSITY  
 OF  
 JOHANNESBURG

---

## CHAPTER 1

### INTRODUCTION

---

#### 1.1 BACKGROUND

Disperse dyes are the class of organic dyes used for man-made fibers such as polyesters, cellulose acetate and nylon materials. The advent of this class of organic dyes dates back to the 1920s through the quest for nonionic, hydrophobic and wash-resistant dyes for coloring polyester and cellulose acetate type of fibers [1-3]. Due to the high degree of non-ionicity and hydrophobicity of polyester, nylon and cellulose acetate fibers, most of the available dyes such as the ionamine and duranol dyes performed fairly for acetate fibers only but showed poor affinity for polyester and nylon materials. Consequently, there was a need for more efficient synthetic dyes for polyester, nylon and even cellulose acetate materials which spiked the discovery of a disperse type of organic dye. Today, various families of disperse dyes have been discovered which include the azo, anthraquinone, nitroarylamino, coumarin, methane, formazan, naphthostyryl, quinophthalone and benzodifuranone disperse dyes. These groups of disperse dyes lack ionic solubilizing groups and are, as a result, sparingly soluble in water [2-4].

The azo class of disperse dyes which consist of at least one azo linkage ( $-N=N-$ ) in their structures attract attention from researchers over any other class due to their ease of manufacture and lower cost compared to other classes. The azo class now constitutes about 60% of the world's total disperse dye consumption [2-5], and they can be found mainly in the forms of aminoazobenzene and azopyridone dyes [2-4].

Aqueous solubility and fastness properties are two key factors in disperse dye applications particularly in textile industries. Aqueous solubility controls the operational cost of dyeing polyester, acetate, and nylon fabrics as it determines the choice and the quantity of dispersing agents required to solubilize the dyes in aqueous medium in order to obtain a homogenous dyeing bath. Fastness on the other hand is a measure of the ability of a dye to resist color depletion under harsh conditions such as heat (sublimation fastness), wash (wash fastness), and light (light fastness).

Low solubility of disperse dyes in water calls for the use of dispersing agents such as turkey red oil, soap, synthetic detergents of the alkylsulphate or alkarylsulphonate, lignin sulphonates or polycondensates of arylsulphonic acids with formaldehyde, and fatty alcohol-ethylene oxide condensates to help in dispersing them into micro particles (particle size of about 1-4  $\mu\text{m}$ ) for easier penetration into their substrates [2, 6, 7]. It follows that the amount of dispersing agent used with a disperse dye depends on the degree of aqueous solubility of the dye. The lower the solubility, the higher the amount of dispersing agent and consequently the higher the cost of dyeing. There are indications that low aqueous solubility can also inhibit the levelling tendency and dyeing rate of a disperse dye [6]. Thus, the use of dispersing agents have been embraced not only to facilitate aqueous solubility but also to promote levelling and avert surface agglomeration of dye particles which leads to poor resistance to rubbing [6].

Chemical reactivity is a measure of the susceptibility of chemical species to a change in electron density and/or electronic configuration. In relation to dyeing, reactivity may be viewed as a measure of the affinity of a dye for certain substrates or its likelihood to adhere firmly onto substrates either through covalent bond formation or by forming strong



intermolecular forces. In relation to photocatalytic degradation, reactivity can be seen as a measure of the binding tendency or adsorption of a dye onto the surface of a photocatalyst, its degradability and its susceptibility to the attack of photo-generated radicals such as the OH radical.

Nonetheless, the reactivity of any chemical system can be evaluated theoretically from selected quantum reactivity descriptors which are classified as global reactivity descriptors (GRD) and local reactivity descriptors (LRD) [8, 9]. The GRD account for the reactivity of a chemical species as a whole. Global reactivity descriptors include the energy gap between frontier molecular orbitals, chemical hardness, chemical softness, chemical potential, electronegativity, electrophilicity index, band gap and dipole moment [8-10]. Using relevant approximation and theorem, the GRD can be determined from the highest occupied molecular orbital (HOMO) and the lowest unoccupied molecular orbital (LUMO) energies or from the energies of the valence and the conduction bands in the case of solid materials as will be discussed later in this work. The LRD are the reactivity parameters that reveal in numeric terms the vulnerability of specific sites (atoms) in a molecule to the attack of a nucleophile, an electrophile or a radical [8, 9]. Examples include local softness, local philicity and Fukui functions.

The use of polar electron-donating and electron-withdrawing substituent groups (EDGs and EWGs, respectively) is a promising way of improving the aqueous solubility of disperse dyes up to an accomplishable limit for nonionic organic compounds. The polar groups are hydrophilic and will therefore enhance solvation of dye molecules, improve aqueous solubility and levelling power, and consequently lower the demand for dispersing agents.

Structural modification of disperse dyes such as the azo class (Figure 1.1) with a good mix of sufficiently polar EDGs (e.g.  $\text{NH}_2$ ,  $\text{NHCH}_3$ ,  $\text{N}(\text{CH}_3)_2$  etc.) and EWGs (e.g.  $\text{CN}$ ,  $\text{NO}_2$  etc.) can impact the reactivity of the dyes. Important dyeing properties such as wash fastness, light fastness, sublimation fastness and levelling power can also be enhanced because the polar substituents will not only increase the molecular weights of the dyes but also contain atomic sites which can promote the van der Waal and dipolar interactions between the dyes and their substrates [2, 4, 5].

Fine tuning of azo disperse dyes with polar EDGs and EWGs can also impact their color brightness and electronic properties such as optical activity and polarizability. This can be explored for development of new disperse dyes of interesting hue and electronic properties for potential applications in textile industries, liquid crystal display (LCD), dye-sensitized solar cells, and laser technology [11-14].

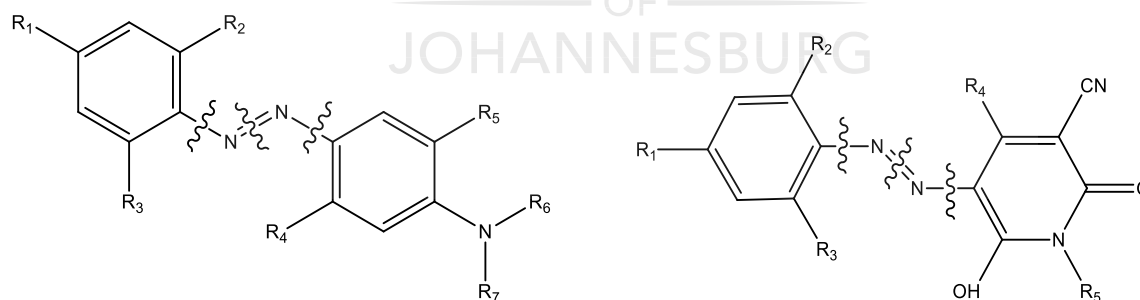


**Figure 1. 1:** The general molecular structures of aminoazobenzene (left) and azopyridone (right) disperse dyes.  $R_1$ ,  $R_2$  and  $R_3$  are EWGs,  $R_4$  and  $R_5$  are EDGs while  $R_6$  and  $R_7$  are alkyl groups or substituted alkyls.

## 1.2 PROBLEM STATEMENT

The low aqueous solubility of disperse dyes has both economic and environmental impact. The economic setback is as a result of the need for dispersing agents to solubilize the dyes, facilitate their penetration through their substrates and increase their levelling power during the dyeing operation. Although, disperse dyes generally have relatively low water pollution tendency due to their low aqueous solubility, the fact that they (particularly the azo class) can still pose some threats when released into the environment cannot be overlooked. They are usually transmitted into the environment through incompetent handling of operators, activities such as grinding/milling of dyes with dispersing agents and cleaning of equipment used during the dyeing operation [15]. They are potential water pollutants since they can effect a change in the color of water, alter its biochemical oxygen demand (BOD) and even affect aquatic life.

Azo disperse dyes are potential causes of bladder cancer and occupational eczema in humans [15]. They persist for a long period of time in the environment due to their high resistance to oxidation at ambient conditions as a result of the electron withdrawing effect of the azo linkage [16] which reduces their vulnerability to electron loss. Therefore, there have been efforts made from across the globe on the means of removing and destroying these dyes from the environment. Among the techniques recommended is the use of adsorbents [17], coagulation and precipitation [18], treatment of waste with chemical oxidants and reductants [19], use of photocatalysts [20, 21], electrochemical treatment [22] and ion pair extraction [23]. Of all these techniques, the use of photocatalysts proves to be more efficient because it ensures complete destruction of the dyes.

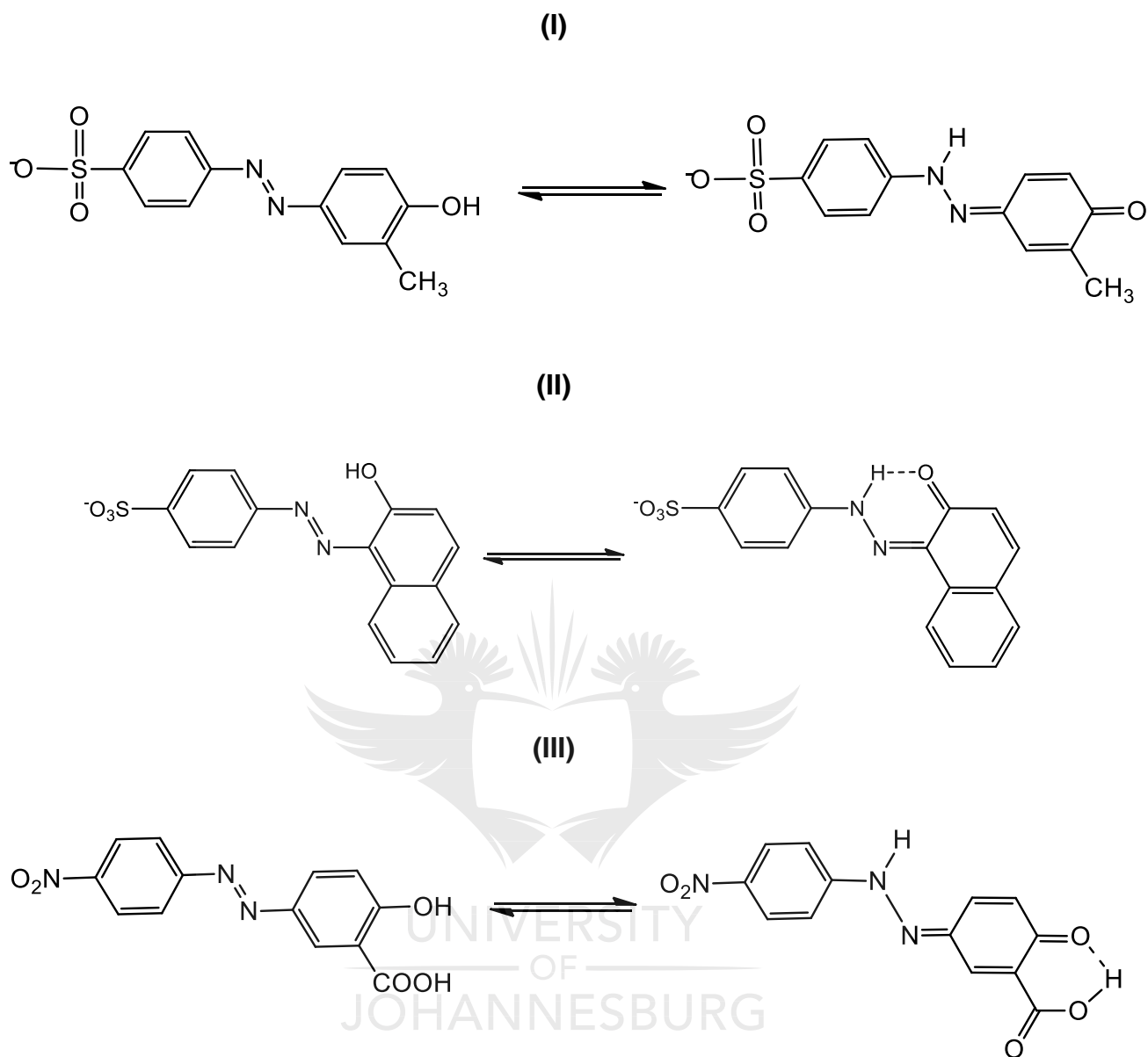
To optimize the use of photocatalysis for environmental remediation, several photocatalysts which make use of the solar energy for activity, have been developed through techniques such as doping and co-doping [24-27], and the use of sensitizers [28]. In the presence of light with sufficient energy, these catalysts generate hydroxyl radicals from water and/or hydroxide ion which causes dye degradation [29, 30]. However, recent findings on photocatalytic degradation of tartrazine using a TiO<sub>2</sub> catalyst showed that increasing the catalyst dosage did not bring about a significant enhancement in the degradation process even at elevated temperature [21]. This indicates that the rate of photocatalytic degradation of dyes does not only depend on variation in some extrinsic factors such as pH, temperature, concentration, catalyst dosage, time, etc. It is therefore necessary to investigate the intrinsic factors which include the reactivity of a dye and that of a photocatalyst as this can help in developing more efficient techniques for removing dye pollutants from the environment.

Many studies have been conducted on optimization of the catalytic strengths of some existing photocatalysts [24-27]. However, it is also necessary to examine the effect of modifying the chemical nature of azo dyes using polar EDGs and EWGs as this can help to address azo disperse dye related environmental pollution through promotion of aqueous solubility, enhancement of adhesion of dye molecules onto substrates, lowering of the demand for dispersing agents and consequently reduction of waste generated during the dyeing operation. In addition, modification of the chemical nature of the dyes can also bring about enhanced dye-catalyst interaction which is necessary for successful degradation.

There are conflicting reports on the degradation mechanism of azo dyes by photo-generated hydroxyl radicals, and no detailed account of the factors responsible for the varying pathways has been provided. Azo dye degradation is experimentally known to occur through the rupture of a C–N or N–N bond (Fig. 1.1). These conflicting pathways have been theoretically investigated for azobenzene, where it was concluded that the N–N bond cleavage predominates the C–N bond cleavage [31]. This can be attributed to the symmetrical nature of azobenzene which naturally gives precedence to the cleavage of the N–N bond. However, since most azo dyes are asymmetrical, using azobenzene as a case study for investigating the pathway(s) of azo dye degradation is considered inadequate.

For instance, in azo dyes such as 2-methyl-4-(4'-sulfophenylazo)phenol, Acid Orange 7 or 8 and Alizarin Yellow R, which can exist in two tautomeric forms i.e. the azo and hydrazone forms (Scheme 1.1) [32-34] due to the presence of a phenolic –OH at an *ortho* or *para* position to the azo bridge, there are conflicting reports on whether the degradation is predominantly through the cleavage of the C–N bond or the N–N bond. A third viewpoint is the one in which the degradation is equally possible via the cleavage of both N–N and C–N bonds in a competitive manner [34].

Intramolecular hydrogen bonding exhibited by some azo dyes is also a potential factor that can dictate the degradation pathway. It is therefore necessary to re-investigate the degradation pathway(s) of azo dyes while taking into consideration the effects of tautomerism and intramolecular hydrogen bonding on the degradation process. This will help to unveil the intrinsic parameter(s) that dictate(s) the pathway of azo dye degradation.



**Scheme 1. 1:** Azo (left) – hydrazone (right) tautomerism in 2-methyl-4-(4'-sulfophenylazo) phenol (I), Acid Orange 7 (II) and Alizarin Yellow R (III).

### 1.3 JUSTIFICATION

To address the problems highlighted above by means of experimentation is relatively cumbersome, cost-intensive, time consuming, and can promote environmental contamination through release of chemical waste into the environment. Alternatively,

theoretical calculation serves as an excellent tool for accomplishing such objectives with relatively little time, energy and cost.

Computational chemistry deals with computer-aided simulation of chemical processes, molecular systems and materials. It uses the theory of molecular mechanics, quantum chemistry or hybrid quantum classical methods incorporated into efficient computer programs, to obtain useful information about chemical systems and also to solve complex chemical problems [35]. Theoretical calculation provides a unique route for designing, characterizing, predicting and understanding the behavior of chemical compounds prior to their synthesis. A plethora of solvation models including Conductor-like Screening Model for Real Solvents (COSMO-RS) [36, 37], Conductor-like Screening Model-Segment Activity Coefficient (COSMO-SAC) [38], Solvation Models 5.42, 6.0 and 8.0 (SM5.42, SM6.0 and SM8.0, respectively) [39-41], 3-Dimensional Reference Interaction Site Models (3D-RISM) [42, 43] and Polarizable Continuum Models (PCMs) [44] have been developed for solvent phase calculations. The advent of these models allows for the prediction of important solution thermodynamic properties such as chemical potential, free energy of solvation, vapor pressure, activity coefficient, free energy of hydration, partition coefficient and aqueous solubility of organic molecules (especially those containing C, H, O, N, F, and Cl as their constituent atoms) with reasonable accuracy and relatively little energy, time and cost [45, 46]. Estimation of these properties has been helpful in assessing the fate of toxic environmental contaminants such as aniline, indole, and organosulphur [47].

The use of theoretical calculations has also been embraced in pharmaceutical industries for predicting the aqueous solubility of drugs [46, 48, 49]. This is necessary because

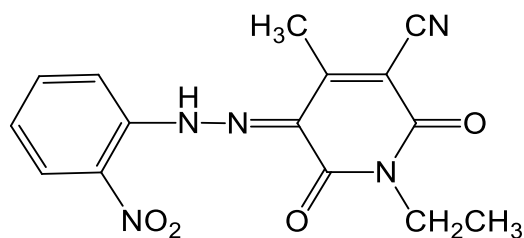
aqueous solubility is key to drug administration and bioavailability in living systems. However, the use of theoretical methods for predicting aqueous solubility of dyes (especially disperse dyes) has not gained appreciable attention. Computational chemistry also provides a relatively cheaper and quicker means of obtaining the electronic properties of organic molecules which can be used to predict their binding ability, chemical reactivity and their tendency to undergo degradation in the presence of different photocatalysts [10, 31, 50].

The current study therefore seeks to embark on a comprehensive theoretical investigation of two azo disperse dyes namely; Disperse Yellow 119 (DY119) and Disperse Red 73 (DR73) (Figure 1.2) and Si, CdSe, CdS, TiO<sub>2</sub>, ZnO, and ZnS catalysts with a view to improving the aqueous solubility and reactivity of the dyes using selected polar substituent groups, suggesting suitable catalysts for their degradation and predicting their degradation pathways using Density Functional Theory (DFT).

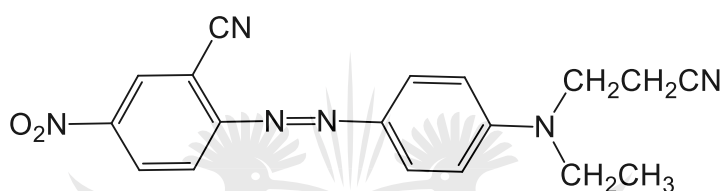
The selected dyes show interesting structural properties which could help to expose the ambiguities in azo dye degradation pathway studies arising from a symmetrical azo linkage (-N=N-), intramolecular hydrogen bonding and tautomerism. In addition to the presence of an unsymmetrical azo linkage, Disperse Red 73 shows no tendency to exhibit azo – hydrazone tautomerism due to the absence of an *ortho* or *para* –OH group (Figure 1.2). On the other hand, Disperse Yellow 119 shows the tendency to exist in both azo and hydrazone tautomeric forms due to the presence of an –OH group at the *ortho* position to the azo linkage (Figure 1.2 and Scheme 1.2). In this work, the most stable tautomeric form, the preferred degradation pathway and the effect of intramolecular



hydrogen bonding on the degradation pathway(s) of the hydrazone form of Disperse Yellow 119 will also be investigated.

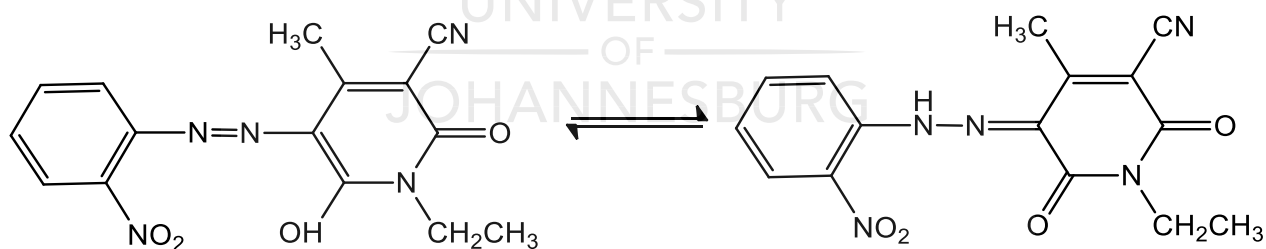


DY119 (Disperse Yellow 119)



DR73 (Disperse Red 73)

**Figure 1. 2:** The molecular structures of DY119 and DR73.



**Scheme 1. 2:** Azo – hydrazone tautomerism involving the azo (left) and the hydrazone (right) tautomers of Disperse Yellow 119 dye.

The selected catalysts have been chosen across a range of band gaps both in the UV and visible region of electromagnetic radiation in order to predict the one(s) with the highest catalytic potential for the degradation of the dyes and their proposed derivatives.

It is anticipated that this study will give rise to new azo disperse dyes with significantly improved aqueous solubility, degradability and dyeing properties for a more economic and more environmentally friendly applications. It will also provide useful guidance in the selection of appropriate photocatalysts for azo disperse dye degradation. Finally, the present study will provide more clarification on the mechanism of degradation of azo disperse dyes by photo-generated OH radicals. To the best of our knowledge as at the time of carrying out this study, this work has not yet been reported.

## **1.4 AIM AND OBJECTIVES OF THE STUDY**

### **1.4.1 AIM**

The aim of this study is to theoretically design new azo disperse dyes with improved solubility and reactivity through systematic structural modification of Disperse Yellow 119 and Disperse Red 73 dyes with polar substituent groups, and also investigate the photodegradation pathways of the selected dyes.

### **1.4.2 OBJECTIVES**

The current work focuses on the following objectives:

1. Determine the aqueous solubility of the selected dyes from COSMO-RS predicted free energy of solvation and vapor pressure using appropriate solubility equation;
2. Evaluate the reactivity of the dyes using some global and local reactivity indices;
3. Determine the changes in the aqueous solubility and reactivity values as a result of the variation of substituent groups;

4. Assess the affinities of the dyes for Si, CdSe, CdS, TiO<sub>2</sub>, ZnO, and ZnS catalysts;
5. Identify the most favorable pathway for the degradation of each dye by hydroxyl radicals and examine the effect of water on the reaction pathway.

## 1.5 OUTLINE OF THE THESIS

This thesis consists of twelve chapters as summarised below:

**Chapter 2** covers a review of relevant literature which forms the basis and motivation for this work.

**Chapter 3** focuses on key quantum chemical theories, methods, equations, and approaches used in this work.

Details of the computational software and the facilities employed for this work are presented in **Chapter 4**.

**Chapters 5 and 6** discuss the results of the method validation study conducted on some azo disperse dyes with known experimental solubility values in order to ensure that the selected level of theory, models, equations and adjustable parameters are reliable for this work.

The effects of electron withdrawing CN and NO<sub>2</sub> substituent groups, and electron donating NH<sub>2</sub>, NHCH<sub>3</sub> and N(CH<sub>3</sub>)<sub>2</sub> groups on the aqueous solubility and reactivity of Disperse Yellow 119 (DY119) dye are discussed in **Chapter 7**. A total of 29 new azo

disperse dyes were reported in this chapter. The photodegradation pathways of the dyes were predicted and appropriate photocatalysts were suggested for their degradation.

An account of the synergistic (i.e. combined) effect of the electron withdrawing CN and NO<sub>2</sub>, and the electron donating NH<sub>2</sub>, NHCH<sub>3</sub> and N(CH<sub>3</sub>)<sub>2</sub> groups on the aqueous solubility and reactivity of Disperse Yellow 119 (DY119) dye is given in **Chapter 8**. A total of 84 additional derivatives was reported in this chapter. Their photodegradation mechanisms and appropriate degradation catalysts were also predicted.

**Chapter 9** presents the effects of electron withdrawing and the electron donating groups on aqueous solubility and reactivity of Disperse Red 73 (DR73) dye. In this chapter, a total of 41 new derivatives of this dye with their probable photodegradation mechanisms and appropriate degradation catalysts were discussed.

In **Chapter 10**, two experimentally proposed mechanisms of azo dye degradation by hydroxyl radical ( $\cdot\text{OH}$ ) were investigated for DY119 dye. This chapter involves the determination of potential energy profiles and optimization of ground state and transition state structures. Effects of intramolecular hydrogen bonding and solvent (water) were discussed. Loss of a nitrogen molecule from the degradation products was also reported.

Theoretical findings on the degradation mechanisms of DR73 dye in the presence of hydroxyl radical ( $\cdot\text{OH}$ ) were presented in **Chapter 11**. Effects of water on the reactions was discussed. Mineralisation processes such as deamination, denitration and removal of a nitrogen molecule from the degradation products were also reported.

Finally, **Chapter 12** presents the overall summary and conclusions drawn from this work.

## 1.6 REFERENCES

1. F. Jones. The solubility and solubilisation of disperse dyes. *Journal of the Society of Dyers and Colourists* **100** (1984) 66-72.
2. J. Koh. Dyeing with disperse dyes; P. Hauser (Ed.), *INTECH Open Access Publisher, Croatia, (2011)*, pp. 195-221. DOI: 10.5772/20458. Available at: <https://www.intechopen.com/books/textile-dyeing/dyeing-with-disperse-dyes>.
3. D. Chattopadhyay. Chemistry of dyeing: Handbook of textile and industrial dyeing: Principles, processes and types of dyes. *Elsevier* **1** (2011) 150.
4. J. Aspland. The structure and properties of disperse dyes and related topics. *Textile Chemistry and Coloration* **25** (1993) 21-25.
5. M. Clark. Handbook of textile and industrial dyeing: principles, processes and types of dyes. *Woodhead Publishing Limited, United Kingdom, (2011)*.
6. C. Bird. The dyeing of acetate rayon with disperse dyes I-aqueous solubility and the influence of dispersing agents II-the relation between aqueous solubility and dyeing properties. *Journal of the Society of Dyers and Colourists* **70** (1954) 68-77.
7. S. A. A. Green and J. W. McBain. Solubilization of water-insoluble dye by pure soaps and detergents of different types. *The Journal of Physical Chemistry* **51** (1947) 286-298.
8. K. Chandrakumar and S. Pal. The concept of density functional theory based descriptors and its relation with the reactivity of molecular systems: A semi-quantitative study. *International Journal of Molecular Sciences* **3** (2002) 324-337.
9. P. K. Chattaraj. Chemical reactivity theory: A density functional view. *CRC Press, United States (2009)*.

10. B. I. Adewale and S. Banjo. Theoretical study on structural and electronic properties of 4-[E-[4-(trifloromethyl)-1, 3-benzothiazol-2-yl] azo] naphthalen-1-ol and 1-[E-[4-(trifloromethyl)-1, 3-benzothiazol-2-yl] azo] naphthalen-2-ol using density functional theory (DFT). *International Journal of Physical Sciences* **8** (2013) 1494-1505.
11. M. R. R. Kooh, V. N. Yoong and P. Ekanayake. Density functional theory (DFT) and time-dependent density functional theory (TDDFT) studies of selected ancient colourants as sensitizers in dye-sensitized solar cells. *Journal of the National Science Foundation of Sri Lanka* **42** (2014) 169-175.
12. J. Xu, H. Zhang, G. Liang, L. Wang, W. Xu, W. Ciu and Z. Li. DFT Studies on the electronic structures of indoline dyes for dye-sensitized solar cells. *Journal of Serbia Chemical Society* **75** (2010) 259-269.
13. M. Inoue and T. Ashida. Development of color resists containing novel dyes for liquid crystal displays. *Sumitomo Kagaku* **2013** (2013) 1-7.
14. V. Chigrinov, H. S. Kwok, H. Takada and H. Takatsu. Photo-aligning by azo-dyes: Physics and applications. *Liquid Crystals Today* **14** (2005) 1-15.
15. H. Øllgaard, L. Frost, J. Galster and O. C. Hansen. Survey of azo-colorants in Denmark. Consumption, use, health and environmental aspects (1998). Available at: <https://www2.mst.dk/udgiv/publications/1999/87-7909-548-8/pdf/87-7909-546-1.pdf>. Accessed on 14 March 2018.
16. J. S. Chang, B. Y. Chen and Y. S. Lin. Stimulation of bacterial decolorization of an azo dye by extracellular metabolites from *Escherichia coli* strain NO<sub>3</sub>. *Bioresource Technology* **91** (2004) 243-248.

17. S. Banerjee and M. Chattopadhyaya. Adsorption characteristics for the removal of a toxic dye, tartrazine from aqueous solutions by a low cost agricultural by-product. *Arabian Journal of Chemistry* **10** (2013) 1629-1638.
18. Y. Anjaneyulu, N. S. Chary and D. S. S. Raj. Decolourization of industrial effluents—available methods and emerging technologies—a review. *Reviews in Environmental Science and Biotechnology* **4** (2005) 245-273.
19. M. A. Salem and A. H. Gemeay. Kinetics of the oxidation of tartrazine with peroxydisulfate in the presence and absence of catalysts. *Chemical Monthly* **131** (2000) 117-129.
20. V. K. Gupta, R. Jain, A. Nayak, S. Agarwal and M. Shrivastava. Removal of the hazardous dye-tartrazine by photodegradation on titanium dioxide surface. *Materials Science and Engineering: C* **31** (2011) 1062-1067.
21. S. K. Al-Dawery. Photo-catalyst degradation of tartrazine compound in wastewater using TiO<sub>2</sub> and UV light. *Journal of Engineering Science and Technology* **8** (2013) 683-691.
22. N. A. Ghalwa, H. M. Abu-Shawish, H. M. Tamous and H. Al Harazeen. Determination of electrochemical degradation of E102 dye at lead dioxide-doped carbon electrodes using some potentiometric and spectrophotometric methods. *Chemistry Journal* **3** (2013) 1-6.
23. P. L. López-de-Alba, L. I. Michelini-Rodriguez, K. Wróbel and J. Amador-Hernández. Extraction of sunset yellow and tartrazine by ion-pair formation with adogen-464 and their simultaneous determination by bivariate calibration and derivative spectrophotometry. *Analyst* **122** (1997) 1575-1579.

24. Z. M. El-Bahy, A. A. Ismail and R. M. Mohamed. Enhancement of titania by doping rare earth for photodegradation of organic dye (Direct Blue). *Journal of Hazardous Materials* **166** (2009) 138-143.
25. M. Hamadani, A. Reisi-Vanani and A. Majedi. Synthesis, characterization and effect of calcination temperature on phase transformation and photocatalytic activity of Cu, S-codoped TiO<sub>2</sub> nanoparticles. *Applied Surface Science* **256** (2010) 1837-1844.
26. Y. Lv, L. Yu, H. Huang, H. Liu and Y. Feng. Preparation, characterization of P-doped TiO<sub>2</sub> nanoparticles and their excellent photocatalytic properties under the solar light irradiation. *Journal of Alloys and Compounds* **488** (2009) 314-319.
27. X. Yang, F. Ma, K. Li, Y. Guo, J. Hu, W. Li, M. Huo and Y. Guo. Mixed phase titania nanocomposite codoped with metallic silver and vanadium oxide: new efficient photocatalyst for dye degradation. *Journal of Hazardous Materials* **175** (2010) 429-438.
28. W. J. Youngblood, S.-H. A. Lee, K. Maeda and T. E. Mallouk. Visible light water splitting using dye-sensitized oxide semiconductors. *Accounts of Chemical Research* **42** (2009) 1966-1973.
29. S. Adhikari and D. Sarkar. Metal oxide semiconductors for dye degradation. *Materials Research Bulletin* **72** (2015) 220-228.
30. M. Kulkarni and P. Thakur. Photocatalytic degradation and mineralization of reactive textile azo dye using semiconductor metal oxide nano particles. *International Journal of Engineering Research General Science* **2** (2014) 245-254.



31. A. S. Özen, V. Aviyente and R. A. Klein. Modeling the oxidative degradation of azo dyes: A density functional theory study. *The Journal of Physical Chemistry A* **107** (2003) 4898-4907.
32. A. S. Özen, V. Aviyente, F. De Proft and P. Geerlings. Modeling the substituent effect on the oxidative degradation of azo dyes. *The Journal of Physical Chemistry A* **108** (2004) 5990-6000.
33. A. S. Özen, V. Aviyente, G. Tezcanli-Güyer and N. H. Ince. Experimental and modeling approach to decolorization of azo dyes by ultrasound: degradation of the hydrazone tautomer. *The Journal of Physical Chemistry A* **109** (2005) 3506-3516.
34. X. Jiao, H. Yu, Q. Kong, Y. Luo, Q. Chen and J. Qu. Theoretical mechanistic studies on the degradation of alizarin yellow R initiated by hydroxyl radical. *Journal of Physical Organic Chemistry* **27** (2014) 519-526.
35. C. David. Computational chemistry: A practical guide for applying techniques to real-world problems. *A John Wiley & Sons Publication*, New York, (2001).
36. A. Klamt. Conductor-like screening model for real solvents: a new approach to the quantitative calculation of solvation phenomena. *The Journal of Physical Chemistry* **99** (1995) 2224-2235.
37. A. Klamt, V. Jonas, T. Bürger and J. C. Lohrenz. Refinement and parametrization of COSMO-RS. *The Journal of Physical Chemistry A* **102** (1998) 5074-5085.
38. E. Mullins, Y. Liu, A. Ghaderi and S. D. Fast. Sigma profile database for predicting solid solubility in pure and mixed solvent mixtures for organic pharmacological compounds with COSMO-based thermodynamic methods. *Industrial & Engineering Chemistry Research* **47** (2008) 1707-1725.

39. C. P. Kelly, C. J. Cramer and D. G. Truhlar. SM6: A density functional theory continuum solvation model for calculating aqueous solvation free energies of neutrals, ions, and solute-water clusters. *Journal of Chemical Theory and Computation* **1** (2005) 1133-1152.
40. A. V. Marenich, R. M. Olson, C. P. Kelly, C. J. Cramer and D. G. Truhlar. Self-consistent reaction field model for aqueous and nonaqueous solutions based on accurate polarized partial charges. *Journal of Chemical Theory and Computation* **3** (2007) 2011-2033.
41. P. Winget, J. D. Thompson, C. J. Cramer and D. G. Truhlar. Parametrization of a universal solvation model for molecules containing silicon. *The Journal of Physical Chemistry A* **106** (2002) 5160-5168.
42. D. S. Palmer, V. P. Sergiievskiy, F. Jensen and M. V. Fedorov. Accurate calculations of the hydration free energies of druglike molecules using the reference interaction site model. *The Journal of Chemical Physics* **133** (2010) 044104(1)- 044104(12).
43. D. S. Palmer, A. I. Frolov, E. L. Ratkova and M. V. Fedorov. Towards a universal method for calculating hydration free energies: a 3D reference interaction site model with partial molar volume correction. *Journal of Physics: Condensed Matter* **22** (2010) 492101(1)- 492101(9).
44. B. Mennucci, E. Cancès and J. Tomasi. Evaluation of solvent effects in isotropic and anisotropic dielectrics and in ionic solutions with a unified integral equation method: theoretical bases, computational implementation, and numerical applications. *The Journal of Physical Chemistry B* **101** (1997) 10506-10517.

45. J. D. Thompson, C. J. Cramer and D. G. Truhlar. Predicting aqueous solubilities from aqueous free energies of solvation and experimental or calculated vapor pressures of pure substances. *The Journal of Chemical Physics* **119** (2003) 1661-1670.
46. D. S. Palmer, J. L. McDonagh, J. B. Mitchell, T. van Mourik and M. V. Fedorov. First-principles calculation of the intrinsic aqueous solubility of crystalline druglike molecules. *Journal of Chemical Theory and Computation* **8** (2012) 3322-3337.
47. J. J. Guerard and J. S. Arey. Critical evaluation of implicit solvent models for predicting aqueous oxidation potentials of neutral organic compounds. *Journal of Chemical Theory and Computation* **9** (2013) 5046-5058.
48. B. Bouillot, S. Teychené and B. Biscans. An evaluation of thermodynamic models for the prediction of drug and drug-like molecule solubility in organic solvents. *Fluid Phase Equilibria* **309** (2011) 36-52.
49. H. Van De Waterbeemd and E. Gifford. ADMET in silico modelling: Towards prediction paradise. *Nature Reviews Drug Discovery* **2** (2003) 192-204.
50. L. H. Mendoza-Huizar. A theoretical study of chemical reactivity of tartrazine through dft reactivity descriptors. *Journal of the Mexican Chemical Society* **58** (2014) 416-423.

---

## CHAPTER 2

### LITERATURE REVIEW

---

#### 2.1 INTRODUCTION

This chapter provides a comprehensive description of the disperse type of organic dyes with more emphasis on the azo class. It discusses photocatalytic degradation, photocatalyst – pollutant interaction and azo dye degradation pathway(s).

#### 2.2 DISPERSE DYES

Disperse dyes constitute the class of non-ionic, hydrophobic, man-made dyes that are mainly used for polyester materials in the form of a fine aqueous dispersion due to their poor aqueous solubility [1-3]. They can also be applied to other artificial hydrophobic fibres which include acetate, nylon, acrylic, modacrylic and polyurethane fibres [2]. Paints, varnishes, plastics, rubber, foods, drugs, papers and cosmetics can also be colored with disperse dyes.

Before application, disperse dyes are usually treated with dispersants such as metamol which helps to transform the dyes into a pasty homogenous mixture. However, carrier agents are usually introduced during application to promote dispersion stability, levelling power, molecular mobility and penetration through the substrate [1, 3-6]. This is further assisted by setting the operational temperature in the range of 80 – 130 °C during the dyeing [1, 3, 4, 7]. Dyeing is said to have occurred when molecules of the dyes have adhered firmly onto the substrate through a non-covalent interaction thought to be van der Waals and dipolar in nature [3].

## 2.3 DISPERSE DYE CLASSIFICATIONS

Disperse dyes can be classified based on thermal stability (i.e. sublimation fastness) relative to molecular size, energy requirement and chemical origin. In one classification, disperse dyes are grouped into classes A, B, C and D, while in another, they are classified as low, medium and high energy disperse dyes. The A class comprises of fast dyeing, low molecular weight and low heat resistant dyes. The D class is the exact opposite of class A, while classes B and C exhibit borderline properties between these two extreme classes. This classification is according to the Imperial Chemical Industries (ICI) [2, 4].

Low energy disperse dyes comprise of less polar, high levelling, rapid dyeing, low heat resistant and low molecular weight dyes. The highly polar, low levelling, slow dyeing, and high heat resistant large dyes constitute the high energy disperse dye group. Moderate energy disperse dyes show intermediate properties between the low and the high energy disperse dyes. This classification is according to Disperse Dyes Committee of Society of Dyers and Colorists [2, 4, 8]. Low energy dyes are used with carrier agents at a temperature of 77 °C, medium energy dyes require a temperature between 104 °C – 110 °C while high energy dyes are used at a temperature above 129 °C [4, 8].

The third mode of classification which is of interest to most researchers, particularly in chemistry, is based on the chemical origin of the dyes. This classification groups disperse dyes into monoazo, disazo, anthraquinone, nitroarylamino, coumarin, methine, benzodifuranone, formazan, quinophthalone and naphthostyryl classes. The monoazo and disazo collectively form the azo class which is the largest group of disperse dyes, accounting for about 60%. Monoazo and disazo contain one and two azo chromophores, respectively, in their structures. Anthraquinone based dyes are the next abundant group,

accounting for about 25%. Nitroarylamino, coumarin, methine, benzodifuranone, formazan, quinophthalone, and naphthostyryl classes account for the remaining 15% [2, 4, 7].

## 2.4 AZO CLASS

The azo class of disperse dyes is characterized by the presence of at least one azo linkage (-N=N-) between two aromatic  $sp^2$ -hybridized carbons in a stable planar trans-geometry (Fig. 2.1), which is envisaged to promote effective electron delocalization and hence boost optical activity [9]. The planarity of azo disperse dyes has also been suggested to be responsible for their ease of penetration through the layers of polyester fibers during dyeing [4].

On the other hand, the nature of the surrounding aromatic substituents (Fig. 2.1) is believed to govern the aqueous solubility property, color type, brightness, binding ability, wavelength of absorption, and even some fastness properties of this group of disperse dyes [3, 4, 10]. For instance, an electron withdrawing group such as  $\text{NO}_2$  will enhance light fastness while electron donating group such as  $\text{NH}_2$  and  $\text{OH}$  will show an opposing effect [4]. This is so because photo-fading of dyes involves electronic excitation, which can be promoted by electron donating substituents. Electron withdrawing substituents contrarily inhibit electronic excitation, which in turn hinders photo-fading. Both  $\text{NO}_2$  and  $\text{NH}_2$  groups are, however expected to promote aqueous solubility due to their substantial polarity. They can also bring about a change in color, brightness and absorption wavelength since they can cause a shift of electron density from one end of the azo bridge to the other, thereby impacting the energy gap between the highest occupied molecular orbital (HOMO) and the lowest unoccupied molecular orbital (LUMO) of a dye [11].

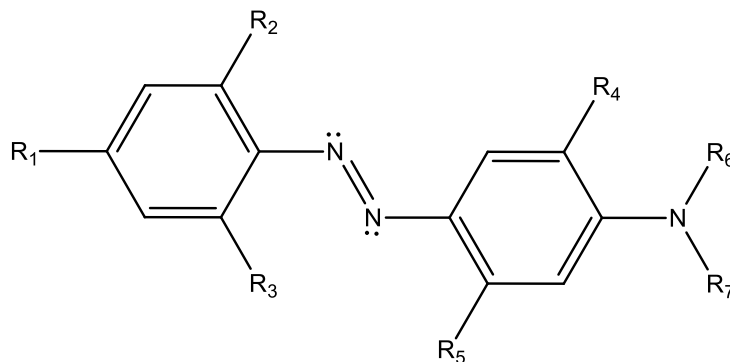


**Figure 2. 1:** General molecular structure of aminoazobenzene dyes. R<sub>1</sub>, R<sub>2</sub> and R<sub>3</sub> could be H or an electron withdrawing group, R<sub>4</sub> and R<sub>5</sub> could be H or an electron donating group, while R<sub>6</sub> and R<sub>7</sub> could be H, alkyl group or substituted alkyl.

Azo disperse dyes exist predominantly in the monoazo form – the one which contains only one azo group per molecule. Monoazo disperse dyes include aminoazobenzene (Fig. 2.1), azopyridone, azothiophene and azobenzothiazole derivatives (Fig. 2.2) [7]. Aminoazobenzene disperse dyes are seconded by the azopyridone derivatives in terms of abundance. They are predominantly used for coloring polyester polymers. Examples include disperse yellow 3, disperse orange 25, disperse red 167, disperse violet 33, and disperse blue 79 [2]. Prominent members of the azopyridone group are disperse yellow 119 and disperse yellow 211 [7, 12, 13]. However, some new members of this group have also been reported recently [14].

Azothiophenes and azobenzothiazoles disperse dyes are scanty. Known members of these groups are disperse green 9 and disperse red 153, respectively [7]. Disazo and triazo dyes, containing two and three chromophoric azo linkages respectively, are relatively less abundant. Some members of the disazo group have been found useful in the production of phase change inks, colored plastics and electro-photographic photoconductors, while the triazo group has been used for coloring nylon 6 [12].

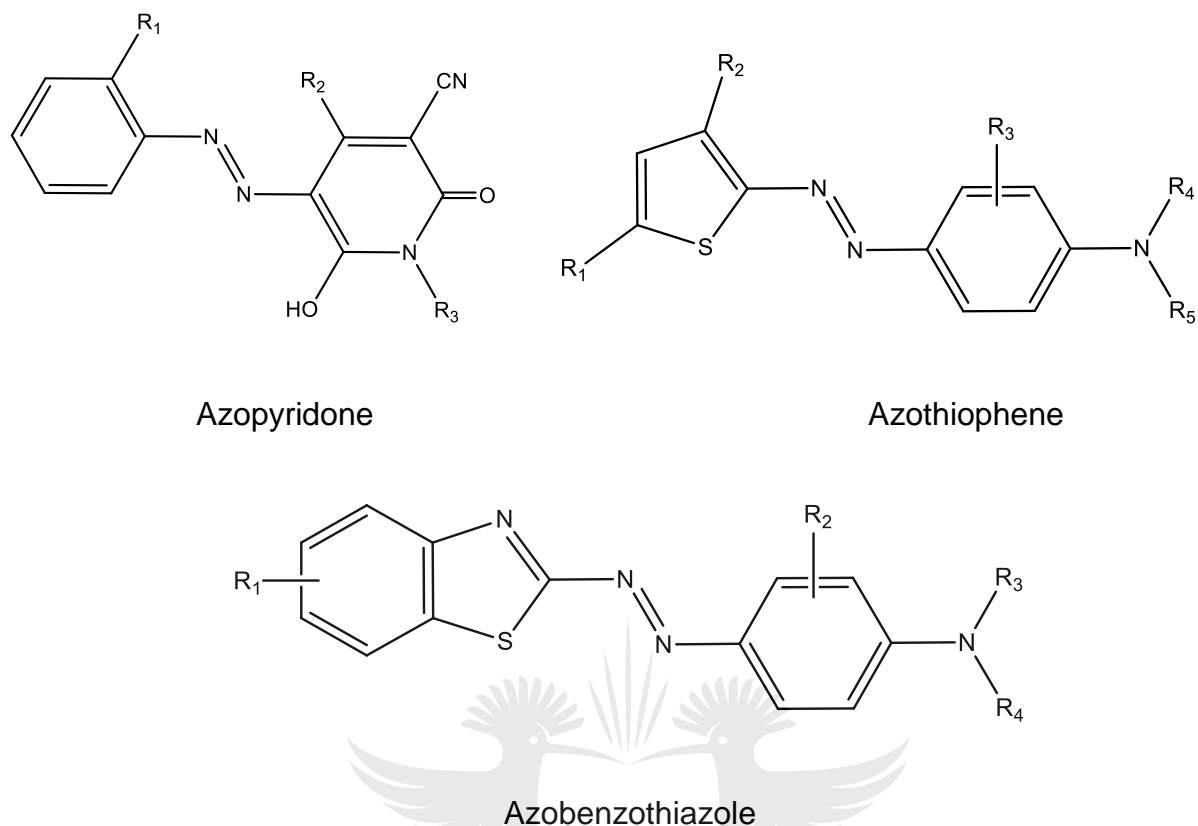


**Figure 2. 2:** Molecular structure of azopyridone, azothiophene and azobenzothiazole dyes.

## 2.5 WHY FOCUS ON AZO DISPERSE DYES

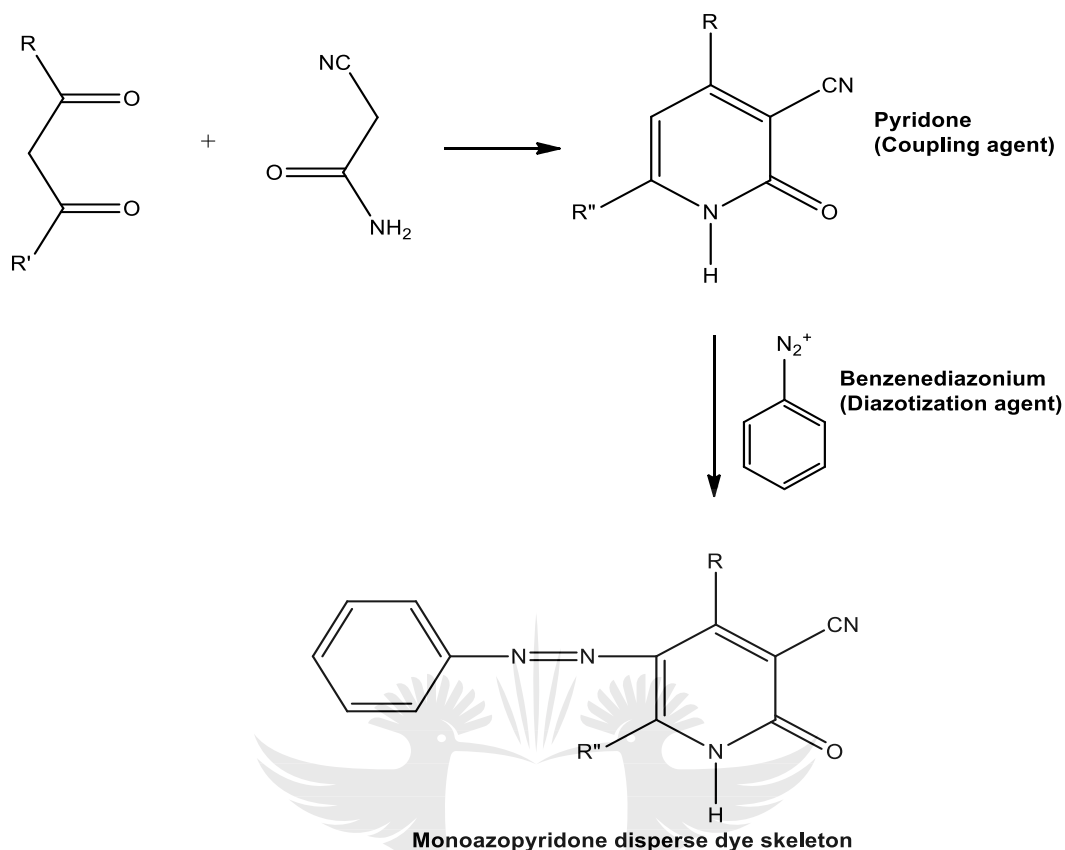
Azo disperse dyes particularly the monoazo class are the dominant class of synthetic azo dyes used for dyeing polyester, nylon and acetate fibres. They account for about 60% of the total commercially available disperse dyes which is about 25% more than the anthraquinone counterpart [2, 7]. This can be attributed to their simplicity, relatively lower cost of production and wider range of applications compared to the anthraquinone counterparts. The range of applications include leather dyeing [15], non-linear optical devices, liquid crystal display [16], high-tech applications such as lasers [17], biological



and medical studies [18], and acid-base, redox and metallochromic indicators in analytical chemistry [19].

Azo disperse dyes can be optimised for various applications through variation of the aromatic ring substituents in their structures [14, 20]. A good combination of electron rich and electron deficient substituent groups will affect the intramolecular charge movement from one end of the azo linkage to the other, thereby impacting the electronic and optical properties of the dye. Changes in solubility and fastness properties could also result depending on the degree of polarity and/or polarizability of the substituents.

Azo disperse dyes are formed by the combination of appropriate diazotization and coupling agents (Scheme 2.1) [12, 14, 20, 21]. The substituent groups are usually incorporated from the start into the diazotization and coupling components. The ease with which this structural adjustment can be carried out explains why the azo class is the subject of most studies on disperse dyes [12, 14, 20-23]. In addition, the perceived tendency of this class of disperse dye to pose environmental and health concerns further justifies the growing attention of researchers in azo disperse dye studies [24-28].



**Scheme 2. 1:** Synthesis of azo pyridone disperse dye from pyridone (coupling agent) and benzenediazonium ion (diazotization agent).

## 2.6 ENVIRONMENTAL AND HEALTH IMPACTS OF AZO DISPERSE DYES

The predominance of azo disperse dyes over their counterparts makes them the first suspect of most environmental pollution. They are less vulnerable to degradation due to the stiffness and the strong electron withdrawing effect of the azo (-N=N-) unit, which tends to decrease the electron density on the neighboring rings.

Azo disperse dyes are not expected to constitute a remarkable environmental (water) pollution problem due to their low aqueous solubility. However, transmission of a significant amount of these dyes to the environment does occur through activities such

as grinding/milling with dispersants, equipment cleaning as well as incompetent handling during the dyeing operation [29]. Dispersants and carrier agents do not only possess undesirable odour, but are also capable of posing danger to the environment and human health. This is because they usually contain toxic chemical substances such as *o*-phenylphenol, biphenyls, phthalates and chlorinated aromatic compounds [4]. This is why high temperature high pressure (HTHP) disperse dyeing method is sometimes preferred as this does not necessarily require the use of carrier agents [2, 4].

Most azo disperse dyes form a suspension or sediments when released into water depending on their molecular weight and particle size. The dissolved portion can render water unsafe for drinking or for any other domestic use due to the intense color of the dyes. It can also raise the chemical/biochemical oxygen demand (COD/BOD) level of aquatic ecosystem, or even block light penetration into the ecosystem.

Azo disperse dyes are derivatives of aromatic amines which suggests that they are potential carcinogenic compounds on their own, and can also give rise to carcinogenic amine products on degradation. Disease conditions such as bladder cancer, contact dermatitis, allergy and occupational eczema in humans have been attributed to exposure to azo dyes through ingestion of contaminated foods or penetration of the dye particles through the skin pores during perspiration [4, 29]. Intestinal and skin bacteria, and also some enzymes secreted by the liver have been identified as possible agents capable of cleaving the azo group to regenerate the carcinogenic aromatic amine components of azo disperse dyes [4].

## 2.7 PHOTOCATALYTIC DEGRADATION

Approximately, 10,000 tons of synthetic dyes are produced annually [30], and about 12% of the used fraction is released into the environment in one way or the other [31]. Since azo dyes constitute the largest population of commercial dyes due to their relative ease of manufacture and wider range of application, the effluents generated from textile industries usually contain high concentrations of azo dyes. Therefore, the effluents are usually toxic, carcinogenic and/or mutagenic in addition to their intense color which can denature water and disrupt aquatic ecosystems.

Numerous treatment methods such as the use of chemical oxidants and reductants [32], adsorption [33], electrochemical treatment [34], coagulation and precipitation [35], ion pair extraction [36] and use of photocatalysts [37, 38] for removing dye molecules from industrial effluents prior to discharge into the environment have been proposed [32-34, 36-39]. However, of all these methods, photocatalytic degradation using photo-active semiconductors or metallic oxides, such as titanium oxide, are considered the most promising technique in terms of efficiency, cost-effectiveness, safety and ability to completely destroy pollutants [37, 38, 40, 41].

Photocatalytic degradation is an advanced oxidation technique which makes use of hydroxyl radicals generated on surfaces of some photo-active metallic oxides and semiconductors in the presence of solar energy to convert toxic pollutants into harmless products. The metal oxides and semiconductors are collectively referred to as photocatalysts because their catalytic activity depends on availability of light. A unique property

of every photocatalyst is the possession of a band gap which is the energy difference between their valence band edge and their conduction band edge (Fig. 2.3) [42].

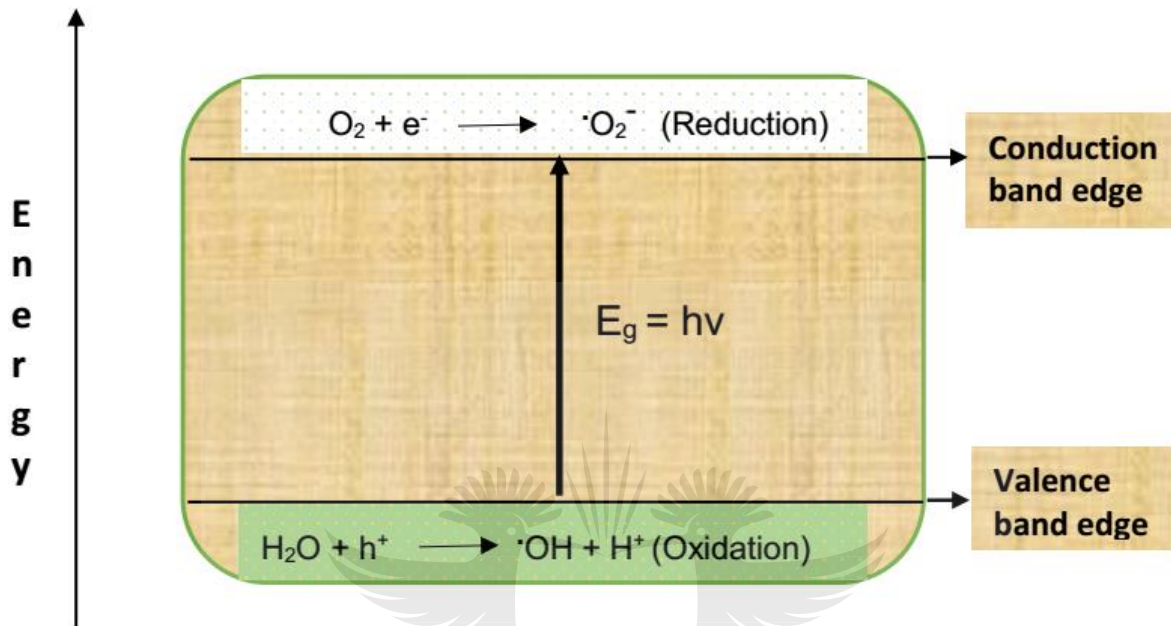
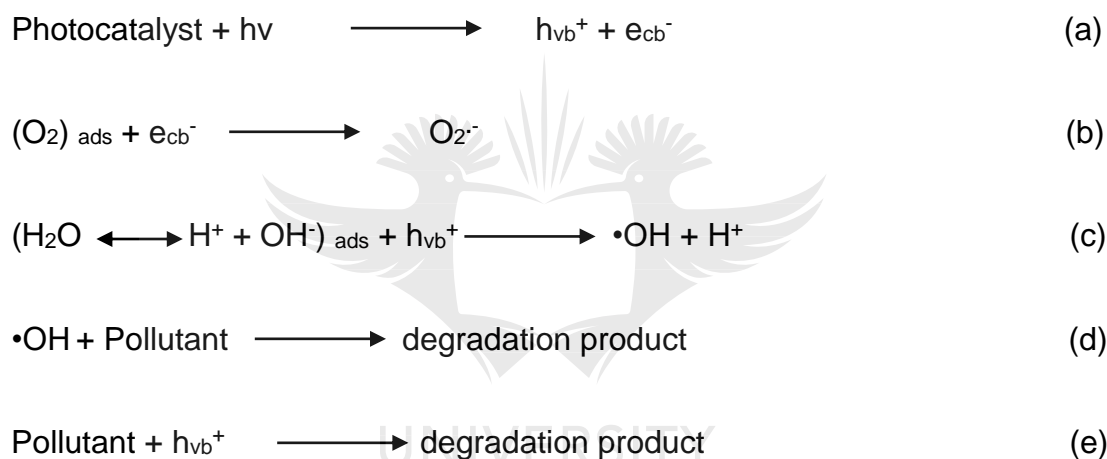


**Figure 2. 3:** A schematic diagram showing the band gap ( $E_g$ ) of a photocatalyst. Reduction of  $O_2$  is caused by the photo-excited electron while oxidation of water is caused by the photo-generated hole.

The energy of solar radiation required for catalytic activity depends on the size of the band gap. Based on this, photocatalysts are generally grouped into ultraviolet (UV) and visible light activated groups. The UV-activated group is the group of photocatalysts having a band gap  $\geq 3.0$  eV while the visible light activated group is the one with a band gap  $< 3.0$  eV [42].

In the presence of a photon of sufficient energy, electrons are excited from the valence band (VB) to the conduction band (CB) of a photocatalyst resulting in the creation of a hole ( $h^+$ ) and an electron ( $e^-$ ) in the VB and CB, respectively (Fig. 2.3, Scheme 2.2a). In

the CB, the generated electron is scavenged by adsorbed oxygen molecules to prevent electron-hole recombination. The oxygen molecule is reduced to a superoxide ion (Scheme 2.2b) which can oxidize the organic pollutant or initiate other radical chain reactions involving  $\text{H}_2\text{O}_2$  and  $\text{O}_3$  [43, 44]. The hole reacts with adsorbed water molecules to produce highly reactive hydroxyl ( $\cdot\text{OH}$ ) radicals (Scheme 2.2c) which are responsible for the degradation (Scheme 2.2d). Degradation can also occur through the direct attack of the generated holes on the pollutant (Scheme 2.2e) [41, 43].



**Scheme 2. 2:** Photocatalytic degradation of a pollutant initiated by photo-generated holes and electrons.

## 2.8 POLLUTANT – PHOTOCATALYST INTERACTION

Significant research efforts have been recorded on photo-catalytic degradation of various pollutants using different photocatalysts where the performance of the photocatalysts were appraised based on some extrinsic properties such as catalyst dosage, pollutant concentration, pH, degradation time, light intensity and temperature [41, 45-47]. However, an important intrinsic property that affects a photocatalytic degradation process, but which has received limited research attention is the philicity of a pollutant for a catalyst. The

greater the philicity of a pollutant for a photocatalyst, the better the interaction and the higher the chance of a successful degradation.

The philicity of a pollutant for a catalyst can be predicted from the interaction tendency between the frontier molecular orbital (FMO) of the pollutant and the energy bands of the photocatalyst. This type of approach was adopted by Oprea *et al.* [48] in their study on the binding of Mordant yellow 10 dye with  $\text{TiO}_2$ , in which the potency of the dye to release electrons into the conduction band of  $\text{TiO}_2$  was evaluated from its FMO.

The FMO of a pollutant comprises its highest occupied molecular orbital (HOMO) and lowest unoccupied molecular orbital (LUMO) [48-50] whereas the energy bands of the photocatalyst consists of the valence band edge (VBE) and the conduction band edge (CBE) (Fig. 2.3) [42]. The HOMO is the part of a molecule with the highest chance of donating an electron while the LUMO is the portion with the highest tendency to accept incoming electrons. In the case of a photocatalyst, the donor site is the valence band because it is the site with the highest electron population. On the other hand, the conduction band is the most electron deficient portion, hence the acceptor site.

The energy gap between the HOMO of a pollutant and the conduction band edge of a catalyst, and that between its LUMO and the valence band edge of the catalyst can provide insight on the probability of electron donation and retro-donation between the pollutant and the catalyst for a favorable adsorption that may lead to degradation. Determination of these interaction parameters for a pollutant can guide the selection of a suitable photocatalyst for degrading the pollutant. This will also be demonstrated in the current study using the selected dyes and photocatalysts.

## 2.9 INTRINSIC PROPERTIES AFFECTING DISPERSE DYE APPLICATIONS

Intrinsic properties are the properties governed exclusively by the chemical nature of a substance. The major intrinsic properties guiding the selection of disperse dyes for various applications are solubility, light fastness, wash fastness and sublimation fastness in addition to color quality. In the case of a monoazo disperse dye, these properties can be controlled by a systematic variation of the substituent groups present in the diazotizing and coupling components of a monoazo dye structure [7, 14, 20-23]. The effect of substituent variation can also manifest in other properties such as chemical reactivity, planarity, optical activity, absorption wavelength and hyperpolarizability as observed by various authors [11, 51-61].

## 2.10 AQUEOUS SOLUBILITY

Aqueous solubility refers to the maximum amount of a given disperse dye that can mix, interact or dissolve completely in a given amount of water to form a saturated solution. It is usually expressed in gram per litre or milligram per litre (g/L or mg/L) [62]. Other units including mole or millimole per litre (mol/L or mmol/L) are also acceptable [3, 5, 24]. Solubility is a temperature dependent property and must therefore be reported in conjunction with the prevailing temperature condition [3, 5, 24]. Aqueous solubility of disperse dyes is a measure of the extent of their hydrophilicity which is governed by the degree of polarity. The higher the polarity, the greater the hydrophilicity and the better the solubility and vice versa.



Aqueous solubility has a great influence on the operational cost of using a given disperse dye because it determines the type and the quantity of dispersing agents required for efficient dyeing. The lower the aqueous solubility, the greater the quantity of dispersing agents needed. Dispersing agents are chemical additives used in conjunction with a disperse dye to enhance its solubility, levelling and substrate penetration power [3]. Examples of such additives include metamol, soap, synthetic detergents of the alkylsulphate or alkarylsulphonate, lignin sulphonates or polycondensates of arylsulphonic acids with formaldehyde, and fatty alcohol-ethylene oxide condensates [2, 4, 5, 63].

### **2.11 LEVELLING AND FASTNESS**

Levelling power is a measure of the ability of a given disperse dye to undergo uniform distribution throughout a substrate without agglomerating on the surface as deposits. To a large extent, levelling power is dependent on solubility [5]. Therefore, it can also be enhanced by the addition of dispersing and carrier agents. The levelling property is affected by molecular size and polarity. Smaller disperse dyes with high polarity are highly levelling while higher molecular weight dyes with low polarity possess low levelling power [8].

The fastness property on the other hand describes the ability of a disperse dye to resist fading under conditions such as light, heat, water, sweat and surface rubbing. These are described as light fastness, sublimation fastness, wash fastness, perspiration fastness and rubbing fastness, respectively [4]. Of these properties, the most commonly used ones by chemists for evaluating disperse dye performances are light and wash fastness [14,

20, 21]. However, sublimation fastness is also paramount as it describes the escape tendency of a disperse dye from a dyed substrate when heated. In addition to size and polarity, fastness properties can also be affected by the nature of substrate. Polyester fibres for example show better wash fastness with disperse dyes due to their higher crystallinity and hydrophobicity compared to their acetate and nylon counterparts [4, 14].

### **2.11.1 LIGHT FASTNESS**

Light fastness refers to the ability of a disperse dye to resist color fading on prolonged exposure to light. It is controlled by numerous factors such as the wavelength of the light, substrate structure, temperature, effective humidity, molecular size, presence of impurities in the form of carrier and dispersants, exposure time, exposed surface area, stability of the aromatic moieties and the nature of the substituents in the dye structure [4]. Light of short wavelengths release larger amounts of energy onto dyed fibre surfaces to bring about accelerated fading compared to those of long wavelengths. A more tightly packed fibre inhibits fading because it possesses well obstructed tiny pores which does not allow free passage of oxygen or moisture. High temperature accelerates fading while low temperature suppresses it.

Effective humidity promotes fading by facilitating the movement of molecular oxygen to excited dye molecules, and also acts as a reaction field in which the fading takes place. Low molecular weight dyes undergo fading faster than higher ones since the rate of fading varies inversely to the radius of dye particles [4]. Impurities such as dispersants, carrier agents and even metals which are retained on the dyed fibre can also enhance fading.

For example, *o*-phenylphenol is known to promote fading of disperse dyed polyester fibres [4].

The longer the exposure time and the larger the exposed surface area, the more the fading. Short time exposure allows excited dye molecules to return to their ground state by releasing their excess energy thereby regaining their lost color. The higher the stability of the aromatic moieties in a disperse dye structure, the smaller the chance of fading. Electron donating groups (EDG) and electron withdrawing groups (EWG) show opposing effects on fading. EDG enhances fading while EWG inhibits it [4, 64].

### 2.11.2 WASH FASTNESS

Wash fastness is a property used to describe the tendency of a dye to retain its color on a dyed substrate when the latter is subjected to washing. This property is dependent not only on the dye solubility, but also on other factors such as the relative strength of dye-substrate and dye-solvent interactions, dye chemistry, dye size, temperature, type of detergent used and the location of the dye on substrate structure [4, 64].

On the basis of solubility, disperse-dyed fibres are expected to show high resistance to color washing due to the low aqueous solubility property of disperse dyes. The relative affinity of a disperse dye for a substrate and the solvent used for washing determines its stability in either phase. An excellent wash fastness is obtained when the interaction between the dye and the substrate is stronger than that between the dye and the solvent. On the other hand, a poor wash fastness is obtained when the dye forms a stronger interaction with a solvent, but a weaker interaction with the substrate. Smaller disperse dyes are leached out of a dyed fibre faster than larger ones. Larger dye

molecules are not easily leached out of fibre openings except at elevated temperatures. Increasing washing temperature opens up the fibre structure in an accelerated manner thereby increasing the rate of dye leaching [64].

### **2.11.3 SUBLIMATION FASTNESS**

Sublimation fastness refers to the ability of a dye to resist loss of color intensity and shade upon exposure to heat. It is a measure of the resistance of a dye to thermal agitation. The sublimation point of a disperse dye is the temperature at which the dye escapes as vapor leading to a lighter shade. This temperature must be well above the operational temperature of dyeing and domestic heat pressing to prevent sublimation.

Sublimation fastness is dependent on the molecular weight and the strength of the intermolecular forces between a disperse dye and a substrate [64]. The higher the molecular weight, the lower the vapor pressure and the better the sublimation fastness. The stronger the binding force between a dye and a substrate, the better the sublimation fastness. Other factors which can also affect sublimation fastness include temperature, time of contact, dye structure and substrate structure [4].

### **2.11.4 PERSPIRATION FASTNESS**

Perspiration fastness deals with the resistivity of a dye to decoloration in the presence of human sweat. Human sweat is considered as an emulsion consisting of ammonia, urea, glucose, chlorides and some trace elements in addition to lactic acid at a pH around 6.14 to 6.57 which is considered as the major component [4]. Loss of color through perspiration is attributed to the synergy effect of body heat and that of the emulsion [4].

## 2.12 CHALLENGES OF AZO DISPERSE DYE APPLICATION

The major concerns associated with the use of disperse dyes particularly the azo class include high cost of application and environmental pollution [2, 4, 65]. These problems are due to low aqueous solubility and poor levelling properties of majority of the dyes which necessitates the addition of dispersing agents. Disperse dyes are generally pre-treated with dispersing or solubilizing agents which may also be added in conjunction with a carrier agent during dyeing to improve their solubility as well as facilitate their penetration through substrates. The use of dispersants and carrier agents leads to high cost of dyeing [2, 4] because different dispersants are usually employed for different dyes, and the quantity of these auxiliary agents required depends on the aqueous solubility of the dye. The smaller the solubility, the larger the quantity of dispersant needed. Since different disperse dyes require specific types of dispersing agents depending on the chemical nature of the dyes [1, 3, 6], the use of a large number of different dyes for a large scale textile production is therefore capital intensive.

Furthermore, research findings have shown that an increase in the concentration of a dispersing agent could lead to a reduction in dye uptake [61]. It is also noteworthy that most of the available carrier agents do not only interfere with the light resistance property of a disperse dye, but also possess undesirable odours and some non-biodegradable toxic chemical components such as chlorinated aromatic compounds, biphenyls, o-phenylphenol etc., which are dangerous to life and the environment [4].

The high temperature high pressure (HTHP) dyeing method has been a common alternative to carrier dyeing, because it can be used without a carrier agent [1, 2, 4].

However, this method is only suitable for disperse dyes with large molecular weights which have high heat resistance capacity. It is not appropriate for disperse dyes whose melting and sublimation temperatures are below the minimum operational temperature of the HTHP machine which is ca 130 °C [4].

In addition, the use of HTHP method is relatively more expensive and more cumbersome as the selection of equipment is based on the type of fabric to dye [4]. In other words, different fabrics may require different HTHP equipment leading to higher production cost. Moreover, the performance of HTHP machines depends largely on the pressure generated from continuous supply of steam by the machine boilers. Therefore, the HTHP method becomes less effective during winter when there is a fall in the operational pressure as a result of steam condensation [4].

### **2.13 PREVIOUS WORK ON IMPROVING AZO DISPERSE DYE APPLICATION**

Addressing both the economic and environmental issues related to azo disperse dyes application requires that their solubility, levelling power and fastness properties be enhanced to limit the use of dispersants and carriers. Solvent dyeing [66-68], supercritical dyeing [69-73] and the use of polar/solubilizing groups [74, 75] have been suggested as alternative techniques to carrier dyeing. Solvent dyeing makes use of organic solvents for dissolution of disperse dyes since these types of solvents possess greater affinity for nonionic and hydrophobic solutes. However, in addition to a relatively high cost of practice, the solvent dyeing technique has not received a monumental commercial application probably due to issues such as toxicity, hazard, flammability, volatility, and

possession of certain characteristic repugnant odors by most organic solvents which are often undesirable for production.

Supercritical dyeing involves the use of supercritical fluid such as supercritical carbon dioxide (SCD) as solvent in place of water or organic solvents during dyeing [71-73]. In addition to relative low cost, non-toxicity and renewability, SCD has been found to have greater affinity for azo disperse dyes and hence, improve their solubility [71, 72]. Moreover, contrary to the use of water or organic solvents, reduction clearing which helps to wash off surface-deposited dye particles and stabilize color intensity is not performed in supercritical dyeing, because in this case, application of dye to fabrics can be controlled better to yield the intended quality [69-72]. However, supercritical carbon dioxide does not occur naturally, but is produced from carbon dioxide gas at a critical temperature and pressure of 304 K and 73.7 bar, respectively [73, 76]. The need to maintain these conditions in order to keep this fluid in its supercritical state for large scale applications is a setback to this technique, as compared to water which is freely and abundantly available in the liquid state.

Most studies on the influence of polar substituent groups have focused mainly on improvement of properties such as color, levelling, dyeability and fastness [14, 20, 22, 55, 60, 61, 77, 78]. This was achieved through incorporation of certain electron withdrawing and electron donating substituent groups into the diazotization and coupling components of the intended azo dyes.

Sakoma *et al.* [14] developed a series of azopyridone disperse dyes using combinations of varying electron-withdrawing groups (EWGs) and electron-donating groups (EDGs).

The EWGs considered included  $-\text{OCH}_3$ ,  $-\text{SO}_3\text{H}$ ,  $-\text{COOH}$ ,  $-\text{OH}$ , and  $\text{Cl}$  while the EDGs are  $\text{CH}_3$  and  $\text{C}_2\text{H}_5$ . The shades of the dyes obtained ranged from light yellow to orange with different combinations of the EDGs and EWGs. Properties such as wavelength of maximum absorption, levelling, light and wash fastness were also enhanced.

In a similar study by Patel *et al.* [20], in which polar substituent effects were investigated on some high molecular weight aminoazobenzene and azopyridone disperse dyes, different combinations of substituent groups were found to impact significant changes in the color and absorption wavelength of the dyes. A marked improvement was also observed in the wash and light fastness properties of the dyes on polyester and nylon fibers. With a variety of coupling components, a set of new azo disperse dyes containing carbonyl and dicyanovinyl groups was synthesized by Choi and co-workers [55]. An increase in electron withdrawing strength of the azo components due to addition of dicyanovinyl substituents was found to promote both bathochromic shifting and color intensity of the derivatives more than those of the parent dyes.

Maradiya and Patel [60] developed a series of new heterocyclic azo disperse dyes by combination of 5-acetyl-2-amino-4-methylthiazole with a variety of N-alkyl derivatives of aniline, where the former and the latter acted as the diazotization and the coupling agents, respectively. Systematic variation of the substituent groups led to a remarkable improvement in the color type and intensity, levelness, fabric penetration power, and wash, light, rubbing, sublimation and perspiration fastness. While a similar result was observed by Modi *et al.* [77] for imidazolone dyes, and Lam *et al.* [78] for pyridone and resorcinol substituted dyes, El-Aspary *et al.* [61] added that electron withdrawing group



substituted azopyridone dyes possess higher light fastness compared to the electron donating group substituted dyes. This implies that the electron withdrawing groups limit the chances of photo-excitation of electrons which causes fading, by decreasing the potential of the dyes to release electrons.

Kim and Park [51] observed that the absorption wavelength, molar extinction coefficient and photodegradation tendency of disperse azo dyes were very sensitive to change in electron donating ability of the coupling component. The dye with phenylindole as coupling component was observed to exhibit excellent dyeing properties and a remarkable light fastness. According to Fadda and Abass [52], a series of new azo disperse dyes containing a pyridine ring in their structures were found to show good affinity towards polyester fibers. Otutu in his synthesis of halogenated disazo disperse dyes from 2,4-dichloroaniline and 3-aminophenol [79], observed that the absorption maxima of the synthesized dyes were found to be sensitive to the nature of the substituents in the diazotizing and coupling components. In addition, the dyes exhibited excellent resistance to photofading, washing, sublimation and good rubbing fastness.

Substitution of aminoazobenzene disperse dyes with a mixture of  $-OCH_3$ ,  $-NHCOCH_3$ ,  $-COOCH_3$ , and  $-NO_2$  groups has been shown to enhance not only some fastness properties, but also the frontier molecular orbitals (i.e. HOMO and LUMO) [22]. Changes in the energies of frontier molecular orbitals have been used by Olasunkanmi *et al.* [49], to predict the corrosion inhibition properties of some food azo dyes in terms of their binding potentials for mild steel surface. Such changes have also been used for

calculating some global reactivity descriptors for predicting the stability and reactivity of various azo dyes [23, 80, 81].

In the above previous studies and many others, an important property for which no considerable account has been given in relation to substituent effect is aqueous solubility. Most of the previous studies were focused on development of more efficient disperse dyes for dyeing hydrophobic substrates particularly polyesters. Until recently, no significant research attention has been given to the development of water soluble disperse dyes which can help in expanding their application. Variations in electron donating and/or electron withdrawing strengths of the coupling and/or diazotising components of azo dyes due to substitution will not only manifest on the color and fastness properties of the dyes, but also on their aqueous solubility, binding capacity and degradability. This is because the substituent groups bring about a change in polarity and chemical reactivity of the dyes, and also contain donor atomic sites which can promote stronger intermolecular forces between a dye and a substrate [4].

Recently, Bianchini *et al.* [74, 75] reported that the introduction of some sugar moieties into azo disperse dye structures led to a significant increase in their aqueous solubility. With the aim of developing disperse dyes that can be used with no dispersing agent, Lee *et al.* [82] observed that modification of some azo disperse dye structures with  $\beta$ -sulfatoethylsulfonyl group enhanced the solubility of the dyes, similar to the observation made by Meena *et al.* [83] in their study on dispersant-free disperse dyes, in which sulfomethylated aniline and sulfomethylated m-toluidine were used as coupling components. Furthermore, a series of dispersant-free azo disperse dyes have also been

developed from 1-substituted-2-hydroxypyrid-6-one and indole derivatives by Lee and co-workers [84, 85].

## 2.14 PREVIOUS THEORETICAL STUDIES ON AZO DYES

A plethora of theoretical studies on azo dyes focusing on investigating structural, binding, reactivity, spectroscopic, electronic and optical properties of these dyes have been reported. Deshmukh and Sekar [11] used DFT to probe the stabilities of the azo and hydrazone tautomeric forms of some aminoazobenzene disperse dyes as well as their electronic excitation properties. All the dyes were found to exist predominantly in the azo form, and frontier molecular orbital calculations revealed that their electron density is mostly concentrated in their donor units. Similar findings were reported by Arslan and co-workers in their study on dimethyl aniline based azo disperse dyes [56], where the dyes were also found to exhibit useful properties for non-linear optical application.

Anouar *et al.* [86] used DFT and time dependent DFT (TD-DFT) to investigate the local reactivity of reactive violet 5R, in addition to its electronic and optical properties. They concluded that the most reactive site in the dye is one of the azo (i.e. N=N) nitrogen atoms. Theoretical calculation was used by Franco and co-workers [87] to investigate the interaction between Disperse Red 73, 78 and 167 dyes, and azoreductase enzyme produced by *Escherichia coli*. Biotransformation of the dyes by the enzyme was observed to be highly favorable, and the biotransformation products were found to possess high affinity for human DNA.

Zhan and co-workers [4] used DFT method to investigate the effects of substitution on hydrolysis and intermolecular interactions in azo dyes containing N-substituted phthalimides as diazotizing component. Substitution with N-alkyl groups was found to have little effect on the absorption maxima whereas the introduction of cyano and bromo groups brought about bathochromic and hypsochromic shifts of the absorption wavelength, respectively. The steric effects of the substituents on dye hydrolysis were found to predominate over their inductive effects and intermolecular interactions between dye molecules were predominantly electrostatic in nature.

Recent theoretical study by Novir and Hashemianzadeh [53] investigated the effects of various anchoring groups such as hydroxamic acid, sulfonic acid, carboxylic acid, biscarbodithiolic acid and phosphonic acid on the lowest unoccupied molecular orbital (LUMO), chemical hardness, excited state life time, electronic and optical properties, light harvesting efficiency and UV-Vis absorption spectra of azo dyes in dye-sensitized solar cells. The dye containing biscarbodithiolic acid was found to have the longest wavelength of maximum absorption, the broadest absorption spectra, the longest excited state life time, and the highest LUMO orbital and light-harvesting performance. In addition, this dye also gave the largest adsorption energy and the highest negative shift of the conduction band when adsorbed onto  $\text{TiO}_2$ .

## 2.15 THE CURRENT STUDY

To achieve an economical and more eco-friendly application, there is a need for new disperse dyes with lower economic and environmental consequences. Provision of useful theoretical data to guide azo disperse dye syntheses, and a simple theoretical approach

for predicting *a priori*, the aqueous solubility, fastness property, degradability and suitable photodegradation catalysts for azo dyes is of paramount importance. Therefore, the current theoretical study is designed to investigate the effects of some polar substituent groups on the aqueous solubility and chemical reactivity of Disperse Yellow 119 (DY119) and Disperse Red 73 (DR73) using Density Functional Theory (DFT). The substituent groups selected are  $-\text{CN}$ ,  $-\text{NO}_2$ ,  $-\text{NH}_2$ ,  $-\text{NHCH}_3$  and  $-\text{N}(\text{CH}_3)_2$  which all contain a nitrogen atom and are expected to also improve the binding capacity of the dyes.

The number of new azo disperse dyes that can be derived through substitution with different combinations of the EDGs ( $-\text{NH}_2$ ,  $-\text{NHCH}_3$  and  $-\text{N}(\text{CH}_3)_2$ ) and the EWGs ( $-\text{CN}$ ,  $-\text{NO}_2$ ) is enormous and almost inexhaustible for any experimental study. However, computational modelling using efficient quantum chemical methods such as DFT can pilot experimental efforts by providing useful and reliable theoretical information on the properties of numerous proposed dyes with relatively lower cost, resource input and in a relatively shorter time frame. The outcome of theoretical screening can help organizations and industries to concentrate only on the proposed dyes that meet some set criteria, thereby preventing waste of materials, effort, time and funds. Theoretical calculations can also provide relevant information such as the likelihood of synthesising the proposed dyes, their degradability, appropriateness of a photocatalyst for their degradation and possible degradation mechanisms.

The scope of this work has been divided into three sections namely; aqueous solubility, chemical reactivity and photodegradation pathway studies, where the reactivity study covers global reactivity, local reactivity and catalytic selectivity studies.

### 2.15.1 AQUEOUS SOLUBILITY STUDY

The conductor-like screening model for realistic solvation (COSMO-RS) [88-90] implemented in the DMol<sup>3</sup> program [89] will be employed in conjunction with the Cramer *et al.* solubility equation (CSE) [91] for the aqueous solubility study.

COSMO-RS model is a non-empirical implicit solvation method used for predicting the thermodynamic properties of solutions and fluids such as vapor pressure, chemical potential, solubility, partition coefficients, solvation free energy, hydration free energy and activity coefficients [89, 92]. This model has been employed in a direct manner for predicting drug and pesticide solubility [92, 93], solubility of some pharmaceutical compounds and flavonoids in ionic liquids [94, 95], solubility of rapeseed oils in various solvents [96] and carbon dioxide absorption by various solvents [97], where the predicted solubility values were reported as mole fraction solubility (i.e. relative solubility).

However, an indirect method of application of COSMO-RS, which involves treatment of some COSMO-RS data such as vapor pressure, solvation free energy and octanol-water partition coefficient, with some solubility equations such as the Cramer *et al.* solubility equation (CSE) [91] and the general solubility equation (GSE) [98], for predicting aqueous solubility in standard units (e.g mol/L, g/L or mg/L) is very rare in the literature. The CSE makes use of a solute vapor pressure and solvation free energy to determine its solubility (Eqn. 2.1) [91], whereas the GSE employs the solute melting point and its octanol-water partition coefficient (Eqn. 2.2) [98]. Selection of CSE for this work is based on the fact that the parameters (i.e. vapor pressure and solvation free energy) required can be obtained

via COSMO-RS calculations. Lack of melting point information in COSMO-RS results prevents utilization of the GSE for this work.

$$S = \frac{P_s}{P^0} e^{-\Delta G_{sol}/RT}$$

Equation 2. 1

$$\text{Log } S = 0.5 - 0.01(m.p^{\circ}C - 25) - \text{Log } P$$

Equation 2. 2

where  $S$  represents the solubility in mol/L,  $P_s$  is the solute vapour pressure,  $P^0 = 24.45$  atm (the pressure of an ideal gas at 1 molar standard state and 298 K),  $\Delta G_{sol}$  is the solvation free energy,  $R$  is the molar gas constant and  $T$  is the temperature.  $\text{Log } P$  is the octanol-water partition coefficient,  $m.p^{\circ}C$  is the melting point of the solute [27].

### 2.15.2 CHEMICAL REACTIVITY STUDY

The reactivity study will be focusing on the evaluation of the overall stability of the dyes (i.e. global reactivity), their affinities for Si, CdSe, CdS, TiO<sub>2</sub>, ZnO and ZnS photocatalysts (i.e. catalytic selectivity) as well as identification of probable sites for the attack of photogenerated hydroxyl radicals during photocatalytic degradation (i.e. local reactivity).

The indices employed for global reactivity evaluation include HOMO-LUMO energy gap, chemical hardness, chemical softness, chemical potential, electronegativity and electrophilicity index [23, 99, 100]. Using relevant approximations, these parameters can be obtained using the HOMO and LUMO energies of the dyes. Catalytic selectivity will be assessed by calculating some interaction parameters using the frontier molecular orbitals (i.e. HOMO and LUMO) of the dyes and the band structures (i.e. VBE and CBE) of the

catalysts. Local reactivity i.e. site propensity to radical attack will be determined through Fukui function calculation using Mulliken atomic charges [99, 100].

The selected catalysts comprise of two groups – the ultraviolet (UV) and the visible light activated groups. The UV activated group comprises the catalysts that have their band gaps within the UV range (i.e. 3.0 – 6.0 eV) of the electromagnetic radiation. Members of this group are TiO<sub>2</sub> (rutile) (3.0 eV), ZnO (3.2 eV) and ZnS (3.6 eV) [42, 45]. The visible light activated group are the ones with band gaps in the visible region (i.e.  $\leq 3.0$  eV) of the radiation. This consists of Si (1.10 eV), CdSe (1.70 eV) and CdS (2.40 eV) [42]. Our objective is to propose the most suitable photocatalyst(s) from this selected set for degrading the selected dyes and their proposed derivatives.

### **2.15.3 PHOTOCATALYTIC DEGRADATION PATHWAYS**

The degradation mechanism of azo dyes when attacked by a photo-generated hydroxyl ( $\cdot\text{OH}$ ) radical is still a subject of intense investigation due to conflicting reported pathways involving either the cleavage of the bond between one of the aromatic moieties and the azo (N=N) group or the bond between the azo nitrogen atoms themselves. These are known as C–N and N–N bond cleavage pathways, respectively (Fig. 2.4).



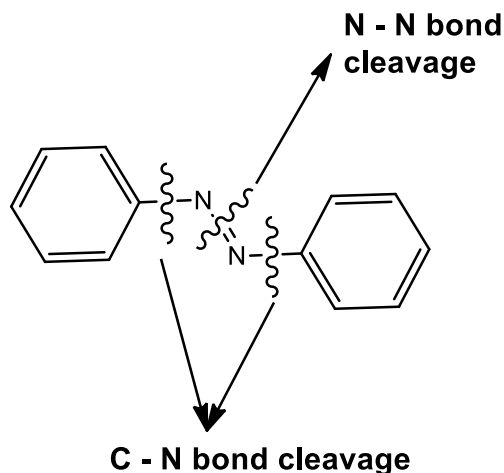


**Figure 2. 4:** C–N and N–N bond cleavage degradation mechanisms of azo dyes.

Based on experimental findings, Spadaro *et al.* [101] proposed the C–N bond cleavage as the preferred degradation pathway for azo dyes both from a kinetic and thermodynamic point of view. This was supported theoretically by Ozen *et al.* [102]. On the contrary, Joseph *et al.* [103] in their study of azo dye degradation by ultrasonically generated  $\cdot\text{OH}$  radicals, reported that the most kinetically and thermodynamically favored pathway is the N–N bond cleavage. This was also supported by theoretical evidence from Ozen *et al.* [104, 105]. A third view point reported by Jiao *et al.* [106] is that both the C–N and N–N bond cleavages are kinetically competitive, with the former having greater thermodynamic favorability [106].

Careful assessment of the above reports revealed that the possible factors which might be responsible for the competing pathways are symmetry and tautomerism. The proposed C–N bond cleavage pathway by Spadaro *et al.* [101] and Ozen *et al.* [102] is suspected to originate from the hydrazone form of the studied dyes as suggested by Jiao *et al.* [106]. The presence of a hydroxyl ( $-\text{OH}$ ) or a carboxyl ( $-\text{COOH}$ ) group in the

structures of some azo dyes can cause the dyes to exist in two tautomeric forms - the azo and the hydrazone forms, such that the latter favors the C-N bond cleavage pathway [102, 104, 106].

On the other hand, the high symmetry of azobenzene about the azo bridge (-N=N-) could naturally give precedence to the cleavage of the N-N bond over the C-N bond. This was not taken into account by Ozen and co-workers [105]. A third factor which is yet to be investigated is the effect of hydrogen bonding which exists in some azo dyes such as disperse yellow 119. The role of this bonding, tautomerism and symmetry will be investigated in this work using the selected dyes in order to provide more clarifications on the preferred degradation pathway(s) of azo dyes. Also, possibility of further disintegration of the bond cleavage products through processes such as deamination and nitrogen evolution will be investigated.

## 2.16 REFERENCES

1. J. Aspland. Disperse dyes and their application to polyester. *Textile Chemist and Colorist* **24** (1992) 18-18.
2. J. Koh. Dyeing with disperse dyes; P. Hauser (Ed.), *INTECH Open Access Publisher*, Croatia, (2011) 195-221. DOI: 10.5772/20458. Available at: <https://www.intechopen.com/books/textile-dyeing/dyeing-with-disperse-dyes>.
3. F. Jones. The solubility and solubilisation of disperse dyes. *Journal of the Society of Dyers and Colourists* **100** (1984) 66-72.

4. M. Clark. Handbook of textile and industrial dyeing: principles, processes and types of dyes. *Woodhead Publishing Limited*, United Kingdom, (2011).
5. C. Bird. The dyeing of acetate rayon with disperse dyes I-aqueous solubility and the influence of dispersing agents II-the relation between aqueous solubility and dyeing properties. *Journal of the Society of Dyers and Colourists* **70** (1954) 68-77.
6. J. Dawson. Fifty years of disperse dyes (1934–1984). *Review of Progress in Coloration and Related Topics* **14** (1984) 90-97.
7. J. Aspland. The structure and properties of disperse dyes and related topics. *Textile Chemistry and Coloration* **25** (1993) 21-25.
8. A. D. Broadbent. Basic principles of textile coloration. *Society of Dyers and Colourists*, Bradford, West Yorkshire, England, (2001).
9. M. R. Almeida, R. Stephani, H. F. Dos Santos and L. F. C. d. Oliveira. Spectroscopic and theoretical study of the azo dye E124 in condensate phase: evidence of a dominant hydrazo form. *The Journal of Physical Chemistry A* **114** (2009) 526-534.
10. D. L. Pavia, G. M. Lampman, G. S. Kriz and R. G. Engel. Fort Worth. Introduction to Organic Laboratory Techniques: Small-Scale Approach. *Chemicke Listy* **104** (2010) 950-953.
11. M. S. Deshmukh and N. N. Sekar. A Combined Experimental and TD-DFT Investigation of Mono Azo Disperse Dyes. *Canadian Chemical Transactions* **1** (2013) 305-325.
12. A. S. Alimmari, A. D. Marinković, D. Ž. Mijin, N. V. Valentić, N. Todorović and G. S. Ušćumlić. Synthesis, structure and solvatochromism of new 5-(4-substituted

- phenylazo)-4-(4-substituted phenyl)-6-hydroxy-3-cyano-2-pyridones. *Journal of the Serbia Chemical Society* **75** (2010) 1019-1032.
13. W. Huang. Structural and computational studies of azo dyes in the hydrazone form having the same pyridine-2, 6-dione component (II): CI disperse yellow 119 and CI disperse yellow 211. *Dyes and Pigments* **79** (2008) 69-75.
  14. K. J. Sakoma, K. A. Bello and M. K. Yakubu. Synthesis of some azo disperse dyes from 1-substituted 2-hydroxy-6-pyridone derivatives and their colour assessment on polyester fabric. *Open Journal of Applied Sciences* **2** (2012) 54-59.
  15. J. Koh and A. J. Greaves. Synthesis and application of an alkali-clearable azo disperse dye containing a fluorosulfonyl group and analysis of its alkali-hydrolysis kinetics. *Dyes and Pigments* **50** (2001) 117-126.
  16. G. W. Gray. Dyes and liquid crystals. *Dyes and Pigments* **3** (1982) 203-209.
  17. Y. Qian, G. Xiao, G. Wang, Y. Sun, Y. Cui and C. Yuan. Synthesis and third-order optical nonlinearity in two-dimensional A- $\pi$ -D- $\pi$ -A carbazole-cored chromophores. *Dyes and Pigments* **71** (2006) 109-117.
  18. K. Nejati, Z. Rezvani and M. Seyedahmadian. The synthesis, characterization, thermal and optical properties of copper, nickel, and vanadyl complexes derived from azo dyes. *Dyes and Pigments* **83** (2009) 304-311.
  19. K. Georgiadou and E. Tsatsaroni. Synthesis, characterisation and application of disperse dyes derived from N-2-hydroxyethyl-1-naphthylamine. *Dyes and Pigments* **50** (2001) 93-97.

20. D. Patel, N. Prajapati, M. Thakor and V. Patel. Formation of some novel disperse azo dyes: Synthesis, characterisation and printing properties. *Journal of Current Chemical and Pharmaceutical Sciences* **2** (2012) 86-91.
21. S. M. Ashkar, M. A. El-Asery, M. M. Touma and M. H. Elnagdi. Synthesis of some novel biologically active disperse dyes derived from 4-Methyl-2, 6-dioxo-1-propyl-1, 2, 5, 6-tetrahydro-pyridine-3-carbonitrile as coupling component and their colour assessment on polyester fabrics. *Molecules* **17** (2012) 8822-8831.
22. M. S. Deshmukh and N. Sekar. A combined experimental and TD-DFT investigation of three disperse azo dyes having the nitroterephthalate skeleton. *Dyes and Pigments* **103** (2014) 25-33.
23. B. I. Adewale and S. Banjo. Theoretical study on structural and electronic properties of 4-[(E)-[4-(trifluoromethyl)-1, 3-benzothiazol-2-yl] azo] naphthalen-1-ol and 1-[(E)-[4-(trifluoromethyl)-1, 3-benzothiazol-2-yl] azo] naphthalen-2-ol using density functional theory (DFT). *International Journal of Physical Sciences* **8** (2013) 1494-1505.
24. G. L. Baughman and T. A. Perenich. Fate of dyes in aquatic systems: I. Solubility and partitioning of some hydrophobic dyes and related compounds. *Environmental Toxicology and Chemistry* **7** (1988) 183-199.
25. J. M. Wattie. A study into respiratory disease in dyehouse operatives exposed to reactive dyes. *Journal of the Society of Dyers and Colourists* **103** (1987) 304-308.
26. B. Hausen and K. Schulz. Allergy to dyes in stockings. *German Medical Weekly* **109** (1984) 1469-1475.

27. B. Hausen, A. Kleinheinz and H. Mensing. Contact Dermatitis by textile dyes (velvet leggings). *Allergo Journal International* **2** (1993) 13-16.
28. E. J. Weber and N. Lee Wolfe. Kinetic studies of the reduction of aromatic azo compounds in anaerobic sediment/water systems. *Environmental Toxicology and Chemistry* **6** (1987) 911-919.
29. H. Øllgaard, L. Frost, J. Galster and O. C. Hansen. Survey of azo-colorants in Denmark. Consumption, use, health and environmental aspects (1998). Available at: <https://www2.mst.dk/udgiv/publications/1999/87-7909-548-8/pdf/87-7909-546-1.pdf>. Accessed on 14 March 2018.
30. M. Doble and A. Kumar. Biotreatment of industrial effluents. *Elsevier*, Netherlands, (2005).
31. I. T. Peternel, N. Koprivanac, A. M. L. Božić and H. M. Kušić. Comparative study of UV/TiO<sub>2</sub>, UV/ZnO and photo-Fenton processes for the organic reactive dye degradation in aqueous solution. *Journal of Hazardous Materials* **148** (2007) 477-484.
32. M. A. Salem and A. H. Gemeay. Kinetics of the oxidation of tartrazine with peroxydisulfate in the presence and absence of catalysts. *Chemical Monthly* **131** (2000) 117-129.
33. S. Banerjee and M. Chattopadhyaya. Adsorption characteristics for the removal of a toxic dye, tartrazine from aqueous solutions by a low cost agricultural by-product. *Arabian Journal of Chemistry* **10** (2013) 1629-1638.
34. N. A. Ghalwa, H. M. Abu-Shawish, H. M. Tamous and H. Al Harazeen. Determination of electrochemical degradation of E102 dye at lead dioxide-doped

- carbon electrodes using some potentiometric and spectrophotometric methods. *Chemistry Journal* **3** (2013) 1-6.
35. Y. Anjaneyulu, N. S. Chary and D. S. S. Raj. Decolourization of industrial effluents—available methods and emerging technologies—a review. *Reviews in Environmental Science and Biotechnology* **4** (2005) 245-273.
36. P. L. López-de-Alba, L. I. Michelini-Rodriguez, K. Wróbel and J. Amador-Hernández. Extraction of sunset yellow and tartrazine by ion-pair formation with adogen-464 and their simultaneous determination by bivariate calibration and derivative spectrophotometry. *Analyst* **122** (1997) 1575-1579.
37. V. K. Gupta, R. Jain, A. Nayak, S. Agarwal and M. Shrivastava. Removal of the hazardous dye-tartrazine by photodegradation on titanium dioxide surface. *Materials Science and Engineering: C* **31** (2011) 1062-1067.
38. S. K. Al-Dawery. Photo-catalyst degradation of tartrazine compound in wastewater using TiO<sub>2</sub> and UV light. *Journal of Engenering Science and Technology* **8** (2013) 683-691.
39. N. Modirshahla, M. Behnajady and S. Kooshaiian. Investigation of the effect of different electrode connections on the removal efficiency of tartrazine from aqueous solutions by electrocoagulation. *Dyes and Pigments* **74** (2007) 249-257.
40. L. Mahlalela and L. Dlamini. Enhanced photocatalytic activity of titania in the presence of KNO<sub>3</sub> on the photodegradation of dyes. *Surfaces and Interfaces* **1** (2016) 21-28.
41. J. Šíma and P. Hasal. Photocatalytic degradation of textile dyes in a TiO<sub>2</sub>/UV system. *Chemical Engineering* **32** (2013) 79-84.

42. X. Li, J. Yu, J. Low, Y. Fang, J. Xiao and X. Chen. Engineering heterogeneous semiconductors for solar water splitting. *Journal of Materials Chemistry A* **3** (2015) 2485-2534.
43. M. Castellote and N. Bengtsson. Principles of TiO<sub>2</sub> photocatalysis. in applications of titanium dioxide photocatalysis to construction materials. *Springer*, Dordrecht, (2011), 5-10.
44. A. Cavicchioli and I. G. Gutz. Effect of scavengers on the photocatalytic digestion of organic matter in water samples assisted by TiO<sub>2</sub> in suspension for the voltammetric determination of heavy metals. *Journal of the Brazilian Chemical Society* **13** (2002) 441-448.
45. K. Mondal and A. Sharma. Photocatalytic oxidation of pollutant dyes in wastewater by TiO<sub>2</sub> and ZnO nano-materials - a mini-review. *Nanoscience & Technology for Mankind, The Academy of Sciences India (NASI)*, Allahabad, India (2014) 36-72.
46. Y. F. Fang, Y. P. Huang, D. F. Liu, Y. Huang, G. Wei and J. David. Photocatalytic degradation of the dye sulforhodamine-B: a comparative study of different light sources. *Journal of Environmental Sciences* **19** (2007) 97-102.
47. O. Tomita, T. Otsubo, M. Higashi, B. Ohtani and R. Abe. Partial oxidation of alcohols on visible-light-responsive WO<sub>3</sub> photocatalysts loaded with palladium oxide cocatalyst. *ACS Catalysis* **6** (2016) 1134-1144.
48. C. I. Oprea, P. Panait, J. Lungu, D. Stamate, A. Dumbravă, F. Cimpoesu and M. A. Gîrțu. DFT study of binding and electron transfer from a metal-free dye with carboxyl, hydroxyl, and sulfonic anchors to a titanium dioxide nanocluster. *International Journal of Photoenergy* **2013** (2013) 1-15.



49. T. Peme, L. O. Olasunkanmi, I. Bahadur, A. S. Adekunle, M. M. Kabanda and E. E. Ebenso. Adsorption and corrosion inhibition studies of some selected dyes as corrosion inhibitors for mild steel in acidic medium: gravimetric, electrochemical, quantum chemical studies and synergistic effect with iodide ions. *Molecules* **20** (2015) 16004-16029.
50. G. Zhang and C. B. Musgrave. Comparison of DFT methods for molecular orbital eigenvalue calculations. *The Journal of Physical Chemistry A* **111** (2007) 1554-1561.
51. S. D. Kim and E. J. Park. Relation between chemical structure of yellow disperse dyes and their lightfastness. *Fibers and Polymers* **2** (2001) 159-163.
52. A. Fadda and N. Abbas. Synthesis of azo disperse dyes containing pyridine ring for dyeing polyester and polyacrylic fibres. *Pigment & Resin Technology* **45** (2016) 10-17.
53. S. B. Novir and S. M. Hashemianzadeh. Computational study of new azo dyes with different anchoring groups for dye-sensitised solar cells. *Molecular Physics* **114** (2016) 650-662.
54. N. Tokay, Z. Seferoğlu, C. Öğretir and N. Ertanb. Quantum chemical studies on the structures of some heterocyclic azo disperse dyes. *Arkivoc* **15** (2008) 9-20.
55. Y. S. Choi, K. S. Lee, H. J. Kim, J. Y. Choi, S. B. Kang, E. J. Lee and G. Keum. Synthesis, spectral property and dyeing assessment of azo disperse dyes containing carbonyl and dicyanovinyl groups. *Bulletin of the Korean Chemical Society* **34** (2013) 863-867.

56. Ö. Arslan, E. Yalçın, N. Seferoglu, M. Yaman and Z. Seferoglu. Molecular structure analysis and spectroscopic properties of monoazo disperse dye from N, N-dimethylaniline. *Gazi University Journal of Science* **30** (2017) 175-189.
57. O. I. Osman. DFT study of the structure, reactivity, natural bond orbital and hyperpolarizability of thiazole azo dyes. *International Journal Of Molecular Sciences* **18** (2017) 239.
58. Y. S. Kim, S. H. Kim, T. K. Kim and Y. A. Son. Characteristics of HOMO and LUMO potentials by altering substituents: computational and electrochemical determination. *Textile Coloration and Finishing* **20** (2008) 41-46.
59. Y. z. Zhan, X. Zhao, B. j. Wang and W. Wang. Computational modelling of the influence of substituent effects on phthalimidylazo disperse dye hydrolysis and interaction energy. *Coloration Technology* **134** (2018) 24-32.
60. H. R. Maradiya and V. S. Patel. Synthesis and dyeing performance of some novel heterocyclic azo disperse dyes. *Journal of the Brazilian Chemical Society* **12** (2001) 710-714.
61. M. Elapasery, S. Shakra, D. Abbas, H. Gaffer and E. Allam. Synthesis of some azo disperse dyes based on pyridone moiety and their application on polyester fabrics. *Egyptian Journal of Chemistry* **60** (2017) 97-102.
62. C. Bird. The dyeing of acetate rayon with disperse dyes I-aqueous solubility and the influence of dispersing agents II-the relation between aqueous solubility and dyeing properties. *Coloration Technology* **70** (1954) 68-77.

63. S. A. A. Green and J. W. McBain. Solubilization of water-insoluble dye by pure soaps and detergents of different types. *The Journal of Physical Chemistry* **51** (1947) 286-298.
64. J. Chakraborty. An overview of dye fastness testing. in handbook of textile and industrial dyeing: principles, processes and types of dyes. *Woodhead Publishing Limited*, United Kingdom, (2011).
65. P. Gregory and P. Gordon. Organic chemistry in colour. *Springer Science & Business Media*, Germany, (1983).
66. C. Shah and D. Jain. Solvent (perchloroethylene) dyeing of disperse dyes on polyester. *Textile Research Journal* **55** (1985) 23-27.
67. H.-D. Weigmann, M. Scott, A. Ribnick and R. Matkowsky. Interactions of nonaqueous solvents with textile fibers: part viii: mechanism of dye diffusion in solvent-treated polyester yarns. *Textile Research Journal* **47** (1977) 745-754.
68. R. B. Love and A. Robson. The use of non-aqueous solvents in dyeing: dyeing of polyester and cotton and polyester fibre blends by the dacsol 2 process. *Journal of the Society of Dyers and Colourists* **94** (1978) 514-520.
69. S. J. Nejad, M. A. Khansary and F. Amiri. Solubility prediction of some disperse azo dyes in supercritical carbon dioxide using equation of states (EOSs). *International Journal of Thermodynamics* **15** (2012) 103-110.
70. A. S. Özcan, A. A. Clifford, K. D. Bartle and D. M. Lewis. Solubility of disperse dyes in supercritical carbon dioxide. *Journal of Chemical & Engineering Data* **42** (1997) 590-592.

71. W. Saus, D. Knittel and E. Schollmeyer. Dyeing with supercritical carbon dioxide- An alternative to high-temperature dyeing of polyester. *Textile Praxis International* **47** (1992) 1052-1054.
72. W. Saus, D. Knittel and E. Schollmeyer. Dyeing of textiles in supercritical carbon dioxide. *Textile Research Journal* **63** (1993) 135-142.
73. M. Banchemo. Supercritical fluid dyeing of synthetic and natural textiles—a review. *Coloration Technology* **129** (2013) 2-17.
74. R. Bianchini, G. Catelani, G. Seu and G. Bartalucci. Coloring agents containing a mono-or disaccharide. *EP1462484A1*, Jouve, Paris, (2004).
75. R. Bianchini, F. Bonaccorsi, G. Catelani, F. Dandrea, J. Isaad, M. Rolla and T. Nocentini. Disperse dyes soluble in water. *EP2085434A1*, Jouve, Paris, (2008).
76. S. Nejad, R. Mohammadikhah, H. Abolghasemi, M. Moosavian and M. Maragheh. A novel equation of state (EOS) for prediction of solute solubility in supercritical carbon dioxide: experimental determination and correlation. *The Canadian Journal of Chemical Engineering* **87** (2009) 930-938.
77. B. Modi, S. Bhalakia, R. Patel and V. Patel. Synthesis of azo disperse dyes with imidazolone moiety and their application on nylon arid polyester fibres. *Indian Journal of Fibre and Textile Research* **23** (1998) 123-127.
78. Y. Y. Lams, P. Nkeonye, K. Bello, M. Yakubu and A. Lawal. Synthesis of disperse dyes from pyridone and resorcinol coupled to diazotized 2-amino-4-chloro-5-formylthiazole and application to polyester. *Advances in Chemistry* **2014** (2014) 1-7.

79. J. Otutu. Synthesis of halogenated disazo disperse dyes derived from 2, 4-dichloroaniline and 3-aminophenol. *Current Research in Chemistry* **4** (2012) 119-127.
80. T. Hihara, Y. Okada and Z. Morita. Reactivity of phenylazonaphthol sulfonates, their estimation by semiempirical molecular orbital PM5 method, and the relation between their reactivity and azo-hydrazone tautomerism. *Dyes and Pigments* **59** (2003) 201-222.
81. T. Hihara, Y. Okada and Z. Morita. A semiempirical molecular orbital study of the photo-reactivity of monoazo reactive dyes derived from  $\gamma$ - and  $\beta$ -acids. *Dyes and Pigments* **73** (2007) 141-161.
82. J. J. Lee, W. J. Lee, J. H. Choi and J. P. Kim. Synthesis and application of temporarily solubilised azo disperse dyes containing  $\beta$ -sulphatoethylsulphonyl group. *Dyes and Pigments* **65** (2005) 75-81.
83. C. Meena, S. Maiti, N. Sekar, S. More and R. Adivarekar. Dispersant-free disperse dyes for polyester an eco-friendly approach. *The Journal of The Textile Institute* **108** (2017) 1144-1149.
84. J. J. Lee, W. J. Lee and J. P. Kim. Dispersant-free dyeing of polyester with temporarily solubilized azo disperse dyes from indole derivatives. *Fibers and Polymers* **4** (2003) 66-70.
85. J. Lee, N. Han, W. Lee, J. Choi and J. Kim. Dispersant-free dyeing of polyester with temporarily solubilised azo disperse dyes from 1-substituted-2-hydroxypyrid-6-one derivatives. *Coloration Technology* **118** (2002) 154-158.

86. H. Anouar, E. Anouar, A. El Hourch and K. El Kacemi. Density functional theory study of Reactive Violet 5R azo dye. *International Journal of Innovation and Applied Studies* **9** (2014) 1362-1367.
87. J. H. Franco, B. F. da Silva, E. F. G. Dias, A. A. de Castro, T. C. Ramalho and M. V. B. Zanoni. Influence of auxochrome group in disperse dyes bearing azo groups as chromophore center in the biotransformation and molecular docking prediction by reductase enzyme: Implications and assessment for environmental toxicity of xenobiotics. *Ecotoxicology and Environmental Safety* **160** (2018) 114-126.
88. A. Klamt, V. Jonas, T. Bürger and J. C. Lohrenz. Refinement and parametrization of COSMO-RS. *The Journal of Physical Chemistry A* **102** (1998) 5074-5085.
89. DMol<sup>3</sup> Guide, Material Studio 8.0. *Accelrys Software, Inc.*, San Diego, United States (2017) 1-161.
90. A. Klamt. The COSMO and COSMO-RS solvation models. *Wiley Interdisciplinary Reviews: Computational Molecular Science* **1** (2011) 699-709.
91. J. D. Thompson, C. J. Cramer and D. G. Truhlar. Predicting aqueous solubilities from aqueous free energies of solvation and experimental or calculated vapor pressures of pure substances. *The Journal of Chemical Physics* **119** (2003) 1661-1670.
92. A. Klamt, F. Eckert, M. Hornig, M. E. Beck and T. Bürger. Prediction of aqueous solubility of drugs and pesticides with COSMO-RS. *Journal of Computational Chemistry* **23** (2002) 275-281.

93. M. Fujisawaa, H. Tsutsumia and T. Kimura. Prediction of solubility of practically insoluble drugs in water/ethanol solvents using non-empirical methods. *Journal of Chemical and Pharmaceutical Research* **3** (2011) 750-758.
94. Z. Guo, B.-M. Lue, K. Thomasen, A. S. Meyer and X. Xu. Predictions of flavonoid solubility in ionic liquids by COSMO-RS: experimental verification, structural elucidation, and solvation characterization. *Green Chemistry* **9** (2007) 1362-1373.
95. M. Lotfi, M. Moniruzzaman and M. S. Rajabi. Predicting the solubility of pharmaceutical compound in ionic liquids using COSMO-RS model. *ARPN Journal of Engineering and Applied Sciences* **11** (2016) 1618-1622.
96. A. G. Sicaire, M. A. Vian, F. Fine, P. Carré, S. Tostain and F. Chemat. Experimental approach versus COSMO-RS assisted solvent screening for predicting the solubility of rapeseed oil. *Oilseeds and Fats, Crops and Lipids* **22** (2015) 1-7.
97. S. Mustapha, P. Okonkwo and S. Waziri. Improvement of carbon dioxide absorption technology using conductor-like screening model for real solvents (COSMO-RS) method. *Journal of Environmental Chemistry and Ecotoxicology* **5** (2013) 96-105.
98. S. H. Yalkowsky and S. C. Valvani. Solubility and partitioning I: solubility of nonelectrolytes in water. *Journal of Pharmaceutical Sciences* **69** (1980) 912-922.
99. K. Chandrakumar and S. Pal. The concept of density functional theory based descriptors and its relation with the reactivity of molecular systems: a semi-quantitative study. *International Journal of Molecular Sciences* **3** (2002) 324-337.

- 
100. P. K. Chattaraj. Chemical reactivity theory: a density functional view. *CRC Press*, Taylor and Francis Group, Boca Raton, (2009).
101. J. T. Spadaro, L. Isabelle and V. Renganathan. Hydroxyl radical mediated degradation of azo dyes: evidence for benzene generation. *Environmental Science & Technology* **28** (1994) 1389-1393.
102. A. S. Özen, V. Aviyente, G. Tezcanli-Güyer and N. H. Ince. Experimental and modeling approach to decolorization of azo dyes by ultrasound: degradation of the hydrazone tautomer. *The Journal of Physical Chemistry A* **109** (2005) 3506-3516.
103. J. M. Joseph, H. Destailats, H.-M. Hung and M. R. Hoffmann. The sonochemical degradation of azobenzene and related azo dyes: rate enhancements via Fenton's reactions. *The Journal of Physical Chemistry A* **104** (2000) 301-307.
104. A. S. Özen, V. Aviyente, F. De Proft and P. Geerlings. Modeling the substituent effect on the oxidative degradation of azo dyes. *The Journal of Physical Chemistry A* **108** (2004) 5990-6000.
105. A. S. Özen, V. Aviyente and R. A. Klein. Modeling the oxidative degradation of azo dyes: A density functional theory study. *The Journal of Physical Chemistry A* **107** (2003) 4898-4907.
106. X. Jiao, H. Yu, Q. Kong, Y. Luo, Q. Chen and J. Qu. Theoretical mechanistic studies on the degradation of alizarin yellow R initiated by hydroxyl radical. *Journal of Physical Organic Chemistry* **27** (2014) 519-526.



---

## CHAPTER 3

### THEORETICAL CHEMISTRY

---

#### 3.1 INTRODUCTION

Theoretical chemistry is the conventional term used to describe a broad area of chemistry which employs fundamental theories of physics and mathematical principles for description of the nature and behavior of chemical systems and processes [1, 2]. The term computational chemistry is preferentially used when a mathematical method has been efficiently developed, automated and implemented on a computer for solving various kinds of chemical problems [1]. This chapter discusses the various theoretical methods known with more emphasis on the density functional theory (DFT) for in-silico studies. It also gives a concise account of various basis sets, solvation models, solubility equations, quantum chemical reactivity parameters and potential energy surfaces which are within the bounds of this work.

#### 3.2 DENSITY FUNCTIONAL THEORY (DFT)

Mathematically, a functional is defined as a function of a function [3]. In relation to density functional theory (DFT), the total energy  $E$ , of a chemical system is a function of the total electron density  $\rho$  in the system, which is in turn a function of the particle position  $r$ . This definition is mathematically expressed as  $E[\rho(r)]$ .

Contrary to wave function-based quantum mechanical methods such as the *ab-initio* [3] and semi-empirical methods [1], DFT protocol determines the quantum mechanical properties of chemical systems from their electron densities which is evaluated as the

square of their wave functions [1-4]. *Ab-initio* methods (e.g. Møller-Plesset and configuration interaction) generally produce greater accuracy compared to the semi-empirical counterparts, but their use is limited by severe computational cost [1, 4]. Hence, they are not suitable for fast calculations because they depend on finding solution of the Schrödinger wave equation, which become increasingly more tedious as system complexity increases due to the difficulty in evaluating the electron-electron repulsion component of the wave equation. Semi-empirical methods (e.g. AM1, PM3, PM6, ZINDO etc.) on the other hand are developed for performing speedy calculations with low accuracy due to the severity of the approximations and empirical constants incorporated in them [1, 4]. Hence, they are not suitable for calculations where high accuracy is needed.

To alleviate the challenges associated with *ab-initio* and semi-empirical methods, Hohenberg and Kohn (1964) [5], followed by Kohn and Sham (1965) [6], introduced the density functional theory which predicts properties of chemical systems from their electron densities instead of wave function. DFT is a robust non-empirical quantum mechanical method. Its accuracy is comparable to *ab-initio* methods, but with significant improvement in speed. This is because DFT narrows down the  $3N$  degree of freedom of an  $N$ -particle body to just three spatial coordinates [3]. Semi-empirical calculations are faster than DFT calculations but with severe reduction in accuracy.

### 3.3 WAVE FUNCTION-BASED ELECTRONIC STRUCTURE CALCULATION

In a simple term, *ab-initio* electronic structure calculations are first principle calculations involving a complete description of an electronic system by a wave function and subsequent treatment of the wave function with the Schrödinger wave equation [1-4]:

$$\hat{H}\Psi(r_i, R_\alpha) = E\Psi(r_i, R_\alpha)$$

Equation 3. 1

where  $\hat{H}$  is the Hamiltonian operator for a particle system represented by the wave function,  $\Psi$ . Operation of the wavefunction by the Hamiltonian operator produces the eigen value i.e. the system energy,  $E$  and the wavefunction,  $\Psi$  itself. A mathematical function of this type is called an eigen function [3].  $r_i$  and  $R_\alpha$  represent the coordinates of the electrons and the nuclei, respectively. The Hamiltonian operator,  $\hat{H}$  contains both kinetic and particle interaction potential energy terms as follows:

$$\hat{H} = -\frac{1}{2} \sum_{i=1}^N \nabla_i^2 - \frac{1}{2} \sum_{\alpha=1}^M \frac{1}{M_\alpha} \nabla_\alpha^2 - \sum_{i=1}^N \sum_{\alpha=1}^M \frac{Z_\alpha}{r_{i\alpha}} + \sum_{i=1}^N \sum_{j>1}^N \frac{1}{r_{ij}} + \sum_{\alpha=1}^M \sum_{\beta>\alpha}^M \frac{Z_\alpha Z_\beta}{R_{\alpha\beta}}$$

Equation 3. 2

The first two terms in equation 3.2 represent the kinetic energy terms of the electrons and nuclei, respectively. The third term describes the electron-nuclear interaction potential energy term while the last two terms represent the electron-electron and the nuclear-nuclear repulsion terms, respectively. The number of electron runs from  $i = 1$  to  $N^{\text{th}}$  electron while the number of nucleus runs from  $\alpha = 1$  and  $\beta > \alpha$  to  $M^{\text{th}}$  nucleus.

Solving equation 3.1 is extremely tedious and virtually impossible for many particle systems. In fact, solution to the equation for a single particle system involves complex mathematical rigor. However, certain approximations are often employed to reduce the complexity of the equation. One such approximation is the Born-Oppenheimer approximation which postulates that the nucleus being much larger in size than the electron, moves relatively more slowly than the latter [1, 3, 4]. This approximation eliminates the kinetic energy term of the nucleus from equation 3.2 and makes the nuclear-nuclear repulsion term a constant. The resulting equation is referred to as

electronic Schrödinger wave equation (eqn. 3.3) because this equation contains only the electronic energy terms (eqn. 3.4). The overall energy of the system is the sum of the energy due to electrons only (i.e.  $E_{elec}$ ) and the constant nuclear-nuclear repulsion energy as given in equation 3.5.

$$\hat{H}_{elec}\Psi_{elec} = E_{elec}\Psi_{elec}$$

Equation 3. 3

$$\hat{H}_{elec} = -\frac{1}{2}\sum_{i=1}^N \nabla_i^2 - \sum_{i=1}^N \sum_{\alpha=1}^M \frac{Z_{\alpha}}{r_{i\alpha}} + \sum_{i=1}^N \sum_{j>1}^N \frac{1}{r_{ij}}$$

Equation 3. 4

$$E_{Tot} = E_{elec} + \sum_{\alpha=1}^M \sum_{\beta>\alpha}^M \frac{Z_{\alpha}Z_{\beta}}{R_{\alpha\beta}}$$

Equation 3. 5

The three energy terms in equation 3.4 represent the sum of electronic kinetic energies, the electron-nuclear attraction and the electron-electron columbic repulsion energies respectively.

Despite the simplification by the Born-Oppenheimer approximation, the solution to the electronic Schrödinger equation is still cumbersome especially for many particle systems due to the increase in exchange and correlation effects as the electron number increases. Electrons are fundamentally identical fermions. This implies that the physical properties of all electronic systems must remain unaltered even when two electrons exchange their positions. For this to be true, the wavefunction must change sign in accordance with the antisymmetry principle [1, 3, 4].

Correlation effects on the other hand accounts for how the motion of each electron, in a collection of N number of electrons, is affected by the remaining N-1 electrons. It

describes how the electrons get in each other's way, interact and repel one another. While it is easier to determine the repulsion energy for systems with very few electrons, its estimation becomes increasingly tedious as the number of electrons increases. Hence, wavefunction-based quantum mechanical methods such as Møller-Plesset, Configuration Interaction and Coupled Cluster, in which the correlation effect is taken into account, are characterized by very high computational cost. Calculation with these methods consumes a lot of time and can only be successful with systems containing atoms in the range of 1 to 100 [1, 4].

Hartree-Fock (HF) approximation, also known as self-consistent field theory was jointly introduced by D.R. Hartree and V.A. Fock for further simplification of the electronic Schrödinger equation [3, 7, 8]. It begins with the Hartree approximation [7] where every electron in a system of N number of electrons is considered as a quasi-independent particle moving in an electric field created by the remaining N-1 electrons. The many electrons wavefunction is decomposed into several one electron wavefunctions (eqn. 3.6) which upon application to equation 3.3, gives rise to the Hartree equation for a single particle (eqn. 3.7).

$$\Psi^H(r_i) = \varphi_1(r_1) \varphi_2(r_2) \cdots \varphi_N(r_N)$$

Equation 3. 6

$$\left[ -\frac{\hbar^2}{2m_e} \nabla^2 - \sum_{i\alpha} \frac{Z_\alpha e^2}{|r_i - R_\alpha|} + \sum_{i,j,(j \neq i)} \int dr_j \frac{|\varphi_j(r_j)|^2}{|r_i - r_j|} \right] \varphi_i(r_i) = E_i \varphi_i(r_i).$$

Equation 3. 7

where  $\hbar$  is Plank's constant,  $h$  divided by  $2\pi$ ;  $m_e$  represents the mass of the electron;  $Z_\alpha$  and  $R_\alpha$  represent the charge and position of a nucleus,  $\alpha$  respectively;  $r_i$  and  $r_j$  are the positions of electrons  $i$  and  $j$  with respective wave functions  $\varphi_i$  and  $\varphi_j$ .

The one-particle equation (i.e eqn. 3.6) can be constructed into a Slater determinant (eqn. 3.8) which satisfies the antisymmetry principle [1-4].

$$\Psi^{HF}(r_i) = \frac{1}{\sqrt{N!}} \begin{vmatrix} \varphi_1(r_1) & \varphi_1(r_2) & \dots & \varphi_1(r_N) \\ \varphi_2(r_1) & \varphi_2(r_2) & \dots & \varphi_2(r_N) \\ \vdots & \vdots & \ddots & \vdots \\ \varphi_N(r_1) & \varphi_N(r_2) & \dots & \varphi_N(r_N) \end{vmatrix}$$

Equation 3. 8

Treatment of the Slater determinant with equation 3.3 (i.e the electronic Schrödinger equation) gives the single electron Hartree-Fock equation 3.9:

$$E_i \varphi_i \left[ -\frac{\hbar^2}{2m_e} \nabla^2 - \sum_{i\alpha} \frac{Z_\alpha e^2}{|r_i - R_\alpha|} + \sum_{i,j,(j \neq i)} \int dr_j \frac{|\varphi_j(r_j)|^2}{|r_i - r_j|} \right] \varphi_i(r_i) - \sum_{i,j,(j \neq i)} \int dr_j \frac{|\varphi_j^*(r_j)\varphi_i(r_j)|}{|r_i - r_j|} \varphi_j(r_i) =$$

Equation 3. 9

The first two terms in the above equation represent the electronic kinetic energy and the electron-nuclear interaction potential energy ( $V_{ext}$ ) operators. This is collectively denoted by a one-electron Hamiltonian operator,  $\hat{H}_0$  in equation 3.10. The third term in equation 3.9 is the electron-electron repulsion energy operator, represented by  $\hat{J}$  in equation 3.10 while the fourth term is the exchange energy operator which accounts for inter-electronic exchange effect. This is denoted by  $\hat{K}$  in equation 3.10.

$$(\hat{H}_0 + \hat{J} - \hat{K}) \varphi_i(r) = E_i \varphi_i(r)$$

Equation 3. 10

$(\hat{H}_0 + \hat{J} - \hat{K})$  is known as the Hartree-Fock (HF) operator,  $\hat{F}$  [3, 7, 8]. That is:

$$\hat{F}\varphi_i(r) = E_i\varphi_i(r)$$

Equation 3. 11

$$\text{where } \hat{F} = (\hat{H}_0 + \hat{J} - \hat{K})$$

Equation 3. 12

Energy,  $E_i$  is the Hartree-Fock energy, denoted as  $E_{HF}$  in equation 3.13. It is equal to the sum of the electronic kinetic energy,  $T_E$ , electron-nuclear interaction energy,  $E_{NE}$ , electron-electron repulsion energy,  $E_{EE}$  and the exchange energy,  $E_K$ . That is:

$$E_{HF} = T_E + E_{NE} + E_{EE} + E_K$$

Equation 3. 13

HF-approximation has some peculiar deficiencies. First, the approximation performs satisfactorily for light atoms. The phenomenon of spin-orbital interaction (i.e. spin-orbit coupling) mars its performance in the case of heavy atoms. Second, the one electron approximation, in which the total wave function is broken down into a product of several one-electron wave functions (eqn. 3.6), is only valid providing that electrons are non-interacting particles. However, electrons do interact and their interactions become increasingly appreciable as the number of electron rises. HF-approximation only accounts for the inter-electronic exchange effect as can be deduced from equation 3.13, but fails to include the effect of electron correlation.

### 3.4 ELECTRON DENSITY-BASED ELECTRONIC STRUCTURE CALCULATION

Density functional theory (DFT) is an electronic structure calculation method that replaces wave function with electron density thereby simplifying the many-electron Schrödinger equation (eqn. 3.3). DFT is a product of the Hohenberg-Kohn (1964) and Kohn-Sham (1965) postulates [5, 6]. DFT is superior to the HF-approximation because it can adequately account for electron correlation effects which is lacking in HF-approximation. The first and second postulates of Hohenberg and Kohn (1964) [5]:

- I. For a system of interacting electrons in an external potential,  $V_{ext}$ , the potential and hence the total energy is a functional of the ground state electron density,  $\rho_0(r)$ .
  
- II. The ground state energy,  $E_0$  of a system of interacting particles is the global minimum of the functional, and this energy can be determined by variational principle. The density  $\rho(r)$  that yields the global minimum energy is the ground state density,  $\rho_0(r)$ .

Based on the above theorems, the ground state energy,  $E_0$  can be expressed mathematically as:

$$E_0 \leq E[\rho(r)] = E_{ne}[\rho(r)] + T_e[\rho(r)] + E_{ee}[\rho(r)]$$

Equation 3. 14

where the first, second and third terms in equation 3.14 represent the nuclear-electron interaction energy functional, electronic kinetic energy functional and electron-electron repulsion energy functional, respectively.

Kohn and Sham [6] simplified the many-particle problem by replacement with non-interacting one-particle equations but with interacting density. The electronic kinetic energy  $T_e$ , is split into a kinetic energy term  $T_s$ , for a non-interacting one-body system, and a kinetic energy correction term  $T_c$ , which accounts for inter-particle interaction effect on the energy (eqn. 3.15). The electron-electron repulsion energy,  $E_{ee}$  is also decomposed into a classical component and non-classical correction term, denoted as  $E_j$  and  $E_x$  respectively (eqn. 3.16).



$$T_e [\rho(r)] = T_s [\rho(r)] + T_c [\rho(r)] \quad \text{Equation 3. 15}$$

and;  $E_{ee} [\rho(r)] = E_J [\rho(r)] + E_x [\rho(r)]$  Equation 3. 16

Combining the two correction terms  $T_c$  and  $E_x$  gives:

$$E_{xc} [\rho(r)] = T_c [\rho(r)] + E_x [\rho(r)] \quad \text{Equation 3. 17}$$

and  $E_x [\rho(r)] = E_{xc} [\rho(r)] - T_c [\rho(r)]$  Equation 3. 18

Substituting equation 3.18 into equation 3.16, and the resulting equation into 3.14 gives:

$$E [\rho(r)] = E_{ne} [\rho(r)] + T_e [\rho(r)] + E_J [\rho(r)] + E_{xc} [\rho(r)] - T_c [\rho(r)] \quad \text{Equation 3. 19}$$

Since from equation 3.15,

$$T_e [\rho(r)] - T_c [\rho(r)] = T_s [\rho(r)] \quad \text{Equation 3. 20}$$

Therefore, equation 3.19 becomes:

$$E [\rho(r)] = E_{ne} [\rho(r)] + T_s [\rho(r)] + E_J [\rho(r)] + E_{xc} [\rho(r)] \quad \text{Equation 3. 21}$$

which on factorization gives;

$$E [\rho(r)] = (T_s + E_{ne} + E_J + E_{xc})[\rho(r)]. \quad \text{Equation 3. 22}$$

The full Kohn-Sham energy functional,  $E [\rho (r)]$  can therefore be expressed as:

$$E [\rho(r)] = \left[ T[\rho(r)] + \int dr V_{ext}(r)\rho(r) + \frac{1}{2} \iint dr_i dr_j \frac{\rho(r_i)\rho(r_j)}{|r_i-r_j|} + E_{xc}[\rho(r)] \right] \quad \text{Equation 3. 23}$$

The density,  $[\rho(r)]$  is expressed as the summation of squares of the single-body orbital as follows:

$$\rho(r) = \sum_{i=1}^N |\varphi_i(r)|^2.$$

Equation 3. 24

By using equation 3.24 in equation 3.23 and applying variational principle to the Kohn-Sham energy functional,  $E[\rho(r)]$ , the resulting single-particle Kohn-Sham (KS) energy equation is:

$$\left[ -\frac{\hbar^2}{2m_e} \nabla^2 - \sum_{i\alpha} \frac{Z_\alpha e^2}{|r_i - R_\alpha|} + \int dr_j \frac{\rho(r_j)}{|r_i - r_j|} + \frac{\delta E_{xc}[\rho]}{\delta \rho} \right] \varphi_i(r_i) = \varepsilon_i \varphi_i(r_i)$$

Equation 3. 25

where the first term in equation 3.25 represents the kinetic energy of the electron, the second term is the electron-nuclear interaction potential,  $V_{ext}$ , the third term is the electron-electron repulsion term, while the fourth term is the exchange and correlation potential,  $v_{xc}$  given as:

$$v_{xc} = \frac{\delta E_{xc}[\rho(r)]}{\delta \rho(r)}$$

Equation 3. 26

In equation 3.26,  $E_{xc}$  represent the exchange-correlation energy. This energy lowers the overall coulombic repulsion in a matter by annulling the repulsive interaction between some of the electrons thereby keeping the matter together in bound state. It accounts for the likelihood of having no collision between electrons to prevent atom collapse. This is why exchange-correlation energy is sometimes described as the “nature’s glue” that naturally holds matter together [9].

While every other term in equation 3.25 can be determined exactly using the HF-approximation, the exact form of  $E_{xc}$  cannot. Hence, different approximations are often

introduced to evaluate this correction term and the performance of any DFT method depends on the severity of the approximations employed.

Equation 3.25 can be solved by an iterative self-consistent procedure starting with making a good guess of the initial density which is used to estimate all the density-dependent terms and the final energy in the equation. The Kohn-Sham orbital,  $\varphi_i$  is then calculated to find a new density using equation 3.24. This process continues until the density gradient closely approaches zero and successive iterations do not bring about substantial changes in the geometry and the total energy of the system [10]. These three conditions are collectively referred to as the convergence criteria.

### 3.5 DENSITY FUNCTIONALS

Various density functionals can be derived through modification of the exchange-correlation term,  $E_{xc}$  in equation 3.25 using different approximations. These approximations could be done to either only the exchange part,  $E_x$ , or the correlation part,  $E_c$  or both. The prominent exchange-correlation approximations include the local density (LDA), generalized-gradient (GGA), hybrid and van der Waal functionals [1, 4, 11].

#### 3.5.1 LOCAL DENSITY APPROXIMATION (LDA)

Local density approximation is the lowest and the simplest level of approximation to the exchange-correlation term,  $E_{xc}$ . This approximation assumes that the electrons in a system are homogenous (i.e uniform) as those of a homogenous electron gas model [6], and by implication, the exchange-correlation energy term of a non-homogenous electronic system is evaluated from the local form of the homogenous electron gas. This

energy term is calculated as the integral over all the system volume with the relevant density at each point similar to that in a uniform electron gas with the same density [11].

$$E_{xc}^{LDA}[\rho(r)] = \int dr \rho(r) \varepsilon_{xc}^{unif} \rho(r)$$

Equation 3. 27

$\varepsilon_{xc}^{unif}$  is the exchange-correlation energy for a homogenous electron gas, the common of which is usually determined by the Ceperley and Alder's Monte Carlo simulation [12]. The associated exchange and correlation parts are given as [11]:

$$\varepsilon_x^{LDA}(r_s) = -\frac{0.9164}{r_s}$$

Equation 3. 28

and:

$$\varepsilon_c^{LDA}(r_s) = \begin{cases} -0.0960 + 0.0622 \ln r_s - 0.0232 r_s + 0.0040 r_s \ln r_s & \text{if } r_s \leq 1 \\ -0.2846 / (1 + 1.0529 \sqrt{r_s} + 0.3334 r_s) & \text{if } r_s \geq 1 \end{cases}$$

Equation 3. 29

where  $r_s$  is a dimensionless parameter known as the Wigner-Seitz radius. It is defined as the radius of a sphere that accommodates exactly one electron, divided by the Bohr radius.  $r_s$  is mathematically related to the electron density  $\rho$  as follows:

$$r_s^3 = 3 / 4\pi\rho$$

Equation 3. 30

Popularly known LDA functionals include the Vosko, Wilks, and Nusair (VWN) [13], Perdew-Zunger (PZ81) [14], Perdew-Wang (PW92) [15] and Cole-Perdew (CP) [16].

### 3.5.2 GENERALIZED-GRADIENT APPROXIMATION (GGA)

LDA has recorded a tremendous success particularly in the study of highly homogenous (such as most bulk metals) and less homogenous (such as semiconductors, ionic salts

and alloys) electron density systems. However, its performance for systems with rapidly changing electron density such as molecules and interaction surfaces is less satisfactory due to its inability to adequately account for the non-uniformity in electron density, non-local exchange-correlation effects and its lack of cancellation for self-interaction [11]. Furthermore, LDA is not suitable for the description of electron-rich species such as anions because it provides an erroneous prediction of their stability [14, 17].

To address the above shortcomings, the density gradient,  $\nabla\rho(r)$  which accounts for non-homogeneity in electronic density is introduced into the integral in equation 3.27, so that the exchange-correlation energy is now dependent on both the local density and the gradient of the density. This is known as generalized-gradient approximation (GGA) [1, 4, 11]. The exchange-correlation energy within the GGA is given as [11]:

$$E_{xc}^{GGA}[\rho(r)] = \int dr f_{xc}(\rho(r), |\nabla\rho(r)|)$$

**Equation 3. 31**

Equation 3.31 shows that the exchange-correlation energy is dependent on both the electron density,  $\rho(r)$  at every points in the molecule and the gradient of the density,  $\nabla\rho(r)$ . Unlike the LDAs, the GGA based functionals performs very well not only for homogenous systems but also for non-homogenous systems such as molecules [11]. Some notable GGA functionals are the Becke exchange with Lee, Yang, Parr correlation functional (BLYP) [1, 18], Perdew and Wang 1991 (PW91) [19], Perdew 1986 and 1991 (P86 and P91) [20, 21], Perdew, Burke and Ernzerhof (PBE) [22] and its modified version RPBE [23].

### 3.5.3 HYBRID DENSITY FUNCTIONALS

A hybrid functional combines the Hartree-Fock (HF) exchange with the exchange and correlation of an LDA or GGA functional. Compared to pure LDA or GGA functionals, hybrid functionals are applicable to a wider range of electronic systems including molecules, ions, radicals, semiconductors, clusters and even polymers, with considerable improvement in accuracy [11]. A typical hybrid functional is the one containing half HF exchange energy and half LDA exchange and correlation energy which was proposed by Becke [24] and is popularly known as the “half and half” form of hybrid functional as shown in equation 3.32:

$$E_{xc}^{Hybrid} = \frac{1}{2}(E_x^{HF} + E_{xc}^{LDA})$$

Equation 3. 32

A number of successful hybrid functionals routinely employed for DFT calculations include B3P91, B3LYP and HSE functionals. The B3P91 is a mixture of three parameters containing HF exchange, the Becke exchange (B88) [25] and the Perdew and Wang correlation (PW91) [19] functionals. On the other hand, the B3LYP uses the Lee, Yang and Parr correlation [26] in place of the PW91. HSE functional is a newly developed hybrid functional by Heyd, Scuseria, and Ernzerhof [27]. In this functional, a much simplified HF exchange known as a screened short range (SR) HF exchange is used instead of the complete HF exchange for evaluating the exchange-correlation energy (eqn. 3.33) [11], which leads to a marked decrease in computational cost.

$$E_{xc}^{SR,HF PBE0} = \frac{1}{4}E_x^{HF,SR} + \frac{3}{4}E_x^{PBE} + E_c^{PBE}$$

Equation 3. 33

$E_{xc}^{SR,HF PBE0}$  is the exchange-correlation energy calculated using short range HF and PBE exchange-correlation functionals,  $E_x^{HF,SR}$  is the short range HF exchange,  $E_x^{PBE}$  is the PBE exchange while  $E_c^{PBE}$  is the PBE correlation functional.

### 3.5.4 VAN DER WAAL DENSITY FUNCTIONALS (vdW-DF)

The van der Waal density functional (vdW-DF) [28, 29] was recently introduced for systems such as biomolecules, soft materials, adsorption surfaces, nano-layers, nano-sheets and nano-clusters which contain large amount of strong local bonds and weak non-local intermolecular forces in the form of van der Waal forces. Adequate account of the effects of these short and long range interaction forces is necessary for accurate description of such systems. The characteristic feature of this functional is the splitting of the correlation energy term,  $E_c$  into a short range,  $E_c^0$  and a long range,  $E_c^{nl}$  portion as shown:

$$E_c[\rho] = E_c^0[\rho] + E_c^{nl}[\rho]$$

Equation 3. 34

The short-ranged part is evaluated by LDA while the long-ranged portion is expressed as:

$$E_c^{nl}[\rho] = \frac{1}{2} \int dr_i dr_j \rho(r_i) \phi(r_i, r_j) \rho(r_j)$$

Equation 3. 35

vdW-DF is a promising functional for computing theoretical binding energies in modelled adsorption processes [11].

## 3.6 BASIS SETS

A basis set is a set of mathematical basis functions used for the description or representation of atomic orbitals in molecules [1, 4]. It is the tool with which a quantum

mechanical method predicts/calculates important properties of chemical systems or processes. An essential property that governs the performance and the efficiency of a basis set is size. Larger basis sets produce more accurate results at higher computational cost because their description of orbitals covers a wider range of location of electrons in space with little or no restriction. Smaller basis sets on the other hand give less accurate orbital description at lower computational cost by imposing more severe restrictions on the location of electrons in space. Moderately sized basis sets offer sufficient accuracy at moderate computational cost, hence, they are the most appropriate basis set for a theoretical calculation.

The types of mathematical functions used for the formation of basis sets are generally grouped into two classes - the Slater-type and the Gaussian-type functions. These functions are popularly known as Slater-type orbitals (STO) and Gaussian-type orbitals (GTO) respectively [4].

### 3.6.1 SLATER-TYPE ORBITALS (STOs)

Slater-type orbitals (STOs) are similar to hydrogenic atomic orbitals and are the type of basis functions used in extended Huckel theory [4]. When the basis functions are made of STOs, the exchange term in the HF-equation (Eqn. 3.10) cannot be solved analytically but by numerical method. However, numerical solution of such exchange term with STOs suffers a significant setback. It is easier to obtain the solution for systems in the atomic and diatomic molecular scales. The solution becomes more tedious as molecular complexity increases above the diatomic scale [4]. The STO in normalized form is mathematically expressed as:



$$\varphi(r, \theta, \phi, \zeta, n, l, m) = Nr^{n-1}e^{-\zeta r}Y_l^m(\theta, \phi)$$

Equation 3. 36

where  $N$  is the normalization constant given by:

$$N = \frac{(2\zeta)^{n+\frac{1}{2}}}{[(2n)!]^{\frac{1}{2}}}$$

Equation 3. 37

$n$  symbolises the principal quantum numbers of the valence orbitals,  $r$  is the radial function,  $Y_l^m(\theta, \phi)$  is the spherical harmonic functions which depends on the azimuthal and magnetic quantum numbers  $l$  and  $m$ , respectively.  $\zeta$  is an atomic number-dependent exponent which is obtained using Slater rules [4].

### 3.6.2 GAUSSIAN TYPE ORBITALS (GTOs)

Standard basis sets use the Gaussian type orbitals (GTOs) to describe atomic orbitals. Gaussian type orbitals are basis functions formed from linear combination of Gaussian functions popularly known as primitives. The basis functions themselves are referred to as contracted functions because they are made up of several Gaussian primitives. Uncontracted functions is the term used when a basis function is formed from a single primitive [4].

Contrary to STOs, GTOs are better candidates for describing larger molecular systems. The replacement of the radial exponential decay term  $e^{-r}$  in STOs with  $e^{-r^2}$  in GTOs gives room for analytical solution of the general exchange integral formed from Gaussian functions. The fact that the pre-exponential term in the GTOs expression (Eqn. 3.37) is a polynomial in the cartesian coordinate as opposed to the spherical polar coordinate in

STOs, further simplifies this solution. The normalized mathematical form of the GTOs in the cartesian form is expressed as [4]:

$$\phi(x, y, z; \alpha, i, j, k) = Nx^i y^j z^k e^{-\alpha r^2} \quad \text{Equation 3. 38}$$

where the normalization constant  $N$  is given by:

$$N = \left(\frac{2\alpha}{\pi}\right)^{3/4} \left[\frac{(8\alpha)^{i+j+k} i! j! k!}{(2i)! (2j)! (2k)!}\right]^{1/2} \quad \text{Equation 3. 39}$$

$r^2$  is the sum of the squares of the three cartesian coordinates,  $x, y$  and  $z$  as shown:

$$r^2 = x^2 + y^2 + z^2 \quad \text{Equation 3. 40}$$

$\alpha$  is the exponent that controls the range of coverage of the GTO while indices  $i, j, k$  are positive integers which controls the orbital nature/symmetry in a cartesian manner. An s-type GTO is the one with a spherical symmetry for which  $i, j, k$  are zero. A GTO is said to have an axial symmetry about one of the cartesian axes when only one of  $i, j, k$  is unity. This results to a p-type GTO in one of the following possibilities:  $p_x$  when  $i = 1$  and  $j = k = 0$ ,  $p_y$  when  $j = 1$  and  $i = k = 0$  or  $p_z$  when  $k = 1$  and  $i = j = 0$ .

There are six possible permutations for a d-type GTO for which the sum of the indices is equal to two. These six combinations which are collectively known as the cartesian d-functions are  $x^2, y^2, z^2, xy, xz,$  and  $yz$  [4]. These functions can be transposed into a group of five canonical d – functions namely;  $xy, xz, yz, x^2 - y^2$  and  $3z^2 - r^2$ . Either the cartesian or the canonical d – functions is suitable for developing a Gaussian basis set [4]. As the sum of the indices rises above two, the difference between the cartesian and canonical functions obtainable increases. In the case of the f-type GTO for which the sum

is three, there are ten cartesian and seven canonical functions as against 15 and 10 respectively for the g-type GTO where the sum is equal to four [4].

### 3.6.3 MINIMAL BASIS SET (MBS)

The minimal basis set otherwise known as STO-3G refers to the basis set with the lowest number of basis functions that can completely accommodate or describe the electrons in an atom without loss of its spherical symmetry. It comprises the 1s function for hydrogen and helium atoms, 1s, 2s, 2p<sub>x</sub>, 2p<sub>y</sub> and 2p<sub>z</sub> functions for the main group elements in period 2 (i.e lithium to neon), 1s, 2s, 2p<sub>x</sub>, 2p<sub>y</sub>, 2p<sub>z</sub>, 3s, 3p<sub>x</sub>, 3p<sub>y</sub> and 3p<sub>z</sub> functions for the elements in period 3 (i.e sodium to argon). Although the 2p orbitals of lithium and beryllium, and the 3p atomic orbitals of sodium and magnesium are not occupied by electrons, they must however be included in the minimal basis set when these atoms are bonded to atoms or groups containing lone-pair of electrons to permit back donation of the lone pair into these empty orbitals [30].

Two prominent limitations exist for the minimal basis set. First, it has a greater affinity for atoms with spherical or nearly spherical molecular environment because the basis functions themselves are spherical or become spherical when combined. The implication of this is that atoms from aspherical molecular environment are not properly described compared to the ones from a spherical molecular environment [30]. Second, the component functions of the basis set are atom centred hence, do not properly account for inter-nuclei electron distribution i.e electrons in a bond [30].

### 3.6.4 SPLIT-VALENCE BASIS SET (SVBS)

The first inadequacy of the minimal basis set which has to do with its discrimination between atoms from spherical and aspherical molecular environment can be overcome by separating the valence electrons into two sets such that each group is represented by a different set of basis functions. The core atomic orbitals are described with one set of basis functions while the valence orbitals are described with two sets of basis functions for the inner and outer portions of the orbitals. The hydrogen atom is described by one s – type function whereas the non-hydrogenic atoms are described by two sets of valence s and p – type functions [30].

Two representatives of the SVBS are the 3-21G and the 6-31G which describe the core atomic orbitals with three and six Gaussian functions respectively. In 3-21G, the valence atomic orbital is expanded by a set of two and one Gaussian function for the inner and the outer portions respectively whereas a set of six and one Gaussian component are used in the case of the 6-31G. The 6-311G uses six Gaussian primitives for the core atomic orbital, and a set of three, one and one Gaussian component for expanding the valence atomic orbital [30].

### 3.6.5 POLARIZATION BASIS SET (PBS)

The polarization basis set helps to overcome the second inadequacy of the minimal or even the split-valence basis set (i.e. their inability to properly account for the electron distributions between atomic nuclei), by providing a d – type function for the main group elements which have s and p – type valence orbitals, and optionally a p – type function for hydrogen atom which has an s–type valence orbital. This allows for a free displacement of electron from the nuclear positions.

Popular examples of the PBS are the 6-31G(d) and 6-31G(d,p) basis sets which are derived from the 6-31G basis set. These two basis sets are identical except that the second contains a p – type polarization function for hydrogen atom in addition to the d – type polarization function for the main group atoms. The same concept applies to the 6-311G(d) and the 6-311G(d,p) basis sets which have one additional Gaussian component for the valence atomic orbital. Inclusion of a p – type polarization function for hydrogen atom may be necessary especially for systems where hydrogen bonding exists [30].

### 3.6.6 DIFFUSE BASIS SET (DBS)

Diffuse functions help to address the inability of a basis set to properly differentiate a loosely held electron from the remaining density which often leads to inaccuracies in computed energies and other quantum chemical properties. Calculations involving anionic systems such as highly excited electronic species often pose difficulties because they are more spatially diffuse compared to ground state molecular orbital species. As a result, incorporation of s and p – type diffuse functions may be necessary for non-hydrogenic atoms and an s – type diffuse function for hydrogen atom [3, 4, 30].

In the Pople system of basis set (i.e. the 6-31G and 6-311G family), a diffuse function is indicated by a “+” sign. A single plus sign indicates the presence of s and p – type diffuse functions for non-hydrogenic atoms as in 6-31+G(d) while a double plus sign implies that an additional s – type diffuse function has been incorporated for hydrogen atom as in the case of 6-31++G(d,p) [3, 4, 30].

In the Dunning system, diffuse functions are specified by adding the prefix “aug”. A typical example is aug-cc-pVTZ which provides diffuse f, d, p and s functions for main group atoms, and diffuse d, p and s functions for hydrogen atom [4, 30]

### 3.6.7 THE DUNNING BASIS SETS (DNBS) [30]

The Dunning basis sets comprises the correlation consistent polarized valence double, triple and quadruple zeta (i.e. cc-pVDZ, cc-pVTZ and cc-pVQZ respectively). They are formulated to yield the lowest possible configuration interaction single and double (CISD) ground-state atomic energies. DBS seems to be more promising in accounting for electron correlation effects especially in free atoms compared to the Pople basis sets such as 6-31G(d). The limitation of the DBS is the fact that they do not share Gaussian exponents between functions with different angular quantum number such as s- and p-type functions unlike the basis sets previously discussed.

### 3.6.8 NUMERICAL BASIS SETS (NBS) [31-33]

Numerical basis sets are high quality basis sets which make use of numerical orbitals as basis functions to represent atomic orbitals, where the functions are generated as values on an atom-centered spherical-polar mesh, rather than as analytical functions as in the case of Gaussian orbitals [33]. Each basis function consists of two portions-the radial and the angular portions. The radial portion is obtained through a numerical solution of the atomic DFT equations [33], while the angular portion is the relevant spherical harmonic,  $Y_{lm}(\theta, \varphi)$ .

NBS are known for their ability to neutralize basis set superposition error (BSSE) better than the Gaussian basis sets. BSSE is defined as the error which arises from mismatch

of basis sets as a result of overlap of atomic basis functions. BSSE could be intermolecular or intramolecular. Intermolecular BSSE occurs when the atomic basis functions involved are from different interacting molecules while intramolecular BSSE on the other hand is the one involving the basis functions of atoms of a single molecule [34, 35]. Each component atom steals basis functions from the neighbouring components thereby increasing its basis set, which leads to underestimation of the molecular energy.

Like the Gaussian sets, NBS provides diffuse orbitals for description of electron density polarization [33]. However, they produce higher accuracy compared to the Gaussian counterparts. Also, calculations with numerical basis sets occur faster than those with their Pople and Dunning counterparts. According to Benedek *et al.* [31], the DNP basis set is much faster both in the worst and in the best scenarios than corresponding Gaussian counterparts. A similar result was reported by Inada and Orita, 2007 [33]. Numerical atomic basis sets, even at their simplest level of the double numerical basis (DN), have the capacity to satisfactorily reproduce properties such as polarizabilities and dipole moments which are essential for accurate description of solvation [36].

### 3.6.9 GENERATION OF NUMERICAL BASIS SETS

Generation of a numerical basis set involves three types of calculations which are neutral atom calculations, dipositive (+2) ion calculations and hydrogenic orbital calculations [32, 33]. A minimal basis set is generated by performing a neutral atom calculation only, whereas a double numerical (DN) basis set is formed by combining the orbitals obtained from a +2 ion calculation with a minimal basis set. Polarization functions and additional orbitals used for the formation of higher numerical basis sets such as the DNP and TNDP

are obtained through a hydrogenic orbital calculation in which the value of a nuclear charge,  $Z$  is optimized by numerical experimentation [33].

In the case of hydrogen atom for instance, the 1s and 2p orbitals obtained by setting  $Z$  to 1.3 in the hydrogenic orbital calculation are used for generating the double numerical and polarization functions respectively. The basis sets for carbon are given in Table 3.1 as an illustration of a heavier atom. The table revealed that the minimal basis set comprising of 1s, 2s, and 2p orbitals is formed by performing a neutral atom calculation. The DN basis set which consists of the first set of additional orbitals 2s' and 2p', is formed by performing a +2 carbon ion ( $C^{2+}$ ) calculation. The first polarization function 3d and the second set of additional orbitals 1s' and 2p'' are obtained by performing a hydrogenic orbital calculation for which the value of  $Z$  is 7. In a similar manner, the second polarization function 3d' and the third additional orbital 2p''' are obtained using  $Z = 5$  for the hydrogenic orbital calculation [33].

The arrows in the table indicates the order of complexity of the basis sets. The DNP is made up of the minimal basis sets, the first additional orbitals 2s' and 2p' and the first polarization function 3d, whereas the TNDP consists of the second additional orbitals, 1s' and 2p'', the second polarization function 3d' and the third additional orbital 2p''' in addition to the DNP.



**Table 3. 1:** Generation of numerical basis set for carbon [33].

Classification	Basis set		Atomic orbital	Method of generation
	DNP	TNDP		
Minimum	↑	↑	1s, 2s, 2p	Obtained with neutral atom calculations
DN	↕	↕	2s', 2p'	Obtained with +2 ion (C <sup>2+</sup> ) calculations
Polarization	↓	↓	3d	Obtained with hydrogenic orbital calculation using nuclear charge, Z = 7
Extension I			1s', 2p''	
Extension II		↓	3d', 2p'''	Hydrogenic orbital calculation using nuclear charge, Z = 5

### 3.7 SOLUBILITY PREDICTION MODELS

Four types of solubility known include intrinsic, thermodynamic, kinetic, and apparent solubility. Intrinsic solubility refers to the solubility of an unionized molecule in a saturated solution [37]. Thermodynamic solubility is the highest amount of the most stable crystalline form of a solute that can be accommodated under an equilibrium condition by a fixed volume of solvent at a fixed pressure and temperature [37]. Kinetic solubility refers to the exact concentration at which an induced precipitate just appeared in a solution. In this case, the exact amount of solute that can be solvated by a solvent has been added such that the solvent can no longer dissolve further additions [37]. Apparent or buffer solubility is the solubility measured for an electrolyte at a certain pH or pKa, and it is also a function of its intrinsic solubility [37]. Of all these types of solubility, the solubility of interest to most theoretical models is the intrinsic type of solubility. Solubility models in

computational chemistry can be grouped into the following categories namely; informatics, explicit and implicit models [38].

### 3.7.1 INFORMATICS

Informatics can be defined as the science of information processing, storage, and data mining [38]. Models belonging to this category predict the intended physical properties of a molecule by correlation with some structural features of the molecule or similar molecules. The most popular among them are the quantitative structure property relationship (QSPR) and quantitative structure activity relationship (QSAR) which predict properties by correlation of structural features with empirical data using methods such as regression analysis [37-39].

The major assumption of QSAR is that molecules with similar structures will exhibit similar chemical or biological behaviors whereas according to QSPR, such molecules will exhibit similar physical properties. It is therefore possible to construct a general model to correlate the structures and properties/activities of some representative molecules (i.e. a training set) and use this model to predict the properties/activities of other similar molecules. QSPR and QSAR models only perform well for molecules which have close structural resemblance to those used in the training set [38] hence, they are not suitable for a general application.

QSPR and QSAR models have been very successful in predicting solubility due to their remarkable prediction strength at a reasonably low computational cost [37, 38]. However, they perform poorly when employed for molecules different from those used in their training set, and also lack full physical interpretation except in few cases. A very popular

QSPR model is the general solubility equation (GSE) by Yalkowsky and co-workers, which predict solubility by making use of the partition coefficient and melting point of a solute as empirical input [40, 41].

### 3.7.2 GENERAL SOLUBILITY EQUATION (GSE)

GSE is used primarily for predicting the aqueous solubility ( $S$ ) of non-ionisable solutes. However, the model has been extended to ionisable solutes and organic nonelectrolytes for which new set GSEs have been developed [37]. Jain and Yalkowsky general solubility equation [41] is based on the melting point ( $m.p$ ) and the partition coefficient ( $\text{Log } P$ ) of a non-ionisable solute in octanol and water (eqn. 3.41). The corresponding equation for ionisable solute is obtained by replacing  $\text{Log } P$  with lipophilicity ( $\text{Log } D$ ) at the pH of the ionisation (eqn. 3.42) [38].

Wang *et al.* [37, 42] modified equation 3.41 into a new GSE by replacing  $\text{Log } P$  with the calculated  $\text{Log } P$  (i.e.  $\text{CLog } P$ ) to give equation 3.43. In another work by Ran and Yalkowsky [43], the GSE for organic nonelectrolytes was proposed, where the partition coefficient ( $\text{Log } P$ ) was replaced by lipophilicity ( $\text{Log } D$ ) as in equation 3.44. To minimize the dependence of the GSE model on experimental lipophilicity and melting point which are often not available for most compounds, Wang *et al.* [42] again proposed another GSE which replaces the melting point term in equation 3.41 with polarizability ( $Pol$ ) to obtain equation 3.45.

$$\log S = 0.5 - 0.01(m.p.^{\circ}C - 25) - \log P \quad \text{Equation 3. 41}$$

$$\log S_{pH(x)} = 0.5 - 0.01(m.p.^{\circ}C - 25) - \log D_{pH(x)} \quad \text{Equation 3. 42}$$

$$\log S = 3.513 - 0.010 \times m.p - 1.112 \times ClogP$$

**Equation 3. 43**

$$\log S = 0.3814 - 1.0223 \log D - 0.00961(m.p - 25)$$

**Equation 3. 44**

$$\log S = 1.095 - 0.008 \times Pol - 1.078 \times ClogP$$

**Equation 3. 45**

### 3.7.3 EXPLICIT SOLVATION MODELS (ESM)

Explicit solvent calculation deals with the investigation of solvent specific effects in an explicit manner i.e. in a manner in which the interaction between a solute and a solvent, and the consequent changes in the solute and solvent properties can be physically studied. ESM employs methods such as the Monte Carlo [38, 44], molecular dynamics, quantum mechanics/molecular mechanics, and the most extensively used solvent is water because its macroscopic properties are well-known as compared to other solvents. Despite offering a very realistic means of probing solvent effects, explicit solvent calculations are usually characterized by high computational cost and convergence problem. Molecular dynamic simulation for instance requires the integration of Newton's laws of motion for all atoms which is done by evaluating all atomic forces at each calculation step. Also, accounting for the non-bonded interactions particularly the long-range electrostatic interactions between atoms is computationally demanding and to address this problem, certain approximations are introduced to confine the system to a finite size and to limit the number of pairwise interactions to those within a specified radius [45]. These are described as the use of boundary conditions and spherical cut-off, respectively. Unfortunately, the use of these approximations often lead to artefacts in results and poor description of dielectric properties, Lennard-Jones interactions and systems with full charges [46].

### 3.7.4 IMPLICIT SOLVATION MODELS (ISM) [4, 38]

Implicit solvation models otherwise known as continuum solvation models are solubility models which consider solvents as continuous isotropic media of known permittivity. The basic assumption of these models is that explicit treatment of solvent effects can be replaced with implicit treatment provided that the continuous medium (i.e. the solvent continuum) replacing the explicit solvent molecules adequately describes equivalent properties. Unlike the explicit models, implicit treatment of solvent does not reveal solvent structural properties and is as a result, much less computationally demanding compared to the explicit counterpart. Prominent examples of ISM are polarizable continuum model (PCM), integral equation formalism for PCM (IEFPCM) and conductor-like screening model (COSMO).

### 3.7.5 POLARIZABLE CONTINUUM MODELS (PCM) [4, 38]

The basic idea of the PCM is that a solvent continuum can be polarized by the charged density of an encapsulated solute, giving rise to a number of solute-solvent interactions that leads to solvation. Consider for instance a positively charged solute,  $Q$  in a polarizable solvent such as water (Fig. 3.1). The solvent molecules move randomly in the absence of the solute, giving an average electric field of zero. However, when the solute is introduced, the negative dipoles of the solvent molecules are orientated around the positively charged solute, leading to a change in orientation of the molecules and a net change in generated electric/reaction field. The polarity and polarizability of the solute increases as does the external electric field strength, leading to an increase in the solute's

dipole moment. The solvent is continuously polarized and more solvent molecules undergo an increased change in orientation to counteract the solute's dipole moment [4]. Solvent polarization, orientation and counteraction of the solute's dipole moment are not spontaneous processes, hence a specific amount of energy is required.

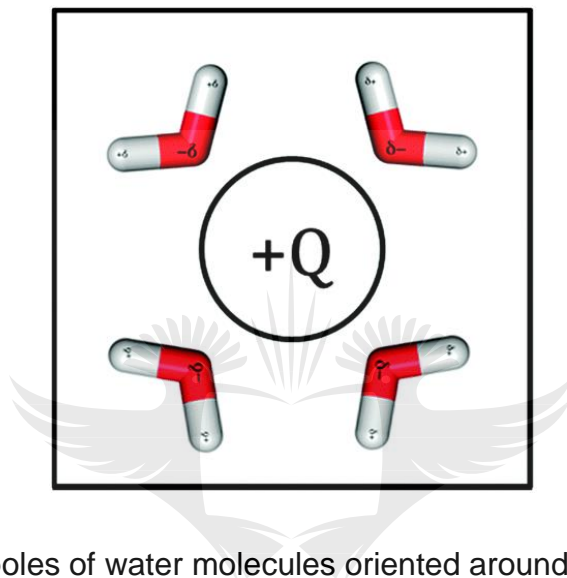


**Figure 3. 1:** Negative poles of water molecules oriented around a solvated charged solute,  $Q^+$  [38].

The solvation free energy,  $G$  of a solute,  $Q$  in a polarizable continuum is given as:

$$G = \frac{1}{2} \int \rho(r)\phi(r)dr$$

**Equation 3. 46**

where  $\rho(r)$  represents the solute charge density at position,  $r$ , in the continuum (i.e. solvent), while  $\phi(r)$  is the electrostatic potential at that position. This energy consists of five components as shown:

$$G(Q) = G_{cav} + G_{el} + G_{dis} + G_{rep} + G_{tm}$$

**Equation 3. 47**

where  $G_{cav}$ ,  $G_{el}$ ,  $G_{dis}$ ,  $G_{rep}$  and  $G_{tm}$  represent the contributions from cavitation, electrostatic interaction, dispersion, repulsion and thermal fluctuation to the solvation free energy.

Two popular models used for applying PCM methods are the Poisson–Boltzmann (PB) and the Generalized Born (GB) models. The accuracy of each model depends on the appropriateness of the cavity constructed around the solute molecule inside an ideal continuum.

### 3.7.6 POISSON-BOLTZMANN (PB) MODELS [38]

The Poisson model (eqns. 3.48-3.50) uses the electrostatic potential term,  $\phi(r)$  with the differential form of Gauss' law to express the electrostatic potential as a function of the charge density,  $\rho(r)$  and dielectric constant,  $\epsilon$ . The Poisson's equation for a linearly responding dielectric medium to an engulfed non-ionic solute is:

$$\nabla^2 \phi(r) = -\frac{4\pi\rho(r)}{\epsilon} \quad \text{Equation 3. 48}$$

For describing the charge distribution in both the solute (i.e. the inside of a cavity) and the solvent (i.e. the cavity surrounding), the equation is:

$$\nabla\epsilon(r) \cdot \nabla\phi(r) = -4\pi\rho(r) \quad \text{Equation 3. 49}$$

For a solution of an ionic solute (i.e. electrolyte) containing mobile ions, the expanded form of the equation known as the Poisson–Boltzmann (PB) equation is given as:

$$\nabla\epsilon(r) \cdot \nabla\phi(r) - \epsilon(r)\lambda(r) \frac{8\pi q^2 I k_B T}{\epsilon k_B T} \frac{1}{q} \sinh \left[ \frac{q\phi(r)}{k_B T} \right] = -4\pi\rho(r) \quad \text{Equation 3. 50}$$

where  $q$  is the ionic charge of the electrolyte,  $\lambda$  is a two-valued function for electrolyte ion accessible and inaccessible areas, where the function is 1 for accessible areas and 0 for

inaccessible areas.  $I$  is the ionic strength,  $k_B$  represents the Boltzmann's constant and  $T$  is the temperature.  $\nabla$  is the differential form of Gauss's law given as:

$$\nabla = \hat{x} \frac{\partial}{\partial x} + \hat{y} \frac{\partial}{\partial y} + \hat{z} \frac{\partial}{\partial z}$$

Equation 3. 51

PB equations perform best for the calculation of electrostatic potential of systems with ideal cavitation i.e. systems for which the solute cavity geometry is almost spherical or ellipsoidal. Estimation of the electrostatic portion of the free energy of solvation (eqn. 3.47) is computationally more expensive and inaccurate for non-ideal cavitation systems. Therefore, some continuum models often employ approximated Poisson's equation such as Onsager model which is a self-consistent reaction field (SCRF) model [47].

### 3.7.7 GENERALIZED BORN (GB) MODEL [38]

The generalized born model is a variant of the Poisson equation which can be solved analytically. This model addresses the inadequacy of the PB model with regards to systems with non-ideal cavitation using the concept of arbitrary cavitation. The term arbitrary cavitation is a process in which a cavity is constructed around a solute like shapes represented by space-filling models which are generated by overlapping atomic spheres at volumes equivalent to van der Waals (vdW) radii.

### 3.7.8 INTEGRAL EQUATION FORMALISM POLARIZABLE CONTINUUM MODELS (IEFPCM)

A major limitation of the dielectric PCM is their assumption that the charge density of a solute is entirely engulfed in the solute cavity whereas in actual sense, electron distributions do extend beyond the solute cavity. IEFPCM is an advanced version of the



dielectric PCM developed by Tomasi *et al.* [48]. This model has been found to perform better in accounting for outlying charges compared to the traditional PCM methods [48]. Another recent advancement is the solvation model based on density (SMD) which combines the IEFPCM theory with a set of optimised atomic Coulomb radii for solving the non-uniform Poisson equation. In this model, non-electrostatic contributions to the free energy of solvation are calculated based on certain parameterized functions which possesses necessary terms needed for describing surface tensions of atoms and molecules, and solvent accessible surface area [49].

### 3.7.9 CONDUCTOR-LIKE SCREENING MODEL (COSMO) [36, 50-53]

The conductor-like screening model (COSMO) and its advanced versions (COSMO for real solvent (COSMO-RS) and COSMO for segment activity coefficient (COSMO-SAC)) developed by Klamt [50, 53] are often regarded as the most successful continuum solvation model [54]. COSMO is a solvation model that describes the behavior of a solute molecule in a perfect conductor (solvent), where the solute is sufficiently polar to be able to interact with the conductor. A polar solute surface possesses unequal distribution of opposite charges due to the difference in the electronegativity of the constituent atoms. When immersed in a conductor, the solute is encapsulated in a molecular-shaped cavity formed inside the conductor (Fig. 3.2) in accordance with some rules and the atomic radii of the constituent atoms (Table 3.2) [55]. The dipole and higher moments of the engulfed solute molecule attract charges from the surrounding solvent molecules to neutralize the charges on the cavity surface. This results in a net surface potential of zero and at this point, the solute molecule is said to be screened, solvated and stabilized by the conductor.

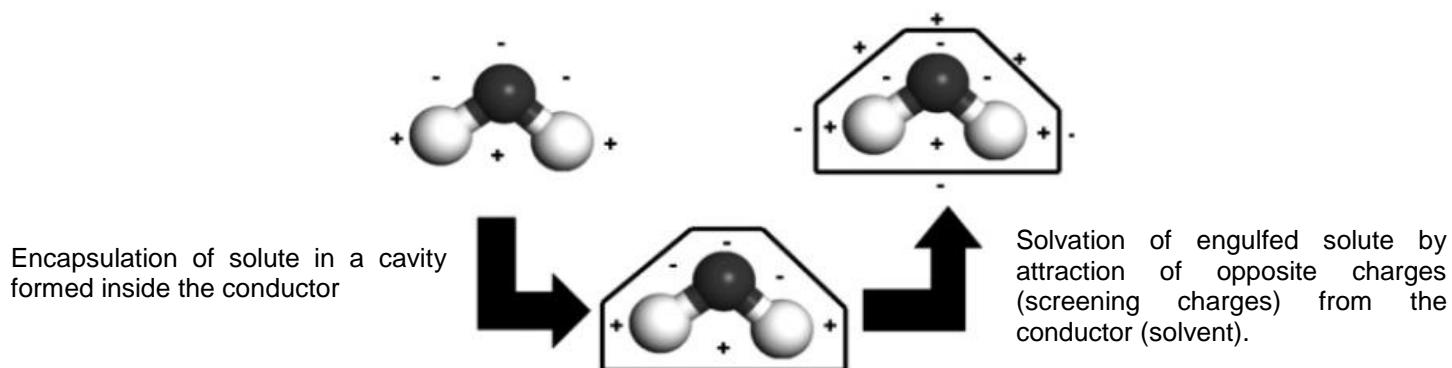


**Figure 3. 2:** A schematic diagram showing an ideally screened and solvated solute in a perfect conductor [55].

**Table 3. 2:** Some elemental atomic radii used for construction of COSMO molecular cavity [55].

Elements	Atomic radius (Å)	Elements	Atomic radius (Å)
H	1.30	S	2.16
C	2.00	P	2.12
N	1.83	Cl	2.05
O	1.72	Br	2.16
F	1.72	I	2.32

The degree of screening depends on the magnitude of the screening charges generated on the cavity surface. The higher the magnitude, the more the screening and vice versa. The screening charge,  $q^*$  is related to the total potential,  $\Phi_{tot}$  generated on the cavity surface, and the potential,  $\Phi_{sol}$  due to charge distribution in the solute only by [36, 55]:

$$\Phi_{sol} + \lambda q^* = \Phi_{tot} = 0$$

**Equation 3. 52**

$\lambda$  represents the coulomb interaction matrix which accounts for the probability of interaction between surface charges.  $\lambda$  is dependent on the geometry of the cavity.

For a dielectric system (solvent) with a finite permittivity value,  $\epsilon$ , the screening charge  $q^*$  is corrected by a scaling factor given by equation 3.53 to obtain the screening charge  $q$  in the finite dielectric.

$$F(\epsilon) = \frac{\epsilon - 1}{\epsilon + 0.5}$$

Equation 3. 53

The distinctive feature of the COSMO is its use of a unique boundary condition which requires that the sum of electrostatic potentials on cavity surfaces inside a conductor is zero (eqn. 3.52). This boundary condition is known as vanishing surface electrostatic potential, and is relatively simple and numerically more stable compared to the traditional dielectric boundary condition used for the electric field in polarizable continuum models. COSMO is reliable, elegant, versatile and computationally less expensive. It is applicable to liquid and solution phase calculations with better numerical accuracy. COSMO method is fully variational because the optimization of the solute charge density is done in a self-consistent manner, in which the screening potential is simultaneously and consistently included in the SCF cycle. COSMO calculations are performed by setting the COSMO dielectric ( $\epsilon$ ) to infinity (i.e.  $\epsilon = \infty$ ) which defines the solvent as a perfect conductor such as water [32, 38]. However, a finite value of  $\epsilon$  could also be used to define any solvent of interest [32, 36].

### 3.7.10 COSMO-RS

Conductor-like screening model for real solvent (COSMO-RS) is a variant of COSMO specifically developed for estimation of thermodynamic properties of pure liquids, liquid mixtures and solutions. It is a non-empirical model which requires only the structures of molecules as the basic input for calculation. COSMO-RS calculations consist of two main steps - a unimolecular quantum chemical COSMO calculation for each component of a system and a statistical thermodynamic treatment of the output of the COSMO calculation [50-52]. COSMO-RS predicts the chemical potential of a solution components from their

surface polarization/screening charge densities which are obtained from quantum chemical COSMO calculation along with their respective absolute energies in the conductor. COSMO-RS treats all interactions (particularly electrostatic and hydrogen bonding) between components of mixtures or solutions, as contact interactions between the component surfaces which can be related to the screening charge densities  $\sigma$  and  $\sigma'$  of the respective surfaces that are in contact [36, 51, 52].

From a statistical thermodynamic point of view, a solute encaged in a solvent (ensemble) is segmented into patches, and the surface charge density,  $\sigma$  on each patch can be obtained by COSMO calculation. The ensemble is characterized based on the distribution of the patches with respect to the surface charge density, and the resulting probability distribution plot is known as the sigma profile,  $p_s(\sigma)$  (Fig. 3.3).

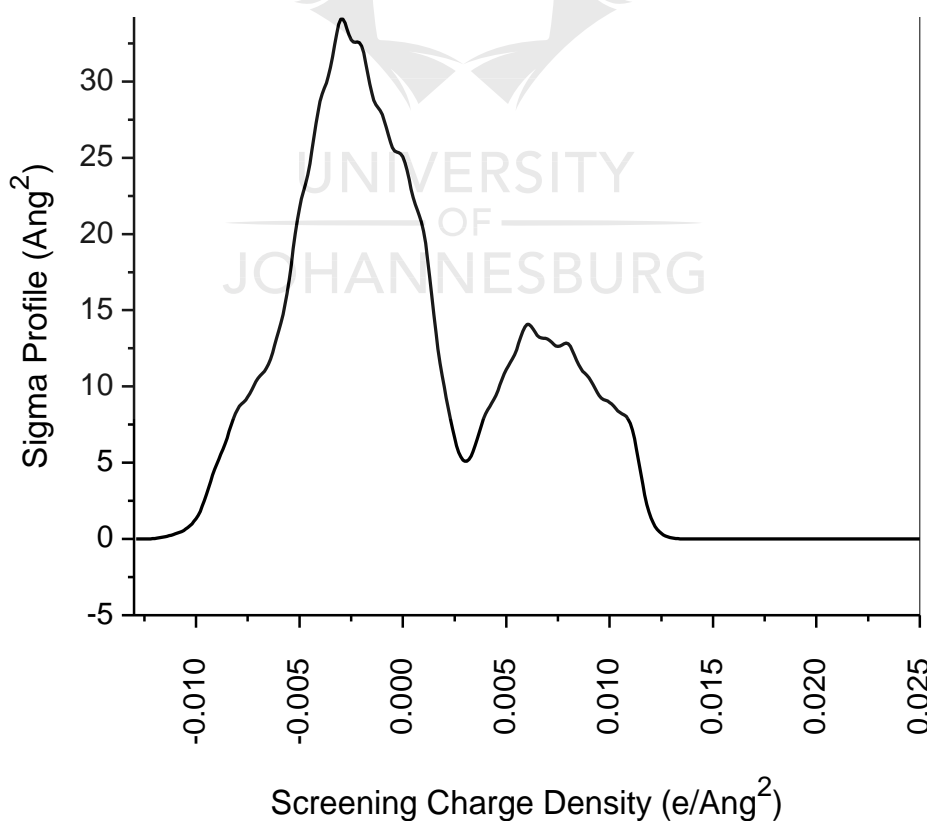


**Figure 3. 3:** A typical sigma profile of a unary solution (disperse yellow 119 in water).

The sigma profile,  $p_s(\sigma)$  for an ensemble (solvent) of  $n$  number of components is related to the surface charge density of each component  $X_i$  by:

$$p_s(\sigma) = \frac{\sum_i^n x_i p^{X_i}(\sigma)}{\sum_i^n x_i}$$

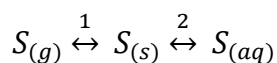
Equation 3. 54

Where  $x_i$  and  $p^{X_i}(\sigma)$  are the molar fraction and sigma profile of each component of the ensemble, respectively.

In the DMol<sup>3</sup> program [32] for instance, the sigma profile is obtained at the end of a COSMO-RS run alongside the output of the calculation itself. Appearance of peaks in the region of zero screening charge density (x-axis) confirms occurrence of screening. Essential thermodynamic properties such as the free energy of hydration, vapor pressure and octanol-water activity coefficient can also be obtained from COSMO-RS calculations. The ability of COSMO-RS to accurately predict these properties without the need for experimental data makes it a very reliable and elegant model for accurate prediction of solution thermodynamic properties.

### 3.7.11 SOLUBILITY AND SOLVATION FREE ENERGY RELATIONSHIP [56]

The thermodynamic relationship between solubility, vapor pressure and solvation free energy serves as a reliable alternative to the general solubility equation for predicting the solubility of different types of solute. This relationship which was first reported by Cramer *et al.* [56] was derived based on a tri-phasic equilibrium system, comprising a pure solute S, its vapor and its aqueous solution (Scheme 3.1) as discussed below.



**Scheme 3. 1:** A tri-phasic equilibrium system of a pure solute S, its vapor and its aqueous solution. Subscripts *s*, ***g*** and ***aq*** indicate solid, gas and aqueous phases, respectively.

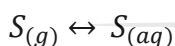
Assuming all phases behave ideally at 1 molar standard state, the standard free energy changes,  $\Delta G_1^0$  and  $\Delta G_2^0$  for processes 1 and 2 in Scheme 3.1 are given as:

$$\Delta G_1^0 = RT \ln \frac{P_s}{P^0 M_s} \quad \text{Equation 3. 55}$$

$$\Delta G_2^0 = -RT \ln \frac{M_s^{aq}}{M_s} \quad \text{Equation 3. 56}$$

where  $P_s$  is the equilibrium vapour pressure of S,  $P^0$  is 24.45 atm which is the pressure of an ideal gas at 1 molar standard state and 298K.  $M_s$  is the molarity of solute S, which can be obtained from the density of the solute,  $M_s^{aq}$  is the solubility of S in molarity unit which is otherwise known as equilibrium aqueous molarity in mole per volume unit. T is the temperature in kelvin and R is the molar gas constant.

Applying the zeroth law to processes 1 and 2 in Scheme 3.1 gives an overall equilibrium equation between the solute vapor and its aqueous solution:



**Scheme 3. 2:** An overall bi-phasic equilibrium equation involving the solute vapor and its aqueous solution.

The total free energy change for the process is the sum of equations 3.55 and 3.56 to give:

$$\Delta G_{Total}^0 = \Delta G_1^0 + \Delta G_2^0 = RT \ln \frac{P_s}{P^0 M_s} - RT \ln \frac{M_s^{aq}}{M_s} \quad \text{Equation 3. 57}$$

Equation 3.57 can be further simplified as:

$$M_s^{aq} = \frac{P_s}{P^0} e^{-\Delta G_{Total}^0 / RT} \quad \text{Equation 3. 58}$$

$\Delta G_{Total}^0$  is the same as the standard state free energy of solvation of the solute, and can therefore be written as  $\Delta G_s^0$ . Similarly,  $M_s^{aq}$  is the same as aqueous solubility,  $S_{aq}$  of the solute in mole per unit volume. Thus, equation 3.58 becomes:

$$S_{aq} = \frac{P_s}{P^0} e^{-\Delta G_s^0/RT}$$

Equation 3. 59

Equation 3.59 shows the dependence of aqueous solubility on solute vapor pressure ( $P_s$ ) and solvation free energy, SFE ( $\Delta G_s^0$ ). Therefore, accurate prediction of the aqueous solubility of a solute can be achieved if its vapor pressure and SFE are known.

### 3.8 CHEMICAL REACTIVITY INDICES (CRI)

Chemical reactivity indices are the set of quantum chemical descriptors used for evaluating/predicting the reactivity of a molecule as an entity (i.e. global reactivity), and/or the reactivity of specific sites in a molecule (i.e. local reactivity). Reactivity parameters are viable tools for probing the connection between structure, reactivity and stability of molecules. Hence, they are very reliable in developing quantitative structure property, structure activity and structure toxicity relations (QSTR) [57]. Examples of global reactivity descriptors include global hardness, global softness, electronegativity, chemical potential, and electrophilicity, while local softness and Fukui function belong to the class of local reactivity descriptors [58].

#### 3.8.1 GLOBAL REACTIVITY DESCRIPTORS (GRD)

Reactivity indices that reveal the overall stability/reactivity of a molecular entity rather than that of the component atoms are called global reactivity descriptors. These descriptors are basically derived from molecular electron affinity,  $A$  and ionization potential,  $I$ , which

are determined theoretically by total electronic energy calculation on the  $N - 1$ ,  $N$  and  $N + 1$  electronic systems in neutral state [57]. A computationally less expensive approach employs the Koopmans' approximation [59], which replaces  $A$  with the negative of lowest unoccupied molecular orbital energy ( $-E_{LUMO}$ ) and  $I$  with the negative of highest occupied molecular orbital energy ( $-E_{HOMO}$ ).  $E_{LUMO}$  and  $E_{HOMO}$  are obtained from DFT calculation on neutral molecules. Prominent members of the global reactivity descriptors are discussed as follows:

- Global hardness, ( $\eta$ ): This is the second-order derivative of the Kohn-Sham (KS) energy,  $E$ , or the first order derivative of the chemical potential,  $\Phi$  with respect to the number of electrons,  $N$  in a system at a constant potential,  $V(\vec{r})$  [57]. It is a parameter that reveals the ability of a molecule to resist a change in electronic configuration and/or electron density when perturbed. Global hardness is mathematically expressed as:

$$\eta = \left( \frac{\partial \Phi}{\partial N} \right)_{V(\vec{r})} = \left( \frac{\partial^2 E}{\partial N^2} \right)_{V(\vec{r})} \approx \frac{I-A}{2} \approx \frac{1}{2} (E_{LUMO} - E_{HOMO})$$

Equation 3. 60

- Global softness, ( $\sigma$ ): This is the reciprocal of global hardness, i.e. a parameter that shows how vulnerable a molecule is to a change in electronic configuration and/or electron density. It is mathematically given as:

$$\sigma = \frac{1}{\eta} = \left( \frac{\partial N}{\partial \Phi} \right)_{V(\vec{r})} = \left( \frac{\partial N^2}{\partial^2 E} \right)_{V(\vec{r})} \approx \frac{2}{I-A} \approx \frac{2}{(E_{LUMO} - E_{HOMO})}$$

Equation 3. 61

- Chemical potential,  $\Phi$  is the first-order derivative of the Kohn-Sham (KS) energy,  $E$  with respect to the electron number at a constant potential,  $V(r)$  [57]. It is a measure



of the electron releasing tendency of a molecule at ground state, and is equal to the negative of electronegativity [57, 60]. Mathematically;

$$\Phi = -\chi = \left(\frac{\partial E}{\partial N}\right)_{V(\vec{r})} \approx \frac{-(I + A)}{2} \approx \frac{E_{HOMO} + E_{LUMO}}{2}$$

Equation 3. 62

- Electronegativity,  $\chi$  refers to the ability to attract electrons. Hence, it is the negative of chemical potential [61].

$$\chi = -\Phi = -\left(\frac{\partial E}{\partial N}\right)_{V(\vec{r})} \approx \frac{(I + A)}{2} \approx -\frac{1}{2}(E_{HOMO} + E_{LUMO})$$

Equation 3. 63

- Electrophilicity index,  $\omega$  reveals the propensity of a molecule towards an incoming nucleophile. It is a measure of the change in stability of a molecule upon the addition of an incoming electron. A low electrophilicity value indicates a good nucleophile while a high value implies a good electrophile. Electrophilicity index is expressed in terms of chemical potential,  $\Phi$  and global hardness,  $\eta$  as [58, 62, 63]:

$$\omega = \frac{\Phi^2}{2\eta}$$

Equation 3. 64

### 3.8.2 LOCAL REACTIVITY DESCRIPTORS (LRD)

Reactivity indices that are concerned with reactivity of specific sites in a molecule are known as local reactivity descriptors. They provide information on the reactivity of the constituent atoms rather than that of the molecule thereby allowing the identification of prospective donor and acceptor sites in the molecule. Prominent members of this group include Fukui functions (FF) and local softness [58].

### 3.8.3 FUKUI FUNCTION

From a DFT perspective, Fukui function is the partial derivative of electron density with respect to the number of electrons in a system under a fixed external potential or the partial derivative of chemical potential,  $\Phi$  with respect to the external potential at fixed number of electron. That is:

$$f(\vec{r}) = \left( \frac{\partial \rho(\vec{r})}{\partial N} \right)_{V(\vec{r})} = \left( \frac{\partial \Phi(\vec{r})}{\partial V(\vec{r})} \right)_N$$

Equation 3. 65

where  $\rho(\vec{r})$  is the electron density,  $N$  is the number of electron and  $V(\vec{r})$  is the external potential.

For a negative change in  $N$ , i.e. when  $N$  increases from  $N$  to  $N-1$ , the Fukui function,  $f^-(\vec{r})$  is given as:

$$f^-(\vec{r}) = \left( \frac{\partial \rho(\vec{r})}{\partial N} \right)_{V(\vec{r})}^- \approx \rho_{HOMO}(\vec{r})$$

Equation 3. 66

For a positive change in  $N$ , i.e. when  $N$  decreases from  $N$  to  $N+1$ , the Fukui function,  $f^+(\vec{r})$  is:

$$f^+(\vec{r}) = \left( \frac{\partial \rho(\vec{r})}{\partial N} \right)_{V(\vec{r})}^+ \approx \rho_{LUMO}(\vec{r})$$

Equation 3. 67

$\rho_{HOMO}$  and  $\rho_{LUMO}$  are the HOMO and LUMO densities, respectively.  $f^-(\vec{r})$  and  $f^+(\vec{r})$  are the Fukui functions for electrophilic and nucleophilic attacks on nucleophilic and electrophilic sites, respectively.

The average of the above equations which gives the Fukui function,  $f^0(\vec{r})$  for radical attack is:

$$f^0(\vec{r}) = \frac{1}{2}[f^+(\vec{r}) + f^-(\vec{r})]^0$$

Equation 3. 68

The condensed forms of the Fukui functions for a specific atomic site are calculated based on Mulliken atomic charges [58]:

$$f^+ = q_k(N + 1) - q_k(N)$$

Equation 3. 69

$$f^- = q_k(N) - q_k(N - 1)$$

Equation 3. 70

$$f^0 = \frac{1}{2}[q_k(N + 1) - q_k(N - 1)]$$

Equation 3. 71

where  $N$  is the number of electron,  $q_k(N - 1)$ ,  $q_k(N)$  and  $q_k(N + 1)$  are the Mulliken charges on atom,  $k$  for  $(N - 1)$  -,  $(N)$  - and  $(N + 1)$  number of electrons, respectively.  $f^+$ ,  $f^-$  and  $f^0$  are the corresponding Fukui functions for nucleophilic, electrophilic and radical attacks, respectively.

A recently proposed local reactivity descriptor which can be used as alternative to Fukui functions is the local electrophilicity,  $\omega_k$  given as [58]:

$$\omega_k^\alpha = \omega f_k^\alpha$$

Equation 3. 72

where  $\omega$  is the global electrophilicity and  $f_k$  is the atom condensed Fukui functions for atom  $k$ .  $\alpha = +, -$  and  $0$  for nucleophilic, electrophilic and radical attacks respectively.

In a given molecule, the site with the biggest value of  $\omega_k^+$ , or  $\omega_k^-$  is the most electrophilic or nucleophilic site, respectively, while the most disposed site to radical attack is the one with the highest value of  $\omega_k^0$ .

Similarly, local softness,  $s$  is another local reactivity parameter that reveals the susceptibility of specific atomic centres in a molecule to reaction. It is expressed as [58]:

$$s_k^\alpha = S f_k^\alpha$$

Equation 3. 73

$S$  is the global softness i.e. the inverse of global hardness and  $f_k$  is the atom condensed Fukui functions.  $\alpha = +, -$  and  $0$  for nucleophilic, electrophilic and radical attacks respectively.

### 3.9 POTENTIAL ENERGY SURFACES (PES)

Simply put, a potential energy surface shows the connection between molecular structure and energy [30]. In a broader sense, a PES is an energy profile diagram which shows the changes in the structure and energy of a reactant molecule as it transits from the reactant state into the product usually via an activated complex known as a transition state. For a multi-step reaction, the structures and energies of the various intermediates involved before the final product are also obtainable from a PES. Potential energy surfaces provide both the kinetic and thermodynamic information associated with a chemical reaction.

#### 3.9.1 POTENTIAL ENERGY SURFACE AND KINETICS

In a single step PES, the energy of the transition state (TS) relative to that of the reactant gives the reaction activation energy (Fig. 3.4), which is the minimum energy required for effective collision between the reactant molecules or the minimum energy needed to overcome the reaction barrier. Activation energy is a kinetic term because it reveals the rate of a reaction (equations 3.74 and 3.75). A slow reaction is characterized by a large activation while a fast reaction occurs with small activation energy. In the case of a multi-step reaction, the activation energy is obtained from the rate limiting step i.e. the step with the highest energy barrier (Fig. 3.5). The relationship between activation energy and reaction rate constant is given by Arrhenius [64] and Eyring [65] as follows:

$$k_{rxn} = A \exp\left(-\frac{\Delta E^\ddagger}{RT}\right) \quad (\text{Arrhenius equation})$$

Equation 3. 74

$$k_{rxn} = \left(\frac{k_B T}{h}\right) \exp\left(-\frac{\Delta G^\ddagger}{RT}\right) \quad (\text{Eyring equation})$$

Equation 3. 75

Where  $k_{rxn}$  is the rate constant,  $k_B$  and  $h$  are the Boltzmann and Planck constants respectively,  $A$  is the Arrhenius factor,  $T$  is the temperature,  $R$  is the molar gas constant,  $\Delta E^\ddagger$  is the activation energy and  $\Delta G^\ddagger$  is the free energy of activation.

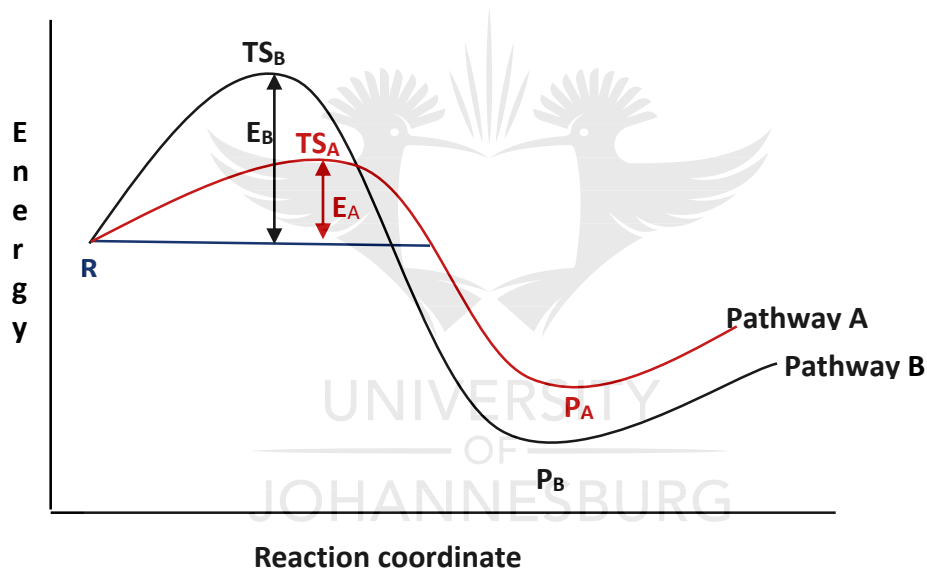


**Figure 3. 4:** A one step reaction PES of reactant R occurring via pathways A and B with activation energies  $E_A$  and  $E_B$  respectively to form products  $P_A$  and  $P_B$ .  $E_A$  is smaller than  $E_B$ , hence  $P_A$  is the kinetic product.  $P_B$  is lower in energy than  $P_A$ , hence it is called a thermodynamic product.

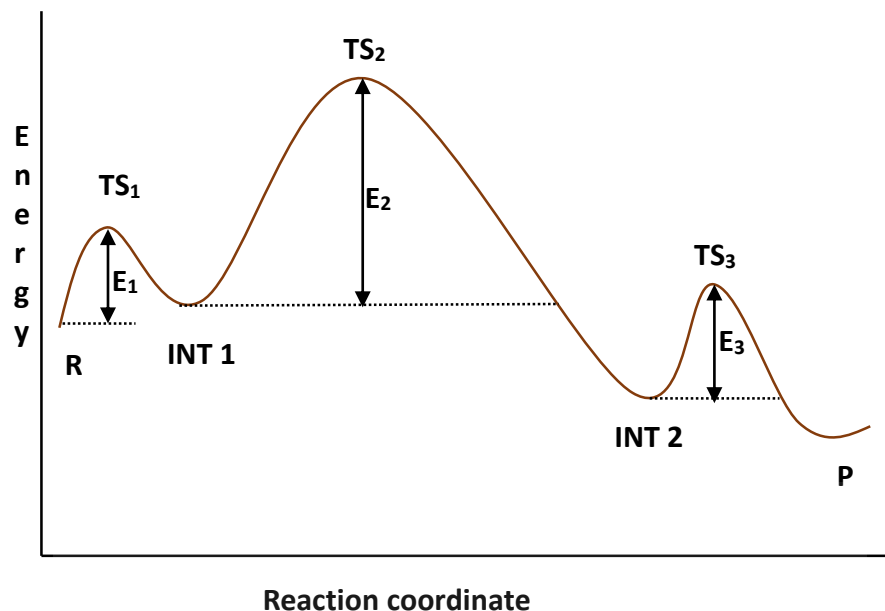


**Figure 3. 5:** A multi-step reaction PES of reactant R where  $E_1$ ,  $E_2$  and  $E_3$  are the activation energies for the three steps.  $E_2$  is larger than  $E_1$  and  $E_3$ , hence, step 2 is the rate limiting step.

### 3.9.2 POTENTIAL ENERGY SURFACE AND THERMODYNAMICS

Thermodynamics reveals the direction of energy flow (i.e. either exothermic or endothermic) and the feasibility of a reaction from the relative stability of the reactant and the product as indicated on the PES by their respective energies (Fig. 3.4) [30]. Unlike reaction kinetics, thermodynamics of reactions is independent of the number of steps involved but strictly on the relative free energies of reactants and products  $\Delta G_{rxn}$  which is the difference between the change in the reaction enthalpy,  $\Delta H_{rxn}$ , and the product of the entropy change,  $\Delta S_{rxn}$  and the absolute temperature,  $T$  [66]. That is:

$$\Delta G_{rxn} = \Delta H_{rxn} - T\Delta S_{rxn}$$

Equation 3. 76

and

$$\Delta H_{rxn} - \Delta E_{rxn} = \Delta(PV)$$

Equation 3. 77

$\Delta E_{rxn}$  is the change in reaction energy and  $\Delta(PV)$  is the change in pressure – volume work which is negligible under normal condition. If the entropic contribution to the reaction free energy is infinitesimally small, then;

$$\Delta G_{rxn} \approx \Delta H_{rxn} \approx \Delta E_{rxn} = \sum E_{product} - \sum E_{reactant}$$

Equation 3. 78

$\sum E_{product}$  and  $\sum E_{reactant}$  are sum of the energies of products and reactants respectively.

Theoretically, it is a common practice to evaluate the thermodynamics of chemical reactions particularly those involving multiple steps using the absolute energies of the reactant(s) and product(s) [67-70].

### 3.9.3 KINETIC AND THERMODYNAMIC CONTROLLED REACTIONS

In chemical reactions, product distributions are often controlled by two different and independent mechanisms namely; thermodynamically favored and kinetically favored mechanisms with the dominant product depending on the reaction conditions [30]. A kinetic controlled reaction is the one that occurred through the lowest possible energy barrier without necessarily forming the most stable product (Fig. 3.4). The product obtained in highest amount in a kinetically-controlled reaction is known as the kinetic product [30]. On the other hand, a thermodynamically controlled reaction is the one that yielded the most stable product (i.e. the thermodynamic product) even if a large energy barrier is involved (Fig. 3.4) [30, 66].

### 3.9.4 REACTIONS WITHOUT ENERGY BARRIER

Chemical reactions with no energy barrier are the ones whose rates depend only on the speed with which reactant molecules diffuse into one another. They are referred to as diffusion controlled reactions [10]. Radical combination and some radical addition reactions are diffusion controlled because they occur with very small or no energy barrier [10]. Nucleophilic substitution reactions which brings about steric relaxation of the substrate also occur without energy barrier [71].

### 3.10 REFERENCES

1. D. C. Young. Computational chemistry: A practical guide for applying techniques to real-world problems. *John Wiley & Sons, Inc.*, United state (2001).
2. F. Jensen. Introduction to computational chemistry. *John Wiley & Sons*, United State, (2007).
3. T. Engel. Quantum chemistry and spectroscopy. *Pearson Education*, India, (2012).
4. C. J. Cramer. Essentials of computational chemistry: theories and models. *John Wiley & Sons*, United State, (2013)
5. P. Hohenberg and W. Kohn. Inhomogeneous electron gas. *Physical Review* **136** (1964) 864-871.
6. W. Kohn and L. J. Sham. Self-consistent equations including exchange and correlation effects. *Physical Review* **140** (1965) 1133-1138.
7. D. R. Hartree. The wave mechanics of an atom with a non-coulomb central field. Part I. Theory and methods. *Mathematical Proceedings of the Cambridge*



- Philosophical Society*, Cambridge University Press, (1928) 89-110.  
Doi.org/10.1017/S030500410001191.
8. V. Fock. Approximation method for the solution of the quantum mechanical multibody problems. *Zeitschrift fur Physik* **61** (1930) 126-148.
  9. S. Kurth and J. P. Perdew. Role of the exchange–correlation energy: Nature's glue. *International Journal of Quantum Chemistry* **77** (2000) 814-818.
  10. W. Henry. and S. Ohlinger. Spartan'10 for Windows, Machintosh and Linux: Tutorial and User's Guide. *Wavefunction, Inc., Irvine, CA, United States* (2011) 423-522.
  11. J. Ren. First-principles modeling of optically active organic molecules in solar cell devices and biological environments. *Ecole Federal Polytechnic of Lausanne, Lausanne, Suisse* (2011) 11-18.
  12. D. M. Ceperley and B. Alder. Ground state of the electron gas by a stochastic method. *Physical Review Letters* **45** (1980) 566-569.
  13. S. H. Vosko, L. Wilk and M. Nusair. Accurate spin-dependent electron liquid correlation energies for local spin density calculations: a critical analysis. *Canadian Journal of Physics* **58** (1980) 1200-1211.
  14. J. P. Perdew and A. Zunger. Self-interaction correction to density-functional approximations for many-electron systems. *Physical Review B* **23** (1981) 5048-5079.
  15. J. P. Perdew and Y. Wang. Accurate and simple analytic representation of the electron-gas correlation energy. *Physical Review B* **45** (1992) 13244-13249.
  16. L. A. Cole and J. Perdew. Calculated electron affinities of the elements. *Physical Review A* **25** (1982) 1265-1271.

17. F. Nogueira, A. Castro and M. A. Marques. Lecture Note in Physics 620: a tutorial on density functional theory. *Springer-Verlag*, Berlin Heidelberg, (2003) 218-256. DOI: 10.1007/3-540-37072-2\_6.
18. C. Lee, W. Yang and R. Parr. Correlation functional. *Physical Review B* **98** (1998) 5648-5652.
19. Y. Wang and J. P. Perdew. Spin scaling of the electron-gas correlation energy in the high-density limit. *Physical Review B* **43** (1991) 8911-8916.
20. J. P. Perdew. Density-functional approximation for the correlation energy of the inhomogeneous electron gas. *Physical Review B* **33** (1986) 8822-8824.
21. J. P. Perdew. Generalized gradient approximations for exchange and correlation: a look backward and forward. *Physica B: Condensed Matter* **172** (1991) 1-6.
22. J. P. Perdew, K. Burke and M. Ernzerhof. Generalized gradient approximation made simple. *Physical Review Letters* **77** (1996) 3865-3868.
23. B. Hammer, L. B. Hansen and J. K. Nørskov. Improved adsorption energetics within density-functional theory using revised Perdew-Burke-Ernzerhof functionals. *Physical Review B* **59** (1999) 7413-7421.
24. A. D. Becke. A new mixing of Hartree–Fock and local density-functional theories. *The Journal of Chemical Physics* **98** (1993) 1372-1377.
25. A. D. Becke. Density-functional exchange-energy approximation with correct asymptotic behavior. *Physical Review A* **38** (1988) 3098-3100.
26. C. Lee, W. Yang and R. G. Parr. Development of the Colle-Salvetti correlation-energy formula into a functional of the electron density. *Physical Review B* **37** (1988) 785-789.

27. J. Heyd, G. E. Scuseria and M. Ernzerhof. Hybrid functionals based on a screened Coulomb potential. *The Journal of Chemical Physics* **118** (2003) 8207-8215.
28. M. Dion, H. Rydberg, E. Schröder, D. C. Langreth and B. I. Lundqvist. Van der Waals density functional for general geometries. *Physical Review Letters* **92** (2004) 246401-246404.
29. Y. Andersson, E. Hult, H. Rydberg, P. Apell, B. I. Lundqvist and D. C. Langreth. Van der Waals interactions in density functional theory. *Physical Review Letters* **76** (1996) 102-105.
30. W. J. Hehre. A guide to molecular mechanics and quantum chemical calculations. *Wavefunction Irvine, CA, United States*, (2003) 40-45. Available at: [https://www.wavefun.com/japan/products/books/AGuidetoMM\\_Cha1-2.pdf](https://www.wavefun.com/japan/products/books/AGuidetoMM_Cha1-2.pdf). Last assessed on August 13, 2018.
31. N. Benedek, I. Snook, K. Latham and I. Yarovsky. Application of numerical basis sets to hydrogen bonded systems: a density functional theory study. *The Journal of Chemical Physics* **122** (2005) 144102-144109.
32. DMol<sup>3</sup> Guide, Material Studio 8.0. *Accelrys Software, Inc.*, San Diego, United States (2017) 1-161.
33. Y. Inada and H. Orita. Efficiency of numerical basis sets for predicting the binding energies of hydrogen bonded complexes: evidence of small basis set superposition error compared to Gaussian basis sets. *Journal of Computational Chemistry* **29** (2008) 225-232.
34. P. Hobza and K. Müller-Dethlefs. Non-covalent interactions: theory and experiment. *Royal Society of Chemistry* **1** (2009) 221-226.

35. R. M. Balabin. Enthalpy difference between conformations of normal alkanes: intramolecular basis set superposition error (BSSE) in the case of n-butane and n-hexane. *The Journal of Chemical Physics* **129** (2008) 164101-164105.
36. A. Klamt, V. Jonas, T. Bürger and J. C. Lohrenz. Refinement and parametrization of COSMO-RS. *The Journal of Physical Chemistry A* **102** (1998) 5074-5085.
37. J. Wang and T. Hou. Recent advances on aqueous solubility prediction. *Combinatorial Chemistry & High Throughput Screening* **14** (2011) 328-338.
38. R. Skyner, J. McDonagh, C. Groom, T. van Mourik and J. Mitchell. A review of methods for the calculation of solution free energies and the modelling of systems in solution. *Physical Chemistry Chemical Physics* **17** (2015) 6174-6191.
39. L. D. Hughes, D. S. Palmer, F. Nigsch and J. B. Mitchell. Why are some properties more difficult to predict than others? A study of QSPR models of solubility, melting point, and Log P. *Journal of Chemical Information and Modeling* **48** (2008) 220-232.
40. S. H. Yalkowsky and S. C. Valvani. Solubility and partitioning I: solubility of nonelectrolytes in water. *Journal of Pharmaceutical Sciences* **69** (1980) 912-922.
41. N. Jain and S. H. Yalkowsky. Estimation of the aqueous solubility I: Application to organic nonelectrolytes. *Journal of Pharmaceutical Sciences* **90** (2001) 234-252.
42. J. Wang, T. Hou and X. Xu. Aqueous solubility prediction based on weighted atom type counts and solvent accessible surface areas. *Journal of Chemical Information And Modeling* **49** (2009) 571-581.
43. Y. Ran, Y. He, G. Yang, J. L. Johnson and S. H. Yalkowsky. Estimation of aqueous solubility of organic compounds by using the general solubility equation. *Chemosphere* **48** (2002) 487-509.

44. D. L. Beveridge and F. DiCapua. Free energy via molecular simulation: applications to chemical and biomolecular systems. *Annual Review of Biophysics and Biophysical Chemistry* **18** (1989) 431-492.
45. P. Mark and L. Nilsson. Structure and dynamics of the TIP3P, SPC, and SPC/E water models at 298 K. *The Journal of Physical Chemistry A* **105** (2001) 9954-9960.
46. D. van der Spoel, P. J. van Maaren and H. J. Berendsen. A systematic study of water models for molecular simulation: derivation of water models optimized for use with a reaction field. *The Journal of Chemical Physics* **108** (1998) 10220-10230.
47. L. Onsager. Electric moments of molecules in liquids. *Journal of the American Chemical Society* **58** (1936) 1486-1493.
48. J. Tomasi, B. Mennucci and R. Cammi. Quantum mechanical continuum solvation models. *Chemical Reviews* **105** (2005) 2999-3094.
49. A. V. Marenich, C. J. Cramer and D. G. Truhlar. Universal solvation model based on solute electron density and on a continuum model of the solvent defined by the bulk dielectric constant and atomic surface tensions. *Journal of Physical Chemistry B* **113** (2009) 6378-6396.
50. J. Andzelm, C. Kölmel and A. Klamt. Incorporation of solvent effects into density functional calculations of molecular energies and geometries. *The Journal of Chemical Physics* **103** (1995) 9312-9320.
51. A. Klamt and F. Eckert. COSMO-RS: a novel and efficient method for the a priori prediction of thermophysical data of liquids. *Fluid Phase Equilibria* **172** (2000) 43-72.

52. A. Klamt. COSMO-RS: from quantum chemistry to fluid phase thermodynamics and drug design. *Elsevier* (2005) 1-246.
53. A. Klamt. The COSMO and COSMO-RS solvation models. *Wiley Interdisciplinary Reviews: Computational Molecular Science* **1** (2011) 699-709.
54. Y. Takano and K. Houk. Benchmarking the conductor-like polarizable continuum model (CPCM) for aqueous solvation free energies of neutral and ionic organic molecules. *Journal of Chemical Theory and Computation* **1** (2005) 70-77.
55. E. Mullins, R. Oldland, Y. Liu, S. Wang, S. I. Sandler, C.-C. Chen, M. Zwolak and K. C. Seavey. Sigma-profile database for using COSMO-based thermodynamic methods. *Industrial and Engineering Chemistry Research* **45** (2006) 4389-4415.
56. J. D. Thompson, C. J. Cramer and D. G. Truhlar. Predicting aqueous solubilities from aqueous free energies of solvation and experimental or calculated vapor pressures of pure substances. *The Journal of Chemical Physics* **119** (2003) 1661-1670.
57. R. Vijayaraj, V. Subramanian and P. Chattaraj. Comparison of global reactivity descriptors calculated using various density functionals: a QSAR perspective. *Journal of Chemical Theory and Computation* **5** (2009) 2744-2753.
58. J. Padmanabhan, R. Parthasarathi, M. Elango, V. Subramanian, B. Krishnamoorthy, S. Gutierrez-Oliva, A. Toro-Labbé, D. Roy and P. Chattaraj. Multiphilic descriptor for chemical reactivity and selectivity. *The Journal of Physical Chemistry A* **111** (2007) 9130-9138.
59. R. G. Pearson. Chemical Hardness. *Wiley Online Library*, United States, (1997).
60. R. G. Parr and Y. Weitao. Density Functional Theory of Atoms and Molecules. *Oxford University Press*, New York (1994) 1-352.

61. R. G. Parr and R. G. Pearson. Absolute hardness: companion parameter to absolute electronegativity. *Journal of the American Chemical Society* **105** (1983) 7512-7516.
62. R. G. Parr, L. V. Szentpaly and S. Liu. Electrophilicity index. *Journal of the American Chemical Society* **121** (1999) 1922-1924.
63. P. Chattaraj, U. Sarkar and D. Roy. Electronic structure principles and aromaticity. *Journal of Chemical Education* **84** (2007) 354-357.
64. S. Arrhenius. Über die Dissociationswärme und den einfluss der temperatur auf den dissociationsgrad der elektrolyte. *Zeitschrift für Physikalische Chemie* **4** (1889) 96-116.
65. H. Eyring. The activated complex in chemical reactions. *The Journal of Chemical Physics* **3** (1935) 107-115.
66. T. Engel and P. J. Reid. Physical Chemistry. San Francisco, United States (2006).
67. A. S. Özen, V. Aviyente, F. De Proft and P. Geerlings. Modeling the substituent effect on the oxidative degradation of azo dyes. *The Journal of Physical Chemistry A* **108** (2004) 5990-6000.
68. A. S. Özen, V. Aviyente and R. A. Klein. Modeling the oxidative degradation of azo dyes: a density functional theory study. *The Journal of Physical Chemistry A* **107** (2003) 4898-4907.
69. A. S. Özen, V. Aviyente, G. Tezcanli-Güyer and N. H. Ince. Experimental and modeling approach to decolorization of azo dyes by ultrasound: degradation of the hydrazone tautomer. *The Journal of Physical Chemistry A* **109** (2005) 3506-3516.

70. X. Jiao, H. Yu, Q. Kong, Y. Luo, Q. Chen and J. Qu. Theoretical mechanistic studies on the degradation of alizarin yellow R initiated by hydroxyl radical. *Journal of Physical Organic Chemistry* **27** (2014) 519-526.
71. O. Wahab, J. Ige, G. Ogunlusi, L. Olasunkanmi and K. Sanusi. Oxatriquinane derivatives: a theoretical investigation of SN<sub>1</sub>-SN<sub>2</sub> reactions borderline. *Walailak Journal of Science and Technology* **15** (2016) 439-453.





---

## CHAPTER 4

### COMPUTATIONAL RESOURCES

---

#### 4.1 INTRODUCTION

Computational resources refer to both the software and the hardware facilities utilized in this project. The software facility comprises the computational software package employed for the calculations, while the hardware facility refers to the cluster used for the calculations. The computational software selected for this project included the BIOVIA Material Studio (MS) package (version 2016) [1] because of its robustness and versatility in terms of its applicability to various types of research problems. This software was installed on a core i5 Dell computer with a system rating of 5.9 and a 64-bit operating system, and the calculations were run on the Lengau cluster at the Centre for High Performance Computing (CHPC) in Cape Town, South Africa. The local desktop computer makes use of Intel processors with processing speed of 3.00 GHz per core, 8.00 GB installed memory (i.e. RAM = 8.00 GB) and 1 TB hard disk. Details of the BIOVIA MS software and the Lengau cluster are provided in the following sections.

#### 4.2 BIOVIA MATERIAL STUDIO [1]

BIOVIA Materials Studio (BIOVIA MS) is a robust modelling package consisting of different computational modules, programs, codes, algorithms and adjustable tools. Some of these include Cambridge Serial Total Energy Package (CASTEP), DMol<sup>3</sup>, Adsorption locator, Kinetix, Forcite, Morphology, Polymorph, Sorption, Reflex, General Utility Lattice Program (GULP) and Gaussian. BIOVIA MS provides a user-friendly

interface which supports Windows, and a visualizer with varieties of modelling and visualization tools for a rapid construction of molecular models and materials (Fig. 4.1). It also provides a more convenient means of accessing the incorporated programs for carrying out quantum mechanical or quantum chemical calculations on constructed models. BIOVIA MS allows for multi-tasking in that several different calculation types can be set up simultaneously at the same time even with different codes. Calculation outputs are returned to the user in an elegant and easily accessible form. In addition to the user-friendly interface, BIOVIA MS also offers an adequate user training guide which enables users to conveniently use the facility in tackling various research problems.

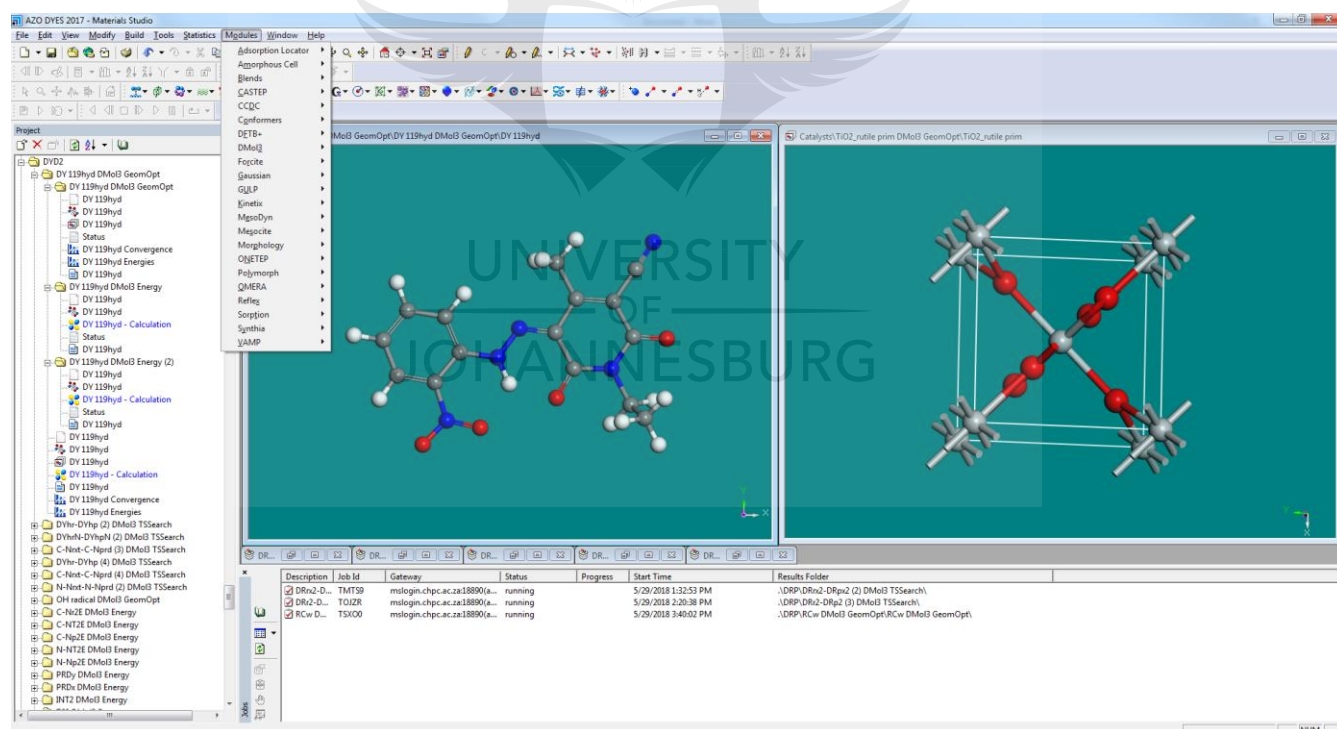


**Figure 4. 1:** The Material Studio Interface

### 4.3 MATERIALS STUDIO DMOL<sup>3</sup> [2]

Materials Studio DMol<sup>3</sup> (MSDMol<sup>3</sup>) is one of the several computational codes in the BIOVIA Materials Studio software [1]. It is a density functional theory (DFT) based modelling program used for predicting properties of materials and simulation of chemical processes. It is a versatile, efficient and elegant computational code that performs simulations with remarkable speed and accuracy even for larger molecules containing over 500 atoms. Because of its applicability to systems in gas, solution and solid phases, it has received a widespread application in chemistry, pharmaceuticals, chemical engineering and materials science for addressing various research problems such as investigating the origin and nature of the geometrical, electronic, optical and chemical properties of systems with no involvement of experimental inputs [2-5]. Despite this, adequate information on selection of key adjustable parameters such as orbital cut-off, solvent radius etc., which govern the accuracy of DMol<sup>3</sup> calculations, is still lacking. Therefore, attempt is made in chapters 5 and 6 of this thesis to address this limitation.

#### 4.3.1 USES OF DMOL<sup>3</sup>

DMol<sup>3</sup> can be employed for a plethora of research goals which include, but are not limited to the following:

- Design of useful compounds such as catalysts, drugs, dyes, polymers etc.
- Process optimization through determination of more efficient synthetic pathway(s).
- Understanding and description of fundamental processes.
- Conformational analysis.
- Modelling catalysis on a metal surface.

- Modelling of ligand binding.
- Understanding crystal polymorphs.
- Development of new solid materials such as semiconductors and superconductors and prediction of their band gaps.
- Homogeneous and heterogeneous catalytic studies.
- Aqueous solubility prediction.
- Evaluation of molecular reactivity through frontier molecular orbital calculations.
- Predict minimum energy structures.
- Investigation of reaction mechanisms and determination of reaction barriers.

#### 4.3.2 ADVANTAGES OF DMOL<sup>3</sup>

- DMol<sup>3</sup> jobs can run on servers located anywhere on a user's network.
- Calculation results are received directly via a users' computer and can also be displayed and analyzed therein.
- Production of high quality graphics of materials and molecular structures, electrostatic potentials, frontier molecular orbital isosurfaces, or electron densities is relatively easy with DMol<sup>3</sup>.
- Models, graphs and animation files obtained from DMol<sup>3</sup> output can easily be shared with other relevant computer applications.

#### 4.3.3 PERFORMANCE OF DMOL<sup>3</sup>

The speed and accuracy of DMol<sup>3</sup> calculations are achieved through the use of numerical basis sets i.e. basis sets that make use of numerical functions as basis functions to

represent atomic orbitals [4-8]. The high accuracy of this group of basis sets is traceable to the fact that the basis functions used for each of the atoms are determined by solving their respective one atomic DFT equations.

In DMol<sup>3</sup>, the total electron density in a system is decomposed into a set of multipolar, atom-centered partial densities which provides a simplistic, but more accurate electron density description, and also promotes good scaling as system size increases. In effect, determination of the coulomb potential scales linearly with system size. Elements of the Hamiltonian matrix are determined using a well-developed, linearly scaling numerical integration algorithm that permits efficient parallelization of the numerical integration procedure.

MSDMol<sup>3</sup> can perform either all electron or pseudopotential calculations using accurate DFT semi-local pseudopotentials (DSPP) [9] or the effective core potentials (ECP) [10, 11].

Geometry and transition state optimizations in DMol<sup>3</sup> are carried out using delocalized internal coordinates for both molecular [12] and periodic [13] models. This is due to the ability of the program to impose Cartesian geometry constraints while performing the optimization in internal coordinates. The transition state search procedure in DMol<sup>3</sup> uses the combination of the linear synchronous transit and quadratic synchronous transit (LST/QST) methods [14, 15] for a rapid determination of transition states.

Finally, implicit solvent phase calculations are performed in DMol<sup>3</sup> with the aid of conductor-like screening model (COSMO) [3]. The COSMO solvation model is applicable to both molecular and periodic systems, which makes it possible to model systems such as polymers and heterogeneous catalysts in solvent phase. DMol<sup>3</sup> also supports the

Klamt's version of the COSMO solvation model which are COSMO for segment activity coefficient (COSMO-SAC) and COSMO for realistic solvation (COSMO-RS) [16]. These versions of COSMO model are regarded as the most successful continuum solvation models. COSMO-SAC is predominantly used for activity coefficient prediction, while COSMO-RS is employed mainly for prediction of physicochemical parameters such as vapor pressure, hydration free energies, partition coefficients, solvation free energies and mole fraction solubility of components of liquid mixtures.

#### 4.3.4 FEATURES OF MSDMOL<sup>3</sup>

Features of MSDMol<sup>3</sup> refer to the types of calculations that can be performed using DMol<sup>3</sup> and the resources available for the calculations such as types of functionals, basis sets, and predictable properties.

#### 4.3.5 CALCULATION TASKS

DMol<sup>3</sup> is capable of performing an unrestricted and restricted DFT calculations, transition state search, geometry optimization, transition state optimization and conformational searches, determination of reaction pathways, vibrational frequency calculations and implicit solvation calculations using COSMO [1].

#### 4.3.6 FUNCTIONALS

The types of DFT functionals available in DMol<sup>3</sup> include local DFT functionals such as PWC and Vosko Wilsk Nusair (VWN), generalized-gradient approximated (GGA) DFT functionals such as Becke and Perdew version of Vosko Wilsk Nusair (VWN-BP),

Becke88 exchange and the Lee-Yang-Parr correlation (BLYP), Perdew–Wang exchange and correlation functional (PW91), Perdew-Burke-Ernzerhof (PBE), Becke-Perdew (BP) exchange functional, etc. [1].

#### **4.3.7 BASIS SETS**

DMol<sup>3</sup> uses numerical type of atomic basis sets for calculations. The most common ones are double numeric basis (DN), double numerical basis with d-type polarization function (DND), double numeric basis with polarization function (DNP) and triple numeric basis with double polarization functions (TNP or TNDP) [1, 4, 5].

#### **4.3.8 PREDICTABLE PROPERTIES**

DMol<sup>3</sup> calculation allows for prediction of properties such as band structures, bond orders, work functions, frontier molecular orbitals, electron density, Fukui functions, electrostatic moments, free energy, heats of formation, heat capacity, enthalpy, entropy, zero point vibrational energies (ZPVE), atomic charges, UV/Vis spectra, excited states, polarizability, hyperpolarizability and lots more [1].

#### **4.4 PROPERTIES OF THE CHPC LENGAU CLUSTER [17]**

The Lengau cluster was launched on 7th of June, 2016 by the CHPC. The peta-scale system of the cluster consists of Dell servers which are powered by Intel processors through Mellanox FDR InfiniBand. The cluster is equipped with 32832 CPU cores, 1368 nodes, 148.5 TB memory and 4 PB lustre storage. Each CPU core processes at a speed of 2.6 GHz with an extra of 2.2 GHz for the FAT nodes which have a total memory of 5

TB and additional 280 CPU cores. A total of 1 to 5 cores will be used in this work for running our DMol<sup>3</sup> calculations on the cluster.

#### 4.5 REFERENCES

1. Materials Studio simulation environment. *Release 2016, Accelrys Software Inc, San Diego, CA, United States (2016).*
2. B. Delley. From molecules to solids with the DMol 3 approach. *The Journal of Chemical Physics* **113** (2000) 7756-7764.
3. O. Wahab, L. Olasunkanmi, K. Govender and P. Govender. DMol<sup>3</sup>/COSMO-RS prediction of aqueous solubility and reactivity of selected azo dyes: effect of global orbital cut-off and COSMO segment variation. *Journal of Molecular Liquids* **249** (2018) 346-360.
4. Y. Inada and H. Orita. Efficiency of numerical basis sets for predicting the binding energies of hydrogen bonded complexes: evidence of small basis set superposition error compared to Gaussian basis sets. *Journal of Computational Chemistry* **29** (2008) 225-232.
5. Y. Luo, S. Yin, W. Lai and Y. Wang. Effects of global orbital cutoff value and numerical basis set size on accuracies of theoretical atomization energies. *Theoretical Chemistry Accounts* **133** (2014) 1580-1590.
6. R. M. Balabin. Enthalpy difference between conformations of normal alkanes: Intramolecular basis set superposition error (BSSE) in the case of n-butane and n-hexane. *The Journal of Chemical Physics* **129** (2008) 164101-164105.



7. P. Hobza and K. Müller-Dethlefs. Non-covalent interactions: theory and experiment. *Royal Society of Chemistry*, **1** (2009) 221-226.
8. B. Delley. Fast calculation of electrostatics in crystals and large molecules. *The Journal of Physical Chemistry* **100** (1996) 6107-6110.
9. B. Delley. Hardness conserving semilocal pseudopotentials. *Physical Review B* **66** (2002) 155125-155128.
10. M. Dolg, U. Wedig, H. Stoll and H. Preuss. Energy-adjusted ab initio pseudopotentials for the first row transition elements. *The Journal of Chemical Physics* **86** (1987) 866-872.
11. A. Bergner, M. Dolg, W. Küchle, H. Stoll and H. Preuß. Ab initio energy-adjusted pseudopotentials for elements of groups 13–17. *Molecular Physics* **80** (1993) 1431-1441.
12. J. Baker, A. Kessi and B. Delley. The generation and use of delocalized internal coordinates in geometry optimization. *The Journal of Chemical Physics* **105** (1996) 192-212.
13. J. Andzelm, R. King-Smith and G. Fitzgerald. Geometry optimization of solids using delocalized internal coordinates. *Chemical Physics Letters* **335** (2001) 321-326.
14. T. A. Halgren and W. N. Lipscomb. The synchronous-transit method for determining reaction pathways and locating molecular transition states. *Chemical Physics Letters* **49** (1977) 225-232.

15. N. Govind, M. Petersen, G. Fitzgerald, D. King-Smith and J. Andzelm. A generalized synchronous transit method for transition state location. *Computational Materials Science* **28** (2003) 250-258.
16. A. Klamt. The COSMO and COSMO-RS solvation models. *Wiley Interdisciplinary Reviews: Computational Molecular Science* **8** (2018) 1-11.
17. CHPC Lengau cluster (2016). <https://www.chpc.ac.za/index.php/resources/lengau-cluster>.



---

## CHAPTER 5

# DMOL<sup>3</sup>/COSMO-RS PREDICTION OF AQUEOUS SOLUBILITY AND REACTIVITY OF SELECTED AZO DYES: EFFECT OF GLOBAL ORBITAL CUT-OFF AND COSMO SEGMENT VARIATION

---

### PREAMBLE

Aqueous solubility and reactivity of four azo dyes were investigated by DMol<sup>3</sup>/COSMO-RS calculation to examine the effects of global orbital cut-off and COSMO segment variation on the accuracies of theoretical solubility and reactivity. The VWN-BP level of theory in conjunction with the double numerical basis set containing polarization function (DNP) was employed for the calculations. The aqueous solubility was calculated from the COSMO-RS data using the Cramer *et al.* solubility equation (CSE) and the general solubility equation (GSE) by Yalkowsky. The results showed that the CSE and the GSE are reliable for predicting solubility (in mol/L) using COSMO-RS data, but their dependence on orbital cut-off differ.

### 5.1 INTRODUCTION

In recent years, quantum chemical prediction of the thermodynamic properties of fluids and solutions using methods based on the conductor-like screening model (COSMO) has received considerable research attention [1-5]. This is due to its ability to generate reliable theoretical data in a shorter time frame with relatively lower cost, and resource input when experimentation is unrealistic or cumbersome. A popular variant of the COSMO model is the conductor-like screening model for realistic solvation (COSMO-RS) [6]. COSMO-RS is a simple and non-empirical solvation model which requires the structure of a solute as

---

The work presented in this chapter has been published.

\*O.O. Wahab, L.O. Olasunkanmi, K.K. Govender and P.P. Govender. *Journal of Molecular Liquids* **249** (2018) 346-360.

the basic information for property calculation. It uses the results of a COSMO calculation to compute solution thermodynamic properties using statistical thermodynamic principles. COSMO-RS has been successfully employed for predicting the solubility of drugs in binary liquid mixtures [1], flavonoids and pharmaceutical compound solubility in ionic liquids [2, 5], solubility of rapeseed oil in various solvents [3], and carbon dioxide (CO<sub>2</sub>) absorption capacity of various solvents [4].

Azo dyes are the most widely used class of organic dyes for textile dyeing [7, 8], corrosion inhibition [9-13], pH and metallochromic indicators [14], sensitizers [15], liquid crystal display (LCD) [16], electrical and optical materials [17], foods and cosmetics [18], and drug delivery [19]. Prediction of aqueous solubility and reactivity properties is an important step towards foreseeing the fate and possible threats of these potential organic pollutants in the environment for better pollution control practice. As far as we know at the time of this work, the theoretical approach reported here for predicting azo dye solubility which involves treatment of DMol<sup>3</sup>/COSMO-RS data with the solubility equations proposed by Cramer and Yalkowsky groups had not been reported.

DMol<sup>3</sup> is a very versatile computational code implemented in the Material Studio (MS) software package [20]. It is known for its capacity to carry out both vacuum and solvent phase calculations on periodic and non-periodic systems using Density Functional Theory (DFT). It performs implicit solvent phase calculations by using the implemented COSMO program. The need for a speedy but accurate calculation remains a dominant challenge for every computation. In the case of DMol<sup>3</sup>/COSMO program, the adjustable parameters that dictate speed and accuracy includes the level of DFT, basis set, global orbital cut-off and COSMO segment. The performances of various basis sets and functionals on the

prediction of some physical parameters have been reported in literature [6, 21-23]. However, reports on the effect of different global orbital cut-offs and COSMO segments on DMol<sup>3</sup>/COSMO-RS calculations of physical parameters, especially solubility are still scanty. The information provided on this subject in the DMol<sup>3</sup> guide [20] is inadequate. While little effort has been made towards unveiling the effect of global orbital cut-off on DMol<sup>3</sup>/DFT calculations by some authors [21, 22], adequate information necessary to guide the selection of appropriate global orbital cut-off and COSMO segment (i.e. number of segment per atomic surface (NSPA)) for DMol<sup>3</sup>/COSMO-RS calculations is still lacking thereby giving room to a selection dilemma, misuse and unreliability of DMol<sup>3</sup>/COSMO-RS calculated results.

To address this menace, the present study investigated the effect of global orbital cut-off and COSMO segment (NSPA) variation on DMol<sup>3</sup>/COSMO-RS predicted aqueous solubility and reactivity properties of four azo dyes namely; (E)-2,2'-((4-((2-chloro-4-nitrophenyl)diazenyl)-3-methylphenyl)azanediyl)diethanol [D1], (E)-2,2'-((4-((2,4-dinitrophenyl)diazenyl)-3-methylphenyl)azanediyl)diethanol [D2], (E)-2,2'-((4-((2,6-dichloro-4-nitrophenyl)diazenyl)-3-methylphenyl)azanediyl)diethanol [D3] and (E)-2,2'-((4-((2-chloro-4,6-dinitrophenyl)diazenyl)-3-methylphenyl)azanediyl)diethanol [D4]. The molecular structures of the dyes are presented in Table 5.1 with their respective physicochemical properties [24]. Although any azo dye could be employed for this study, the selection of the set of dyes (D1, D2, D3 and D4) employed in this study is however based on availability of their experimental solubility data, which eases adequate assessment of the performance, validity and reliability of the theoretical technique adopted in this study. In addition, these dyes have structural resemblance, differing only

by one substituent and/or substituent position. Our motive with regards to the solubility study was to calculate theoretical aqueous solubility expressed in the standard solubility unit (i.e. mol/L or mg/L) from COSMO-RS data using the solubility equation proposed by Cramer *et al.* [25]. This was deemed necessary to provide a better and simpler theoretical approach for predicting aqueous solubility in standard units as opposed to the more rigorous non standard mole fraction solubility system adopted by previous COSMO-RS studies [1-3, 5].

**Table 5. 1:** Molecular structures of studied dyes and their physicochemical properties [24].

Dyes	Molecular structures	Molecular weights (g/mol)	Melting point (°C)	Experimental solubility (mg/L) in water at 25°C
D1		378.50	188	0.2
D2		389.00	189	0.5
D3		413.26	147	1.0
D4		423.50	184	0.2

The performance of the Cramer *et al.* solubility equation (CSE) [25] is compared to that of an empirical general solubility equation (GSE) proposed by Yalkowsky [26, 27] to identify which of the two equations is more suitable for COSMO-RS solubility prediction. Since the studied dyes are aminoazobenzene based dyes which are known for their tendency to form carcinogenic amine products upon degradation [28], assessment of their reactivity was therefore necessary to understand their fate in the environment. Their chemical reactivity was evaluated using some global reactivity indices such as the highest occupied molecular orbital (HOMO) and lowest unoccupied molecular orbital (LUMO) energies, HOMO-LUMO energy gap, chemical hardness and softness, electronegativity, chemical potential and electrophilicity index. These parameters, which have been successfully used for probing the reactivity of azo dyes [9, 29, 30], were calculated in both vacuum and aqueous phases to identify which of these two media favors the stability of the studied dyes. Response to change in global orbital cut-off and NSPA is also examined to identify the best/optimum cut-off and NSPA for predicting the aqueous solubility and reactivity of azo dyes.

## 5.2 COMPUTATIONAL DETAILS

The DMol<sup>3</sup> program incorporated in the Material Studio (MS) computational package [20] was employed for this study. All calculations were performed using the Becke-Perdew [31, 32] version of the Volsko-Wilk-Nusair functional [33] (VWN-BP) in conjunction with double numerical basis with polarization functions (DNP) basis set (version 4.0.0). VWN-BP is the functional recommended in the DMol<sup>3</sup> manual for COSMO-RS calculations [20]. It has been successfully used for predicting the thermodynamic phase behavior of

different sets of organic molecules [34]. DNP belongs to the class of numerical basis sets that are known for their ability to yield more accurate results at a significantly lower computational cost compared to their Pople basis set counterparts [6, 20-22, 35]. DNP also outperforms other numerical basis sets in terms of a balance between accuracy and speed and has been found as efficient for DMol<sup>3</sup> calculations [6, 20-22, 35].

The structures of the four dyes were built in the MS workspace, refined to bring them closer to their equilibrium geometries and then subjected to full optimization without symmetry constraints. The resulting equilibrium geometries were confirmed by the absence of imaginary vibrational frequencies. Since the geometry parameters and thus, minimum energy of a molecule vary from one phase to another, full geometry optimizations were performed both in the gas and aqueous phases. The optimizations were carried out at various global orbital cut-off values (3.0, 3.5, 4.5, 5.5, 6.5, 7.0 and 8.0 Å) in order to investigate the effect of orbital cut-off value.

For the COSMO-RS calculations, COSMO dielectric,  $\epsilon$  was set to 78.4 (the dielectric of water) and COSMO segment i.e. the number of surface segments per atomic sphere (NSPA) was varied between the recommended value of 92 and 1082 [6, 34].

Two different models were used for the prediction of solubility of the studied dyes in water. The models are the Cramer *et al.* solubility equation (CSE) [25] and the general solubility equation (GSE) proposed by Yalkowsky [26, 27]. The solubility values ( $S_{\text{CSE}}$  and  $S_{\text{GSE}}$ ) obtained from the two models were compared.

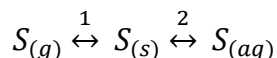
The Cramer *et al.* solubility equation expresses the solubility of a pure non-ionic solute in water ( $S_{\text{aq}}$ ) as [25]:

$$S_{\text{aq}} = \frac{P_s}{p^0} e^{-\Delta G_s^0/RT}$$

Equation 5. 1



where  $P_s$  is the equilibrium vapor pressure of the solute,  $P^0$  is ideal gas pressure at 1 molar standard state and 298 K, having numerical value of 24.45 atm,  $\Delta G_s^0$  is the standard-state aqueous free energy of solvation of the solute,  $R$  is the gas constant, and  $T$  is absolute temperature.  $\Delta G_s^0$  is the sum of standard free energy changes for the tri-phasic system:



Equation 5. 2

which represents the pure solute in equilibrium with its vapor and aqueous solution. This model is discussed in detail elsewhere [25].

The solvation free energy (SFE, denoted by  $\Delta G_s$ ) of the optimized dyes was calculated from their total energies in gas and water phases according to the following equation [20]:

$$\Delta G_s = (E + \Delta G_{NSE}) - E^0$$

Equation 5. 3

where  $E$  is the total energy of the molecule in the solvent phase (COSMO energy),  $\Delta G_{NSE}$  is the non-electrostatic contribution to SFE due to dispersion and cavity formation effects and  $E^0$  is the total energy of the molecule in gas phase. Values of  $\Delta G_{NSE}$  are produced along with the total COSMO energy in the COSMO output. COSMO-RS calculations also produced calculated vapour pressure of the molecule. Therefore, the CSE predicted aqueous solubility ( $S_{CSE}$ ) values of the dyes were obtained using equation 5.1.

The GSE predicted solubility ( $S_{GSE}$ ) values of the dyes were obtained according to the equation [26]:

$$\text{Log } S = 0.5 - 0.01(m.p^0C - 25) - \text{Log } P$$

Equation 5. 4

where  $S$  is the solubility,  $\text{Log } P$  is the octanol-water partition coefficient (obtained from COSMO-RS calculations),  $m.p^0C$  is the melting point of the solute in degree celsius (*vide*

*supra* Table 5.1), 0.5 is the excess of the base ten logarithm of the calculated solubility value over that of the experimental value for a solid or liquid rigid nonelectrolyte, 0.01 is the approximated entropy of fusion constant and 25 is the constant room temperature (in degree celsius) [27].

The polarizability,  $\alpha$  of the dyes was determined from the COSMO-RS calculated vapour pressure,  $p$  using the Liang and Gallagher equation [36]:

$$\text{Log } p = -0.401\alpha + 3.940$$

**Equation 5. 5**

The reactivity indices were calculated from the HOMO and LUMO energies using equations 5.6 to 5.10 [29, 30, 37-46].

$$\text{Global hardness } (\eta) = -\frac{1}{2}(E_{HOMO} - E_{LUMO})$$

**Equation 5. 6**

$$\text{Global softness } (\sigma) = \frac{1}{\eta} = -2/(E_{HOMO} - E_{LUMO})$$

**Equation 5. 7**

$$\text{Electronegativity } (\chi) = -\frac{1}{2}(E_{HOMO} + E_{LUMO})$$

**Equation 5. 8**

$$\text{Chemical potential } (\mu) = -\chi = \frac{1}{2}(E_{HOMO} + E_{LUMO})$$

**Equation 5. 9**

$$\text{Global electrophilicity index } (\omega) = \frac{\chi^2}{2\eta}$$

**Equation 5. 10**

## 5.3 RESULTS AND DISCUSSIONS

### 5.3.1 AQUEOUS SOLUBILITY STUDY

Table 5.2 compares the best calculated  $S_{CSE}$  and  $S_{GSE}$  averages obtained for the studied dyes with their respective experimental solubility at 25 °C. The averages were calculated as the sum of solubility values obtained across all NSPA studied divided by the number of NSPA (Appendices: Tables A.1 – A.4). The table revealed that the most comparable  $S_{CSE}$  average to experimental data was obtained at a cut-off of 5.5 Å for D1, 4.5 Å for D2, 3.5 Å for D3 and 3.0 Å for D4. These cut-off values yielded average  $S_{CSE}$  values of 0.09 mg/L, 0.53 mg/L, 0.98 mg/L and 0.25 mg/L for D1, D2, D3 and D4, respectively. Selection of the best cut-off value was not only based on the size of the average but also on the general performance of the cut-off across all NSPA studied. This is why 4.5 Å was selected instead of 7.0 Å as the best cut-off for D2 despite the latter giving a lower average  $S_{CSE}$  of 0.50 mg/L (Appendices: Table A.2). The  $S_{CSE}$  values are generally in good agreement with the experimental values.

**Table 5. 2:** Comparison of the best  $S_{CSE}$  and  $S_{GSE}$  results obtained for D1, D2, D3 and D4 with their respective experimental solubility ( $S_{Expt.}$ ) at 25 °C.

Dyes	Mwt. (g/mol)	$S_{Expt.}$ (mg/L)	Log $S_{Expt.}$ (mol/L)	$S_{CSE}$ cut-off (Å)	$S_{CSE}$ (mg/L)	Log $S_{CSE}$ (mol/L)	$\frac{\text{Log } S_{CSE}}{\text{Log } S_{Expt}}$	$S_{GSE}$ cut-off (Å)	$S_{GSE}$ (mg/L)	Log $S_{GSE}$ (mol/L)	$\frac{\text{Log } S_{GSE}}{\text{Log } S_{Expt}}$
D1	378.50	0.20	-6.28	5.5	0.09	-6.62	1.05	5.5	0.10	-6.58	1.05
D2	389.00	0.50	-5.89	4.5	0.53	-5.87	1.00	4.5	0.68	-5.76	0.98
D3	413.26	1.00	-5.62	3.5	0.98	-5.62	1.00	5.5	0.12	-6.54	1.16
D4	423.50	0.20	-6.33	3.0	0.25	-6.23	0.98	4.5	0.20	-6.33	1.00

Inspection of the results in Table 5.2 showed that the best cut-off for the  $S_{CSE}$  also produced reasonable  $S_{GSE}$  values for D1 and D2. This was however, not the case with D3 and D4 where the  $S_{GSE}$  values are much smaller than the experimental at the cut-off values (i.e. 3.5 Å and 3.0 Å) adjudged best for their respective  $S_{CSE}$  results (Appendices: Tables A.3 and A.4). Possible explanation for this discrepancy is the inability of the lower cut-off values to adequately estimate the partition coefficient ( $\text{Log } P$ ) of D3 and D4 probably due to their larger weights because at higher orbital cut-off, the GSE yielded better solubility values especially for D4 at 4.5 Å. The  $S_{GSE}$  for D3 was also enhanced by cut-off increase to an average value of 0.12 mg/L at a cut-off of 5.5 Å beyond which there was no significant change in the solubility. This suggests that the maximum obtainable  $S_{GSE}$  value for D3 is 0.12 mg/L which is largely deviated from experimental value. However, base ten logarithm in mol/L of this value is just about 1.16 times that of the experimental value of the same unit (i.e.  $\text{Log } S_{GSE} = 1.16 \text{ Log } S_{\text{Expt}}$  (Table 5.2)) which is still in the range of allowed values for compounds containing polarizable groups [47, 48]. The  $\text{Log } S_{GSE}$  values for D1, D2 and D4 are 1.05  $\text{Log } S_{\text{Exp}}$ , 0.98  $\text{Log } S_{\text{Expt}}$  and 1  $\text{Log } S_{\text{Expt}}$  respectively which justify the strong agreement between their calculated  $S_{GSE}$  values and their respective experimental values (Table 5.2).

Since for all the studied dyes, the minimum cut-off value which gave reliable  $S_{GSE}$  as evident from Table 5.2 was 4.5 Å, it can therefore be deduced that a cut-off value  $\geq 4.5$  Å should be selected for the calculation of  $\text{Log } P$  and hence solubility of a non-ionic solute when using the GSE. However, the choice of cut-off for solubility prediction using the CSE seems to be sensitive to the molecular size. The results presented in Table 5.2 revealed that the size of the best cut-off for CSE decreases with increasing molecular size of the

dyes. In other words, CSE required 5.5 Å and 4.5 Å for D1 (378.50 g) and D2 (389.00 g), respectively whereas the required cut-off for D3 (413.26 g) and D4 (423.50 g) are 3.5 Å and 3.0 Å, respectively. The possible factor responsible for this trend will be discussed in later sections.

Recalling that the CSE relies completely on the theoretical data of this work as opposed to the GSE which has an experimental term (i.e. melting point), it is interesting to see that the CSE did not only compete well with the GSE in reproducing the experimental solubility of D1 at the same cut-off of 5.5 Å but even outperformed the GSE in the case of D2 at 4.5 Å (Table 5.2). At a different cut-off value though, the CSE also predicted the solubility of D3 better than the GSE, while both models agree well with the experimental value in the case of D4.

### 5.3.2 EFFECT OF ORBITAL CUT-OFF VARIATION

The performances of the CSE and the GSE are compared in Figure 5.1 in terms of their capacity to reproduce the experimental solubility and their response to orbital cut-off variation. The figure illustrates the variation of  $\text{Log } S_{\text{CSE}}$  and  $\text{Log } S_{\text{GSE}}$  values with orbital cut-off for D1, D2, D3 and D4. For all the dyes, the  $S_{\text{GSE}}$  values increased with increasing orbital cut-off contrary to the irregular trend shown by  $S_{\text{CSE}}$ . This difference is not unexpected since the values were obtained using different equations which are governed by different theoretical parameters. In this work, the theoretical variable that dictate the accuracy of the GSE results is the octanol-water partition coefficient,  $\text{Log } P$ . According to equation 5.4, the bigger the magnitude of  $\text{Log } P$ , the smaller the  $S_{\text{GSE}}$  value will be. This

confirmed by the opposing trend shown by  $\text{Log } P$  and  $\text{Log } S_{\text{GSE}}$  with respect to cut-off in Figure 5.2.

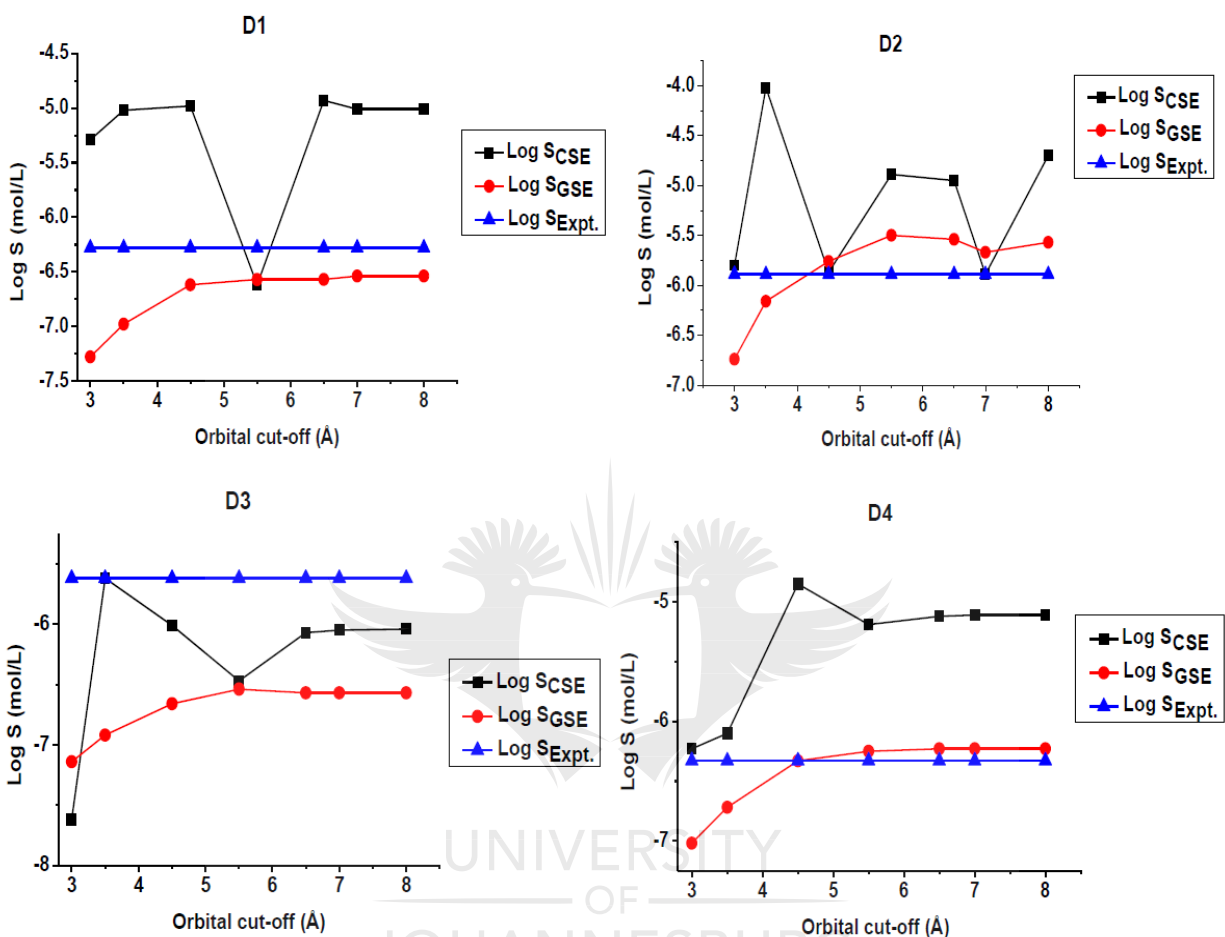


**Figure 5. 1:** Base ten logarithm of the aqueous solubility values for D1, D2, D3 and D4 as a function of orbital cut-off.

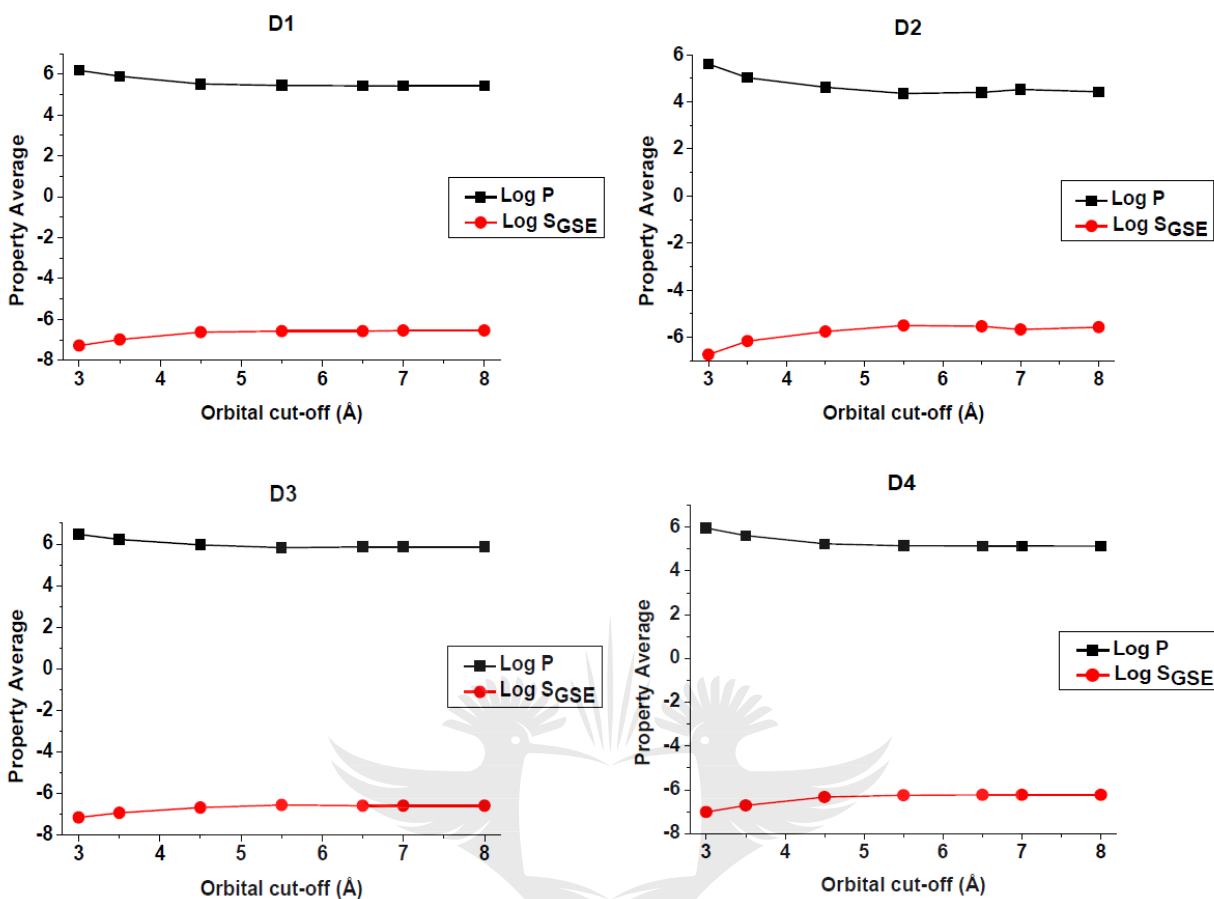


**Figure 5. 2:** Log S<sub>GSE</sub> and Log P for D1, D2, D3 and D4 as a function of orbital cut-off.

In the case of CSE the accuracy of the results is governed by both solvation free energy (SFE) and vapor pressure. Therefore, the magnitude of the S<sub>CSE</sub> depends on the relative changes in both parameters as the cut-off increases. Assessment of Figure 5.3 showed that the vapor pressure generally decreased downward with increasing cut-off to a point of saturation at 5.5 Å beyond which further changes become insignificant. This was not the case for SFE whose magnitude depends on both gas and aqueous phase absolute energies (equation 5.3). The fact that there was no further change in vapor pressure from cut-off 5.5 Å upward suggests why this cut-off is the recommended value for DMol<sup>3</sup>/COSMO-RS calculations [20].

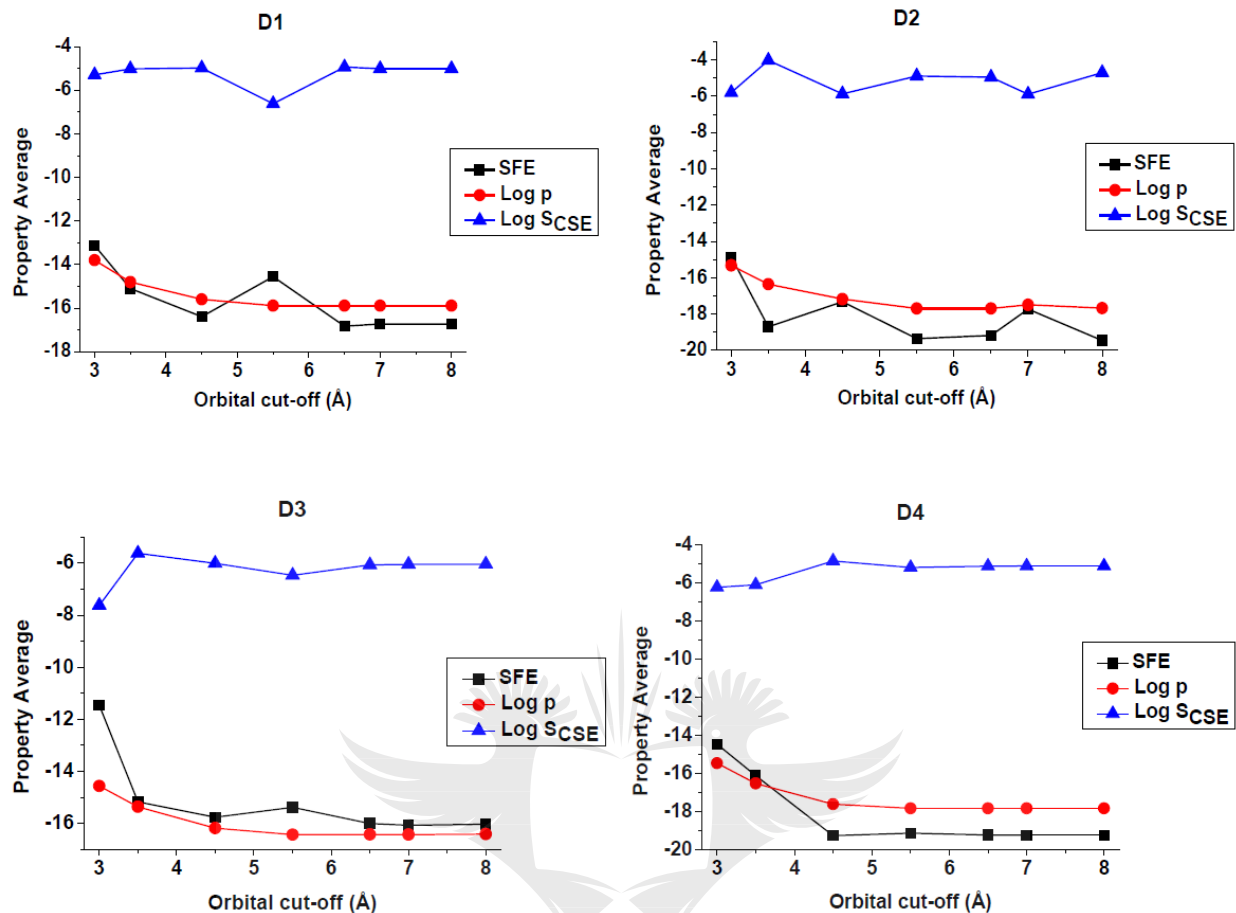


**Figure 5. 3:** Solvation free energy, vapor pressure (Log p) and Log Sc<sub>CSE</sub> for D1, D2, D3 and D4 as a function of orbital cut-off.

For aqueous solubility determination using the CSE, five key deductions can be made from Figure 5.3 on how the changes in SFE and vapor pressure determine the result. First, a largely negative SFE with a low vapor pressure produces a large Sc<sub>CSE</sub> value. This is evident at cut-off 3.5 Å and 4.5 Å in D1, 3.5 Å in D2 and 4.5 Å in D4. Second, a less negative SFE with a low vapor pressure leads to a small Sc<sub>CSE</sub> value. This can be seen at cut-off 5.5 Å in D1, 4.5 Å and 7.0 Å in D2, and 3.5 Å in D4. Third, a large increase in the negative SFE against a constant vapor pressure produces a large Sc<sub>CSE</sub> value as can be observed at cut-off 6.5 Å and above in D1, 5.5 Å, 6.5 Å and 8.0 Å in D2 and 5.5 Å and



above in D4. Fourth, a small increase in SFE magnitude accompanied by a large decrease in vapor pressure resulted in a low  $S_{CSE}$ . This is the case with D3 at cut-off 3.5 Å and above. Fifth, a less negative SFE with a large vapor pressure also results in a low  $S_{CSE}$ . This is obvious in D2, D3 and D4 at cut-off 3.0 Å. Generally for every cut-off value, the bigger the negative SFE produced, the smaller the corresponding vapor pressure and vice versa. Hence, the most appropriate cut-off for estimating solubility using the CSE is the one that neither overestimates the negative SFE nor underestimates the vapor pressure. These cut-off values are 5.5 Å for D1, 4.5 Å for D2, 3.5 Å for D3 and 3.0 Å for D4 (Table 5.2).

The absolute energies of the dyes in gas and aqueous phases relative to cut-off (Appendix: Table A.5) reveals the cause of the indefinite trend of SFE with cut-off. The aqueous phase energies presented in Table A.5 (Appendix) have been corrected for dispersion and cavity formation effects before they were used to determine the SFE through equation 5.3. For D1 and D2, careful inspection of the table revealed that the aqueous phase energy decreased downwards with increasing cut-off size up to 6.5 Å for D1 and 7.0 Å for D2, beyond which further changes are insignificant. This suggests that the optimum cut-off values for obtaining the aqueous phase (COSMO) energy of D1 and D2 are 6.5 Å and 7.0 Å, respectively. Unfortunately for D1, these optimum cut-off values and higher ones overestimated the gas phase energy compared to 5.5 Å hence their larger negative SFE (Fig. 5.3). The lowest gas phase energy was obtained for D1 at 5.5 Å which also predicted a reasonable aqueous phase energy. However, in the case of D2, the optimum cut-off also gave the lowest energy gas phase geometry. Since accurate SFE calculation depends on accurate description of solvation which in turn depend on

accurate gas phase geometry, the cut-off that yielded the most stable gas phase geometry of a solute is the more appropriate cut-off which is 5.5 Å for D1 and 7.0 Å for D2. These cut-off values reproduced the experimental solubility values very well with the CSE (Fig. 5.1). It should however be noted from Table A.5 (Appendix) that, cut-off 4.5 Å which is selected as the best  $S_{CSE}$  cut-off for D2 (Table 5.2) did not give the lowest gas and aqueous phase energies as 7.0 Å because the best cut-off for SFE may not necessarily produce the best  $S_{CSE}$  value as this also depends on the vapor pressure.

A similar trend of energy decrease was observed in D3 both in the gas and aqueous phases (Appendix: Table A.5). However, in this case, the changes in the absolute energies are relatively small especially at 4.5 Å and above. The difference between the highest and the lowest SFE average obtained with 3.5 Å and 7.0 Å, respectively is just 0.9 kcal/mol (Fig. 5.3, Appendix: Table A.3). This suggests the possibility of all the cut-off values excluding 3.0 Å which grossly underestimated the results, to predict close  $S_{CSE}$  values depending on their vapor pressure as confirmed by the Log  $S_{CSE}$  values for D3 in Figure 5.3. Inspection of Table A.5 (Appendix) for D4 also revealed a continuous decrease of the absolute energies both in the gas and aqueous phases as the cut-off increased downward. Therefore, the cut-off value of 7.0 Å which gave the lowest gas and aqueous phase energies is expected to yield the best  $S_{CSE}$  average if its predicted vapor pressure value is sufficiently large. This is however, not the case as evident from Figure 5.1 where the cut-off value that produced the best  $S_{CSE}$  values was found to be 3.0 Å because it predicted appropriately both the vapor pressure and SFE. We therefore concluded that the best cut-off value for solubility calculation using the CSE is the one

that yielded the right combination of SFE and vapor pressure for each dye. No general rule is available yet to identify this cut-off however, there are indications from our findings that this cut-off is sensitive to molecular size as previously mentioned.

We therefore recommend based on our findings that a cut-off  $\leq 3.0$  Å should be used with the CSE for solutes of molecular weight greater than 420 g/mol whereas a cut-off range from 3.1 Å to 3.5 Å should be selected for molecular weights between 400 g/mol to 420 g/mol. A cut-off value of 4.5 Å should be appropriate for solutes of molecular weights in the region of 385 g/mol to 395 g/mol while a 5.5 Å should be sufficient for molecular weights around 370 g/mol to 380 g/mol. Molecular weights below 370 g/mol may require the use of higher cut-off values. Investigation of this possibility is currently in progress.

### 5.3.3 EFFECT OF NSPA (COSMO SEGMENT) VARIATION

To investigate the effect of varying NSPA on DMol<sup>3</sup>/COSMO-RS results and hence on CSE and GSE predicted aqueous solubility, the NSPA was varied beyond the recommended value of 92 [20]. The NSPA studied are 92, 272 (*ca*  $3 \times 92$ ), 362 (*ca*  $4 \times 92$ ), 482 (*ca*  $5 \times 92$ ), 482 (*ca*  $7 \times 92$ ) and 1082 (*ca*  $12 \times 92$ ) which have all been parameterized for DMol<sup>3</sup>/COSMO-RS calculation [20].

For all the dyes, the response of the calculated solubility values to change in NSPA is virtually the same across all cut-off values except at 3.0 Å for D1 (Appendices: Table A.1) and the few outlying values observed with D2 (Appendices: Table A.2) due to overestimation by some of the cut-off values. Therefore, our discussion of the NSPA effect is based only on the best cut-off value for each dye. Figures 5.4a and 5.4b show the variation of the best Log  $S_{CSE}$  and Log  $S_{GSE}$  values with NSPA. Inspection of the

figures revealed a very low sensitivity of Log  $S_{CSE}$  and Log  $S_{GSE}$  to change in NSPA. In other words, the popularly known NSPA of 92 was found to produce  $S_{CSE}$  and  $S_{GSE}$  values which do not change significantly at higher NSPA, suggesting that this recommended NSPA is truly sufficient for DMol<sup>3</sup>/COSMO-RS.

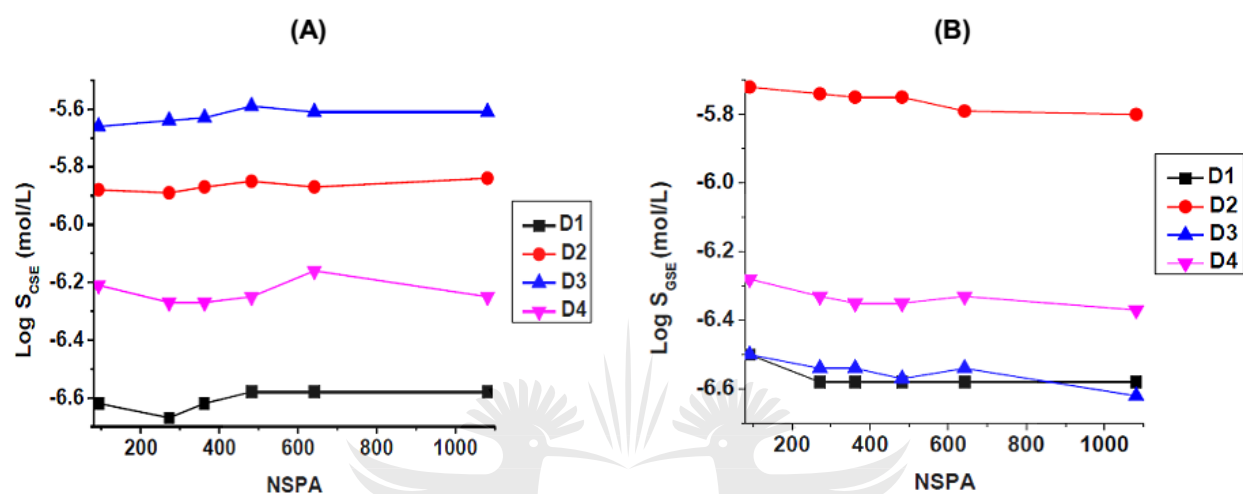


**Figure 5. 4:** Best Log  $S_{CSE}$  (A) and Log  $S_{GSE}$  (B) values obtained for D1, D2, D3 and D4 as functions of NSPA.

It is important to also examine the trend of some solvation related properties with respect to cut-off and NSPA variation as this will further reveal the effect of these adjustable parameters on DMol<sup>3</sup>/COSMO-RS results. These properties include the screening charge, the dipole moment and the polarizability. The screening charge ( $q$ ) is the most essential microscopic property of a solute molecule used in COSMO-RS calculations. It is the tool with which the COSMO program measures the extent of solvation of a solute when embedded in a perfect conductor (solvent). The larger the magnitude of  $q$ , the more the screening, the better the solvation and the lower the COSMO energy, and vice versa. Dipole moment,  $\mu$ , is a quantity that gives insight on the extent of solute polarity. A large  $\mu$  indicates high polarity while low polarity is implied by small  $\mu$  value. Polarizability,  $\alpha$ , is

a property that reveals the response of a molecule to the application of an electric field (solvent in this case). That is, the change in polarity of a molecule upon interaction with an electric field. The larger the value, the better the interaction, the higher the polarity and the more favorable the solvation experienced by the molecule. The variation of the screening charges, dipole moments and polarizabilities of the studied dyes with NSPA at each cut-off value are shown in Figures 5.5, 5.6 and 5.7, respectively.

It is clear from Figure 5.5 that the magnitude of the negative screening charge increased with cut-off up to 6.5 Å beyond which further cut-off increase brought no significant change in the charge magnitude. This is in agreement with trend of aqueous phase absolute energies presented in Table A.5 (Appendix). In the direction of increasing NSPA, there was also an initial increase in the charge magnitude from 92 to 362 segments after which the magnitude decreased continuously at NSPAs 482, 642 and 1082. This suggests that a total 362 surface segments per atom described the solvation of the dyes better than the other NSPAs as confirmed by the lowest aqueous phase energies obtained with the same NSPA at virtually all the cut-offs studied (Appendix: Table A.5).

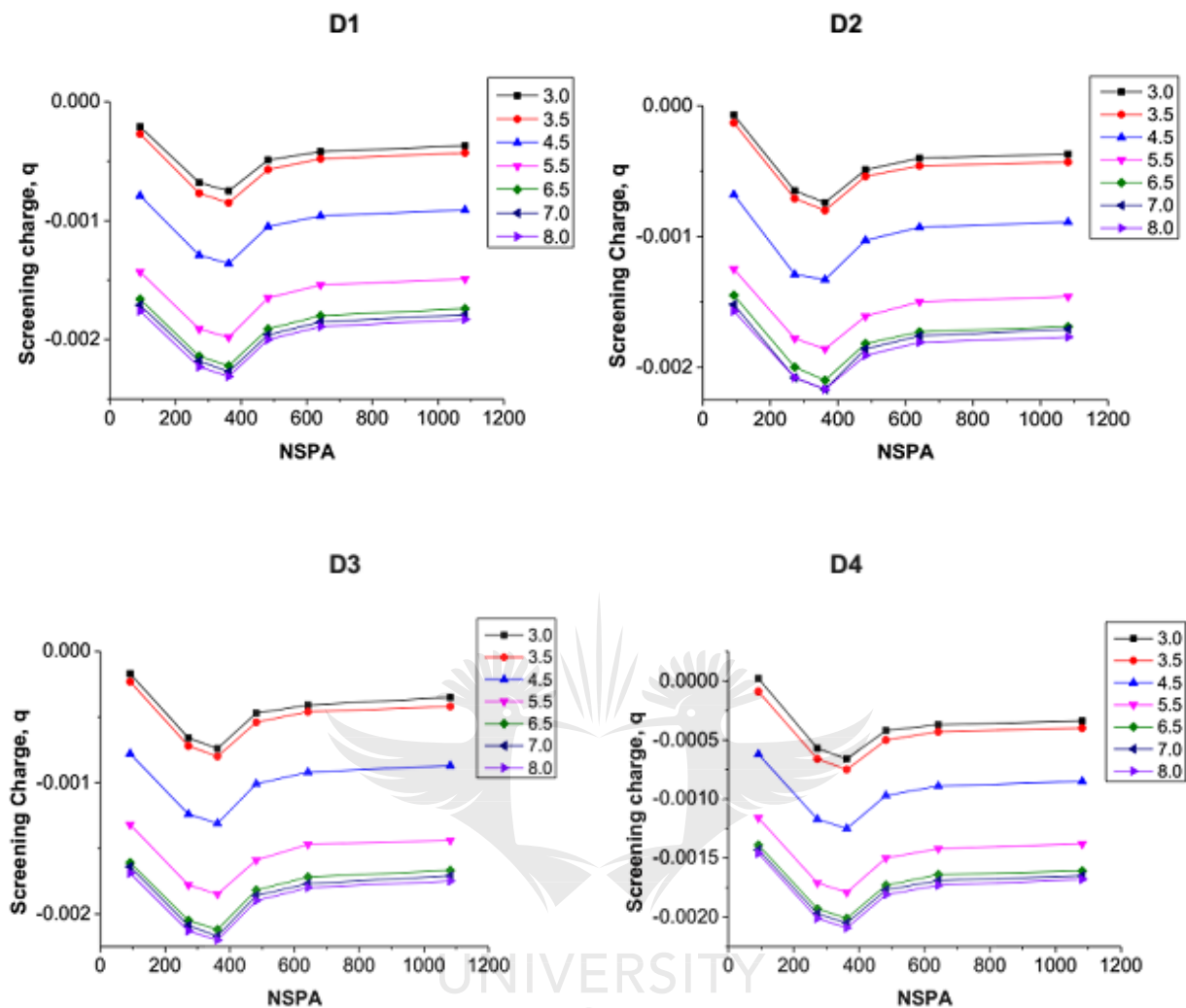


**Figure 5. 5:** COSMO screening charges for D1, D2, D3 and D4 as a function of NSPA.

Figure 5.6 revealed that the dyes are more polar in the aqueous phase due to the increase in dipole moment as they transitioned from the gas phase to the aqueous phase. This is also in conformity with the absolute energy trend given in Table A.5 (Appendix). On average, the dipole moment showed a low sensitivity to change in NSPA, while cut-off variation seemed to produce a similar effect on both the gas phase dipole moment and  $\text{Log } S_{\text{CSE}}$  values as can be observed from comparison of Figures 5.3 and 5.6 at the best cut-off values as 5.5 Å for D1, 4.5 Å and 7.0 Å for D2, 3.5 Å for D3 and 3.0 Å for D4. This points to the reliability of gas phase dipole moment calculation as a tool for predicting solvation and

hence, solubility. The slight disagreement observed between the aqueous phase dipole moment and the Log S<sub>CSE</sub> values are due to overestimation in the aqueous phase by some cut-off values such as 5.5 Å for D1 and 3.0 Å in the case of D3 (Fig. 5.6). For all the dyes, the highest aqueous phase dipole moment was obtained at a cut-off value of 5.5 Å beyond which there was a slight drop in dipole moment. This could also explain why 5.5 Å is the recommended cut-off value for DMol<sup>3</sup>/COSMO-RS calculations as pointed out earlier.

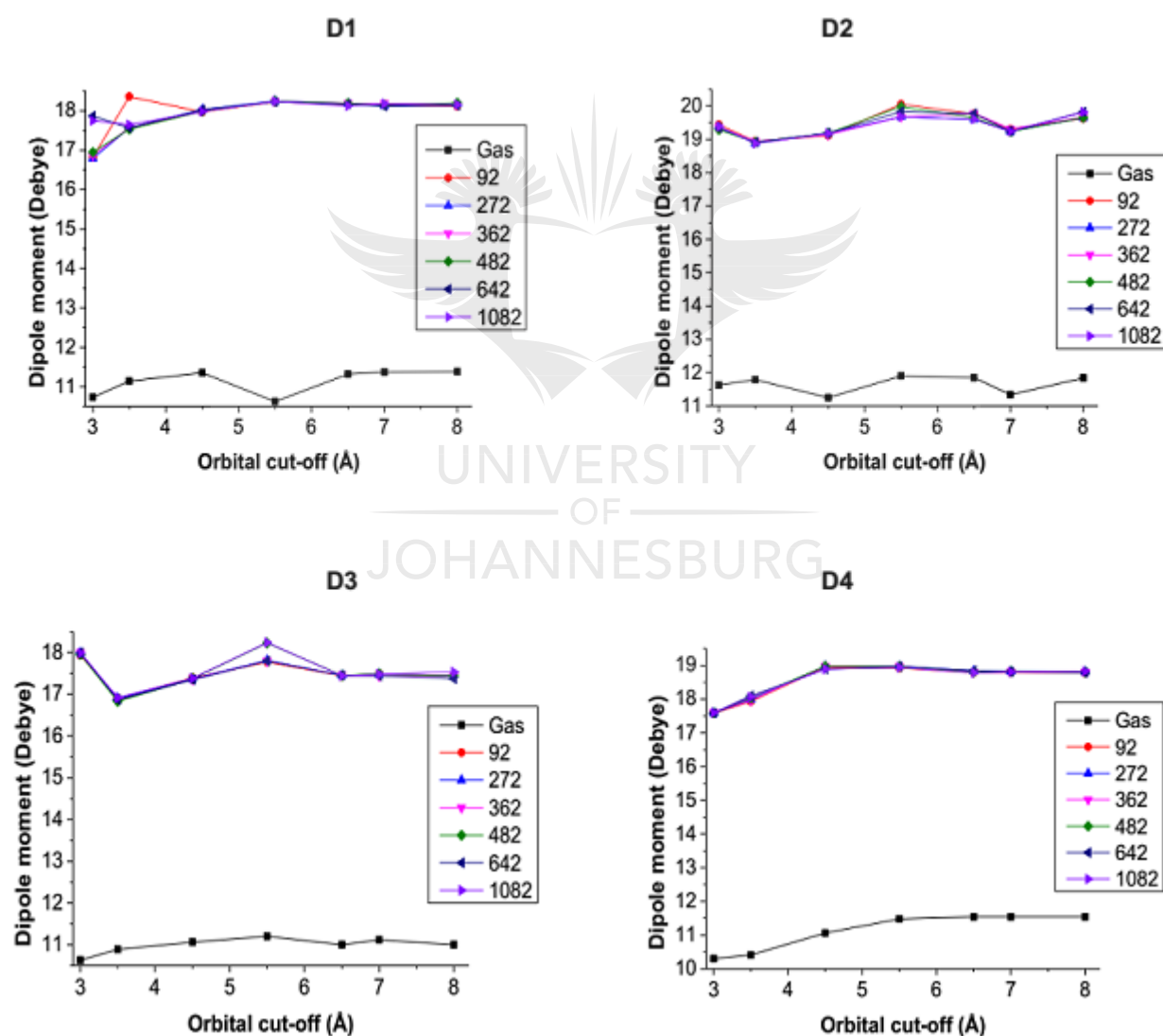
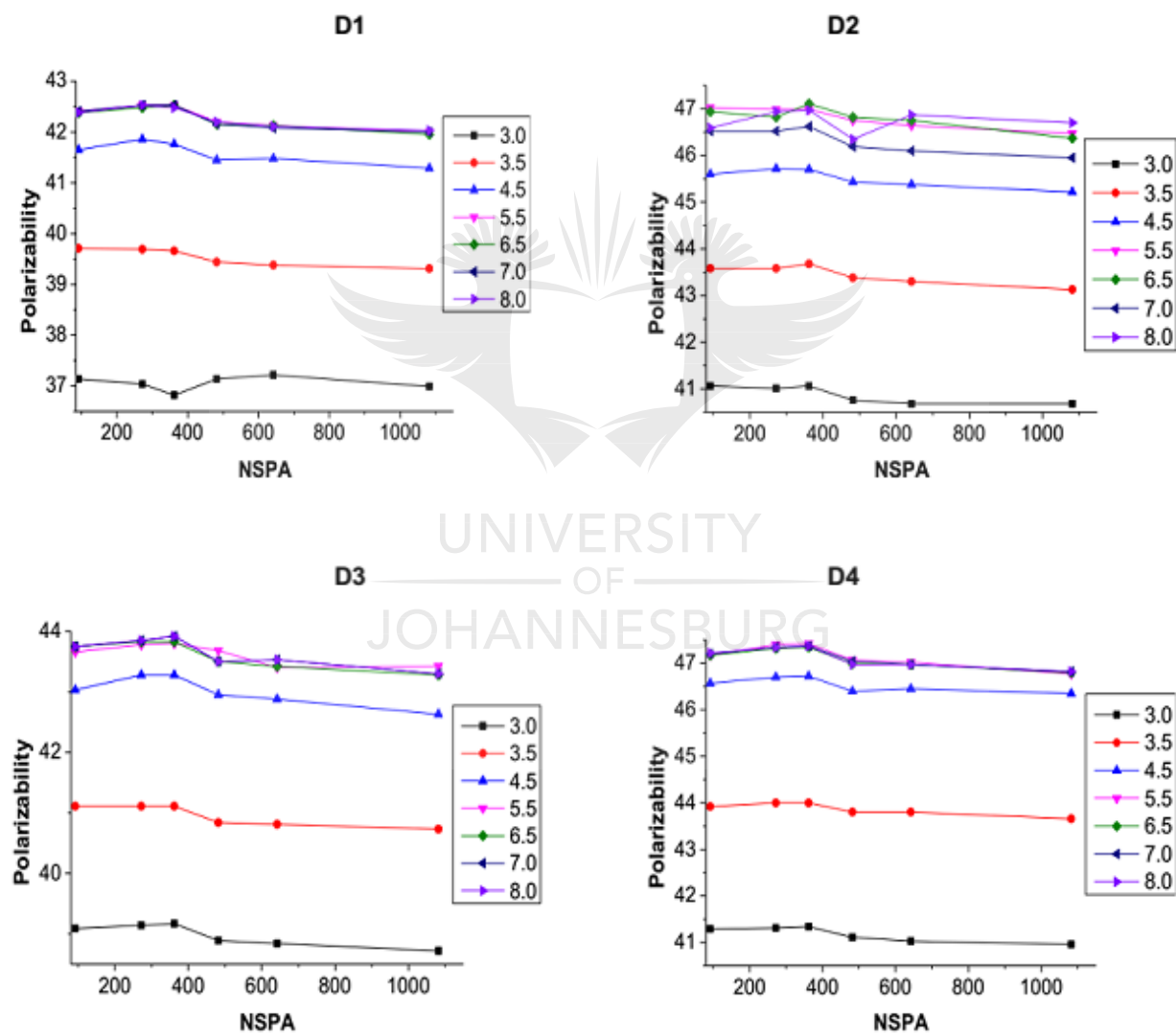


Figure 5. 6: Dipole moments for D1, D2, D3 and D4 as a function of Orbital cut-off.

In the direction of increasing cut-off, the polarizability of the dyes increases to an optimum value at a cut-off of 5.5 Å beyond which further changes are insignificant (Fig. 5.7). This confirms 5.5 Å as being sufficient for describing the interaction of the dyes with the solvent (water). Increasing NSPA values does not bring about a marked change in polarizability suggesting that the lower NSPA values are sufficient for the solvent phase calculation.



**Figure 5. 7:** Calculated polarizability values for D1, D2, D3 and D4 as a function of NSPA.



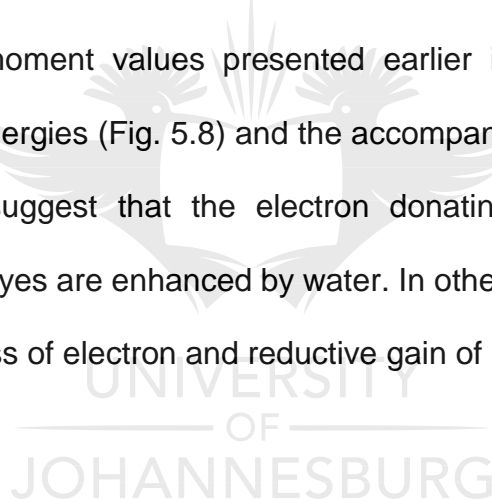
### 5.3.4 CHEMICAL REACTIVITY STUDY

The studied dyes belong to the class of azo dyes which are potential generators of carcinogenic amine molecules upon degradation. Appraisal of their reactivity was therefore necessary to expose their fate in the environment as this can promote better environmental management practice. Since water is an essential part of the environment which supports life, the reactivity of the dyes was studied both in the gas and aqueous phases to compare their stability in both media. It was also deemed necessary to investigate the effect of varying orbital cut-off and NSPA as this is expected to provide the necessary guide on the choice of these parameters for future reactivity studies that will be employing the service of the DMol<sup>3</sup> computational program. The reactivity of the studied dyes were evaluated in terms of some quantum chemical reactivity indices which include HOMO and LUMO energies, HOMO-LUMO energy gaps, global hardness and softness, electronegativity, chemical potential and global electrophilicity index.

The HOMO is an important reactivity index which reveals the portion of a molecule with the highest vulnerability to electron loss, while the LUMO shows the part of a molecule with the highest potency towards an incoming electron. The higher the HOMO energy, the greater the chance of electron donation and the lower the LUMO energy, the more the likelihood of accepting electron. The HOMO – LUMO energy gap,  $E_g$  is another essential reactivity parameter which reveals the overall stability of a molecule. The smaller the energy gap, the higher the reactivity and the larger the energy gap, the higher the stability. Global hardness,  $\eta$ , is a reactivity index that shows the resistance capacity of a molecule to a change in electron density or ground state electronic configuration while global softness,  $\sigma$ , reveals a molecule's vulnerability to such a change. The higher

the size of  $\eta$ , the more stable is a molecule and the higher the magnitude of  $\sigma$ , the more reactive the molecule. Electronegativity,  $\chi$ , describes the tendency of a molecule to pull an electron towards itself while chemical potential,  $\mu$ , reveals the ability to lose electrons from the occupied orbitals. The global electrophilicity,  $\omega$ , index describes the potency of a molecule towards an incoming electron. A high  $\omega$  value indicates a good electrophile while small value of  $\omega$  implies a good nucleophile.

The results in Figures 5.8 – 5.10 generally revealed that the studied dyes are more reactive in aqueous medium compared to vacuum. This could be due to the increased polarity of the dyes as a result of their interaction with water as confirmed by their larger aqueous phase dipole moment values presented earlier in Figure 5.6. The higher aqueous phase HOMO energies (Fig. 5.8) and the accompanying lower LUMO energies (Fig. 5.9), respectively suggest that the electron donating and electron accepting capacities of the studied dyes are enhanced by water. In other words, the dyes are more prone to both oxidative loss of electron and reductive gain of electron in water.



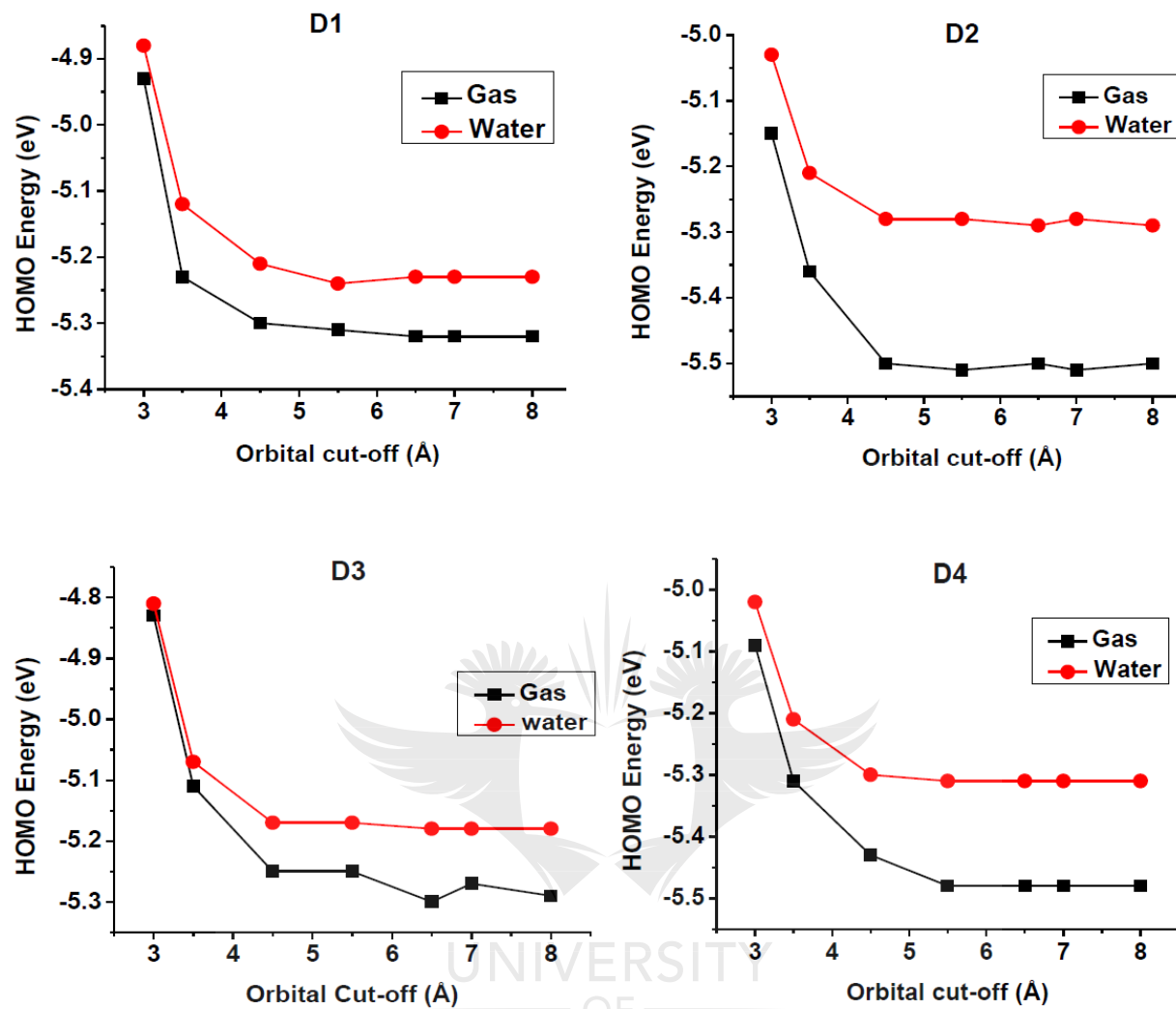


Figure 5. 8: HOMO energy as a function of orbital cut-off.

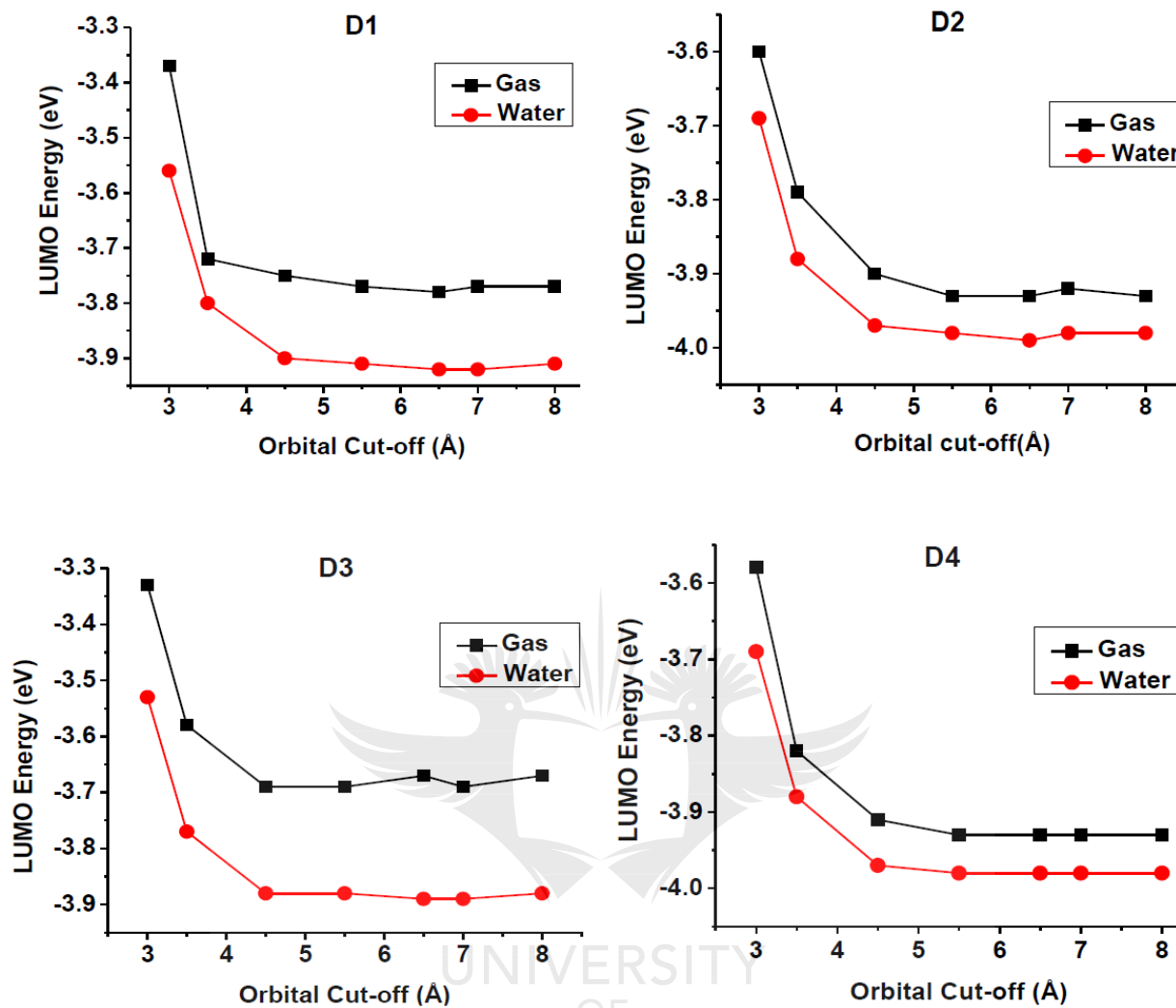
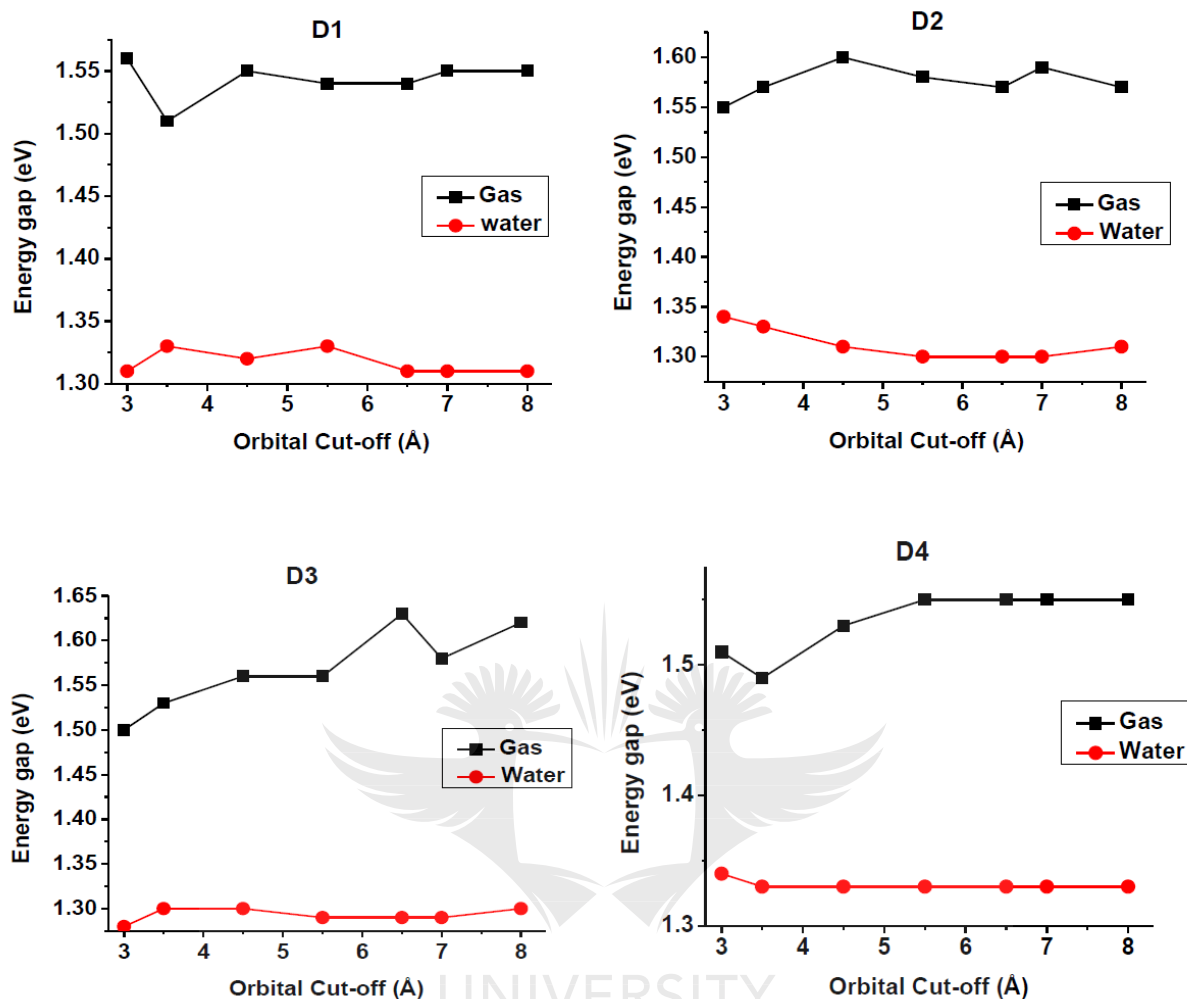


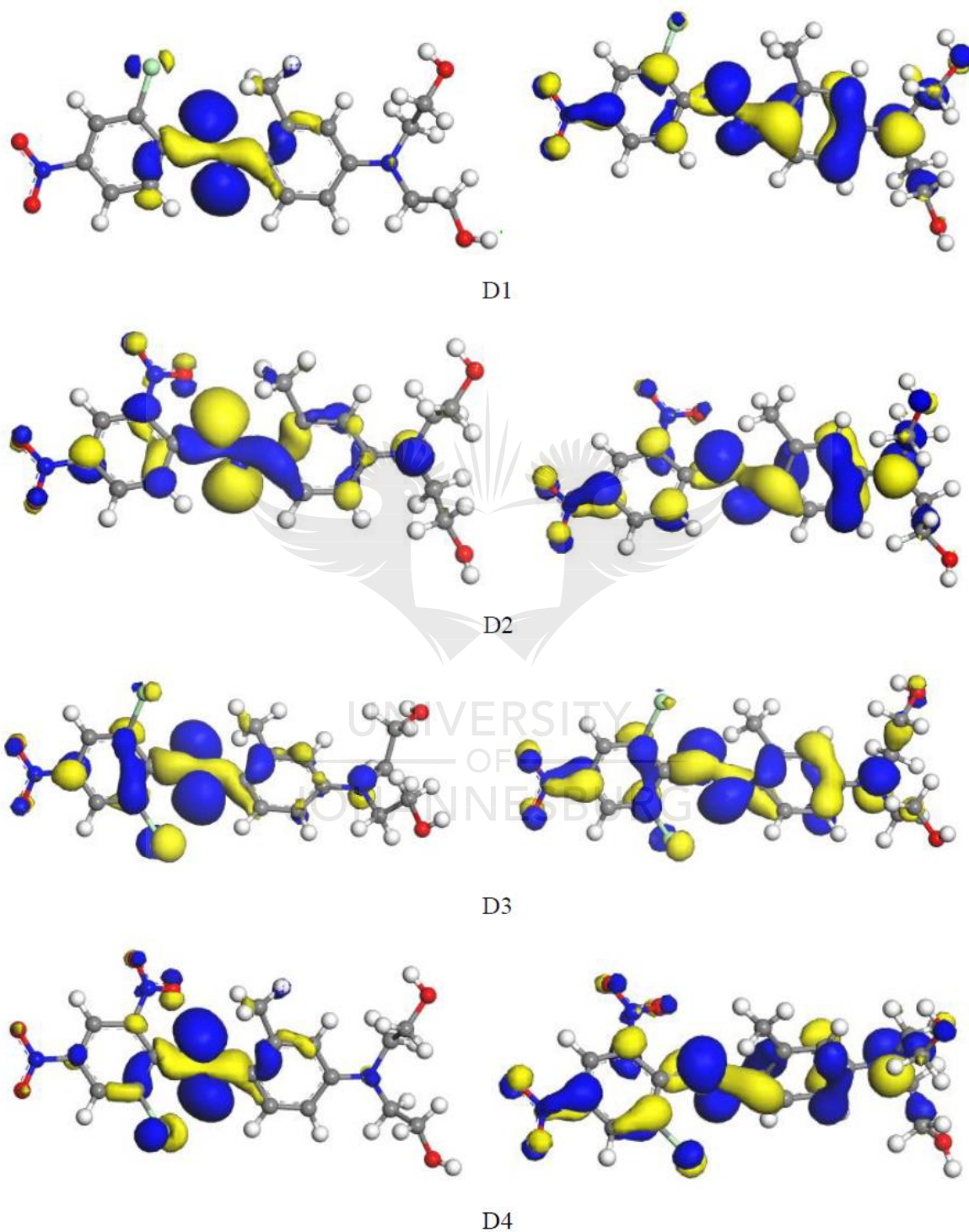
Figure 5. 9: LUMO energy as a function of orbital cut-off.



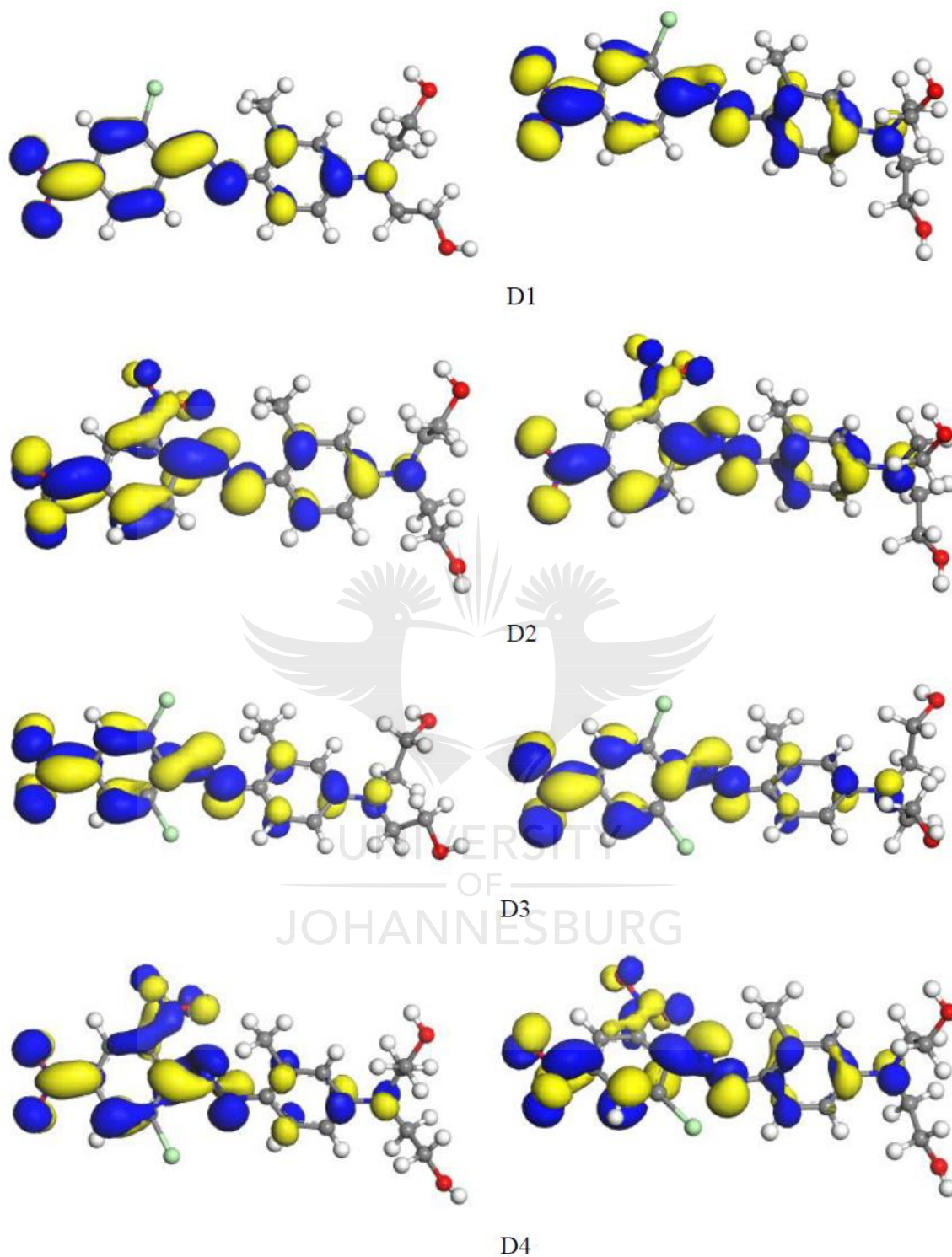
**Figure 5. 10:** HOMO-LUMO energy gap as a function of orbital cut-off.

Photo-catalytic degradation of the dyes which relies largely on favorable interactions between the dyes and a catalyst will consequently be promoted in aqueous environment. In the presence of water, the dyes can donate electron(s) more readily to the metal atom of the catalyst due to their higher aqueous phase HOMO energy (Fig. 5.11). At the same time they can also accept donated electron(s) from the catalyst due to their lower aqueous phase LUMO energies (Fig. 5.12) thereby forming a strong interaction which leads to degradation. Figures 5.11 and 5.12 revealed a general increase in the frontier molecular

orbitals (FMOs) electron density distribution in aqueous phase compared to the gas phase. This might be responsible for the increased activity of the dyes in aqueous phase.



**Figure 5. 11:** Isosurfaces of the HOMOs of D1, D2, D3 and D4 in gas (left) and water (right) taken at isovalue of 0.03.



**Figure 5. 12:** Isosurfaces of the LUMOs of D1, D2, D3 and D4 in gas (left) and water (right) taken at isovalue of 0.03.

The smaller aqueous phase HOMO-LUMO energy gap values generally showed that the dyes are less stable in water compared to gas suggesting a higher probability to degrade faster in the former. This is further supported by their smaller aqueous phase hardness and the corresponding higher softness values (Appendix: Tables A.6 – A.9). Similarly, the lower aqueous phase electronegativity values observed in the tables and the accompanying higher chemical potential suggests a greater electron releasing power in water. Finally, the aqueous phase electrophilicity index values are indications of increased potency towards a nucleophilic attack.

In the direction of increasing cut-off, the HOMO-LUMO energy gap (Fig. 5.10), the global hardness and the softness (Appendix: Tables A.6 – A.9) showed no substantial change especially in the aqueous phase. However, the HOMO and LUMO energies (Figs. 5.8 and 5.9), and the chemical potential decreased while electronegativity, and electrophilicity index increased in the same direction up to a cut-off value of 4.5 Å beyond which further cut-off increase yielded no significant changes in the parameters (Appendix: Tables A.6 – A.9). This suggests that a minimum cut-off value of 4.5 Å should be selected for a DMol<sup>3</sup>/DFT investigation of molecular reactivity.

Figure 5.13 and Tables A.6 – A.9 (Appendix) revealed that the reactivity predictors are insensitive to a change in NSPA. This implies that there is no link between the reactivity parameters and NSPA.



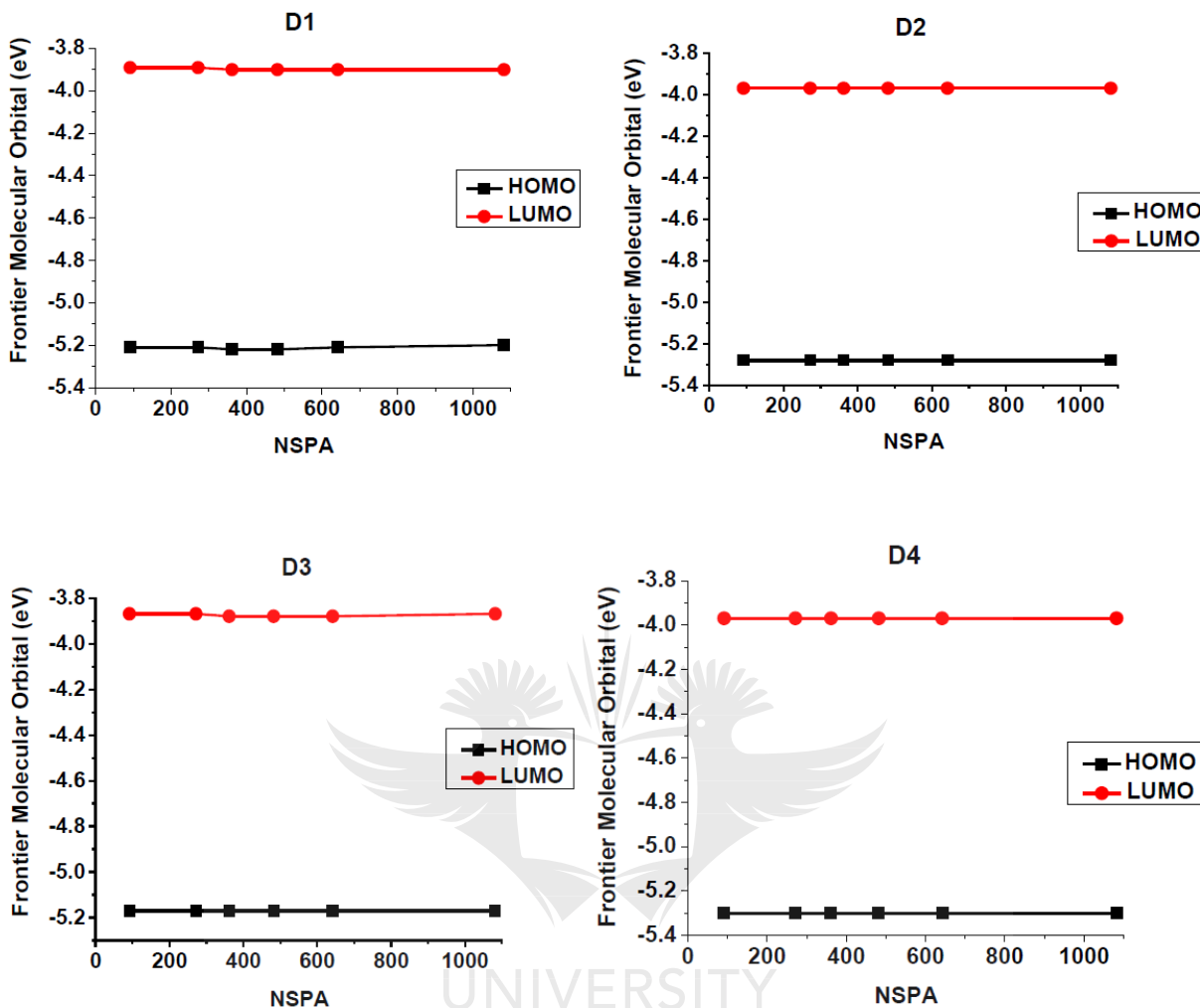


**Figure 5. 13:** Aqueous phase frontier molecular orbitals of the dyes as a function of NSPA at a cut-off value of 4.5 Å.

### 5.3.5 EFFECTS OF NO<sup>2-</sup> AND Cl<sup>-</sup> SUBSTITUENTS ON SOLUBILITY AND REACTIVITY OF D1-D4

Careful inspection of Table 5.1 revealed that both D3 and D4 differ structurally from D1 and D2 respectively by only one Cl<sup>-</sup> group. However, this substituent seems to impact the solubility of D3 and D4 differently. It increases the solubility of D3 relative to D1 but decreases that of D4 relative to D2 (Table 5.3). Similar comparison shows that D2 and D3 are more soluble than D1 and D4 respectively. However in these cases, the

differences in solubility stems from replacement of a Cl<sup>-</sup> group in D1 and D3 by an NO<sub>2</sub><sup>-</sup> group in the D2 and D4 respectively (Table 5.1). To explain the influence of these functional groups on the solubility and reactivity of D1 – D4, the screening charges, the dipole moments, the polarizability, and the solvation free energies obtained for the dyes at a cut-off value of 5.5 Å, and the HOMO and LUMO energies obtained at the optimum reactivity cut-off value of 4.5 Å (Appendices: Tables A.6 – A.9), are presented along with their best calculated solubility values in Table 5.3.

**Table 5.3:** Calculated solubility ( $S_{\text{CSE}}$  and  $S_{\text{GSE}}$ ), screening charge,  $q$ , dipole moment,  $\mu$ , polarisability,  $\alpha$ , solvation free energy (SFE), HOMO and LUMO energies for D1, D2, D3 and D4 at 25°C.

Dyes	$S_{\text{CSE}}$ (mg/L)	$S_{\text{GSE}}$ (mg/L)	$Q$	$\mu$ (Debye)	$\alpha$	SFE (kcal/mol)	HOMO (eV)		LUMO (eV)	
							Gas	Water	Gas	Water
D1	0.09	0.10	-0.0020	10.62	42.26	-14.56	-5.30	-5.21	-3.75	-3.90
D2	0.53	0.68	-0.0019	11.90	46.78	-19.36	-5.50	-5.28	-3.90	-3.97
D3	0.98	0.12	-0.0019	11.20	43.62	-15.38	-5.25	-5.17	-3.69	-3.87
D4	0.25	0.20	-0.0018	11.48	47.09	-19.13	-5.43	-5.30	-3.92	-3.97

Comparing D3 and D1, the lower screening charge obtained for D3 can be attributed to the electron withdrawing influence of the extra Cl<sup>-</sup> group which further decreases the charge density of the dye by attracting more electrons away from the azo bridge (i.e – N = N –). A monoazo dye consists of two opposite aromatic moieties (i.e the accepting and donating rings), sandwiched by the azo bridge. The accepting ring is the portion with electron withdrawing substituent (s) whereas the donating ring is the one with the electron donating substituent(s). The net dipole moment between these two parts depends on their overall charge density difference which is governed by both the nature and the number

of active substituents on each moiety. For D3, the accepting part is one Cl<sup>-</sup> more than that D1, therefore, more electrons are displaced towards the accepting part of D3 leading to a large charge separation between its accepting and donating parts. This explains why D3 has higher dipole moment and SFE, and has more solubility than D1. On the other hand, the extra Cl<sup>-</sup> group in D4 yields a lower dipole moment, SFE and solubility values relative to D2. This suggests that the Cl<sup>-</sup> acts as an electron donor rather than an acceptor for D4.

The higher solubility value observed for D2 compared to D1 can be attributed to its relatively small screening charge and the resultant larger dipole moment, polarizability and SFE values compared to D1 which suggests NO<sub>2</sub> as being more electron withdrawing than Cl<sup>-</sup>. Similarly, the relatively large dipole moment, polarizability and SFE values obtained for D4 compared to D3, also confirms NO<sub>2</sub> as being the stronger electron withdrawing substituent.

Furthermore, the lower HOMO and LUMO energies obtained for D2 and D4 both in gas and water, compared to D1 and D3 respectively, suggests that NO<sub>2</sub><sup>-</sup> causes more electron deficiency than Cl<sup>-</sup> due to its higher electron withdrawing power. Lower HOMO energy suggests lower chance of donating electrons while lower LUMO energies indicates higher propensity towards incoming electrons. Finally, the increase in HOMO and LUMO energies observed for D3 compared to D1 suggests that the additional Cl<sup>-</sup> in the former tends to minimize the influence of the accepting moiety by partial donation of electron to the azo bridge. Similar reason holds for the difference in HOMO energy observed between D4 and D2.

## 5.4 CONCLUSION

The effect of global orbital cut-off and NSPA variation on DMol<sup>3</sup>/COSMO-RS predicted aqueous solubility (in mg/L) of four azo dyes have been investigated using the solubility equations proposed by Cramer *et al.* (CSE) and the general solubility equation (GSE) by Yalkowsky. The reactivity of the dyes was also investigated. The results showed that both CSE and GSE are reliable for predicting aqueous solubility *via* COSMO-RS calculations but their dependence on orbital cut-off values differ. Where the best cut-off values are the same for both equations, the CSE was found to show higher prediction strength. While the GSE calculated solubility increased with cut-off value to a point of saturation, the CSE results showed no constant trend. However, there are indications that the choice of appropriate cut-off for the CSE depends on molecular size of the solute. The results of the reactivity study revealed that the dyes are more reactive in water than in gas phase. The COSMO-RS results, the calculated solubility and the reactivity indices were generally found to be almost insensitive to a change in NSPA whereas significant changes in most of the reactivity indices occurred up to a cut-off value of 4.5 Å.

## 5.5 REFERENCES

1. M. Fujisawaa, H. Tsutsumia and T. Kimura. Prediction of solubility of practically insoluble drugs in water/ethanol solvents using non-empirical methods. *Journal of Chemical and Pharmaceutical Research* **3** (2011) 750-758.
2. Z. Guo, B. M. Lue, K. Thomasen, A. S. Meyer and X. Xu. Predictions of flavonoid solubility in ionic liquids by COSMO-RS: experimental verification, structural elucidation, and solvation characterization. *Green Chemistry* **9** (2007) 1362-1373.

3. A. G. Sicaire, M. A. Vian, F. Fine, P. Carré, S. Tostain and F. Chemat. Experimental approach versus COSMO-RS assisted solvent screening for predicting the solubility of rapeseed oil. *Oilseeds and Fats, Crops and Lipids* **22** (2015) 1-7.
4. S. Mustapha, P. Okonkwo and S. Waziri. Improvement of carbon dioxide absorption technology using conductor-like screening model for real solvents (COSMO-RS) method. *Journal of Environmental Chemistry and Ecotoxicology* **5** (2013) 96-105.
5. M. Lotfi, M. Moniruzzaman and M. S. Rajabi. Predicting the solubility of pharmaceutical compound in ionic liquids using COSMO-RS model. *ARPN Journal of Engineering and Applied Sciences* **11** (2016) 1618-1622.
6. A. Klamt, V. Jonas, T. Bürger and J. C. Lohrenz. Refinement and parametrization of COSMO-RS. *The Journal of Physical Chemistry A* **102** (1998) 5074-5085.
7. K. J. Sakoma, K. A. Bello and M. K. Yakubu. Synthesis of some azo disperse dyes from 1-substituted 2-hydroxy-6-pyridone derivatives and their colour assessment on polyester fabric. *Open Journal of Applied Sciences* **2** (2012) 54-59.
8. Y. S. Choi, K. S. Lee, H. J. Kim, J. Y. Choi, S. B. Kang, E. J. Lee and G. Keum. Synthesis, spectral property and dyeing assessment of azo disperse dyes containing carbonyl and dicyanovinyl groups. *Bulletin of the Korean Chemical Society* **34** (2013) 863-867.
9. T. Peme, L. O. Olasunkanmi, I. Bahadur, A. S. Adekunle, M. M. Kabanda and E. E. Ebenso. Adsorption and corrosion inhibition studies of some selected dyes as corrosion inhibitors for mild steel in acidic medium: gravimetric, electrochemical,

- quantum chemical studies and synergistic effect with iodide ions. *Molecules* **20** (2015) 16004-16029.
10. S. S. Al-Juaid. Mono azo dyes compounds as corrosion inhibitors for dissolution of aluminium in sodium hydroxide solutions. *Portugaliae Electrochimica Acta* **25** (2007) 363-373.
  11. A. Fouda, H. Ali, R. Awad and A. Ahmed. New benzonitrile azo dyes as corrosion inhibitors for carbon steel in hydrochloric acid solutions. *International Journal of Electrochemical Science* **9** (2014) 1117-1131.
  12. A. Abdul Nabi and A. Hussain. Synthesis, Identification and study of some new azo dyes as corrosion inhibitors for carbon-steel in acidic media. *Journal of Basrah Researches (Sciences)* **38** (2012) 125-146.
  13. M. Abdallah, A. Fouda, S. Shama and E. Afifi. Azodyes as corrosion inhibitors for dissolution of c-steel in hydrochloric acid solution. *African Journal of Pure and Applied Chemistry* **2** (2008) 83-91.
  14. K. Georgiadou and E. Tsatsaroni. Synthesis, characterisation and application of disperse dyes derived from N-2-hydroxyethyl-1-naphthylamine. *Dyes and Pigments* **50** (2001) 93-97.
  15. M. R. R. Kooh, V. N. Yoong and P. Ekanayake. Density functional theory (DFT) and time-dependent density functional theory (TDDFT) studies of selected ancient colourants as sensitizers in dye-sensitized solar cells. *Journal of the National Science Foundation of Sri Lanka* **42** (2014) 169-175.
  16. V. Chigrinov, H. S. Kwok, H. Takada and H. Takatsu. Photo-aligning by azo-dyes: Physics and applications. *Liquid Crystals Today* **14** (2005) 1-15.

17. H. A. Badran, A. Y. Taha, A. F. Abdulkader and C. A. Emshary. Preparation and study of the electrical and optical properties of a new azo dye (4-acetaminophenol–[2-(4-azo)]-4-amino dipheyl sulfone). *Journal of Ovonic Research* **8** (2012) 161-170.
18. A. H. Wolff and F. W. Oehme. Carcinogenic chemicals in food as an environmental health issue. *Journal of the American Veterinary Medical Association* **164** (1974) 623-631.
19. G. Mooter, B. Maris, C. Samyn, P. Augustijns and R. Kinget. Use of azo polymers for colon-specific drug delivery. *Journal of Pharmaceutical Sciences* **86** (1997) 1321-1327.
20. DMol<sup>3</sup> Guide, Material Studio 8.0. *Accelrys Software, Inc.*, San Diego, United States (2017) 1-161.
21. Y. Luo, S. Yin, W. Lai and Y. Wang. Effects of global orbital cutoff value and numerical basis set size on accuracies of theoretical atomization energies. *Theoretical Chemistry Accounts* **133** (2014) 1580-1587.
22. V. A. Basiuk and L. V. Henao-Holguín. Effects of orbital cutoff in DMol3 DFT calculations: a case study of meso-tetraphenylporphine–C60 complex. *Journal of Computational and Theoretical Nanoscience* **10** (2013) 1266-1272.
23. J. Andzelm, C. Kölmel and A. Klamt. Incorporation of solvent effects into density functional calculations of molecular energies and geometries. *The Journal of Chemical Physics* **103** (1995) 9312-9320.

24. C. Bird. The Dyeing of Acetate Rayon with Disperse Dyes I-Aqueous Solubility and the Influence of Dispersing Agents II-The Relation between Aqueous Solubility and Dyeing Properties. *Coloration Technology* **70** (1954) 68-77.
25. J. D. Thompson, C. J. Cramer and D. G. Truhlar. Predicting aqueous solubilities from aqueous free energies of solvation and experimental or calculated vapor pressures of pure substances. *The Journal of Chemical Physics* **119** (2003) 1661-1670.
26. D. L. Peterson and S. H. Yalkowsky. Comparison of two methods for predicting aqueous solubility. *Journal of Chemical Information And Computer Sciences* **41** (2001) 1531-1534.
27. S. H. Yalkowsky and S. C. Valvani. Solubility and partitioning I: solubility of nonelectrolytes in water. *Journal of Pharmaceutical Sciences* **69** (1980) 912-922.
28. J. Koh. Dyeing with disperse dyes. *INTECH Open Access Publisher*, (2011)
29. B. I. Adewale and S. Banjo. Theoretical study on structural and electronic properties of 4-[(E)-[4-(trifloromethyl)-1, 3-benzothiazol-2-yl] azo] naphthalen-1-ol and 1-[(E)-[4-(trifloromethyl)-1, 3-benzothiazol-2-yl] azo] naphthalen-2-ol using density functional theory (DFT). *International Journal of Physical Sciences* **8** (2013) 1494-1505.
30. L. H. Mendoza-Huizar. A Theoretical Study of Chemical Reactivity of Tartrazine Through DFT Reactivity Descriptors. *Journal of the Mexican Chemical Society* **58** (2014) 416-423.
31. A. D. Becke. Density-functional thermochemistry. III. The role of exact exchange. *The Journal of Chemical Physics* **98** (1993) 5648-5652.



32. J. P. Perdew. Density-functional approximation for the correlation energy of the inhomogeneous electron gas. *Physical Review B* **33** (1986) 8822-8824.
33. S. H. Vosko, L. Wilk and M. Nusair. Accurate spin-dependent electron liquid correlation energies for local spin density calculations: a critical analysis. *Canadian Journal of Physics* **58** (1980) 1200-1211.
34. E. Mullins, R. Oldland, Y. Liu, S. Wang, S. I. Sandler, C.-C. Chen, M. Zwolak and K. C. Seavey. Sigma-profile database for using COSMO-based thermodynamic methods. *Industrial and Engineering Chemistry Research* **45** (2006) 4389-4415.
35. Y. Inada and H. Orita. Efficiency of numerical basis sets for predicting the binding energies of hydrogen bonded complexes: evidence of small basis set superposition error compared to Gaussian basis sets. *Journal of Computational Chemistry* **29** (2008) 225-232.
36. C. Liang and D. A. Gallagher. QSPR prediction of vapor pressure from solely theoretically-derived descriptors. *Journal of Chemical Information And Computer Sciences* **38** (1998) 321-324.
37. R. G. Parr and R. G. Pearson. Absolute hardness: companion parameter to absolute electronegativity. *Journal of the American Chemical Society* **105** (1983) 7512-7516.
38. R. G. Parr, R. A. Donnelly, M. Levy and W. E. Palke. Electronegativity: the density functional viewpoint. *The Journal of Chemical Physics* **68** (1978) 3801-3807.
39. R. G. Parr, L. V. Szentpaly and S. Liu. Electrophilicity index. *Journal of the American Chemical Society* **121** (1999) 1922-1924.

40. J. L. Gázquez. Perspectives on the density functional theory of chemical reactivity. *Journal of the Mexican Chemical Society* **52** (2008) 3-10.
41. P. Geerlings, F. De Proft and W. Langenaeker. Conceptual density functional theory. *Chemical reviews* **103** (2003) 1793-1874.
42. P. K. Chattaraj. Chemical reactivity theory: a density functional view. *CRC Press*, Taylor and Francis Group, Boca Raton, (2009) pp. 7-22.
43. P. W. Ayers and R. G. Parr. Variational principles for describing chemical reactions: the Fukui function and chemical hardness revisited. *Journal of the American Chemical Society* **122** (2000) 2010-2018.
44. P. K. Chattaraj, H. Lee and R. G. Parr. HSAB principle. *Journal of the American Chemical Society* **113** (1991) 1855-1856.
45. J. L. Gázquez and F. Mendez. The hard and soft acids and bases principle: an atoms in molecules viewpoint. *The Journal of Physical Chemistry* **98** (1994) 4591-4593.
46. F. Mendez and J. L. Gázquez. Chemical reactivity of enolate ions: the local hard and soft acids and bases principle viewpoint. *Journal of the American Chemical Society* **116** (1994) 9298-9301.
47. R. Skyner, J. McDonagh, C. Groom, T. van Mourik and J. Mitchell. A review of methods for the calculation of solution free energies and the modelling of systems in solution. *Physical Chemistry Chemical Physics* **17** (2015) 6174-6191.
48. J. Ali, P. Camilleri, M. B. Brown, A. J. Hutt and S. B. Kirton. Revisiting the general solubility equation: in silico prediction of aqueous solubility incorporating the effect

of topographical polar surface area. *Journal of Chemical Information and Modeling*  
**52** (2012) 420-428.



---

## CHAPTER 6

# PREDICTION OF AQUEOUS SOLUBILITY BY TREATMENT OF COSMO-RS DATA WITH EMPIRICAL SOLUBILITY EQUATIONS: THE ROLES OF GLOBAL ORBITAL CUT-OFF AND COSMO SOLVENT RADIUS

---

### PREAMBLE

Aqueous solubility values of low molecular weight dyes were predicted by the treatment of relevant COSMO-RS data with Cramer *et al.* solubility equation (CSE) and general solubility equation (GSE). The COSMO-RS data were obtained with DMol<sup>3</sup> computational code using VWN-BP level of theory with double numerical basis set containing polarization functions (DNP). The aim was to investigate the performances of CSE and GSE, compare their solubility prediction strengths and examine the roles of global orbital cut-off and COSMO solvent radius (CSR) on their predictions. Our findings revealed that aqueous solubility (in mol/L) of azo dyes can be accurately predicted using CSE or GSE with some COSMO-RS data, and that global orbital cut and COSMO solvent radius are essential parameters for accurate prediction.

### 6.1 INTRODUCTION

Conductor-like screening model (COSMO) developed by the Klamt group [1-3] remains the most successful continuum solvation model (CSM) for a number of reasons, which

---

The work presented in this chapter has been published.

\*O.O. Wahab, L.O. Olasunkanmi, K.K. Govender and P.P. Govender. *Theoretical Chemistry Account* **138** (2019) 80(1) - 80(13).

include algorithmic simplicity, numerical stability and high insensitivity to outlying charge errors [3]. A popular advancement of COSMO known as conductor-like screening model for realistic solvation (COSMO-RS) [3-5] is used to predict thermodynamic properties, solvation energies, vapor pressure, partition coefficients, hydration free energies and solubility of pure liquids, mixtures or solutions using unimolecular quantum chemical calculations and statistical thermodynamics. Compared to other CSMs, the ability of COSMO-RS to predict these important physicochemical properties with greater accuracy at various temperatures has motivated tremendous research applications which include prediction of drug solubility in liquid mixtures [6], acyclovir solubility in ionic liquids [7], solubility of imidazolium-based ionic liquids in model fuel hydrocarbons [8], flavonoids and pharmaceutical compounds solubility in ionic liquids [9, 10], micelle-water partition coefficients [11], solubility of rapeseed oil in various solvents [12], cyclohexane-water distribution coefficients [13], carbon dioxide (CO<sub>2</sub>) absorption capacity of various solvents [14], lipophilicity [15], solubility of drugs and pesticides [16], basicity of aqueous solution [17], partition and distribution coefficients in different solvent pairs [18], aqueous solubility of hexafluorobenzene [19] and azo dyes [20].

Two popularly known computational programs that use COSMO-RS to predict thermodynamic properties of liquid mixtures and solutions are DMol<sup>3</sup> [21] and COSMOtherm [22], where the former is more versatile because it can perform both gaseous and solvent phase calculations on both periodic and non-periodic structures using density functional theory (DFT) [21, 23]. In addition, DMol<sup>3</sup> uses numerical basis sets which are regarded as one of the best classes of basis sets for theoretical calculations [5, 21, 24-26]. However, the use of DMol<sup>3</sup> for accurate COSMO-RS calculations is still limited probably due to lack of adequate theoretical guide on selection

of some necessary adjustable parameters such as global orbital cut-off, COSMO segment and solvent radius which govern the accuracy of DMol<sup>3</sup>/COSMO-RS predictions. Global orbital cut-off defines the extent of numerical integration of the numerical basis sets [26], i.e. the fraction of molecular orbitals that should be taken into consideration by the basis set. COSMO segment specifies the number of segments/grids required per atomic surface in a molecule inside a perfect conductor (solvent) [5, 23, 27, 28]. Solvent radius (also known as solvent probe radius) is a parameter which specifies the size of a sphere that is approximately used to describe the effective size of the solvent molecule [27, 29] and the default solvent radius for COSMO calculations is 1.3 Å [23].

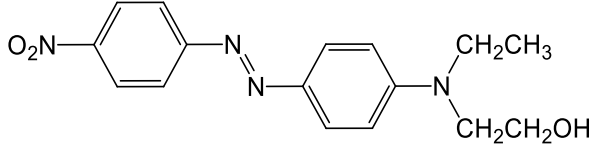
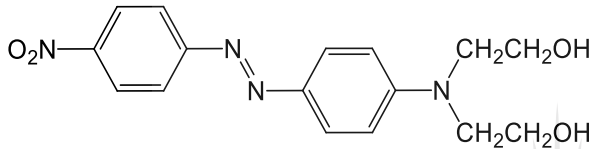
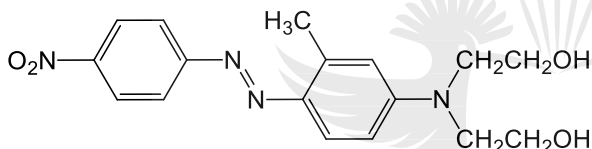
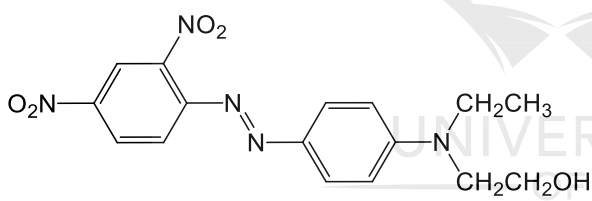
COSMO-RS can be directly or indirectly used to predict solubility. Direct use of COSMO-RS involves evaluation of relative solubility (i.e. mole fraction solubility) of components of mixtures from their respective chemical potential [6, 9, 10, 12, 16, 19, 27]. Indirect application of COSMO-RS involves treatment of COSMO-RS data such as solvation free energies (SFE), vapor pressure and octanol-water partition coefficient of a solute with known empirical solubility equations [20]. The advantage of this technique is that it provides room for calculating solubility in standard units (mol/L or mg/L) from COSMO-RS data unlike the non-standard mole fraction solubility system adopted by the direct technique. There are considerable reports on the direct use of COSMO-RS for prediction of solubility [6, 9, 10, 12, 16, 19, 27]. However, reports on indirect application of COSMO-RS for this purpose are very scanty. One of the few reports on it is our recent work on the prediction of aqueous solubility and reactivity of some azo dyes [20] in which the performances of Cramer *et al.* solubility equation (CSE) [30] and general solubility

equation (GSE) by Yalkowsky [31] were compared and the effects of global orbital cut-off and COSMO segment variation on the predicted properties were examined.

The results obtained in our recent study [20] proposed that the best cut-off value for COSMO-RS/CSE predicted solubility was inversely proportional to the molecular weight of the studied dyes. To consolidate on the fact, the present study is designed to further probe the role of global orbital cut-off on COSMO-RS/CSE predicted solubility using four lower molecular weight azo dyes. This will aid better understanding of the behavior of COSMO-RS/CSE predicted solubility with respect to cut-off variation and provide reliable theoretical basis for selection of appropriate cut-off value for COSMO-RS/CSE calculations.

The low molecular weight azo dyes selected for this study are (E)-2-(ethyl(4-((4-nitrophenyl)diazenyl)phenyl)amino)ethanol [B1], (E)-2,2'-((4-((4-nitrophenyl)diazenyl)phenyl)azanediyl)diethanol [B2], (E)-2,2'-((3-methyl-4-((4-nitrophenyl)diazenyl)phenyl)azanediyl)diethanol [B3] and (E)-2-((4-((2,4-dinitrophenyl)diazenyl)phenyl)(ethyl)amino)ethanol [B4], whose molecular structures and some physicochemical properties are contained in Table 6.1 [32]. Selection of these dyes was strictly based on availability of experimental solubility values which provides room for proper performance evaluation of the theoretical model adopted for the study. The role of solvent radius in DMol<sup>3</sup>/COSMO-RS calculations and the response of the CSE and the GSE to change in solvent radius in relation to predicted solubility are also investigated.

**Table 6. 1:** Molecular structures of studied dyes and their physicochemical properties [32].

Dyes	Molecular structures	Molecular weights (g/mol)	Melting point (°C)	Experimental solubility (mg/L) in water at 25°C
B1		314	163	0.3
B2		330	207	0.4
B3		344	160	1.2
B4		359	145	0.6

## 6.2 COMPUTATIONAL DETAILS

With the DMol<sup>3</sup> program [23] incorporated in the Material Studio (MS) 2016 software package [33], all calculations were carried out at Becke and Perdew [34-39] form of Volsko, Wilk and Nusair (VWN-BP) level of density functional theory [40] using double numerical basis with polarization functions (DNP) (version 4.0.0) [23, 24, 28] basis set. VWN-BP is very suitable for COSMO-RS calculations using DMol<sup>3</sup> [23, 28]. It has a remarkable prediction accuracy for thermodynamic phase behaviors [27] and has successfully been used for predicting aqueous solubility of some azo dyes by indirect



application of COSMO-RS [20]. DNP is one of the best members of the numerical basis sets, which are known for high prediction accuracy, ability to eliminate basis set superposition errors (BSSE) and greater calculation speed compared to their Pople basis set counterparts [24, 41]. Even at their simplest level of the double numerical basis (DN), numerical basis sets have the capacity to satisfactorily reproduce properties such as dipole moments and polarizabilities which are essential for accurate description of solvation [5]. With moderate speed and high accuracy, DNP is very efficient for DMol<sup>3</sup> calculations [25, 26] especially with VWN-BP functional in predicting solubility via COSMO-RS calculations [20].

The molecular structures of B1 – B4 were modelled, cleaned and then subjected to full gas phase geometry optimization without symmetry constraints. The optimizations were carried out at different global orbital cut-off values (3.5, 4.5, 5.5, 6.5, 7.0 and 8.0 Å) and the optimized geometries were confirmed by the absence of imaginary vibrational frequencies. The gas phase optimized geometries of the dyes were then re-optimized in water to adequately account for possible changes in their global minimum energies, geometrical parameters, dipole moments, polarizabilities and solvation free energies. This was achieved by setting COSMO dielectric,  $\epsilon$  to 78.4 (permittivity of water) and incorporating the recommended atomic radii [27] of the constituent atoms (i.e. H, C, N and O) of the dyes in the input files for proper cavitation of the solutes (dyes) in the conductor (water) in order to ensure accurate description of the solvation process. To investigate the role of solvent radius, the COSMO solvent radius parameter was varied from 0.5 to 1.9, which include the recommended default value of 1.3 for COSMO and COSMO-RS calculations [23].

The Cramer *et al.* solubility equation (CSE) [30] and the general solubility equation (GSE) [31] were employed for prediction of aqueous solubility of the studied dyes using COSMO and COSMO-RS data and the solubility values ( $S_{CSE}$  and  $S_{GSE}$ ) obtained from the two equations were compared.

The Cramer *et al.* solubility equation is an exponential equation that expresses the solubility of a pure non-ionic solute in water ( $S_{aq}$ ) in terms of its vapor pressure, free energy of solvation and temperature as [30]:

$$S_{aq} = \frac{P_s}{P^0} e^{-\Delta G_s^0/RT}$$

**Equation 6. 1**

where  $P_s$  is the equilibrium vapor pressure of the solute,  $P^0$  is ideal gas pressure at 1 molar standard state and 298 K, having numerical value of 24.45 atm,  $\Delta G_s^0$  is the standard-state aqueous free energy of solvation of the solute, R is the gas constant, and T is absolute temperature.  $\Delta G_s^0$  is the sum of standard free energy changes (solvation free energies) for a tri-phasic system comprising of a pure solid solute in equilibrium with its vapour and aqueous solution [30]:



The solvation free energies (denoted by  $\Delta G_s$ ) of the optimized dyes were determined from their respective absolute energies in gas and water phases using equation 6.3 [20, 23]:

$$\Delta G_s = (E + \Delta G_{NSE}) - E^0$$

**Equation 6. 3**

where  $E^0$  is the absolute energy of the dye in gas phase,  $E$  is the absolute energy in the solvent phase (i.e. total COSMO energy) and  $\Delta G_{NSE}$  is the non-electrostatic contribution to SFE due to dispersion and cavity formation effects. COSMO-RS calculations yielded predicted vapor pressure and octanol-water partition coefficients ( $\text{Log } P$ ) of the dyes.

Hence, the CSE predicted aqueous solubility ( $S_{CSE}$ ) values of the dyes were obtained using equation 6.1 while the GSE predicted solubility ( $S_{GSE}$ ) values were obtained according to the equation [31]:

$$\text{Log } S = 0.5 - 0.01(m.p^{\circ}C - 25) - \text{Log } P \quad \text{Equation 6. 4}$$

where  $S$  is the solubility,  $\text{Log } P$  is the octanol-water partition coefficient,  $m.p^{\circ}C$  is the melting point of the solute in degree celsius (See Table 6.1), 0.5 is the excess of the base ten logarithm of the calculated solubility value over that of the experimental value for a solid or liquid rigid nonelectrolyte, 0.01 is the approximated entropy of fusion constant and 25 is the constant room temperature (in degree celsius) [42].

## 6.3 RESULTS AND DISCUSSION

### 6.3.1 AQUEOUS SOLUBILITY STUDY

The performances of the Cramer *et al.* solubility equation (CSE) and the general solubility equation (GSE) in terms of relative accuracy of the solubility values derived from the two equations using COSMO and/or COSMO-RS data are compared in Figure 6.1. The results in Figure 6.1 are the logarithmic values (base 10), i.e.  $\log S_{CSE}$  and  $\log S_{GSE}$  of the average solubility obtained using both CSE and GSE at different global orbital cut-offs compared with the respective experimental solubility values of the studied dyes at 298 K. The averages were calculated at each orbital cut-off as the sum of solubility values obtained across all the COSMO solvent radii (CSR) considered divided by the number of CSR (Appendix: Tables A.10 – A.13). Figure 6.1 reveals that for all the studied dyes, there is a better agreement between the GSE predicted solubility (i.e.  $\text{Log } S_{GSE}$ ) and the experimental values, which suggests the GSE as having better prediction accuracy for

solubility of the dyes compared to CSE. Exemptions to this general observation are the result for B2 at cut-off values  $\geq 7.0$  Å where both equations seem to exhibit similar prediction capacities, and B4 at cut-off value of 3.5 Å where the CSE showed greater prediction strength. The relatively large deviation of the  $\text{Log } S_{\text{GSE}}$  value at this cut-off from the experimental solubility may be due to slight overestimation of the octanol-water partition coefficient ( $\text{Log } P$ ) from which the  $S_{\text{GSE}}$  value was calculated. According to equation 6.4, the larger the  $\text{Log } P$ , the smaller the  $S_{\text{GSE}}$  [20].

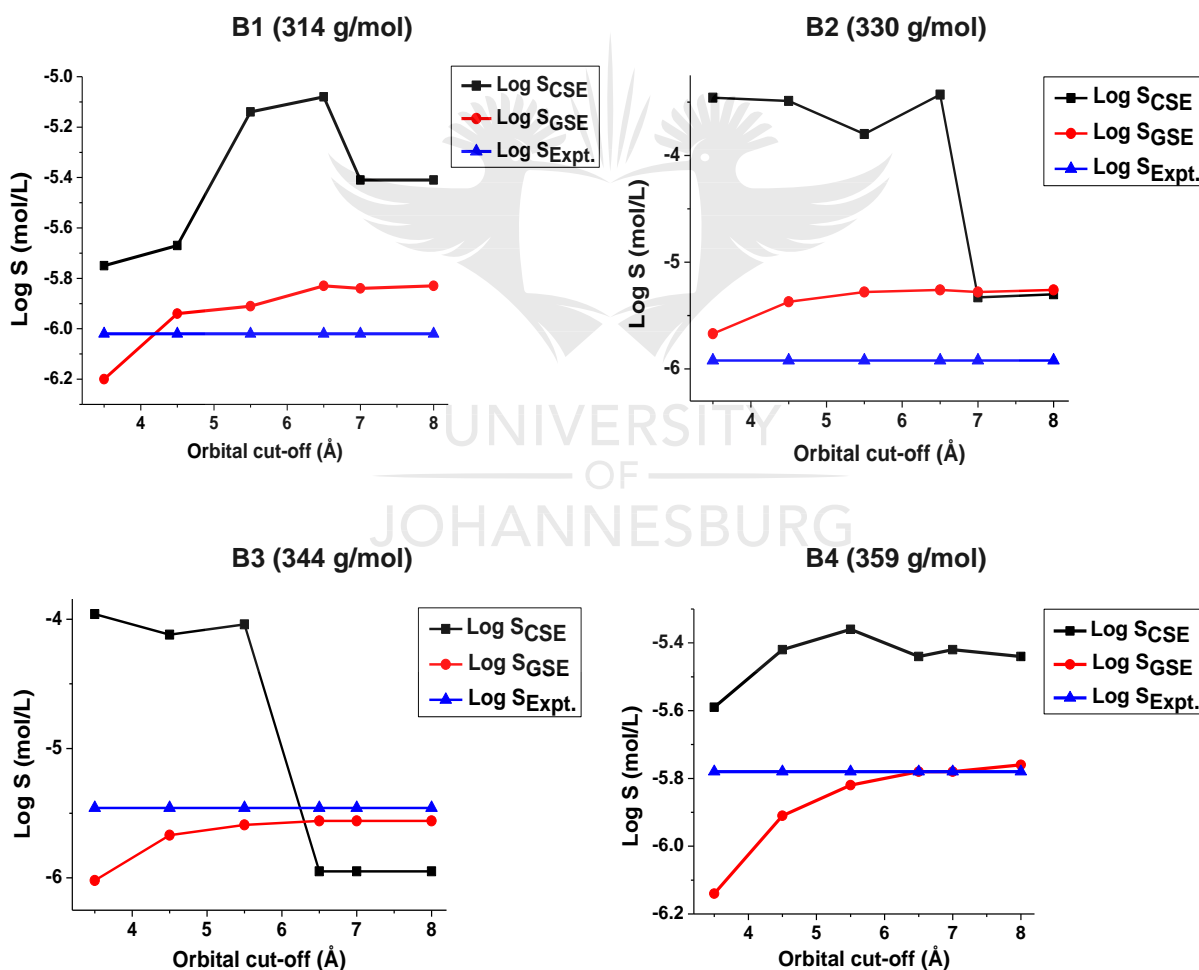


**Figure 6. 1:** Base ten logarithm of average CSE and GSE predicted solubility values for B1, B2, B3 and B4 at 298 K.

### 6.3.2 EFFECT OF CUT-OFF ON CSE PREDICTED SOLUBILITY ( $S_{CSE}$ )

The change in  $\log S_{CSE}$  values with respect to variation in cut-off value is depicted in Figure 6.2. In agreement with previous findings [20], the results show that CSE predicted solubility does not exhibit a definite trend with cut-off variation, but exhibits different trends from one dye to another. This is due to variation in the relative strengths of the cut-off values to adequately predict solvation free energies (SFEs) and vapor pressure which are the properties that determine the magnitude of  $S_{CSE}$  values (eqn. 6.1). The most appropriate CSE cut-off for each dye is the one that sufficiently predicts its SFE and vapor pressure even if this cut-off does not produce the optimum values of predicted SFE and/or vapor pressure [20].

Careful inspection of Figure 6.2 revealed a strong agreement between the  $S_{CSE}$  values and the experimental solubility values at cut-off values  $\geq 7.0 \text{ \AA}$  for B2 and  $\geq 6.5 \text{ \AA}$  for B3 and B4. Although better  $S_{CSE}$  values were obtained for B1 at cut-off values  $\leq 4.5 \text{ \AA}$ , the  $S_{CSE}$  values obtained for this dye at cut-off values  $\geq 7.0 \text{ \AA}$  also compare well with experimental results unlike values obtained at  $5.5 \text{ \AA}$  and  $6.5 \text{ \AA}$ . Similarly, a cut-off value of  $3.5 \text{ \AA}$  yielded better results for B4 compared to the values  $\geq 6.5 \text{ \AA}$ , however, the performances of this and other lower cut-off values are poorer for B2 and B3. Thus, for the sake of consistency and appreciable accuracy, the minimum cut-off value which seems to be more appropriate on average for these low molecular weight dyes is  $7.0 \text{ \AA}$ , which validates our previous postulate that recommended a minimum CSE cut-off value of  $7.0 \text{ \AA}$  for azo dyes with molecular weights less than  $370 \text{ g/mol}$  [13]. Even though smaller cut-off values such as  $3.5 \text{ \AA}$  may sometimes reproduce the experimental value better than the higher ones, the reliability of this cut-off especially for low molecular weight azo dyes

is not guaranteed, because it usually overestimates CSE predicted solubility values as evident in B2 and B3 (Fig. 6.2). This observation is also in accord with previous findings [20] in which cut-off value of 3.5 Å grossly overestimated the solubility of azo dyes with molecular weights < 400 g/mol.

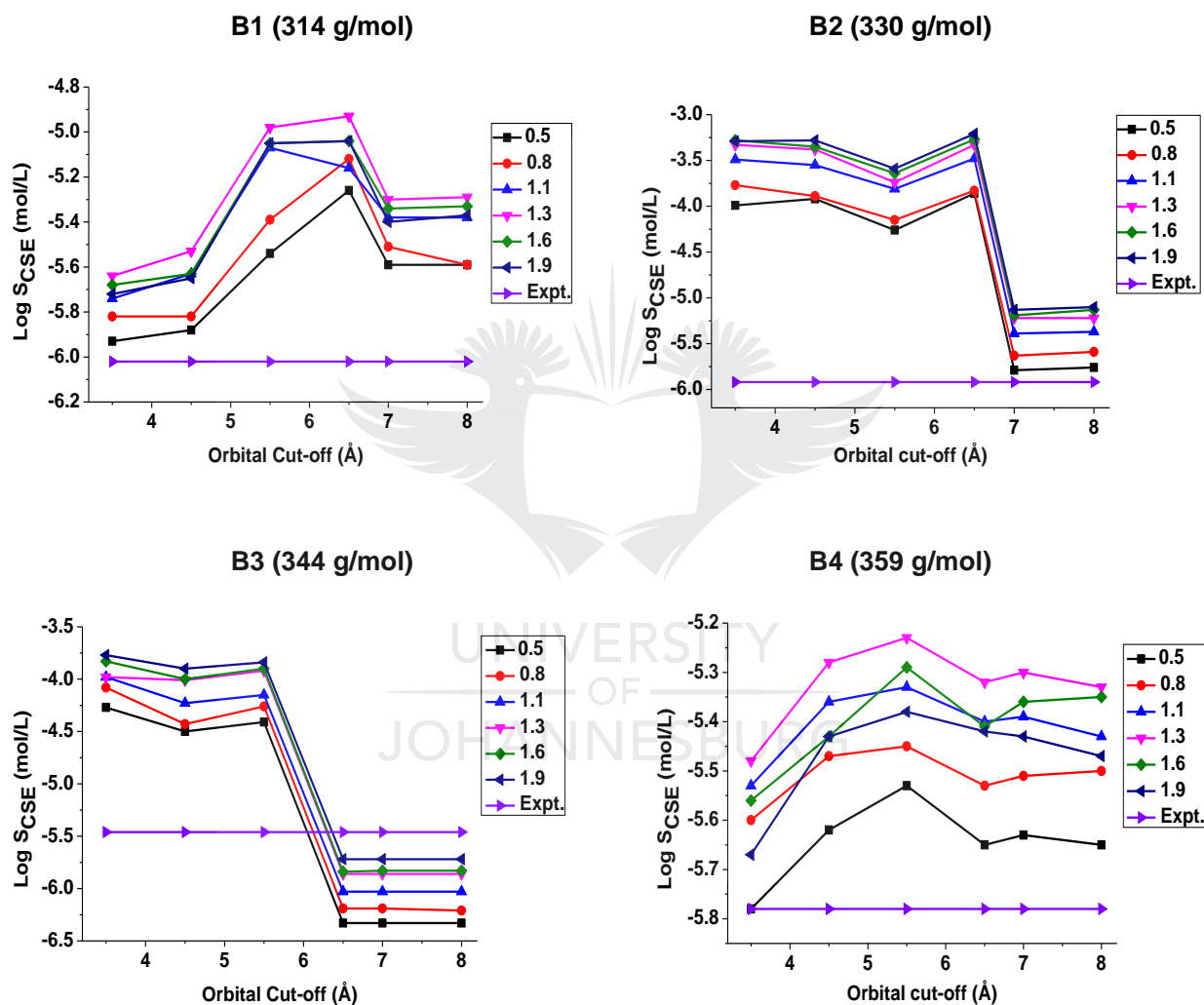


**Figure 6. 2:** Variation of  $\log S_{CSE}$  values of B1, B2, B3 and B4 with orbital cut-off.

Comparing B1 and B2, to B3 and B4 (Fig. 6.2), it is evident on average that the minimum appropriate cut-off value for B3 and B4 is 6.5 Å unlike B1 and B2 where the value is

7.0 Å. The fact that B3 and B4 are larger than B1 and B2, and that the minimum appropriate cut-off value for each pair follows an opposite trend agrees with the fact that the size of appropriate COSMO and COSMO-RS cut-off for CSE calculation is inversely related to the molecular weight of azo dyes [20]. That is, the bigger the molecular size, the smaller the CSE cut-off value suitable for accurate or near accurate prediction of its CSE based solubility value.

### 6.3.3 EFFECT OF CUT-OFF ON GSE PREDICTED SOLUBILITY ( $S_{GSE}$ )

Figure 6.3 shows the change in  $\log S_{GSE}$  values with orbital cut-off variation. The trend of the profiles in Figure 6.3 reveals that  $\log S_{GSE}$  exhibits a constant trend with cut-off variation across all CSR studied. But unlike  $\log S_{CSE}$ , the best CSR value is not the same for all the studied dyes. The best CSR values are 1.3 for B1, 1.9 for B2, 0.5 and 0.8 for B3 and 1.1 for B4. However, it is important to note that  $\log S_{GSE}$  values obtained for these dyes with most of the CSR studied are highly satisfactory because they compare very well with experimental solubility values (Fig. 6.3).

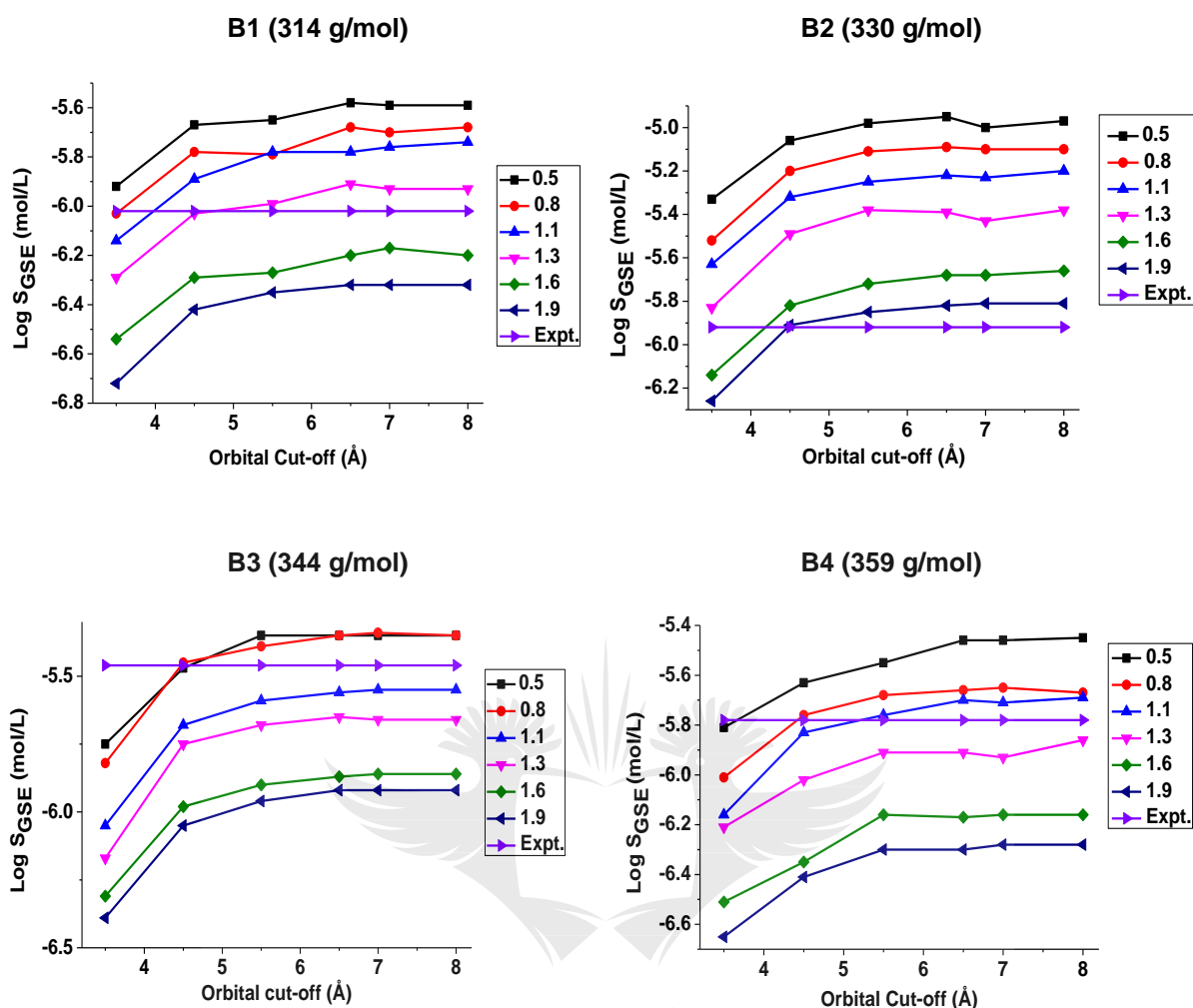


**Figure 6. 3:** Log  $S_{GSE}$  for B1, B2, B3 and B4 as a function of orbital cut-off.

It can be observed from Figure 6.3 that log  $S_{GSE}$  increases with an increase in cut-off value and reached an optimum value at a cut-off value of 5.5 Å beyond which further increase in cut-off brought no substantial increase in log  $S_{GSE}$  values. This suggests 5.5 Å as being the optimum cut-off value for predicting the aqueous solubility of the studied dyes using COSMO-RS/GSE model. However, this optimum cut-off does not seem to be the best cut-off for the dyes because log  $S_{GSE}$  values obtained at a cut-off value of 4.5 Å are closer to the experimental values (Fig. 6.3), which suggests 4.5 Å as the most appropriate cut-off value for the COSMO-RS/GSE model. Since this cut-off is also the



best minimum  $S_{GSE}$  cut-off for higher molecular weight azo dyes [20], it can be concluded that selection of appropriate global orbital cut-off for predicting the aqueous solubility of azo dyes using COSMO-RS/GSE technique is independent of molecular weights of the dyes and a minimum cut-off value of 4.5 Å must be selected for this technique because it guarantees higher accuracy. Although accurate predicted solubility (i.e.  $S_{GSE}$ ) values were obtained with a cut-off value of 3.5 Å for some of the dyes such as B1 and B4 at CSR values of 0.8 and 0.5, respectively, this cut-off value is inconsistent (Fig 6.3) and hence unreliable compared to 4.5 Å especially for higher molecular weight azo dyes [20].

#### **6.3.4 EFFECT OF COSMO SOLVENT RADIUS ON CSE PREDICTED SOLUBILITY ( $S_{CSE}$ )**

The response of CSE predicted solubility ( $S_{CSE}$ ) to change in COSMO solvent radius (CSR) is shown in Figure 6.4 where the predicted solubility values are presented as  $\log S_{CSE}$  obtained across the range of orbital cut-off studied. As can be observed from Figure 6.4,  $\log S_{CSE}$  increases with increase in CSR and approaches a plateau at CSR value of 1.3. There was a slight decrease in  $S_{CSE}$  values of B1 and B4 at CSR > 1.3. This may be responsible for the choice of 1.3 as the default CSR value for COSMO calculations [23]. Unfortunately, this CSR did not strongly reproduce the experimental solubility values compared to the lower CSR and the higher ones in the cases of B1 and B4.  $S_{CSE}$  values obtained at lower CSR compare better with experimental solubility values especially at CSR of 0.5 because lower CSR allows the solute (dye) to interact more strongly with the solvent thereby promoting solvent polarization and hence the solvation of the solute as confirmed by the relatively low solvation free energies (SFE) for the lower CSR (Appendix: Tables A.10 – A.13).

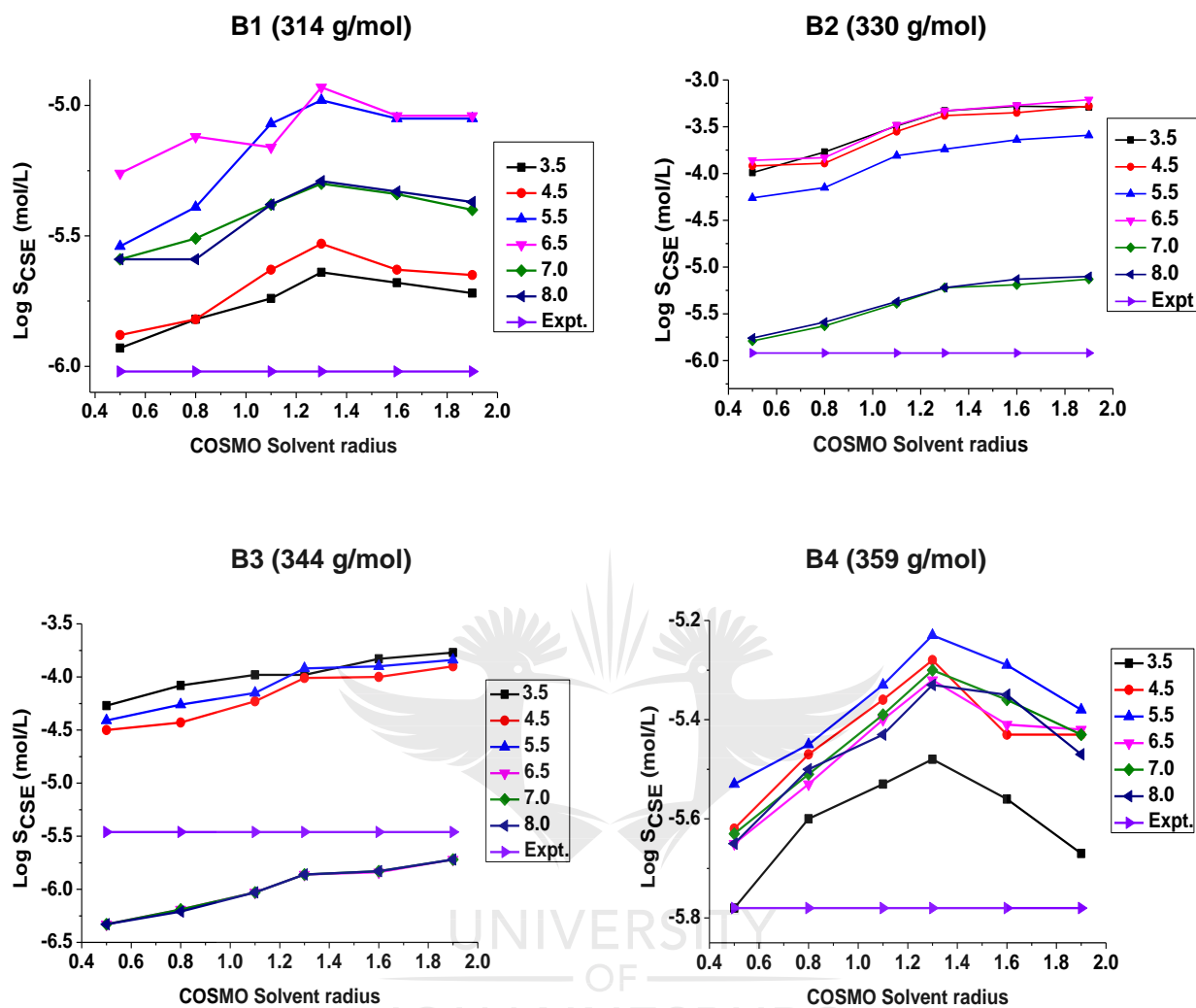


**Figure 6. 4:** Log  $S_{cSE}$  for B1, B2, B3 and B4 as a function of COSMO solvent radius.

The more negative screening charge (Fig. 6.5) and larger dipole moment (Fig. 6.6) values obtained with CSR < 1.3 further confirm stronger solute-solvent electrostatic interaction due to increased solvent polarization at lower CSR. The fact that the strongest interaction is produced by CSR of 0.5 as revealed by corresponding screening charge, dipole moment and SFE values (Fig. 6.5 and 6.6, and Appendix: Tables A.10 – A.13) explains why this CSR yielded the most accurate Log  $S_{cSE}$  values for all the dyes with the

exception of B3 at cut-off values  $> 5.5 \text{ \AA}$  where better results were obtained with  $\text{CSR} \geq 1.3$ .

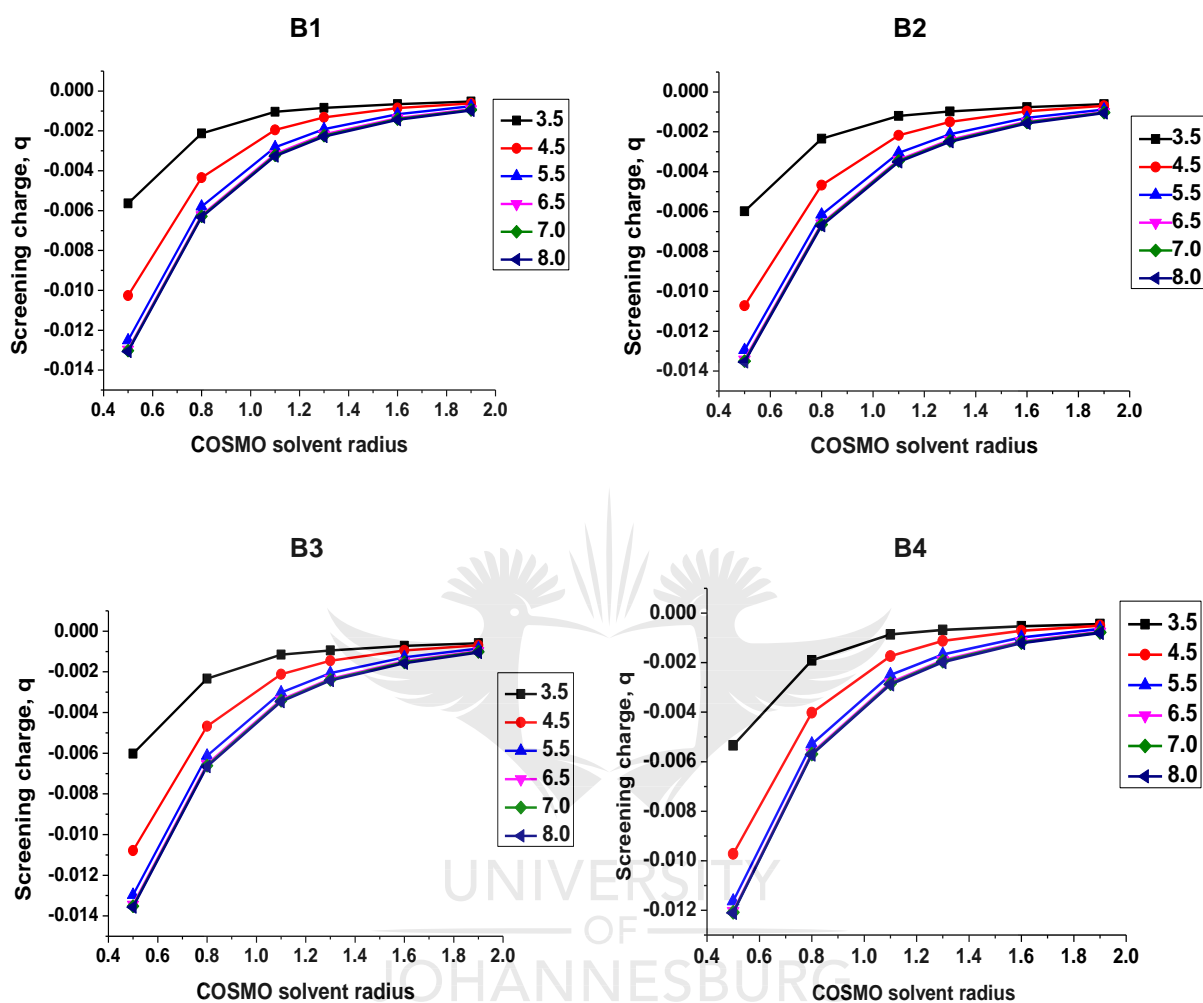


**Figure 6. 5:** COSMO screening charges for B1, B2, B3 and B4 as a function of COSMO solvent radius.

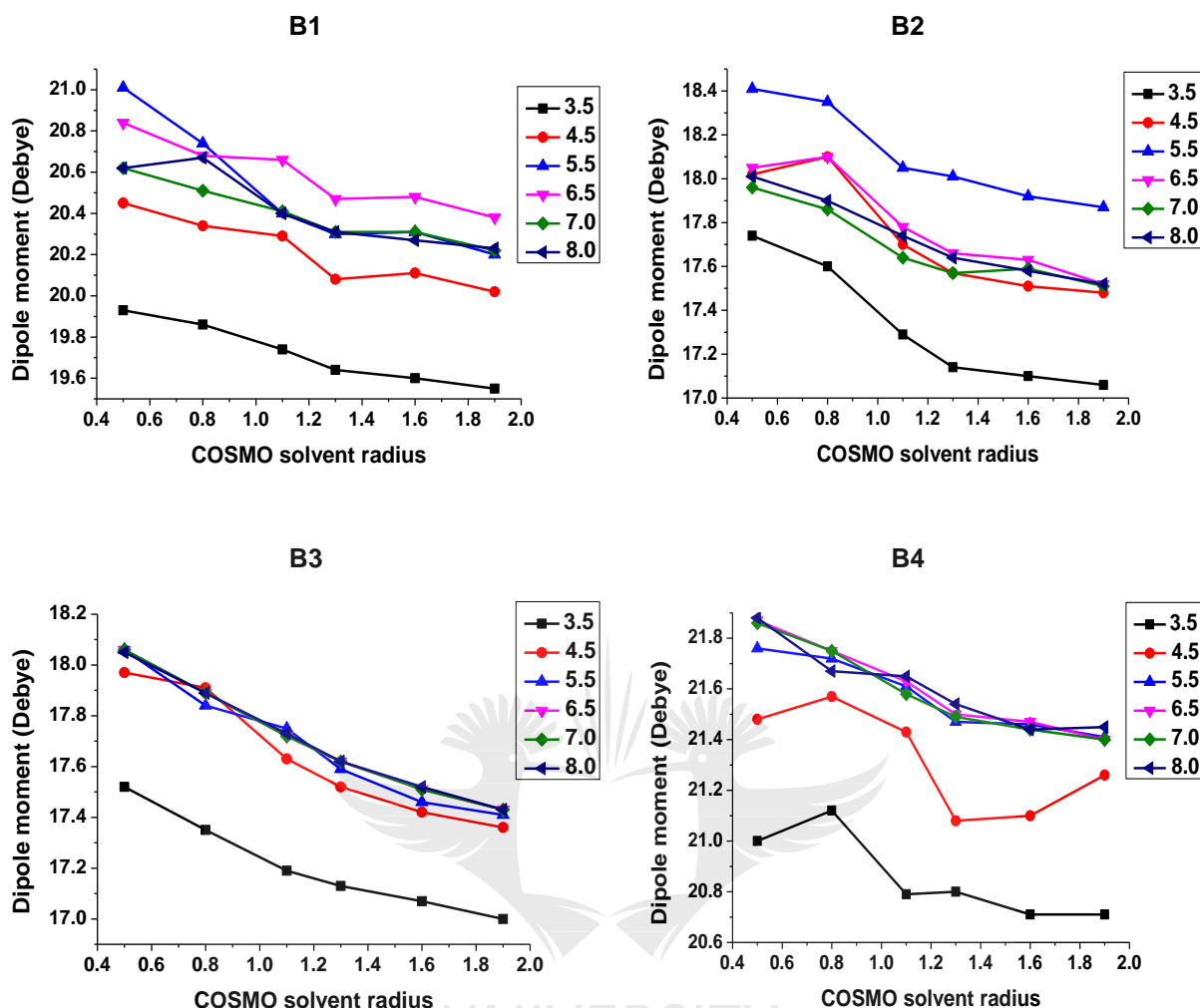


**Figure 6. 6:** Dipole moments for B1, B2, B3 and B4 as a function of COSMO solvent radius.

As CSR increases, solute-solvent electrostatic interactions become increasingly weaker because the solvent molecules are far away from the solute particles depending on the magnitude of the CSR increment. The solvent becomes increasingly less polarized leading to a continuous decrease in screening charge (Fig. 6.5), dipole moment (Fig. 6.6) and SFE magnitudes (Appendix: Tables A.10 – A.13). Despite this decrease, the solubility values obtained at the higher CSR are large, which may be due to overestimation of the vapor pressure (Appendix: Tables A.10 – A.13) by the larger CSR. Vapor pressure

overestimation usually result in a large  $S_{CSE}$  value unless the SFE magnitude is sufficiently small [20].

The trends observed for B1 and B4 at  $CSR > 1.3$  suggest that their vapour pressure is less overestimated by these COSMO solvent radii. Careful inspection of Tables A.10 and A.13 (Appendix) for B1 and B4, respectively, revealed a geometric increase in vapor pressure by a factor  $\geq 2$  up to CSR of 1.3, beyond which the increase in successive vapor pressure values is less than a factor of 2. Since a similar drop in Log  $S_{CSE}$  values at  $CSR > 1.3$  is not observed in B2 and B3 (Fig. 6.4) where a similar geometric increase in vapor pressure was obtained up to the highest CSR value of 1.9 (Appendix: Tables A.11 and A.12), we therefore suspect that the difference in vapor pressure and Log  $S_{CSE}$  trend between B1 and B4, and B2 and B3 at  $CSR > 1.3$  might be due to differences in molecular structures. B2 and B3 are structurally similar because they both possess two terminal hydroxyl groups, unlike B1 and B4 which possess only one terminal hydroxyl group (Fig. 6.7). Based on this structural difference, we can attribute the trend of vapor pressure and hence Log  $S_{CSE}$  observed for B1 and B4 at  $CSR > 1.3$  to absence of a second terminal hydroxyl group. The mechanism of how this affects vapor pressure estimation at these CSR is not yet known. It is noteworthy, however that Log  $S_{CSE}$  values obtained for B1 and B4 with  $CSR > 1.3$  are in stronger agreement with their respective experimental solubility values (Fig. 6.4) compared to values obtained with CSR of 1.3. For the sake of consistency, accuracy and reliability, we recommend a CSR value  $< 1.3$  for predicting the aqueous solubility of aminoazobenzene dyes using COSMO and COSMO-RS with Cramer *et al.* solubility equation and a CSR of 0.5 seems to be the best.

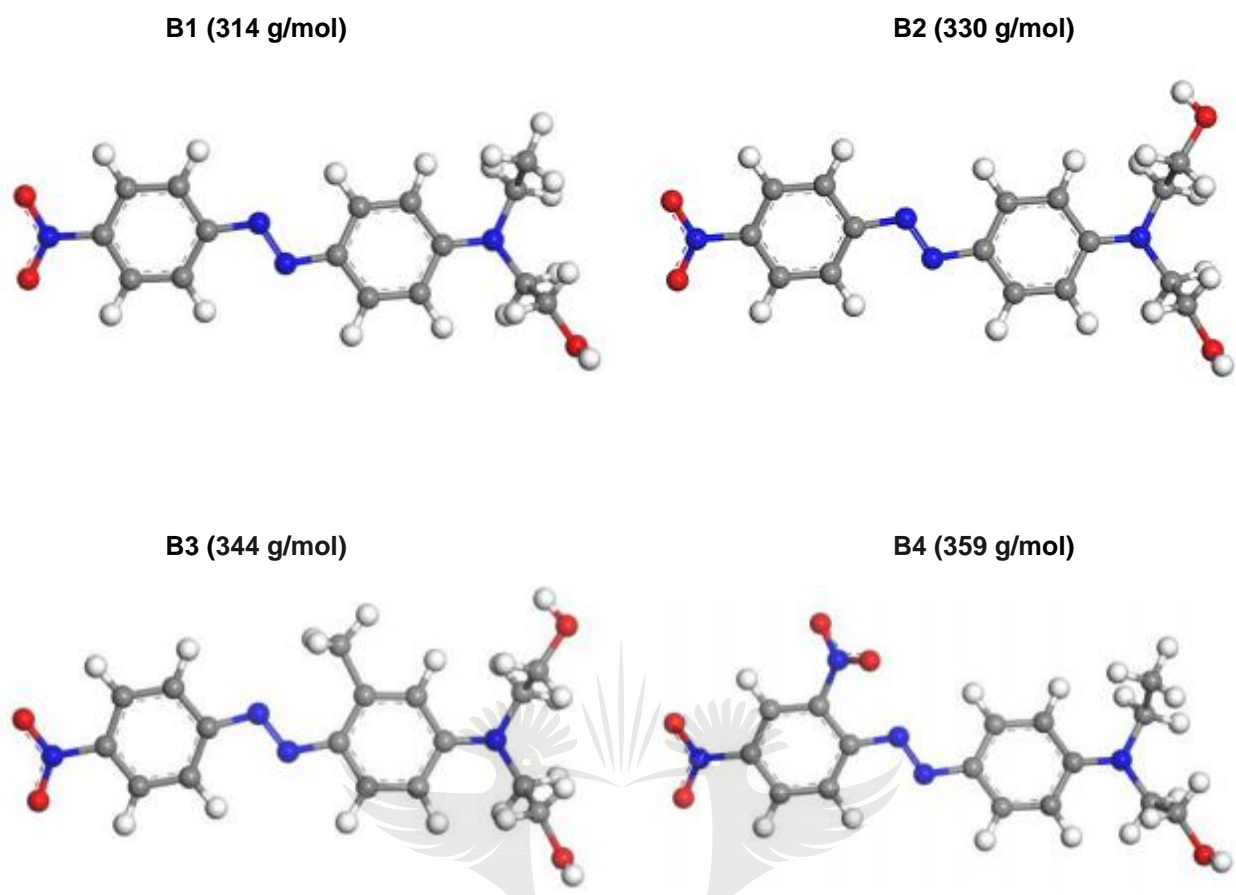


**Figure 6. 7:** Molecular structures of B1, B2, B3 and B4 with their respective Molecular weights.

### 6.3.5 EFFECT OF CSR ON GSE PREDICTED SOLUBILITY ( $S_{GSE}$ )

In the discussion of the effect of global orbital cut-off, the minimum appropriate cut-off for applying COSMO-RS/GSE technique for the solubility prediction has been identified as 4.5 Å. Therefore, for simplicity, the effects of COSMO solvent radius on GSE predicted solubility will be discussed in relation to this minimum cut-off. Figure 6.8 shows the response of Log  $S_{GSE}$  to change in COSMO solvent radius. For all the studied dyes, the figure revealed a general decrease in Log  $S_{GSE}$  with increase in CSR. This is not unexpected because the octanol-water partition coefficients (Log P) (Appendix: Tables A.10 – A.13) from which the  $S_{GSE}$  values were evaluated using equation 6.4 increases in

the same direction. The observed decrease in  $\text{Log } S_{\text{GSE}}$  with CSR may also be due to a similar decrease in negative screening charge and dipole moment which indicates a continuous decrease in solvent polarization and electrostatic interaction between the dyes and the solvent (water) as CSR increases. Careful inspection of Figure 6.8 showed that the range of CSR that yielded appreciable  $\text{Log } S_{\text{GSE}}$  values is not the same for all the dyes. The  $\text{Log } S_{\text{GSE}}$  values obtained for the studied dyes compare better with their respective experimental solubility values at CSR from 0.8 to 1.6 for B1,  $\geq 1.3$  for B2, and  $\leq 1.3$  for B3 and B4 whereas the best CSR are 1.3, 1.9, 0.5 and 0.8 for B1, B2, B3 and B4, respectively (Fig. 6.8). Unlike  $\text{Log } S_{\text{CSE}}$  values which increased with CSR and are closer to the experimental solubility values at lower CSR (Fig. 6.4),  $\text{Log } S_{\text{GSE}}$  values do not exhibit a definite trend with CSR. However for all these dyes, the only CSR which appreciably reproduced the experimental solubility values is 1.3 which may be the reason why this value is the default CSR for COSMO calculations [20].

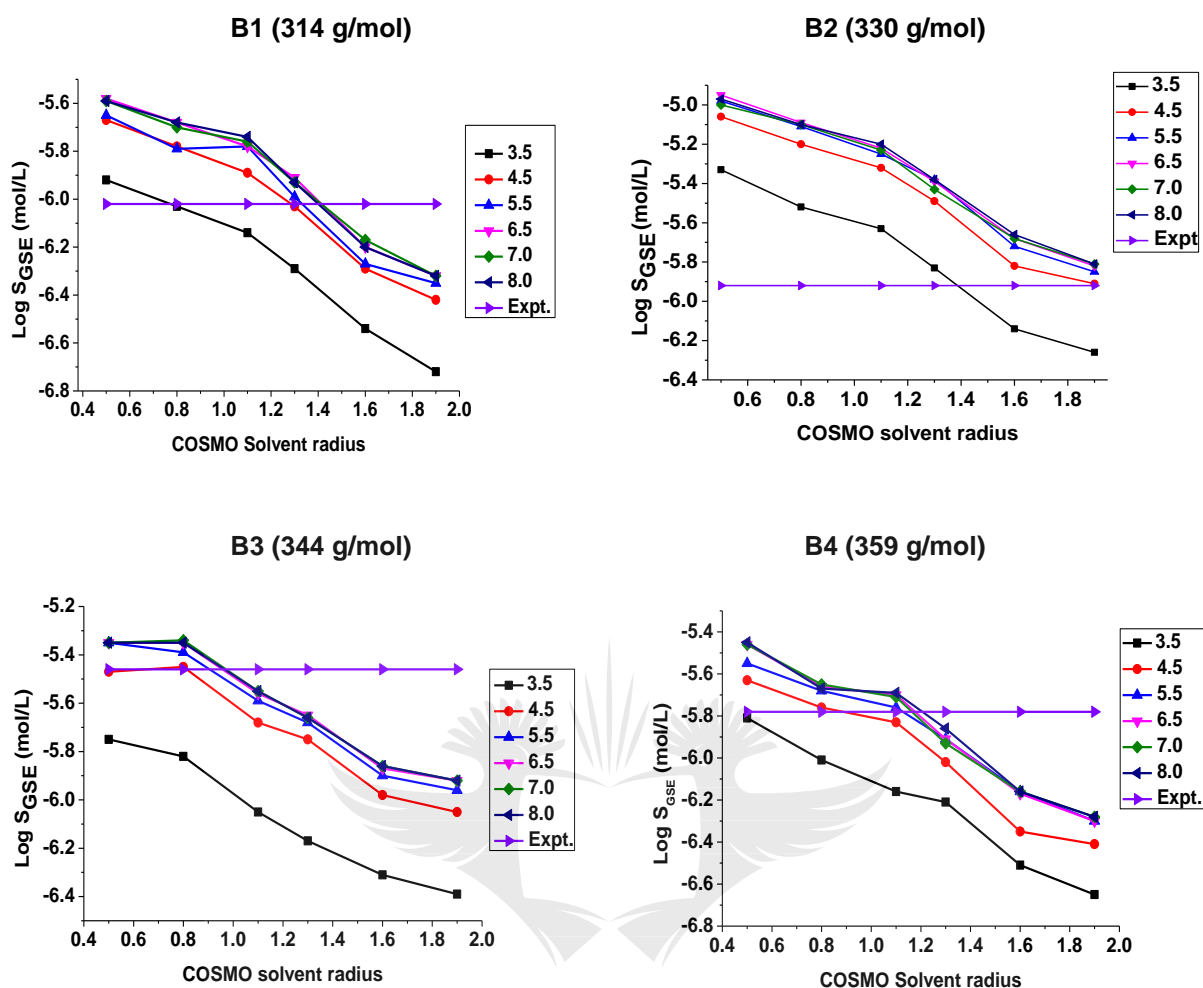


Figure 6. 8: Log S<sub>GSE</sub> for B1, B2, B3 and B4 as a function of COSMO solvent radius.

## 6.4 CONCLUSION

The roles of global orbital cut-off and COSMO solvent radius on predicted aqueous solubility (in mol/L) have been investigated for four low molecular weight aminoazobenzene dyes where the aqueous solubility prediction was achieved by treatment of DMol<sup>3</sup>/COSMO-RS data with Cramer *et al.* solubility equation (CSE) and general solubility equation (GSE) by Yalkowsky. The results revealed that both CSE and GSE are valid for predicting aqueous solubility (in mol/L) using COSMO-RS data, but their



responses to orbital cut-off and COSMO solvent radius vary. While the GSE predicted solubility increased with increase in cut-off value up to cut-off of 5.5 Å, the CSE results showed no constant trend of dependence on cut-off values for all the studied dyes. However, the dependence of appropriate CSE cut-off selection on solute molecular weight and the recommendation of a global orbital cut-off value of 7.0 Å for azo dyes with molecular weights less than 370 g/mol has been validated in this work.

## 6.5 REFERENCES

1. A. Klamt and G. Schüürmann. COSMO: a new approach to dielectric screening in solvents with explicit expressions for the screening energy and its gradient. *Journal of the Chemical Society, Perkin Transactions 2* (1993) 799-805.
2. J. Andzelm, C. Kölmel and A. Klamt. Incorporation of solvent effects into density functional calculations of molecular energies and geometries. *The Journal of Chemical Physics* **103** (1995) 9312-9320.
3. A. Klamt. The COSMO and COSMO-RS solvation models. *Wiley Interdisciplinary Reviews: Computational Molecular Science* **1** (2011) 699-709.
4. A. Klamt. Conductor-like screening model for real solvents: a new approach to the quantitative calculation of solvation phenomena. *The Journal of Physical Chemistry* **99** (1995) 2224-2235.
5. A. Klamt, V. Jonas, T. Bürger and J. C. Lohrenz. Refinement and parametrization of COSMO-RS. *The Journal of Physical Chemistry A* **102** (1998) 5074-5085.

6. M. Fujisawa, H. Tsutsumi and T. Kimura. Prediction of solubility of practically insoluble drugs in water/ethanol solvents using non-empirical methods. *Journal of Chemical and Pharmaceutical Research* **3** (2011) 750-758.
7. M. Lotfi, M. Moniruzzaman, M. Sivapragasam, S. Kandasamy, M. A. Mutalib, N. B. Alitheen and M. Goto. Solubility of acyclovir in nontoxic and biodegradable ionic liquids: COSMO-RS prediction and experimental verification. *Journal of Molecular Liquids* **243** (2017) 124-131.
8. Z. Song, Q. Zeng, J. Zhang, H. Cheng, L. Chen and Z. Qi. Solubility of imidazolium-based ionic liquids in model fuel hydrocarbons: A COSMO-RS and experimental study. *Journal of Molecular Liquids* **224** (2016) 544-550.
9. M. Lotfi, M. Moniruzzaman and M. S. Rajabi. Predicting the solubility of pharmaceutical compound in ionic liquids using COSMO-RS model. *ARPN Journal of Engineering and Applied Sciences* **11** (2016) 1618-1622.
10. Z. Guo, B.-M. Lue, K. Thomasen, A. S. Meyer and X. Xu. Predictions of flavonoid solubility in ionic liquids by COSMO-RS: experimental verification, structural elucidation, and solvation characterization. *Green Chemistry* **9** (2007) 1362-1373.
11. L. Mokrushina, M. Buggert, I. Smirnova, W. Arlt and R. Schomäcker. COSMO-RS and UNIFAC in prediction of micelle/water partition coefficients. *Industrial & Engineering Chemistry Research* **46** (2007) 6501-6509.
12. A. G. Sicaire, M. A. Vian, F. Fine, P. Carré, S. Tostain and F. Chemat. Experimental approach versus COSMO-RS assisted solvent screening for predicting the solubility of rapeseed oil. *Oilseeds and Fats, Crops and Lipids* **22** (2015) 1-7.

13. A. Klamt, F. Eckert, J. Reinisch and K. Wichmann. Prediction of cyclohexane-water distribution coefficients with COSMO-RS on the SAMPL5 data set. *Journal of Computer-Aided Molecular Design* **30** (2016) 959-967.
14. S. Mustapha, P. Okonkwo and S. Waziri. Improvement of carbon dioxide absorption technology using conductor-like screening model for real solvents (COSMO-RS) method. *Journal of Environmental Chemistry and Ecotoxicology* **5** (2013) 96-105.
15. C. Wittekindt and A. Klamt. COSMO-RS as a Predictive Tool for Lipophilicity. *Molecular Informatics* **28** (2009) 874-877.
16. A. Klamt, F. Eckert, M. Hornig, M. E. Beck and T. Bürger. Prediction of aqueous solubility of drugs and pesticides with COSMO-RS. *Journal of Computational Chemistry* **23** (2002) 275-281.
17. F. Eckert and A. Klamt. Accurate prediction of basicity in aqueous solution with COSMO-RS. *Journal of Computational Chemistry* **27** (2006) 11-19.
18. S. Tshepelevitsh, K. Hernits and I. Leito. Prediction of partition and distribution coefficients in various solvent pairs with COSMO-RS. *Journal of Computer-Aided Molecular Design* **32** (2018) 711-722.
19. B. Schröder, M. G. Freire, F. R. Varanda, I. M. Marrucho, L. M. Santos and J. A. Coutinho. Aqueous solubility, effects of salts on aqueous solubility, and partitioning behavior of hexafluorobenzene: experimental results and COSMO-RS predictions. *Chemosphere* **84** (2011) 415-422.
20. O. Wahab, L. Olasunkanmi, K. Govender and P. Govender. DMol<sup>3</sup>/COSMO-RS prediction of aqueous solubility and reactivity of selected Azo dyes: Effect of global

- orbital cut-off and COSMO segment variation. *Journal of Molecular Liquids* **249** (2018) 346-360.
21. B. Delley. From molecules to solids with the DMol 3 approach. *The Journal of Chemical Physics* **113** (2000) 7756-7764.
  22. F. Eckert and A. Klamt. COSMOtherm, Version C3.0, Release 13.01; COSMOlogic GmbH & Co. KG., Leverkusen, Germany, (2013). <http://www.cosmologic.de>. Last accessed on May 27, 2018.
  23. DMol<sup>3</sup> Guide. Material Studio 8.0. *Accelrys Software, Inc.*, San Diego, United States (2017) 1-161.
  24. Y. Inada and H. Orita. Efficiency of numerical basis sets for predicting the binding energies of hydrogen bonded complexes: evidence of small basis set superposition error compared to Gaussian basis sets. *Journal of Computational Chemistry* **29** (2008) 225-232.
  25. Y. Luo, S. Yin, W. Lai and Y. Wang. Effects of global orbital cutoff value and numerical basis set size on accuracies of theoretical atomization energies. *Theoretical Chemistry Accounts* **133** (2014) 1580-1587.
  26. V. A. Basiuk and L. V. Henao-Holguín. Effects of orbital cutoff in DMol<sup>3</sup> DFT calculations: a case study of meso-tetraphenylporphine–C60 complex. *Journal of Computational and Theoretical Nanoscience* **10** (2013) 1266-1272.
  27. E. Mullins, Y. Liu, A. Ghaderi and S. D. Fast. Sigma profile database for predicting solid solubility in pure and mixed solvent mixtures for organic pharmacological compounds with COSMO-based thermodynamic methods. *Industrial & Engineering Chemistry Research* **47** (2008) 1707-1725.

28. E. Mullins, R. Oldland, Y. Liu, S. Wang, S. I. Sandler, C.-C. Chen, M. Zwolak and K. C. Seavey. Sigma-profile database for using COSMO-based thermodynamic methods. *Industrial and Engineering Chemistry Research* **45** (2006) 4389-4415.
29. S. Bhat and E. O. Purisima. Molecular surface generation using a variable-radius solvent probe. *Proteins: Structure, Function, and Bioinformatics* **62** (2006) 244-261.
30. J. D. Thompson, C. J. Cramer and D. G. Truhlar. Predicting aqueous solubilities from aqueous free energies of solvation and experimental or calculated vapor pressures of pure substances. *The Journal of Chemical Physics* **119** (2003) 1661-1670.
31. D. L. Peterson and S. H. Yalkowsky. Comparison of two methods for predicting aqueous solubility. *Journal of Chemical Information and Computer Sciences* **41** (2001) 1531-1534.
32. C. Bird. The Dyeing of Acetate Rayon with Disperse Dyes I-Aqueous Solubility and the Influence of Dispersing Agents II-The Relation between Aqueous Solubility and Dyeing Properties. *Journal of the Society of Dyers and Colourists* **70** (1954) 68-77.
33. Materials Studio simulation environment. *Release 2016, Accelrys Software Inc., San Diego, CA, United States* (2016).
34. A. D. Becke. Density functional calculations of molecular bond energies. *The Journal of Chemical Physics* **84** (1986) 4524-4529.
35. A. D. Becke. Density-functional exchange-energy approximation with correct asymptotic behavior. *Physical Review A* **38** (1988) 3098-3100.

36. A. D. Becke. Density-functional thermochemistry. The effect of the Perdew–Wang generalized-gradient correlation correction. *The Journal of Chemical Physics* **97** (1992) 9173-9177.
37. A. D. Becke. Density-functional thermochemistry. The role of exact exchange. *The Journal of Chemical Physics* **98** (1993) 5648-5652.
38. A. D. Becke. A new mixing of Hartree–Fock and local density-functional theories. *The Journal of Chemical Physics* **98** (1993) 1372-1377.
39. J. P. Perdew. Density-functional approximation for the correlation energy of the inhomogeneous electron gas. *Physical Review B* **33** (1986) 8822-8824.
40. S. H. Vosko, L. Wilk and M. Nusair. Accurate spin-dependent electron liquid correlation energies for local spin density calculations: a critical analysis. *Canadian Journal of Physics* **58** (1980) 1200-1211.
41. N. Benedek, I. Snook, K. Latham and I. Yarovsky. Application of numerical basis sets to hydrogen bonded systems: a density functional theory study. *The Journal of Chemical Physics* **122** (2005) 144102-144109.
42. S. H. Yalkowsky and S. C. Valvani. Solubility and partitioning I: solubility of nonelectrolytes in water. *Journal of Pharmaceutical Sciences* **69** (1980) 912-922.

---

## CHAPTER 7

# COMPUTATIONAL STUDY OF THE EFFECTS OF SUBSTITUENT GROUPS ON SOLUBILITY AND REACTIVITY OF DISPERSE YELLOW 119 DYE

---

### PREAMBLE

Effects of substituent groups on aqueous solubility and chemical reactivity of disperse yellow 119 (DY119) dye has been theoretically investigated using the VWN-BP functional together with DNP basis set. The aim was to theoretically develop a set of new azo disperse dyes with improved aqueous solubility and degradability for more economic and more eco-friendly application. Appropriateness of some photocatalysts for their photodegradation was examined, and their possible photodegradation mechanisms were also predicted. Most of the studied derivatives were found to be more susceptible to photodegradation compared to the parent DY119 but only 50% of them were predicted to be more water-soluble than the parent dye. The electron withdrawing group substituted derivatives are predicted to be vulnerable to degradation via a C–N bond cleavage mechanism whereas the electron donating group substituted counterparts will most likely degrade through an N–N bond rupture pathway. ZnO showed highest catalytic affinity for the dyes.

### 7.1 INTRODUCTION

Being an abundant gift of nature, water remains the dominant dissolution medium for dyes. The use of non-aqueous solvents (i.e. solvent dyeing) and supercritical CO<sub>2</sub> fluid

has not received wide spread commercial application [1]. Carrier and dispersing agents often used to promote disperse dye solubility has both economic and environmental consequences [2,3]. High temperature and high pressure (HTHP) machines often employed for carrier free disperse dyeing is not suitable for dyes with low thermal stability due to the phenomenon of decomposition [3]. In addition to its relatively high cost, the machine also becomes less efficient during winter when condensation of the generated steam causes a drop in the operational pressure [3]. Supercritical CO<sub>2</sub> is not naturally occurring but produced from gaseous CO<sub>2</sub> at a critical temperature and pressure of 304 K and 73.7 bar, respectively [4-7] using specialized equipment. Maintenance cost and the lack of technical knowhow are obvious challenges to most users. To promote a less cumbersome, more economic and environmentally friendly dyeing practice, there is a need for disperse dyes with improved aqueous solubility and wash resistance properties to minimize the need for carrier agents.

Exposure to azo disperse dyes has been suspected as a potential cause of diseases such as bladder cancer and eczema in humans [3,8]. Several treatment methods have been proposed for dye pollutants [9-16], but photocatalytic degradation technique with the use of efficient, low cost and non-toxic photocatalysts such as TiO<sub>2</sub> and ZnO [11,17,14,18-21] is one of the most reliable methods. This is because it ensures complete destruction or denaturation of the pollutants (dyes). However, necessary guidelines on the selection of appropriate photodegradation catalysts is lacking. Evaluation of dye-catalyst interactions could help in understanding why some photocatalysts are more effective than others and as a result serves as a reliable theoretical guide for selecting a suitable catalyst for photodegradation processes.



Prediction of aqueous solubility, reactivity and thermodynamic properties of existing and novel dyes has both economic and environmental merits. It can pilot research scopes and efforts to concentrate on newly predicted dyes that exhibit certain advantageous characteristics. This, in a way, will cut down research cost and time, reduce redundancy in research activities, promote industrial applications of dyes and predict the fate of dyes in the environment. There are reports on the dyeing performance of some new disperse dyes on different fibers [22-24]. However, no theoretical study has been reported on disperse yellow (DY) 119 or any of its derivatives. More so, studies that focus on the prediction of aqueous solubility, relative reactivity and photodegradation potentials of DY119 derivatives in relation to the effects of substituent groups are very rare.

In view of the problem statements, the present work presents theoretical investigations of aqueous solubility, reactivity and thermodynamic stability of 29 azopyridone disperse dyes (E1 – E29) and the unsubstituted (parent) DY119 (Fig. 7.1). The 29 new dyes are electron withdrawing group (EWG) and electron donating group (EDG) substituted derivatives of DY119. As posited in the literature [25], the EWGs are substituted at positions R<sub>1</sub> and R<sub>3</sub> on the accepting moiety of DY119 while the EDGs are substituted at position R<sub>4</sub> and R<sub>5</sub> on the donating moiety. Since EWGs are *meta* directors [26], the NO<sub>2</sub> group on the accepting part of DY119 suggests positions R<sub>1</sub> and R<sub>3</sub> as the only reasonable vacant positions for further EWG substitution. On the other hand, EDGs are *ortho/para* directors [26], hence their substitution at positions R<sub>4</sub> and R<sub>5</sub>. Susceptibility of the dyes to photocatalytic degradation and suitability of some selected catalysts for the process are also discussed. Photodegradation pathways were predicted and the prospective sites for radical attacks during photocatalytic degradation were identified.

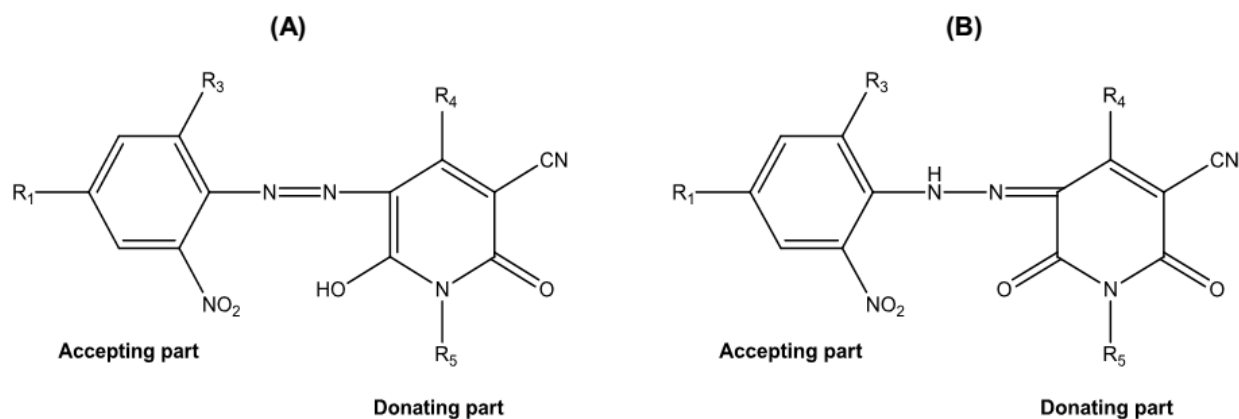


**Figure 7. 1:** General molecular structures of the azo (A) and hydrazone (B) forms of the studied dyes.

DY119:  $R_1 = R_3 = \text{H}$ ,  $R_4 = \text{CH}_3$  and  $R_5 = \text{C}_2\text{H}_5$ ; **E1**:  $R_1 = \text{H}$ ,  $R_3 = \text{NO}_2$ ,  $R_4 = \text{CH}_3$  and  $R_5 = \text{C}_2\text{H}_5$ ; **E2**:  $R_1 = \text{H}$ ,  $R_3 = \text{CN}$ ,  $R_4 = \text{CH}_3$  and  $R_5 = \text{C}_2\text{H}_5$ ; **E3**:  $R_1 = \text{NO}_2$ ,  $R_3 = \text{H}$ ,  $R_4 = \text{CH}_3$  and  $R_5 = \text{C}_2\text{H}_5$ ; **E4**:  $R_1 = \text{CN}$ ,  $R_3 = \text{H}$ ,  $R_4 = \text{CH}_3$  and  $R_5 = \text{C}_2\text{H}_5$ ; **E5**:  $R_1 = R_3 = \text{NO}_2$ ,  $R_4 = \text{CH}_3$  and  $R_5 = \text{C}_2\text{H}_5$ ; **E6**:  $R_1 = R_3 = \text{CN}$ ,  $R_4 = \text{CH}_3$  and  $R_5 = \text{C}_2\text{H}_5$ ; **E7**:  $R_1 = \text{NO}_2$ ,  $R_3 = \text{CN}$ ,  $R_4 = \text{CH}_3$  and  $R_5 = \text{C}_2\text{H}_5$ ; **E8**:  $R_1 = \text{CN}$ ,  $R_3 = \text{NO}_2$ ,  $R_4 = \text{CH}_3$  and  $R_5 = \text{C}_2\text{H}_5$ ; **E9**:  $R_1 = R_3 = \text{H}$ ,  $R_4 = \text{NH}_2$  and  $R_5 = \text{C}_2\text{H}_5$ ; **E10**:  $R_1 = R_3 = \text{H}$ ,  $R_4 = \text{NHCH}_3$  and  $R_5 = \text{C}_2\text{H}_5$ ; **E11**:  $R_1 = R_3 = \text{H}$ ,  $R_4 = \text{N}(\text{CH}_3)_2$  and  $R_5 = \text{C}_2\text{H}_5$ ; **E12**:  $R_1 = R_3 = \text{H}$ ,  $R_4 = \text{CH}_3$  and  $R_5 = \text{NH}_2$ ; **E13**:  $R_1 = R_3 = \text{H}$ ,  $R_4 = \text{CH}_3$  and  $R_5 = \text{NHCH}_3$ ; **E14**:  $R_1 = R_3 = \text{H}$ ,  $R_4 = \text{CH}_3$  and  $R_5 = \text{NH}(\text{CH}_3)_2$ ; **E15**:  $R_1 = R_3 = \text{H}$ ,  $R_4 = \text{NH}_2$  and  $R_5 = \text{CH}_3$ ; **E16**:  $R_1 = R_3 = \text{H}$ ,  $R_4 = \text{NHCH}_3$  and  $R_5 = \text{CH}_3$ ; **E17**:  $R_1 = R_3 = \text{H}$ ,  $R_4 = \text{N}(\text{CH}_3)_2$  and  $R_5 = \text{CH}_3$ ; **E18**:  $R_1 = R_3 = \text{H}$ ,  $R_4 = \text{C}_2\text{H}_5$  and  $R_5 = \text{NH}_2$ ; **E19**:  $R_1 = R_3 = \text{H}$ ,  $R_4 = \text{C}_2\text{H}_5$  and  $R_5 = \text{NHCH}_3$ ; **E20**:  $R_1 = R_3 = \text{H}$ ,  $R_4 = \text{C}_2\text{H}_5$  and  $R_5 = \text{NH}(\text{CH}_3)_2$ ; **E21**:  $R_1 = R_3 = \text{H}$ ,  $R_4 = R_5 = \text{NH}_2$ ; **E22**:  $R_1 = R_3 = \text{H}$ ,  $R_4 = \text{NH}_2$  and  $R_5 = \text{NHCH}_3$ ; **E23**:  $R_1 = R_3 = \text{H}$ ,  $R_4 = \text{NH}_2$  and  $R_5 = \text{NH}(\text{CH}_3)_2$ ; **E24**:  $R_1 = R_3 = \text{H}$ ,  $R_4 = \text{NHCH}_3$ ,  $R_5 = \text{NH}_2$ ; **E25**:  $R_1 = R_3 = \text{H}$ ,  $R_4 = R_5 = \text{NHCH}_3$ ; **E26**:  $R_1 = R_3 = \text{H}$ ,  $R_4 = \text{NHCH}_3$  and  $R_5 = \text{NH}(\text{CH}_3)_2$ ; **E27**:  $R_1 = R_3 = \text{H}$ ,  $R_4 = \text{NH}(\text{CH}_3)_2$ ,  $R_5 = \text{NH}_2$ ; **E28**:  $R_1 = R_3 = \text{H}$ ,  $R_4 = \text{NH}(\text{CH}_3)_2 = R_5 = \text{NHCH}_3$ ; **E29**:  $R_1 = R_3 = \text{H}$ ,  $R_4 = R_5 = \text{NH}(\text{CH}_3)_2$ .

## 7.2 COMPUTATIONAL DETAILS

The DMol<sup>3</sup> computational code [27] incorporated in the Material studio 2016 package was employed for this study. The geometries of the studied dyes were optimized both in the gas and aqueous phases at the GGA/VWN-BP level of theory [27] using the DNP basis set [27,28]. A global orbital cut-off value of 7.0 Å was used for the calculations. Aqueous phase optimization was carried out using the COSMO-RS code implemented in DMol<sup>3</sup>

program module by setting the COSMO dielectric constant to 78.4 (i.e. dielectric of water). A total of 92 surface segments per atom (i.e. NSPA = 92) was used and the recommended radii [29,30] for the component atoms of the studied dyes were included in the COSMO calculation for proper description of molecular cavitation.

The solvation free energies (SFEs) of the dyes were obtained using equation 7.1 [27]. The aqueous solubility (in mg/L) was calculated from the SFEs and the COSMO-RS vapor pressure using the Cramer *et al.* solubility equation (CSE) (Eqn. 7.2) [31]. The Gibb's free energies were calculated using equation 7.3 [27].

$$\Delta G_{sol} = (E + \Delta G_{NSE}) - E^0 \quad \text{Equation 7.1}$$

$$S_{aq} = \frac{P_s}{P^0} e^{-\Delta G_{sol}/RT} \quad \text{Equation 7.2}$$

$$G = H - TS \quad \text{Equation 7.3}$$

$\Delta G_{sol}$  in equation 7.1 is the solvation free energy,  $E$  is the energy in the aqueous phase (i.e COSMO energy),  $E^0$  is the energy in gas phase,  $\Delta G_{NSE}$  is the non-electrostatic contribution to SFE due to dispersion and cavity formation effects,  $S_{aq}$  in equation 7.2 is the aqueous solubility in mol/L,  $P_s$  is the solute (dye) vapor pressure obtained from COSMO-RS calculation in this study,  $P^0 = 24.45$  atm (the pressure of an ideal gas at 1 molar standard state and 298 K),  $R$  and  $T$  are the molar gas constant and temperature respectively.  $G$ ,  $H$  and  $S$  in equation 7.3 are the Gibb's free energy, enthalpy and entropy of the solute, respectively.

The polarizabilities of the dyes were calculated from their respective vapor pressure using the Liang and Gallagher relation (eqn. 7.4) [32]. The global reactivity indices, which comprise the energy gap between the highest occupied molecular orbital (HOMO) and

lowest unoccupied molecular orbital (LUMO), global hardness and softness, global electronegativity, chemical potential and global electrophilicity index were calculated from the HOMO and LUMO energies using equations 7.5 – 7.10 [33-38].

$$\alpha = (3.940 - \text{Log } P_s)/0.401 \quad \text{Equation 7. 4}$$

$\alpha$  represents solute polarizability and  $P_s$  is as defined previously.

$$\text{Energy gap } (E_g) = (E_{LUMO} - E_{HOMO}) \quad \text{Equation 7. 5}$$

$$\text{Global hardness } (\eta) = \frac{1}{2}(E_{LUMO} - E_{HOMO}) \quad \text{Equation 7. 6}$$

$$\text{Global softness } (\sigma) = \frac{1}{\eta} = 2/(E_{LUMO} - E_{HOMO}) \quad \text{Equation 7. 7}$$

$$\text{Electronegativity } (\chi) = -\frac{1}{2}(E_{HOMO} + E_{LUMO}) \quad \text{Equation 7. 8}$$

$$\text{Chemical potential } (\Phi) = -\chi = \frac{1}{2}(E_{HOMO} + E_{LUMO}) \quad \text{Equation 7. 9}$$

$$\text{Global electrophilicity index } (\omega) = \frac{\Phi^2}{2\eta} \quad \text{Equation 7. 10}$$

The semiconductors considered in this study include Si, CdSe, CdS, TiO<sub>2</sub>, ZnO and ZnS. These photocatalysts were selected across a range of band gaps in both the UV and the visible region of the solar radiation. Their band structures which comprise the conduction band minimum (CBM), the valence band minimum (VBM) and the band gap were also calculated with the DMol<sup>3</sup> program using the selected level of DFT. The primitive cells of Si and CdSe were used for the calculations while the most stable surface morphologies were employed in the case of CdS, TiO<sub>2</sub> (rutile), ZnO and ZnS [39-43] because they produced more accurate theoretical band gap at minimal computational cost.

The atom condensed Fukui functions for radical,  $f^0$ , attack was determined from the Mulliken's atomic charges using equations 7.11 [44].

$$f^0 = \frac{1}{2} [q_k(N + 1) - q_k(N - 1)]$$

Equation 7. 11

where  $N$  is the number of electron,  $q_k(N + 1)$  and  $q_k(N - 1)$  are the Mulliken charges on atom  $k$ , for  $(N + 1)$  - and  $(N - 1)$  - electron systems respectively.

## 7.3 RESULTS AND DISCUSSIONS

### 7.3.1 AQUEOUS SOLUBILITY STUDY

The vapor pressure, solvation free energies, aqueous solubility and Gibb's free energies obtained for DY119 and its studied derivatives (Fig. 7.1) are presented in Table 7.1. The screening charges, dipole moments and polarizabilities calculated for the dyes are given in Table 7.2.

The results in Table 7.1 revealed that the vapor pressure of the studied derivatives are generally lower than that of the parent dye, which suggests that the derivatives will have greater heat resistance (i.e. higher sublimation fastness) than DY119. The reduction in vapor pressure in the presence of the substituents could be attributed to increase in molecular weight and enhanced polarizability (Table 7.2). High molecular weight disperse dyes are known to possess higher thermal stability than their low molecular weight counterparts [2]. Also, a high polarizability value suggests the likelihood of a solute to strongly interact with a polar solvent and get solvated.

**Table 7. 1:** Aqueous solubility ( $S_{aq}$ ), SFE ( $\Delta G_{sol}$ ), vapour pressure ( $p$ ) and the Gibb's free energies ( $G_{gas}$ ) obtained for DY119 and its studied derivatives at 25 °C.

Dye	R <sub>1</sub>	R <sub>2</sub>	R <sub>3</sub>	R <sub>4</sub>	R <sub>5</sub>	Mwt. (g/mol)	$p \times 10^{-11}$ (atm)	$\Delta G_{sol}$ (kcal/mol)	$S_{aq}$ (mg/L)	$\Delta G_{gas}$ (kcal/mol)
DY119	H	NO <sub>2</sub>	H	CH <sub>3</sub>	C <sub>2</sub> H <sub>5</sub>	327.30	1.92	-11.38	57.33	-37.07
EWG substitution										
E1	H	NO <sub>2</sub>	NO <sub>2</sub>	CH <sub>3</sub>	C <sub>2</sub> H <sub>5</sub>	372.30	0.31	-12.75	106.52	-35.58
E2	H	NO <sub>2</sub>	CN	CH <sub>3</sub>	C <sub>2</sub> H <sub>5</sub>	352.31	0.34	-12.94	152.40	-33.59
E3	NO <sub>2</sub>	NO <sub>2</sub>	H	CH <sub>3</sub>	C <sub>2</sub> H <sub>5</sub>	372.30	0.037	-13.20	27.19	-36.61
E4	CN	NO <sub>2</sub>	H	CH <sub>3</sub>	C <sub>2</sub> H <sub>5</sub>	352.31	0.046	-13.69	73.19	-34.71
E5	NO <sub>2</sub>	NO <sub>2</sub>	NO <sub>2</sub>	CH <sub>3</sub>	C <sub>2</sub> H <sub>5</sub>	417.29	0.067	-13.43	81.39	-38.37
E6	CN	NO <sub>2</sub>	CN	CH <sub>3</sub>	C <sub>2</sub> H <sub>5</sub>	377.32	0.023	-15.12	438.81	-36.44
E7	NO <sub>2</sub>	NO <sub>2</sub>	CN	CH <sub>3</sub>	C <sub>2</sub> H <sub>5</sub>	397.31	0.029	-14.33	153.40	-36.03
E8	CN	NO <sub>2</sub>	NO <sub>2</sub>	CH <sub>3</sub>	C <sub>2</sub> H <sub>5</sub>	397.31	0.039	-14.20	165.62	-37.24
EDG substitution										
E9	H	NO <sub>2</sub>	H	NH <sub>2</sub>	C <sub>2</sub> H <sub>5</sub>	328.29	0.0023	-14.67	17.85	-33.31
E10	H	NO <sub>2</sub>	H	NHCH <sub>3</sub>	C <sub>2</sub> H <sub>5</sub>	342.31	0.0022	-14.36	10.54	-34.05
E11	H	NO <sub>2</sub>	H	N(CH <sub>3</sub> ) <sub>2</sub>	C <sub>2</sub> H <sub>5</sub>	356.34	0.0065	-12.99	3.21	-35.41
E12	H	NO <sub>2</sub>	H	CH <sub>3</sub>	NH <sub>2</sub>	314.26	0.26	-13.56	296.26	-31.68
E13	H	NO <sub>2</sub>	H	CH <sub>3</sub>	NHCH <sub>3</sub>	328.29	0.16	-13.11	89.06	-33.98
E14	H	NO <sub>2</sub>	H	CH <sub>3</sub>	N(CH <sub>3</sub> ) <sub>2</sub>	342.31	0.45	-12.17	53.37	-35.19
E15	H	NO <sub>2</sub>	H	NH <sub>2</sub>	CH <sub>3</sub>	314.26	0.0028	-15.27	57.32	-31.45
E16	H	NO <sub>2</sub>	H	NHCH <sub>3</sub>	CH <sub>3</sub>	328.29	0.0028	-14.86	29.96	-31.04
E17	H	NO <sub>2</sub>	H	N(CH <sub>3</sub> ) <sub>2</sub>	CH <sub>3</sub>	342.31	0.012	-13.64	17.05	-34.17
E18	H	NO <sub>2</sub>	H	C <sub>2</sub> H <sub>5</sub>	NH <sub>2</sub>	328.29	0.18	-13.15	107.19	-34.28
E19	H	NO <sub>2</sub>	H	C <sub>2</sub> H <sub>5</sub>	NHCH <sub>3</sub>	342.31	0.10	-12.72	30.03	-35.04
E20	H	NO <sub>2</sub>	H	C <sub>2</sub> H <sub>5</sub>	N(CH <sub>3</sub> ) <sub>2</sub>	356.34	0.27	-11.82	18.46	-35.30
E21	H	NO <sub>2</sub>	H	NH <sub>2</sub>	NH <sub>2</sub>	315.25	0.00020	-17.09	88.86	-30.22
E22	H	NO <sub>2</sub>	H	NH <sub>2</sub>	NHCH <sub>3</sub>	329.27	0.000030	-16.65	6.62	-31.47

E23	H	NO <sub>2</sub>	H	NH <sub>2</sub>	N(CH <sub>3</sub> ) <sub>2</sub>	343.30	0.000058	-15.80	3.18	-34.14
E24	H	NO <sub>2</sub>	H	NHCH <sub>3</sub>	NH <sub>2</sub>	329.27	0.00016	-16.92	55.72	-33.09
E25	H	NO <sub>2</sub>	H	NHCH <sub>3</sub>	NHCH <sub>3</sub>	343.30	0.000053	-16.28	6.53	-35.04
E26	H	NO <sub>2</sub>	H	NHCH <sub>3</sub>	N(CH <sub>3</sub> ) <sub>2</sub>	357.33	0.000090	-15.89	5.97	-32.92
E27	H	NO <sub>2</sub>	H	N(CH <sub>3</sub> ) <sub>2</sub>	NH <sub>2</sub>	343.30	0.00099	-16.11	91.50	-33.84
E28	H	NO <sub>2</sub>	H	N(CH <sub>3</sub> ) <sub>2</sub>	NHCH <sub>3</sub>	357.33	0.00030	-17.46	282.27	-33.42
E29	H	NO <sub>2</sub>	H	N(CH <sub>3</sub> ) <sub>2</sub>	N(CH <sub>3</sub> ) <sub>2</sub>	371.35	0.0015	-16.99	663.06	-35.75

**Table 7. 2:** Screening charges,  $q$ , polarizability,  $\alpha$ , and dipole moment,  $\mu$  of DY119 and its studied derivatives at 25 °C.

Dye No.	R1	R2	R3	R4	R5	Screening charge, $q$	$\alpha$	$\mu$ (Debye)
DY119	H	NO <sub>2</sub>	H	CH <sub>3</sub>	C <sub>2</sub> H <sub>5</sub>	-0.00119	29.37	6.80
EWG substitution								
E1	H	NO <sub>2</sub>	NO <sub>2</sub>	CH <sub>3</sub>	C <sub>2</sub> H <sub>5</sub>	-0.00100	31.34	7.51
E2	H	NO <sub>2</sub>	CN	CH <sub>3</sub>	C <sub>2</sub> H <sub>5</sub>	-0.00103	31.24	7.71
E3	NO <sub>2</sub>	NO <sub>2</sub>	H	CH <sub>3</sub>	C <sub>2</sub> H <sub>5</sub>	-0.00081	33.64	0.35
E4	CN	NO <sub>2</sub>	H	CH <sub>3</sub>	C <sub>2</sub> H <sub>5</sub>	-0.00090	33.41	0.91
E5	NO <sub>2</sub>	NO <sub>2</sub>	NO <sub>2</sub>	CH <sub>3</sub>	C <sub>2</sub> H <sub>5</sub>	-0.00063	33.00	2.91
E6	CN	NO <sub>2</sub>	CN	CH <sub>3</sub>	C <sub>2</sub> H <sub>5</sub>	-0.00077	34.16	3.43
E7	NO <sub>2</sub>	NO <sub>2</sub>	CN	CH <sub>3</sub>	C <sub>2</sub> H <sub>5</sub>	-0.00068	33.91	3.27
E8	CN	NO <sub>2</sub>	NO <sub>2</sub>	CH <sub>3</sub>	C <sub>2</sub> H <sub>5</sub>	-0.00071	33.59	3.15
EDG substitution								
E9	H	NO <sub>2</sub>	H	NH <sub>2</sub>	C <sub>2</sub> H <sub>5</sub>	-0.00125	36.65	7.57
E10	H	NO <sub>2</sub>	H	NHCH <sub>3</sub>	C <sub>2</sub> H <sub>5</sub>	-0.00128	36.70	8.05
E11	H	NO <sub>2</sub>	H	N(CH <sub>3</sub> ) <sub>2</sub>	C <sub>2</sub> H <sub>5</sub>	-0.00130	35.52	7.91
E12	H	NO <sub>2</sub>	H	CH <sub>3</sub>	NH <sub>2</sub>	-0.00116	31.53	7.54
E13	H	NO <sub>2</sub>	H	CH <sub>3</sub>	NHCH <sub>3</sub>	-0.00117	32.05	7.76
E14	H	NO <sub>2</sub>	H	CH <sub>3</sub>	N(CH <sub>3</sub> ) <sub>2</sub>	-0.00130	30.93	6.14

E15	H	NO <sub>2</sub>	H	NH <sub>2</sub>	CH <sub>3</sub>	-0.00120	36.44	7.99
E16	H	NO <sub>2</sub>	H	NHCH <sub>3</sub>	CH <sub>3</sub>	-0.00122	36.44	8.42
E17	H	NO <sub>2</sub>	H	N(CH <sub>3</sub> ) <sub>2</sub>	CH <sub>3</sub>	-0.00122	34.86	8.21
E18	H	NO <sub>2</sub>	H	C <sub>2</sub> H <sub>5</sub>	NH <sub>2</sub>	-0.00120	31.93	7.46
E19	H	NO <sub>2</sub>	H	C <sub>2</sub> H <sub>5</sub>	NHCH <sub>3</sub>	-0.00122	32.57	7.70
E20	H	NO <sub>2</sub>	H	C <sub>2</sub> H <sub>5</sub>	N(CH <sub>3</sub> ) <sub>2</sub>	-0.00135	31.49	6.23
E21	H	NO <sub>2</sub>	H	NH <sub>2</sub>	NH <sub>2</sub>	-0.00123	39.30	8.13
E22	H	NO <sub>2</sub>	H	NH <sub>2</sub>	NHCH <sub>3</sub>	-0.00124	41.35	8.29
E23	H	NO <sub>2</sub>	H	NH <sub>2</sub>	N(CH <sub>3</sub> ) <sub>2</sub>	-0.00128	40.64	7.63
E24	H	NO <sub>2</sub>	H	NHCH <sub>3</sub>	NH <sub>2</sub>	-0.00124	39.54	8.89
E25	H	NO <sub>2</sub>	H	NHCH <sub>3</sub>	NHCH <sub>3</sub>	-0.00125	40.74	8.90
E26	H	NO <sub>2</sub>	H	NHCH <sub>3</sub>	N(CH <sub>3</sub> ) <sub>2</sub>	-0.00131	40.16	8.31
E27	H	NO <sub>2</sub>	H	N(CH <sub>3</sub> ) <sub>2</sub>	NH <sub>2</sub>	-0.00125	38.06	8.42
E28	H	NO <sub>2</sub>	H	N(CH <sub>3</sub> ) <sub>2</sub>	NHCH <sub>3</sub>	-0.00126	38.86	8.57
E29	H	NO <sub>2</sub>	H	N(CH <sub>3</sub> ) <sub>2</sub>	N(CH <sub>3</sub> ) <sub>2</sub>	-0.00138	37.11	7.89

Therefore, keeping other factors such as effect of steric hindrance constant, a highly polarizable solute will be highly soluble in a polar solvent. In this regard, the relatively large aqueous solubility values obtained for the EWG substituted derivatives (Table 7.1) apart from E3 might be due to their large polarizability values (Table 7.2) compared to the parent dye. The relatively small solubility value obtained for E3 is suspected to result from its extremely low polarity compared to the parent dye as suggested by its dipole moment value in Table 7.2.

Though, the slightly more negative screening charge, the larger dipole moment and higher polarizability of most of the EDG substituted derivatives compared to DY119 (Table 7.2) might be prognostic of greater solvation and higher solubility of the derivatives, the conversely observed lower aqueous solubility of most of these derivatives, particularly



those containing  $\text{NHCH}_3$  and  $\text{N}(\text{CH}_3)_2$  groups in comparison to the parent dye might be due to relatively large steric hindrance to solvation caused by these substituents.

The magnitude of steric hindrance caused by the EDG substituents at positions  $\text{R}_4$  and  $\text{R}_5$  are compared in Figure 7.2 in terms of their torsion angles relative to the molecular plane. The closer the angle to  $180^\circ$ , the more the alignment of the substituent along the molecular plane and the less the steric effect. Large deviation from  $180^\circ$  is indicative of large steric effect at the concerned substituent position.

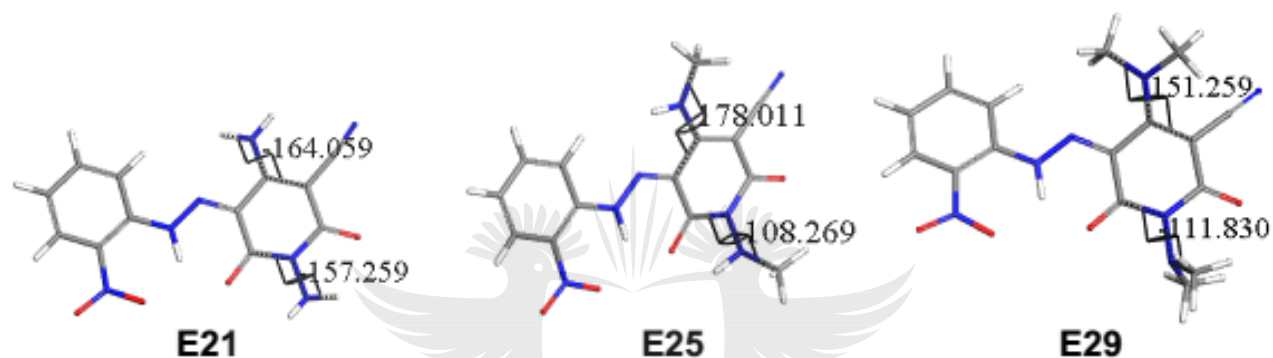


**Figure 7. 2:** Optimized structures of E21, E25 and E29 showing the torsion angles of  $\text{NH}_2$ ,  $\text{NHCH}_3$  and  $\text{N}(\text{CH}_3)_2$  substituents respectively, at positions  $\text{R}_4$  and  $\text{R}_5$ .

The remarkable increase in solubility obtained when the EDG substituents are attached to position  $\text{R}_5$  as in derivatives such as E12-E14 and E18-E20 compared to E15-E17 and E9-E11 respectively can be ascribed to the electron withdrawing influence of the two neighboring carbonyl groups, which decreases the electron density at the pyridone nitrogen center (i.e. position  $\text{R}_5$ ) (Fig. 7.1). This nitrogen center consequently abstracts electrons by means of an inductive effect from the attached substituent groups which increases the polarity of the  $\text{N} - \text{N}$  bond (Fig. 7.3). Figure 7.3 showed that the  $\text{C} - \text{N}$  bond formed between the EDG substituents and the donor ring at positions  $\text{R}_4$  is shorter than the corresponding  $\text{N} - \text{N}$  bond formed at position  $\text{R}_5$ . The longer the bond, the more the influence of the carbonyl group and the greater the ionic character and the polarity of the

bond. This implies that the N – N bond has greater ionic character as a result of its higher polarity compared to the C – N bond.

The electron withdrawing influence of the carbonyl groups will be minimal on position R<sub>4</sub> from a proximity perspective (Fig. 7.1). Therefore, the electron donating effect of the substituents will increase the polarity of the azo bridge better when attached to position R<sub>4</sub> compared to R<sub>5</sub>. This explains why the dipole moment values for E15-E17 and E9-E11 are greater than those of E12-E14 and E18-E20 respectively (Table 7.2).

The slightly more negative screening charge obtained for E9-E11 and E15-E17 compared respectively to E18-E20 and E12-E14 also confirms a higher electronic effect for the EDGs when substituted at position R<sub>4</sub>. The generally higher solubility values obtained for the NH<sub>2</sub> substituted derivatives compared to NHCH<sub>3</sub> and N(CH<sub>3</sub>)<sub>2</sub> substituted counterparts confirm lower steric contribution by NH<sub>2</sub> as a result of its relatively small size (Fig. 7.2).

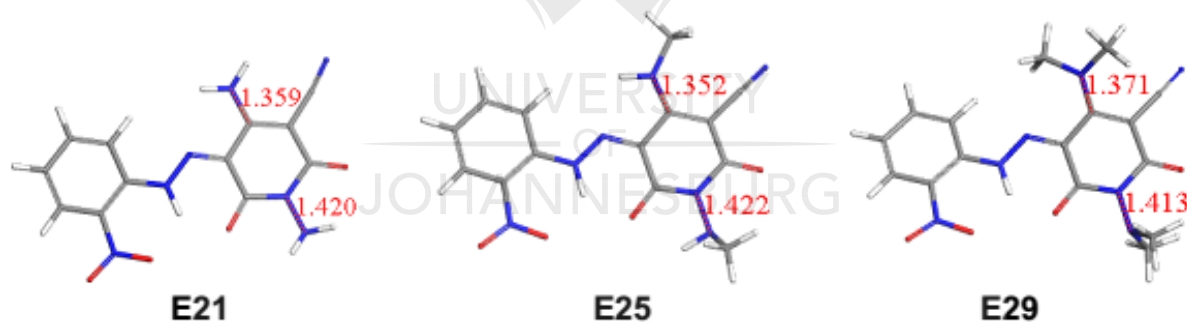


**Figure 7. 3:** Optimized structures of E21, E25 and E29 showing the lengths of the C – N and N – N bond formed at positions R<sub>4</sub> and R<sub>5</sub> respectively, by NH<sub>2</sub>, NHCH<sub>3</sub> and N(CH<sub>3</sub>)<sub>2</sub> substituents.

In addition, the NH<sub>2</sub> substituted derivatives have more sites available for hydrogen bonding interaction with water molecules compared to the NHCH<sub>3</sub> and N(CH<sub>3</sub>)<sub>2</sub> substituted counterparts (Fig. 7.4). NH<sub>2</sub> has one more available site (i.e. 1H atom) than NHCH<sub>3</sub>, but two more hydrogen bonding sites (i.e. 2H atoms) than N(CH<sub>3</sub>)<sub>2</sub>. This may

also be responsible for the relatively large solubility values obtained for the  $\text{NH}_2$  substituted derivatives.

The screening charges for the EWG derivatives vary by less than a factor of two compared to the parent dye and most of these derivatives also show smaller dipole moment than the parent dye. This could be ascribed to the decrease in charge separation between the donor and acceptor moieties of the dyes (Fig. 7.1) as the electron density is drifted towards the accepting part of the dyes by the EWGs. The dipole moment vector of azo dyes (Fig. 7.5) lies along the azo bridge through which intra-molecular charge migration occurs between the donor and acceptor moieties. This implies that the overall polarity of an entire azo dye molecule depends on the polarity of the azo linkage (i.e. the  $-\text{N}=\text{N}-$  group), which in turn depends on the charge separation between donor and acceptor units of the dye. The arrow in Figure 7.5 shows the part of the dye with the higher charge density which is the donor in the cases of the parent dye and its EDG derivatives. However, when the acceptor is substituted with more EWGs, more electrons are pulled from the donor towards the acceptor. This tends to balance the charge density on both sides of the molecule thereby decreasing the overall charge density and the net dipole moment magnitude leading to small screening charge in the solvent. In contrary, substituting the parent dye with the EDGs increases the charge density on the donor side of the dye. This results in a large charge separation between the two sides of the dye as confirmed by the relatively large dipole moment and screening charge values of the EDG substituted derivatives in Table 7.2.

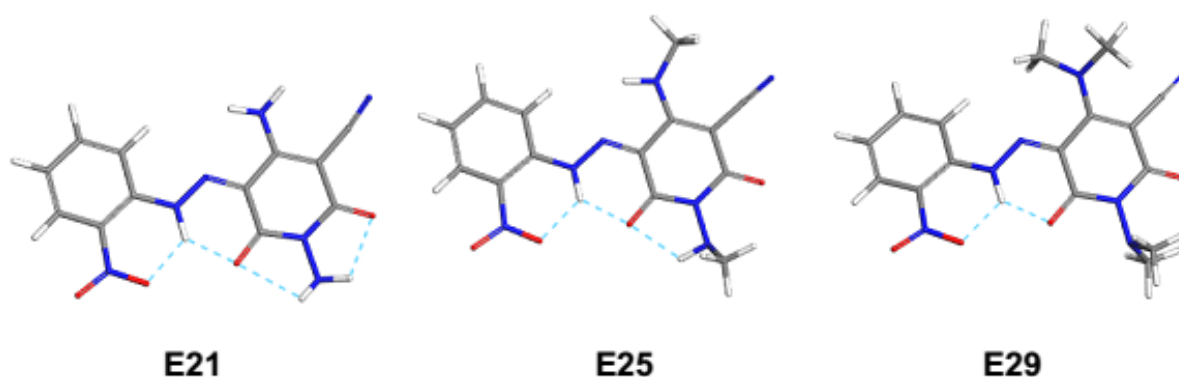


**Figure 7. 4:** Optimized structures of E21, E25 and E29 showing the available sites for hydrogen bonding.

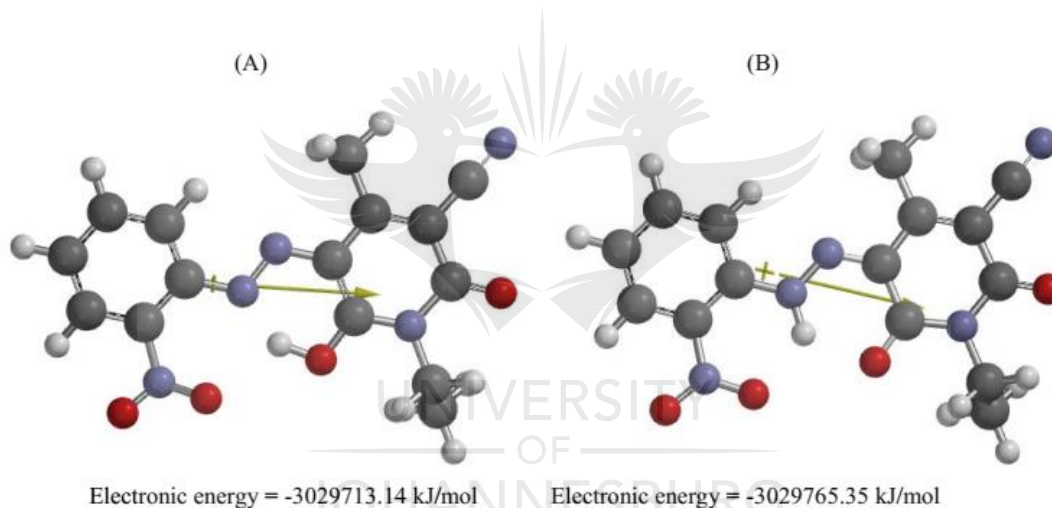


**Figure 7. 5:** Equilibrium geometries of (A) azo and (B) hydrazone tautomeric forms of DY119 dye (obtained at B3LYP/6-31G\* level of theory) showing the direction of dipole moment vectors. The absolute energy difference between A and B is ~52 kJ/mol.

It should be noted that the size of the screening charge depends on the total charge density in a solute whereas the dipole moment magnitude depends on the charge density difference between the donor and the acceptor moieties.

The results in Figure 7.5 also revealed that the hydrazone form of DY119 is more stable than the azo form by ca. 52.21 kJ/mol. This is confirmed by the VWN-BP/DNP calculation

which gave no distinct equilibrium geometry for the azo form, suggesting the hydrazone form as the most stable geometry (Fig. 7.6), which is in strong agreement with existing experimental findings [45]. It appears that the hydrogen atom of the hydroxyl group (in the azo form) tends to reunite with the azo nitrogen next to the acceptor moiety to regenerate the hydrazone form. This hydrogen atom consequently formed intramolecular hydrogen bonding with the two adjacent oxygen atoms from the acceptor and the donor moieties (Fig. 7.6B), serving as a bridging atom between them and the hydrazone nitrogen to form two six-membered rings, which confers higher stability on the hydrazone form. The zero energy difference between Figures 7.6A and 7.6B as well as the zero difference in the lengths of the hydrogen bonds in the figures confirms the hydrazone form as the most stable geometry. The absence of the azo form from the VWN-BP/DNP calculation may be attributed to the lower accuracy of VWN-BP which is a GGA functional compared to B3LYP which is a hybrid functional.

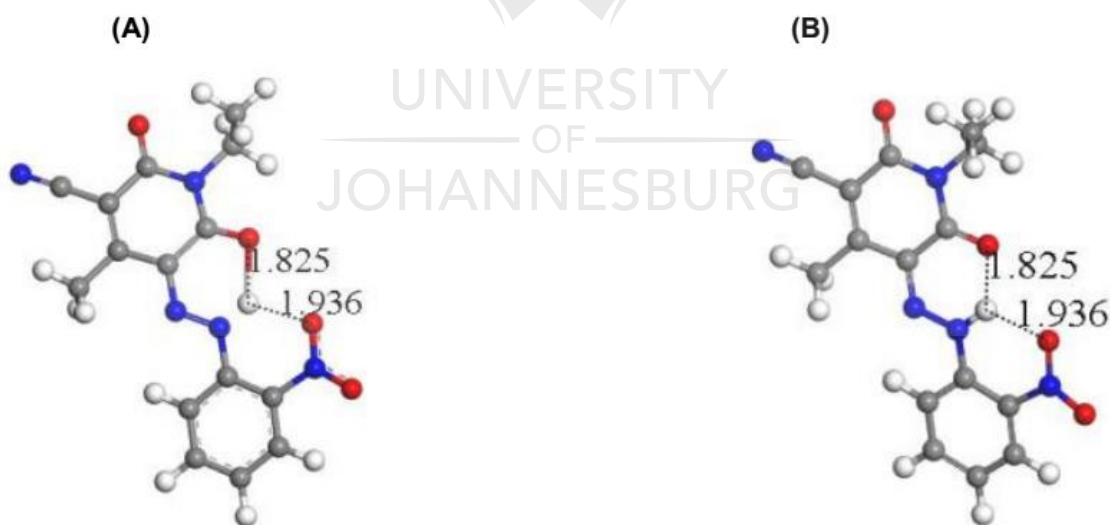


**Figure 7. 6:** VWN-BP/DNP optimized geometries of the azo (A) and hydrazone (B) forms of DY119.

To better understand the varying effect of the substituents on the solubility, the predicted electronegativities,  $\chi$ , chemical potentials,  $\Phi$ , dipole moments,  $\mu$ , solvation free energies in water,  $\Delta G_{\text{sol}}$ , and the literature Hammett constants,  $\tau$  [46], for the electron withdrawing and electron donating substituents studied are compared in Table A.14 (Appendix). For the electron withdrawing substituents i.e. CN and NO<sub>2</sub>, the table revealed that the dipole moment and the solvation free energy magnitude of the CN substituent are greater than those of NO<sub>2</sub>. This suggests that the CN group will enhance the solubility better than NO<sub>2</sub> as confirmed by the trend observed in Table 7.1 where the CN substituted derivatives generally produced higher solubility values. The electronegativity values and the Hammett constants in Table 7.3 revealed that NO<sub>2</sub> possesses higher electron withdrawing strength which leads to a smaller screening charge and lower dipole moment (Table 7.2), and consequently lower solubility values for the NO<sub>2</sub> derivatives compared to their CN substituted counterparts (Table 7.1).

Positional effect of substituents on solubility is also observed in the EWG derivatives in Table 7.1 where substitution at position R<sub>3</sub> (*ortho* position) yielded a higher solubility value compared to that at R<sub>1</sub> (*para* position). The drop in solubility observed for E3 and E4 compared to E1 and E2 respectively, can also be attributed to the large decrease in the vapour pressure as the substituents switched to position R<sub>1</sub> (Table 7.1).

In the case of the electron donating substituents (i.e. NH<sub>2</sub>, NHCH<sub>3</sub> and N(CH<sub>3</sub>)<sub>2</sub>), the dipole moment values in Table 7.3 revealed that the polarity of these substituents follows the order NHCH<sub>3</sub> > NH<sub>2</sub> > N(CH<sub>3</sub>)<sub>2</sub>, which suggests that NHCH<sub>3</sub> will be the most solvated member of this series, as confirmed by the solvation free energy ( $\Delta G_{\text{sol}}$ ) trend in the same table. Unfortunately, the above trend is contrary to the solubility trend observed in Table 7.1, in which the NH<sub>2</sub> substituted derivatives have the largest solubility values compared

to their  $\text{NHCH}_3$  and  $\text{N}(\text{CH}_3)_2$  counterparts. This may be attributed to the relatively small size of the  $\text{NH}_2$  substituent which also explains why its solvation free energy is nearly the same as that of  $\text{NHCH}_3$ , despite the substantial difference in their dipole moments. The higher steric hindrance to solvation offered by  $\text{N}(\text{CH}_3)_2$  substituent is suspected to be responsible for its relatively less negative  $\Delta G_{\text{sol}}$  values in Table 7.3 and its corresponding lower solubility values in Table 7.1. The chemical potential and the Hammett constants for  $\text{NH}_2$ ,  $\text{NHCH}_3$  and  $\text{N}(\text{CH}_3)_2$  (Table 7.3) revealed their respective electron donating capacities. According to Table 7.3,  $\text{N}(\text{CH}_3)_2$  substituent has the highest chemical potential which suggest that it has the highest donating power. This is suspected to be responsible for the large screening charge values observed for E11, E14, E17, E20, E23, E26 and E29 (Table 7.2). A similar explanation holds for the  $\text{NHCH}_3$  substituent which produced a smaller effect compared to  $\text{N}(\text{CH}_3)_2$  because of its lower electron donating capacity. The relatively low polarity of  $\text{N}(\text{CH}_3)_2$  as indicated by the dipole moment values given in Table 7.3 also justifies why the  $\text{N}(\text{CH}_3)_2$  derivatives generally yielded low solubility values compared to their  $\text{NH}_2$  and  $\text{NHCH}_3$  counterparts (Table 7.2). The low polarity of  $\text{N}(\text{CH}_3)_2$  may be due to the relative positions of the surrounding  $\text{CH}_3$  groups which tend to balance the charge densities on both sides of the nitrogen atom thereby giving rise to a weak dipole (Fig. 7.7). In the case of  $\text{NHCH}_3$ , the charge densities on both sides of the central nitrogen atom are unequal thereby giving rise to a larger dipole moment. The dipole moment vector shown in Figure 7.7 for  $\text{NHCH}_3$  is pointing towards the side with the higher charge density which is the more electronegative nitrogen atom. Comparing the symmetrical substituents (i.e.  $\text{NH}_2$  and  $\text{N}(\text{CH}_3)_2$ ), the lower polarity of the N-C bonds in  $\text{N}(\text{CH}_3)_2$  compared to the N-H bond in  $\text{NH}_2$ , explains why the dipole moment of  $\text{NH}_2$  is larger than that of  $\text{N}(\text{CH}_3)_2$  (Table 7.3).

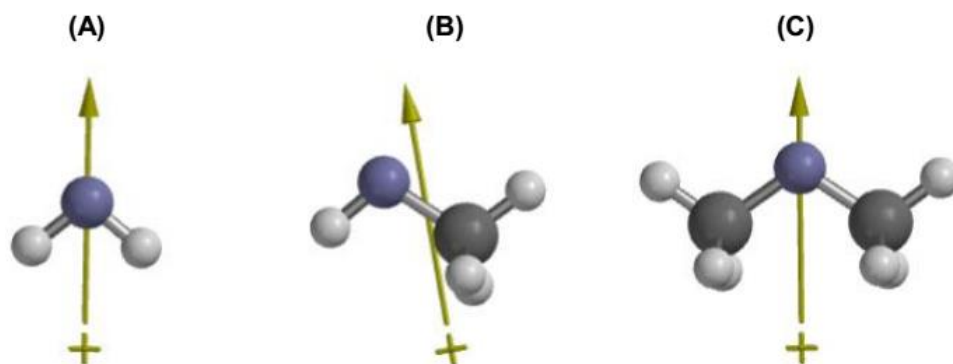


**Figure 7. 7:** Optimized geometries of  $\text{NH}_2^-$  (A),  $\text{NHCH}_3^-$  (B) and  $\text{N}(\text{CH}_3)_2^-$  (C) (obtained at B3LYP/6-31G(d) level of theory) showing their respective dipole moment vectors. The dipole moment vector of  $\text{NHCH}_3^-$  (B) lying along the C–N bond is stronger than those of  $\text{NH}_2^-$  (A) and  $\text{N}(\text{CH}_3)_2^-$  (C) which are perpendicular to the central oxygen atom.

Comparing the  $\text{CH}_3$  substituted derivatives with the corresponding  $\text{C}_2\text{H}_5$  counterparts, the relatively high solubility values obtained with the  $\text{CH}_3$  substituent may be due to the relatively low steric hindrance to solvation offered by  $\text{CH}_3$ . However, the slight differences in screening charge and dipole moment values observed between the  $\text{CH}_3$  and  $\text{C}_2\text{H}_5$  substituted derivatives suggests that the electron donating strengths of  $\text{CH}_3$  and  $\text{C}_2\text{H}_5$  are comparable.

The remarkable increase in solubility observed for E27 and E28 compared to E23 and E26 may be due to the increase in dipole moment (Table 7.2) when the EDG substituents switched their positions. This suggests that substitution of  $\text{N}(\text{CH}_3)_2$  at position  $\text{R}_4$  as in E27 and E28 favors higher polarity compared to its substitution at position  $\text{R}_5$ . The relatively small dipole moment and polarizability values obtained for E29 compared to E27 and E28 (Table 7.2) is prognostic of lower solubility. Therefore, the large solubility value obtained for E29 compared to E27 and E28 (Table 7.1) may be due to overestimated vapor pressure.

The negative Gibb's free energy obtained for the parent dye and its studied derivatives suggests that they are thermodynamically stable (Table 7.1). However, the stability



seems to be enhanced by the electron withdrawers as a result of displacement of more electrons towards the accepting part of the dye which tends to balance the charge densities on both sides of the molecules. The fact that NO<sub>2</sub> is more electron-withdrawing than CN explains why the Gibb's free energies for the NO<sub>2</sub> substituted derivatives are more negative.

### 7.3.2 CORRELATION OF AQUEOUS SOLUBILITY WITH DIPOLE MOMENT ( $\mu$ ), POLARIZABILITY ( $\alpha$ ) AND SCREENING CHARGES ( $q$ )

To further investigate the dependence of aqueous solubility of dyes on some physicochemical parameters, an attempt was made to correlate the predicted aqueous solubility with dipole moment, polarizability and screening charges. The analyses were carried out using the XLSTAT codes [47]. The results revealed that there is no linear relationship between aqueous solubility and the selected parameters. However, non-linear empirical equations were found, relating aqueous solubility and the parameters for some sets of dyes. Dyes with electron withdrawing substituents (E1 – E8) showed strong non-linear dependence on  $\mu$ ,  $\alpha$  and  $q$  as shown in Figure 7.8, and in accordance with the empirical equation:

$$S = 5.84 \times 10^5 - 1.07 \times 10^7 q - 3.52 \times 10^4 \alpha + 341.56\mu - 6.56 \times 10^9 q^2 + 526.87 \alpha^2 - 76.99\mu^2$$

Equation 7. 12

where  $S$  is the predicted solubility obtained from CSE (eqn. 7.2). Similarly, R<sub>4</sub> or R<sub>5</sub> electron donating methyl or amino substituted dyes (E12 – E17) and those with R<sub>4</sub> or R<sub>5</sub> electron donating ethyl or non-identical amino groups (E9 – E11 and E18 – E20) showed strong dependence on  $\mu$ ,  $\alpha$  and  $q$  as adjudged by the R<sup>2</sup> value of 1.000 (Fig. 7.9). The relationships between  $S$ ,  $\mu$ ,  $\alpha$  and  $q$  for these groups of dyes are:

$$S = 6.17 \times 10^4 + 1.01 \times 10^8 q + 117.14 \alpha + 42.17 \mu + 3.96 \times 10^{10} q^2 - 1.36 \alpha^2 \quad (\text{for E12 – E17})$$

Equation 7. 13

and;

$$S = 1.68 \times 10^6 + 3.35 \times 10^9 q + 1.98 \times 10^4 \alpha + 1.44 \times 10^3 \mu + 1.37 \times 10^{12} q^2 - 281 \alpha^2 \quad (\text{for E9 – E11, and E18 – E20})$$

Equation 7. 14

showing that their solubility values have some linear relationships with  $\mu$ , but non-linear relationships with  $\alpha$  and  $q$ .

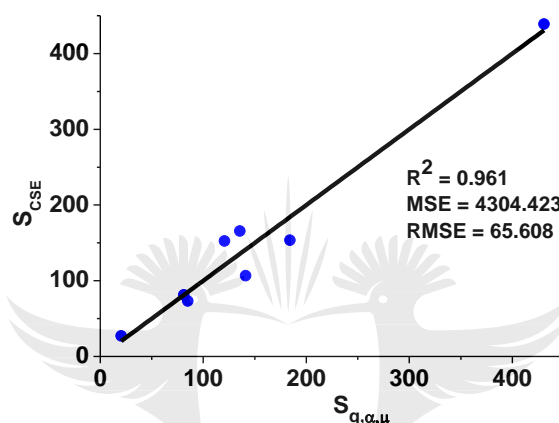


**Figure 7. 8:** Dependence of solubility of the EWG substituted derivatives on screening charge, dipole moment and polarizability\*.

\* $S_{CSE}$  = CSE predicted solubility based on equation 7.2,  $S_{q,\alpha,\mu}$  = predicted solubility from QSPR-model based on equation 7.12.

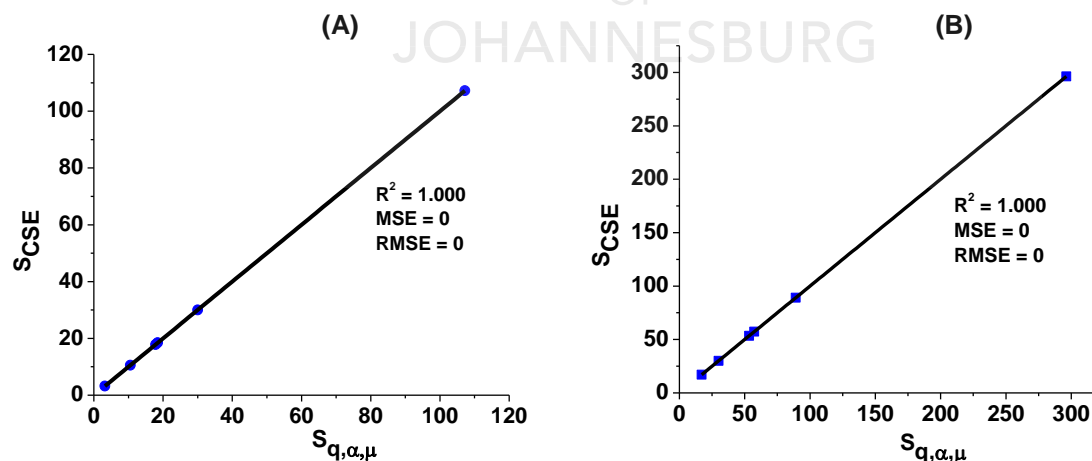


**Figure 7. 9:** Dependence of solubility of some EDG substituted derivatives on screening charge, dipole moment and polarizability. Plot A is for E12 – E17 while B is for E9 – E11, and E18 – E20\*.

\* $S_{CSE}$  = CSE predicted solubility based on equation 7.2,  $S_{q,\alpha,\mu}$  = predicted solubility from QSPR-model based on equations 7.13 and 7.14 for plots A and B, respectively.

### 7.3.3 CHEMICAL REACTIVITY STUDY

Global reactivity parameters of the studied dyes are provided in Table 7.3. The HOMO energy of a molecule is a predictor of its tendency to release electrons while the LUMO energy shows its propensity to accept an incoming electron. The higher the HOMO energy, the greater the chance of electron donation and the lower the LUMO energy, the more the likelihood of accepting an electron. The HOMO – LUMO energy gap,  $E_g$  is a parameter that reveals the overall stability of a molecule and its chance of undergoing electronic excitation. The wider the energy gap, the higher the stability and the lesser the chance of electronic excitation. Global hardness,  $\eta$  and softness,  $\sigma$  are both measures of molecular reactivity. The larger the value of  $\eta$ , or the smaller the  $\sigma$ , the less reactive the molecule. Electronegativity,  $\chi$  describes the power of a molecule to pull an electron towards itself, while chemical potential,  $\Phi$  reveals its ability to release an electron. Global electrophilicity,  $\omega$  index describes the potency of a molecule towards an incoming electron i.e. the attack of a nucleophile. A high  $\omega$  value indicates a good electrophile while small value of  $\omega$  implies a good nucleophile.

**Table 7. 3:** HOMO energies ( $E_{\text{HOMO}}$ ), LUMO energies ( $E_{\text{LUMO}}$ ), HOMO-LUMO energy gap ( $E_g$ ) and hardness ( $\eta$ ) of DY119 and its studied derivatives.

Dye No.	R <sub>1</sub>	R <sub>2</sub>	R <sub>3</sub>	R <sub>4</sub>	R <sub>5</sub>	$E_{\text{HOMO}}$ (eV)		$E_{\text{LUMO}}$ (eV)		$E_g$ (eV)		$\eta$ (eV)	
						Gas	Water	Gas	Water	Gas	Water	Gas	Water
DY119	H	NO <sub>2</sub>	H	CH <sub>3</sub>	C <sub>2</sub> H <sub>5</sub>	-6.25	-6.03	-4.37	-4.22	1.88	1.81	0.94	0.91
EWG Substitution													
E1	H	NO <sub>2</sub>	NO <sub>2</sub>	CH <sub>3</sub>	C <sub>2</sub> H <sub>5</sub>	-6.47	-6.23	-4.59	-4.39	1.88	1.84	0.94	0.92
E2	H	NO <sub>2</sub>	CN	CH <sub>3</sub>	C <sub>2</sub> H <sub>5</sub>	-6.47	-6.21	-4.60	-4.36	1.87	1.85	0.94	0.93
E3	NO <sub>2</sub>	NO <sub>2</sub>	H	CH <sub>3</sub>	C <sub>2</sub> H <sub>5</sub>	-6.70	-6.32	-4.82	-4.47	1.88	1.85	0.94	0.93
E4	CN	NO <sub>2</sub>	H	CH <sub>3</sub>	C <sub>2</sub> H <sub>5</sub>	-6.61	-6.22	-4.73	-4.38	1.88	1.84	0.94	0.92
E5	NO <sub>2</sub>	NO <sub>2</sub>	NO <sub>2</sub>	CH <sub>3</sub>	C <sub>2</sub> H <sub>5</sub>	-6.88	-6.52	-5.04	-4.67	1.84	1.85	0.92	0.93
E6	CN	NO <sub>2</sub>	CN	CH <sub>3</sub>	C <sub>2</sub> H <sub>5</sub>	-6.78	-6.39	-4.93	-4.52	1.85	1.87	0.93	0.94
E7	NO <sub>2</sub>	NO <sub>2</sub>	CN	CH <sub>3</sub>	C <sub>2</sub> H <sub>5</sub>	-6.88	-6.48	-5.03	-4.62	1.85	1.86	0.93	0.93
E8	CN	NO <sub>2</sub>	NO <sub>2</sub>	CH <sub>3</sub>	C <sub>2</sub> H <sub>5</sub>	-6.79	-6.43	-4.94	-4.56	1.85	1.87	0.93	0.94
EDG Substitution													
E9	H	NO <sub>2</sub>	H	NH <sub>2</sub>	C <sub>2</sub> H <sub>5</sub>	-6.12	-5.94	-4.31	-4.13	1.81	1.81	0.91	0.91
E10	H	NO <sub>2</sub>	H	NHCH <sub>3</sub>	C <sub>2</sub> H <sub>5</sub>	-5.91	-5.83	-4.21	-4.09	1.70	1.74	0.85	0.87
E11	H	NO <sub>2</sub>	H	N(CH <sub>3</sub> ) <sub>2</sub>	C <sub>2</sub> H <sub>5</sub>	-5.75	-5.67	-4.11	-4.05	1.64	1.62	0.82	0.81
E12	H	NO <sub>2</sub>	H	CH <sub>3</sub>	NH <sub>2</sub>	-6.26	-6.07	-4.47	-4.27	1.79	1.80	0.90	0.90
E13	H	NO <sub>2</sub>	H	CH <sub>3</sub>	NHCH <sub>3</sub>	-6.08	-6.03	-4.43	-4.26	1.65	1.77	0.83	0.89
E14	H	NO <sub>2</sub>	H	CH <sub>3</sub>	N(CH <sub>3</sub> ) <sub>2</sub>	-5.57	-5.50	-4.33	-4.21	1.24	1.29	0.62	0.65
E15	H	NO <sub>2</sub>	H	NH <sub>2</sub>	CH <sub>3</sub>	-6.09	-5.94	-4.32	-4.14	1.77	1.80	0.89	0.90
E16	H	NO <sub>2</sub>	H	NHCH <sub>3</sub>	CH <sub>3</sub>	-5.93	-5.84	-4.23	-4.09	1.70	1.75	0.85	0.88
E17	H	NO <sub>2</sub>	H	N(CH <sub>3</sub> ) <sub>2</sub>	CH <sub>3</sub>	-5.81	-5.68	-4.16	-4.06	1.65	1.62	0.83	0.81
E18	H	NO <sub>2</sub>	H	C <sub>2</sub> H <sub>5</sub>	NH <sub>2</sub>	-6.23	-6.06	-4.45	-4.26	1.78	1.80	0.89	0.90
E19	H	NO <sub>2</sub>	H	C <sub>2</sub> H <sub>5</sub>	NHCH <sub>3</sub>	-6.08	-6.03	-4.42	-4.26	1.66	1.77	0.83	0.89
E20	H	NO <sub>2</sub>	H	C <sub>2</sub> H <sub>5</sub>	N(CH <sub>3</sub> ) <sub>2</sub>	-5.58	-5.50	-4.32	-4.22	1.26	1.28	0.63	0.64
E21	H	NO <sub>2</sub>	H	NH <sub>2</sub>	NH <sub>2</sub>	-6.00	-5.83	-4.38	-4.16	1.62	1.67	0.81	0.84
E22	H	NO <sub>2</sub>	H	NH <sub>2</sub>	NHCH <sub>3</sub>	-5.83	-5.82	-4.35	-4.16	1.48	1.66	0.74	0.83

E23	H	NO <sub>2</sub>	H	NH <sub>2</sub>	N(CH <sub>3</sub> ) <sub>2</sub>	-5.52	-5.44	-4.30	-4.13	1.22	1.31	0.61	0.66
E24	H	NO <sub>2</sub>	H	NHCH <sub>3</sub>	NH <sub>2</sub>	-5.81	-5.70	-4.28	-4.11	1.53	1.59	0.77	0.80
E25	H	NO <sub>2</sub>	H	NHCH <sub>3</sub>	NHCH <sub>3</sub>	-5.75	-5.71	-4.27	-4.11	1.48	1.60	0.74	0.80
E26	H	NO <sub>2</sub>	H	NHCH <sub>3</sub>	N(CH <sub>3</sub> ) <sub>2</sub>	-5.45	-5.41	-4.20	-4.09	1.25	1.32	0.63	0.66
E27	H	NO <sub>2</sub>	H	N(CH <sub>3</sub> ) <sub>2</sub>	NH <sub>2</sub>	-5.76	-5.60	-4.22	-4.09	1.54	1.51	0.77	0.76
E28	H	NO <sub>2</sub>	H	N(CH <sub>3</sub> ) <sub>2</sub>	NHCH <sub>3</sub>	-5.67	-5.60	-4.18	-4.09	1.49	1.51	0.75	0.76
E29	H	NO <sub>2</sub>	H	N(CH <sub>3</sub> ) <sub>2</sub>	N(CH <sub>3</sub> ) <sub>2</sub>	-5.40	-5.43	-4.10	-4.05	1.30	1.38	0.65	0.69

$E_g = E_{LUMO} - E_{HOMO}$  energy gap,  $\eta$  = global hardness

From Table 7.3, the  $E_{HOMO}$  and  $E_{LUMO}$  of the EWG substituted derivatives are generally lower than those of the parent dye, which suggests that the derivatives will have a greater affinity for electrons than the parent dye. The derivatives are more liable to undergo reduction by electron addition than the parent dye. However, the parent dye appears to be a better electron donor due to its higher  $E_{HOMO}$ . This suggests that the parent dye is more susceptible to oxidation than the derivatives. The reduction in  $E_{HOMO}$  and  $E_{LUMO}$  of the derivatives arising from the EWG effects is not unexpected. The electron withdrawing substituents reduce the electron density in the ring and consequently reduce the electron donating ability at the reactive center. The higher electron withdrawing potential of NO<sub>2</sub> substituent compared to CN substituent is also confirmed by the lower  $E_{HOMO}$  and  $E_{LUMO}$  of the NO<sub>2</sub> substituted derivatives. In contrast, the  $E_{HOMO}$  values of nearly all the EDG substituted derivatives are higher than that of the parent dye due to increase in electron density at the active sites of the molecules and hence, increase in electron donating ability of the entire dye molecule. Due to higher  $E_{HOMO}$  and  $E_{LUMO}$  compared to the parent dye, most of the EDG derivatives will be more oxidizable and less reducible. The effect of the EDGs generally follows the order  $N(CH_3)_2 > NHCH_3 > NH_2$  which follows their electron donating capacities discussed previously.

Using the HOMO – LUMO energy gap ( $E_g$ ) as a measure of relative stability of the studied dyes, it can be observed that the EWGs only have little effects on the overall reactivity as the  $E_g$  for the derivatives are not significantly different from that of the parent dye (Table 7.3). This suggests that the EWG substituents changed the position of both the HOMO and LUMO energies by approximately equal magnitude. On the other hand, the EDG substituted derivatives appears to be more reactive than the unsubstituted dye with the EDG derivatives having smaller energy gap. Possible implication is that the derivatives will not only possess a higher substrate binding potential but will also be more vulnerable to degradation due to their relatively lower stability. This is an advantage since it suggests the derivatives to be the better candidates for the various industrial applications such as fabric and leather dyeing, paints and coating coloring, and even for liquid crystal displays (LCD). In addition, the chance of photo-excitation of electrons, which leads to fading, is higher for the EDG derivatives as a result of their relatively small HOMO–LUMO energy gap which implies low stability and shorter life time compared to the parent. Unfortunately, this also means a reduction in light fastness which is an essential property in textile applications. However, we believe that this property can be improved by substituting the parent dye with both EWGs and EDGs.

Since the energy gap is dependent on the positions of the HOMO and LUMO relative to each other, the net effect of the substituents on the energy gap therefore depends on the relative changes in the HOMO and LUMO energies. If the changes in the HOMO and the LUMO energies are equal, a zero change in the energy gap results. This is the trend observed for E1, E3 and E4 in gas, and E9 in water. However, if the change in the HOMO energy is not accompanied by an equal change in the LUMO, a change in energy gap

occurs depending on the relative changes in the HOMO and the LUMO energies. This explains the trend observed for the other derivatives.

In addition to the relatively higher aqueous solubility and lower vapor pressure (i.e. higher thermal stability) observed earlier in Table 7.1 for the EWG substituted derivatives, these derivatives are also predicted to be more resistant to photo-excitation which leads to fading (i.e. have higher light fastness) in aqueous medium, due to their larger HOMO-LUMO energy gap and higher hardness (Table 7.3) values in water. Except for E11 and E17, Table 7.3 similarly revealed that the EDG substituted derivatives will be more resistant to photo-excitation in the presence of water due to their higher aqueous phase HOMO-LUMO energy gap and hardness values.

The trends observed in the electronegativity and chemical potential (Table 7.4) is also a consequence of the varying electron withdrawing and donating capacities of the substituents. The presence of additional electron withdrawing substituent in E1 – E8 compared to the parent dye increases the electron withdrawing power of these derivatives but decreases their power to release electrons as confirmed by their electronegativity and chemical potential values respectively. The relatively smaller electronegativity coupled with the higher chemical potential of most of the CN substituted derivatives is a manifestation of the low electron withdrawing power of the CN substituent compared to the NO<sub>2</sub> counterpart. In contrary, the relatively small electronegativity and the accompanying higher chemical potential of the EDG substituted derivatives compared to the parent simply suggest that the EDG substituents NH<sub>2</sub>, NHCH<sub>3</sub> and N(CH<sub>3</sub>)<sub>2</sub> possess higher electron donating capacity compared to the CH<sub>3</sub> and C<sub>2</sub>H<sub>5</sub>. The aberrancy observed in the cases of E12 and E18 have been discussed previously.

**Table 7. 4:** Softness,  $\sigma$ , electronegativity,  $\chi$ , chemical potential,  $\Phi$ , and electrophilicity indices,  $\omega$ , of DY119 and its studied derivatives.

Dye No.	$\sigma$ (eV <sup>-1</sup> )		$\chi$ (eV)		$\Phi$ (eV)		$\omega$ (eV)	
	Gas	Water	Gas	Water	Gas	Water	Gas	Water
DY 119	1.06	1.10	5.31	5.13	-5.31	-5.13	15.00	14.46
EWG substitution								
E1	1.06	1.09	5.53	5.31	-5.53	-5.31	16.27	15.32
E2	1.06	1.08	5.54	5.29	-5.54	-5.29	16.33	15.04
E3	1.06	1.08	5.76	5.40	-5.76	-5.40	17.65	15.68
E4	1.06	1.09	5.67	5.30	-5.67	-5.30	16.27	15.27
E5	1.09	1.08	5.96	5.60	-5.96	-5.60	19.31	16.86
E6	1.08	1.06	5.86	5.46	-5.86	-5.46	18.46	15.86
E7	1.08	1.08	5.96	5.55	-5.96	-5.55	19.10	16.56
E8	1.07	1.06	5.87	5.50	-5.87	-5.50	18.53	16.09
EDG substitution								
E9	1.10	1.10	5.22	5.04	-5.22	-5.04	14.97	13.96
E10	1.18	1.15	5.06	4.96	-5.06	-4.96	15.06	14.14
E11	1.22	1.23	4.93	4.86	-4.93	-4.86	14.82	14.58
E12	1.11	1.11	5.37	5.17	-5.37	-5.17	16.02	14.85
E13	1.20	1.12	5.26	5.15	-5.26	-5.15	16.67	14.90
E14	1.61	1.54	4.95	4.86	-4.95	-4.86	19.76	18.17
E15	1.12	1.11	5.21	5.04	-5.21	-5.04	15.25	14.11
E16	1.18	1.14	5.08	4.97	-5.08	-4.97	15.18	14.03
E17	1.20	1.23	4.99	4.87	-4.99	-4.87	15.00	14.64
E18	1.12	1.11	5.34	5.16	-5.34	-5.16	16.02	14.79
E19	1.20	1.12	5.25	5.15	-5.25	-5.15	16.60	14.90
E20	1.59	1.56	4.95	4.86	-4.95	-4.86	19.45	18.45
E21	1.23	1.19	5.19	5.00	-5.19	-5.00	16.63	14.88
E22	1.35	1.20	5.09	4.99	-5.09	-4.99	17.51	15.00



E23	1.64	1.51	4.91	4.79	-4.91	-4.79	19.76	17.38
E24	1.30	1.25	5.05	4.91	-5.05	-4.91	16.56	15.07
E25	1.35	1.25	5.01	4.91	-5.01	-4.91	16.96	15.07
E26	1.59	1.52	5.43	4.75	-5.43	-4.75	23.40	17.09
E27	1.30	1.32	4.99	4.85	-4.99	-4.85	16.17	15.48
E28	1.33	1.32	4.93	4.85	-4.93	-4.85	16.20	15.48
E29	1.54	1.45	4.75	4.74	-4.75	-4.74	17.36	16.28

Careful inspection of the table revealed that the chemical potential of the EDG substituted derivatives increases as electron donating capacity increases from  $\text{NH}_2$  to  $\text{N}(\text{CH}_3)_2$  while their electronegativity decreases in the same order. This is not unexpected since the ability to attract an electron is inversely related to the ability to donate an electron.

The calculated electrophilicity indices suggest both the EWG and the EDG substituted derivatives as being more electrophilic than the parent dye. This implies that the derivatives are more vulnerable to a nucleophilic attack and as a result will undergo easier reductive degradation.

The observed changes in the reactivity indices of some of the derivatives with the same chemical make-up such as E9 and E18, E10 and E19, E11 and E20, E12 and E15, E13 and E16, E14 and E17 and the likes could also be attributed to the EDG substituents exhibiting different electron-donating character at positions  $\text{R}_4$  and  $\text{R}_5$  depending on their involvement in intramolecular hydrogen bonding with neighboring oxygen atoms. The substituents (excluding  $\text{N}(\text{CH}_3)_2$ ) seems to experience a reduction in their electron donating strength when attached to position  $\text{R}_5$  due to their involvement in intramolecular hydrogen bonding with the surrounding carbonyl oxygen (Fig. 7.4). This explains why the HOMO and LUMO energies for E18, E19, E12 and E13 are lower than those of E9, E10,

E15 and E16 respectively. In addition, the more the involvement in the hydrogen bonding, the lower the donating power. This explains why the HOMO and LUMO energies for E12 and E18 are lower than those of E13 and E19 respectively which suggests  $\text{NH}_2$  as being more involved in the hydrogen bonding as confirmed by Figure 7.4. Non-involvement of the  $\text{N}(\text{CH}_3)_2$  substituent at position  $\text{R}_5$  in intramolecular hydrogen bonding (Fig. 7.4), suggests higher donating strength for  $\text{N}(\text{CH}_3)_2$  compared to  $\text{NH}_2$  and  $\text{NHCH}_3$  at that position. This may be responsible for the relatively high HOMO energy of E14 and E20. However, this increase in HOMO energy is accompanied by a decrease in LUMO when compared to E17 and E11 respectively, suggesting that  $\text{N}(\text{CH}_3)_2$  substitution at  $\text{R}_5$  raises the HOMO energy level, whereas its substitution at  $\text{R}_4$  raises the LUMO energy level. Comparing derivatives such as E23 and E26 to E27 and E28 respectively revealed that position  $\text{R}_5$  has more influence on the frontier molecular orbitals especially the HOMO, than position  $\text{R}_4$ .

While the HOMO-LUMO energy gap and hardness of the parent dye are slightly decreased by water to enhance its reactivity, most of the derivatives do not undergo any remarkable change in these parameters in the presence of water. The exceptions to these include E13, E19, E22 and E25. The fact that these four derivatives has  $\text{NHCH}_3$  substituent at position  $\text{R}_5$  suggests that substitution of the parent dye at position  $\text{R}_5$  by this substituent will significantly reduce the reactivity of the dye in water. The electronegativity of the parent dye and those of the studied derivatives are generally smaller in water and are accompanied by a corresponding increase in chemical potential (Table 7.4). Similarly, the electrophilicity indices are also smaller in water compared to the gas phase. These collectively suggest that the studied dyes will be more susceptible to oxidation but less vulnerable to reduction in water than in gas.

### 7.3.4 PREDICTION OF SUITABLE CATALYST FOR PHOTOCATALYTIC DEGRADATION OF THE DYES

Table A.15 (Appendix) gives the calculated band structures for Si, CdSe, CdS, TiO<sub>2</sub> (rutile), ZnO and ZnS photocatalysts. The table revealed a strong agreement between the calculated and the reported experimental band gaps of the catalysts, which validates the selected level of theory for this study.

The energy gap between the HOMO of the studied dyes and the conduction band edge (CBE) of the catalysts ( $\beta$ ) as well as the gap between the LUMO and the valence band edges (VBE) of the catalysts ( $\alpha$ ) are presented in Table 7.5. These comprise both the ultraviolet (UV) and the visible light activated groups. Members of the UV activated group include TiO<sub>2</sub>, ZnO and ZnS whose band gap values are 3.0 eV and above. Si, CdSe and CdS form the visible light activated group since their band gap values are less than 3.0 eV (Table 7.5) [48].

The relative affinities of the studied dyes for the photocatalysts are evaluated in Table 7.5 with a view to identify the catalyst(s) with the highest catalytic potential for their degradation. The chance of a favorable interaction between the dyes and the catalysts depends on the magnitude of  $\alpha$  and  $\beta$ .  $\alpha$  represents the energy gap between the LUMO (i.e. the electron deficient portion) of the dyes and the valence band edges (i.e. the electron rich portion) of the catalysts while  $\beta$  is the energy gap between the conduction band edges (i.e. the electron deficient part) of the catalysts and the HOMO (i.e. the electron rich portion) of the dyes. The smaller the  $\alpha$  value, the greater the chance of electron donation into the LUMO of the dyes. Similarly, the smaller the  $\beta$  value, the higher the likelihood of electron donation into the conduction band edges of the catalysts.

**Table 7. 5:** Calculated energy gaps between the FMO (i.e. HOMO and LUMO) of the studied dyes and the band edges of the catalysts.

Dye	$\alpha^*_{Si}$	$\beta^{**}_{Si}$	$\alpha^*_{CdSe}$	$\beta^{**}_{CdSe}$	$\alpha^*_{CdS}$	$\beta^{**}_{CdS}$	$\alpha^*_{TiO_2}$	$\beta^{**}_{TiO_2}$	$\alpha^*_{ZnO}$	$\beta^{**}_{ZnO}$	$\alpha^*_{ZnS}$	$\beta^{**}_{ZnS}$
No.	(eV)	(eV)	(eV)	(eV)	(eV)	(eV)	(eV)	(eV)	(eV)	(eV)	(eV)	(eV)
DY119	0.67	2.01	0.45	3.01	1.48	2.76	3.43	1.23	-0.17	5.26	0.90	4.62
EWG substituted derivatives												
E1	0.45	2.23	0.23	3.23	1.26	2.98	3.21	1.45	-0.39	5.48	0.68	4.84
E2	0.44	2.23	0.22	3.23	1.25	2.98	3.20	1.45	-0.40	5.48	0.67	4.84
E3	0.22	2.46	0.00	3.46	1.03	3.21	2.98	1.68	-0.62	5.71	0.45	5.07
E4	0.31	2.37	0.25	3.37	1.12	3.12	3.07	1.59	-0.53	5.62	0.54	4.98
E5	0.00	2.64	-0.22	3.64	0.81	3.39	2.76	1.86	-0.84	5.89	0.23	5.25
E6	0.11	2.54	-0.11	3.54	0.92	3.29	2.87	1.76	-0.73	5.79	0.34	5.15
E7	0.01	2.64	-0.21	3.64	0.82	3.39	2.77	1.86	-0.83	5.89	0.24	5.25
E8	0.10	2.55	-0.12	3.55	0.91	3.30	2.86	1.77	-0.74	5.80	0.33	5.16
EDG substituted derivatives												
E9	0.73	1.88	0.51	2.88	1.54	2.63	3.49	1.10	-0.11	5.13	0.96	4.49
E10	0.83	1.67	0.61	2.67	1.64	2.42	3.59	0.89	-0.01	4.92	1.06	4.28
E11	0.93	1.51	0.71	2.51	1.74	2.26	3.69	0.73	0.09	4.76	1.16	4.12
E12	0.57	2.02	0.35	3.02	1.38	2.77	3.33	1.24	-0.27	5.27	0.80	5.33
E13	0.61	1.84	0.39	2.84	1.42	2.59	3.37	1.06	-0.23	5.09	0.84	4.45
E14	0.71	1.33	0.49	2.33	1.52	2.08	3.47	0.55	-0.13	4.58	0.94	3.94
E15	0.72	1.85	0.50	2.85	1.53	2.60	3.48	1.07	-0.12	5.10	0.95	4.46
E16	0.81	1.69	0.59	2.69	1.62	2.44	3.57	0.91	-0.03	4.94	1.04	4.30
E17	0.88	1.57	0.66	2.57	1.69	2.32	3.64	0.79	0.04	4.82	1.11	4.18
E18	0.59	1.99	0.37	2.99	1.40	2.74	3.35	1.21	-0.25	5.24	0.82	4.60
E19	0.62	1.84	0.40	2.84	1.43	2.59	3.38	1.06	-0.22	5.09	0.85	4.45
E20	0.72	1.34	0.50	2.34	1.53	2.09	3.48	0.56	-0.12	4.59	0.95	3.95
E21	0.66	1.76	0.44	2.76	1.47	2.51	3.42	0.98	-0.18	5.01	0.89	4.37
E22	0.69	1.59	0.47	2.59	1.50	2.34	3.45	0.81	-0.15	4.84	0.92	4.20

E23	0.74	1.28	0.52	2.28	1.55	2.03	3.50	0.50	-0.10	4.53	0.97	3.89
E24	0.76	1.57	0.54	2.57	1.57	2.32	3.52	0.79	-0.08	4.82	0.99	4.18
E25	0.77	1.51	0.55	2.51	1.58	2.26	3.53	0.73	-0.07	4.76	1.00	4.12
E26	0.84	1.21	0.62	2.21	1.65	1.96	3.60	0.43	0.00	4.46	1.07	3.82
E27	0.82	1.52	0.60	2.52	1.63	2.27	3.58	0.74	-0.02	4.77	1.05	4.13
E28	0.86	1.43	0.64	2.43	1.67	2.18	3.62	0.65	0.02	4.68	1.09	4.04
E29	0.94	1.16	0.72	2.16	1.75	1.91	3.70	0.38	0.10	4.41	1.17	3.77

$$\alpha^* = E_{\text{LUMO}} - E_{\text{VBE}} \text{ and } \beta^{**} = E_{\text{CBE}} - E_{\text{HOMO}}$$

The smaller the  $\alpha$  value, the greater the chance of electron donation into the LUMO of the dyes. Similarly, the smaller the  $\beta$  value, the higher the likelihood of electron donation into the conduction band edges of the catalysts. For a given dye-catalyst pair, the molecular orbital/band edge combination (i.e. LUMO/VBE or HOMO/CBE) with the smaller energy gap is the most preferred combination for interaction.

From the visible light activated group in Table 7.5, the  $\alpha_{\text{Si}}$  and  $\beta_{\text{Si}}$  values (for Si) and the  $\alpha_{\text{CdSe}}$  values for (CdSe) suggest that they are better candidates for the photodegradation of the dyes compared to CdS. However, the interaction between both catalysts and the studied dyes will preferably involve their VBEs and the LUMOs of the dyes. In addition, Si has the highest chance of HOMO-CBE type of overlap compared to other visible light activated catalysts studied as revealed by the  $\beta$  values. Comparing pairs with similar interaction modes, the  $\alpha$  and  $\beta$  values in the table suggest ZnO and TiO<sub>2</sub> as not only the more appropriate UV-activated catalysts but also the overall best of the studied catalysts for degrading the dyes. Such high photocatalytic abilities of ZnO and TiO<sub>2</sub> is in consonant with literature facts [20,21]. ZnO will most preferably interact with the LUMOs of the dyes whereas TiO<sub>2</sub> will most likely interact with their HOMOs as revealed by their  $\alpha$  and  $\beta$

values respectively. ZnS also showed evidence of appreciable activity via a LUMO-VBE type overlap as indicated by the relatively small size of  $\alpha_{\text{ZnS}}$ .

The  $\beta$  values generally suggest that the HOMOs of the CN substituted derivatives have greater affinity for the studied catalysts compared to the  $\text{NO}_2$  counterparts which are suggested by the  $\alpha$  values as having the greater tendency to accept electrons from catalysts for interaction. The  $\beta$  values for the EDG substituted derivatives decreases with increasing order of electron donating capacity i.e.  $\text{NH}_2 < \text{NHCH}_3 < \text{N}(\text{CH}_3)_2$  while the converse is true for their  $\alpha$  values. These general differences in the  $\alpha$  and  $\beta$  values of the studied dyes are consequences of their varying electron withdrawing and electron donating capacities of the substituents similar to the trends observed in their HOMO and LUMO energies, electronegativity and chemical potential (Tables 7.3 and 7.4) which were discussed earlier.

### 7.3.5 SITE EVALUATION FOR RADICAL ATTACK AND PREDICTION OF DEGRADATION PATHWAY

Photodegradation of azo dyes usually occur through the attack of photogenerated radicals at sites  $\text{C}_4$ ,  $\text{N}_7$ ,  $\text{N}_8$  and  $\text{C}_9$  in the dye structures (Fig. 7.10) [49, 50]. Therefore, the Mulliken radical Fukui functions ( $f^0$ ) of these sites are presented in Table 7.6 where the sites with the highest activity are in bold. Since the main goal of this aspect is to identify the most plausible center for the attack of a photo-generated hydroxyl ( $\cdot\text{OH}$ ) radical and hence predict the degradation way(s) of the studied dyes, our discussions were therefore focused only on the Fukui function for radical attack and no account is given on the Fukui functions for nucleophilic and electrophilic attacks.

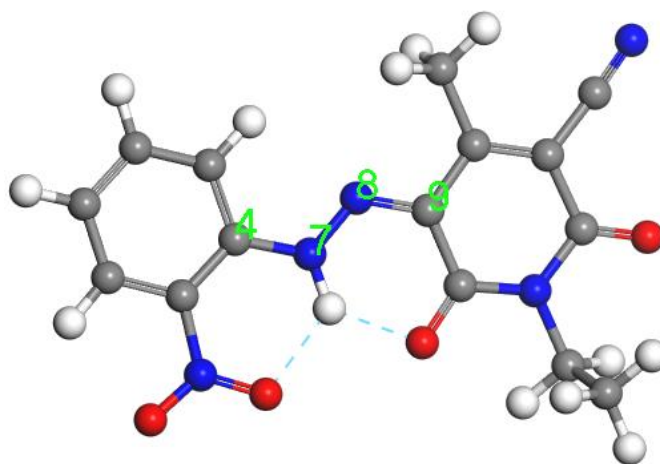


**Figure 7. 10:** Optimized model of DY119 showing the showing the prospective sites for radical attack. The constituent atoms are hydrogen (white), carbon (grey), nitrogen (blue) and oxygen (red).

**Table 7. 6:** Radical attack Fukui functions,  $f^0$  for the most active sites in the studied dyes.

Dye	$f^0$			
	C4	N7	N8	C9
DY119	0.021	0.022	0.038	<b>0.045</b>
EWG substitution				
E1	0.021	0.017	0.032	<b>0.040</b>
E2	0.021	0.018	0.036	<b>0.042</b>
E3	0.022	0.018	0.039	<b>0.042</b>
E4	0.022	0.019	0.037	<b>0.043</b>
E5	0.024	0.013	0.033	<b>0.036</b>
E6	0.021	0.015	0.036	<b>0.039</b>
E7	0.023	0.014	0.036	<b>0.038</b>
E8	0.022	0.015	0.031	<b>0.037</b>
EDG substitution				
E9	0.020	0.015	0.034	<b>0.035</b>
E10	0.019	0.010	<b>0.029</b>	0.028
E11	0.019	0.009	<b>0.031</b>	0.027
E12	0.017	0.017	<b>0.041</b>	0.031

E13	0.017	0.014	<b>0.040</b>	0.027
E14	0.015	0.008	<b>0.039</b>	0.018
E15	0.019	0.015	<b>0.035</b>	0.034
E16	0.018	0.011	<b>0.030</b>	0.028
E17	0.018	0.010	<b>0.032</b>	0.027
E18	0.017	0.017	<b>0.041</b>	0.030
E19	0.017	0.014	<b>0.039</b>	0.027
E20	0.015	0.008	<b>0.039</b>	0.018
E21	0.016	0.011	<b>0.037</b>	0.024
E22	0.016	0.008	<b>0.035</b>	0.023
E23	0.017	0.005	<b>0.035</b>	0.024
E24	0.016	0.008	<b>0.032</b>	0.023
E25	0.017	0.007	<b>0.031</b>	0.022
E26	0.018	0.004	<b>0.032</b>	0.024
E27	0.016	0.008	<b>0.032</b>	0.021
E28	0.017	0.007	<b>0.032</b>	0.022
E29	0.017	0.004	<b>0.033</b>	0.022

Assessment of Table 7.6 showed that the most active sites towards a radical attack in both the parent dye and its EWG substituted derivatives is C<sub>9</sub> (Fig. 7.10) whereas the N<sub>8</sub> seems to be the most likely site for such attack on the EDG counterparts. This suggests that the attack of a photo-generated hydroxyl radical on the parent dye and the EWG analogues will occur with a lower activation energy at C<sub>9</sub> and thereby favor the cleavage C<sub>9</sub> – N<sub>8</sub> bond (i.e. a C–N bond cleavage mechanism). In contrary, the table showed that N<sub>8</sub> is more poised towards a radical attack in the case of the EDG analogues hence, the activation energy for ·OH attack on that center will be lower than that for the competing



C<sub>9</sub> and the attack will give rise to an N–N bond cleavage mechanism (i.e. the cleavage of the N<sub>7</sub> – N<sub>8</sub> bond).

It is therefore reasonable to conclude that the EWGs will favor the C–N bond cleavage pathway while the EDGs will give precedence to the competing N–N bond cleavage pathway. The variation observed in the values of  $f^0$  is also due to the difference in the electron withdrawing and electron donating strengths of the substituents and the positional effects previously discussed. The electron withdrawers decrease the charge density on the donating part of the dye making it more disposed to incoming electrons. This explains why C<sub>9</sub> is the most deficient site in E1 – E8. Conversely, the electron donors increase the charge density on the donating part making it less prone to incoming electrons. This explains the trend observed for N<sub>8</sub> and C<sub>9</sub> in E9 – E29 where C<sub>9</sub> becomes less deficient compared to N<sub>8</sub> as a result of donation from the electron donating substituents. NO<sub>2</sub> is more electron withdrawing than CN hence, it seems to stabilize the C<sub>9</sub> center better. This explains the smaller  $f^0$  values observed for the NO<sub>2</sub> derived dyes. Similarly, N(CH<sub>3</sub>)<sub>2</sub> is the most electron donating substituent among the EDGs studied. It will therefore decrease the potency of the attack center towards an incoming electron, hence the least  $f^0$  values observed for the N(CH<sub>3</sub>)<sub>2</sub> substituted derivatives. The fact that C<sub>9</sub> is the most vulnerable site in parent dye suggests CH<sub>3</sub> and C<sub>2</sub>H<sub>5</sub> as being less electron donating compared to NH<sub>2</sub>, NHCH<sub>3</sub> and N(CH<sub>3</sub>)<sub>2</sub>.

## 7.4 CONCLUSION

The effects of some electron withdrawing (EW) and electron donating (ED) polar substituents on aqueous solubility and reactivity of disperse yellow 119 (DY119) have been investigated using DFT/COSMO-RS method with the aid of DMol<sup>3</sup> program. The

relative affinities of the studied dyes for some photocatalysts and the susceptibility of atomic sites in the dyes to radical attack were also evaluated. The following conclusions can be derived from the study:

1. Aqueous solubility of the dyes depends on both electronic and steric effects of the substituents, which in turn depend on the nature and position of the substituents.
2. Except for the DY119 derivative with only  $-\text{NO}_2$  substitution at  $\text{R}_1$ , all the other investigated  $-\text{NO}_2$  and/or  $-\text{CN}$  substituted derivatives of DY119 showed better aqueous solubility than the parent dye. More so,  $-\text{CN}$  group enhanced solubility more than  $-\text{NO}_2$  group.
3. Modification of DY119 by replacement of the  $-\text{CH}_3$  group at  $\text{R}_4$  with an amino substituent only decreased aqueous solubility tendency, while substitution with  $-\text{NH}_2$  and  $-\text{NHCH}_3$  at position  $\text{R}_5$  of DY119 increased the solubility. However, substitution with  $-\text{N}(\text{CH}_3)_2$  at  $\text{R}_5$  resulted in a derivative with decreased solubility due to steric hindrance.
4. A modified DY119 with  $-\text{N}(\text{CH}_3)_2$  substituents at both positions  $\text{R}_4$  and  $\text{R}_5$  showed the highest aqueous solubility tendency.
5. Aqueous solubility of a dye appeared to depend on the synergy of screening charges, polarizability and dipole moment of the dye, and none of the three properties is sufficient to adjudge the relative solubility of dyes.
6. All the DY119 derivatives with EW groups showed lower  $E_{\text{HOMO}}$  and  $E_{\text{LUMO}}$  than the parent dye, while all the derivatives with ED groups showed higher  $E_{\text{HOMO}}$  and  $E_{\text{LUMO}}$  than the parent dye, except E12, E13, E18, E19 and E21, which showed lower  $E_{\text{LUMO}}$ .

7. ZnO and TiO<sub>2</sub> showed the highest potentials as photocatalysts for the degradation of the studied dyes.
8. EW substituted DY119 derivatives are most likely to degrade via the C–N bond cleavage, while the ED substituted derivatives would prefer degradation via the N-N rupture upon radical attack.

## 7.5 REFERENCES

1. S.M. Burkinshaw. Physico-chemical aspects of textile coloration. *John Wiley & Sons*, United States, (2016).
2. J. Koh. Dyeing with disperse dyes; P. Hauser (Ed.), *INTECH Open Access Publisher*, Croatia, (2011), pp. 195-221. DOI: 10.5772/20458. Available at: <https://www.intechopen.com/books/textile-dyeing/dyeing-with-disperse-dyes>.
3. M. Clark. Handbook of textile and industrial dyeing: principles, processes and types of dyes. *Woodhead Publishing Limited*, United Kingdom, (2011).
4. W. Saus, D. Knittel and E. Schollmeyer. Dyeing with supercritical carbon dioxide—an alternative to high-temperature dyeing of polyester. *Textile Praxis International* **47** (1992) 1052-1054.
5. W. Saus, D. Knittel and E. Schollmeyer. Dyeing of textiles in supercritical carbon dioxide. *Textile Research Journal* **63** (1993) 135-142.
6. M. Banhero. Supercritical fluid dyeing of synthetic and natural textiles—a review. *Coloration Technology* **129** (2013) 2-17.
7. S. Özcan, A. A. Clifford, K. D. Bartle and D. M. Lewis. Solubility of disperse dyes in supercritical carbon dioxide. *Journal of Chemical and Engineering Data* **42** (1997) 590-592.

8. H. Øllgaard, L. Frost, J. Galster and O. C. Hansen. Survey of azo-colorants in Denmark. Consumption, use, health and environmental aspects (1998). Available at: <https://www2.mst.dk/udgiv/publications/1999/87-7909-548-8/pdf/87-7909-546-1.pdf>. Accessed on 14 March 2018.
9. Y. Anjaneyulu, N. S. Chary and D. S. S. Raj. Decolourization of industrial effluents—available methods and emerging technologies – a review. *Reviews in Environmental Science and Biotechnology* **4** (2005) 245-273.
10. N. A. Ghalwa, H. M. Abu-Shawish, H. M. Tamous and H. Al-Harazeen. Determination of electrochemical degradation of E102 dye at lead dioxide-doped carbon electrodes using some potentiometric and spectrophotometric methods. *Chemistry Journal* **3** (2013) 1-6.
11. S. K. Al-Dawery. Photo-Catalyst degradation of tartrazine compound in wastewater using TiO<sub>2</sub> and UV light. *Journal of Engineering Science and Technology* **8** (2013) 683-691.
12. S. Banerjee and M. Chattopadhyaya. Adsorption characteristics for the removal of a toxic dye, tartrazine from aqueous solutions by a low cost agricultural by-product. *Arabian Journal of Chemistry* **10** (2013) 1629-1638.
13. Cavicchioli and I. G. Gutz. Effect of scavengers on the photocatalytic digestion of organic matter in water samples assisted by TiO<sub>2</sub> in suspension for the voltammetric determination of heavy metals. *Journal of Brazilian Chemical Society* **13** (2002) 441-448.
14. V. K. Gupta, R. Jain, A. Nayak, S. Agarwal and M. Shrivastava. Removal of the hazardous dye-tartrazine by photodegradation on titanium dioxide surface. *Material Science Engineering C* **31** (2011) 1062-1067.

15. J. M. Joseph, H. Destailats, H.M. Hung and M. R. Hoffmann. The sonochemical degradation of azobenzene and related azo dyes: rate enhancements via Fenton's reactions. *Journal of Physical Chemistry A* **104** (2000) 301-307.
16. N. Modirshahla, M. Behnajady, S. Kooshaiian. Investigation of the effect of different electrode connections on the removal efficiency of Tartrazine from aqueous solutions by electrocoagulation. *Dyes and Pigments* **74** (2007) 249-257.
17. S. Adhikari and D. Sarkar. Metal oxide semiconductors for dye degradation. *Material Research Bulletin* **72** (2015) 220-228.
18. M. Kulkarni and P. Thakur. Photocatalytic degradation and mineralization of reactive textile azo dye using semiconductor metal oxide nano particles. *International Journal of Engineering Research and General Science* **2** (2014) 245-254.
19. L. Mahlalela and L. Dlamini. Enhanced photocatalytic activity of titania in the presence of  $\text{KNO}_3$  on the photodegradation of dyes. *Surfaces and Interfaces* **1** (2016) 21-28.
20. K. Mondal and A. Sharma. Photocatalytic oxidation of pollutant dyes in wastewater by  $\text{TiO}_2$  and  $\text{ZnO}$  nano-materials - a mini-review. *Nanoscience & Technology for Mankind, The Academy of Sciences India (NASI)*, Allahabad, India (2014) 36-72.
21. T. Peternel, N. Koprivanac, A. M. L. Božić and H. M. Kušić. Comparative study of UV/ $\text{TiO}_2$ , UV/ $\text{ZnO}$  and photo-fenton processes for the organic reactive dye degradation in aqueous solution, *Journal of Hazardous Materials* **148** (2007) 477-484.

22. D. Patel, N. Prajapati, M. Thakor and V. Patel. Formation of some novel disperse azo dyes: synthesis, characterisation and printing properties. *Journal of Current Chemical and Pharmaceutical Sciences* **2** (2012) 86-91.
23. K. J. Sakoma, K. A. Bello and M. K. Yakubu. Synthesis of some azo disperse dyes from 1-substituted 2-hydroxy-6-pyridone derivatives and their colour assessment on polyester fabric. *Open Journal of Applied Sciences* **2** (2012) 54-59.
24. Y. S. Choi, K. S. Lee, H. J. Kim, J. Y. Choi, S. B. Kang, E. J. Lee and G. Keum. Synthesis, spectral property and dyeing assessment of azo disperse dyes containing carbonyl and dicyanovinyl groups. *Bulletin of Korean Chemical Society* **34** (2013) 863-867.
25. J. Aspland. The structure and properties of disperse dyes and related topics. *Textile Chemistry and Coloration* **25** (1993) 21-25.
26. M.B. Smith and J. March. March's advanced organic chemistry: reactions, mechanisms, and structure. *John Wiley & Sons*, United State, (2007).
27. DMol<sup>3</sup> Guide, Material Studio 8.0. *Accelrys Software, Inc.*, San Diego, United States (2017) 1-161.
28. Y. Inada and H. Orita. Efficiency of numerical basis sets for predicting the binding energies of hydrogen bonded complexes: evidence of small basis set superposition error compared to Gaussian basis sets. *Journal of Computational Chemistry* **29** (2008) 225-232.
29. Klamt, V. Jonas, T. Bürger and J. C. Lohrenz. Refinement and parametrization of COSMO-RS. *Journal of Physical Chemistry A* **102** (1998) 5074-5085.

30. E. Mullins, R. Oldland, Y. Liu, S. Wang, S. I. Sandler, C.C. Chen, M. Zwolak and K. C. Seavey. Sigma-profile database for using COSMO-based thermodynamic methods. *Industrial and Engineering Chemistry Research* **45** (2006) 4389-4415.
31. J. D. Thompson, C. J. Cramer and D. G. Truhlar. Predicting aqueous solubilities from aqueous free energies of solvation and experimental or calculated vapor pressures of pure substances. *Journal of Chemical Physics* **119** (2003) 1661-1670.
32. Liang and D.A. Gallagher. QSPR prediction of vapor pressure from solely theoretically-derived descriptors. *Journal of Chemical Information and Computer Sciences* **38** (1998) 321-324.
33. P. K. Chattaraj. Chemical reactivity theory: A density functional view. *CRC Press*, United States, (2009).
34. R. G. Parr and R. G. Pearson. Absolute hardness: companion parameter to absolute electronegativity. *Journal of American Chemical Society* **105** (1983) 7512-7516.
35. R. G. Parr, R. A. Donnelly, M. Levy and W. E. Palke. Electronegativity: the density functional viewpoint. *Journal of Chemical Physics* **68** (1978) 3801-3807.
36. R. G. Parr, L. V. Szentpaly and S. Liu. Electrophilicity index. *Journal of American Chemical Society* **121** (1999) 1922-1924.
37. J. L. Gázquez. Perspectives on the density functional theory of chemical reactivity. *Journal of Mexican Chemical Society* **52** (2008) 3-10.

38. L.H. Mendoza-Huizar. A theoretical study of chemical reactivity of tartrazine through DFT reactivity descriptors. *Journal of Mexican Chemical Society* **58** (2014) 416-423.
39. S. Kumar and J. Sharma. Stable phase CdS nanoparticles for optoelectronics: a study on surface morphology, structural and optical characterization. *Material Science-Poland* **34** (2016) 368-373.
40. U. Diebold. The surface science of titanium dioxide. *Surface Science Report* **48** (2003) 53-229.
41. M. Grunze, W. Hirschwald and D. Hofmann. Zinc oxide: surface structure, stability and mechanisms of surface reactions. *Journal Crystal Growth* **52** (1981) 241-249.
42. J.V. Lauritsen, S. Porsgaard, M.K., M.C. Jensen, R. Bechstein, K. Meinander, B.S. Clausen, S. Helveg, R. Wahl and G. Kresse. Stabilization principles for polar surfaces of ZnO. *ACS nano* **5** (2011) 5987-5994.
43. K. Wright, G. Watson, S. Parker and D. Vaughan. Simulation of the structure and stability of sphalerite (ZnS) surfaces. *American Mineralogist* **83** (1998) 141-146.
44. P. W. Ayers and R. G. Parr. Variational principles for describing chemical reactions: the Fukui function and chemical hardness revisited. *Journal of American Chemical Society* **122** (2000) 2010-2018.
45. W. Huang. Structural and computational studies of azo dyes in the hydrazone form having the same pyridine-2, 6-dione component (II): CI disperse yellow 119 and CI disperse yellow 211. *Dyes and Pigments* **79** (2008) 69-75.



46. D.H. McDaniel and H.C. Brown. An extended table of Hammett substituent constants based on the ionization of substituted benzoic acids. *Journal of Organic Chemistry* **23** (1958) 420-427.
47. XLSTAT 2012: Leading data analysis and statistical solution for Microsoft excel, *Addinsoft SRL*, (2012). <https://www.xlstat.com>. Last assessed on May 25, 2018.
48. X. Li, J. Yu, J. Low, Y. Fang, J. Xiao, X. Chen. Engineering heterogeneous semiconductors for solar water splitting. *Journal of Material Chemistry A* **3** (2015) 2485-2534.
49. A .S. Özen, V. Aviyente, F. De Proft and P. Geerlings. Modeling the substituent effect on the oxidative degradation of azo dyes. *Journal of Physical Chemistry A* **108** (2004) 5990-6000.
50. X. Jiao, H. Yu, Q. Kong, Y. Luo, Q. Chen and J. Qu. Theoretical mechanistic studies on the degradation of alizarin yellow R initiated by hydroxyl radical. *Journal of Physical Organic Chemistry* **108** (2014) 519-526.

---

## CHAPTER 8

# SYNERGISTIC EFFECT OF OPPOSITE POLAR SUBSTITUENTS ON SELECTED PROPERTIES OF DISPERSE YELLOW 119 DYE

---

### PREAMBLE

By theoretically exploring the synergistic effects of electron donating (ED) and electron withdrawing (EW) substituent effects on intramolecular charge movement in Disperse yellow (DY)119 dye, series of new azopyridone disperse dyes with improved aqueous solubility and chemical reactivity has been predicted using VWN-BP/DNP level of theory. Effects of substituents on all predicted properties generally showed great sensitivity to the nature of substituent and substitution positions in DY119 structure.

### 8.1 INTRODUCTION

Azo dyes remain the most essential group of dyes for various industrial applications ranging from textile dyeing [1-4], corrosion inhibition [5-10], pH and metallochromic indicators [11], sensitizers [12], liquid crystal display (LCD) [13], electrical and optical materials [14], foods and cosmetics [15], and drug production and delivery [16]. However, their effectiveness for most of these applications rely to a very large extent on their aqueous solubility properties. The introduction of organic solvents and supercritical fluid [17-20] as alternative dissolution agents in place of water seems to be only effective for limited applications. Despite their benefits in textile dyeing, organic solvents and supercritical fluid are yet to receive a widespread commercial application due to their

---

The work presented in this chapter has been published.

\*O.O. Wahab, L.O. Olasunkanmi, K.K. Govender and P.P. Govender. *Chemical Physics Letters* **704** (2018) 55-61.

relatively higher cost and lower availability compared to natural water. Some of the organic solvents are also characterized by repugnant odors, which limit their acceptance by most end users. While the use of carrier and dispersing agents for enhancing disperse dye solubility has both economic and environmental defects [1,21], the use of high temperature and high pressure (HTHP) noncarrier dyeing is not a better alternative either, especially for dyes with low heat resistance due to the likelihood of decomposition [21]. Besides its relatively higher cost and complexity compared to aqueous dyeing, HTHP machines usually become less efficient during winter as a result of the drop in the operational pressure caused by the condensation of generated steam [21]. Since water remains the most abundant, naturally available, nontoxic, odorless, and universal solvent for azo dye applications, it is necessary to optimize aqueous solubility properties of azo dyes for a more economic and environmentally benign application.

Azo disperse dyes have allegedly been the cause of disease causing conditions such as allergy, contact dermatitis, bladder cancer and eczema in humans [21,22]. Of all the several pollutant treatment methods available [23-30], the use of efficient, low cost and non-toxic photocatalysts [25,28,31-35] appears to be the most promising because it ensures total elimination of pollutants. For a proper and more effective photocatalysis, selection guidelines for efficient photocatalysts are paramount. Theoretical assessment of the relative affinities of different photocatalysts for a pollutant could help to identify the one with the highest efficiency for its degradation prior to detail experimentation.

In a separate theoretical study on 29 derivatives of DY119 (Fig. 8.1) and 6 known photocatalysts (Chapter 7), we have investigated the separate effects of electron withdrawing -CN and -NO<sub>2</sub>, and electron donating -NH<sub>2</sub>, -NHCH<sub>3</sub> and -N(CH<sub>3</sub>)<sub>2</sub>

substituents on the aqueous solubility, reactivity, thermodynamic stability, and catalyst selectivity properties of DY119. In the present chapter, DMol<sup>3</sup> simulations were carried out on 84 additional modelled derivatives of the dye to examine the combined effect of the electron withdrawing and the electron donating substituents on the same properties. The aim is to theoretically develop new azo disperse dyes with much improved aqueous solubility and fastness properties, predict their vulnerability to degradation, propose suitable photocatalysts for their degradation, identify the most vulnerable sites towards the attack of photo-generated radicals and hence predict their photodegradation pathways. The molecular structure of DY119 is shown below:

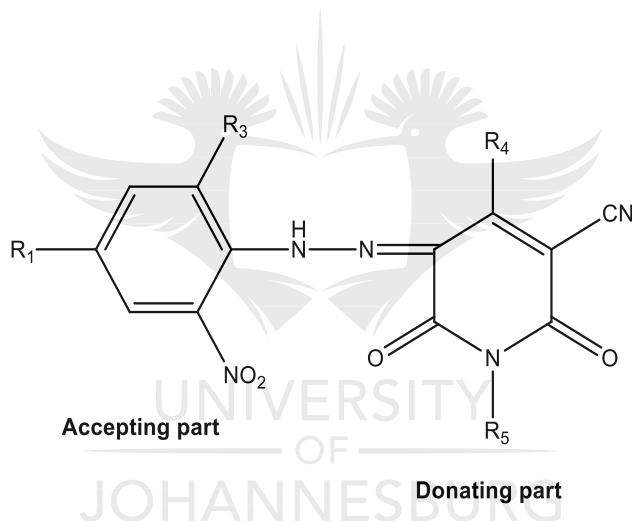


**Figure 8. 1:** General molecular structure of DY 119 ( $R_1 = R_3 = \text{H}$ ,  $R_4 = \text{CH}_3$  and  $R_5 = \text{C}_2\text{H}_5$ ) and its studied derivatives.

## 8.2 COMPUTATIONAL DETAILS

The DMol<sup>3</sup> code [36] implemented in the Material studio (2016 version) package was employed for this study. The molecular geometries of the studied dyes were optimized both in the gas and aqueous phases at the GGA/VWN-BP level of theory [36] using the DNP basis set [36,37]. A global orbital cut-off value of 7.0 Å was used for the calculations. The solvent phase optimization was carried out using the COSMO-RS program

implemented in DMol<sup>3</sup>, where water was selected as the solvent by setting the COSMO dielectric constant to 78.4. A total of 92 surface segments per atom (i.e. NSPA = 92) were used and the recommended radii for the component atoms [38,39] of the studied dyes were included in the COSMO calculation for a proper description of molecular cavitation.

### 8.2.1 PROCEDURE FOR CALCULATING THE AQUEOUS SOLUBILITY AND GIBB'S FREE ENERGIES

The solvation free energies (SFEs) of the dyes in water were determined from the energies of their optimized geometries using equation 8.1 [36]. The vapor pressure of the dyes were obtained from COSMO-RS calculation based on equation 8.2 [40] using appropriate keywords [36, 40] in the DMol<sup>3</sup>/COSMO-RS input file. The aqueous solubility, in mg/L, was determined from the calculated vapor pressure and the SFEs using the Cramer *et al.* solubility equation (CSE) (eqn. 8.3) [41]. The Gibb's free energies were calculated from the enthalpy and entropy values obtained for the dyes in vacuum using equation 8.4 [36].

$$\Delta G_{sol} = (E + \Delta G_{NSE}) - E^0 \quad \text{Equation 8. 1}$$

$$P_s = x_s \exp\left(\frac{\mu_s^{solv} - \mu_s^{gas}}{RT}\right) \quad \text{Equation 8. 2}$$

$$S_{aq} = \frac{P_s}{P^0} e^{-\Delta G_{sol}/RT} \quad \text{Equation 8. 3}$$

$$G = H - TS \quad \text{Equation 8. 4}$$

where  $\Delta G_{sol}$  is the solvation free energy,  $E$  is the energy in the aqueous phase (i.e COSMO energy),  $E^0$  is the energy in vacuum,  $\Delta G_{NSE}$  is the nonelectrostatic contribution to SFE due to dispersion and cavity formation effects and is produced alongside with

COSMO energy in the COSMO output.  $P_s$  represents solute vapour pressure (in atm),  $x_s$  and  $\mu_s^{solv}$  represent the mole fraction and the pseudochemical potential of the solute in the solvent, respectively.  $\mu_s^{gas}$  is the pseudochemical potential of the solute in vacuum,  $S_{aq}$  is the aqueous solubility in mol/L,  $P^0$  is the pressure of an ideal gas at 1 molar standard state and 298 K and is equal to 24.45 atm.  $R$  and  $T$  are the molar gas constant and temperature, respectively.  $G$  is the Gibb's free energy,  $H$  is the enthalpy and  $S$  is the entropy of the solute at 25 °C.

## 8.2.2 PROCEDURE FOR PREDICTING THE CHEMICAL REACTIVITY

By applying Koopmans' and finite difference approximation [42, 43], the global reactivity indices which comprise the HOMO–LUMO energy gap, global hardness and softness, global electronegativity, chemical potential and global electrophilicity index were evaluated from the HOMO and LUMO energies using equations 8.5 – 8.10 [43].

$$\text{Energy gap } (E_g) = (E_{LUMO} - E_{HOMO}) \quad \text{Equation 8. 5}$$

$$\text{Global hardness } (\eta) = -\frac{1}{2}(E_{HOMO} - E_{LUMO}) \quad \text{Equation 8. 6}$$

$$\text{Global softness } (\sigma) = \frac{1}{\eta} = -2/(E_{HOMO} - E_{LUMO}) \quad \text{Equation 8. 7}$$

$$\text{Electronegativity } (\chi) = -\frac{1}{2}(E_{HOMO} + E_{LUMO}) \quad \text{Equation 8. 8}$$

$$\text{Chemical potential } (\Phi) = -\chi = \frac{1}{2}(E_{HOMO} + E_{LUMO}) \quad \text{Equation 8. 9}$$

$$\text{Global electrophilicity index } (\omega) = \frac{\chi^2}{2\eta} \quad \text{Equation 8. 10}$$

where  $E_{HOMO}$  and  $E_{LUMO}$  are the HOMO and LUMO energies respectively.

The atom condensed Fukui function for radical attacks,  $f^0$ , was obtained from the Mulliken's atomic charges using equation 8.11 [44].

$$f^0 = \frac{1}{2} [q_k(N + 1) - q_k(N - 1)]$$

Equation 8. 11

where  $N$  is the number of electrons,  $q_k(N + 1)$  and  $q_k(N - 1)$  are the Mulliken charges on atom  $k$  for  $(N+1)$  and  $(N-1)$  numbers of electrons, respectively.

## 8.3 RESULTS AND DISCUSSIONS

### 8.3.1 AQUEOUS SOLUBILITY STUDY

The results of the aqueous solubility and thermodynamic studies for 84 derivatives of DY119 (Fig. 8.1) are provided in Table A.16 (Appendix). The relative performances of -CN and -NO<sub>2</sub> with the electron donating substituents (EDS) studied are compared and presented in Figure 8.2, based on their relative influence on the aqueous solubility property. The figure shows the aqueous solubility values for group A and the group B derivatives in which the electron withdrawing substituents (EWS) occupy positions R<sub>1</sub> (*para* to N-N) and R<sub>3</sub> (*ortho* to N-N), respectively in DY119 (Fig. 8.1). There are 13 representatives in each group where each representative consists of one -NO<sub>2</sub> and one -CN substituted members. Members of the same representative have identical EDS and substituent position but differ from members of other representatives. Members of each group A and group B representatives are listed with their respective solubility values in Table 8.1.

In general, the figure revealed that the electron withdrawing -CN substituent performed better with the electron donating substituents studied in enhancing the aqueous solubility

of the dye compared to  $-\text{NO}_2$ . The figure also showed that nearly all the group B derivatives are more soluble than their respective group A counterparts probably due to decrease in the electron withdrawing influence of the substituents when attached to position  $R_3$  (i.e. *ortho* to N-N) as indicated by the relatively larger screening charge magnitude and dipole moment values of these derivatives (Figs. 8.3 and 8.4).

A decrease in the electron withdrawing powers of the substituents (i.e.  $-\text{CN}$  and  $-\text{NO}_2$ ) favors larger negative screening charge and dipole moment values for the derivatives in which they are substituted *ortho* to the N-N bridge due to the following:

- 1) The electron is less depleted from the N-N bridge which implies higher charge density in the system compared to when the substituent is *para* to the bridge.
- 2) The electron density difference between the accepting and the donating parts of the dye at the N-N linkage (Fig. 8.1) is large as a result of electron deficiency in the accepting part which favors a larger dipole moment value unlike when the substituent is *para* to the bridge.



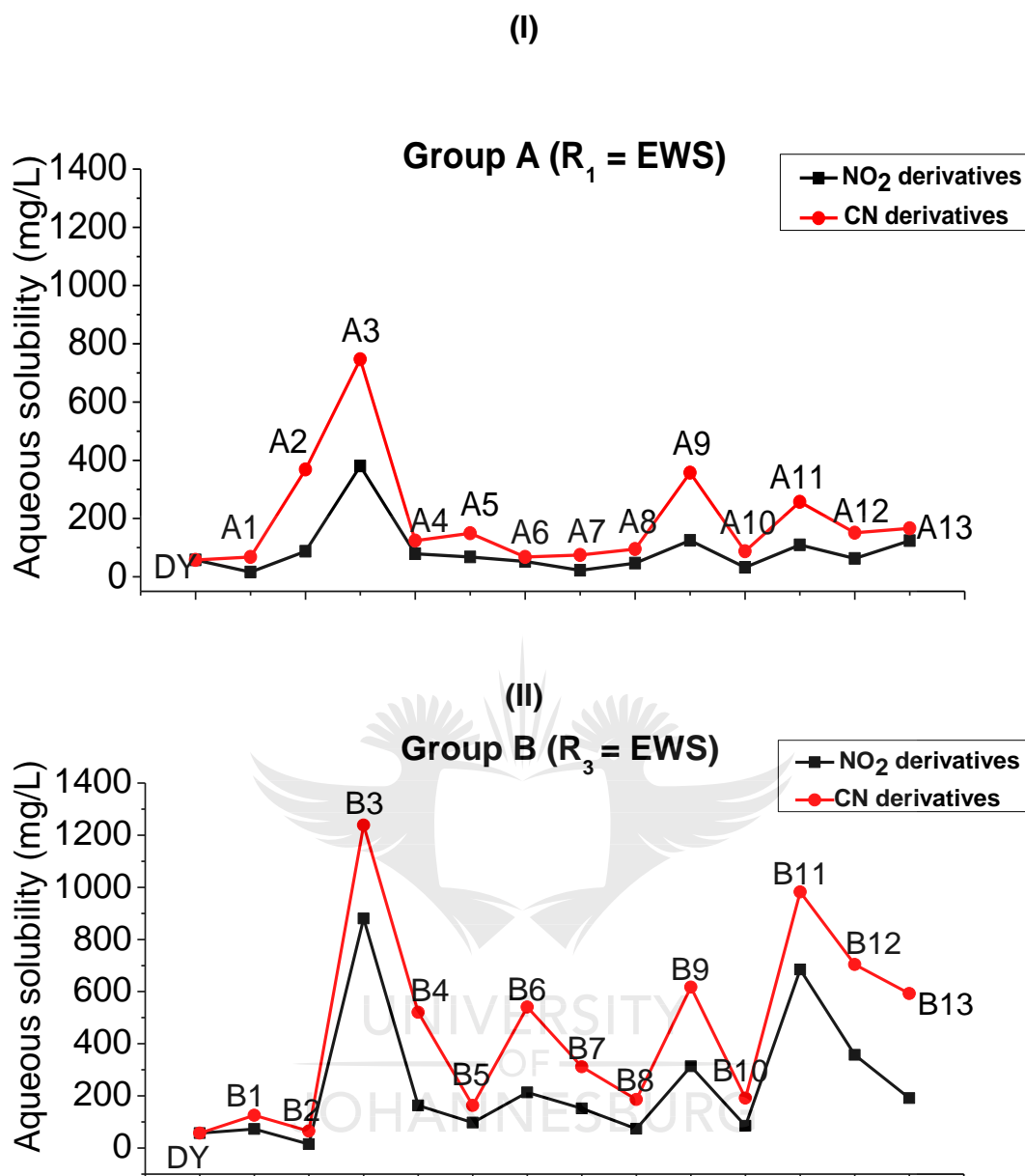


**Figure 8. 2:** Comparison of aqueous solubility values of Group A (I) and Group B (I) derivatives of DY119\*

\*groups A1 and B1:  $R_4 = \text{NH}_2$  and  $R_5 = \text{C}_2\text{H}_5$ , groups A2 and B2:  $R_4 = \text{N}(\text{CH}_3)_2$  and  $R_5 = \text{C}_2\text{H}_5$ , groups A3 and B3:  $R_4 = \text{CH}_3$  and  $R_5 = \text{NH}_2$ , groups A4 and B4:  $R_4 = \text{CH}_3$  and  $R_5 = \text{NHCH}_3$ , groups A5 and B5:  $R_4 = \text{CH}_3$  and  $R_5 = \text{N}(\text{CH}_3)_2$ , groups A6 and B6:  $R_4 = \text{NH}_2$  and  $R_5 = \text{CH}_3$ , groups A7 and B7:  $R_4 = \text{NHCH}_3$  and  $R_5 = \text{CH}_3$ , groups A8 and B8:  $R_4 = \text{N}(\text{CH}_3)_2$  and  $R_5 = \text{CH}_3$ , groups A9 and B9:  $R_4 = \text{C}_2\text{H}_5$  and  $R_5 = \text{NH}_2$ , groups A10 and B10:  $R_4 = \text{C}_2\text{H}_5$  and  $R_5 = \text{NHCH}_3$ , groups A11 and B11:  $R_4 = R_5 = \text{NH}_2$ , groups A12 and B12:  $R_4 = \text{NHCH}_3$  and  $R_5 = \text{NH}_2$ , and groups A13 and B13:  $R_4 = \text{N}(\text{CH}_3)_2$  and  $R_5 = \text{NH}_2$ .

**Table 8. 1:** Predicted solubility values of members of groups A and B derivatives of DY119 at 25 °C.

Members with R <sub>1</sub> = EWS					Members with R <sub>3</sub> = EWS				
Group A	R <sub>1</sub> = NO <sub>2</sub>	S <sub>aq</sub> (mg/L)	R <sub>1</sub> = CN	S <sub>aq</sub> (mg/L)	Group B	R <sub>3</sub> = NO <sub>2</sub>	S <sub>aq</sub> (mg/L)	R <sub>3</sub> = CN	S <sub>aq</sub> (mg/L)
A1	E30	16.24	E36	67.55	B1	E72	73.19	E78	125.52
A2	E32	87.41	E38	368.30	B2	E74	14.96	E80	65.20
A3	E33	380.00	E39	746.52	B3	E75	880.66	E81	1238.10
A4	E34	78.99	E40	123.71	B4	E76	163.68	E82	520.40
A5	E35	67.82	E41	149.44	B5	E77	97.55	E83	163.75
A6	E42	52.59	E48	68.04	B6	E84	212.96	E90	540.91
A7	E43	21.85	E49	74.30	B7	E85	152.18	E91	311.92
A8	E44	47.00	E50	94.92	B8	E86	74.17	E92	185.93
A9	E45	124.62	E51	357.42	B9	E87	313.51	E93	617.16
A10	E46	31.88	E52	87.76	B10	E88	85.59	E94	191.63
A11	E54	109.31	E63	257.02	B11	E96	684.42	E105	982.61
A12	E57	62.97	E66	150.71	B12	E99	357.19	E108	704.04
A13	E60	123.53	E69	166.03	B13	E102	191.11	E111	564.90

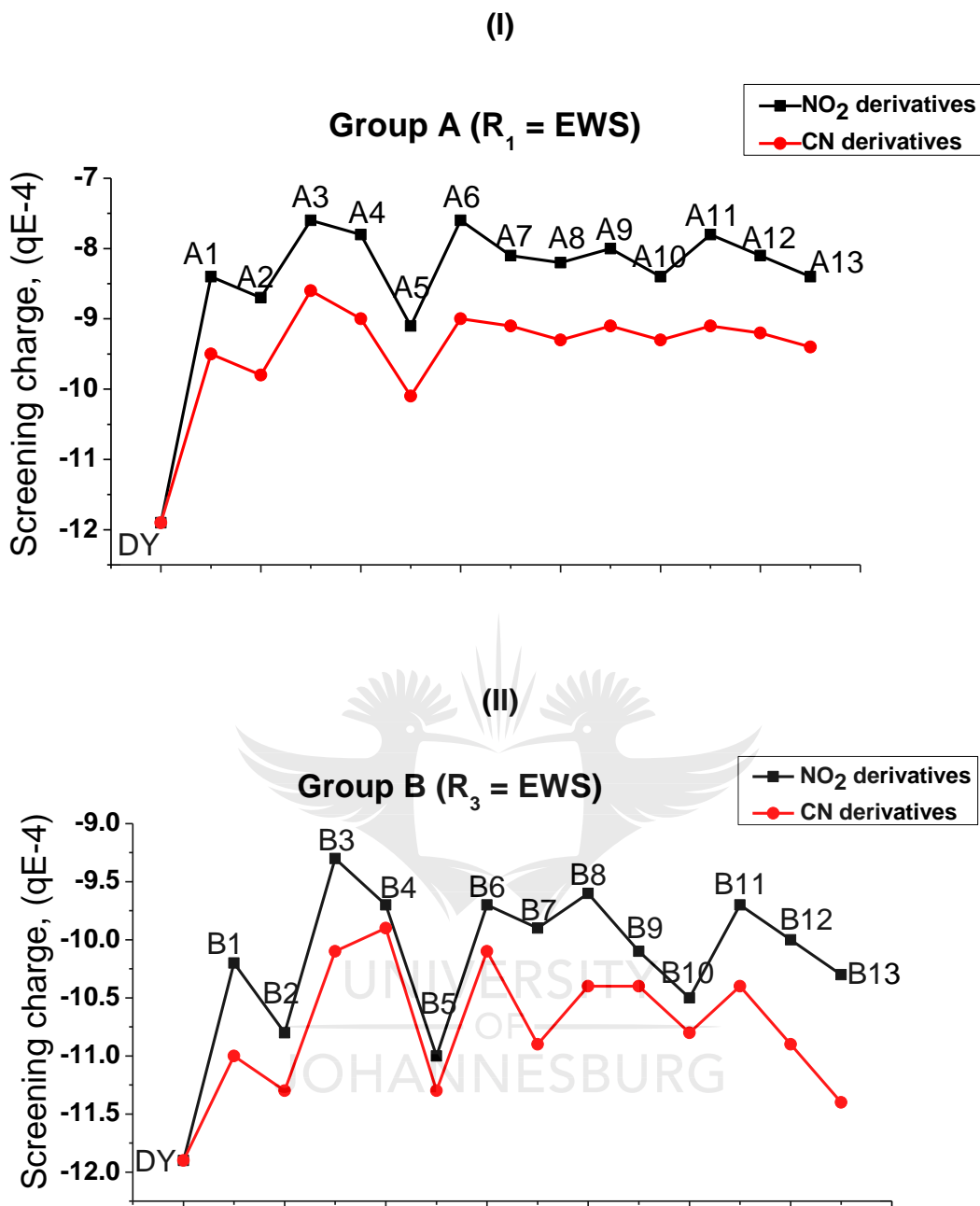


**Figure 8. 3:** Comparison of the screening charges of Group A (I) and Group B (II) derivatives.

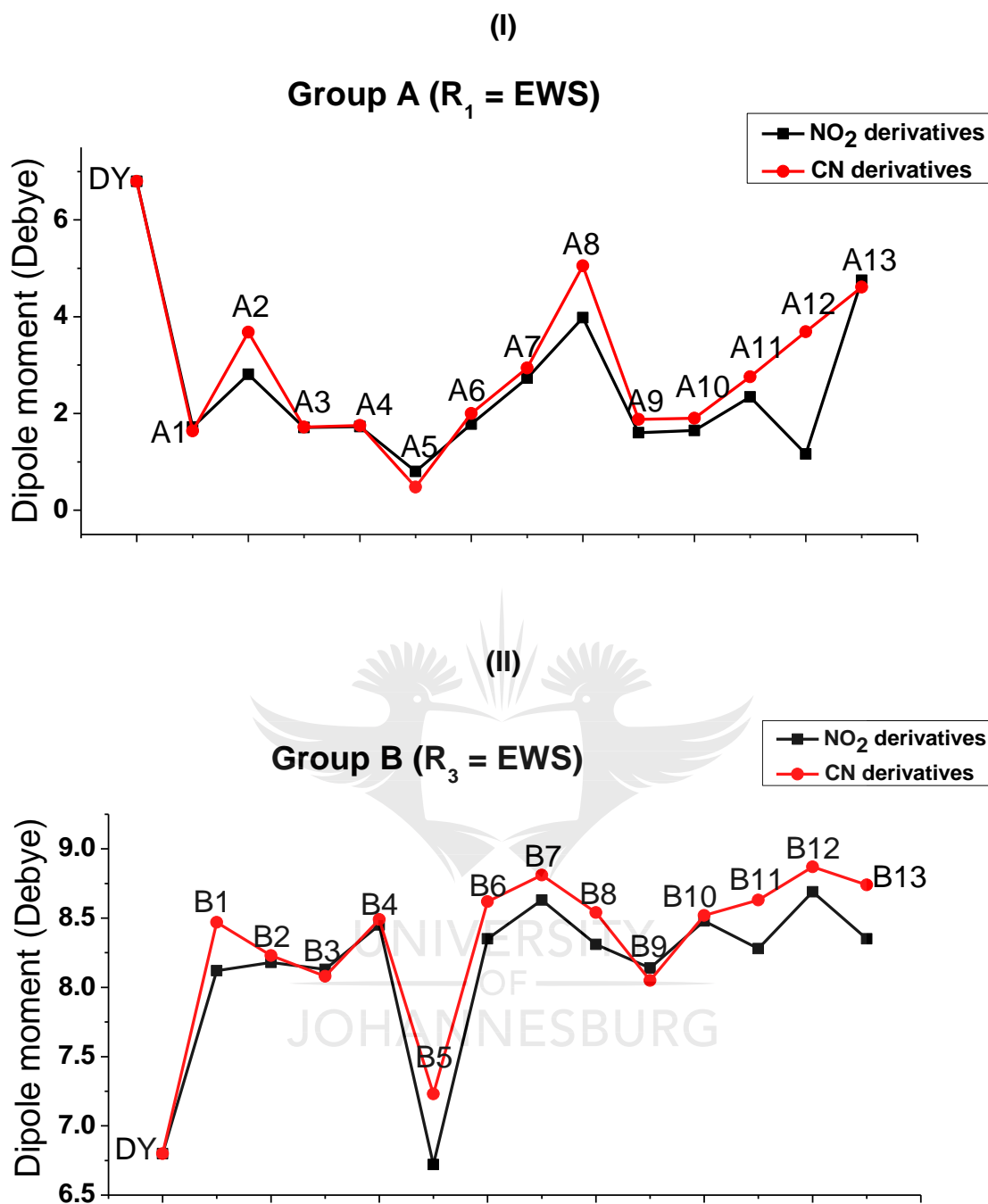


**Figure 8. 4:** Comparison of the dipole moments of Group A (I) and Group B (II) derivatives.

The trend observed between CN and  $\text{NO}_2$  substituted derivatives is in consonant with the electron withdrawing capacity difference between the substituents. CN is less electron withdrawing, more polar and more readily solvated compared to  $\text{NO}_2$  as suggested by its

electronegativity, dipole moment and solvation free energy, respectively (Appendix: Table A.14). Hence the higher solubility values observed for the CN substituted derivatives (Fig. 8.2). Due to its relatively stronger electron withdrawing power, NO<sub>2</sub> depletes the charge density of the dyes more than CN, thereby inhibiting the solvation process as indicated by the relatively small negative SFE (Appendix: Table A.17), screening charge (Fig. 8.3), and dipole moment (Fig. 8.4) values of the NO<sub>2</sub> substituted derivatives.

Of all the electron donating groups combined with CN and NO<sub>2</sub>, NH<sub>2</sub> was found to promote the solubility better than NHCH<sub>3</sub> and N(CH<sub>3</sub>)<sub>2</sub> while the CH<sub>3</sub> substituent outperformed C<sub>2</sub>H<sub>5</sub> except in few cases (Appendix: Table A.16). The differences in solubility observed are of both electronic and steric origins. Compared to NHCH<sub>3</sub> and N(CH<sub>3</sub>)<sub>2</sub>, NH<sub>2</sub> has the lowest electron donating power (i.e. lowest chemical potential), but offers appreciable polarity, hence a relatively large SFE in water (Appendix: Table A.14). These justify the relatively large aqueous solubility values obtained for groups A3, A9, A11, and A12, and all the group B members possessing NH<sub>2</sub> substituent in their structures (Fig. 8.2). Despite having the highest polarity (Appendix: Table A.14), NHCH<sub>3</sub> offers higher steric hindrance due to its larger size compared to NH<sub>2</sub> (Fig. 8.5), hence the lower solubility observed for the NHCH<sub>3</sub> substituted derivatives compared to the NH<sub>2</sub> counterparts (Fig. 8.2).

The relatively large solubility values obtained for A2 (Fig. 8.2(I)) which possesses N(CH<sub>3</sub>)<sub>2</sub> substituent at position R<sub>4</sub> (Fig. 8.1) compared to A1 where the position is occupied by NH<sub>2</sub> suggest that the electron donating effect of the N(CH<sub>3</sub>)<sub>2</sub> substituent is higher than that of NH<sub>2</sub>, and also predominates over its steric effect at that position. This is confirmed by the relatively large negative screening charge and dipole moment values of A2 compared to A1 (Fig. 8.3(I) and 8.4(II)). Since a similar trend is not observed between groups B2 and B1 (Fig. 8.2(II)) because the electron withdrawing substituent (i.e. CN or NO<sub>2</sub>) is

attached to position R<sub>3</sub> (Fig. 8.1), the predominance of electronic effect of -N(CH<sub>3</sub>)<sub>2</sub> at position R<sub>4</sub> in group A2 can therefore be ascribed to the strong electron withdrawing influence of the EWS at R<sub>1</sub> (Fig. 8.1). In the case of group B derivatives, the large steric hindrance of N(CH<sub>3</sub>)<sub>2</sub> seems to have outweighed its electron donating impact especially when the substituent is attached to R<sub>5</sub> (Fig. 8.5). This explains why the solubility values of groups B5 and B8 are smaller than those of B3 and B6 respectively (Fig 8.2(II), Table 8.1).

The drastic increase in solubility obtained for groups A3 and B3, A9 and B9, A11 and B11 (Fig. 8.2) and the other derivatives (Appendix: Table A.16) in which the NH<sub>2</sub> substituent is attached to position R<sub>5</sub> could be attributed to the synergy of electron withdrawing effects of the two neighboring carbonyl groups in the dye structures (Fig. 8.1), which increases the polarity of the substituent at R<sub>5</sub> through inductive effect (Fig. 8.6). Such effect is expected to be less pronounced at position R<sub>4</sub> from proximity view point which explains why substitution of NH<sub>2</sub> at R<sub>4</sub> produced lower solubility (Appendix: Table A.16).

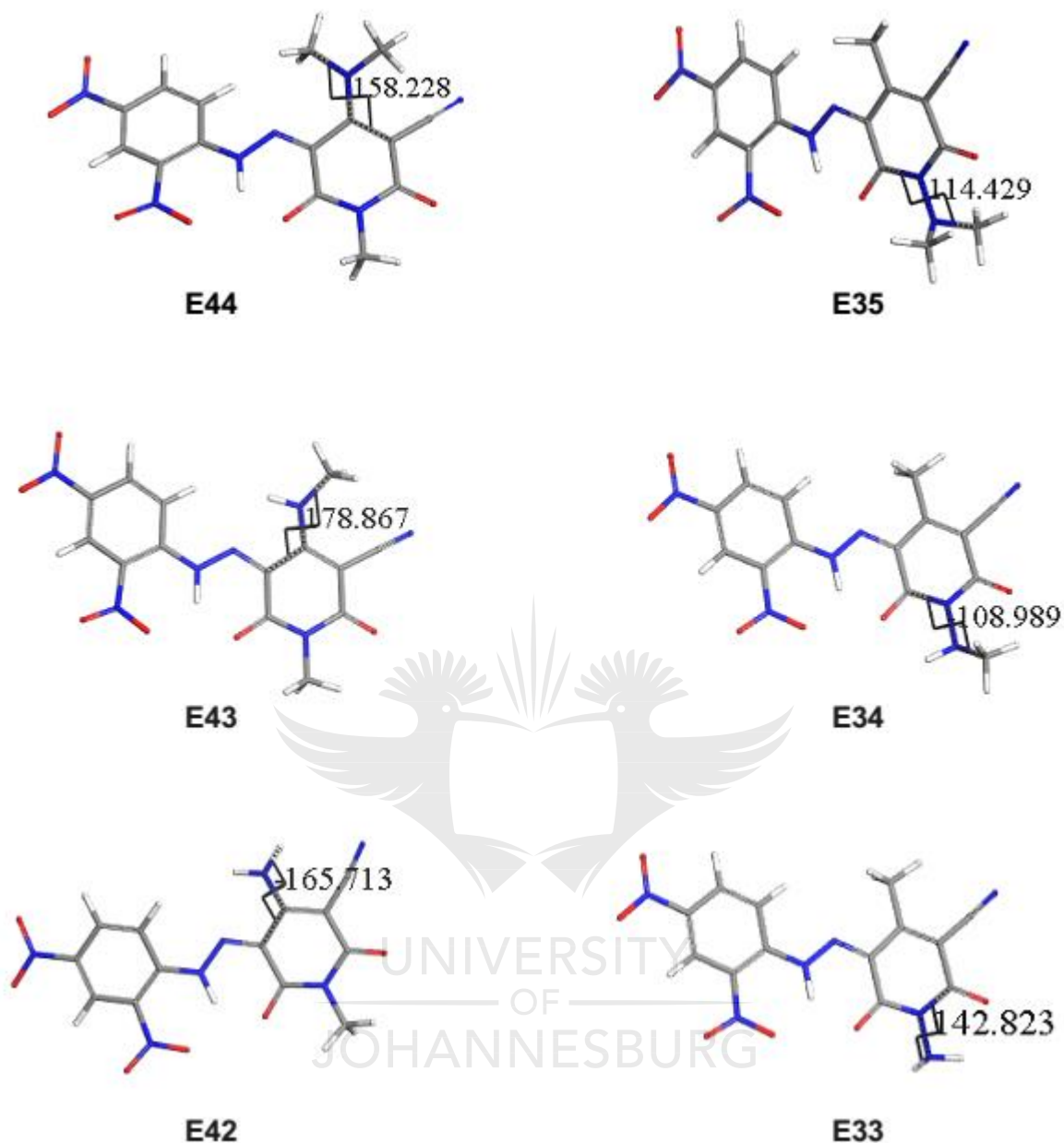


**Figure 8. 5:** Some optimized NH<sub>2</sub>, NHCH<sub>3</sub> and N(CH<sub>3</sub>)<sub>2</sub> substituted derivatives for which the substituents occupy positions R<sub>4</sub> (left) and R<sub>5</sub> (right) in the dye structures. The colors of the constituent atoms carbon, hydrogen, nitrogen and oxygen are grey, white, blue and red, respectively. Torsion angles between the planes of the ring and amine substituent group are shown. The closer the magnitude of the torsion angles to 0° or 180°, the more the orientation of the substituent along the molecular plane and the smaller the steric hindrance.

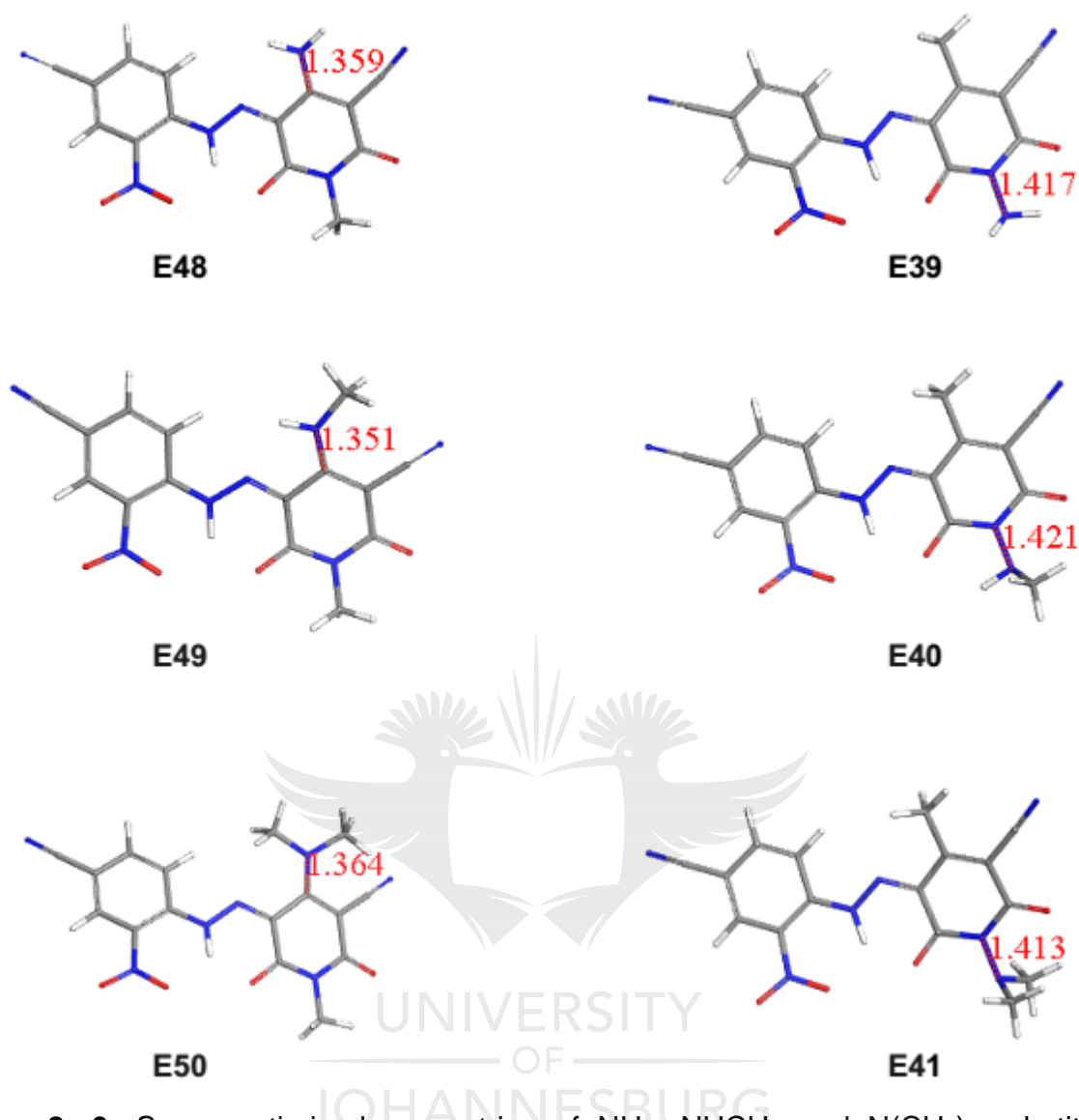


**Figure 8. 6:** Some optimized geometries of  $\text{NH}_2$ ,  $\text{NHCH}_3$  and  $\text{N}(\text{CH}_3)_2$  substituted derivatives showing the lengths of the bonds formed between the substituents and the donor unit at substitution positions  $\text{R}_4$  (left) and  $\text{R}_5$  (right) in the dye structures. The colors of the constituent atoms carbon, hydrogen, nitrogen and oxygen are grey, white, blue and red, respectively. The longer the bond, the higher the polarity.

The relatively small screening charge values obtained for the  $\text{NH}_2$  derivatives compared to those of the  $\text{NHCH}_3$  and  $\text{N}(\text{CH}_3)_2$  counterparts (Appendix: Table A.17) confirms that  $\text{NH}_2$  is the least electron donating. On the other hand, the relatively high screening charge values for the  $\text{NHCH}_3$  and  $\text{N}(\text{CH}_3)_2$  derivatives suggest that they are populated with more



electrons by the substituents due to their higher electron donating capacities compared to  $\text{NH}_2$ . The inflow of more electrons from these substituents into the donor part tend to increase the charge density difference between the accepting and the donating parts of the dyes (Fig. 8.1) thereby giving rise to strong dipoles. This explains the relatively large dipole moment and screening charge magnitude obtained for E31, E32, E37, E38, E43, E44, E49 and E50 (Appendix: Table A.17), where the substituents are attached to position  $\text{R}_4$  (Fig. 8.1).

Smaller dipole moment values were obtained for derivatives such as E34, E35, E40, E41, E46, E47, E52, and E53 in which the substituents are attached to position  $\text{R}_5$  (Fig. 8.1) because the electron donating influence of the substituents is counteracted by steric effects at this position and their proximity to the influence of the electron withdrawing carbonyl groups (Fig. 8.6). This leads to lower charge density difference between both parts of the dyes and consequently a smaller dipole moment along the N-N bridge. Similar positional effect is also responsible for the dipole moment difference observed between E55 and E57, E56 and E60, E64 and E66, and E65 and E69 (Appendix: Table A.17). The fact that E57, E60, E66, and E69 are more soluble than E55, E56, E64 and E65, respectively (Appendix: Table A.16), suggests that the electron donating influence is higher and the steric hindrance to solvation is minimal when the bulky  $\text{NHCH}_3$  and  $\text{N}(\text{CH}_3)_2$  substituents are attached to position  $\text{R}_4$  as confirmed by their respective SFE values in the same table.

The vapor pressure obtained for the derivatives are significantly lower than that of the parent dye (Appendix: Table A.16), which suggests that the derivatives will have greater resistance to heat (i.e. higher sublimation fastness). Also, most of the  $-\text{NO}_2$  substituted

derivatives show higher heat resistance tendency compared to their -CN substituted counterparts particularly when the substituents are *para* to the azo linkage.

The calculated Gibb's free energies suggest that the derivatives possess appreciable thermodynamic stability, with some of them being more stable than the parent dye (Appendix: Table A.16). However, the stability appears to be more enhanced by NO<sub>2</sub> with NHCH<sub>3</sub> and N(CH<sub>3</sub>)<sub>2</sub> substituents due to their relatively higher electron withdrawing and electron donating strengths respectively, which tends to balance the charge densities on both sides of the dye molecule.

### 8.3.2 GLOBAL REACTIVITY STUDY

The detailed results of the reactivity study are presented in Table A.18 (Appendix). Figures 8.7 and 8.8 compares the HOMO and LUMO energies of the derivatives with those of the parent dye which is indicated as DY in the figures. Group C comprises all the compounds in group A and the remaining derivatives with R<sub>1</sub> = EWS (Appendix: Table A.18). Similarly, group D consists of the group B compounds plus the remaining ones with R<sub>3</sub> = EWS. Not all the derivatives have solubility values greater than that of DY119 and since the solubility values of the CN substituted derivatives are generally higher than those the NO<sub>2</sub> counterparts, only the CN substituted derivatives with aqueous solubility greater than that of DY119 and their corresponding NO<sub>2</sub> counterparts were shown in Figure 8.2.

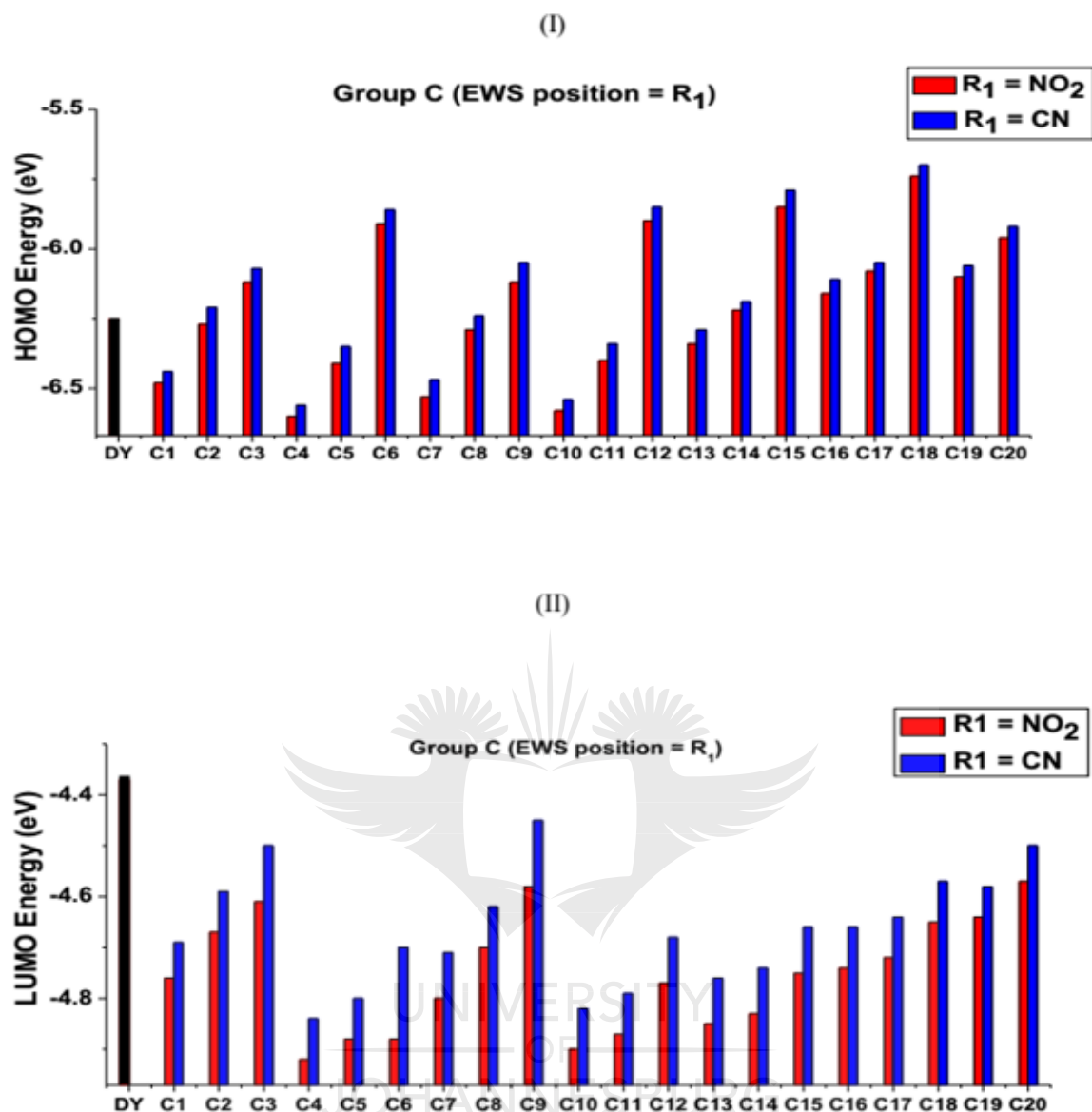


**Figure 8. 7:** HOMO (I) and LUMO (II) energies of Group C derivatives\*\*.

\*\*C1: R<sub>4</sub> = NH<sub>2</sub> and R<sub>5</sub> = C<sub>2</sub>H<sub>5</sub>, C2: R<sub>4</sub> = NHCH<sub>3</sub> and R<sub>5</sub> = C<sub>2</sub>H<sub>5</sub>, C3: R<sub>4</sub> = N(CH<sub>3</sub>)<sub>2</sub> and R<sub>5</sub> = C<sub>2</sub>H<sub>5</sub>, C4: R<sub>4</sub> = CH<sub>3</sub> and R<sub>5</sub> = NH<sub>2</sub>, C5: R<sub>4</sub> = CH<sub>3</sub> and R<sub>5</sub> = NHCH<sub>3</sub>, C6: R<sub>4</sub> = CH<sub>3</sub> and R<sub>5</sub> = N(CH<sub>3</sub>)<sub>2</sub>, C7: R<sub>4</sub> = NH<sub>2</sub> and R<sub>5</sub> = CH<sub>3</sub>, C8: R<sub>4</sub> = NHCH<sub>3</sub> and R<sub>5</sub> = CH<sub>3</sub>, C9: R<sub>4</sub> = N(CH<sub>3</sub>)<sub>2</sub> and R<sub>5</sub> = CH<sub>3</sub>, C10: R<sub>4</sub> = C<sub>2</sub>H<sub>5</sub> and R<sub>5</sub> = NH<sub>2</sub>, C11: R<sub>4</sub> = C<sub>2</sub>H<sub>5</sub> and R<sub>5</sub> = NHCH<sub>3</sub>, C12: R<sub>4</sub> = C<sub>2</sub>H<sub>5</sub> and R<sub>5</sub> = N(CH<sub>3</sub>)<sub>2</sub>, C13: R<sub>4</sub> = R<sub>5</sub> = NH<sub>2</sub>, C14: R<sub>4</sub> = NH<sub>2</sub> and R<sub>5</sub> = NHCH<sub>3</sub>, C15: R<sub>4</sub> = NH<sub>2</sub> and R<sub>5</sub> = N(CH<sub>3</sub>)<sub>2</sub>, C16: R<sub>4</sub> = NHCH<sub>3</sub> and R<sub>5</sub> = NH<sub>2</sub>, C17: R<sub>4</sub> = R<sub>5</sub> = NHCH<sub>3</sub>, C18: R<sub>4</sub> = NHCH<sub>3</sub> and R<sub>5</sub> = N(CH<sub>3</sub>)<sub>2</sub>, C19: R<sub>4</sub> = N(CH<sub>3</sub>)<sub>2</sub> and R<sub>5</sub> = NH<sub>2</sub>, and C20: R<sub>4</sub> = N(CH<sub>3</sub>)<sub>2</sub> and R<sub>5</sub> = NHCH<sub>3</sub>.

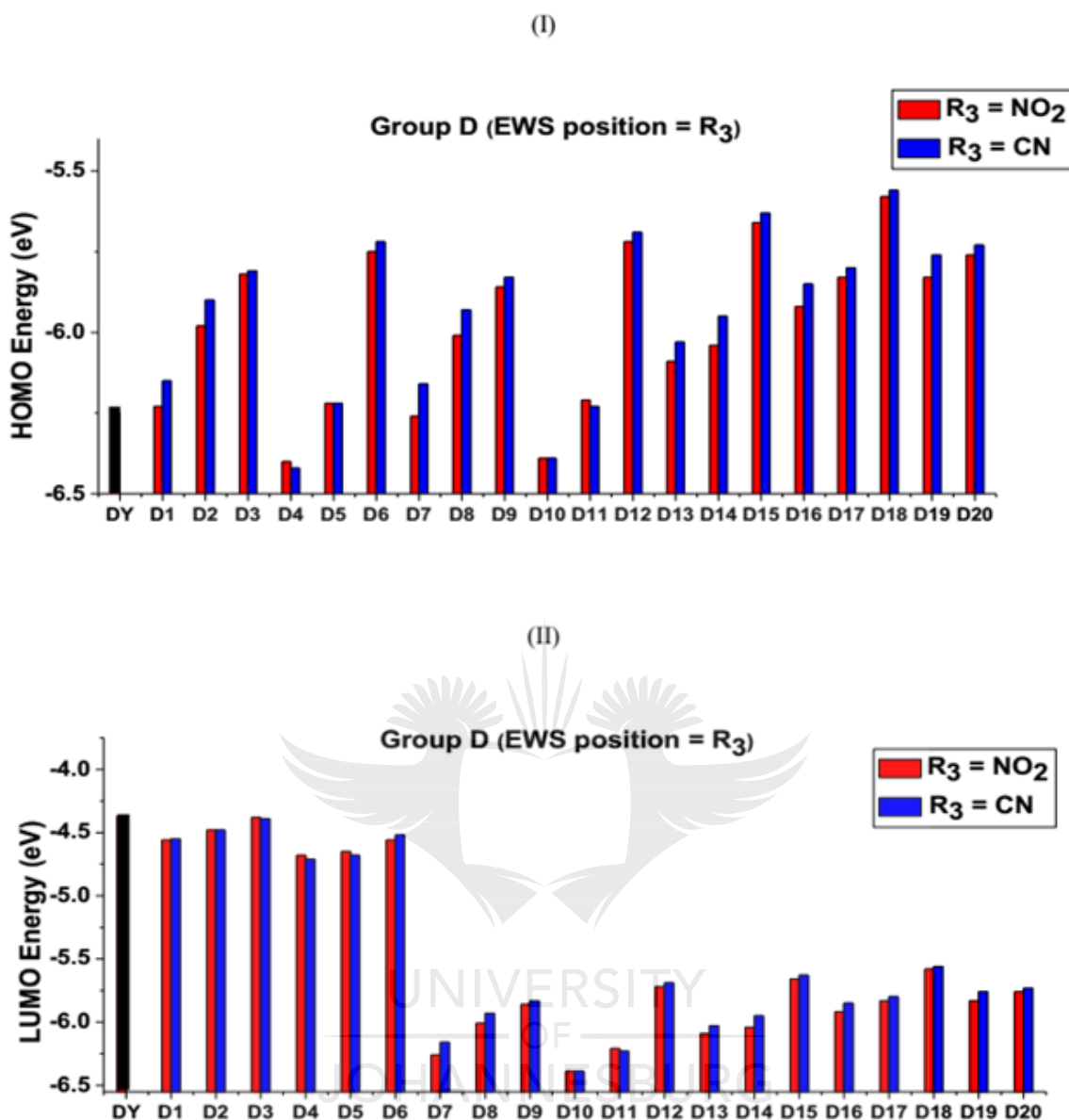


**Figure 8. 8:** HOMO (I) and LUMO (II) energies of Group D derivatives\*\*\*.

\*\*\*D1: R<sub>4</sub> = NH<sub>2</sub> and R<sub>5</sub> = C<sub>2</sub>H<sub>5</sub>, D2: R<sub>4</sub> = NHCH<sub>3</sub> and R<sub>5</sub> = C<sub>2</sub>H<sub>5</sub>, D3: R<sub>4</sub> = N(CH<sub>3</sub>)<sub>2</sub> and R<sub>5</sub> = C<sub>2</sub>H<sub>5</sub>, D4: R<sub>4</sub> = CH<sub>3</sub> and R<sub>5</sub> = NH<sub>2</sub>, D5: R<sub>4</sub> = CH<sub>3</sub> and R<sub>5</sub> = NHCH<sub>3</sub>, D6: R<sub>4</sub> = CH<sub>3</sub> and R<sub>5</sub> = N(CH<sub>3</sub>)<sub>2</sub>, D7: R<sub>4</sub> = NH<sub>2</sub> and R<sub>5</sub> = CH<sub>3</sub>, D8: R<sub>4</sub> = NHCH<sub>3</sub> and R<sub>5</sub> = CH<sub>3</sub>, D9: R<sub>4</sub> = N(CH<sub>3</sub>)<sub>2</sub> and R<sub>5</sub> = CH<sub>3</sub>, D10: R<sub>4</sub> = C<sub>2</sub>H<sub>5</sub> and R<sub>5</sub> = NH<sub>2</sub>, D11: R<sub>4</sub> = C<sub>2</sub>H<sub>5</sub> and R<sub>5</sub> = NHCH<sub>3</sub>, D12: R<sub>4</sub> = C<sub>2</sub>H<sub>5</sub> and R<sub>5</sub> = N(CH<sub>3</sub>)<sub>2</sub>, D13: R<sub>4</sub> = R<sub>5</sub> = NH<sub>2</sub>, D14: R<sub>4</sub> = NH<sub>2</sub> and R<sub>5</sub> = NHCH<sub>3</sub>, D15: R<sub>4</sub> = NH<sub>2</sub> and R<sub>5</sub> = N(CH<sub>3</sub>)<sub>2</sub>, D16: R<sub>4</sub> = NHCH<sub>3</sub> and R<sub>5</sub> = NH<sub>2</sub>, D17: R<sub>4</sub> = R<sub>5</sub> = NHCH<sub>3</sub>, D18: R<sub>4</sub> = NHCH<sub>3</sub> and R<sub>5</sub> = N(CH<sub>3</sub>)<sub>2</sub>, D19: R<sub>4</sub> = N(CH<sub>3</sub>)<sub>2</sub> and R<sub>5</sub> = NH<sub>2</sub>, and D20: R<sub>4</sub> = N(CH<sub>3</sub>)<sub>2</sub> and R<sub>5</sub> = NHCH<sub>3</sub>.

According to the figures, the LUMO energies of the derivatives are generally lower than that of the parent dye, suggesting that the derivatives are better electron acceptors and

hence, more susceptible to reductive degradation. This general decrease in LUMO energies (Fig. 8.7(II) and 8.8(II)) and the decrease in HOMO energies observed for derivatives such as C1, C4, C5, C7, C10, C11, C13, D4 and D10 (Fig. 8.7(I) and 8.8(I)) suggest the prevailing effect of CN or NO<sub>2</sub> over that of the electron donors. The higher HOMO energies observed for the other derivatives in Figures 8.7(I) and 8.8(I) indicate that the effects of the electron donors become more appreciable especially when the EWS are switched to position R<sub>3</sub>. Also, as electron donating power increased from NH<sub>2</sub> to N(CH<sub>3</sub>)<sub>2</sub>, the effects of CN and NO<sub>2</sub> on the HOMO energy was sufficiently counteracted, hence, the relatively higher HOMO energies obtained for derivatives such as C3, C6, C9, C12, C14-C20 and their corresponding group D derivatives, which implies that these derivatives are more prone to oxidative degradation compared to DY119.

The differences observed between the HOMO and LUMO energies of the NO<sub>2</sub> and CN substituted derivatives reflect the variation in the electron withdrawing capacities of the substituents. NO<sub>2</sub> is more electron withdrawing hence, decreased the energies more than CN. Among the EDS, NH<sub>2</sub> offers the least counteraction to electron withdrawing effect, hence, the relatively lower energies obtained for its derivatives compared to those of NHCH<sub>3</sub> and N(CH<sub>3</sub>)<sub>2</sub> substituted counterparts (Fig. 8.7 and 8.8).

Comparison of Figures 8.7 and 8.8 revealed that substitution of the EWS at R<sub>1</sub> yielded lower HOMO and LUMO energies, which confirms that the electron withdrawing powers of NO<sub>2</sub> and CN are higher when they are *para* to the N-N bridge (Fig. 8.1).

The HOMO and the LUMO energies of both DY119 and the derivatives are generally higher in water (Appendix: Table A.18a) indicating that the influence of the EDS was more facilitated against that of the EWS by water molecules. This suggests that the dyes will be more susceptible to oxidation in an aqueous environment.

The HOMO – LUMO energy gap, hardness (Appendix: Table A.18a) and softness (Appendix: Table A.18b) suggest that the derivatives are less stable compared to the parent, which implies that they will be more vulnerable to photo-excitation and hence photodegradation. However, this vulnerability seems to be lower in water for almost all the derivatives as indicated by the relatively higher energy gap values obtained in water. The results of electronegativity and chemical potential (Appendix: Table A.18b) showed that most of the derivatives are more electronegative and less electropositive than the parent dye. The trends observed in these properties reflect the net influence of the electron withdrawing and electron donating substituents combined, where the former seems to predominate in most of the derivatives. Also, substitution of the EWS at position R<sub>3</sub> yielded lower electronegativity values compared to their substitution at R<sub>1</sub> due to the reduction in their electron withdrawing powers when attached to position R<sub>3</sub>. The results of electrophilicity calculation shown in Table A.18b (Appendix) revealed that the derivatives are generally more electrophilic than the parent dye, which suggests their higher susceptibility to nucleophilic attack.

### 8.3.3 LOCAL REACTIVITY STUDY

Assessment of Table A.19 (Appendix) showed that the most disposed site towards a radical attack in DY119 is the carbon atom C<sub>9</sub> (Fig. 8.9), whereas the nitrogen atom N<sub>8</sub> is the most probable site for such attack on the derivatives with few exceptions. This suggests that the attack of a photo-generated hydroxyl radical which leads to degradation will occur with the lowest activation energy at C<sub>9</sub> on the parent dye and N<sub>8</sub> on the derivatives to favor the cleavage of C<sub>9</sub> – N<sub>8</sub> and N<sub>8</sub> – N<sub>7</sub> bonds, respectively. These are known as C – N and N – N bond cleavage degradation mechanisms [45-48].

The variation observed in the values of  $f^o$  for the derivatives is the net effect of combining the electron withdrawing and the electron donating substituents where the latter have the dominant influence. C<sub>9</sub> belongs to the donating part of the studied dyes. This site is less shielded in the parent dye from the electron withdrawing influence of NO<sub>2</sub> and CN due to the relatively low electron donating power of CH<sub>3</sub> and C<sub>2</sub>H<sub>5</sub> compared to NH<sub>2</sub>, NHCH<sub>3</sub> and N(CH<sub>3</sub>)<sub>2</sub> groups. Hence, it is the most electron deficient center in the parent dye as indicated by the  $f^o$  value (Appendix: Table A.19). The influence of the electron withdrawing substituents on C<sub>9</sub> was significantly counteracted by the highly electron donating NH<sub>2</sub>, NHCH<sub>3</sub> and N(CH<sub>3</sub>)<sub>2</sub> substituents. This explains why C<sub>9</sub> is less vulnerable to radical attack compared to N<sub>8</sub> in almost all the derivatives.

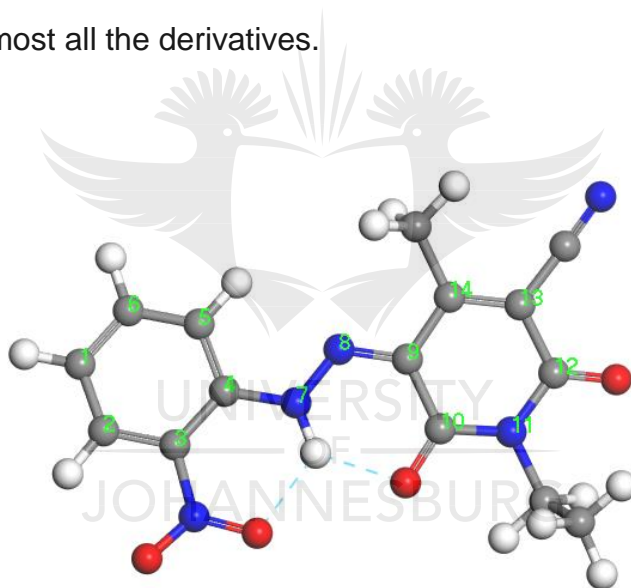


**Figure 8. 9:** An optimized geometry of DY119 showing the probable sites C<sub>4</sub>, N<sub>7</sub>, N<sub>8</sub> and C<sub>9</sub> for radical attack. The constituent atoms are carbon (grey), hydrogen (white), nitrogen (blue) and oxygen (red).

Although the electron withdrawing substituents are less active when they are *ortho* to the N-N group, their proximity to a reactive site can dictate the propensity of the site to radical attack. This is suspected to be the case for E74, E86, E99 – E101, E103, E104 and E108 (Appendix: Table A.19) where the EWS are *ortho* (i.e. position R<sub>3</sub>) to the N-N bridge.

### 8.3.4 CATALYTIC SELECTIVITY

The calculated band structures for Si, CdSe, CdS, TiO<sub>2</sub> (rutile), ZnO and ZnS photocatalysts are provided in Table A.15 (Appendix). Table A.20 (Appendix) gives account of the energy gap between the HOMO of the studied dyes and the conduction band edge (CBE) of the catalysts and that between the LUMO and the valence band edges (VBE) of the catalysts. Si, CdSe and CdS are visible light activated catalysts because their band gap values are less than 3.0 eV [49] whereas TiO<sub>2</sub> (rutile), ZnO and ZnS represent the UV activated catalysts since their band gap values are 3.0 eV and above [34,49].

The chance of a favorable interaction between the dyes and the catalysts depends on the size of  $\alpha$  and  $\beta$  (Appendices: Table A.20). The smaller the  $\alpha$ , the greater the chance of electron donation into the LUMO of the dyes. Similarly, the smaller the  $\beta$  value, the more the likelihood of electron donation into the CBE of the catalysts. For a given dye-catalyst pair, the molecular orbital/band edge combination (i.e. LUMO/VBE or HOMO/CBE) with the smaller energy gap is the most preferred combination for interaction.

Among the visible light activated representatives, the  $\alpha_{\text{Si}}$  and  $\beta_{\text{Si}}$  and the  $\alpha_{\text{CdSe}}$  values for Si and CdSe respectively, suggest that they are better candidates for photodegradation compared to CdS. However, the interaction of the dyes with these catalysts will preferably involve their LUMOs and the VBE of the catalysts. In addition, Si has the highest chance of HOMO-CBE type of overlap as revealed by the  $\beta$  values. By comparing similar molecular orbital-band edge pair for all the studied catalysts, TiO<sub>2</sub> and ZnO do not only appear as the more appropriate UV-activated, but also the overall best catalysts for degrading the dyes. However, the former will most preferably interact with the dye HOMOs whereas the latter will most likely interact with their LUMOs as revealed by their



$\beta$  and  $\alpha$  values, respectively. Such high photocatalytic abilities of ZnO and TiO<sub>2</sub> is in agreement with that reported in literature [34,35].

#### 8.4 CONCLUSION

DMol<sup>3</sup> computational code had been used to predict aqueous solubility, chemical reactivity, photodegradation mechanism and catalytic selectivity of 84 derivatives of DY119 dye by varying the electron donating and electron withdrawing substituents and their positions on the dye molecule. The following points summarize the key findings of the study:

1. All 84 new derivatives studied were found to be more reactive than the parent dye, but 28 of these derivatives showed lower aqueous solubility.
2. A -CN substituted DY119 dye promises to be a more soluble dye in aqueous system than a corresponding -NO<sub>2</sub> substituted counterpart.
3. In conjunction with -CN and/or -NO<sub>2</sub>, -NH<sub>2</sub> substituent improved aqueous solubility better than -NHCH<sub>3</sub> and -N(CH<sub>3</sub>)<sub>2</sub> groups.
4. The effect of substituents on reactivity of the dyes could be of electronic and/or steric origins, but the electronic factor appeared to prevail over the steric effect.
5. DY119 was predicted to be amenable to degradation via a C-N bond cleavage, while the degradation of the derivatives appeared to be more feasible via an N-N bond cleavage.
6. Both TiO<sub>2</sub> and ZnO are the most suitable catalysts for degradation of the dyes, though both catalysts might have different modes of interaction with the dyes.

## 8.5 REFERENCES

1. J. Koh. Dyeing with disperse dyes; P. Hauser (Ed.), *INTECH Open Access Publisher*, Croatia, (2011), pp. 195-221. DOI: 10.5772/20458. Available at: <https://www.intechopen.com/books/textile-dyeing/dyeing-with-disperse-dyes>.
2. D. Patel, N. Prajapati, M. Thakor and V. Patel. Formation of some novel disperse azo dyes: synthesis, characterisation and printing properties. *Journal of Current Chemical and Pharmaceutical Sciences* **2** (2012) 86-91.
3. K. J. Sakoma, K. A. Bello and M. K. Yakubu. Synthesis of some azo disperse dyes from 1-substituted 2-hydroxy-6-pyridone derivatives and their colour assessment on polyester fabric. *Open Journal of Applied Sciences* **2** (2012) 54-59.
4. Y. S. Choi, K. S. Lee, H. J. Kim, J. Y. Choi, S. B. Kang, E. J. Lee and G. Keum. Synthesis, spectral property and dyeing assessment of azo disperse dyes containing carbonyl and dicyanovinyl groups. *Bulletin of the Korean Chemical Society* **34** (2013) 863-867.
5. T. Peme, L. O. Olasunkanmi, I. Bahadur, A. S. Adekunle, M. M. Kabanda and E. E. Ebenso. Adsorption and corrosion inhibition studies of some selected dyes as corrosion inhibitors for mild steel in acidic medium: gravimetric, electrochemical, quantum chemical studies and synergistic effect with iodide ions. *Molecules* **20** (2015) 16004-16029.
6. S. S. Al-Juaid. Mono azo dyes compounds as corrosion inhibitors for dissolution of aluminium in sodium hydroxide solutions. *Portugaliae Electrochimica Acta* **25** (2007) 363-373.

7. A. Fouda, H. Ali, R. Awad and A. Ahmed. New benzonitrile azo dyes as corrosion inhibitors for carbon steel in hydrochloric acid solutions. *International Journal of Electrochemical Science* **9** (2014) 1117-1131.
8. P. S. Desai and R. Vashi. Disperse dyes as corrosion inhibitors for aluminum alloy in trichloroacetic acid system. *Asian Journal of Chemistry* **20** (2008) 3387-3394.
9. A. Abdul Nabi and A. Hussain. Synthesis, identification and study of some new azo dyes as corrosion inhibitors for carbon-steel in acidic media. *Journal of Basrah Researches (Sciences)* **38** (2012) 125-146.
10. M. Abdallah, A. Fouda, S. Shama and E. Afifi. Azodyes as corrosion inhibitors for dissolution of c-steel in hydrochloric acid solution. *African Journal of Pure and Applied Chemistry* **2** (2008) 83-91.
11. K. Georgiadou and E. Tsatsaroni. Synthesis, characterisation and application of disperse dyes derived from N-2-hydroxyethyl-1-naphthylamine. *Dyes and Pigments* **50** (2001) 93-97.
12. M. R. R. Kooh, V. N. Yoong and P. Ekanayake. Density functional theory (DFT) and time-dependent density functional theory (TDDFT) studies of selected ancient colourants as sensitizers in dye-sensitized solar cells. *Journal of the National Science Foundation of Sri Lanka* **42** (2014) 169-175.
13. V. Chigrinov, H. S. Kwok, H. Takada and H. Takatsu. Photo-aligning by azo-dyes: physics and applications. *Liquid Crystals Today* **14** (2005) 1-15.
14. H. A. Badran, A. Y. Taha, A. F. Abdulkader and C. A. Emshary. Preparation and study of the electrical and optical properties of a new azo dye (4-acetaminophenol–[2-(4-azo)]-4-amino dipheyl sulfone). *Journal of Ovonic Research* **8** (2012) 161-170.

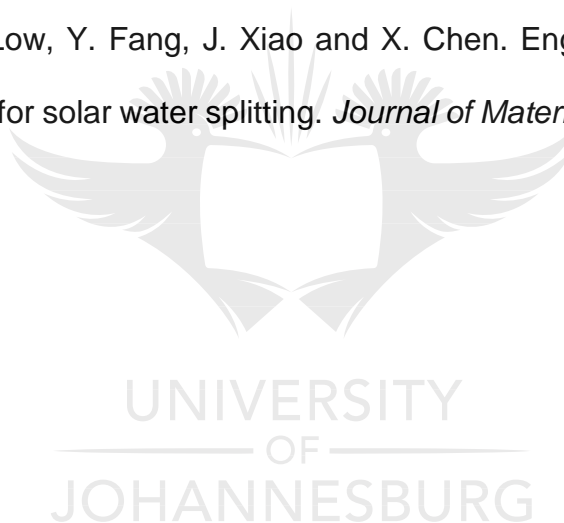
15. A. H. Wolff and F. W. Oehme. Carcinogenic chemicals in food as an environmental health issue. *Journal of the American Veterinary Medical Association* **164** (1974) 623-629.
16. G. Mooter, B. Maris, C. Samyn, P. Augustijns and R. Kinget. Use of azo polymers for colon-specific drug delivery. *Journal of Pharmaceutical Sciences* **86** (1997) 1321-1327.
17. W. Saus, D. Knittel and E. Schollmeyer. Dyeing of textiles in supercritical carbon dioxide. *Textile Research Journal* **63** (1993) 135-142.
18. W. Saus, D. Knittel and E. Schollmeyer. Dyeing with supercritical carbon dioxide—an alternative to high-temperature dyeing of polyester. *Textile Praxis International* **47** (1992) 1052-1054.
19. M. Banchemo. Supercritical fluid dyeing of synthetic and natural textiles—a review. *Coloration Technology* **129** (2013) 2-17.
20. A. S. Özcan, A. A. Clifford, K. D. Bartle and D. M. Lewis. Solubility of disperse dyes in supercritical carbon dioxide. *Journal of Chemical & Engineering Data* **42** (1997) 590-592.
21. M. Clark. Handbook of textile and industrial dyeing: principles, processes and types of dyes. *Woodhead Publishing Limited, United Kingdom*, (2011).
22. H. Øllgaard, L. Frost, J. Galster and O. C. Hansen. Survey of azo-colorants in Denmark. *Consumption, use, health and environmental aspects* (1998). Available at: <https://www2.mst.dk/udgiv/publications/1999/87-7909-548-8/pdf/87-7909-546-1.pdf>. Accessed on 14 March 2018.

23. Y. Anjaneyulu, N. S. Chary and D. S. S. Raj. Decolourization of industrial effluents—available methods and emerging technologies—a review. *Reviews in Environmental Science and Biotechnology* **4** (2005) 245-273.
24. N. A. Ghalwa, H. M. Abu-Shawish, H. M. Tamous and H. Al Harazeen. Determination of electrochemical degradation of E102 dye at lead dioxide-doped carbon electrodes using some potentiometric and spectrophotometric methods. *Chemistry Journal* **3** (2013) 1-6.
25. S. K. Al-Dawery. Photo-Catalyst degradation of tartrazine compound in wastewater using TiO<sub>2</sub> and UV light. *Journal of Engineering Science and Technology* **8** (2013) 683-691.
26. S. Banerjee and M. Chattopadhyaya. Adsorption characteristics for the removal of a toxic dye, tartrazine from aqueous solutions by a low cost agricultural by-product. *Arabian Journal of Chemistry* (2013) 1-10.
27. A. Cavicchioli and I. G. Gutz. Effect of scavengers on the photocatalytic digestion of organic matter in water samples assisted by TiO<sub>2</sub> in suspension for the voltammetric determination of heavy metals. *Journal of the Brazilian Chemical Society* **13** (2002) 441-448.
28. V. K. Gupta, R. Jain, A. Nayak, S. Agarwal and M. Shrivastava. Removal of the hazardous dye-tartrazine by photodegradation on titanium dioxide surface. *Materials Science and Engineering: C* **31** (2011) 1062-1067.
29. J. M. Joseph, H. Destailats, H.M. Hung and M. R. Hoffmann. The sonochemical degradation of azobenzene and related azo dyes: rate enhancements via Fenton's reactions. *The Journal of Physical Chemistry A* **104** (2000) 301-307.

30. N. Modirshahla, M. Behnajady and S. Kooshaiian. Investigation of the effect of different electrode connections on the removal efficiency of tartrazine from aqueous solutions by electrocoagulation. *Dyes and Pigments* **74** (2007) 249-257.
31. S. Adhikari and D. Sarkar. Metal oxide semiconductors for dye degradation. *Materials Research Bulletin* **72** (2015) 220-228.
32. M. Kulkarni and P. Thakur. Photocatalytic degradation and mineralization of reactive textile azo dye using semiconductor metal oxide nano particles. *International Journal of Engineering Research and General Science* **2** (2014) 245-254.
33. L. Mahlalela and L. Dlamini. Enhanced photocatalytic activity of titania in the presence of  $\text{KNO}_3$  on the photodegradation of dyes. *Surfaces and Interfaces* **1** (2016) 21-28.
34. K. Mondal and A. Sharma. Photocatalytic oxidation of pollutant dyes in wastewater by  $\text{TiO}_2$  and  $\text{ZnO}$  nano-materials-a mini-review. *Nanoscience & Technology for Mankind, The Academy of Sciences India (NASI), Allahabad, India* (2014) 36-72.
35. I. T. Peternel, N. Koprivanac, A. M. L. Božić and H. M. Kušić. Comparative study of UV/ $\text{TiO}_2$ , UV/ $\text{ZnO}$  and photo-fenton processes for the organic reactive dye degradation in aqueous solution. *Journal of Hazardous Materials* **148** (2007) 477-484.
36. DMol<sup>3</sup> Guide, Material Studio 8.0. *Accelrys Software Inc.*, San Diego, United States (2017) 1-161.
37. Y. Inada and H. Orita. Efficiency of numerical basis sets for predicting the binding energies of hydrogen bonded complexes: evidence of small basis set

- superposition error compared to Gaussian basis sets. *Journal of Computational Chemistry* **29** (2008) 225-232.
38. E. Mullins, R. Oldland, Y. Liu, S. Wang, S. I. Sandler, C.C. Chen, M. Zwolak and K. C. Seavey. Sigma-profile database for using COSMO-based thermodynamic methods. *Industrial and Engineering Chemistry Research* **45** (2006) 4389-4415.
39. A. Klamt, V. Jonas, T. Bürger and J. C. Lohrenz. Refinement and parametrization of COSMO-RS. *The Journal of Physical Chemistry A* **102** (1998) 5074-5085.
40. COSMO-RS Manual, Release 2017. *Software for Chemistry and Materials* (2018). [http://www.scm.com/doc/COSMO-RS/\\_downloads/COSMO-RS.pdf](http://www.scm.com/doc/COSMO-RS/_downloads/COSMO-RS.pdf). Last accessed on 1 May, 2018.
41. J. D. Thompson, C. J. Cramer and D. G. Truhlar. Predicting aqueous solubilities from aqueous free energies of solvation and experimental or calculated vapor pressures of pure substances. *The Journal of Chemical Physics* **119** (2003) 1661-1670.
42. R. G. Pearson. Chemical hardness. *Wiley Online Library*, United States (1997).
43. P. K. Chattaraj. Chemical reactivity theory: a density functional view. *CRC Press*, United States, (2009).
44. P. W. Ayers and R. G. Parr. Variational principles for describing chemical reactions: the Fukui function and chemical hardness revisited. *Journal of the American Chemical Society* **122** (2000) 2010-2018.
45. A. S. Özen, V. Aviyente and R. A. Klein. Modeling the oxidative degradation of azo dyes: A density functional theory study. *The Journal of Physical Chemistry A* **107** (2003) 4898-4907.

46. A. S. Özen, V. Aviyente, F. De Proft and P. Geerlings. Modeling the substituent effect on the oxidative degradation of azo dyes. *The Journal of Physical Chemistry A* **108** (2004) 5990-6000.
47. X. Jiao, H. Yu, Q. Kong, Y. Luo, Q. Chen and J. Qu. Theoretical mechanistic studies on the degradation of alizarin yellow R initiated by hydroxyl radical. *Journal of Physical Organic Chemistry* **27** (2014) 519-526.
48. A. S. Özen, V. Aviyente, G. Tezcanli-Güyer and N. H. Ince. Experimental and modeling approach to decolorization of azo dyes by ultrasound: degradation of the hydrazone tautomer. *The Journal of Physical Chemistry A* **109** (2005) 3506-3516.
49. X. Li, J. Yu, J. Low, Y. Fang, J. Xiao and X. Chen. Engineering heterogeneous semiconductors for solar water splitting. *Journal of Materials Chemistry A* **3** (2015) 2485-2534.





---

## CHAPTER 9

# THEORETICAL MODELLING OF SUBSTITUENT EFFECTS ON AQUEOUS SOLUBILITY, CHEMICAL REACTIVITY AND ABSORPTION WAVELENGTH OF DISPERSE RED 73

---

### PREAMBLE

Effects of some polar electron withdrawing ( $X^-$ ) and electron donating ( $X^+$ ) substituents on aqueous solubility, thermodynamic stability and chemical reactivity of (E)-2-((4-((2-cyanoethyl)(ethyl)amino)phenyl)diazanyl)-5-nitrobenzonitrile popularly known as disperse red 73 (DR73) dye were theoretically investigated using the VWN-BP functional together with DNP basis set. This study is in view of introducing new aminoazobenzene disperse dyes with improved aqueous solubility, dyeing performance and photodegradation tendency.

### 9.1 INTRODUCTION

Disperse dyes are sparingly soluble nonionic dyes that are mainly used for coloring hydrophobic materials such as polyesters, nylons, acrylics and cellulose acetates. Due to their low aqueous solubility, they do not form a homogenous dye solution with ordinary water. Therefore, dispersing/solubilizing and carrier agents are usually added to obtain a finely and evenly dispersed homogenous medium for easier penetration of dye molecules into the substrates at a temperature above the glass transition temperature ( $T_g$ ) of the substrates [1-5]. Unfortunately, addition of dispersing/solubilizing agents does not only

---

The work presented in this has been published.

\*O.O. Wahab, L.O. Olasunkanmi, K.K. Govender and P.P. Govender. *Molecular Physics* (2019) 1-22.  
<https://doi.org/10.1080/00268976.2019.1626508>.

increase production costs, but can also interfere with safety [1, 3-5] because, most of the carrier agents contain toxic substances such as o-phenylphenol, phthalates, biphenyls and chlorinated aromatic compounds [2, 6]. In addition, most carriers are non-biodegradable, and are also capable of plasticizing fibers, which consequently lowers the  $T_g$  of the fibers [5, 6].

Non-carrier dyeing methods which make use of organic solvent, supercritical fluid and conventional machinery such as high temperature and high pressure (HTHP) machine at a temperature between 120 °C-130 °C have been introduced [1, 2, 7-11]. However, each of these alternatives has peculiar limitations compared to the use of water which is the almost exclusive vehicle for dyeing. For instance, solvent dyeing method using organic solvents has not received an extensive commercial application [7] probably due to hazard, toxicity, volatility and flammability concerns, as well as possession of certain repugnant odors which are undesirable to consumers.

Supercritical dyeing involves the use of supercritical carbon dioxide ( $CO_2$ ) which is not freely existing like water, but obtained from gaseous  $CO_2$  at a critical temperature and pressure of 304 K and 73.7 bar, respectively [8-11]. However, this technique is relatively more expensive and is ineffective for polar fibers such as cotton and other cellulosic materials, and does not yield appreciable solubility for polar dyes as reported by Burkinshaw [7]. High temperature and high pressure dyeing has been an effective method of coloration without the use of carriers. However, beside relatively high cost of machinery, a large amount of heat is required in this method for keeping the dye bath at the operation temperature [5]. Hence, this method is not advisable for dyes with low heat resistance capacity due to the risk thermal decomposition. In addition, HTHP machines

are usually less efficient during winter as a result of condensation of the generated steam and the consequent drop in the operational pressure [2], which mars successful dyeing. Water is the most abundant, most accessible, naturally occurring, non-hazardous, non-flammable and non-toxic universal solvent that can readily be used for dissolution of dyes. Therefore, the need for disperse dyes with improved aqueous solubility cannot be overemphasized because it can help to promote a more economic and more eco-friendly dispersant-free dyeing, and also help to widen the range of application of the dyes. Recognition of this need has spiked considerable research efforts on development of more water-soluble and dispersant-free disperse dyes [3, 12-18], while other studies have focused on the use of various chemical additives such as alcohols and surfactants as solubilizing agents [19-23].

Development of more water-soluble and dispersant-free disperse dyes have been achieved through incorporation of various solubilizing groups into disperse dye structures to enhance their aqueous solubility [3, 12-18]. Bianchini and co-workers [3, 12] reported that incorporation of some sugar moieties into the structures of azo disperse dyes led to a significant increase in their aqueous solubility. Lee *et al.* [15] observed that modification of some azo disperse dyes with  $\beta$ -sulfatoethylsulfonyl group enhanced the solubility of the dyes, similar to what was observed by Meena *et al.* [4] in their study on dispersant-free disperse dyes, in which sulfomethylated aniline and sulfomethylated m-toluidine were used as coupling components. Furthermore, a series of dispersant-free azo disperse dyes have been developed from 1-substituted-2-hydroxypyrid-6-one and indole derivatives by Lee and co-workers [17, 18].

Systematic modification of a disperse dye structure with polar groups will not only promote the aqueous solubility of the dye but can also help to enhance its ability to form stronger

dipolar, hydrogen bonding and van der Waal interactions with substrates [2]. It is also well known that incorporation of polar electron donating and electron withdrawing groups into a disperse dye structure can positively impact interesting properties such as color, dyeability, reactivity, planarity, optical response, binding affinity, hyperpolarizability, light fastness, wash fastness, and sublimation fastness. The effects of various substituent groups on these essential properties have been immensely investigated by different authors [24-35].

Like most other organic dyes, disperse dyes are potential environmental contaminants. The azo class show high resistance to degradation due to the stiffness of the azo ( $-N=N$ ) unit, and are potential sources of health issues such as bladder cancer, contact dermatitis, allergy and eczema in humans [2, 36]. In addition, their degradation in the environment can also give rise to toxic amine compounds with great carcinogenic and mutagenic potentials [37]. Therefore, effluents from dye houses are usually treated using methods such as adsorption [38, 39], coagulation/flocculation [38, 39], biological treatment [37-39], chemical oxidation [39] etc. However, these treatment methods have peculiar limitations. For instance, the use of adsorption or coagulation method usually leads to generation of secondary pollutant in the form of sludge. Chemical treatment brings about exposure to chemicals. Biodegradation method which makes use of bio-active enzymes such as azoreductase does not ensure total mineralization of dye because the enzyme is specific for the azo group [37, 39]. This method gives rise to bond cleavage products of high carcinogenic and mutagenic threats [37].

Recently, photocatalytic degradation using efficient, low cost photo-active materials such as ZnO [40-42],  $TiO_2$  [43-45], CdS [46-48] etc. has emerged as a more preferred method for dye degradation because it guarantees total transformation of pollutant into harmless

minerals. This method has been successfully employed for degradation of disperse dyes [49-52].

In photocatalysis, a pollutant is degraded by active radicals such as  $\bullet\text{OH}$  radical which is produced by photo-splitting of water molecules on the surface of a photo-excited catalyst [45, 53, 54]. Degradation of azo dye occurs when the radical attacks the dye through one of the nitrogen atoms in the azo chromophore ( $\text{N}=\text{N}$ ), or via a ring carbon next to it. This leads to an N-N or a C-N bond cleavage degradation mechanism, respectively [53-57]. Since photo-active materials are numerous with varying catalytic potential, useful guidelines on the choice of suitable materials for photodegradation is therefore necessary. Hence, the current study has demonstrated a simple and reliable theoretical means of predicting the suitability of a photo-active material for photodegradation.

Prediction of important physicochemical properties of existing and novel dyes can streamline research coverage, efforts and expenses, reduce wastage in research activities, optimize industrial applications and promote environmental safety by ensuring that attention is concentrated on newly predicted dyes that manifest certain meritorious characteristics. Therefore, the current work presents theoretical evaluations of aqueous solubility, chemical reactivity, absorption wavelength and thermodynamic stability for new derivatives of DR73, which comprise electron withdrawing cyano- and nitro- groups and/or electron donating amino and alkyl substituted amino groups. It has been reported [1, 53, 58] that electron withdrawing ( $X^-$ ) groups occupy *meta* positions relative to one another in the acceptor unit of aminoazobenzene dyes, while electron donating ( $X^+$ ) groups occupy *para* positions relative to one another in the donor unit. Hence the substitution of the  $X^-$  groups at position  $R_3$  and  $X^+$  groups at positions  $R_4$  and  $R_5$  in Figure 1. Position  $R_6$  is occupied by a CN group in DR73 while  $R_7$  is occupied by a hydrogen

atom. Position  $R_7$  can also be substituted with simple polar groups such as  $-CN$ ,  $-OH$  and halogens [1, 53, 58]. In this work however, only a  $-CN$  group is considered for this position in order to symmetrize the terminal cyanoalkylamine group. Susceptibility of the dyes to photocatalytic degradation and appropriateness of some photo-active materials for the process are also assessed. Photodegradation pathways were predicted and the probable sites for radical attacks during photocatalytic degradation were identified.

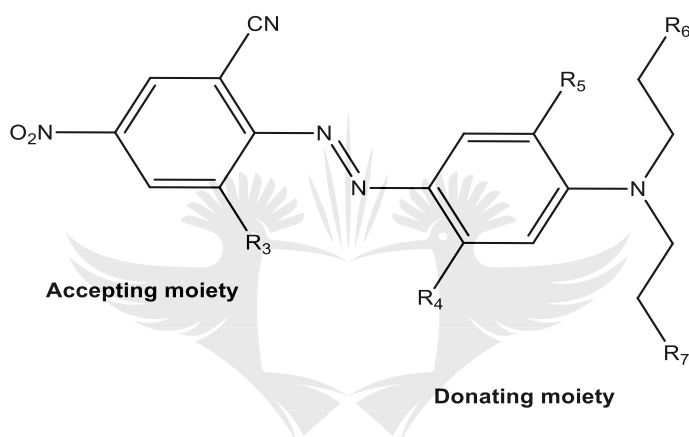


**Figure 9. 1:** General molecular structure of the studied dyes. For DR73,  $R_3 = R_4 = R_5 = R_7 = H$  and  $R_6 = CN$ . For the derivatives,  $R_6$  is unchanged,  $R_3 = X^-$ ,  $R_4$  and/or  $R_5 = X^+$ , and  $R_7 = H$  or  $CN$ .

## 9.2 COMPUTATIONAL DETAILS

Aqueous solubility and reactivity calculations were performed with the DMol<sup>3</sup> module [59] of the Material studio (2016) modelling package [60] using GGA/VWN-BP functional [59] with DNP basis set [59, 61]. This level of theory was selected because it is the recommended level of theory for COSMO calculations [59], and has been used successfully for predicting aqueous solubility of some azo disperse dyes via COSMO-RS calculation [62]. The geometries of DR73 and its studied derivatives were first optimized in gas phase, and then in water at the selected level of theory. All optimized geometries

were confirmed to be true ground state structures by the absence of imaginary frequencies. The aqueous phase optimization was carried out using the COSMO-RS program of the DMol<sup>3</sup> code and using the COSMO dielectric constant of 78.4 for water. A global orbital cut-off value of 7.0 Å was used for all but the aqueous solubility determination, where the value was varied from 3.0 Å to 7.0 Å depending on the molecular weight of the solute. Based on previous findings [62], a cut-off value of 3.0 Å was used for derivatives with molecular weights around 420 g and above, 3.5 Å for those with molecular weights between 395 g and 419 g, 4.5 Å for those with molecular weights between 380 g and 394 g, 5.5 Å for those with molecular weights between 375 g and 380 g and 7.0 Å for those with molecular weight of 374 g and below. The number of surface segment per atom (NSPA) was set to 92 with a COSMO solvent radius of 0.5. The radii of the constituent atoms (H, C, N, and O) [63] of the studied dyes were taken into account during the COSMO-RS calculation for a proper description of solute cavitation inside the conductor (water).

Solvation free energies (SFEs) in water were calculated using equation 9.1 [59]. The aqueous solubility in mol/L was determined from the SFEs and COSMO-RS calculated vapor pressure using the Cramer *et al.* solubility equation (CSE) (eqn. 9.2) [64]. Thermodynamic stability was evaluated based on Gibb's free energy calculations using equation 9.3 [59].

$$\Delta G_{sol} = (E + \Delta G_{NSE}) - E^0$$

**Equation 9. 1**

$$S_{aq} = \frac{P_s}{P^0} e^{-\Delta G_{sol}/RT}$$

**Equation 9. 2**

$$G = H - TS$$

**Equation 9. 3**

$\Delta G_{sol}$  is the solvation free energy,  $E$  is the energy in water (i.e COSMO energy),  $E^0$  is the energy in vacuum,  $\Delta G_{NSE}$  is the nonelectrostatic contribution to SFE due to dispersion and cavitation effects,  $S_{aq}$  is the aqueous solubility in mol/L,  $P_s$  is the solute vapor pressure (in atm) obtained from COSMO-RS calculation,  $P^0$  with numerical value of 24.45 atm is the pressure of an ideal gas at 1 molar standard state and 298 K,  $R$  and  $T$  are the molar gas constant and temperature, respectively,  $G$  is the Gibb's free energy,  $H$  is the enthalpy, and  $S$  is the entropy of the solute.

The polarizability of the studied dyes were determined from their respective vapor pressure using the Liang and Gallagher model (eqn. 9.4) [65]. Taking Koopmans' and finite difference approximations into consideration [66], the global reactivity indices which comprise the energy gap, global hardness and softness, global electronegativity, chemical potential and global electrophilicity index were evaluated from the highest occupied molecular orbital (HOMO) and lowest unoccupied molecular orbital (LUMO) energies using equations 9.5 – 9.10 [67].

$$\alpha = (3.940 - \text{Log } P_s)/0.401 \quad \text{Equation 9. 4}$$

where  $\alpha$  represents solute polarizability and  $P_s$  is as defined previously.

$$\text{Energy gap } (E_g) = E_{LUMO} - E_{HOMO} \quad \text{Equation 9. 5}$$

$$\text{Global hardness } (\eta) = -\frac{1}{2}(E_{HOMO} - E_{LUMO}) \quad \text{Equation 9. 6}$$

$$\text{Global softness } (\sigma) = \frac{1}{\eta} = -2/(E_{HOMO} - E_{LUMO}) \quad \text{Equation 9. 7}$$

$$\text{Electronegativity } (\chi) = -\frac{1}{2}(E_{HOMO} + E_{LUMO}) \quad \text{Equation 9. 8}$$

$$\text{Chemical potential } (\Phi) = -\chi = \frac{1}{2}(E_{HOMO} + E_{LUMO}) \quad \text{Equation 9. 9}$$



$$\text{Global electrophilicity index } (\omega) = \frac{\chi^2}{2\eta}$$

Equation 9. 10

where  $E_{HOMO}$  and  $E_{LUMO}$  are the HOMO and LUMO energies respectively.

The semiconductors considered in this study include Si, CdSe, CdS, TiO<sub>2</sub>, ZnO and ZnS. They were selected across a range of band gap in both the UV and the visible region of the solar radiation. Their band structures which comprise the conduction band minimum (CBM), the valence band minimum (VBM) and the band gaps were also calculated with the DMol<sup>3</sup> program using the selected level of DFT. The primitive cells of Si and CdSe were used for the calculations while the most stable surface morphologies were employed in the case of CdS, TiO<sub>2</sub> (rutile), ZnO and ZnS [68-72] because they produced more accurate theoretical band gap at minimal computational cost.

Site vulnerability to hydroxyl radical attack was evaluated based on Fukui function for radical attack,  $f^0$ , obtained using equation 9.11 [73].

$$f^0 = \frac{1}{2} [q_k(N+1) - q_k(N-1)]$$

Equation 9. 11

where  $N$  is the number of electron,  $q_k(N+1)$  and  $q_k(N-1)$  are the Mulliken charges on atom  $k$  for  $(N+1)$  and  $(N-1)$  numbers of electrons, respectively.

It has been observed that hybrid functionals such as B3LYP and PBE0 are more reliable for predicting absorption wavelengths [24, 27, 28, 74, 75] compared to pure LDA and GGA functionals which underestimate HOMO-LUMO energy gap and consequently lead to overestimation of absorption wavelength [76]. Therefore, the B3LYP level of theory in conjunction with 6-31G\*, which is a polarized split valence basis set, was used for the calculation of absorption wavelength. For this purpose, Spartan 14 software produced by Wavefunction, Inc. Irvine, CA, USA, was employed because it offers a relatively less

rigorous means of calculating this property using hybrid functionals. TD-DFT calculation of absorption wavelength using DMol<sup>3</sup> was computationally unaffordable.

Two approaches were adopted for calculating the absorption wavelength. In the first approach, the wavelength was calculated directly using the configuration interaction singles (CIS) method for excited states whereas in the second approach, the wavelength was estimated from HOMO-LUMO energy gap using equation 9.12. This is because the characteristic absorption wavelengths of most azo dyes are due to electronic transition from HOMO to LUMO (i.e.  $n \rightarrow \pi^*$  transition) [24, 27, 30] which is usually the most allowed and the most intense electronic transition with the largest oscillator strength. The absorption wavelengths calculated via the two approaches are designated as  $\lambda_{CIS}$  and  $\lambda_{H-L}$ , respectively.

$$\Delta E_{H-L} = \frac{hc}{\lambda_{H-L}}$$

Equation 9. 12

where  $\Delta E_{H-L}$  is the predicted energy of electronic excitation from HOMO to LUMO and is estimated as the HOMO-LUMO energy difference,  $h = 6.626 \times 10^{-34} J s$  is the Planck's constant,  $c = 2.998 \times 10^{10} m s^{-1}$  is the speed of light in vacuum and  $\lambda_{H-L}$  represents the corresponding absorption wavelength.

## 9.3 RESULTS AND DISCUSSIONS

### 9.3.1 AQUEOUS SOLUBILITY STUDY

The calculated vapor pressure, aqueous solubility and Gibb's free energies for DR73 and its studied derivatives are given in Table 9.1. The substituent groups studied comprise the electron withdrawing (i.e. CN and NO<sub>2</sub>) and the electron donating (i.e. NH<sub>2</sub>, NHCH<sub>3</sub> and N(CH<sub>3</sub>)<sub>2</sub>) series which were substituted on the acceptor and the donor moieties of

DR73. Since electron withdrawing substituent groups (i.e.  $X^-$ ) occupy *meta* positions relative to one another [77], they were substituted at position R<sub>3</sub> on the acceptor moiety of DR73 (Fig. 9.1). On the contrary, electron donating substituent groups (i.e.  $X^+$ ) occupy *ortho* or *para* positions relative to one another [77], hence, the terminal alkyl amino group in the donor moiety suggests position R<sub>5</sub> as having greater chance for substitution than R<sub>4</sub>.

In addition, the isosurface of the HOMO of DR73 (shown in Fig. 9.2) revealed that position R<sub>3</sub> in the acceptor moiety is more susceptible to electron withdrawers compared to other vacant positions in the moiety. Similarly, the isosurface of the LUMO indicated that position R<sub>5</sub> in the donor moiety is more predisposed to electron donating groups compared to other vacant sites in the moiety. The effects of these various substituent positions on the calculated properties are also examined.

**Table 9. 1:** Aqueous solubility ( $S_{aq}$ ), SFE ( $\Delta G_{sol}$ ), vapour pressure ( $p$ ) and the Gibb's free energies ( $\Delta G_{gas}$ ) obtained for DR73 and its studied derivatives at 25 °C.

Dyes	R3	R4	R5	R6	R7	Mwt. (g/mol)	pE-16 (atm)	$\Delta G_{sol}$ (kcal/mol)	$S_{aq}$ (mg/L)	$\Delta G_{gas}$ (kcal/mol)
DR73	H	H	H	CN	H	348.36	0.54	-18.41	24.65	-33.83
X <sup>-</sup> substitution										
F1	NO <sub>2</sub>	H	H	CN	H	393.36	0.0054	-22.00	119.74	-38.05
F2	CN	H	H	CN	H	373.37	0.015	-20.76	38.87	-36.18
F3	H	H	H	CN	CN	373.37	0.00023	-24.24	212.91	-37.68
F4	NO <sub>2</sub>	H	H	CN	CN	418.37	0.000023	-24.58	42.37	-39.17
F5	CN	H	H	CN	CN	398.38	0.0000036	-26.46	151.19	-37.61
X <sup>+</sup> substitution										
F6	H	NH <sub>2</sub>	H	CN	H	363.38	0.00029	-20.64	0.60	-34.98
F7	H	NHCH <sub>3</sub>	H	CN	H	377.40	0.00023	-20.79	0.63	-36.85

F8	H	N(CH <sub>3</sub> ) <sub>2</sub>	H	CN	H	391.43	0.00040	-19.74	0.19	-39.03
F9	H	H	NH <sub>2</sub>	CN	H	363.38	0.044	-18.85	4.40	-34.40
F10	H	H	NHCH <sub>3</sub>	CN	H	377.40	0.043	-17.07	0.22	-37.45
F11	H	H	N(CH <sub>3</sub> ) <sub>2</sub>	CN	H	391.43	0.18	-16.04	0.17	-38.23
F12	H	NH <sub>2</sub>	H	CN	CN	388.39	0.0000001	-29.46	650.14	-37.42
F13	H	NHCH <sub>3</sub>	H	CN	CN	402.41	0.0000022	-27.14	294.35	-37.44
F14	H	N(CH <sub>3</sub> ) <sub>2</sub>	H	CN	CN	416.44	0.0000020	-26.74	140.90	-38.64
F15	H	H	NH <sub>2</sub>	CN	CN	388.39	0.000041	-24.96	133.22	-37.65
F16	H	H	NHCH <sub>3</sub>	CN	CN	402.41	0.00020	-23.16	32.19	-37.70
F17	H	H	N(CH <sub>3</sub> ) <sub>2</sub>	CN	CN	416.44	0.0018	-20.13	1.79	-40.81
X <sup>-</sup> versus X <sup>+</sup> substitution										
F18	NO <sub>2</sub>	NH <sub>2</sub>	H	CN	H	408.38	0.0027	-21.50	26.71	-38.29
F19	NO <sub>2</sub>	NHCH <sub>3</sub>	H	CN	H	422.40	0.082	-17.32	0.72	-41.27
F20	NO <sub>2</sub>	N(CH <sub>3</sub> ) <sub>2</sub>	H	CN	H	436.43	0.0099	-18.21	0.40	-40.97
F21	NO <sub>2</sub>	H	NH <sub>2</sub>	CN	H	408.38	0.0029	-19.47	0.93	-38.47
F22	NO <sub>2</sub>	H	NHCH <sub>3</sub>	CN	H	422.40	0.078	-16.78	0.28	-40.18
F23	NO <sub>2</sub>	H	N(CH <sub>3</sub> ) <sub>2</sub>	CN	H	436.43	0.33	-15.64	0.18	-41.15
F24	NO <sub>2</sub>	NH <sub>2</sub>	H	CN	CN	433.39	0.000027	-25.77	384.57	-41.05
F25	NO <sub>2</sub>	NHCH <sub>3</sub>	H	CN	CN	447.41	0.000058	-24.72	144.74	-42.43
F26	NO <sub>2</sub>	N(CH <sub>3</sub> ) <sub>2</sub>	H	CN	CN	461.44	0.0000021	-25.09	10.10	-41.83
F27	NO <sub>2</sub>	H	NH <sub>2</sub>	CN	CN	433.39	0.00019	-22.88	20.52	-39.75
F28	NO <sub>2</sub>	H	NHCH <sub>3</sub>	CN	CN	447.41	0.000046	-21.96	1.08	-41.24
F29	NO <sub>2</sub>	H	N(CH <sub>3</sub> ) <sub>2</sub>	CN	CN	461.44	0.00038	-21.13	2.27	-43.01
F30	CN	NH <sub>2</sub>	H	CN	H	388.39	0.0035	-22.77	281.36	-37.49
F31	CN	NHCH <sub>3</sub>	H	CN	H	402.41	0.088	-17.83	1.74	-39.40
F32	CN	N(CH <sub>3</sub> ) <sub>2</sub>	H	CN	H	416.44	0.0027	-19.56	1.03	-41.54
F33	CN	H	NH <sub>2</sub>	CN	H	388.39	0.0011	-21.56	11.45	-36.81
F34	CN	H	NHCH <sub>3</sub>	CN	H	402.41	0.0017	-18.29	0.07	-39.18

F35	CN	H	N(CH <sub>3</sub> ) <sub>2</sub>	CN	H	416.44	0.048	-17.41	0.48	-39.89
F36	CN	NH <sub>2</sub>	H	CN	CN	413.39	0.0000064	-26.79	487.03	-40.53
F37	CN	NHCH <sub>3</sub>	H	CN	CN	427.42	0.00049	-22.07	13.29	-40.79
F38	CN	N(CH <sub>3</sub> ) <sub>2</sub>	H	CN	CN	441.45	0.000022	-23.33	5.18	-42.25
F39	CN	H	NH <sub>2</sub>	CN	CN	413.39	0.0000059	-25.27	34.45	-40.10
F40	CN	H	NHCH <sub>3</sub>	CN	CN	427.42	0.000099	-22.88	10.55	-42.18
F41	CN	H	N(CH <sub>3</sub> ) <sub>2</sub>	CN	CN	441.45	0.00086	-21.67	12.26	-43.06

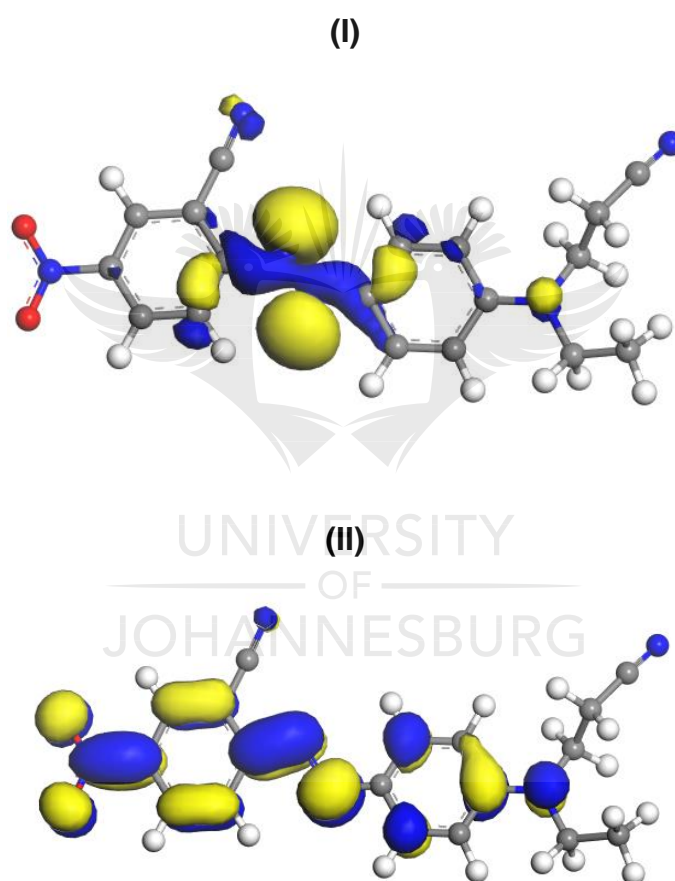


**Figure 9. 2:** HOMO (I) and LUMO (II) isosurfaces of DR73 showing the electron-rich and electron-deficient parts of the molecule. The HOMO and LUMO isovalue is 0.03.

### 9.3.2 EFFECTS OF X- GROUPS ON SOLUBILITY

Substitution of NO<sub>2</sub> and CN at position R<sub>3</sub> in DR73 enhances the aqueous solubility of the dye as can be observed for F1, F2, F4 and F5. Comparing F1 and F2, the higher solubility value for F1 suggests that NO<sub>2</sub> enhances the solubility better than CN. However, the converse is true for F4 and F5 where the latter possesses higher solubility value, which suggests CN as the better electron withdrawer for promoting the solubility. To understand this conflicting solubility trend between these pairs of derivatives, assessment of their screening charges, dipole moments and polarizabilities (Table 9.2) is necessary. Considering the dipole moment vector shown in Figure A.1 (Appendix), which indicates higher electron density for the acceptor moiety, substitution of the X<sup>-</sup> groups at position R<sub>3</sub> in DR73 will result in the drifting of electron cloud towards the accepting moiety of the dye.

**Table 9. 2:** Screening charges,  $q$ , polarizability,  $\alpha$ , and dipole moment,  $\mu$  of DR73 and its studied derivatives at 25 °C.

Dyes	R3	R4	R5	R6	R7	Screening charge, $q$	$\mu$ (Debye)	$\alpha$
DR73	H	H	H	CN	H	-0.00113	11.70	43.21
X <sup>-</sup> substitution								
F1	NO <sub>2</sub>	H	H	CN	H	-0.00082	10.78	48.20
F2	CN	H	H	CN	H	-0.00083	10.23	47.09
F3	H	H	H	CN	CN	-0.00090	6.96	51.61
F4	NO <sub>2</sub>	H	H	CN	CN	-0.00062	5.92	54.11
F5	CN	H	H	CN	CN	-0.00064	5.45	56.17
X <sup>+</sup> substitution								
F6	H	NH <sub>2</sub>	H	CN	H	-0.00114	13.48	51.36
F7	H	NHCH <sub>3</sub>	H	CN	H	-0.00115	14.13	51.61
F8	H	N(CH <sub>3</sub> ) <sub>2</sub>	H	CN	H	-0.00116	14.86	51.02

F9	H	H	NH <sub>2</sub>	CN	H	-0.00127	10.08	45.92
F10	H	H	NHCH <sub>3</sub>	CN	H	-0.00126	9.74	45.95
F11	H	H	N(CH <sub>3</sub> ) <sub>2</sub>	CN	H	-0.00128	11.37	44.40
F12	H	NH <sub>2</sub>	H	CN	CN	-0.00101	8.72	60.00
F13	H	NHCH <sub>3</sub>	H	CN	CN	-0.00093	9.38	56.65
F14	H	N(CH <sub>3</sub> ) <sub>2</sub>	H	CN	CN	-0.00097	9.95	56.75
F15	H	H	NH <sub>2</sub>	CN	CN	-0.00102	5.28	53.48
F16	H	H	NHCH <sub>3</sub>	CN	CN	-0.00107	5.08	51.77
F17	H	H	N(CH <sub>3</sub> ) <sub>2</sub>	CN	CN	-0.00108	5.86	49.39
X <sup>-</sup> versus X <sup>+</sup> substitution								
F18	NO <sub>2</sub>	NH <sub>2</sub>	H	CN	H	-0.00096	12.13	48.95
F19	NO <sub>2</sub>	NHCH <sub>3</sub>	H	CN	H	-0.00094	13.01	45.25
F20	NO <sub>2</sub>	N(CH <sub>3</sub> ) <sub>2</sub>	H	CN	H	-0.00095	13.30	47.54
F21	NO <sub>2</sub>	H	NH <sub>2</sub>	CN	H	-0.00094	9.75	48.87
F22	NO <sub>2</sub>	H	NHCH <sub>3</sub>	CN	H	-0.00092	10.11	45.30
F23	NO <sub>2</sub>	H	N(CH <sub>3</sub> ) <sub>2</sub>	CN	H	-0.00096	10.43	43.74
F24	NO <sub>2</sub>	NH <sub>2</sub>	H	CN	CN	-0.00075	6.91	53.93
F25	NO <sub>2</sub>	NHCH <sub>3</sub>	H	CN	CN	-0.00077	7.94	53.11
F26	NO <sub>2</sub>	N(CH <sub>3</sub> ) <sub>2</sub>	H	CN	CN	-0.00073	8.58	56.70
F27	NO <sub>2</sub>	H	NH <sub>2</sub>	CN	CN	-0.00076	5.52	51.82
F28	NO <sub>2</sub>	H	NHCH <sub>3</sub>	CN	CN	-0.00074	5.54	53.36
F29	NO <sub>2</sub>	H	N(CH <sub>3</sub> ) <sub>2</sub>	CN	CN	-0.00078	5.78	51.07
F30	CN	NH <sub>2</sub>	H	CN	H	-0.00101	11.97	48.67
F31	CN	NHCH <sub>3</sub>	H	CN	H	-0.00100	12.63	45.17
F32	CN	N(CH <sub>3</sub> ) <sub>2</sub>	H	CN	H	-0.00094	13.17	48.95
F33	CN	H	NH <sub>2</sub>	CN	H	-0.00098	9.03	49.92
F34	CN	H	NHCH <sub>3</sub>	CN	H	-0.00095	8.33	49.45
F35	CN	H	N(CH <sub>3</sub> ) <sub>2</sub>	CN	H	-0.00098	10.38	45.83

F36	CN	NH <sub>2</sub>	H	CN	CN	-0.00079	6.65	55.49
F37	CN	NHCH <sub>3</sub>	H	CN	CN	-0.00081	7.53	50.80
F38	CN	N(CH <sub>3</sub> ) <sub>2</sub>	H	CN	CN	-0.00074	8.28	54.16
F39	CN	H	NH <sub>2</sub>	CN	CN	-0.00078	5.07	55.58
F40	CN	H	NHCH <sub>3</sub>	CN	CN	-0.00075	5.39	52.53
F41	CN	H	N(CH <sub>3</sub> ) <sub>2</sub>	CN	CN	-0.00078	5.40	50.19

The Hammett constant,  $\tau$  [78] and the electronegativity,  $\chi$  values shown in Table A.14 (Appendix) suggest that NO<sub>2</sub> has higher electron withdrawing power compared to CN. Therefore, NO<sub>2</sub> will cause greater depletion of electron cloud, which will result in a larger charge density difference between the accepting and the donating moieties. This explains why the dipole moment values for the NO<sub>2</sub> substituted derivatives are higher than those of the CN counterparts (Table 9.2). The relatively large screening charge values obtained for the CN substituted derivatives also confirm lower electron withdrawing strength for CN (Table 9.2).

Based on these observations, NO<sub>2</sub> is expected to promote the solubility more than CN, which is the trend observed for F1 and F2. However, the introduction of additional CN substituent at position R<sub>7</sub> in F4 and F5 seems to favor higher polarizability for F5 (Table 9.2) which suggests stronger interaction with water. This explains why the solvation free energy magnitude and the solubility values for F5 are larger than those of F4 (Table 9.1). The increased bulkiness of the acceptor unit of F4 compared F5 due to the relatively larger size of NO<sub>2</sub> compared to CN may also be responsible for the lower solubility enhancement effect of the R<sub>7</sub> –CN substituent on F4. Similarly, the relatively small polarizability value obtained for the parent dye compared to F1, F2, F4 and F5 accounts for the lesser solubility of the former despite its larger screening charge and dipole



moment. This may be due to the lower number of polar substituent groups in the parent dye compared to the derivatives. Introduction of an extra -CN substituent at position R<sub>7</sub> further decreased both the charge density in the molecule and the charge density difference between the donating and the accepting terminals of the azo bridge as revealed by the relatively small screening charge and the dipole moment values obtained for F3, F4 and F5 compared to DR73, F1 and F2, respectively. However, the consequent increase in polarizability for F3, F4 and F5 might be responsible for their large SFE values.

### 9.3.3 EFFECTS OF X<sup>+</sup> GROUPS ON SOLUBILITY

Since electron donating substituent groups are *ortho* or *para* directors, the presence of a terminal cyanoalkylamino group in the donating moiety of DR73 (Fig. 9.1) suggests that further substitution of an X<sup>+</sup> group will be more effective if the substitution occurs at position R<sub>5</sub> which is *ortho* to the terminal substituent. In other words, the electron donating impact of the incoming substituent will be more significant when attached to position R<sub>5</sub> unlike R<sub>4</sub> which is *meta* to the terminal substituent.

The chemical potential ( $\Phi$ ) and the Hammett constants ( $\tau$ ) for the X<sup>+</sup> substituents (Appendix: Table A.14) suggest that the NH<sub>2</sub> substituent possesses a lower electron donating capacity compared to NHCH<sub>3</sub> and N(CH<sub>3</sub>)<sub>2</sub>. The aqueous solubility values obtained for the X<sup>+</sup> substituted derivatives are generally smaller than that of the parent dye suggesting that the substituents (particularly NHCH<sub>3</sub> and N(CH<sub>3</sub>)<sub>2</sub>) reduce the solubility (Table 9.1). This may be attributed to increased steric hindrance to solvation caused by NHCH<sub>3</sub> and N(CH<sub>3</sub>)<sub>2</sub>, which is believed to be higher when they are substituted at position R<sub>5</sub> due to the proximity of this position to the bulky terminal alkyl amino group (Fig. 9.3).

The more negative solvation free energies (SFE) of F6 – F8 compared to F9 – F11, respectively (Table 9.1), are not only due to lower steric hindrance to solvation of the former, but also to the decrease in the electron donating impact of the substituents at position R<sub>4</sub> which resulted in the inability of the substituents to sufficiently counteract the electron withdrawing impact of the accepting moiety. This led to larger charge separation between the accepting and the donating parts as confirmed by the relatively large dipole moment and polarizability values obtained for F6 – F8 (Table 9.2).

The dipole moment ( $\mu$ ) and the solvation free energy ( $\Delta G_{\text{sol}}$ ) values given in Table A.14 (Appendix) revealed that the polarity and the degree of solvation of the X<sup>+</sup> substituents follow the order NHCH<sub>3</sub> > NH<sub>2</sub> > N(CH<sub>3</sub>)<sub>2</sub>, which suggests that the solubility value of an NHCH<sub>3</sub> substituted derivative will be higher than those of NH<sub>2</sub> and N(CH<sub>3</sub>)<sub>2</sub> substituted counterparts. This is in agreement with the solubility trend observed for F6 – F8 (Table 9.1). However, the increase in steric hindrance when the substituents are switched to position R<sub>5</sub> may be responsible for why F10 produced a lower solubility value compared to F9 despite NHCH<sub>3</sub> having the higher dipole moment value (Appendix: Table A.14). The relatively large solubility of F9 may be attributed to the small size of the NH<sub>2</sub> substituent, which also explains why the solvation free energy of this substituent is negligibly different from that of NHCH<sub>3</sub> (Appendix: Table A.14) despite the significant difference in their dipole moments.

Position of substituent = R<sub>4</sub>

Position of substituent = R<sub>5</sub>

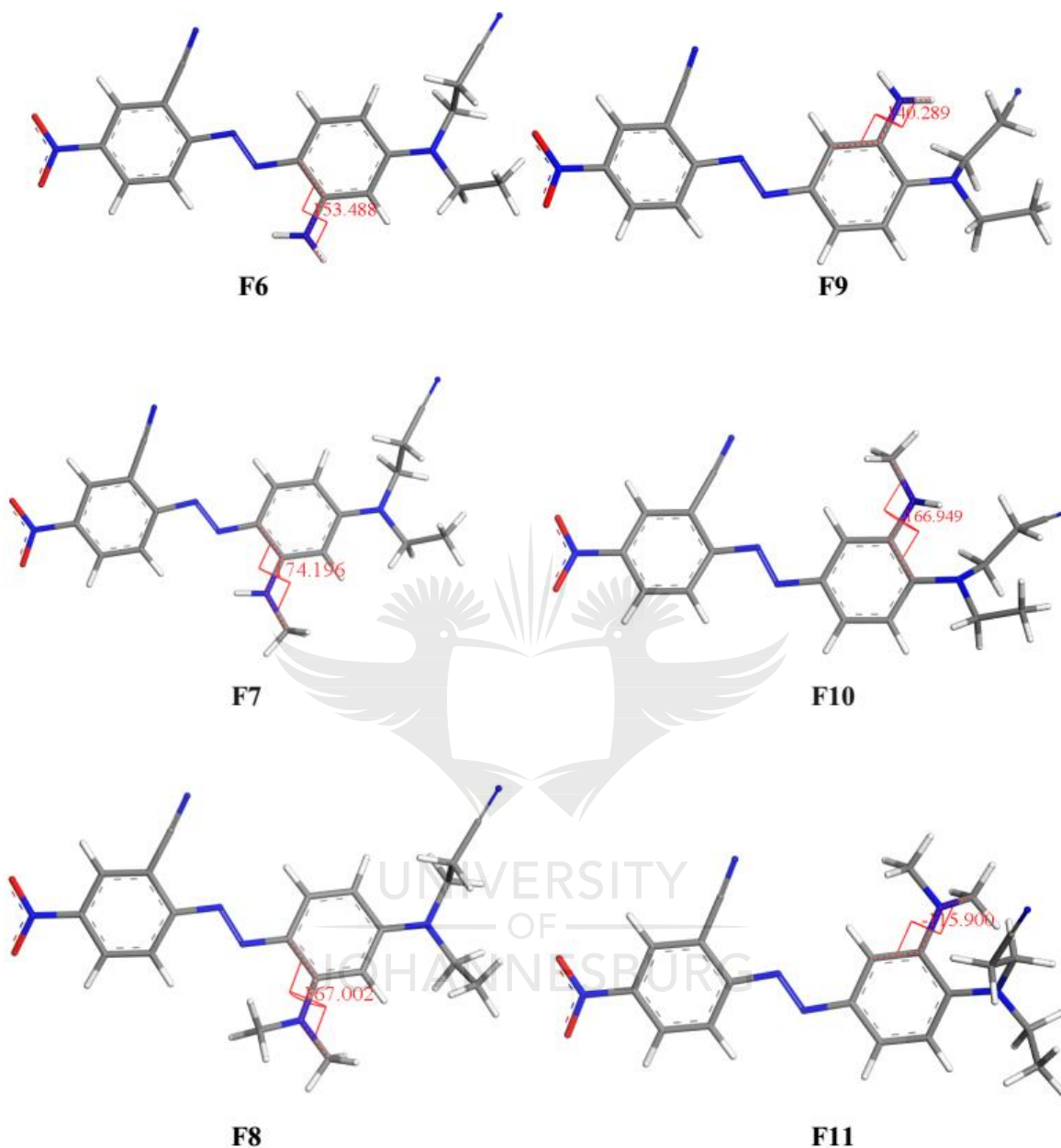


**Figure 9. 3:** Models of some X<sup>+</sup> substituted DR73 showing different torsion angles between the planes of the ring and the amine substituents due to varying magnitude of steric effect at positions R<sub>4</sub> (left) and R<sub>5</sub> (right). The closer the angles to 0° or 180°, the more the orientation of the substituent along the molecular plane and the less the steric effect.

The relatively large screening charge magnitude, low dipole moment and polarizability values obtained for F9 – F11 confirm higher electron donating impact for the substituents when substituted *ortho* to the terminal alkyl amino group (i.e. position R<sub>5</sub>). Figure 9.4 shows the lengths of the C – N bonds formed by the X<sup>+</sup> substituents with the donating ring of DR73. It is evident from the figure that the C – N bond formed at position R<sub>5</sub> is longer than the one at position R<sub>4</sub> which suggests greater ionic character for this bond at R<sub>5</sub> due to higher electron donating power of the substituents at this position.

The relatively large dipole moment and polarizability values (Table 9.2) coupled with the lower steric effect of F6 (Fig. 9.3), suggest that this derivative will be more soluble compared to F9. This is contrary to the trend observed in Table 9.1 which may be due to slight underestimation of the vapor pressure and/or SFE values of F6.

Comparing F6 – F11 to F12 – F17, respectively, in Table 9.1, it is clear that the introduction of additional electron withdrawing - CN substituent to F6 – F11 at position R<sub>7</sub> (Fig. 9.1) brought about remarkable increase in the SFE and the aqueous solubility of these derivatives where the highest increase was obtained with NH<sub>2</sub> substituent as can be observed for F12 and F15. This further confirms NH<sub>2</sub> as the best candidate of the X<sup>+</sup> series for promoting the aqueous solubility. CN introduction at position R<sub>7</sub> further decreases the charge density of the system and charge separation magnitude between the donating and the accepting moieties of the dye. This results in a decrease in screening charge magnitude and dipole moment for F12 – F17 relative to F6 – F11, respectively (Table 9.2). However, the relatively large polarizability values for F12 – F17 due to the extra polarizable CN substituent explains why these derivatives produced larger SFE and solubility values compared to F6 – F11, respectively. The variations observed between F12 – F14 and F15 – F17 in terms of screening charge, dipole moment, polarizability and

the resultant SFE and aqueous solubility values are due to varying electron donating impact of the X<sup>+</sup> groups at positions R<sub>4</sub> and R<sub>5</sub> which were explained earlier.

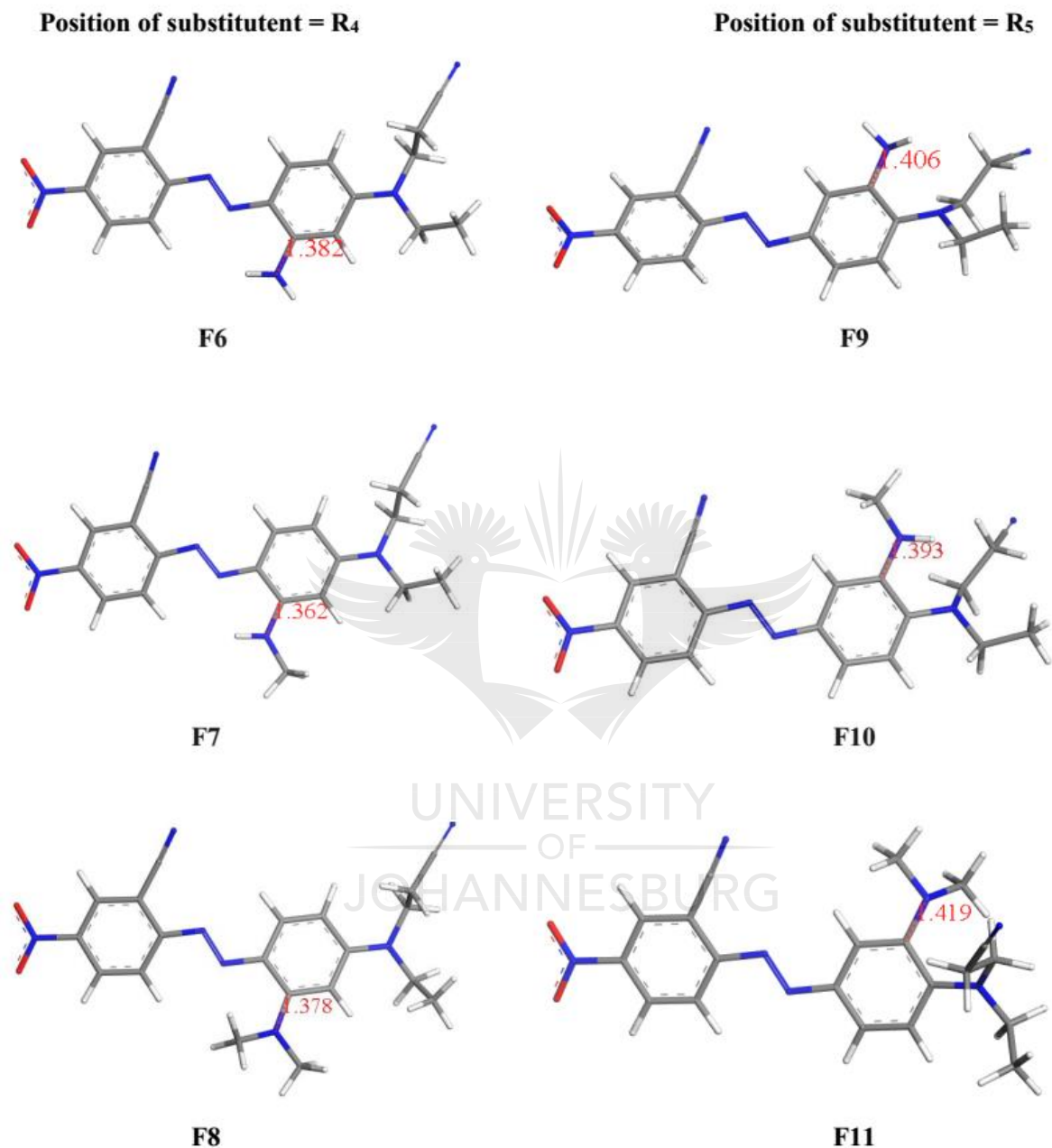


**Figure 9. 4:** Models of some X<sup>+</sup> substituted DR73 showing the lengths of the C – N bonds formed by the X<sup>+</sup> substituents at positions R<sub>4</sub> (left) and R<sub>5</sub> (right), where the bonds formed at R<sub>5</sub> are longer than those at R<sub>4</sub>.

### 9.3.4 EFFECTS OF X<sup>-</sup> AND X<sup>+</sup> GROUPS ON SOLUBILITY

Introduction of electron withdrawing NO<sub>2</sub> substituent to derivatives F6 – F17 brought about no significant improvement in the solubility (with the exception of F18 compared to F6) and in fact in most cases, the solubility was further decreased by this substituent (Table 9.1). This is probably because the substituent decreased the charge density in the azo (-N = N-) region by inductively withdrawing electrons towards the acceptor unit of the dye, which led to smaller screening charge values for F18 – F29 compared to F6 – F17, respectively (Table 9.2). The charge density difference between the acceptor and donor moieties consequently become smaller as confirmed by the low dipole moment values for F18 – F23 compared to F6 – F11. The unexpected increase in solubility of F18 compared to F6 may be ascribed to slightly overestimated SFE value of the former. On the other hand, the extra CN – substituent at position R<sub>7</sub> in F24 – F29 did not only decrease the screening charge further, but also attracted a significant number of electrons to the donor fragment to counteract the electron withdrawing effect of NO<sub>2</sub>. This explains why both the screening charge and dipole moment values for F24 – F29 are smaller than those of F18 – F23 respectively (Table 9.2). The polarizability trend however, revealed why derivatives F24 – F29 possess larger SFE values and are as a result, more soluble than F18 – F23 (Table 9.1).

Similar results were obtained when the NO<sub>2</sub> substituent was replaced by the CN substituent at position R<sub>3</sub> as in F30 – F41. However in this case, the solubility values are higher than those of the NO<sub>2</sub> substituted counterparts (i.e. F18 – F29) especially with NH<sub>2</sub> as the electron donating substituent (Table 9.1). Comparison between F30 – F41 and F18 – F29, respectively, in Table 9.2 revealed, with very few exceptions, that the -CN substituent favors larger screening charge, dipole moment, polarizability and hence

higher aqueous solubility values compared to NO<sub>2</sub>. This confirms that the -CN substituent is better than NO<sub>2</sub> for enhancing aqueous solubility. The dipole moments ( $\mu$ ) and the solvation free energies ( $\Delta G_{\text{sol}}$ ) presented in Table A.14 (Appendix), which suggest that the CN substituent is more polar and more solvated, justify why almost all the CN substituted derivatives possess larger solubility values compared to their NO<sub>2</sub> substituted counterparts.

### 9.3.5 PREDICTION OF HEAT RESISTANCE CAPACITY AND THERMODYNAMIC STABILITY OF THE DYES

The results in Table 9.1 showed that the vapor pressure of the derivatives is generally lower than that of DR73, which suggests that the derivatives will have greater thermal resistance capacity (i.e. higher sublimation fastness) than the parent dye. However, the decrease in vapor pressure is more pronounced in derivatives in which position R<sub>7</sub> (Fig. 9.1) is replaced by a CN substituent, because this replacement enhances the polarizability of the derivatives leading to an increase in solvation as confirmed by the relatively large negative SFE values for derivatives such as F3-F5, F12-F16, F24-F28 and F36-F40. At constant temperature and pressure, a low vapor pressure suggests that a solute is present in low concentration in the vapor phase, which is an indication of high solvation.

The negative Gibb's free energy obtained for the derivatives (Table 9.1) suggests that they are thermodynamically stable as DR73. However, substitution with different combinations of X<sup>-</sup> and X<sup>+</sup> enhances the thermodynamic stability compared to an isolated substitution with X<sup>-</sup> or X<sup>+</sup> groups. NO<sub>2</sub> is more electron-withdrawing than CN, hence it stabilizes the dye better by withdrawing sufficient electrons towards the acceptor moiety

which decreases the charge separation between the donor and acceptor moieties. This explains why the Gibb's free energies for the NO<sub>2</sub> substituted derivatives are more negative.

### 9.3.6 CHEMICAL REACTIVITY STUDY

The HOMO and LUMO energies, HOMO-LUMO energy gap and global hardness values obtained for DR73 and its studied derivatives are presented in Tables 9.3. The bigger the HOMO energy, the higher the probability of donating an electron and the lower the LUMO energy, the more the propensity towards incoming electrons. The HOMO – LUMO energy gap,  $E_g$  is an essential indicator of the net stability of a molecule and its probability to undergo electronic excitation. The larger the energy gap, the higher the stability, the lower the reactivity and the less the chance of excitation. Global hardness,  $\eta$ , is a measure of a molecule's resistivity towards a change in the number and/or configuration of electrons while global softness,  $\sigma$ , reveals a molecule's vulnerability to such. The higher the hardness or the lower the softness, the less the reactivity. Electronegativity,  $\chi$  describes the ability of a molecule to attract electrons towards itself while chemical potential,  $\Phi$  which is also known as electropositivity, reveals its ability to release electrons. The global electrophilicity index,  $\omega$ , reveals the extent of electron deficiency or unsaturation in a molecule because it shows its susceptibility to a nucleophilic attack. A large value of  $\omega$  implies a good electrophile while a small  $\omega$  indicates a good nucleophile.

### 9.3.7 EFFECTS OF X- SUBSTITUTION ON REACTIVITY

From Table 9.3, the relatively low HOMO and LUMO energies observed both in gas and water for the X-substituted derivatives suggests that their probability to donate an



electron is lower while their tendency of accepting electrons is higher compared to DR73 which seems to be a stronger electron donor and a weaker electron acceptor. This implies that the parent dye is more prone to oxidative degradation while the derivatives are more susceptible to reductive degradation as a result of high electron deficiency caused by the electron withdrawing NO<sub>2</sub> and CN substituents. However, the impact of these substituents on the HOMO and LUMO energies vary. NO<sub>2</sub> lowers the HOMO energy more than CN, suggesting derivatives F1 and F4 as being less vulnerable to oxidation compared to F2 and F5 respectively. On the other hand, CN decreases the LUMO energy more than NO<sub>2</sub>, hence the greater chance of reduction for F2 and F5 relative to F1 and F4 respectively.

Following the HOMO and LUMO energy trends, the table further suggests the CN substituted derivatives as having greater binding potential towards substrates through both the HOMO and the LUMO compared to the NO<sub>2</sub> counterparts. The relatively high HOMO energies obtained for F2 and F5, and the accompanying lower LUMO energies compared to F1 and F4 respectively suggest greater probability of concerted electron donation and retro-donation processes between F2 and F5 and a substrate. Comparing F3 to DR73, it is evident from the table that the extra electron withdrawing -CN substituent at position R<sub>7</sub> in F3 (Fig. 9.1) is responsible for the observed decrease in HOMO and LUMO energies of this derivative, which suggests it as being less predisposed to oxidation but more susceptible to reduction than DR73.

The HOMO-LUMO energy gap, the hardness and the softness (Tables 9.3 and A.21(Appendix)), clearly revealed that the NO<sub>2</sub> substituted derivatives (F1 and F4) are more stable and less vulnerable to photo-excitation especially in gas compared to the CN substituted counterparts (F2 and F5). This suggests longer life time, higher light fastness,

but lower photodegradation tendency for the NO<sub>2</sub> derivatives. The differences in electronegativity and chemical potential (Appendix: Table A.21) between the NO<sub>2</sub> and CN substituted derivatives are insignificant, which suggest negligible differences in electron attracting and electron releasing abilities.

The calculated electrophilicity indices revealed that the derivatives are more electrophilic than the parent dye, with the CN-substituted ones being the most electrophilic. This suggests the parent dye as being a better nucleophile compared to the derivatives.

The differences observed between the HOMO-LUMO energy gap, hardness, softness, electronegativity, chemical potential and electrophilicity values of F3, F4 and F5 compared to DR73, F1 and F2 are the resultant effects of the extra electron withdrawing -CN substituent at position R<sub>7</sub> in F3, F4 and F5.

The HOMO and the LUMO energies of both the parent dyes and the X-substituted derivatives are higher in water than gas phase (Table 9.3), which suggests that water enhances the chance of oxidation, but reduces the chance of reduction. In other words, the dyes are more susceptible to oxidative degradation in water, but reductive degradation in gas.

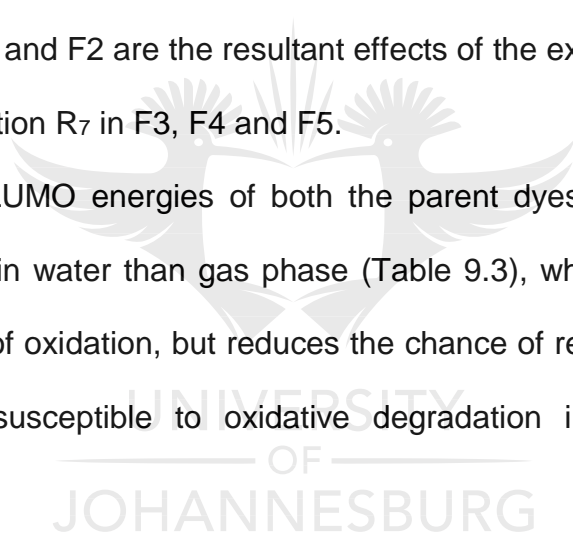


**Table 9. 3:** HOMO energies ( $E_{\text{HOMO}}$ ), LUMO energies ( $E_{\text{LUMO}}$ ), HOMO-LUMO energy gap ( $E_g$ ) and hardness ( $\eta$ ) of DR73 and its studied derivatives.

Dyes	R <sub>3</sub>	R <sub>4</sub>	R <sub>5</sub>	R <sub>6</sub>	R <sub>7</sub>	HOMO (eV)		LUMO (eV)		E <sub>g</sub> (eV)		$\eta$ (eV)	
						Gas	Water	Gas	Water	Gas	Water	Gas	Water
DR73	H	H	H	CN	H	-5.80	-5.43	-4.16	-4.10	1.64	1.33	0.82	0.67
X <sup>-</sup> Substitution													
F1	NO <sub>2</sub>	H	H	CN	H	-5.99	-5.60	-4.40	-4.27	1.59	1.33	0.80	0.67
F2	CN	H	H	CN	H	-5.96	-5.59	-4.45	-4.27	1.51	1.32	0.76	0.66
F3	H	H	H	CN	CN	-6.02	-5.56	-4.37	-4.16	1.65	1.40	0.83	0.70
F4	NO <sub>2</sub>	H	H	CN	CN	-6.23	-5.74	-4.60	-4.34	1.63	1.40	0.82	0.70
F5	CN	H	H	CN	CN	-6.17	-5.71	-4.65	-4.34	1.52	1.37	0.76	0.69
X <sup>+</sup> Substitution													
F6	H	NH <sub>2</sub>	H	CN	H	-5.65	-5.34	-4.05	-3.97	1.60	1.37	0.80	0.69
F7	H	NHCH <sub>3</sub>	H	CN	H	-5.47	-5.23	-3.97	-3.91	1.50	1.32	0.75	0.66
F8	H	N(CH <sub>3</sub> ) <sub>2</sub>	H	CN	H	-5.42	-5.20	-3.88	-3.87	1.54	1.33	0.77	0.67
F9	H	H	NH <sub>2</sub>	CN	H	-5.75	-5.25	-4.26	-4.14	1.49	1.11	0.75	0.56
F10	H	H	NHCH <sub>3</sub>	CN	H	-5.56	-5.14	-4.23	-4.13	1.33	1.01	0.67	0.51
F11	H	H	N(CH <sub>3</sub> ) <sub>2</sub>	CN	H	-5.51	-5.10	-4.14	-4.07	1.37	1.03	0.69	0.52
F12	H	NH <sub>2</sub>	H	CN	CN	-5.80	-5.37	-4.20	-3.99	1.60	1.38	0.80	0.69
F13	H	NHCH <sub>3</sub>	H	CN	CN	-5.68	-5.30	-4.17	-3.98	1.51	1.32	0.76	0.66
F14	H	N(CH <sub>3</sub> ) <sub>2</sub>	H	CN	CN	-5.64	-5.26	-4.05	-3.93	1.59	1.33	0.80	0.67
F15	H	H	NH <sub>2</sub>	CN	CN	-5.97	-5.38	-4.42	-4.17	1.55	1.21	0.78	0.61
F16	H	H	NHCH <sub>3</sub>	CN	CN	-5.81	-5.20	-4.44	-4.18	1.37	1.02	0.69	0.51
F17	H	H	N(CH <sub>3</sub> ) <sub>2</sub>	CN	CN	-5.76	-5.19	-4.37	-4.15	1.39	1.04	0.70	0.52
X <sup>-</sup> versus X <sup>+</sup> Substitution													
F18	NO <sub>2</sub>	NH <sub>2</sub>	H	CN	H	-5.81	-5.52	-4.28	-4.15	1.53	1.37	0.77	0.69
F19	NO <sub>2</sub>	NHCH <sub>3</sub>	H	CN	H	-5.65	-5.45	-4.20	-4.10	1.45	1.35	0.73	0.68
F20	NO <sub>2</sub>	N(CH <sub>3</sub> ) <sub>2</sub>	H	CN	H	-5.59	-5.34	-4.12	-4.02	1.47	1.32	0.74	0.66
F21	NO <sub>2</sub>	H	NH <sub>2</sub>	CN	H	-5.87	-5.37	-4.48	-4.31	1.39	1.06	0.70	0.53

F22	NO <sub>2</sub>	H	NHCH <sub>3</sub>	CN	H	-5.62	-5.22	-4.38	-4.27	1.24	0.95	0.62	0.48
F23	NO <sub>2</sub>	H	N(CH <sub>3</sub> ) <sub>2</sub>	CN	H	-5.66	-5.23	-4.38	-4.25	1.28	0.98	0.64	0.49
F24	NO <sub>2</sub>	NH <sub>2</sub>	H	CN	CN	-6.05	-5.60	-4.48	-4.20	1.57	1.40	0.79	0.70
F25	NO <sub>2</sub>	NHCH <sub>3</sub>	H	CN	CN	-5.86	-5.49	-4.39	-4.17	1.47	1.32	0.74	0.66
F26	NO <sub>2</sub>	N(CH <sub>3</sub> ) <sub>2</sub>	H	CN	CN	-5.75	-5.40	-4.27	-4.07	1.48	1.33	0.74	0.67
F27	NO <sub>2</sub>	H	NH <sub>2</sub>	CN	CN	-6.16	-5.48	-4.68	-4.39	1.48	1.09	0.74	0.55
F28	NO <sub>2</sub>	H	NHCH <sub>3</sub>	CN	CN	-5.97	-5.33	-4.64	-4.38	1.33	0.95	0.67	0.48
F29	NO <sub>2</sub>	H	N(CH <sub>3</sub> ) <sub>2</sub>	CN	CN	-5.90	-5.30	-4.58	-4.32	1.32	0.98	0.66	0.49
F30	CN	NH <sub>2</sub>	H	CN	H	-5.81	-5.53	-4.27	-4.12	1.54	1.41	0.77	0.71
F31	CN	NHCH <sub>3</sub>	H	CN	H	-5.67	-5.45	-4.21	-4.08	1.46	1.37	0.73	0.69
F32	CN	N(CH <sub>3</sub> ) <sub>2</sub>	H	CN	H	-5.58	-5.32	-4.12	-4.00	1.46	1.32	0.73	0.66
F33	CN	H	NH <sub>2</sub>	CN	H	-5.89	-5.37	-4.52	-4.30	1.37	1.07	0.69	0.54
F34	CN	H	NHCH <sub>3</sub>	CN	H	-5.73	-5.24	-4.49	-4.28	1.24	0.96	0.62	0.48
F35	CN	H	N(CH <sub>3</sub> ) <sub>2</sub>	CN	H	-5.67	-5.24	-4.39	-4.24	1.28	1.00	0.64	0.50
F36	CN	NH <sub>2</sub>	H	CN	CN	-6.01	-5.60	-4.46	-4.18	1.55	1.42	0.78	0.71
F37	CN	NHCH <sub>3</sub>	H	CN	CN	-5.87	-5.49	-4.40	-4.13	1.47	1.36	0.74	0.68
F38	CN	N(CH <sub>3</sub> ) <sub>2</sub>	H	CN	CN	-5.74	-5.37	-4.30	-4.07	1.44	1.30	0.72	0.65
F39	CN	H	NH <sub>2</sub>	CN	CN	-6.16	-5.48	-4.70	-4.38	1.46	1.10	0.73	0.55
F40	CN	H	NHCH <sub>3</sub>	CN	CN	-5.98	-5.33	-4.71	-4.38	1.27	0.95	0.64	0.48
F41	CN	H	N(CH <sub>3</sub> ) <sub>2</sub>	CN	CN	-5.93	-5.29	-4.62	-4.29	1.31	1.00	0.66	0.50

While no change is observed between the LUMO energies of the NO<sub>2</sub>-substituted derivatives (i.e. F1 and F4) and their corresponding CN-substituted counterparts (i.e. F2 and F5, respectively), the CN-substituted derivatives seem to possess greater electron releasing tendency in water and consequently more vulnerable to oxidation compared to the NO<sub>2</sub>-substituted counterparts due to the low electron withdrawing impact of CN. Overall, the dyes are more reactive and more prone to photo-excitation in water compared

to gas as revealed by the low aqueous phase HOMO-LUMO energy gap, hardness and softness values (Tables 9.3 and A.21 (Appendix)). The aqueous phase electronegativity and chemical potential values confirm low vulnerability to reduction and high susceptibility to oxidation in water compared to gas. Both the parent dye and the X-substituted derivatives appear to be more electrophilic in water which suggests higher potency towards a nucleophilic attack. The additional electron withdrawing CN substituent at position R<sub>7</sub>, which increases electron deficiency for F3, explains why this derivative is more electronegative but less electropositive compared to DR73 in both gas and water.

### 9.3.8 EFFECTS OF X<sup>+</sup> SUBSTITUTION ON REACTIVITY

Substitution of NH<sub>2</sub>, NHCH<sub>3</sub> and N(CH<sub>3</sub>)<sub>2</sub> groups at positions R<sub>4</sub> and R<sub>5</sub> in DR73 leads to increase in HOMO and LUMO energies, where the increase is directly proportional to the electron donating powers of the substituents as observed for F6 – F8 and F9 – F11 (Table 9.3). This suggests that the derivatives are better electron donors and are as a result, more predisposed to oxidation but less vulnerable to reduction in both gas and water compared to the parent dye. The highest values of HOMO and LUMO energies obtained for F8 and F11 is due to the highest electron donating strength of N(CH<sub>3</sub>)<sub>2</sub> among the three amino substituents. The apparent higher HOMO and LUMO energies obtained in the gas phase for F6 – F8 compared to F9 – F11 respectively, suggest that the electron donating effect of the X<sup>+</sup> groups is higher at position R<sub>4</sub> in the gas phase, whereas the opposite is the case in water where the HOMO energies for F9 – F11 are higher, suggesting greater donating impact at position R<sub>5</sub> in water. This is in line with the earlier assumption that the X<sup>+</sup> groups demonstrate higher electron donating influence at position R<sub>5</sub> (Fig. 9.1). Although, the aqueous phase LUMO energies for F9 – F11 are still smaller

than those of F6 – F8 respectively, thorough inspection of the results revealed that the LUMO energies for F9 – F11 increase from gas to water by a larger magnitude compared to F6 – F8. This also indicates that the donating impact is more enhanced by water when the substituents are attached to position R<sub>5</sub>.

Except for F6 – F8 in water, the relatively low HOMO-LUMO energy gap and hardness (Table 9.3), and the resulting higher softness (Appendix: Table A.21) obtained for F6 – F11 compared to DR73, implies that the derivatives will be more reactive and more vulnerable to photo-excitation, where F9 – F11, which contain the substituents at position R<sub>5</sub>, are expected to be the most vulnerable derivatives in this group. The insignificant change in reactivity observed especially for F7 and F8 compared to DR73 in water may be due to reduction in the electron donating impact of the substituents at position R<sub>4</sub> which leads to small changes in the HOMO energies. In general, the reactivity parameters suggest that both the parent and the derivatives are more reactive in water than in gas.

With F9 as the only exception in the gas phase, the electronegativity and chemical potential results obtained in both gas and water phases revealed that the X<sup>+</sup>-substituted derivatives are less electronegative than the parent dye. This may be due to increased electron population in the derivatives as a result of the electron donating effect of the substituents. The relatively large electronegativity values obtained for F9-F11 compared to F6-F8 may be due to increase in the net nuclear charges generated in the former by their relatively large electron density as revealed by their screening charges (Table 9.2). Both sets of derivatives differ only in the positions of their substituents. The results of electrophilicity suggest F6 – F8 as being more nucleophilic than DR73, which is more nucleophilic than F9 – F11 both in the gas and water phases.

Introduction of  $-\text{CN}$  group to F6 – F11 at position R<sub>7</sub> (Fig. 9.1) lowers the HOMO and LUMO energies with no marked changes observed in the energy gap, hardness and softness (Table 9.3) especially in water. This implies that the extra electron withdrawing CN substituent reduces the chance of oxidation, promotes the likelihood of reduction, but produces no significant change in the overall stability of the derivatives. However, substantial changes occur in electronegativity, chemical potential and electrophilicity as can be observed for F12 – F17 compared to F6 – F11, respectively (Appendix: Table A.21) which shows F12 – F17 as being more electronegative, less electropositive and more electrophilic than F6 – F11.

### 9.3.9 EFFECTS OF X<sup>-</sup> AND X<sup>+</sup> ON REACTIVITY

Replacing the hydrogen atom at position R<sub>3</sub> in F6 – F11 with electron withdrawing NO<sub>2</sub> substituent decreases the HOMO and the LUMO energies, the energy gap, the hardness, and the chemical potential, but increases the softness, the electronegativity and the electrophilicity especially in the gas phase, as can be observed for F18 – F23 (Tables 9.3 and A.21 (Appendix)). This suggests that these derivatives are less prone to oxidation, more susceptible to reduction, more chemically reactive, less electropositive, and less nucleophilic compared to F6 – F11. Comparing derivatives F18 – F23 to F30 – F35, respectively, shows clearly that replacement of the NO<sub>2</sub> substituent in the former with CN substituent in the latter, brings about no substantial change in the reactivity parameters, which suggests that both the NO<sub>2</sub> and the CN substituents produce nearly the same effect on F6 – F11.

Compared to DR73 in the gas phase, substitution of both of X<sup>-</sup> and X<sup>+</sup> groups results in a general decrease in the LUMO energy and an increase in the HOMO energy except for

derivatives F18, F21, F30 and F33 where the  $X^+$  component is  $\text{NH}_2$  which has lower electron donating power. The relatively low LUMO energies of the derivatives suggest that they are more susceptible to reduction while their higher HOMO energies suggest higher vulnerability to oxidation compared to the parent dye. Since these opposing changes in the LUMO and the HOMO energies are characteristic effects of electron withdrawing substituents and electron donating substituents, respectively, it is reasonable to conclude that the influence of the higher  $X^+$  groups (i.e.  $\text{NHCH}_3$  and  $\text{N}(\text{CH}_3)_2$ ) on the HOMO energy predominates that of the  $X^-$  groups (i.e.  $\text{NO}_2$  and  $\text{CN}$ ), whereas the inverse is the case for the LUMO energy. The decrease in HOMO-LUMO energy gap and hardness (Table 9.3), and the consequent increase in softness values (Appendix: Table A.21) obtained for F18 – F23 and F30 – F35 compared to DR73 revealed that these derivatives are less stable, more predisposed to photo-excitation and hence, will have shorter lifetime in the environment.

Except for F19, F20, F31 and F32 where the higher  $X^+$  groups (i.e.  $\text{NHCH}_3$  and  $\text{N}(\text{CH}_3)_2$ ) are attached to position  $\text{R}_4$ , the derivatives appear to be more electronegative and less electropositive than the parent dye which seems to be a better nucleophile as revealed by the electrophilicity results (Appendix: Table A.21). Electron withdrawing substituents ( $X^-$ ) decrease the power of a molecule to release electrons, but increase its power to attract them. The more the  $X^-$  groups in a molecule, the more electrons will be attracted and vice versa. Addition of electron donating substituents ( $X^+$ ) reduces the power to attract electrons, and the extent of the reduction depends on the donating capacity of the  $X^+$  substituent in relation to its position in the molecule. For instance, the decrease in electronegativity and the consequent increase in electropositivity observed for F19, F20, F31 and F32 compared to DR73 may be ascribed to the higher electron donating



influence of  $\text{NHCH}_3$  and  $\text{N}(\text{CH}_3)_2$  which tend to decrease the impact of the electron withdrawing  $\text{NO}_2$  and  $\text{CN}$  substituents. In addition, careful inspection of Table A.21 (Appendix) also showed that the chemical potential increases with decreasing electronegativity for the  $\text{X}^-$  plus  $\text{X}^+$  substituted derivatives, as electron donating power of the  $\text{X}^+$  component increases.

Transiting from gas to water, the overall reactivity of F18 – F23 and F30 – F35 increases with increase in oxidation tendency as the likelihood of reduction decreases, while the ability to release electrons and the vulnerability to a nucleophilic attack increase. This is because water reduces the HOMO-LUMO energy gap, the hardness and the electronegativity, but increases the HOMO and LUMO energies, the softness, the chemical potential and the electrophilicity as revealed by Tables 9.3 and A.21 (Appendix). However, careful inspection of the tables showed that the impact of water on these reactivity parameters varies with the electron donating capacity of the  $\text{X}^+$  components as clearly revealed by F18 – F20, F21 – F23, F30 – F32 and F33 – F35. The observed changes in the reactivity parameters discussed above are consequences of enhanced electron donating influence of the  $\text{X}^+$  components caused by water.

Similar arguments as in above are also valid for derivatives F24 – F29 and F36 – F41, but in these cases, the extra electron withdrawing  $\text{CN}$  substituent attached to position  $\text{R}_7$  (Fig. 9.1) further decreases the HOMO and LUMO energies, and the chemical potential, increases the electronegativity and electrophilicity, but brings about no marked changes in the energy gap, the hardness and the softness. The  $\text{CN}$  substituent at  $\text{R}_7$  makes the derivatives more electron deficient, hence, the observed changes in the reactivity parameters.

### 9.3.10 PREDICTION OF SUITABLE CATALYSTS FOR PHOTOCATALYTIC DEGRADATION OF THE DYES

The band structures for Si, CdSe, CdS, TiO<sub>2</sub>, ZnO and ZnS semiconductors which comprise the valence band edge, the conduction band edge and the band gap are given in Table A.15 (Appendix). Si, CdSe and CdS have band gap values < 3.0 eV hence, they are visible light (Vis) active [79]. The band gap values for TiO<sub>2</sub>, ZnO and ZnS are > 3.0 eV hence, they are ultraviolet (UV) active [79]. The energy differences between the HOMOs (i.e. the electron rich portion) of the studied dyes and the conduction band minima (CBM) (i.e. the electron deficient part) of the catalysts ( $\beta$ ) as well as the difference between the LUMOs (i.e. the electron deficient portion) and the valence band maxima (VBE) (i.e. the electron rich portion) of the catalysts ( $\alpha$ ) are given in Table 9.4. The relative affinities of the studied dyes for the semiconductors are evaluated from  $\alpha$  and  $\beta$  to identify the catalyst(s) with the highest catalytic potential for their degradation. The likelihood of a spontaneous interaction between the catalysts and the dyes is dependent on the size of  $\alpha$  and/or  $\beta$ . The smaller the value of  $\alpha$ , the higher the likelihood of electron donation into the LUMO of the dyes. Similarly, the smaller the magnitude of  $\beta$ , the greater the probability of electron donation into the conduction band minima of the catalysts. For a given dye-catalyst pair, the frontier molecular orbital/band edge combination (i.e. LUMO/VBE or HOMO/CBE) with the smaller energy gap is the most preferred combination for interaction.

According to Table 9.4, the  $\alpha_{\text{Si}}$ ,  $\beta_{\text{Si}}$ , and  $\alpha_{\text{CdSe}}$  values for Si and CdSe respectively, suggest that they are better candidates among the visible light activated catalysts for the photodegradation of the dyes compared to CdS. However, the interaction of these catalysts with the dyes will preferably occur via a LUMO-VBM interaction mode. In

addition, the HOMO of Si may also be involved in the interaction to favor a HOMO-CBM type of overlap compared to CdSe and CdS as suggested by the  $\beta$  values. In the case of the UV-activated series, the  $\alpha$  values suggest ZnO as having the highest affinity for the dyes through a LUMO-VBM interaction mode, while the  $\beta$  values favor TiO<sub>2</sub> as the catalyst with the highest chance of interacting with the HOMOs of the dyes using the CBM. Overall, the most appropriate of the studied semiconductors for degrading the dyes is ZnO because it produces the smallest energy gap with the dyes. Such exceptional photocatalytic potential of ZnO is in accordance with what has been reported elsewhere [80, 81].

The  $\alpha$  and  $\beta$  values generally suggest that the HOMOs and the LUMOs of the NO<sub>2</sub> substituted derivatives have lower affinity for the studied catalysts compared to those of the CN counterparts. This suggests the CN substituted derivatives as being more vulnerable to interaction with the catalysts which leads to degradation.

For the X<sup>+</sup> substituted derivatives, the  $\beta$  values decrease with increasing order of electron donating capacity of the substituents (i.e. NH<sub>2</sub> < NHCH<sub>3</sub> < N(CH<sub>3</sub>)<sub>2</sub>) whereas the  $\alpha$  values show an opposite trend. The variation in the  $\alpha$  and  $\beta$  values are reflections of the trends observed in the HOMO and LUMO energies (Table 9.4) discussed earlier.

**Table 9. 4:** Calculated energy gaps between the FMO (i.e. HOMO and LUMO) of the studied dyes and the band edges of the catalysts.

Dyes	$\alpha^*_{Si}$	$\beta^{**}_{Si}$	$\alpha^*_{CdSe}$	$\beta^{**}_{CdSe}$	$\alpha^*_{CdS}$	$\beta^{**}_{CdS}$	$\alpha^*_{TiO_2}$	$\beta^{**}_{TiO_2}$	$\alpha^*_{ZnO}$	$\beta^{**}_{ZnO}$	$\alpha^*_{ZnS}$	$\beta^{**}_{ZnS}$
	(eV)	(eV)	(eV)	(eV)	(eV)	(eV)	(eV)	(eV)	(eV)	(eV)	(eV)	(eV)
DR73	0.88	1.56	0.66	2.56	1.69	2.31	3.64	0.78	0.04	4.81	1.13	4.17
X <sup>-</sup> substituted derivatives												
F1	0.64	1.75	0.42	2.75	1.45	2.50	3.40	0.97	-0.20	5.00	0.89	4.36
F2	0.59	1.72	0.37	2.72	1.40	2.47	3.35	0.94	-0.25	4.97	0.84	4.33
F3	0.67	1.78	0.45	2.78	1.48	2.53	3.43	1.00	-0.17	5.03	0.92	4.39
F4	0.44	1.99	0.22	2.99	1.25	2.74	3.20	1.21	-0.40	5.24	0.69	4.60
F5	0.39	1.93	0.17	2.93	1.20	2.68	3.15	1.15	-0.45	5.18	0.64	4.54
X <sup>+</sup> substituted derivatives												
F6	0.99	1.41	0.77	2.41	1.80	2.16	3.75	0.63	0.15	4.66	1.24	4.02
F7	1.07	1.23	0.85	2.23	1.88	1.98	3.83	0.45	0.23	4.48	1.32	3.84
F8	1.19	1.18	0.94	2.18	1.97	1.93	3.92	0.40	0.32	4.43	1.41	3.79
F9	0.78	1.51	0.56	2.51	1.59	2.26	3.54	0.73	-0.06	4.76	1.03	4.12
F10	0.81	1.32	0.59	2.32	1.62	2.07	3.57	0.54	-0.03	4.57	1.06	3.93
F11	0.90	1.27	0.68	2.27	1.71	2.02	3.66	0.49	0.06	4.52	1.15	3.88
F12	0.84	1.56	0.62	2.56	1.65	2.31	3.60	0.78	0.00	4.81	1.09	4.17
F13	0.87	1.44	0.65	2.44	1.68	2.19	3.63	0.66	0.03	4.69	1.12	4.05
F14	0.99	1.40	0.77	2.40	1.80	2.15	3.75	0.62	0.15	4.65	1.24	4.01
F15	0.62	1.73	0.40	2.73	1.43	2.48	3.38	0.95	-0.22	4.98	0.87	4.34
F16	0.60	1.57	0.38	2.57	1.41	2.32	3.36	0.79	-0.24	4.82	0.85	4.18
F17	0.67	1.52	0.45	2.52	1.48	2.27	3.43	0.74	-0.17	4.77	0.92	4.13
X <sup>-</sup> versus X <sup>+</sup> Substitution												
F18	0.76	1.57	0.54	2.57	1.57	2.32	3.52	0.79	-0.08	4.82	1.01	4.18
F19	0.84	1.41	0.62	2.41	1.65	2.16	3.60	0.63	0.00	4.66	1.09	4.02
F20	0.92	1.35	0.70	2.35	1.73	2.10	3.68	0.57	0.08	4.60	1.17	3.96
F21	0.56	1.63	0.34	2.63	1.37	2.38	3.32	0.85	-0.28	4.88	0.81	4.24

F22	0.66	1.38	0.44	2.38	1.47	2.13	3.42	0.60	-0.18	4.63	0.91	3.99
F23	0.66	1.42	0.44	2.42	1.47	2.17	3.42	0.64	-0.18	4.67	0.91	4.03
F24	0.56	1.81	0.34	2.81	1.37	2.56	3.32	1.03	-0.28	5.06	0.81	4.42
F25	0.65	1.62	0.43	2.62	1.46	2.37	3.41	0.84	-0.19	4.87	0.90	4.23
F26	0.77	1.51	0.55	2.51	1.58	2.26	3.53	0.73	-0.07	4.76	1.02	4.12
F27	0.36	1.92	0.14	2.92	1.17	2.67	3.12	1.14	-0.48	5.17	0.61	4.53
F28	0.40	1.73	0.18	2.73	1.21	2.48	3.16	0.95	-0.44	4.98	0.65	4.34
F29	0.46	1.66	0.24	2.66	1.27	2.41	3.22	0.88	-0.38	4.91	0.71	4.27
F30	0.77	1.57	0.55	2.57	1.58	2.32	3.53	0.79	-0.07	4.82	1.02	4.18
F31	0.83	1.43	0.61	2.43	1.64	2.18	3.59	0.65	-0.01	4.68	1.08	4.04
F32	0.92	1.34	0.70	2.34	1.73	2.09	3.68	0.56	0.08	4.59	1.17	3.95
F33	0.52	1.65	0.30	2.65	1.33	2.40	3.28	0.87	-0.32	4.90	0.77	4.26
F34	0.55	1.49	0.33	2.49	1.36	2.24	3.31	0.71	-0.29	4.74	0.80	4.10
F35	0.65	1.43	0.43	2.43	1.46	2.18	3.41	0.65	-0.19	4.68	0.90	4.04
F36	0.58	1.77	0.36	2.77	1.39	2.52	3.34	0.99	-0.26	5.02	0.83	4.38
F37	0.64	1.63	0.42	2.63	1.45	2.38	3.40	0.85	-0.20	4.88	0.89	4.24
F38	0.74	1.50	0.52	2.50	1.55	2.25	3.50	0.72	-0.10	4.75	0.99	4.11
F39	0.34	1.92	0.12	2.92	1.15	2.67	3.10	1.14	-0.50	5.17	0.59	4.53
F40	0.33	1.74	0.11	2.74	1.14	2.49	3.09	0.96	-0.51	4.99	0.58	4.35
F41	0.42	1.69	0.20	2.69	1.23	2.44	3.18	0.91	-0.42	4.94	0.67	4.30

$$\alpha^* = E_{\text{LUMO}} - E_{\text{VBE}} \text{ and } \beta^{**} = E_{\text{CBE}} - E_{\text{HOMO}}$$

### 9.3.11 SITE SELECTIVITY STUDY FOR RADICAL ATTACK AND PREDICTION OF PHOTODEGRADATION PATHWAY

The Fukui functions for prospective sites for radical attack are provided in Table 9.5. These sites are C4, N7, N8 and C9 (Fig. 9.5). In the parent dye and most of the studied derivatives, the most vulnerable sites to the attack of photo-generated hydroxyl radicals are the azo nitrogen atoms especially the one next to the donor moiety (i.e. N8), which

will result to an N – N bond cleavage photodegradation pathway. On the other hand, derivatives such as F18, F25 and F31 will give precedence to a C – N bond cleavage mechanism because the most susceptible center to radical attack is their C9 atom. However, there are chances that some of the studied derivatives such as F7, F13, F20, F24, F30 and F37 will favor a competing N – N and C – N bond cleavage photodegradation pathway as a result of slight differences in the Fukui functions of their C9 and N7 radical attack centers.

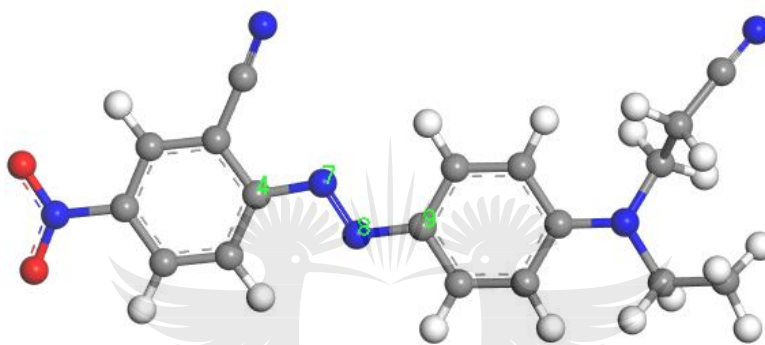


**Figure 9. 5:** Optimized model of DR73 showing the prospective sites for attack of radicals. Constituent atoms are carbon (grey), hydrogen (white), nitrogen (blue) and oxygen (red).

The higher vulnerability to radical attack observed for the azo nitrogen atoms in most of the studied derivatives may be due to the electron withdrawing impact of the acceptor moiety on the azo bridge, coupled with those of the CN substituent at position R<sub>6</sub> and the extra CN substituent at position R<sub>7</sub> in some of the derivatives. It should be recalled that substitution of the donor moiety with additional CN group at position R<sub>7</sub> reduces the electron donating impact of the donor moiety. This explains why electron donations from this moiety could not sufficiently shield the N8 atom from radical attack. Nevertheless, this atom should be less susceptible to radical attack compared to N7 which is closer to the acceptor ring. However, it seems the N7 atom inductively attracts electrons from N8

thereby making N8 more vulnerable to radical attack. The relatively small Fukui function values obtained for the  $X^+$  substituted derivatives and the  $X^-$  plus  $X^+$  substituted derivatives compared to the  $X^-$  substituted counterparts (Table 9.5) are reflections of the electron donating influence of the  $X^+$  groups which tend to minimize the electron withdrawing influence of the acceptor moiety.

**Table 9. 5:** Fukui functions,  $f^0$  for prospective sites for radical attack in the studied dyes.

Dye No.	R3	R4	R5	R6	R7	$f^0$			
						C4	N7	N8	C9
DR73	H	H	H	CN	H	0.025	0.057	0.058	0.034
X <sup>-</sup> substituted derivatives									
F1	NO <sub>2</sub>	H	H	CN	H	0.022	0.046	0.049	0.035
F2	CN	H	H	CN	H	0.023	0.054	0.060	0.035
F3	H	H	H	CN	CN	0.025	0.061	0.064	0.032
F4	NO <sub>2</sub>	H	H	CN	CN	0.020	0.051	0.058	0.032
F5	CN	H	H	CN	CN	0.023	0.058	0.066	0.034
X <sup>+</sup> substituted derivatives									
F6	H	NH <sub>2</sub>	H	CN	H	0.023	0.045	0.040	0.039
F7	H	NHCH <sub>3</sub>	H	CN	H	0.022	0.039	0.032	0.040
F8	H	N(CH <sub>3</sub> ) <sub>2</sub>	H	CN	H	0.024	0.042	0.044	0.037
F9	H	H	NH <sub>2</sub>	CN	H	0.021	0.045	0.046	0.026
F10	H	H	NHCH <sub>3</sub>	CN	H	0.021	0.035	0.041	0.022
F11	H	H	N(CH <sub>3</sub> ) <sub>2</sub>	CN	H	0.021	0.035	0.040	0.024
F12	H	NH <sub>2</sub>	H	CN	CN	0.023	0.044	0.040	0.039
F13	H	NHCH <sub>3</sub>	H	CN	CN	0.022	0.040	0.034	0.039
F14	H	N(CH <sub>3</sub> ) <sub>2</sub>	H	CN	CN	0.023	0.046	0.049	0.035
F15	H	H	NH <sub>2</sub>	CN	CN	0.022	0.050	0.055	0.028
F16	H	H	NHCH <sub>3</sub>	CN	CN	0.020	0.037	0.043	0.020

F17	H	H	N(CH <sub>3</sub> ) <sub>2</sub>	CN	CN	0.020	0.037	0.044	0.021
X <sup>-</sup> versus X <sup>+</sup> Substitution									
F18	NO <sub>2</sub>	NH <sub>2</sub>	H	CN	H	0.022	0.038	0.032	0.041
F19	NO <sub>2</sub>	NHCH <sub>3</sub>	H	CN	H	0.021	0.034	0.026	0.040
F20	NO <sub>2</sub>	N(CH <sub>3</sub> ) <sub>2</sub>	H	CN	H	0.021	0.035	0.035	0.034
F21	NO <sub>2</sub>	H	NH <sub>2</sub>	CN	H	0.020	0.037	0.039	0.025
F22	NO <sub>2</sub>	H	NHCH <sub>3</sub>	CN	H	0.021	0.028	0.034	0.022
F23	NO <sub>2</sub>	H	N(CH <sub>3</sub> ) <sub>2</sub>	CN	H	0.020	0.029	0.036	0.023
F24	NO <sub>2</sub>	NH <sub>2</sub>	H	CN	CN	0.021	0.040	0.036	0.039
F25	NO <sub>2</sub>	NHCH <sub>3</sub>	H	CN	CN	0.021	0.035	0.028	0.039
F26	NO <sub>2</sub>	N(CH <sub>3</sub> ) <sub>2</sub>	H	CN	CN	0.020	0.037	0.041	0.034
F27	NO <sub>2</sub>	H	NH <sub>2</sub>	CN	CN	0.019	0.041	0.044	0.025
F28	NO <sub>2</sub>	H	NHCH <sub>3</sub>	CN	CN	0.019	0.032	0.039	0.020
F29	NO <sub>2</sub>	H	N(CH <sub>3</sub> ) <sub>2</sub>	CN	CN	0.019	0.030	0.040	0.021
F30	CN	NH <sub>2</sub>	H	CN	H	0.023	0.042	0.041	0.40
F31	CN	NHCH <sub>3</sub>	H	CN	H	0.023	0.036	0.034	0.040
F32	CN	N(CH <sub>3</sub> ) <sub>2</sub>	H	CN	H	0.022	0.037	0.042	0.035
F33	CN	H	NH <sub>2</sub>	CN	H	0.020	0.040	0.045	0.026
F34	CN	H	NHCH <sub>3</sub>	CN	H	0.020	0.033	0.040	0.022
F35	CN	H	N(CH <sub>3</sub> ) <sub>2</sub>	CN	H	0.020	0.033	0.041	0.024
F36	CN	NH <sub>2</sub>	H	CN	CN	0.023	0.044	0.043	0.039
F37	CN	NHCH <sub>3</sub>	H	CN	CN	0.022	0.038	0.035	0.039
F38	CN	N(CH <sub>3</sub> ) <sub>2</sub>	H	CN	CN	0.021	0.039	0.046	0.033
F39	CN	H	NH <sub>2</sub>	CN	CN	0.019	0.044	0.051	0.025
F40	CN	H	NHCH <sub>3</sub>	CN	CN	0.019	0.036	0.043	0.021
F41	CN	H	N(CH <sub>3</sub> ) <sub>2</sub>	CN	CN	0.019	0.036	0.046	0.023



### 9.3.12 PREDICTION OF THE ABSORPTION WAVELENGTHS OF SELECTED DISPERSE RED DYES

To verify the reliability of the B3LYP/6-31G\* for predicting absorption wavelength of azo dyes, this level of theory was tested on a number of disperse azo dyes which are mostly of disperse red family with known experimental absorption wavelength. The selected dyes are azobenzene (AZB), Disperse red 1 (DR1), Disperse red 19 (DR19), Disperse red 78 (DR78), Disperse red 13 (DR13), Disperse red 73 (DR73), dye X and dye Y with molecular structures shown in Figure A.2 (Appendices).

The calculated absorption wavelengths ( $\lambda_{CIS}$  and  $\lambda_{H-L}$ ) for the test molecules are compared with their respective experimental values in Table 9.6. Except for dyes X and Y whose  $\lambda_{CIS}$  values deviate largely from both  $\lambda_{H-L}$  and  $\lambda_{Expt}$  values, it is evident from the table that  $\lambda_{CIS}$  and  $\lambda_{H-L}$  values of the dyes are in good agreement with each other and with their respective experimental values, which validates the selected level of theory.

Since the  $\lambda_{H-L}$  values compare very well with the  $\lambda_{Expt}$  values for most of the dyes, and also reproduced the experimental values better than  $\lambda_{CIS}$ , it is reasonable to conclude that the HOMO-LUMO energy gap is a reliable parameter for predicting the absorption wavelengths of azo dyes, and that the  $\lambda_{CIS}$  values are probably due to electronic transition from the HOMO to the LUMO of AZB, DR1, DR19, DR78, DR13 and DR73, which corresponds to  $n \rightarrow \pi^*$  transition. Also, since the experimental absorption wavelengths were obtained in the presence of solvent, the bathochromic shift observed between the predicted wavelengths and the experimental values may be attributed to solvent effect. For instance, the experimental absorption wavelength of AZB which corresponds to a  $\pi \rightarrow \pi^*$  was obtained as 314 nm in ethanol [82]. The excellent agreement between this value and the predicted values in Table 9.6 is indicative of a negligible solvent effect on the

absorption wavelength of AZB which is not unexpected considering the absence of polar groups in the dye structure (Appendices: Fig. A.2).

**Table 9. 6:** Comparison of predicted and experimental absorption wavelengths of some test azo disperse dyes.

Dyes	$\lambda_{cis}$ (nm)	H-L gap (eV)	$\lambda_{H-L}$ (nm)	$\lambda_{Expt.}$ (nm)
AZB	309	3.95	314	260-420 [82-84]
DR1	422	2.90	428	390-550 [76, 85]
DR19	421	2.92	425	285, 495 [82]
DR78	423	2.91	426	481 [37]
DR13	434	2.80	443	520 [86]
DR73	427	2.84	437	500 [37]
Dye X	323	3.12	397	432 [25]
Dye Y	328	2.96	419	449 [25]

### 9.3.13 EFFECTS OF SUBSTITUTION ON THE ABSORPTION WAVELENGTH OF DR73

It is a literature fact that the absorption wavelength of monoazo dye depends on the type of substituent groups present in the dye as well as the substitution position. Tuning the electron withdrawing ability of the diazotizing component and/or the electron donating capacity of the coupling component of an azo dye using different electron withdrawing and electron donating substituent groups can have tremendous impact on its absorption wavelength and intensity among other properties [24-29]. The predicted absorption wavelength for DR73 and its studied analogues are presented in Table 9.7 alongside with the corresponding excitation energies between the HOMOs and LUMOs of dyes. It has been observed from Table 9.6 that HOMO-LUMO energy gap yielded better theoretical absorption wavelength for azo disperse dyes compared to the direct approach which

employs CIS calculation. Therefore, the effect of the studied substituents on the absorption wavelength of DR73 will be discussed using  $\lambda_{H-L}$  values.

**Table 9. 7:** Predicted dipole moment ( $\mu$ ), HOMO-LUMO energy gap ( $H-L$  gap) and absorption wavelength ( $\lambda_{CIS}$  and  $\lambda_{H-L}$ ) of DR73 and its studied analogues.

Dye	R3	R4	R5	R6	R7	$\mu$ (Debye)	$\lambda_{CIS}$ (nm)	Intensity	H-L gap (eV)	$\lambda_{H-L}$ (nm)
DR73	H	H	H	CN	H	10.85	426.77	1.29	2.84	436.62
X <sup>-</sup> substituted derivatives										
F1	NO <sub>2</sub>	H	H	CN	H	8.89	441.65	1.02	2.78	446.04
F2	CN	H	H	CN	H	8.34	439.18	1.38	2.70	459.25
F3	H	H	H	CN	CN	5.91	414.92	1.31	2.97	417.51
F4	NO <sub>2</sub>	H	H	CN	CN	4.37	429.33	1.01	2.90	427.59
F5	CN	H	H	CN	CN	4.48	430.69	1.32	2.82	439.72
X <sup>+</sup> substituted derivatives										
F6	H	NH <sub>2</sub>	H	CN	H	12.47	438.74	0.89	2.75	450.91
F7	H	NHCH <sub>3</sub>	H	CN	H	13.36	417.77	0.92	2.81	441.28
F8	H	N(CH <sub>3</sub> ) <sub>2</sub>	H	CN	H	10.44	433.61	1.28	2.78	446.04
F9	H	H	NH <sub>2</sub>	CN	H	6.74	357.83	0.64	2.73	454.21
F10	H	H	NHCH <sub>3</sub>	CN	H	6.34	427.70	0.62	2.53	490.12
F11	H	H	N(CH <sub>3</sub> ) <sub>2</sub>	CN	H	9.44	433.15	0.84	2.61	475.09
F12	H	NH <sub>2</sub>	H	CN	CN	7.61	437.63	0.85	2.82	439.72
F13	H	NHCH <sub>3</sub>	H	CN	CN	8.45	403.31	0.79	2.86	433.57
F14	H	N(CH <sub>3</sub> ) <sub>2</sub>	H	CN	CN	8.33	405.14	0.89	2.75	450.91
F15	H	H	NH <sub>2</sub>	CN	CN	3.86	355.30	0.98	2.89	429.06
F16	H	H	NHCH <sub>3</sub>	CN	CN	3.93	412.97	0.68	2.64	469.70
F17	H	H	N(CH <sub>3</sub> ) <sub>2</sub>	CN	CN	4.39	423.25	0.91	2.70	459.26
X <sup>-</sup> and X <sup>+</sup> substituted derivatives										
F18	NO <sub>2</sub>	NH <sub>2</sub>	H	CN	H	10.27	419.38	1.00	2.77	447.65
F19	NO <sub>2</sub>	NHCH <sub>3</sub>	H	CN	H	11.25	442.80	0.59	2.72	455.88

F20	NO <sub>2</sub>	N(CH <sub>3</sub> ) <sub>2</sub>	H	CN	H	11.52	424.26	0.49	2.68	462.69
F21	NO <sub>2</sub>	H	NH <sub>2</sub>	CN	H	7.69	435.74	0.39	2.52	492.06
F22	NO <sub>2</sub>	H	NHCH <sub>3</sub>	CN	H	7.87	443.93	0.51	2.42	512.40
F23	NO <sub>2</sub>	H	N(CH <sub>3</sub> ) <sub>2</sub>	CN	H	8.00	450.75	0.76	2.50	496.00
F24	NO <sub>2</sub>	NH <sub>2</sub>	H	CN	CN	5.90	411.81	0.98	2.81	441.28
F25	NO <sub>2</sub>	NHCH <sub>3</sub>	H	CN	CN	6.47	428.88	0.44	2.76	449.27
F26	NO <sub>2</sub>	N(CH <sub>3</sub> ) <sub>2</sub>	H	CN	CN	6.50	424.72	0.73	2.67	464.42
F27	NO <sub>2</sub>	H	NH <sub>2</sub>	CN	CN	3.53	425.67	0.46	2.64	469.70
F28	NO <sub>2</sub>	H	NHCH <sub>3</sub>	CN	CN	3.80	429.81	0.54	2.51	494.02
F29	NO <sub>2</sub>	H	N(CH <sub>3</sub> ) <sub>2</sub>	CN	CN	3.87	440.38	0.77	2.60	476.92
F30	CN	NH <sub>2</sub>	H	CN	H	10.79	427.96	1.30	2.65	467.92
F31	CN	NHCH <sub>3</sub>	H	CN	H	11.10	425.77	1.03	2.76	449.27
F32	CN	N(CH <sub>3</sub> ) <sub>2</sub>	H	CN	H	11.12	429.08	0.78	2.69	460.97
F33	CN	H	NH <sub>2</sub>	CN	H	7.86	438.13	0.57	2.47	502.02
F34	CN	H	NHCH <sub>3</sub>	CN	H	7.98	445.41	0.71	2.38	521.01
F35	CN	H	N(CH <sub>3</sub> ) <sub>2</sub>	CN	H	8.10	448.16	0.99	2.46	504.06
F36	CN	NH <sub>2</sub>	H	CN	CN	6.01	418.63	1.09	2.69	460.97
F37	CN	NHCH <sub>3</sub>	H	CN	CN	6.17	414.73	0.88	2.80	442.86
F38	CN	N(CH <sub>3</sub> ) <sub>2</sub>	H	CN	CN	6.57	418.67	1.03	2.65	467.92
F39	CN	H	NH <sub>2</sub>	CN	CN	3.73	428.87	0.60	2.58	480.62
F40	CN	H	NHCH <sub>3</sub>	CN	CN	3.93	434.18	0.67	2.47	502.02
F41	CN	H	N(CH <sub>3</sub> ) <sub>2</sub>	CN	CN	4.25	440.00	1.01	2.53	490.11

Substitution of the X<sup>-</sup> groups at position R<sub>3</sub> in DR73 resulted to a decrease in dipole moment and HOMO-LUMO energy gap, where the highest decrease was obtained with CN probably because this substituent group exhibited higher electron withdrawing ability than NO<sub>2</sub> at this position. As dipole moment and HOMO-LUMO gap decreased from DR73 to F1 and F2, and from F3 to F4 and F5, the absorption wavelength is red-shifted in that

order. This suggests that absorption wavelength is inversely proportional to HOMO-LUMO gap and dipole moment. Recall from Figure A.1 (Appendix) that electron density is higher in the acceptor moiety compared to the donor moiety of DR73. Therefore, substitution of the X<sup>-</sup> groups at position R<sub>3</sub> in this dye will bring about a decrease of electron density in the acceptor ring and consequently a reduction in charge density difference and dipole moment between the acceptor and the donor moieties.

The presence of an extra terminal electron withdrawing -CN substituent at position R<sub>7</sub> decreased the charge density in the donor ring. The cooperative electron withdrawing effects of this substituent and the X<sup>-</sup> groups at position R<sub>3</sub> resulted in smaller dipole moments, larger HOMO-LUMO energy gaps and consequently the hypsochromic shift in wavelength observed for F3, F4 and F5 compared to DR73, F1 and F2, respectively.

Substitution of DR73 with electron donating NH<sub>2</sub>, NHCH<sub>3</sub> and N(CH<sub>3</sub>)<sub>2</sub> groups yielded lower HOMO-LUMO energy gap and hence, red-shifted absorption wavelength values for the X<sup>+</sup> substituted derivatives with few exceptions. Lower dipole moment, smaller H-L energy gap and more pronounced bathochromic shift were obtained when the X<sup>+</sup> groups were switched to position R<sub>5</sub> as in F9-F11, F16 and F17, compared to F6-F8, F13 and F14, respectively, which confirms that the substituent groups have more electron donating ability at this position.

Similar explanation hold for derivatives F21-F23, F27-F29, F33-F35 and F39-F41 compared to F18-F20, F24-F26, F30-F32 and F38-F38, respectively. However, in these cases, the presence of an electron withdrawing NO<sub>2</sub> or CN substituent at position R<sub>3</sub> in the diazotizing component further red-shifted the absorption wavelength by further decreasing the HOMO-LUMO energy gap as can be observed from Table 9.7.

The increase in electron donating impact of the substituents at position R<sub>5</sub> resulted in a greater ability of the substituents to sufficiently annul the electron withdrawing impact of the accepting moiety, leading to smaller charge separation between the accepting and the donating units, as confirmed by the relatively small dipole moment obtained for F9 – F11, F15-F17, F21-F23, F27-F29, F33-F35 and F39-F41 compared to F6-F8, F12-F14, F18-F20, F24-F26, F30-F32 and F36-F38, respectively (Table 9.7). The differences observed between F12-F17 and F6-F11, F24-F29 and F18-F23, and F36-F41 and F30-F35, are due to the influence of the additional terminal CN group discussed previously. Careful inspection of Table 9.7 revealed that NHCH<sub>3</sub> yielded the highest HOMO-LUMO energy gap, hence the least bathochromic shift compared to NH<sub>2</sub> and N(CH<sub>3</sub>)<sub>2</sub> when they are substituted at R<sub>4</sub>, but the smallest energy gap and hence the largest red shifting when switched to R<sub>5</sub>. This suggests that NHCH<sub>3</sub> has the least electron donating ability at R<sub>4</sub> but the highest ability at R<sub>5</sub>.

#### 9.4 CONCLUSION

In this work, the effects of some polar electron withdrawing and electron donating substituents on predicted aqueous solubility, thermodynamic stability, chemical reactivity and absorption wavelength of disperse red 73 (DR73) have been investigated. The role of substituent positions on the predicted properties was also examined. Significant number of the studied derivatives were predicted to be more soluble in water, while almost all of them showed evidence of higher chemical reactivity (i.e. degradability) and thermal stability (higher sublimation fastness) compared to the parent molecule. All the derivatives appeared to be thermodynamically more stable than the parent dye. A bathochromic shift of absorption wavelength was observed with both the electron

withdrawing and electron donating substituents considered with few exceptions. Electron withdrawing  $-\text{CN}$  substituent promoted the aqueous solubility and red-shifted the absorption wavelength of DR73 dye more than the  $-\text{NO}_2$  counterpart. In the case of the electron donating substituents,  $-\text{NH}_2$  improved aqueous solubility better than  $-\text{NHCH}_3$  and  $-\text{N}(\text{CH}_3)_2$  groups, whereas the highest bathochromic shift was obtained with  $-\text{NHCH}_3$  when substituted *ortho* to the terminal alkylamino group (i.e. at position  $\text{R}_5$ ) in the coupling component. Predicted properties were generally found to be sensitive to a change in substituent position as a result of changes in electronic and/or steric effects. 85% of the studied derivatives and the unsubstituted dye were predicted to be susceptible to photodegradation through an N-N bond cleavage pathway, about 7% of them gave precedence to a C-N bond cleavage pathway while the remaining derivatives showed evidence of competing C-N and N-N bond cleavage photodegradation pathways. Overall, ZnO showed the highest binding tendency and is as result the best candidate for their degradation. We conclude that the results of this work could be useful in developing new azo disperse dyes with interesting physicochemical properties for more economic and eco-friendly application.

## 9.5 REFERENCES

1. J. Koh. Dyeing with disperse dyes; P. Hauser (Ed.), *INTECH Open Access Publisher*, Croatia, (2011) 195-221. DOI: 10.5772/20458. Available at: <https://www.intechopen.com/books/textile-dyeing/dyeing-with-disperse-dyes>.
2. M. Clark. Handbook of textile and industrial dyeing: principles, processes and types of dyes. *Woodhead Publishing Limited*, United Kingdom, (2011).

3. R. Bianchini, F. Bonaccorsi, G. Catelani, F. Dandrea, J. Isaad, M. Rolla and T. Nocentini. Disperse dyes soluble in water. *EP2085434A1*, Jouve, Paris, (2008).
4. C. Meena, S. Maiti, N. Sekar, S. More and R. Adivarekar. Dispersant-free disperse dyes for polyester an eco-friendly approach. *The Journal of the Textile Institute* **108** (2017) 1144-1149.
5. S. Radei, F. J. Carrión-Fité, M. Ardanuy and J. M. Canal. Kinetics of low temperature polyester dyeing with high molecular weight disperse dyes by solvent microemulsion and agrosourced auxiliaries. *Polymers* **10** (2018) 200(1)-200(11).
6. F. J. Carrion-Fite and S. Radei. Development auxiliaries for dyeing polyester with disperse dyes at low temperatures. *IOP Conference Series: Materials Science and Engineering* **254** (2017) 082006(1)-082006(6). Doi:10.1088/1757-899X/254/8/082006.
7. S. M. Burkinshaw. Physico-chemical aspects of textile coloration. *John Wiley & Sons*, United States, (2016).
8. W. Saus, D. Knittel and E. Schollmeyer. Dyeing with supercritical carbon dioxide- An alternative to high-temperature dyeing of polyester. *Textile Praxis International* **47** (1992) 1052-1054.
9. W. Saus, D. Knittel and E. Schollmeyer. Dyeing of textiles in supercritical carbon dioxide. *Textile Research Journal* **63** (1993) 135-142.
10. M. Banchemo. Supercritical fluid dyeing of synthetic and natural textiles—a review. *Coloration Technology* **129** (2013) 2-17.
11. A. S. Özcan, A. A. Clifford, K. D. Bartle and D. M. Lewis. Solubility of disperse dyes in supercritical carbon dioxide. *Journal of Chemical & Engineering Data* **42** (1997) 590-592.



12. R. Bianchini, G. Catelani, G. Seu and G. Bartalucci. Coloring agents containing a mono-or disaccharide. *EP1462484A1*, Jouve, Paris, (2004).
13. H. Wang, Z. Han and X. Pan. Cyanation of water-soluble disperse dyes. *Dyes and Pigments* **41** (1999) 35-39.
14. H. S. Kim, Y. K. Park, A. R. Jo and J. J. Lee. Dispersant-free dyeing of poly (lactic acid) knitted fabric with temporarily solubilized azo disperse dyes. *Fibers and Polymers* **18** (2017) 1263-1268.
15. J. J. Lee, W. J. Lee, J. H. Choi and J. P. Kim. Synthesis and application of temporarily solubilised azo disperse dyes containing  $\beta$ -sulphatoethylsulphonyl group. *Dyes and Pigments* **65** (2005) 75-81.
16. W. Lee and J. Kim. Dispersant-free dyeing of polyester with temporarily solubilised disperse dyes. *Coloration Technology* **115** (1999) 370-373.
17. J. Lee, N. Han, W. Lee, J. Choi and J. Kim. Dispersant-free dyeing of polyester with temporarily solubilised azo disperse dyes from 1-substituted-2-hydroxypyrid-6-one derivatives. *Coloration technology* **118** (2002) 154-158.
18. J. J. Lee, W. J. Lee and J. P. Kim. Dispersant-free dyeing of polyester with temporarily solubilized azo disperse dyes from indole derivatives. *Fibers and Polymers* **4** (2003) 66-70.
19. T. Takagishi, A. Katayama, M. Matsuo, K. Konishi and N. Kuroki. Effects of alcohols on the aqueous solubility of disperse dyes. *Colloid and Polymer Science* **232** (1969) 699-703.
20. A. R. Tehrani-Bagha and K. Holmberg. Solubilization of hydrophobic dyes in surfactant solutions. *Materials* **6** (2013) 580-608.

21. A. Datyner. The solubilization of disperse dyes by dispersing agents at 127 °C. *Journal of the Society of Dyers and Colourists* **94** (1978) 256-260.
22. T. S. Choi, Y. Shimizu, H. Shirai and K. Hamada. Solubilization of disperse dyes in cationic gemini surfactant micelles. *Dyes and Pigments* **45** (2000) 145-152.
23. M. Marti, A. de la Maza, J. Parra and L. Coderch. Liposome as dispersing agent into disperse dye formulation. *Textile Research Journal* **81** (2011) 379-387.
24. M. S. Deshmukh and N. N. Sekar. A Combined Experimental and TD-DFT Investigation of Mono Azo Disperse Dyes. *Canadian Chemical Transactions* **1** (2013) 305-325.
25. S. D. Kim and E. J. Park. Relation between chemical structure of yellow disperse dyes and their lightfastness. *Fibers and Polymers* **2** (2001) 159-163.
26. A. Fadda and N. Abbas. Synthesis of azo disperse dyes containing pyridine ring for dyeing polyester and polyacrylic fibres. *Pigment & Resin Technology* **45** (2016) 10-17.
27. S. B. Novir and S. M. Hashemianzadeh. Computational study of new azo dyes with different anchoring groups for dye-sensitised solar cells. *Molecular Physics* **114** (2016) 650-662.
28. N. Tokay, Z. Seferoğlu, C. Öğretir and N. Ertanb. Quantum chemical studies on the structures of some heterocyclic azo disperse dyes. *Arkivoc* **15** (2008) 9-20.
29. Y. S. Choi, K. S. Lee, H. J. Kim, J. Y. Choi, S. B. Kang, E. J. Lee and G. Keum. Synthesis, spectral property and dyeing assessment of azo disperse dyes containing carbonyl and dicyanovinyl groups. *Bulletin of the Korean Chemical Society* **34** (2013) 863-867.

30. Ö. Arslan, E. Yalçın, N. Seferoglu, M. Yaman and Z. Seferoglu. Molecular structure analysis and spectroscopic properties of monoazo disperse dye from N, N-Dimethylaniline. *Gazi University Journal of Science* **30** (2017) 175-189.
31. O. I. Osman. DFT study of the structure, reactivity, natural bond orbital and hyperpolarizability of thiazole azo dyes. *International Journal of Molecular Sciences* **18** (2017) 239(1)-239(16).
32. Y.S. Kim, S.H. Kim, T.K. Kim and Y.A. Son. Characteristics of HOMO and LUMO potentials by altering substituents: computational and electrochemical determination. *Textile Coloration and Finishing* **20** (2008) 41-46.
33. Y. Z. Zhan, X. Zhao, B.J. Wang and W. Wang. Computational modelling of the influence of substituent effects on phthalimidylazo disperse dye hydrolysis and interaction energy. *Coloration Technology* **134** (2018) 24-32.
34. H. R. Maradiya and V. S. Patel. Synthesis and dyeing performance of some novel heterocyclic azo disperse dyes. *Journal of the Brazilian Chemical Society* **12** (2001) 710-714.
35. M. Elapasery, S. Shakra, D. Abbas, H. Gaffer and E. Allam. Synthesis of some azo disperse dyes based on pyridone moiety and their application on polyester fabrics. *Egyptian Journal of Chemistry* **60** (2017) 97-102.
36. H. Øllgaard, L. Frost, J. Galster and O. C. Hansen. Survey of azo-colorants in Denmark. Consumption, use, health and environmental aspects (1998). Available at: <https://www2.mst.dk/udgiv/publications/1999/87-7909-548-8/pdf/87-7909-546-1.pdf>. Last accessed on March 14, 2018.
37. J. H. Franco, B. F. da Silva, E. F. G. Dias, A. A. de Castro, T. C. Ramalho and M. V. B. Zanoni. Influence of auxochrome group in disperse dyes bearing azo groups

- as chromophore center in the biotransformation and molecular docking prediction by reductase enzyme: implications and assessment for environmental toxicity of xenobiotics. *Ecotoxicology and Environmental Safety* **160** (2018) 114-126.
38. S.T. Ong, P.S. Keng, W.N. Lee, S.T. Ha and Y.T. Hung. Dye waste treatment. *Water* **3** (2011) 157-176.
39. Y. Anjaneyulu, N. S. Chary and D. S. S. Raj. Decolourization of industrial effluents—available methods and emerging technologies—a review. *Reviews in Environmental Science and Biotechnology* **4** (2005) 245-273.
40. B. Hameed, U. Akpan and K. P. Wee. Photocatalytic degradation of Acid red 1 dye using ZnO catalyst in the presence and absence of silver. *Desalination and Water Treatment* **27** (2011) 204-209.
41. G. P. Pandey, A. K. Singh, L. Deshmukh, A. Asthana and S. R. Deo. Photocatalytic degradation of an azo dye with ZnO nanoparticles, *AIP Conference Proceedings*, **1536** (2013) 243-244. Doi: 10.1063/1.4810191.
42. K. Intarasuwan, P. Amornpitoksuk, S. Suwanboon and P. Graidist. Photocatalytic dye degradation by ZnO nanoparticles prepared from  $X_2C_2O_4$  (X= H, Na and  $NH_4$ ) and the cytotoxicity of the treated dye solutions. *Separation and Purification Technology* **177** (2017) 304-312.
43. M. B. Mukhlish, F. Najnin, M. Rahman and M. Uddin. Photocatalytic degradation of different dyes using  $TiO_2$  with high surface area: a kinetic study. *Journal of Scientific Research* **5** (2013) 301-314.
44. E. Fosso-Kankeu, F. Waanders and M. Geldenhuys. Photocatalytic degradation of dyes using  $TiO_2$  nanoparticles of different shapes. *7th International Conference on*

- Latest Trends in Engineering and Technology (ICLTET'2015)*, Pretoria, South Africa (2015), 84-89. Doi: 10.15242/IIE.E1115022.
45. E. M. Saggiaro, A. S. Oliveira, T. Pavesi, C. G. Maia, L. F. V. Ferreira and J. C. Moreira. Use of titanium dioxide photocatalysis on the remediation of model textile wastewaters containing azo dyes. *Molecules* **16** (2011) 10370-10386.
46. E. Repo, S. Rengaraj, S. Pulkka, E. Castangnoli, S. Suihkonen, M. Sopanen and M. Sillanpää. Photocatalytic degradation of dyes by CdS microspheres under near UV and blue LED radiation. *Separation and Purification Technology* **120** (2013) 206-214.
47. S. Aggarwal. Photo Catalytic Degradation of Methyl Orange by Using CdS Semiconductor Nanoparticles Photo catalyst. *International Research Journal of Engineering and Technology* **3** (2016) 451-454.
48. B. Patil and S. Acharya. Photocatalytic behaviour of CdS/ZnS nanocomposite for dye degradation in presence of visible light. *AIP Conference Proceedings*, **1728** (2016) 020648(1) - 020648(4). Doi: 10.1063/1.4946699.
49. Y. Kambalagere, B. Channappa, K. M. Mahadevan and M. Narayanappa. Decolorization of synthetic Coralene Violet 3R and Disperse Blue 2BL azo dyes using photoactive Calcium Aluminate nanoparticle in presence of sunlight. *International Journal of Advances in Chemical Engineering & Biological Sciences* **3** (2016) 108-112.
50. N. Madhusudhana, K. Yogendra, K. Mahadevan, S. Naik and H. Gopalappa. Photocatalytic degradation of coralene dark red 2B dye using calcium aluminate ( $\text{CaAl}_2\text{O}_4$ ) catalyst. *Journal of Environmental Science: An Indian Journal* **6** (2011) 1-5.

51. N. Madhusudhana, K. Yogendra, K. Mahadevan and S. Naik. Photocatalytic degradation of Coralene Dark red 2B azo dye using calcium zincate nanoparticle in presence of natural sunlight: an aid to environmental remediation. *International Journal of Chemical Engineering and Applications* **2** (2011) 294-298.
52. N. Madhusudhana, K. Yogendra and K. M. Mahadevan. Photocatalytic degradation of violet GL2B azo dye by using calcium aluminate nanoparticle in presence of solar light. *Research Journal of Chemical Sciences* **2** (2012) 72-77.
53. A. S. Özen, V. Aviyente and R. A. Klein. Modeling the oxidative degradation of azo dyes: A density functional theory study. *The Journal of Physical Chemistry A* **107** (2003) 4898-4907.
54. A. S. Özen, V. Aviyente, F. De Proft and P. Geerlings. Modeling the substituent effect on the oxidative degradation of azo dyes. *The Journal of Physical Chemistry A* **108** (2004) 5990-6000.
55. X. Jiao, H. Yu, Q. Kong, Y. Luo, Q. Chen and J. Qu. Theoretical mechanistic studies on the degradation of alizarin yellow R initiated by hydroxyl radical. *Journal of Physical Organic Chemistry* **27** (2014) 519-526.
56. A. S. Özen, V. Aviyente, G. Tezcanli-Güyer and N. H. Ince. Experimental and modeling approach to decolorization of azo dyes by ultrasound: degradation of the hydrazone tautomer. *The Journal of Physical Chemistry A* **109** (2005) 3506-3516.
57. S. Padmaja and S. A. Madison. Hydroxyl radical-induced oxidation of azo dyes: a pulse radiolysis study. *Journal of Physical Organic Chemistry* **12** (1999) 221-226.
58. J. Aspland. The structure and properties of disperse dyes and related topics. *Textile Chemistry and Coloration* **25** (1993) 21-25.

59. DMol<sup>3</sup> Guide. Material Studio 8.0. *Accelrys Software, Inc.*, San Diego, United States (2017) 1-161.
60. Materials Studio simulation environment. *Release 2016, Accelrys Software Inc.*, San Diego, CA, United States, (2016).
61. Y. Inada and H. Orita. Efficiency of numerical basis sets for predicting the binding energies of hydrogen bonded complexes: evidence of small basis set superposition error compared to Gaussian basis sets. *Journal of Computational Chemistry* **29** (2008) 225-232.
62. O. Wahab, L. Olasunkanmi, K. Govender and P. Govender. DMol<sup>3</sup>/COSMO-RS prediction of aqueous solubility and reactivity of selected Azo dyes: Effect of global orbital cut-off and COSMO segment variation. *Journal of Molecular Liquids* **249** (2018) 346-360.
63. E. Mullins, R. Oldland, Y. Liu, S. Wang, S. I. Sandler, C.-C. Chen, M. Zwolak and K. C. Seavey. Sigma-profile database for using COSMO-based thermodynamic methods. *Industrial and Engineering Chemistry Research* **45** (2006) 4389-4415.
64. J. D. Thompson, C. J. Cramer and D. G. Truhlar. Predicting aqueous solubilities from aqueous free energies of solvation and experimental or calculated vapor pressures of pure substances. *The Journal of Chemical Physics* **119** (2003) 1661-1670.
65. C. Liang and D. A. Gallagher. QSPR prediction of vapor pressure from solely theoretically-derived descriptors. *Journal of Chemical Information And Computer Sciences* **38** (1998) 321-324.
66. R. G. Pearson. Chemical hardness. Wiley-VCH Verlag GmbH, Weinheim, (1997).

67. P. K. Chattaraj. Chemical reactivity theory: a density functional view. *CRC Press*, Taylor and Francis Group, Boca Raton, (2009).
68. S. Kumar and J. Sharma. Stable phase CdS nanoparticles for optoelectronics: a study on surface morphology, structural and optical characterization. *Materials Science-Poland* **34** (2016) 368-373.
69. U. Diebold. The surface science of titanium dioxide. *Surface science reports* **48** (2003) 53-229.
70. M. Grunze, W. Hirschwald and D. Hofmann. Zinc oxide: Surface structure, stability, and mechanisms of surface reactions. *Journal of Crystal Growth* **52** (1981) 241-249.
71. J. V. Lauritsen, S. Porsgaard, M. K. Rasmussen, M. C. Jensen, R. Bechstein, K. Meinander, B. S. Clausen, S. Helveg, R. Wahl and G. Kresse. Stabilization principles for polar surfaces of ZnO. *ACS nano* **5** (2011) 5987-5994.
72. K. Wright, G. Watson, S. Parker and D. Vaughan. Simulation of the structure and stability of sphalerite (ZnS) surfaces. *American Mineralogist* **83** (1998) 141-146.
73. P. W. Ayers and R. G. Parr. Variational principles for describing chemical reactions: the Fukui function and chemical hardness revisited. *Journal of the American Chemical Society* **122** (2000) 2010-2018.
74. V. Wathélet, J. Preat, M. Bouhy, M. Fontaine, E. A. Perpète, J. M. André and D. Jacquemin. Assessment of PBE0 for evaluating the absorption spectra of carbonyl molecules. *International Journal of Quantum Chemistry* **106** (2006) 1853-1859.
75. N. A. Sanchez-Bojorge, L. M. Rodriguez-Valdez, D. Glossman-Mitnik and N. Flores-Holguin. Theoretical calculation of the maximum absorption wavelength for



- Cyanidin molecules with several methodologies. *Computational and Theoretical Chemistry* **1067** (2015) 129-134.
76. J. Ojanen and T. T. Rantala. Electronic structure and absorption spectrum of disperse red 1: comparison of computational approaches. *Open Chemical Physics Journal* **2** (2009) 37-46.
77. M. B. Smith and J. March. March's advanced organic chemistry: reactions, mechanisms, and structure. *John Wiley & Sons, United State*, (2007).
78. D. H. McDaniel and H. C. Brown. An extended table of hammett substituent constants based on the ionization of substituted benzoic acids. *The Journal of Organic Chemistry* **23** (1958) 420-427.
79. X. Li, J. Yu, J. Low, Y. Fang, J. Xiao and X. Chen. Engineering heterogeneous semiconductors for solar water splitting. *Journal of Materials Chemistry A* **3** (2015) 2485-2534.
80. K. Mondal and A. Sharma. Photocatalytic oxidation of pollutant dyes in wastewater by TiO<sub>2</sub> and ZnO nano-materials-a mini-review. *Nanoscience & Technology for Mankind, The Academy of Sciences India (NASI), Allahabad, India* (2014) 36-72.
81. I. T. Peternel, N. Koprivanac, A. M. L. Božić and H. M. Kušić. Comparative study of UV/TiO<sub>2</sub>, UV/ZnO and photo-fenton processes for the organic reactive dye degradation in aqueous solution. *Journal of Hazardous Materials* **148** (2007) 477-484.
82. N. Jaggi, M. Giri and K. Yadav. Absorption and fluorescence spectra of disperse red 19-An azo dye. *Indian Journal of Pure & Applied Physics* **51** (2013) 833-836.

83. I. Lednev, T. Ye, P. Matousek, M. Towrie, S. Umapathy, R. Hester and J. Moore. Science - lasers for science facility programme. *CLF Annual Report* (1996) 124-125. Available at: [http://www.dmpotonics.com/Ultrafast\\_spectroscopy/53.pdf](http://www.dmpotonics.com/Ultrafast_spectroscopy/53.pdf).
84. P. Birnbaum, J. Linford and D. Style. The absorption spectra of azobenzene and some derivatives. *Transaction of the Faraday Society* **49** (1953) 735-744.
85. C. V. Uliana, G. S. Garbellini and H. Yamanaka. Spectrophotometric evaluation of the behavior of disperse red 1 dye in aqueous media and its interaction with calf thymus ds-DNA. *Journal of Brazilian Chemical Society* **23** (2012) 1469-1475.
86. D. Patterson and R. Sheldon, *Journal of the Society of Dyers and Colourists* **76** (1960) 178-181.



---

## CHAPTER 10

# A DFT STUDY OF DISPERSE YELLOW 119 DEGRADATION MECHANISM BY HYDROXYL RADICAL ATTACK

---

### PREAMBLE

The energetics of two experimentally proposed mechanisms of azo dye degradation by hydroxyl ( $\bullet\text{OH}$ ) radical were investigated for disperse yellow 119 (DY119) dye using a DFT method. The two degradation pathways are the ones in which the attack of the radical on the dye occurs through one of the azo ( $\text{N}=\text{N}$ ) nitrogen leading to an  $\text{N}-\text{N}$  bond cleavage mechanism, or through a ring carbon next to the azo group, giving rise to a  $\text{C}-\text{N}$  bond rupture mechanism. Potential energy profiles (PEP) for these two possibilities were calculated and compared to determine the more energetically favored mechanism for DY119 degradation. Local reactivity indices and energetic parameters revealed that the  $\text{C}-\text{N}$  bond cleavage mechanism is the preferred photodegradation pathway for DY119.

### 10.1 INTRODUCTION

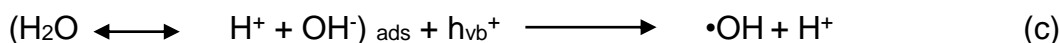
Photocatalytic oxidation is an advanced oxidation technique for the treatment of organic pollutants before being released to the environment. It involves photochemical generation of  $\bullet\text{OH}$  radicals using efficient, low cost, light-active semiconductor or metal oxide particles such as  $\text{TiO}_2$  and  $\text{ZnO}$  as catalysts [1-8]. Upon illumination with light of appropriate wavelength, electrons migrate from the valence band (VB) to the conduction band (CB) of a catalyst where they are scavenged by adsorbed oxygen molecules to

---

The work presented in this chapter has been published.

\*O.O. Wahab, L.O. Olasunkanmi, K.K. Govender and P.P. Govender. *ChemistrySelect* **2000** (2018) 1-11.

prevent their recombination with generated holes in the VB (Scheme 10.1b). Reaction of the holes with adsorbed water molecules gives rise to highly reactive hydroxyl ( $\bullet\text{OH}$ ) radicals (Scheme 10.1c) which cause pollutant degradation (Scheme 10.1d) [9].



**Scheme 10. 1:** Photocatalytic production of  $\bullet\text{OH}$  radical.

Production of  $\bullet\text{OH}$  radical can also be achieved through chemical methods, radiolysis, and ultrasonic irradiation [10-13]. Two or more techniques are often combined to increase  $\bullet\text{OH}$  radical production in order to promote decolorization and mineralization of pollutants [14-16]. It should be noted however, that the reaction of generated  $\bullet\text{OH}$  radicals with organic pollutants is independent of the method of  $\bullet\text{OH}$  production during degradation. For instance, reaction of  $\bullet\text{OH}$  radicals with azo dyes is believed to occur via two experimentally proposed pathways involving the attack of the radical on one of the azo ( $\text{N}=\text{N}$ ) nitrogen or on the ring carbon next to the azo chromophore [16-18]. This gives rise to a N-N or C-N bond cleavage degradation pathway, respectively, regardless of how the radical is produced.

Reaction of  $\bullet\text{OH}$  radical with azo dyes consists of two steps (i) the radical addition step which leads to adduct formation and (ii) the bond cleavage step which leads to adduct fragmentation [10, 19, 20]. The radical addition results in decolorization of the dye [18]

while the bond cleavage step leads to mineralization of the addition product. For a given azo dye, it is necessary to determine the more preferred mechanism (i.e attack on N or C) for decolorization and subsequent mineralization of the dye as this can help to predict the degradation product(s).

Several experimental studies [16-18, 21, 22] particularly that reported by Panajkar and Mohan [18] have suggested that oxidative degradation of azo dyes occurs predominantly via the N-N bond cleavage pathway in which ~60% of the generated  $\bullet\text{OH}$  radicals attack the azo group, while about 40% of the radicals attack the carbon atoms linked to the azo chromophore. Spadaro *et al.* [23] proposed that the attack of  $\bullet\text{OH}$  radical on azobenzene favors C-N bond cleavage mechanism which leads to formation of benzene, whereas Joseph *et al.* [16] proposed an N-N cleavage pathway leading to production of nitrosobenzene.

Theoretical calculations using DFT methods have been reported on different azo benzene derivatives to determine the more energetically preferred degradation pathway and to investigate factors such as substituent effect, tautomerism and molecular charge that can influence the choice of degradation mechanism. These include the works of Ozen *et al.* [19, 22] and Jiao *et al.* [20].

Reaction of  $\bullet\text{OH}$  radical with unsubstituted azobenzene dye was reported to favor the N-N bond cleavage pathway in preference to the C-N bond cleavage [10], and similar results were found with some substituted azo benzene derivatives [19]. Previous theoretical studies by Ozen *et al.* [22] and Jiao *et al.* [20] gave conflicting reports on the degradation mechanisms of azo dyes such as Acid Orange 7, Acid Orange 8 and Alizarin Yellow R, which exist predominantly in hydrazone tautomeric form. Ozen *et al.* [22] concluded that the reactions of Acid Orange 7 and 8 with  $\bullet\text{OH}$  radical gave precedence to a C-N bond

cleavage mechanism both kinetically and thermodynamically. On the contrary, Jiao *et al.* [20] in their study on neutral and anionic forms of Alizarin Yellow R reported that the C-N and the N-N bond cleavage pathways are kinetically competitive, but the former was found to be more thermodynamically favored for the anionic form and the hydrazone tautomer only. That is, the C-N bond cleavage pathway for the neutral form shows lower thermodynamic favorability.

In view of the foregoing, it is obvious that the degradation mechanism of azo dyes which exist mainly in hydrazone form is still complicated. As a result, further investigations are necessary in order to address the mechanistic ambiguities. The present work therefore investigated theoretically, the mechanism of  $\bullet\text{OH}$  radical reactions with C.I. Disperse yellow 119 (DY119) - an azopyridone disperse dye that exists mainly in hydrazone form (Fig. 10.1) [24]. The choice of DY119 for the present work was motivated by the fact that degradation pathway studies on azopyridone disperse dyes are very rare. Most of the previous studies have focused on azobenzene derivatives. Like other azo disperse dyes, DY119 is mainly used in the textile industry for coloring polyester, nylon and cellulose acetate materials [25, 26]. Since this dye possesses intramolecular hydrogen bonding, the role of this bonding in its degradation mechanism was also examined. Possibility of molecular nitrogen evolution through subsequent attack of  $\bullet\text{OH}$  radical on a C-N bond cleavage product was also investigated.

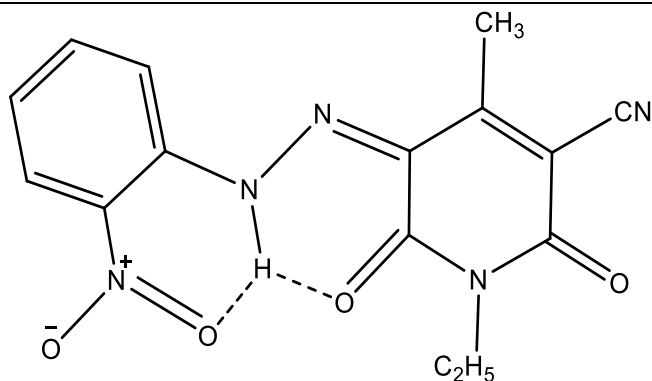


**Figure 10. 1:** Molecular structure of disperse yellow 119 (DY119).

## 10.2 COMPUTATIONAL DETAILS

### 10.2.1 COMPUTATIONAL SOFTWARE

DMol<sup>3</sup> computational program [27] available in the Material studio (2016) package [28] was employed in this study. It makes use of density functional theory (DFT) methods which are more appropriate for calculations on open shell systems such as radicals [10, 29]. As opposed to wave function based ab-initio methods, DFT methods predict properties of systems using electron densities and are not prone to spin contamination which undermines the Hartree-Fock methods [10, 30]. Also, DFT methods produce higher result accuracy at a relatively low computational cost even for large systems.

Selection of DMol<sup>3</sup> was further motivated by the fact that this computational code has a unique, well-developed and efficient transition state search procedure comprising the linear synchronous transit (LST) and the quadratic synchronous transit (QST) methods [31, 32] for rapid location of transition states. DMol<sup>3</sup> also makes use of numerical basis sets which are considered more superior to Gaussian basis sets both in terms of accuracy and speed [33]. Numerical basis sets are also known for their ability to eliminate basis set superposition errors (BSSE) [33]. Finally, DMol<sup>3</sup> uses the conductor-like screening model

(COSMO) which is regarded as the most successful continuum solvation models for implicit solvent phase calculations [34].

### 10.2.2 CALCULATION PROCEDURE

Potential energy profile calculations (i.e. transition state search), transition state confirmation and full optimization of relevant stationary point geometries (i.e. ground state and intermediate geometries) in the energy profiles were carried out at the VWN-BP level of theory [27] using double numerical basis set containing polarization functions (DNP) [27, 33]. Fukui function calculation at the same level of theory was used to determine the propensity of the prospective reaction centers in DY119 to •OH radical attack. The Fukui function for radical attack ( $f^0$ ) was calculated according to the following equation [10, 35]

:

$$f^0 = 1/2 [q_k(N + 1) - q_k(N - 1)]$$

Equation 10. 1

where N is the number of electrons,  $q_k(N + 1)$ , and  $q_k(N - 1)$  are the Mulliken charges on atom k for N+1 and N-1 number of electrons, respectively. The most reactive sites were identified and employed for the calculations.

Reactant geometries were optimized and confirmed by absence of imaginary frequencies before subjected to energy profile calculations. Transition state structures were confirmed by frequency calculations and also verified through a unique transition state confirmation procedure involving the use of the nudged elastic band (NEB) method [36] to ascertain the link between the structures and their associated minimum geometries (i.e. reactants, intermediates and products) on energy profiles, and to reveal other transition state structure(s) that may also be present along the reaction path. Single point energy calculations in solvent phase were carried out on the stationary point geometries obtained



in the gas phase to examine the effect of water on the reaction. This was achieved with the aid of conductor-like screening model (COSMO), using a COSMO dielectric constant of 78.4 to specify water.

### 10.3 RESULTS AND DISCUSSIONS

#### 10.3.1 DETERMINATION OF SITE PROPENSITY TO RADICAL ATTACK

Due to differences in the chemical constituents of the aromatic rings of DY119, the chemical environments and hence, the susceptibility of the prospective reaction sites C<sub>4</sub>, N<sub>7</sub>, N<sub>8</sub> and C<sub>9</sub> in the dye (Fig. 10.2) differ. Thus, the propensity of these sites towards a radical attack was evaluated to identify the one with the highest susceptibility to •OH radical attack.

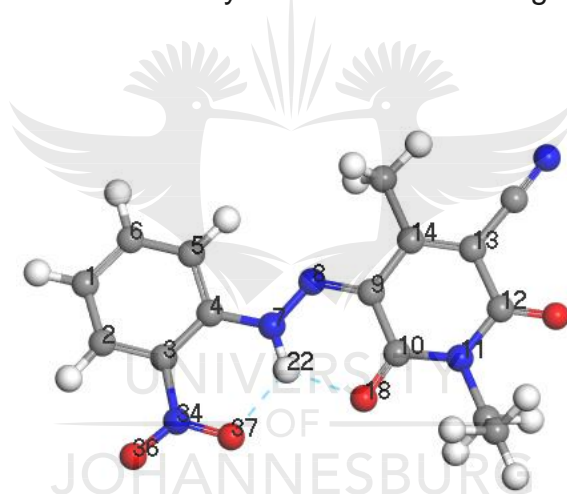


**Figure 10. 1:** Optimized geometry of DY119 showing the prospective reaction sites for •OH radical. Atoms colored in white, grey, blue and red are hydrogen, carbon, nitrogen and oxygen, respectively.

The Mulliken radical attack Fukui functions calculated for the prospective reaction sites are provided in Table 10.1. For the dye to degrade via a C–N bond cleavage mechanism, the attack of •OH radical must occur on either C<sub>4</sub> or C<sub>9</sub>, whereas the available sites for N–N bond rupture pathway are N<sub>7</sub> and N<sub>8</sub>. However, the table revealed N<sub>8</sub> and C<sub>9</sub> as the sites with greater propensity for radical attack compared to N<sub>7</sub> and C<sub>4</sub>, respectively.

Therefore, only the N<sub>8</sub> and C<sub>9</sub> reaction sites were considered for the degradation study.

Similarly, further inspection of the table revealed that C<sub>9</sub> is more vulnerable to radical attack than N<sub>8</sub>, which suggests that the attack of •OH radical attack on C<sub>9</sub> will occur with lower activation energy to favor the C–N bond cleavage degradation mechanism. This was verified by comparing the energetics of C–N and N–N bond cleavage degradation mechanisms which was discussed later in section 10.3.4.

**Table 10. 1:** Mulliken radical attack Fukui functions,  $f^0$  for the prospective reaction sites in DY119

Atoms	$f^0$
C <sub>4</sub>	0.021
N <sub>7</sub>	0.022
N <sub>8</sub>	0.038
C <sub>9</sub>	0.045

### 10.3.2 C-N BOND RUPTURE DEGRADATION MECHANISM

The potential energy profiles (PEP) for the reaction of •OH radical with DY119 via the C<sub>9</sub> center are shown in Figure 10.3 and Scheme 10.2. The PEPs in the figure consist of a radical addition step occurring through a transition state structure, TS<sub>1C</sub>, with a low imaginary frequency of -81 cm<sup>-1</sup>, and an adduct fragmentation step in which the addition product, INT<sub>1C</sub> undergoes a C–N bond cleavage reaction via a transition state structure, TS<sub>3C</sub> to form product P<sub>1C</sub>, respectively. For the first time, a proton transfer step which appears to be the rate limiting step of the reaction is also observed. This additional step preceding the bond cleavage, involves isomerization of the addition product, INT<sub>1C</sub> from its hydrazone tautomeric form to its corresponding azo form, INT<sub>2C</sub>, through a genuine transition state structure, TS<sub>2C</sub> (Fig. 10.3, Scheme 10.2), with an imaginary frequency of

$-243.32 \text{ cm}^{-1}$ , corresponding to vibration of the  $\text{N}_7 - \text{H}_{22}$  bond (Fig. 10.2), which confirms

the departure of the proton.

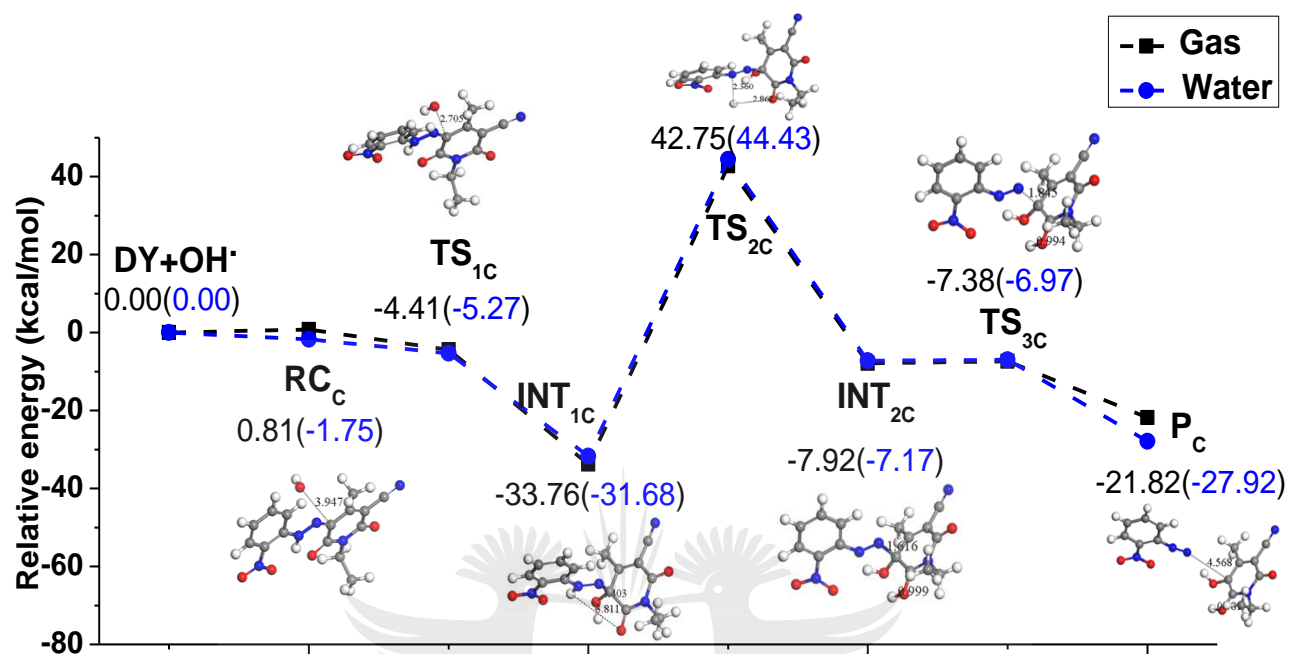
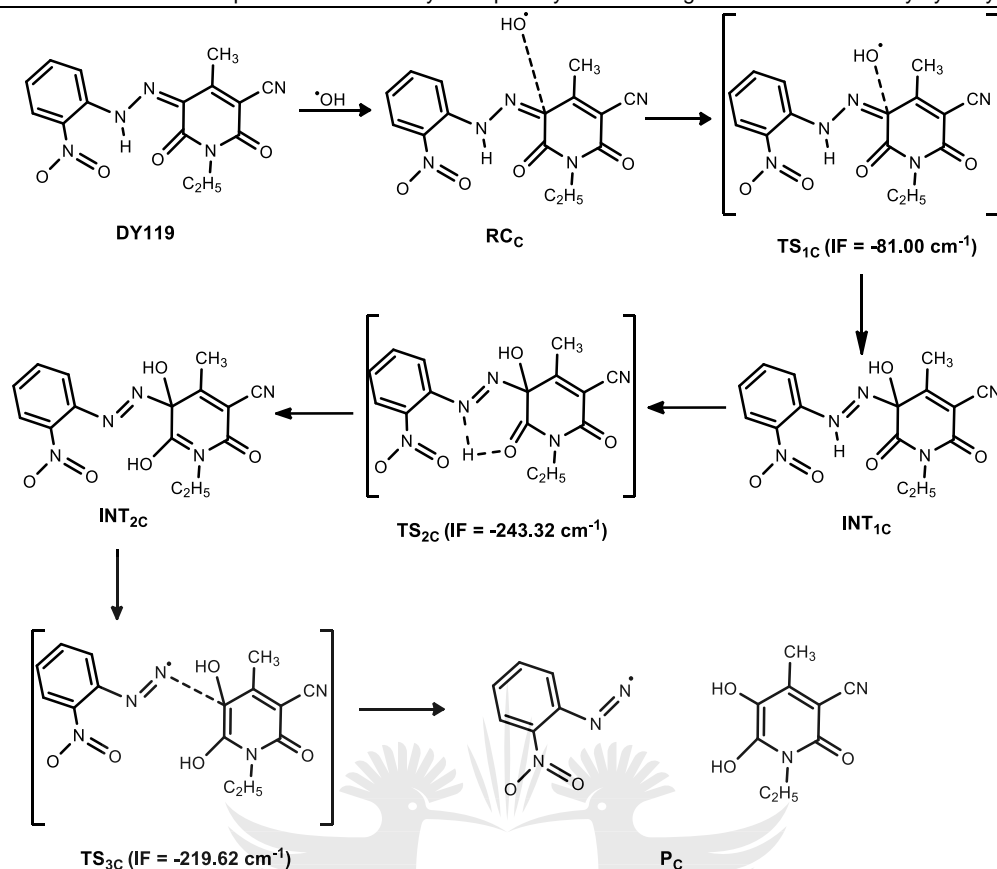


**Figure 10.2:** Potential energy profile for  $\bullet\text{OH}$  radical initiated degradation of DY119 via a C–N bond cleavage mechanism.

UNIVERSITY  
OF  
JOHANNESBURG



**Scheme 10. 2:** C–N bond rupture degradation mechanism.

### 10.3.3 EFFECT OF WATER ON C–N BOND RUPTURE DEGRADATION MECHANISM

The presence of water has varying impacts on the energies of the stationary point structures. It lowers the energies of the pre-reaction complex (RC<sub>c</sub>), transition states TS<sub>1c</sub>, and the cleavage product, P<sub>1c</sub>, but raises the energies of the  $\cdot\text{OH}$  adducts (i.e. INT<sub>1c</sub> and INT<sub>2c</sub>) and their accompanying transition state structures (i.e. TS<sub>2c</sub> and TS<sub>3c</sub>). The energy lowering effect produced by water on TS<sub>1c</sub> may be attributed to the extra stabilization offered by the hydrogen bonding between water molecules and the hydrazine hydrogen.

Kinetically, the presence of water raises the energy barrier for  $\bullet\text{OH}$  radical addition to the  $\text{C}_9$  center by  $\sim 1.7$  kcal/mol, but increases the rate of the C–N bond cleavage step by producing a reduction of  $\sim 1$  kcal/mol in the activation energy for the formation of  $\text{P}_{1\text{C}}$ .

#### 10.3.4 N-N BOND RUPTURE DEGRADATION MECHANISM

The potential energy profile obtained for the reaction between  $\bullet\text{OH}$  radical and DY119 through the attack of the radical on  $\text{N}_8$ , is presented in Figure 10.4 and Scheme 10.3. The PEP shows a radical addition step which occurs through a transition state,  $\text{TS}_{1\text{N}}$ , and the N–N bond cleavage step occurring through a transition state,  $\text{TS}_{3\text{N}}$ . For the radical addition step, transition state confirmation using the NEB method revealed a new intermediate ( $\text{INT}_{\text{C}}$ ) between the transition state,  $\text{TS}_{1\text{N}}$  and the addition product,  $\text{INT}_{1\text{N}}$ . Formation of  $\text{INT}_{\text{C}}$  between the approaching  $\bullet\text{OH}$  radical and  $\text{C}_9$  when the radical was at a bond distance of 2.393 Å from the target site i.e.  $\text{N}_8$ , confirms greater thermodynamic preference for the attack of the radical on  $\text{C}_9$  compared to  $\text{N}_8$ , which is in accord with the Fukui function trend discussed previously. Transformation of this intermediate to  $\text{INT}_{1\text{N}}$  occurred with activation energy of  $\sim 27$  kcal/mol and 24 kcal/mol in vacuum and water, respectively via a transition state,  $\text{TS}_{\text{NC}}$ , which has imaginary frequency value of  $-154.41$   $\text{cm}^{-1}$ , corresponding to the reaction coordinate.

In the case of N–N bond cleavage step, transition state confirmation using the same method revealed a new cyclic transition state ( $\text{TS}_{2\text{N}}$ ) located between the addition product,  $\text{INT}_{1\text{N}}$  and its distorted isomer,  $\text{INT}_{2\text{N}}$ . This new transition state gave a large imaginary frequency value of  $-367.21$   $\text{cm}^{-1}$  corresponding to the vibrations of  $\text{N}_7$ – $\text{H}_{22}$  and  $\text{H}_{22}$ – $\text{O}_{37}$  bonds combined, which are caused by the shortening of  $\text{HO}$ – $\text{N}_8$  bond to a bond length of 1.432 Å (Appendix: Fig. A.3). This led to contraction of the  $\text{N}_8$ – $\text{N}_7$  bond, and a

subsequent push of the hydrazine hydrogen (i.e. H<sub>22</sub>) atom towards the neighboring oxygen (i.e. O<sub>37</sub>), causing it to act as a bridging atom between N<sub>7</sub> and O<sub>37</sub> to give the bicyclic transition state (TS<sub>2N</sub>) (Fig. 10.4 and Scheme 10.3).

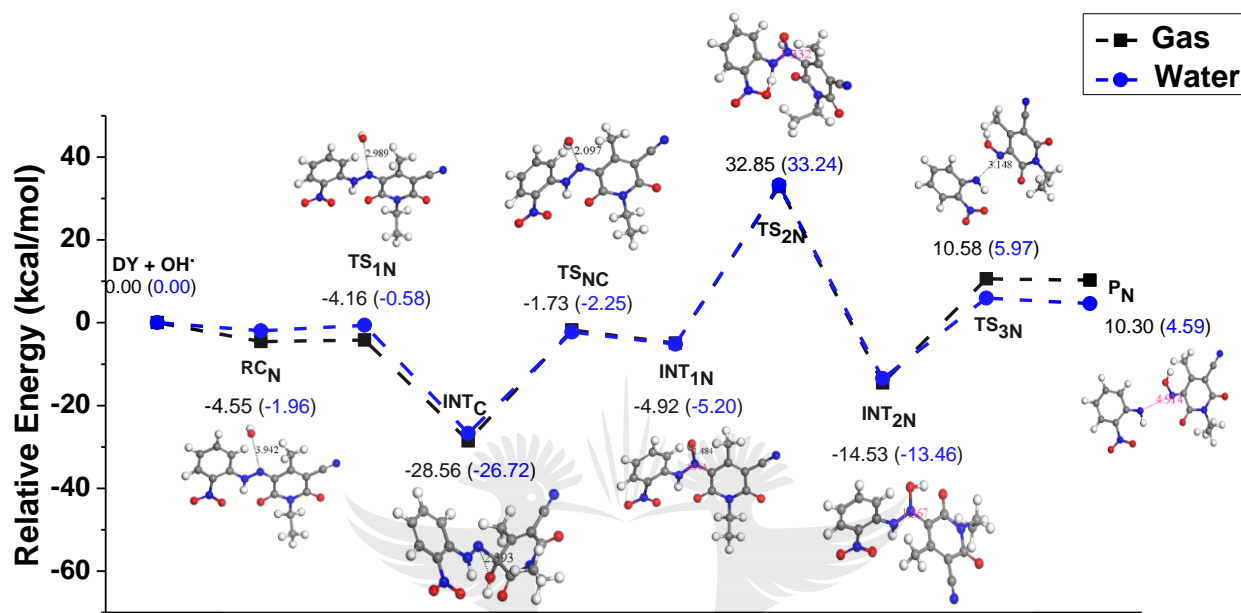
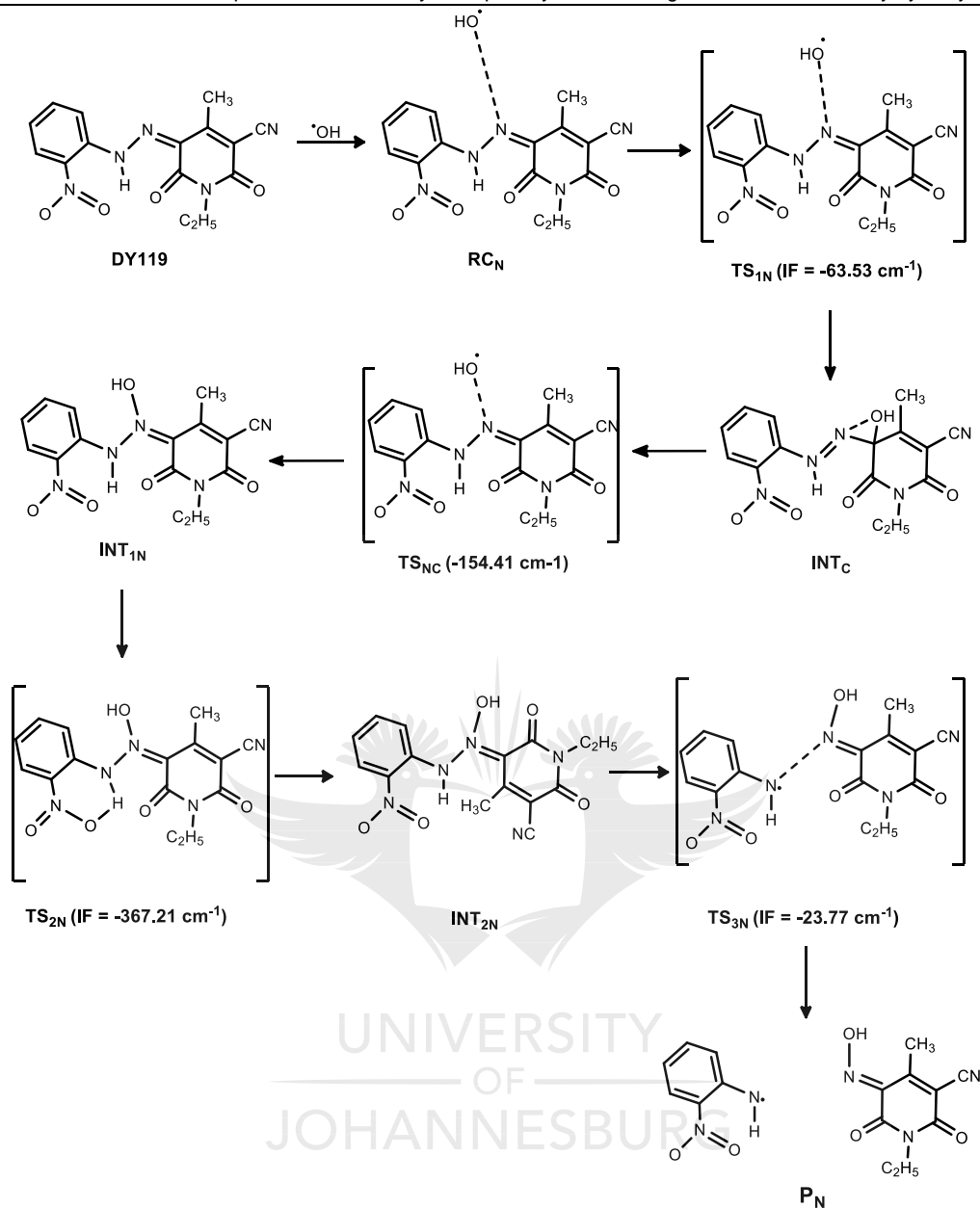


**Figure 10.3:** Potential energy profile for •OH radical initiated degradation of DY119 via an N–N bond cleavage mechanism.

Some observable changes in the geometry of the addition product, INT<sub>1N</sub> as it transitioned to its distorted form, INT<sub>2N</sub> are shown in Figure A.4 (Appendix). These geometrical changes may be attributed to the lower stability of INT<sub>1N</sub> compared to INT<sub>2N</sub> as indicated by their respective energies (Fig. 10.4).



**Scheme 10. 3:** N–N bond rupture degradation mechanism.

### 10.3.5 EFFECT OF WATER ON N–N BOND RUPTURE DEGRADATION MECHANISM

Similar to the effect observed in the C–N bond cleavage mechanism, the introduction of water lowers the total activation energies for the attack of  $\cdot\text{OH}$  radical on N<sub>8</sub> site and subsequent fragmentation of the addition product by  $\sim 1.4 \text{ kcal/mol}$  and  $\sim 5.7 \text{ kcal/mol}$ ,

respectively. However, the energies of the stationary point geometries are raised by this solvent with the exception of INT<sub>1N</sub>, TS<sub>3N</sub> and P<sub>N</sub> (Fig. 10.4).

### 10.3.6 COMPARISON OF C–N AND N–N BOND RUPTURE DEGRADATION MECHANISMS

The activation energies for the radical addition ( $\Delta E_{RA}^\ddagger$ ) and the bond cleavage ( $\Delta E_{BC}^\ddagger$ ) steps, and the overall activation energies ( $\Delta E_A^\ddagger$ ) for both C–N and N–N bond cleavage degradation mechanisms of DY119 (Fig. 10.3 and 10.4) are compared in Table 10.2. The radical addition step is the step that leads to the formation of INT<sub>1C</sub> and INT<sub>1N</sub> (Fig. 10.3 and 10.4), while the bond cleavage step refers to the C–N or the N–N bond cleavage step. The overall activation energy is the total activation energy for each mechanism i.e. the sum of all activation energies involved in the conversion of DY119 to the final degradation products (i.e. P<sub>C</sub> and P<sub>N</sub>) in the figures. The relative energies, E<sub>AP</sub> and E<sub>B<sub>CP</sub></sub> of the addition and bond cleavage products, respectively, are also compared in the table for the two pathways. The purpose of these comparisons is to identify the degradation mechanism with the highest kinetic and/or thermodynamic priorities for DY119. Values enclosed in parentheses in the table are aqueous phase results.

The  $\Delta E_{RA}^\ddagger$ ,  $\Delta E_{BC}^\ddagger$ , E<sub>AP</sub> and E<sub>B<sub>CP</sub></sub> values in Table 10.2 revealed that •OH radical attack through the N<sub>8</sub> center of DY119 is kinetically less favorable than the attack through the C<sub>9</sub> center, which occurred almost without energy barriers and yielded more stable addition and bond cleavage product. Similarly, the relatively lower overall activation energy,  $\Delta E_A^\ddagger$  for C–N bond cleavage step compared to that of N–N bond cleavage, also rules in favor of the C–N bond cleavage degradation mechanism.



**Table 10. 2:** Energetic parameters for the C-N and the N-N bond cleavage degradation mechanisms.

Parameters (kcal/mol)	•OH attack on C <sub>9</sub> / C-N bond cleavage mechanism	•OH attack on N <sub>8</sub> / N-N bond cleavage mechanism
$\Delta E_{RA}^{\ddagger}$	-5.22 (-3.52) <sup>a</sup>	0.39 (1.38) <sup>aa</sup>
$\Delta E_{BC}^{\ddagger}$	0.54 (0.20) <sup>b</sup>	25.11 (19.43) <sup>bb</sup>
$\Delta E_A^{\ddagger}$	71.83 (72.79) <sup>c</sup>	90.10 (83.72) <sup>cc</sup>
$E_{AP}$	-33.76 (-31.68)	-28.56 (-26.72)
$E_{BCP}$	-21.82 (-27.92)	10.30 (4.59)

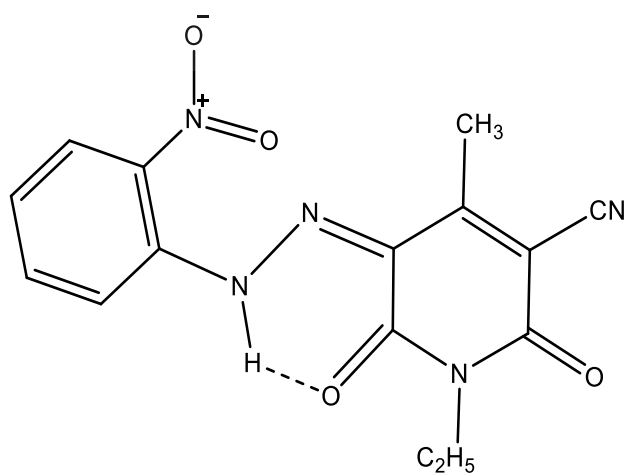
<sup>a</sup>TS<sub>1C</sub> - RC<sub>C</sub>, <sup>aa</sup>[(TS<sub>1N</sub> - RC<sub>N</sub>) + (TS<sub>NC</sub> - INT<sub>C</sub>)]

<sup>b</sup>TS<sub>3C</sub> - INT<sub>2C</sub>, <sup>bb</sup>(TS<sub>3N</sub> - INT<sub>2N</sub>)

<sup>c</sup>[(TS<sub>1C</sub> - RC<sub>C</sub>) + (TS<sub>2C</sub> - INT<sub>1C</sub>) + (TS<sub>3C</sub> - INT<sub>2C</sub>)], <sup>cc</sup>[(TS<sub>1N</sub> - RC<sub>N</sub>) + (TS<sub>NC</sub> - INT<sub>C</sub>) + (TS<sub>2N</sub> - INT<sub>1N</sub>) + (TS<sub>3N</sub> - INT<sub>2N</sub>)]

### 10.3.7 EFFECT OF HYDROGEN BONDING

To investigate the role of intramolecular hydrogen bonding in DY119 on its degradation mechanism, a conformer of this molecule (Fig. 10.5) in which the nitrophenyl moiety has been rotated by 180° about the C<sub>4</sub>-N<sub>7</sub> bond (Fig. 10.2), was considered. In this conformer, the hydrogen bond observed between the hydrazine unit and the nitro group in DY119 (Fig. 10.1) is absent. The potential energy profiles obtained for the reaction of •OH radical with this conformer via the C-N and N-N bond rupture pathways are presented in Figures 10.6 and 10.7.

**Figure 10. 4:** Molecular structure of disperse yellow 119 conformer (DYIS).

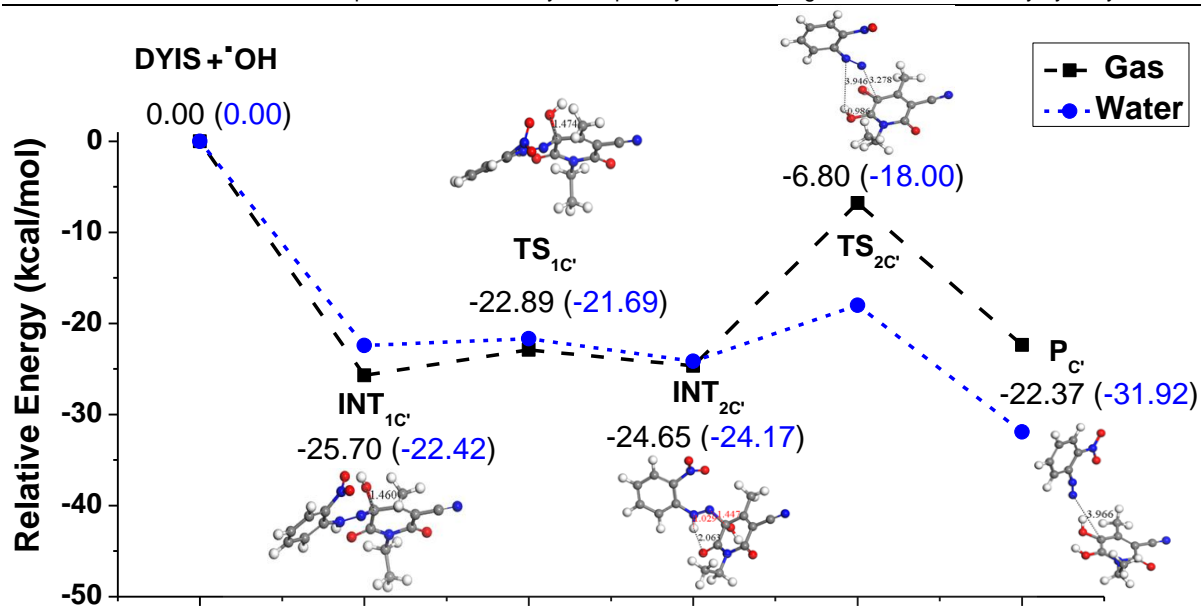


**Figure 10. 5:** Potential energy profile for •OH radical initiated degradation of DYIS via a C–N bond cleavage mechanism.

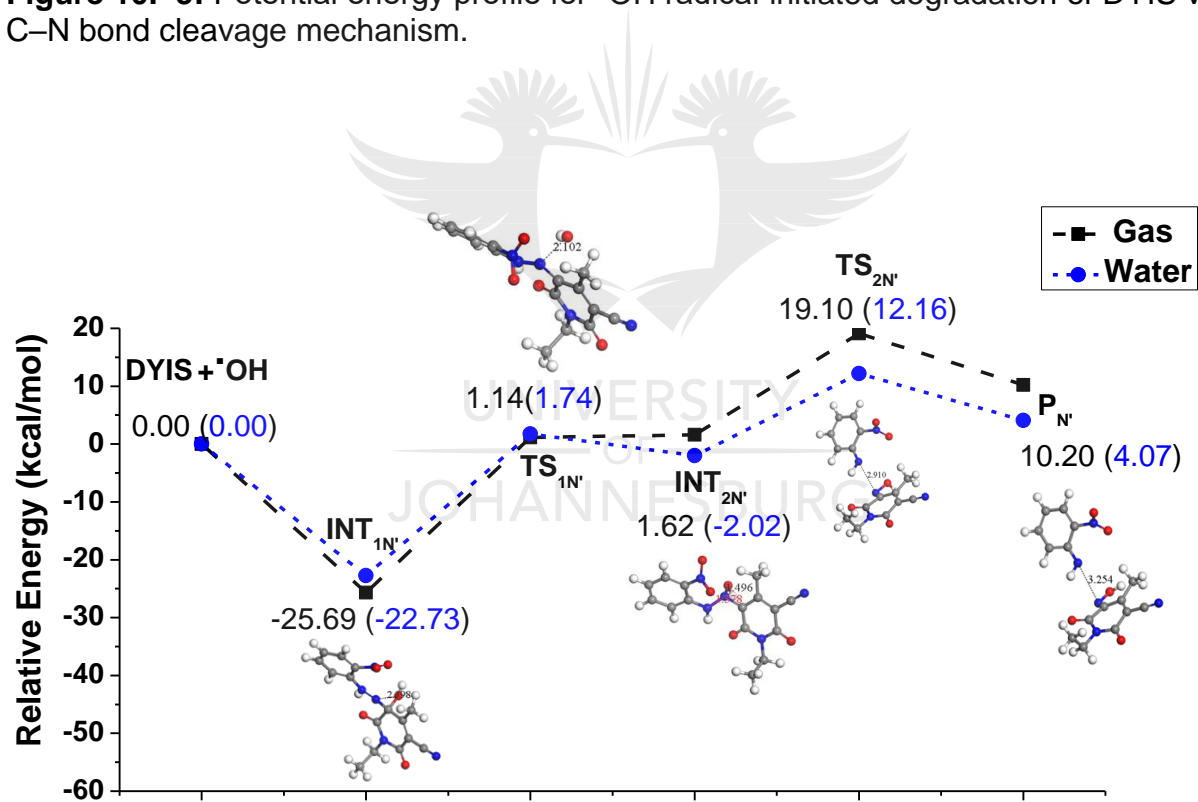


**Figure 10. 6:** Potential energy profile for •OH radical initiated degradation of DYIS via an N–N bond cleavage mechanism.

The key findings are:

- 1) For the C-N bond cleavage mechanism (Fig. 10.6), no pre-reaction complex and transition state structures were observed for the formation of the radical addition product (i.e. INT<sub>1C'</sub>).
- 2) The addition product undergoes a geometrical rearrangement involving rotation of the attached •OH radical about the C<sub>9</sub> center for increased activity.
- 3) The proton transfer step which converts the addition product (INT<sub>1C'</sub>) to its azo tautomeric form occurred simultaneously with the C-N bond cleavage in a concerted manner (Fig. 10.6), and the required activation energy is about 59 kcal/mol and 70 kcal/mol lower in vacuum and water, respectively, compared to the sum of activation energies for the proton transfer and C – N bond cleavage steps in the case of unsubstituted DY119 (Fig. 10.3). Figure A.5 (Appendix) shows a negligible change in the N–H bond length and a continuous decrease in stability of the addition product as the H–O bond distance decreases. This affirms the absence of an isolated proton transfer step in this case.
- 4) For the N-N bond cleavage pathway (Fig. 10.7), a radical addition product, (INT<sub>1N'</sub>) confirming the preferential attack of the radical on the C<sub>9</sub> instead of the N<sub>8</sub> center was observed without a pre-reaction complex and a transition state. This occurred when the radical was at a bond distance of 2.398 Å from N<sub>8</sub>, similar to what was observed in the case of DY119. Transition of this intermediate product to INT<sub>2N'</sub> and finally to P<sub>N'</sub> occurred uphill (Fig. 10.7) with activation energies of ~44 kcal/mol and ~39 kcal/mol in gas and water, respectively.

- 5) No cyclic transition state structure similar to  $TS_{2N}$  (Fig. 10.3) was observed, and the total activation energy for the N–N bond cleavage mechanism is reduced by ~46 kcal/mol and ~45 kcal/mol in vacuum and water, respectively.
- 6) As previously observed for DY119, water produced an accelerating effect on both the C–N and the N–N bond cleavage mechanisms, and a stabilizing effect on the cleavage products.
- 7) Overall, absence of one intramolecular hydrogen bond in DY119 isomer led to a general decrease in activation energies of both the C–N and the N–N bond cleavage pathways, but no marked changes in the stability of the cleavage products.

### 10.3.8 EVOLUTION OF NITROGEN MOLECULE

Using the product of the C–N bond cleavage mechanism shown in Figure 10.3, the possibility of loss of a nitrogen molecule upon further attack of  $\bullet\text{OH}$  radical on the product was investigated. This was considered necessary for achieving total degradation of the dye because it involves the removal of the main chromophoric group (i.e.  $\text{N}=\text{N}$ ) which is responsible for physicochemical properties such as color and low reactivity of the dye.

Figure 10.8 presents the calculated potential energy profile for the reaction between  $\bullet\text{OH}$  radical and the nitrodiazenyl radical portion of the C–N bond cleavage product (i.e.  $P_{1C}$ ) shown in Figure 10.3. It can be observed from Figure 10.8 that the attack of the  $\bullet\text{OH}$  radical on this fragment led to the formation of 2-nitrophenol with loss of nitrogen molecule. The result of frequency calculation gave a large imaginary frequency of  $ca - 321 \text{ cm}^{-1}$  for the transition state (i.e.  $TS_{N=N}$ ) which corresponds to the reaction coordinate (i.e. vibration of the  $\text{HO}-\text{C}_4$  bond). The estimated activation energy for this reaction is

~14 kcal/mol and ~12 kcal/mol in gas and water, respectively, and the reaction is highly spontaneous as suggested by the very low energy of the product ( $P_{N=N}$ ) compared to the reactant.

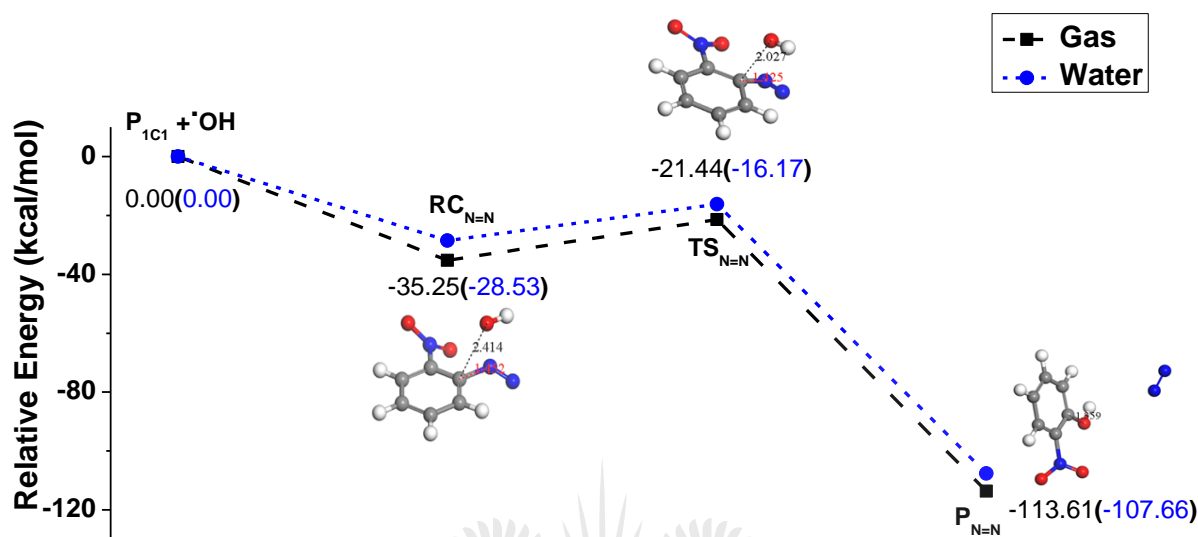


**Figure 10. 7:** Potential energy profile for  $\bullet OH$  radical initiated loss of nitrogen molecule.

As previously observed in Figure 10.3, mineralization of the radical addition product ( $INT_{1C}$ ) which began with a proton transfer isomerization step is very slow because it requires a very large activation energy. Hence, the chance of production of the nitrodiazanyl radical is very slim. However, knowing from this study that the nitrodiazanyl radical (when formed) can be converted to 2-nitrophenol which is a toxic pollutant with several health consequences [37], the need for special treatment of effluents containing DY119 and related dyes before discharge into the environment is recommended.

## 10.4 CONCLUSION

Relative favorability of C-N and N-N degradation pathways for DY 119 when reacted with  $\bullet OH$  radical has been investigated theoretically. Substantial theoretical evidences

including local reactivity indices, stability of radical addition products, stability of degradation products and activation energies suggested that C–N bond cleavage mechanism is more favorable than N–N bond cleavage pathway. Removal of one intramolecular hydrogen bond from DY119 structure led to an increase in the rate of both the C–N and the N–N bond rupture mechanisms, but with prevalence of the C–N bond. Loss of a nitrogen molecule from the C–N bond cleavage product was found to be highly spontaneous. The progress rates for both mechanisms were observed to be higher in aqueous phase than gas phase and the cleavage products are more stable in aqueous phase.

## 10.5 REFERENCES

1. L. Mahlalela and L. Dlamini. Enhanced photocatalytic activity of titania in the presence of  $\text{KNO}_3$  on the photodegradation of dyes. *Surfaces and Interfaces* **1** (2016) 21-28.
2. I. Poulios and I. Aetopoulou. Photocatalytic degradation of the textile dye reactive orange 16 in the presence of  $\text{TiO}_2$  suspensions. *Environmental Technology* **20** (1999) 479-487.
3. K. Tanaka, K. Padermpole and T. Hisanaga. Photocatalytic degradation of commercial azo dyes. *Water Research* **34** (2000) 327-333.
4. C. Bauer, P. Jacques and A. Kalt. Photooxidation of an azo dye induced by visible light incident on the surface of  $\text{TiO}_2$ . *Journal of Photochemistry and Photobiology A: Chemistry* **140** (2001) 87-92.

5. S. Ruan, F. Wu, T. Zhang, W. Gao, B. Xu and M. Zhao. Surface state studies of TiO<sub>2</sub> nanoparticles and photocatalytic degradation of methyl orange in aqueous TiO<sub>2</sub> dispersions. *Materials Chemistry and Physics* **69** (2001) 7-9.
6. N. Daneshvar, D. Salari and A. Khataee. Photocatalytic degradation of azo dye acid red 14 in water on ZnO as an alternative catalyst to TiO<sub>2</sub>. *Journal of Photochemistry and Photobiology A: Chemistry* **162** (2004) 317-322.
7. S. Chakrabarti and B. K. Dutta. Photocatalytic degradation of model textile dyes in wastewater using ZnO as semiconductor catalyst. *Journal of Hazardous Materials* **112** (2004) 269-278.
8. M. Behnajady, N. Modirshahla and R. Hamzavi. Kinetic study on photocatalytic degradation of CI Acid Yellow 23 by ZnO photocatalyst. *Journal of Hazardous Materials* **133** (2006) 226-232.
9. K. Mondal and A. Sharma. Photocatalytic oxidation of pollutant dyes in wastewater by TiO<sub>2</sub> and ZnO nano-materials-a mini-review. *Nanoscience & Technology for Mankind, The Academy of Sciences India (NASI)*, Allahabad, India (2014) 36-72.
10. A. S. Özen, V. Aviyente and R. A. Klein. Modeling the oxidative degradation of azo dyes: A density functional theory study. *The Journal of Physical Chemistry A* **107** (2003) 4898-4907.
11. C.H. Wu, P. A. Hong and M.Y. Jian. Decolorization of Reactive Red 2 in Fenton and Fenton-like systems: effects of ultrasound and ultraviolet irradiation. *Reaction Kinetics, Mechanisms and Catalysis* **106** (2012) 11-24.
12. H. Destailats, A. G. Turjanski, D. A. Estrin and M. R. Hoffmann. Molecular structure effects on the kinetics of hydroxyl radical addition to azo dyes. *Journal of Physical Organic Chemistry* **15** (2002) 287-292.

13. S. Padmaja and S. A. Madison. Hydroxyl radical-induced oxidation of azo dyes: a pulse radiolysis study. *Journal of Physical Organic Chemistry* **12** (1999) 221-226.
14. E. Naffrechoux, S. Chanoux, C. Petrier and J. Suptil. Sonochemical and photochemical oxidation of organic matter. *Ultrasonics Sonochemistry* **7** (2000) 255-259.
15. H. Destailats, A. Colussi, J. M. Joseph and M. R. Hoffmann. Synergistic effects of sonolysis combined with ozonolysis for the oxidation of azobenzene and methyl orange. *The Journal of Physical Chemistry A* **104** (2000) 8930-8935.
16. J. M. Joseph, H. Destailats, H.M. Hung and M. R. Hoffmann. The sonochemical degradation of azobenzene and related azo dyes: rate enhancements via Fenton's reactions. *The Journal of Physical Chemistry A* **104** (2000) 301-307.
17. H. Zhan, K. Chen and H. Tian. Photocatalytic degradation of acid azo dyes in aqueous TiO<sub>2</sub> suspension II. The effect of pH values. *Dyes and Pigments* **37** (1998) 241-247.
18. M. Panajkar and H. Mohan. Investigations of transients produced on reactions of OH radicals with azobenzene in aqueous solutions. *Indian Journal of Chemistry* **32A** (1993) 25-27.
19. A. S. Özen, V. Aviyente, F. De Proft and P. Geerlings. Modeling the substituent effect on the oxidative degradation of azo dyes. *The Journal of Physical Chemistry A* **108** (2004) 5990-6000.
20. X. Jiao, H. Yu, Q. Kong, Y. Luo, Q. Chen and J. Qu. Theoretical mechanistic studies on the degradation of alizarin yellow R initiated by hydroxyl radical. *Journal of Physical Organic Chemistry* **27** (2014) 519-526.



21. W. Z. Tang and R. Z. Chen. Decolorization kinetics and mechanisms of commercial dyes by H<sub>2</sub>O<sub>2</sub>/iron powder system. *Chemosphere* **32** (1996) 947-958.
22. A. S. Özen, V. Aviyente, G. Tezcanli-Güyer and N. H. Ince. Experimental and modeling approach to decolorization of azo dyes by ultrasound: degradation of the hydrazone tautomer. *The Journal of Physical Chemistry A* **109** (2005) 3506-3516.
23. J. T. Spadaro, L. Isabelle and V. Renganathan. Hydroxyl radical mediated degradation of azo dyes: evidence for benzene generation. *Environmental Science & Technology* **28** (1994) 1389-1393.
24. W. Huang. Structural and computational studies of azo dyes in the hydrazone form having the same pyridine-2, 6-dione component (II): CI Disperse Yellow 119 and CI Disperse Yellow 211. *Dyes and Pigments* **79** (2008) 69-75.
25. K. J. Sakoma, K. A. Bello and M. K. Yakubu. Synthesis of some azo disperse dyes from 1-substituted 2-hydroxy-6-pyridone derivatives and their colour assessment on polyester fabric. *Open Journal of Applied Sciences* **2** (2012) 54-59.
26. D. Patel, N. Prajapati, M. Thakor and V. Patel. Formation of some novel disperse azo dyes: Synthesis, characterisation and printing properties. *Journal of Current Chemical and Pharmaceutical Sciences* **2** (2012) 86 - 91.
27. DMol<sup>3</sup> Guide, Material Studio 8.0. *Accelrys Software, Inc.*, San Diego, United States (2017) 1-161.
28. Materials Studio simulation environment. *Release 2016, Accelrys Software Inc.*, San Diego, CA, United States, (2016).
29. M. H. Lim, S. E. Worthington, F. J. Dulles and C. J. Cramer. Density-functional calculations of radicals and diradicals. *ACS Symposium Series* **629** (1996) 402-422.

30. T. Bally and W. T. Borden. Calculations on open-shell molecules: A Beginner's Guide. *Reviews in Computational Chemistry*, **13** (2007) 1-97.
31. T. A. Halgren and W. N. Lipscomb. The synchronous-transit method for determining reaction pathways and locating molecular transition states. *Chemical Physics Letters* **49** (1977) 225-232.
32. N. Govind, M. Petersen, G. Fitzgerald, D. King-Smith and J. Andzelm. A generalized synchronous transit method for transition state location. *Computational Materials Science* **28** (2003) 250-258.
33. Y. Inada and H. Orita. Efficiency of numerical basis sets for predicting the binding energies of hydrogen bonded complexes: evidence of small basis set superposition error compared to Gaussian basis sets. *Journal of Computational Chemistry* **29** (2008) 225-232.
34. A. Klamt. The COSMO and COSMO-RS solvation models. *Wiley Interdisciplinary Reviews: Computational Molecular Science* **8** (2018) 1338(1)-1338(11).
35. P. W. Ayers and R. G. Parr. Variational principles for describing chemical reactions: the Fukui function and chemical hardness revisited. *Journal of the American Chemical Society* **122** (2000) 2010-2018.
36. H. Jónsson, G. Mills and K. W. Jacobsen. Nudged elastic band method for finding minimum energy paths of transitions. in Classical and quantum dynamics in condensed phase simulations. *World Scientific* (1998) 385-404. Doi: 10.1142/9789812839664\_0016.
37. Agency for toxic substances and disease registry. Toxicological profile for nitrophenols: 2-nitrophenol and 4-nitrophenol. *US Public Health Service*, Atlanta,

Chapter 10: A DFT study of disperse yellow 119 degradation mechanism by hydroxyl radical attack  
GA, USA, (1992). <https://www.atsdr.cdc.gov/toxprofiles/tp50-p.pdf>. Last accessed  
on August 17, 2018.



---

## CHAPTER 11

# A DFT STUDY OF HYDROXYL RADICAL DEGRADATION OF DISPERSE RED 73 (DR73)

---

### PREAMBLE

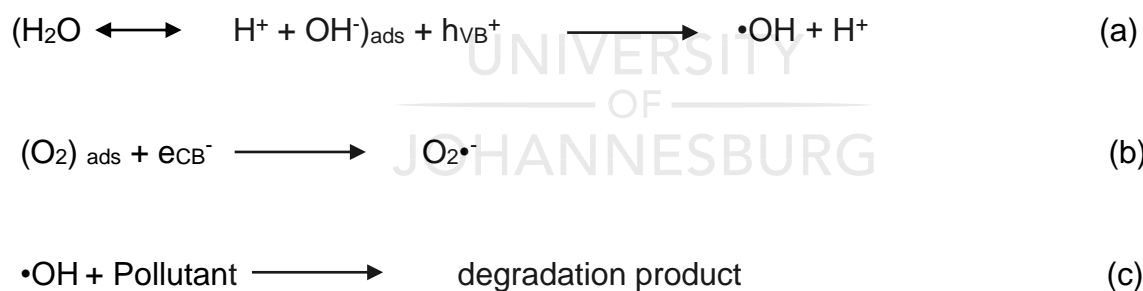
Using DFT calculations, the degradation mechanisms of disperse red 73 (DR73) dye upon exposure to hydroxyl radical attack is investigated in this chapter. The energetics of two experimentally proposed azo dye degradation pathways involving the attack of the radical on one of the azo (N=N) nitrogen, or on a ring carbon attached to the azo group, leading to an N-N or C-N bond cleavage, respectively, were compared. This was necessary to determine the more energetically preferred degradation pathway for DR73 and hence, predict the degradation products. The results showed that the addition of •OH radical to the dye via one of the azo (N=N) nitrogen will occur more fervently compared to its addition through a ring carbon attached to it. However, the subsequent cleavage of the N-N bond was found to be kinetically and thermodynamically less favored compared to the C-N bond cleavage arising from the attack of the radical on a ring carbon attached to the azo group.

### 11.1 INTRODUCTION

Disperse red 73 (DR73) is considered as an azo disperse dye with high mutagenic potential [1], and their biotransformation with enzymes such as azoreductase also leads to generation of carcinogenic amine products which can endanger life and the environment [2]. Therefore, adequate treatment of industrial wastes containing this dye is

necessary to detoxify the effluents prior to discharge into the environment. Advanced oxidation processes such as photocatalytic oxidation which makes use of nontoxic photo-active metallic oxides or semiconductors as catalysts [3-10] has proven to be very effective and efficient for this purpose because it guarantees total elimination or detoxification of pollutants.

Photochemical production of  $\bullet\text{OH}$  radical occurs from the splitting of adsorbed water molecules on the surface of a photo-excited catalyst (Scheme 11.1a), when the catalyst is illuminated with light of sufficient energy. Electrons are promoted from the valence band (VB) to the conduction band (CB) of the catalyst where they are entrapped by adsorbed oxygen molecules (Scheme 11.1b), to prevent their recombination with generated holes in the VB. Reaction of photo-generated  $\bullet\text{OH}$  radical with the pollutant leads to pollutant degradation (Scheme 11.1c) [11].



**Scheme 11. 1:** Photochemical production of  $\bullet\text{OH}$  radical during a photocatalytic degradation process.

$\bullet\text{OH}$  radicals can also be generated radiolytically, chemically, by ultrasonic irradiation [12-15] or by the use of combination of methods [16-18]. Irrespective of the method of production, a photo-generated  $\bullet\text{OH}$  radical can only bring about degradation of an azo dye in two ways. It can either attack the dye through a ring carbon next to the azo ( $\text{N}=\text{N}$ )

chromophore, or via one of the azo nitrogen [18-20]. This leads to a C-N or an N-N bond rupture degradation mechanism, respectively.

Reaction of  $\bullet\text{OH}$  radical with azo dyes can generally be divided into two major steps - the radical addition and the bond rupture steps [12, 21, 22]. The addition step forms a colorless  $\bullet\text{OH}$  adduct [20], while the bond cleavage step leads to adduct fragmentation. Determination of the preferred mechanism (i.e. C-N or N-N bond cleavage) for a given azo dye is necessary to predict its degradation product(s) for appropriate decisions on safety.

A plethora of experimental reports on azo dye degradation by  $\bullet\text{OH}$  radicals [18-20, 23, 24] have proposed an N-N bond cleavage pathway in which ca 60% of the radicals attack the azo chromophore, while the remaining 40% attack the carbon atom linked to the chromophore [20]. Spadaro *et al.* [25] proposed a dominant C-N bond cleavage mechanism for the reaction of  $\bullet\text{OH}$  radical with azobenzene.

Theoretical studies using DFT methods have been conducted on different azobenzene derivatives to predict the preferred degradation pathway and to examine the effects of substituent groups, molecular charge and tautomerism on the degradation mechanisms [21, 22, 24]. Reaction of  $\bullet\text{OH}$  radical with both unsubstituted and substituted azobenzene dye was predicted to favor the N-N bond cleavage pathway [12, 21]. However, theoretical study by Ozen *et al.* [24] reported the predominance of the C-N bond cleavage mechanism over the N-N counterpart for azo dyes that exist predominantly in hydrazone tautomeric form.

On the contrary, Jiao *et al.* [22] in a similar study on Alizarin Yellow R concluded that the N-N and the C-N bond rupture mechanisms have close kinetic chances, but the latter showed lower thermodynamic priority for the neutral form of the dye.

From the foregoing findings, it can be deduced that the degradation mechanism varies from one azo dye to another depending on the components of the dye structure and its tautomeric form. In other words, the degradation pathway of an azo dye may not necessarily be the same as that of other similar members. Therefore, more investigations are required to resolve these mechanistic issues.

In response to the above, we investigated in a separate study, the degradation mechanism(s) of Disperse yellow 119 dye which exists in hydrazone tautomeric form, and found that the most preferred degradation mechanism for this dye is the C-N bond cleavage pathway. As a step further, the current study investigated theoretically, the mechanism of  $\bullet\text{OH}$  radical reaction with Disperse red 73 which exists in azo tautomeric form (Fig. 11.1) [2, 26]. Possibility of occurrence of deamination and nitrogen evolution processes from further attack of  $\bullet\text{OH}$  radical on the bond cleavage products was also investigated.

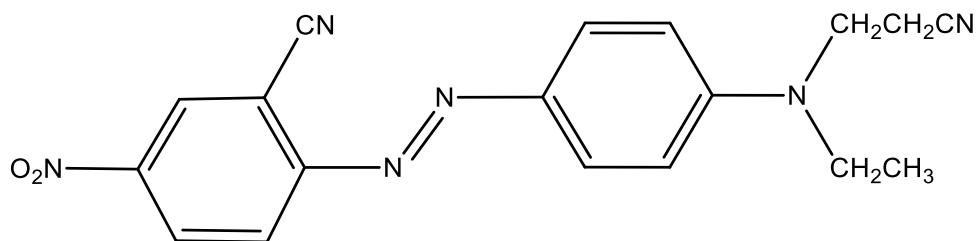


**Figure 11. 1:** Molecular structure of Disperse red 73 (DR73).

## 11.2 COMPUTATIONAL DETAILS

### 11.2.1 COMPUTATIONAL SOFTWARE

This study was carried out using the DMol<sup>3</sup> computational code [27] implemented in Material Studio (2016 version) [28], because it uses density functional theory (DFT) methods which are more suitable for open shell electronic systems such as radicals [12, 29] for performing calculations. In addition to their higher calculation accuracy at moderate speed, DFT methods are not vulnerable to spin contamination which is a major limitation of Hartree-Fock methods [12, 30].

Utilisation of DMol<sup>3</sup> was also due to its possession of a powerful transition state search scheme which combines the linear synchronous transit (LST) and the quadratic synchronous transit (QST) methods [31, 32] for a quick determination of transition states. DMol<sup>3</sup> also employs the numerical types of basis sets which provide greater accuracy and speed compared to the Gaussian counterparts [33]. Numerical basis sets possess a remarkable ability to neutralize basis set superposition errors (BSSE) [33].

Finally, DMol<sup>3</sup> employs the conductor-like screening model (COSMO) which is considered as the most accomplished implicit solvation model for solvent phase calculations [34].

### 11.2.2 CALCULATION PROCEDURE

All calculations were performed using the VWN-BP functional [27] with double numerical basis set containing polarization functions (DNP) [27, 33].

Susceptibility of the prospective reaction sites in DR73 to a radical attack was first evaluated to determine the site(s) with the highest propensity to the attack of •OH radical.



This was achieved by calculating their atom condensed Fukui functions for radical attack using Mulliken atomic charges according to equation 11.1 [12, 35];

$$f^0 = \frac{1}{2} [q_k(N + 1) - q_k(N - 1)]$$

Equation 11. 1

where  $f^0$  is the Fukui function for radical attack,  $q_k(N + 1)$ , and  $q_k(N - 1)$  are the Mulliken charges on atom k for  $(N + 1)$  and  $(N - 1)$  number of electrons, respectively. Sites with the highest reactivity were then selected for the degradation pathway study.

The potential energy profiles for the addition of  $\bullet\text{OH}$  radical to DR73 through the selected sites, and the subsequent fragmentation of the resulting adduct via a C-N or N-N bond rupture pathway were calculated. All transition state structures were verified by frequency calculations. A unique transition state confirmation scheme which uses the nudged elastic band (NEB) method [36] was used to ascertain the connection between the transition states and their associated intermediates or products, and to reveal other possible transition state structure(s) that may be present along the reaction path. Relevant stationary point geometries (i.e. reactants, intermediates, transition states and products) in the energy profiles were subjected to full optimization. Effect of water on the reaction was investigated by means of single point energy calculations using COSMO with a COSMO dielectric constant of 78.4 (i.e. dielectric constant water).

## 11.3 RESULTS AND DISCUSSIONS

### 11.3.1 ASSESSMENT OF SITE SUSCEPTIBILITY TO RADICAL ATTACK

The results of site activity evaluation for DR73 are presented in Table 11.1 in which only the prospective reaction sites (C<sub>4</sub>, N<sub>7</sub>, N<sub>8</sub> and C<sub>9</sub>) involved in degradation are shown. This is to determine the most vulnerable carbon and/or nitrogen center to the attack of •OH radical, since the prospective reaction sites have different chemical environments, as a result of differences in the chemical constituents of the surrounding rings (Fig. 11.2).

**Table 11. 1:** Mulliken radical attack Fukui functions,  $f^0$  for the prospective reaction sites in DR73.

Atoms	$f^0$
C <sub>4</sub>	0.025
N <sub>7</sub>	0.057
N <sub>8</sub>	0.058
C <sub>9</sub>	0.034

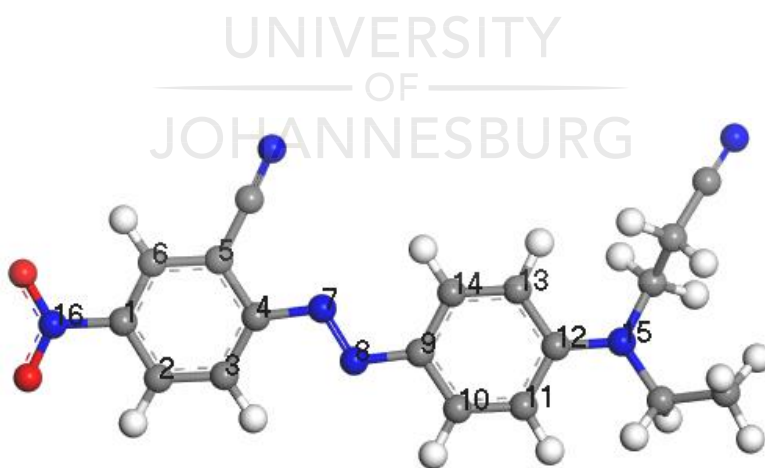


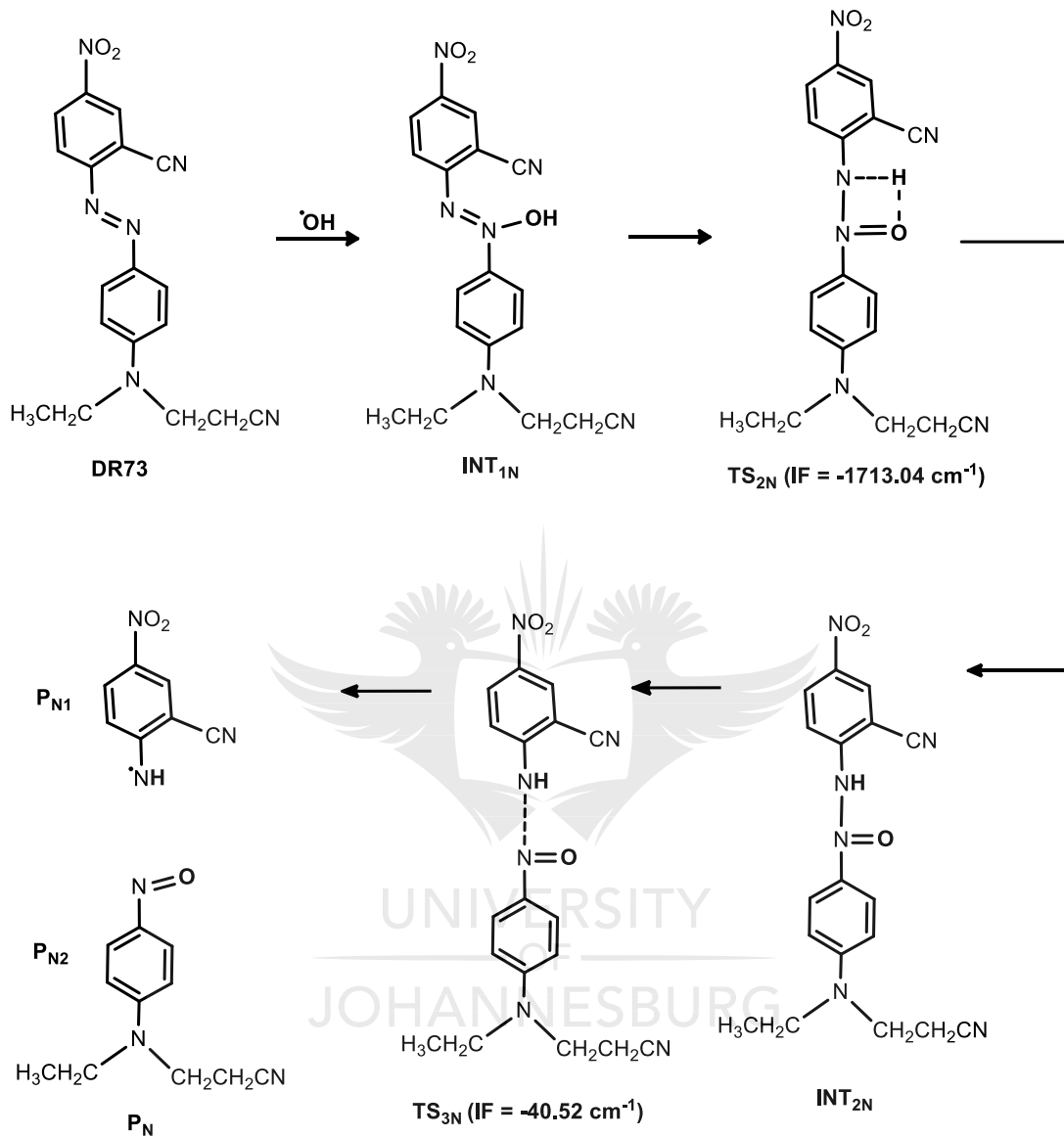
**Figure 11. 2:** Optimized geometry of DR73 showing the prospective reaction sites for •OH radical. Atoms colored in white, grey, blue and red are hydrogen, carbon, nitrogen and oxygen, respectively.

According to Table 11.1, the most favorable site for the attack of  $\bullet\text{OH}$  radical for a C–N bond rupture degradation mechanism is the  $\text{C}_9$  center whereas both the  $\text{N}_7$  and the  $\text{N}_8$  sites can spontaneously give rise to an N–N bond rupture mechanism. However,  $\text{N}_8$  seems to be a little more reactive than  $\text{N}_7$  and as a result, this is the site chosen for the N–N bond rupture mechanism.

The results in Table 11.1 also revealed that the  $\text{N}_8$  center is more vulnerable to radical attack compared to  $\text{C}_9$ . Hence, the attack of  $\bullet\text{OH}$  radical on  $\text{N}_8$  will be more spontaneous, and may give precedence to the N–N bond rupture mechanism.

### 11.3.2 N-N BOND RUPTURE DEGRADATION MECHANISM

The modelled energy profile for the reaction of  $\bullet\text{OH}$  radical with DR73 via the  $\text{N}_8$  center (Scheme 11.2), is shown in Figure 11.3. As evident from the figure, the attack of the radical on the  $\text{N}_8$  center occurred downhill without a pre-reaction complex and transition state, which is indicative of a barrierless radical addition process. This may be due to the high reactivity of the  $\text{N}_8$  center discussed previously. The radical addition product,  $\text{INT}_{1\text{N}}$  undergoes self-protonation by transfer of a hydrogen atom from the attached OH group to the  $\text{N}_7$  center through a cyclic transition state structure,  $\text{TS}_{2\text{N}}$  (Scheme 11.2). The protonation product,  $\text{INT}_{2\text{N}}$  finally undergoes an  $\text{N}_7$ – $\text{N}_8$  bond cleavage via a transition state structure,  $\text{TS}_{3\text{N}}$ , to form the cleavage product,  $\text{P}_\text{N}$ . Since a similar proton transfer which seems to be the rate limiting step has been reported for unsubstituted/symmetrical azobenzene [12], it is therefore reasonable to conclude that this step is intrinsic of the N–N degradation pathway of every azo dye (symmetrical or asymmetrical) that exist in the azo form only.



**Scheme 11. 2:** N–N bond rupture degradation mechanism.

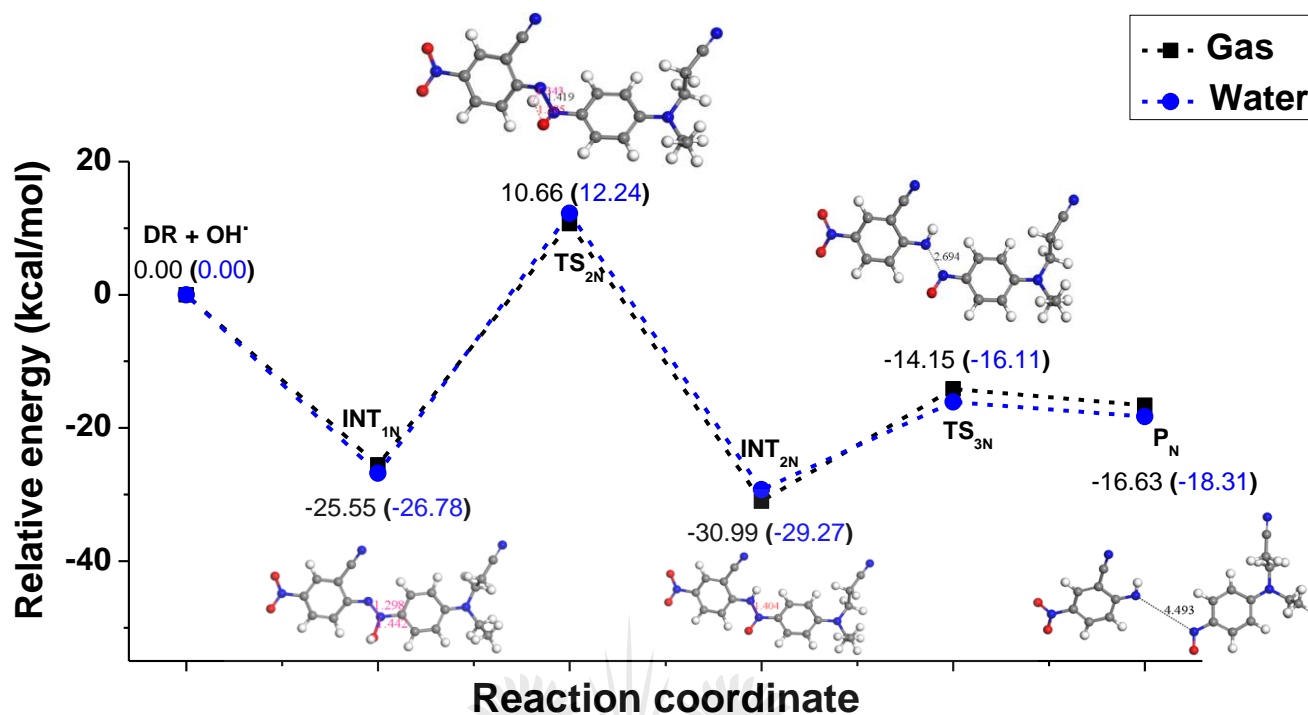


**Figure 11. 3:** Potential energy profile for •OH radical initiated degradation of DR73 via an N–N bond cleavage mechanism.

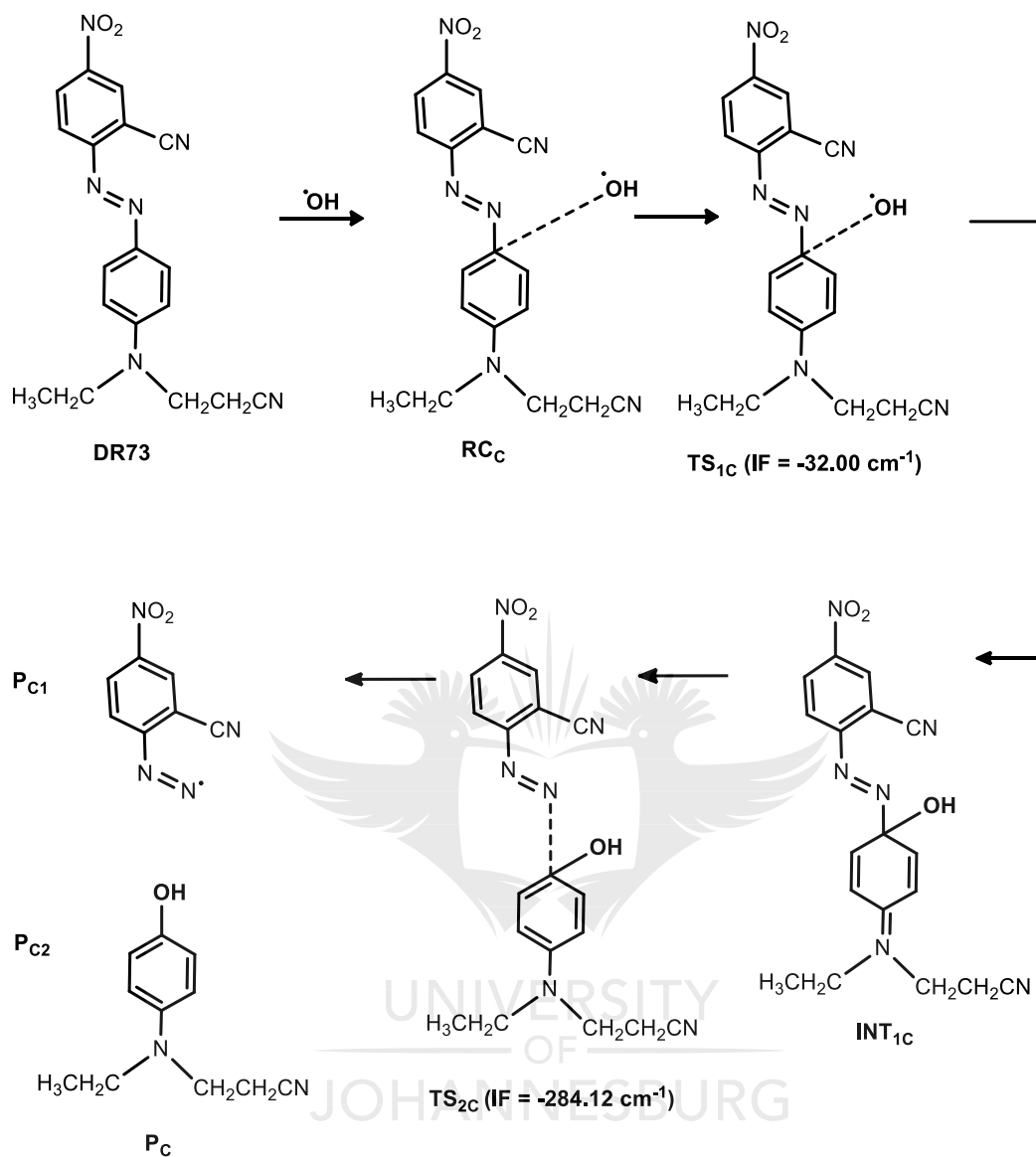
### 11.3.3 EFFECT OF WATER ON N–N BOND RUPTURE DEGRADATION MECHANISM

As can be observed from Figure 11.3, the introduction of water raises the activation energy of the protonation step by ~ 3 kcal/mol but lowers that of the N–N bond cleavage step by ~ 4 kcal/mol. This implies that the protonation reaction is inhibited by water probably due to existence of hydrogen bonding between the solvent and the hydroxyl hydrogen atom. Inspection of the figure revealed a decrease in the energy of the radical addition product, INT<sub>1N</sub>, and an increase in that of the protonation transition state, TS<sub>2N</sub> in water, which led to the observed increase in the activation energy of protonation in the solvent. On the other hand, the decrease in the activation energy for the N–N bond cleavage is indicative of increased ease of polarization of the bond in the presence of water. Contrary to the trend observed for the protonation step, the energy of the reactant

for the cleavage step i.e. the protonation product,  $INT_{2N}$  is raised while that of the transition state,  $TS_{3N}$  is lowered by water. This explains the observed decrease in the activation energy for the N-N bond cleavage in water. The increase in the stability of the cleavage product,  $P_N$  in water coupled with the observed decrease in the activation energy of cleavage suggests that polarization of the N-N bond is thermodynamically and kinetically enhanced by water.

#### 11.3.4 C-N BOND RUPTURE DEGRADATION MECHANISM

The result of  $\bullet OH$  radical reaction with DR73 via the  $C_9$  reactive center of the dye (Scheme 11.3) is presented in Figure 11.4. Contrary to the trend observed for the N-N bond cleavage mechanism in which the attack of the radical occurred on the  $N_8$  reaction site without a pre-reaction complex and a transition state (Fig. 11.3), the energy profile in Figure 11.4 shows a radical addition step that occurred through a pre-reaction complex,  $RC_C$  and a transition state,  $TS_{1C}$ , which led to the radical addition product,  $INT_{1C}$ . This is followed by the cleavage of the bond between the  $C_9$  and the  $N_8$  sites via a transition state,  $TS_{2C}$  leading to the formation of the cleavage product,  $P_C$ . Transition state confirmation using the NEB method revealed that all the transition states in Figure 11.4 are directly linked to their respective reactants and products.



**Scheme 11. 3:** C–N bond rupture degradation mechanism.

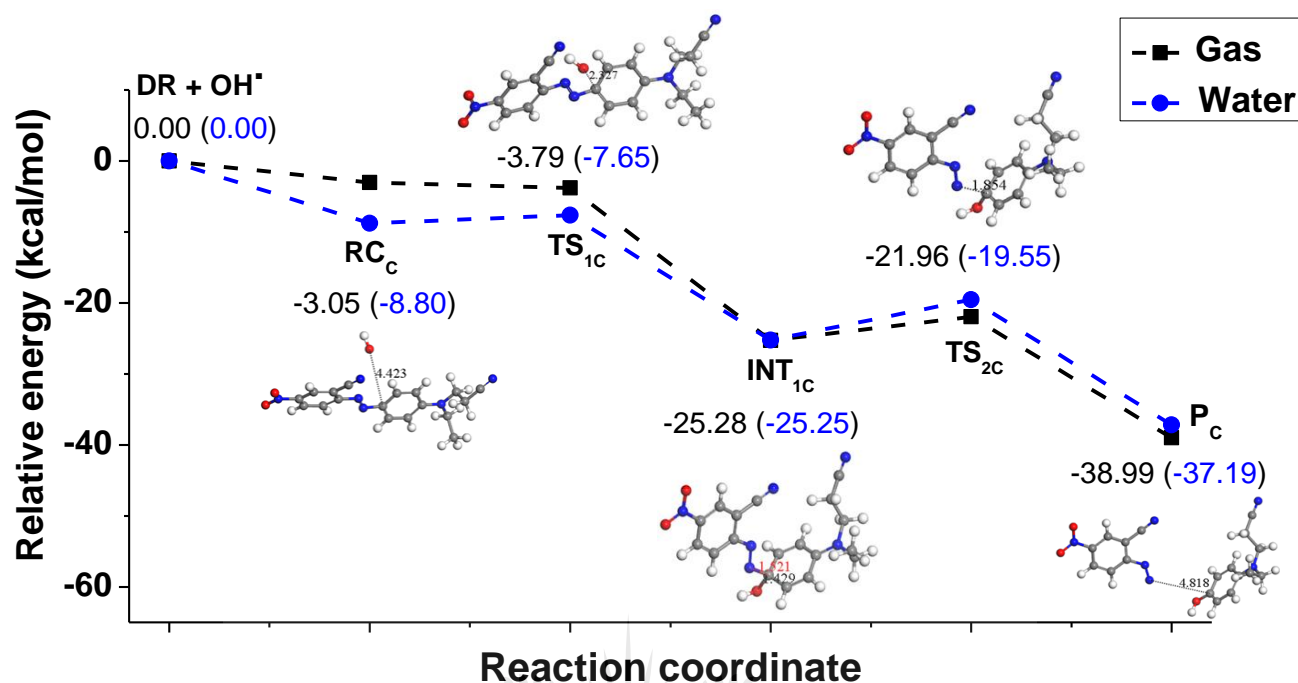


**Figure 11. 4:** Potential energy profile for  $\bullet\text{OH}$  radical initiated degradation of DR73 via a C–N bond rupture mechanism.

### 11.3.5 EFFECT OF WATER ON C–N BOND RUPTURE DEGRADATION MECHANISM

From the results shown in Figure 11.4, the introduction of water raises both the activation energies for the radical addition and the C–N bond cleavage by  $\sim 1.9$  kcal/mol and  $\sim 2.4$  kcal/mol, respectively, which suggests that these processes are inhibited by water.

In other words, the approach of the  $\bullet\text{OH}$  radical towards the reaction site (i.e. C<sub>9</sub>) and the subsequent polarization of the C<sub>9</sub>–N<sub>8</sub> bond are kinetically hindered by water. Contrary to the trend observed in the gas phase, the energy of the transition state, TS<sub>1c</sub> relative to the pre-reaction complex, RC<sub>c</sub> is higher in the aqueous phase, which explains the increase in activation energy observed in this medium. In the case of the bond cleavage step, the introduction of water led to a significant increase in the energy of the transition



state,  $TS_{2C}$ , but a negligible increase in that of the intermediate,  $INT_{1C}$ . This accounts for the observed increase in the activation energy for the bond cleavage in water.

Thermodynamically, water enhances the stability of the stationary point geometries (i.e.  $RC_C$  and  $TS_{1C}$ ) of the radical addition, but lowers the stability of those of the bond cleavage (i.e.  $INT_{1C}$ ,  $TS_{2C}$  and  $P_C$ ) (Fig. 11.4).

### 11.3.6 COMPARISON BETWEEN THE N-N AND THE C-N BOND RUPTURE DEGRADATION MECHANISMS

To determine the most preferred degradation mechanism (i.e. N-N or C-N) for DR73, the energetics of the competing mechanisms are compared kinetically and thermodynamically in Table 11.2 to identify the one with the highest kinetic and/or thermodynamic favorability. The kinetic parameters in the table are the activation energies for the radical addition ( $\Delta E_{RA}^\ddagger$ ) and the bond rupture ( $\Delta E_{BR}^\ddagger$ ) steps, and the total activation energies ( $\Delta E_A^\ddagger$ ) for each mechanism. Again, the radical addition step is the step that produces the intermediates,  $INT_{1N}$  and  $INT_{1C}$  in Figures 11.3 and 11.4, respectively, while the bond cleavage step is the final step in each figure. The total activation energy for each mechanism is the sum of activation energies involved in the complete transformation of DR73 to the final degradation products,  $P_C$  and  $P_N$ .

Thermodynamic favorability is predicted based on the relative energies,  $E_{AP}$  and  $E_{BRP}$  of the addition and the bond rupture products, respectively (Table 11.2). Values given in parentheses in the table are the results obtained in water.

From Table 11.2, the absence of a  $\Delta E_{RA}^\ddagger$  value for the N-N rupture mechanism which indicates a lack of energy barrier to  $\bullet OH$  radical addition (Fig. 11.3), confirms greater

**Table 11. 2:** Energetic parameters for the C-N and the N-N bond rupture degradation mechanisms.

Parameters (kcal/mol)	•OH attack on N <sub>8</sub> (N-N rupture)	•OH attack on C <sub>9</sub> (C-N rupture)
$\Delta E_{RA}^\ddagger$	-	-0.74 (1.15) <sup>xx</sup>
$\Delta E_{BR}^\ddagger$	16.84 (13.16) <sup>y</sup>	3.32 (5.70) <sup>yy</sup>
$\Delta E_A^\ddagger$	53.05 (52.18) <sup>z</sup>	2.58 (6.85) <sup>zz</sup>
$E_{AP}$	-25.55 (-26.78)	-25.28 (-25.25)
$E_{BRP}$	-16.63 (-18.31)	-38.99 (-37.19)

<sup>xx</sup>(TS<sub>1C</sub> – RC<sub>C</sub>)<sup>y</sup>TS<sub>3N</sub> – INT<sub>2N</sub>, <sup>yy</sup>(TS<sub>2C</sub> – INT<sub>1C</sub>)<sup>z</sup>[(TS<sub>2N</sub> – INT<sub>1N</sub>) + (TS<sub>3N</sub> – INT<sub>2N</sub>)], <sup>zz</sup>[(TS<sub>1C</sub> – RC<sub>C</sub>) + (TS<sub>2C</sub> – INT<sub>1C</sub>)]

kinetic preference for the attack of the radical on N<sub>8</sub> compared to C<sub>9</sub>, which is in accord with the Fukui function trend shown in Table 11.1. However, the very low  $\Delta E_{RA}^\ddagger$  value for C-N rupture mechanism (particularly in gas) equally suggests a high kinetic probability for the radical attack on C<sub>9</sub>, while the slight difference in the  $E_{AP}$  values suggests that the attack of the radical on both sites are thermodynamically competitive.

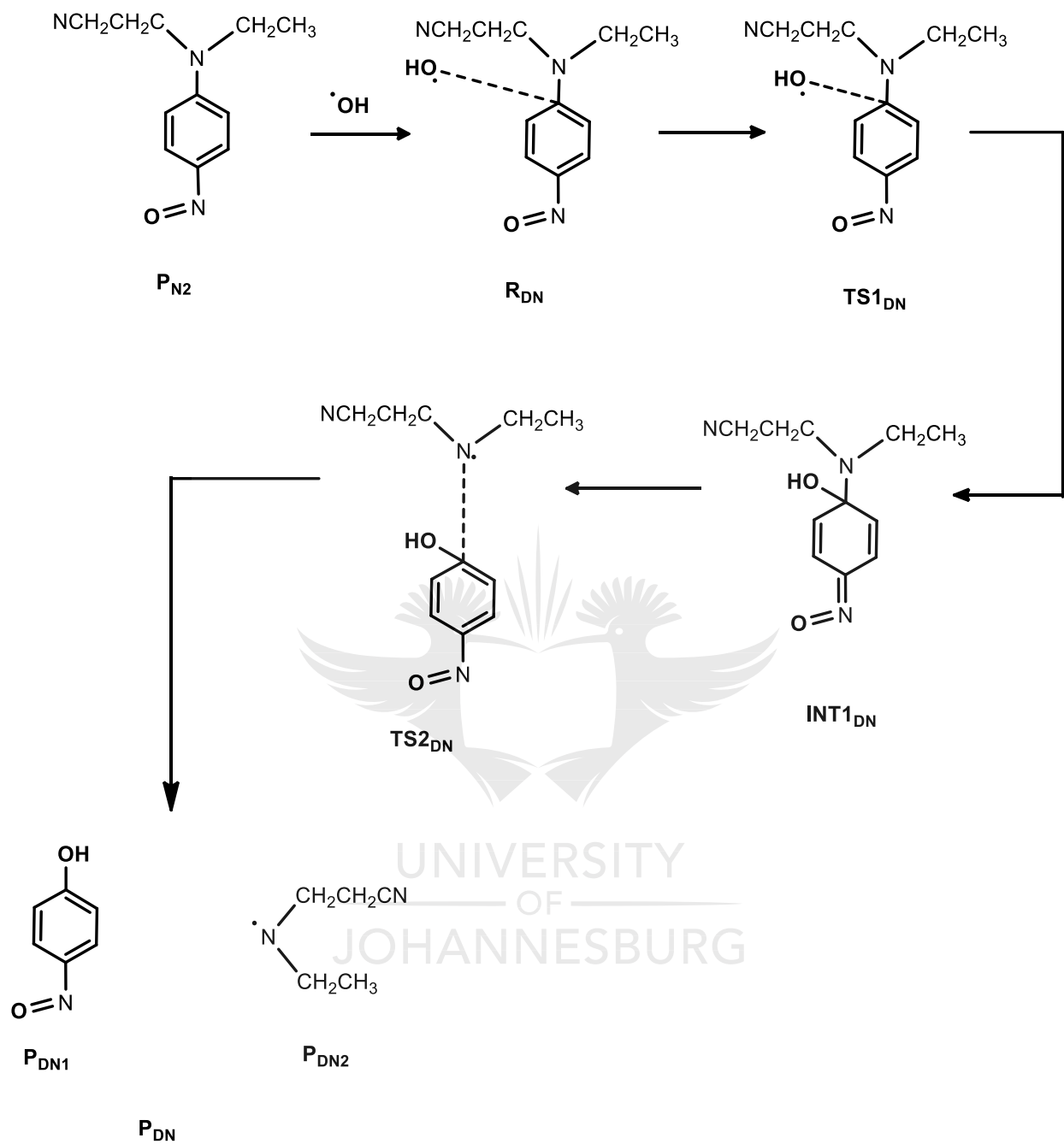
Values of the activation energies,  $\Delta E_{BR}^\ddagger$  for the bond rupture step, and the relative energies,  $E_{BRP}$  of the resulting products suggests that the C-N bond rupture is kinetically and thermodynamically more favored and more preferred compared to the N-N bond rupture.

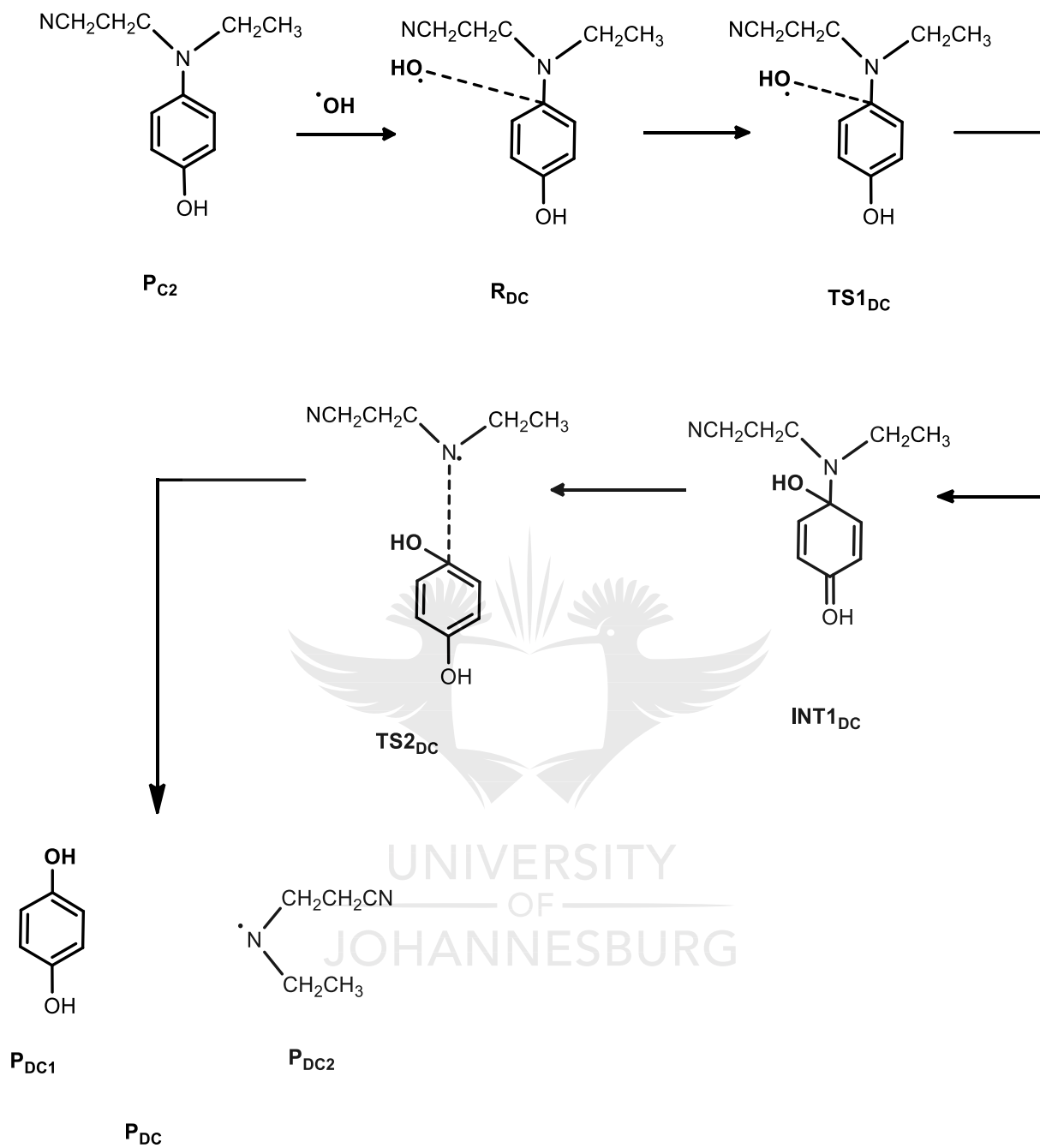
Overall, the total activation energies,  $\Delta E_A^\ddagger$  and the  $E_{BRP}$  values revealed that the C-N bond rupture degradation mechanism is kinetically and thermodynamically more feasible compared to the N-N counterpart. Although, the addition of •OH radical which leads to decoloration of a dye will occur more rapidly and fervently via the N<sub>8</sub> site as informed by the lack of energy barrier in the radical addition step (Fig. 11.2), the subsequent cleavage of the N-N bond is both kinetically and thermodynamically less favored.

### 11.3.7 DEAMINATION

To explore the likelihood of further disintegration of the bond cleavage products,  $P_{N_2}$  and  $P_{C_2}$  (Schemes 11.2 and 11.3, respectively) into simpler forms, they were subjected to deamination through the attack of  $\bullet OH$  radical on the  $C_{12}$  reaction site (Fig. 11.2, Schemes 11.4 and 11.5). The resulting potential energy profiles are presented in Figures 11.5 and 11.6, respectively. Each energy profile consists of two segments. The first segment is the radical addition step which yielded an  $\bullet OH$  radical containing adduct (i.e.  $INT_{DN}$  or  $INT_{DC}$ ), while the second segment is the adduct fragmentation step which led to the removal of the substituted amino moiety. It is evident from both energy profiles that the latter step is the rate determining step, and unlike for  $P_{C_2}$ , this step is endothermic and hence, thermodynamically unfavorable for  $P_{N_2}$ .



Scheme 11. 4:  $\cdot\text{OH}$  radical initiated deamination of  $\text{P}_{\text{N}2}$ .

Scheme 11. 5:  $\cdot\text{OH}$  radical initiated deamination of  $\text{Pc}_2$ .

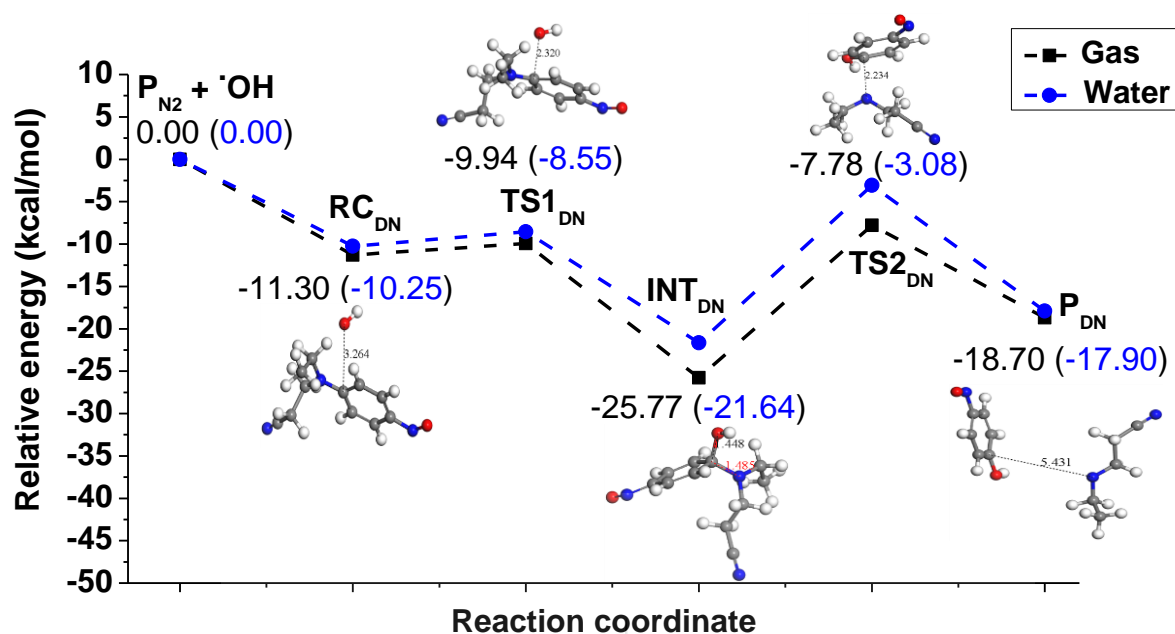


Figure 11. 5: Potential energy profile for •OH radical initiated deamination of P<sub>N2</sub>.

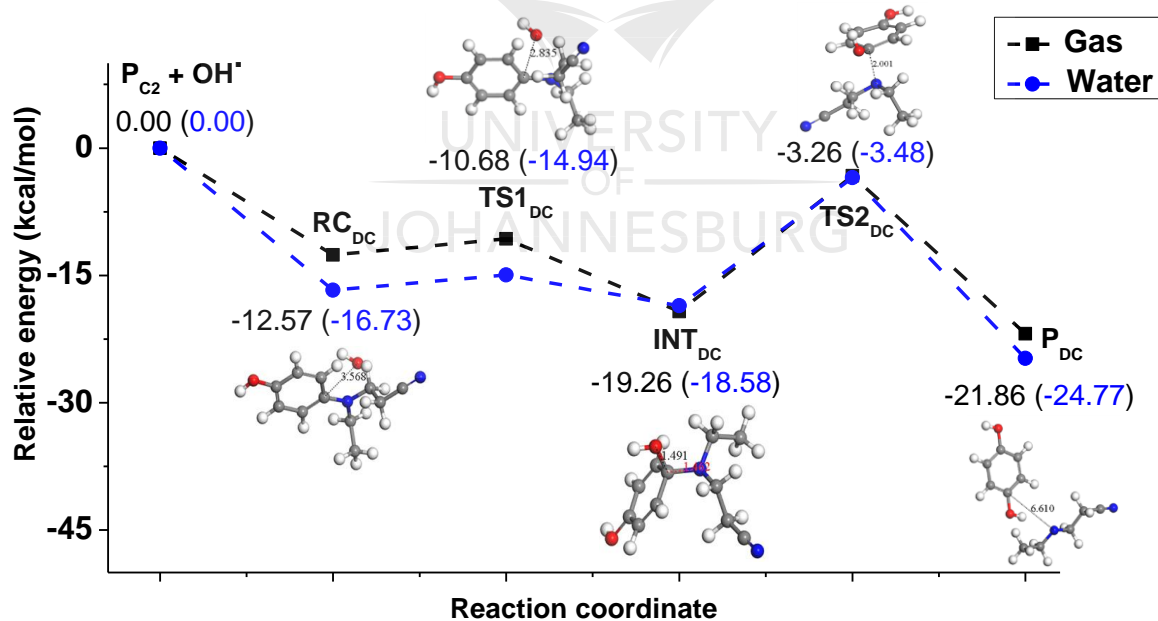


Figure 11. 6: Potential energy profile for •OH radical initiated deamination of P<sub>C2</sub>.

Also, by comparing their activation energies for the adduct fragmentation ( $\Delta E_{AF}^\ddagger$ ) step, and their overall activation energies ( $\Delta E_A^\ddagger$ ), it is obvious from Table 11.3 that the deamination of  $P_{C2}$  is kinetically more favored than that of  $P_{N2}$ , even though their radical addition steps have close kinetic chances as suggested by their  $\Delta E_{RA}^\ddagger$  values. Values given in parentheses in the table are the activation energies obtained in water.

**Table 11. 3:** Activation parameters for the deamination of  $P_{N2}$  and  $P_{C2}$  by  $\bullet OH$  radical.

Parameters (kcal/mol)	$P_{N2}$	$P_{C2}$
$\Delta E_{RA}^\ddagger$	1.36 (1.70) <sup>a</sup>	1.89 (1.79) <sup>aa</sup>
$\Delta E_{AF}^\ddagger$	17.99 (18.56) <sup>b</sup>	16.00 (15.10) <sup>bb</sup>
$\Delta E_A^\ddagger$	19.35 (20.26) <sup>c</sup>	17.89 (16.89) <sup>cc</sup>

<sup>a</sup>( $TS1_{DN} - RC_{DN}$ ), <sup>aa</sup>( $TS1_{DC} - RC_{DC}$ )

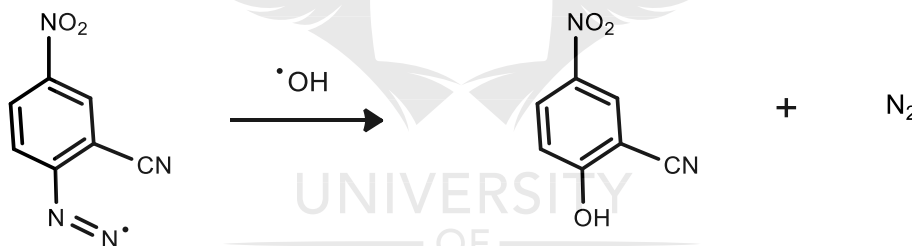
<sup>b</sup>( $TS2_{DN} - INT_{DN}$ ), <sup>bb</sup>( $TS2_{DC} - INT_{DC}$ )

<sup>c</sup>[( $TS1_{DN} - RC_{DN}$ ) + ( $TS2_{DN} - INT_{DN}$ )], <sup>cc</sup>[( $TS1_{DC} - RC_{DC}$ ) + ( $TS2_{DC} - INT_{DC}$ )]

The introduction of water produced a contrasting effect on the deamination of  $P_{N2}$  and  $P_{C2}$  as can be observed from Figures 11.5 and 11.6. It destabilized the deamination of  $P_{N2}$  by raising the energies of the stationary point geometries (Fig. 11.5), but stabilized that of  $P_{C2}$  by lowering the energies of the geometries in the energy profile (Fig. 11.6). Consequently, the deamination of  $P_{N2}$  is inhibited by water while that of  $P_{C2}$  is kinetically enhanced by the solvent as revealed by the activation energies in parentheses (Table 11.3).

### 11.3.8 LOSS OF MOLECULAR NITROGEN

To deradicalize the cyanonitrodiazenyl portion (i.e.  $P_{C1}$ ) of the C-N bond rupture product (Figure 11.4), and investigate the likelihood of removal of the chromophoric azo ( $N=N$ ) group, the C-N bond cleavage product,  $P_{C1}$  (Scheme 11.3) was also subjected to  $\bullet OH$  radical attack through the  $C_4$  reaction site (Fig. 11.2) to expel the azo ( $N=N$ ) group as molecular nitrogen (Scheme 11.6). The results of this investigation shown in Figure 11.7 clearly revealed that the displacement of the azo group by the  $\bullet OH$  radical is very rapid and highly spontaneous, since the reaction proceeded downhill with no energy barrier to produce cyanonitrophenol and nitrogen molecules. The slightly higher energy barrier located between  $P_{N=N}$  and  $P_R$  is due to rotation of the phenolic  $-OH$  about the  $C_4$  axis.



**Scheme 11. 6:**  $\bullet OH$  radical initiated removal of molecular nitrogen from the C-N bond cleavage product,  $P_{C1}$ .



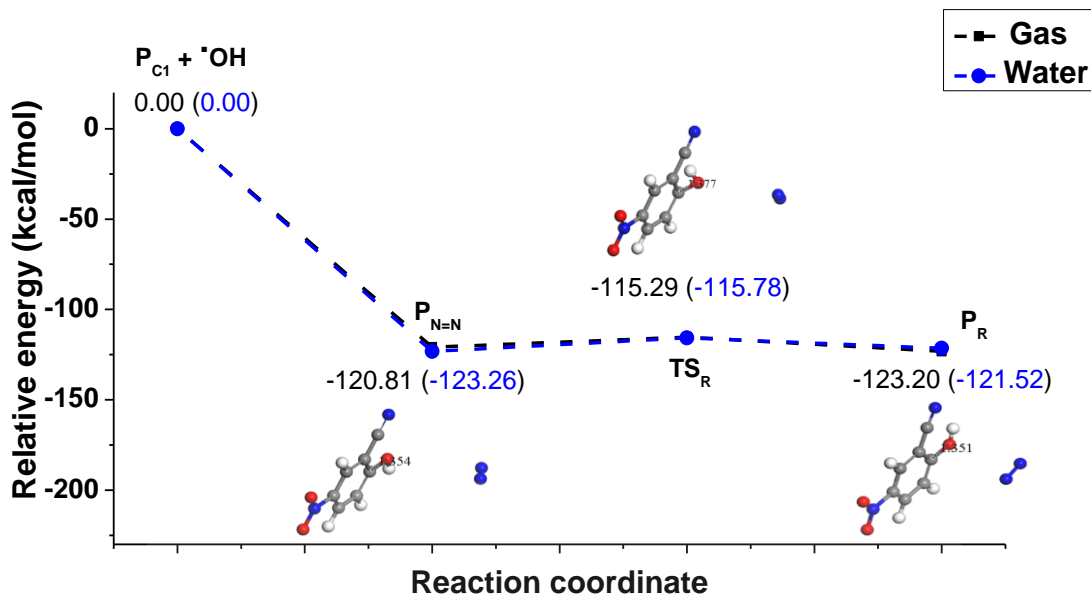


**Figure 11. 7:** Potential energy profile for  $\cdot OH$  radical initiated loss of nitrogen molecule from the C–N bond cleavage product,  $P_{C1}$ .

### 11.3.9 IMPLICATIONS OF DEAMINATION AND NITROGEN EVOLUTION PROCESSES

It has been established from the discussions so far that the deamination and nitrogen evolution reactions of DR73 degradation products, particularly those arising from the C–N bond cleavage mechanism, are kinetically and thermodynamically favorable. In other words, production of 1,4-benzenediol (i.e. quinol) (Fig. 11.6) and cyanonitrophenol (Fig. 11.7) which are toxic to human health [37-39] is highly possible. Therefore, the use of photocatalytic degradation method only may not be sufficient for total conversion of DR73 into harmless products. Rather, the use of a combination of treatment methods might be more appropriate for effluents containing this dye for adequate safety prior to their release into the environment.

## 11.4 CONCLUSION

The preferred mechanism for the degradation of Disperse red 73 (DR73) by  $\bullet\text{OH}$  radical has been theoretically investigated. The feasibility of mineralisation processes such as deamination and nitrogen evolution have also been predicted. Substantial theoretical evidence including local reactivity parameters, barrierless radical addition step and stability of the addition products suggested that the attack of the radical will preferentially occur on an azo nitrogen atom. However, the subsequent N-N bond cleavage step is kinetically and thermodynamically less favored compared to the competing C-N bond cleavage pathway. Since the radical addition step for this pathway is kinetically and thermodynamically comparable to that of the N-N bond, and its overall activation energy is drastically lower, we therefore conclude that the degradation of DR73 by  $\bullet\text{OH}$  radical will occur to a larger extent via the C-N bond cleavage mechanism. Formation of compounds such as 1,4-benzenediol and cyanonitrophenol through deamination and nitrogen evolution reactions of the C-N bond cleavage products was found to be kinetically and thermodynamically favorable.

## 11.5 REFERENCES

1. J. H. Franco, B. F. da Silva, R. V. Oliveira, G. Meireles, D. P. de Oliveira, A. A. de Castro, T. C. Ramalho and M. V. Zanoni. Identification of biotransformation products of disperse dyes with rat liver microsomes by LC-MS/MS and theoretical studies with DNA: structure-mutagenicity relationship using Salmonella/microsome assay. *Science of the Total Environment* **613** (2018) 1093-1103.
2. J. H. Franco, B. F. da Silva, E. F. G. Dias, A. A. de Castro, T. C. Ramalho and M. V. B. Zanoni. Influence of auxochrome group in disperse dyes bearing azo groups as chromophore center in the biotransformation and molecular docking prediction by reductase enzyme: implications and assessment for environmental toxicity of xenobiotics. *Ecotoxicology and Environmental Safety* **160** (2018) 114-126.
3. L. Mahlalela and L. Dlamini. Enhanced photocatalytic activity of titania in the presence of  $\text{KNO}_3$  on the photodegradation of dyes. *Surfaces and Interfaces* **1** (2016) 21-28.
4. I. Poullos and I. Aetopoulou. Photocatalytic degradation of the textile dye reactive orange 16 in the presence of  $\text{TiO}_2$  suspensions. *Environmental Technology* **20** (1999) 479-487.
5. K. Tanaka, K. Padermpole and T. Hisanaga. Photocatalytic degradation of commercial azo dyes. *Water Research* **34** (2000) 327-333.
6. C. Bauer, P. Jacques and A. Kalt. Photooxidation of an azo dye induced by visible light incident on the surface of  $\text{TiO}_2$ . *Journal of Photochemistry and Photobiology A: Chemistry* **140** (2001) 87-92.

7. S. Ruan, F. Wu, T. Zhang, W. Gao, B. Xu and M. Zhao. Surface state studies of TiO<sub>2</sub> nanoparticles and photocatalytic degradation of methyl orange in aqueous TiO<sub>2</sub> dispersions. *Materials Chemistry and Physics* **69** (2001) 7-9.
8. N. Daneshvar, D. Salari and A. Khataee. Photocatalytic degradation of azo dye acid red 14 in water on ZnO as an alternative catalyst to TiO<sub>2</sub>. *Journal of Photochemistry And Photobiology A: Chemistry* **162** (2004) 317-322.
9. S. Chakrabarti and B. K. Dutta. Photocatalytic degradation of model textile dyes in wastewater using ZnO as semiconductor catalyst. *Journal of Hazardous Materials* **112** (2004) 269-278.
10. M. Behnajady, N. Modirshahla and R. Hamzavi. Kinetic study on photocatalytic degradation of CI Acid Yellow 23 by ZnO photocatalyst. *Journal of Hazardous Materials* **133** (2006) 226-232.
11. K. Mondal and A. Sharma. Photocatalytic oxidation of pollutant dyes in wastewater by TiO<sub>2</sub> and ZnO nano-materials—a mini-review. *Nanoscience & Technology for Mankind, The Academy of Sciences India (NASI), Allahabad, India* (2014) 36-72.
12. A. S. Özen, V. Aviyente and R. A. Klein. Modeling the oxidative degradation of azo dyes: A density functional theory study. *The Journal of Physical Chemistry A* **107** (2003) 4898-4907.
13. C.H. Wu, P. A. Hong and M.Y. Jian. Decolorization of Reactive Red 2 in Fenton and Fenton-like systems: effects of ultrasound and ultraviolet irradiation. *Reaction Kinetics, Mechanisms and Catalysis* **106** (2012) 11-24.

14. H. Destailats, A. G. Turjanski, D. A. Estrin and M. R. Hoffmann. Molecular structure effects on the kinetics of hydroxyl radical addition to azo dyes. *Journal of Physical Organic Chemistry* **15** (2002) 287-292.
15. S. Padmaja and S. A. Madison. Hydroxyl radical-induced oxidation of azo dyes: a pulse radiolysis study. *Journal of Physical Organic Chemistry* **12** (1999) 221-226.
16. E. Naffrechoux, S. Chanoux, C. Petrier and J. Suptil. Sonochemical and photochemical oxidation of organic matter. *Ultrasonics Sonochemistry* **7** (2000) 255-259.
17. H. Destailats, A. Colussi, J. M. Joseph and M. R. Hoffmann. Synergistic effects of sonolysis combined with ozonolysis for the oxidation of azobenzene and methyl orange. *The Journal of Physical Chemistry A* **104** (2000) 8930-8935.
18. J. M. Joseph, H. Destailats, H.-M. Hung and M. R. Hoffmann. The sonochemical degradation of azobenzene and related azo dyes: rate enhancements via Fenton's reactions. *The Journal of Physical Chemistry A* **104** (2000) 301-307.
19. H. Zhan, K. Chen and H. Tian. Photocatalytic degradation of acid azo dyes in aqueous TiO<sub>2</sub> suspension II. The effect of pH values. *Dyes and Pigments* **37** (1998) 241-247.
20. M. Panajkar and H. Mohan. Investigations of transients produced on reactions of OH radicals with azobenzene in aqueous solutions. *Indian Journal of Chemistry* **32A** (1993) 25-27.
21. A. S. Özen, V. Aviyente, F. De Proft and P. Geerlings. Modeling the substituent effect on the oxidative degradation of azo dyes. *The Journal of Physical Chemistry A* **108** (2004) 5990-6000.

22. X. Jiao, H. Yu, Q. Kong, Y. Luo, Q. Chen and J. Qu. Theoretical mechanistic studies on the degradation of alizarin yellow R initiated by hydroxyl radical. *Journal of Physical Organic Chemistry* **27** (2014) 519-526.
23. W. Z. Tang and R. Z. Chen. Decolorization kinetics and mechanisms of commercial dyes by H<sub>2</sub>O<sub>2</sub>/iron powder system. *Chemosphere* **32** (1996) 947-958.
24. A. S. Özen, V. Aviyente, G. Tezcanli-Güyer and N. H. Ince. Experimental and modeling approach to decolorization of azo dyes by ultrasound: degradation of the hydrazone tautomer. *The Journal of Physical Chemistry A* **109** (2005) 3506-3516.
25. J. T. Spadaro, L. Isabelle and V. Renganathan. Hydroxyl radical mediated degradation of azo dyes: evidence for benzene generation. *Environmental Science & Technology* **28** (1994) 1389-1393.
26. J.-E. Lee, H. J. Kim, M. R. Han, S. Y. Lee, W. J. Jo, S. S. Lee and J. S. Lee. Crystal structures of Cl disperse red 65 and Cl disperse red 73. *Dyes and Pigments* **80** (2009) 181-186.
27. DMol<sup>3</sup> Guide, Material Studio 8.0. *Accelrys Software, Inc.*, San Diego, United States (2017) 1-161.
28. Materials Studio simulation environment. *Release 2016, Accelrys Software Inc.*, San Diego, CA, United States, (2016).
29. M. H. Lim, S. E. Worthington, F. J. Dulles and C. J. Cramer. Density-functional calculations of radicals and diradicals. *ACS Symposium Series* **629** (1996) 402-422.
30. T. Bally and W. T. Borden. Calculations on open-shell molecules: a beginner's guide. *Reviews in Computational Chemistry*, **13** (2007) 1-97.

31. T. A. Halgren and W. N. Lipscomb. The synchronous-transit method for determining reaction pathways and locating molecular transition states. *Chemical Physics Letters* **49** (1977) 225-232.
32. N. Govind, M. Petersen, G. Fitzgerald, D. King-Smith and J. Andzelm. A generalized synchronous transit method for transition state location. *Computational Materials Science* **28** (2003) 250-258.
33. Y. Inada and H. Orita. Efficiency of numerical basis sets for predicting the binding energies of hydrogen bonded complexes: evidence of small basis set superposition error compared to Gaussian basis sets. *Journal of Computational Chemistry* **29** (2008) 225-232.
34. A. Klamt. The COSMO and COSMO-RS solvation models. *Wiley Interdisciplinary Reviews: Computational Molecular Science* **8** (2018) 1338(1)-1338(11).
35. P. W. Ayers and R. G. Parr. Variational principles for describing chemical reactions: the Fukui function and chemical hardness revisited. *Journal of the American Chemical Society* **122** (2000) 2010-2018.
36. H. Jónsson, G. Mills and K. W. Jacobsen. Nudged elastic band method for finding minimum energy paths of transitions. in Classical and quantum dynamics in condensed phase simulations. *World Scientific* (1998) 385-404. Doi: [10.1142/9789812839664\\_0016](https://doi.org/10.1142/9789812839664_0016).
37. F. Vega-Lopez and S. Ritchie. Dermatological problems. in Manson's tropical infectious diseases. (Twenty-third Edition). *Elsevier*, (2014) 995-1026.
38. I. Duarte, R. Lazzarini and A. Rotter. Dermatological drugs, topical agents, and cosmetics. in Side effects of drugs annual. *Elsevier*, (2010), 295-304.

39. Agency for toxic substances and disease registry. Toxicological Profile for Nitrophenols: 2-Nitrophenol and 4-Nitrophenol. *US Public Health Service*, Atlanta, GA, USA, (1992). <https://www.atsdr.cdc.gov/toxprofiles/tp50-p.pdf>. Last accessed on August 17, 2018.





### CONCLUSIONS AND RECOMMENDATIONS

---

#### 12.1 CONCLUSIONS

Effects of electron withdrawing  $-\text{NO}_2$  and  $-\text{CN}$ , and electron donating  $-\text{NH}_2$ ,  $-\text{NHCH}_3$  and  $-\text{N}(\text{CH}_3)_2$  substituents on aqueous solubility and chemical reactivity of Disperse yellow 119 (DY119) and Disperse red 73 (DR73) dyes have been investigated using Density functional theory (DFT) and conductor-like screening model for realistic solvation (COSMO-RS) methods with the aid of the DMol<sup>3</sup> program. The photodegradation mechanisms of both dyes as well as the factors affecting the mechanism were also studied. The following sections contain the details of the various aspects of the study and their key findings.

##### 12.1.1 AQUEOUS SOLUBILITY STUDY

Aqueous solubility in mol/L was determined by indirect application of COSMO-RS which involves treatment of relevant COSMO-RS data with known empirical solubility equations. Since this approach is being reported for the first time, it was first tested on azo dyes with known experimental solubility data to determine and compare the prediction capacities of the tested solubility models before utilization for this study. Natural and positional influences of the substituents on aqueous solubility were analyzed based on electronic and steric considerations as reflected in physicochemical properties such as screening charge, dipole moment and polarizability, and geometrical properties such as bond lengths and torsion angles at substitution positions.

Significant number of the substituted DY119 and DR73 analogues were predicted to be more water soluble than the parent dyes. A  $-\text{CN}$  substituted dye promises to be a more soluble dye in an aqueous system than a corresponding  $-\text{NO}_2$  substituted counterpart due to variation in the electronic influence of the substituents. On the other hand,  $-\text{NH}_2$  improved aqueous solubility better than  $-\text{NHCH}_3$  and  $-\text{N}(\text{CH}_3)_2$  groups in the electron donating series due to its relatively lower steric effect. Aqueous solubility of the studied dye seemed to be dependent on the cooperation between screening charges, dipole moments and polarisabilities of the dyes, and none of these three properties is singly sufficient to adjudge the relative solubility of dyes. Predicted solubility showed great sensitivity to substitution position in the parent dye structures as a result of changes in electronic and steric effects. All the studied derivatives showed evidence of higher thermal stability (i.e. sublimation fastness) compared to the parent dyes.

### 12.1.2 CHEMICAL REACTIVITY STUDY

The chemical reactivity study comprises the global reactivity, local reactivity and catalytic selectivity. Global reactivity was analyzed using some quantum chemical based reactivity descriptors such as HOMO-LUMO energy gap, global hardness, global softness, molecular electronegativity, chemical potential and electrophilicity. Local reactivity and probable photodegradation mechanisms were investigated using atom condensed Fukui functions which were calculated from Mulliken atomic charges. Affinities of the studied dyes for Si, CdSe, CdS,  $\text{TiO}_2$ , ZnO and ZnS catalysts were evaluated from the energy differences between the frontier molecular orbitals of the dyes and the band edges of the catalysts.

Most of the studied derivatives of DY119 and DR73 were predicted to be chemically more reactive (i.e. more degradable) than the parent dyes. The EWG substituted DY119 derivatives and the unsubstituted DY119 were predicted to be vulnerable to a C–N bond cleavage degradation mechanism, while the EDG substituted derivatives gave priority to N–N bond rupture degradation pathway. DY119 derivatives containing both EWG and EDG in their structures appeared to favor the N–N bond cleavage pathway, indicating the prevalence of the EDG effect. Most of the DR73 derivatives favored an N–N bond cleavage pathway, few of them gave precedence to a C–N bond cleavage and very few showed evidence of competing C–N and N–N bond cleavages.

The reactivity patterns of the studied DY119 and DR73 derivatives were predominantly due to the electronic influence of the substituent groups, and were also sensitive to a change in substituent position in the parent dye structures. With different molecular orbital-band edge combinations, CdSe was predicted to be the most appropriate visible light activated catalyst, whereas TiO<sub>2</sub> and ZnO showed the highest philicity for the dyes among the UV activated photodegradation catalysts considered.

### 12.1.3 PHOTODEGRADATION PATHWAY STUDY

The potential energy profiles for OH radical degradation of DY119 and DR73 via the C–N and N–N bond cleavage degradation mechanisms were calculated using DFT. Further decomposition of the C–N or N–N bond cleavage products through OH radical initiated loss of nitrogen molecule and deamination was also studied. In agreement with the local reactivity prediction, thermodynamic and kinetic evidence including stability of radical addition products, stability of degradation products and activation energies indicated that the C–N bond cleavage pathway is the preferred degradation mechanism for DY119.

Elimination of intramolecular hydrogen bond from the structure of this dye resulted to a decrease in the activation energies of both the N–N and the C–N bond cleavage pathways, but with prevalence of the latter.

In the case of DR73 degradation, a barrier less radical addition step and a relatively more stable addition product showed that OH radical attack will preferentially occur on an azo nitrogen atom which is also in agreement with the local reactivity prediction. However, the accompanying N-N bond cleavage step was found to be kinetically and thermodynamically less favored compared to the competing C-N bond cleavage. Since the radical addition step for this pathway was kinetically and thermodynamically comparable to that of the N-N, and its overall activation energy is much lower than that of the N-N, we therefore conclude that the degradation of DR73 by •OH radical will occur to a larger extent via the C-N bond cleavage mechanism.

Further decomposition of the C-N and N-N bond cleavage products through removal of molecular nitrogen and deamination reactions was found to be kinetically and thermodynamically feasible, which suggests that mineralisation of the bond cleavage products will occur readily. Introduction of water was found to promote the degradation reactions by lowering the overall activation energies of both mechanisms, and the energies of the degradation products.

## 12.2 RECOMMENDATIONS

Considering that most of the derivatives introduced in this work showed better aqueous solubility, substrate binding ability and photodegradability compared to their parents DY119 and DR73 dyes, they can therefore be considered as promising alternative azo dyes for a more economic and more environmentally friendly applications.

Also, since other properties such as absorption wavelength can also be impacted by substitution as observed for DR73, further studies are therefore necessary particularly on the electronic excitation, hyperpolarizability and non-linear optical properties of the studied derivatives in order to evaluate their potential for technological and optical applications.

Finally, it has been theoretically shown in this work that hydroxyl radical degradation of DY119 and DR73 could lead to generation of toxic by-products. Hence, the use of a combination of treatment methods might be more appropriate for effluents containing these dyes for adequate safety prior to their release into the environment.



## APPENDIX

**Table A. 1:** Solvation free energy (SFE), vapor pressure (p), octanol-water partition coefficient (Log P) and aqueous solubility ( $S_{CSE}$  and  $S_{GSE}$ ) at 25 °C for D1 (Molecular weight. = 378.50 g).

Calculated properties	$\epsilon = 78.4$						Average values	Experimental solubility* (mg/L)
	NSPA							
	92	272	362	482	642	1082		
	Space cut-off = 3.0 (Å)							
SFE (kcal/mol)	-13.94	-13.77	-13.56	-13.50	-12.10	-11.89	-13.13	0.2
P x 10 <sup>-14</sup> (atm)	1.46	1.60	1.97	1.46	1.36	1.68	1.59	
S <sub>CSE</sub> (mg/L)	3.81	3.13	2.70	1.81	0.16	0.14	1.96	
Log P	6.17	6.15	6.20	6.16	6.16	6.22	6.18	
S <sub>GSE</sub> (mg/L)	0.02	0.02	0.02	0.02	0.02	0.02	0.02	
	Space cut-off = 3.5 (Å)							
SFE (kcal/mol)	-14.19	-15.37	-15.37	-15.24	-15.24	-15.20	-15.10	
P x 10 <sup>-14</sup> (atm)	0.14	0.14	0.14	0.18	0.18	0.20	0.16	
S <sub>CSE</sub> (mg/L)	0.54	4.05	4.17	4.13	4.31	4.32	3.59	
Log P	5.79	5.90	5.88	5.91	5.91	5.92	5.89	
S <sub>GSE</sub> (mg/L)	0.05	0.04	0.04	0.03	0.03	0.03	0.04	
	Space cut-off = 4.5 (Å)							
SFE (kcal/mol)	-16.41	-16.49	-16.45	-16.35	-16.35	-16.28	-16.39	
P x 10 <sup>-14</sup> (atm)	0.023	0.019	0.021	0.027	0.027	0.032	0.025	
S <sub>CSE</sub> (mg/L)	3.82	3.64	3.73	4.16	4.07	4.33	3.96	
Log P	5.47	5.50	5.53	5.53	5.53	5.55	5.52	
S <sub>GSE</sub> (mg/L)	0.10	0.09	0.08	0.08	0.08	0.08	0.09	
	Space cut-off = 5.5 (Å)							
SFE (kcal/mol)	-14.59	-14.63	-14.65	-14.53	-14.49	-14.45	-14.56	
P x 10 <sup>-14</sup> (atm)	0.011	0.010	0.010	0.014	0.015	0.016	0.013	
S <sub>CSE</sub> (mg/L)	0.09	0.08	0.09	0.10	0.10	0.10	0.09	
Log P	5.38	5.43	5.44	5.46	5.47	5.47	5.44	
S <sub>GSE</sub> (mg/L)	0.12	0.10	0.10	0.10	0.10	0.10	0.10	
	Space cut-off = 6.5 (Å)							
SFE (kcal/mol)	-16.86	-16.91	-16.91	-16.80	-16.77	-16.73	-16.83	
P x 10 <sup>-14</sup> (atm)	0.012	0.011	0.010	0.014	0.015	0.017	0.013	
S <sub>CSE</sub> (mg/L)	4.20	4.17	3.98	4.67	4.54	5.00	4.43	
Log P	5.39	5.44	5.42	5.43	5.44	5.43	5.43	
S <sub>GSE</sub> (mg/L)	0.11	0.10	0.11	0.10	0.10	0.10	0.10	
	Space cut-off = 7.0 (Å)							
SFE (kcal/mol)	-16.75	-16.78	-16.82	-16.71	-16.67	-16.63	-16.73	
P x 10 <sup>-14</sup> (atm)	0.011	0.010	0.010	0.014	0.015	0.016	0.013	
S <sub>CSE</sub> (mg/L)	3.39	3.19	3.41	4.01	4.01	4.02	3.67	
Log P	5.39	5.44	5.43	5.40	5.42	5.45	5.42	
S <sub>GSE</sub> (mg/L)	0.11	0.10	0.10	0.11	0.11	0.10	0.11	
	Space cut-off = 8.0 (Å)							
SFE (kcal/mol)	-16.78	-16.81	-16.82	-16.70	-16.69	-16.65	-16.74	
P x 10 <sup>-14</sup> (atm)	0.012	0.010	0.011	0.014	0.015	0.016	0.013	
S <sub>CSE</sub> (mg/L)	3.67	3.36	3.58	3.75	4.04	4.06	3.74	
Log P	5.39	5.43	5.41	5.41	5.43	5.44	5.42	
S <sub>GSE</sub> (mg/L)	0.11	0.10	0.11	0.11	0.10	0.10	0.11	

**Table A. 2:** Solvation free energy (SFE), vapor pressure (p), octanol-water partition coefficient (Log P) and aqueous solubility ( $S_{CSE}$  and  $S_{GSE}$ ) at 25 °C for D2 (Molecular weight. = 389.00 g).

Calculated properties	$\epsilon = 78.4$						Average values	Experimental solubility <sup>a</sup> (mg/L)
	NSPA							
	92	272	362	482	642	1082		
	Space cut-off = 3.0 (Å)							
SFE (kcal/mol)	-14.95	-14.97	-14.99	-14.84	-14.83	-14.77	-14.86	0.5
P x 10 <sup>-16</sup> (atm)	3.93	4.11	3.93	5.18	5.55	5.55	4.71	
S <sub>CSE</sub> (mg/L)	0.58	0.63	0.62	0.63	0.67	0.60	0.62	
Log P	5.55	5.62	5.61	5.63	5.62	5.64	5.61	
S <sub>GSE</sub> (mg/L)	0.08	0.07	0.07	0.07	0.07	0.06	0.07	
	Space cut-off = 3.5 (Å)							
SFE (kcal/mol)	-18.74	-18.78	-18.79	-18.69	-18.66	-18.60	-18.71	
P x 10 <sup>-16</sup> (atm)	0.38	0.38	0.35	0.46	0.50	0.58	0.44	
S <sub>CSE</sub> (mg/L)	34.18	36.57	33.90	37.79	38.49	40.82	36.96	
Log P	5.00	5.01	5.03	5.03	5.04	5.06	5.03	
S <sub>GSE</sub> (mg/L)	0.28	0.28	0.26	0.26	0.26	0.25	0.27	
	Space cut-off = 4.5 (Å)							
SFE (kcal/mol)	-17.35	-17.40	-17.42	-17.30	-17.26	-17.21	-17.32	
P x 10 <sup>-16</sup> (atm)	0.059	0.053	0.054	0.070	0.073	0.084	0.066	
S <sub>CSE</sub> (mg/L)	0.51	0.50	0.52	0.55	0.53	0.56	0.53	
Log P	4.58	4.60	4.61	4.61	4.65	4.66	4.62	
S <sub>GSE</sub> (mg/L)	0.74	0.71	0.69	0.69	0.63	0.62	0.68	
	Space cut-off = 5.5 (Å)							
SFE (kcal/mol)	-19.29	-19.49	-19.50	-19.27	-19.30	-19.30	-19.36	
P x 10 <sup>-16</sup> (atm)	0.016	0.016	0.016	0.021	0.023	0.027	0.020	
S <sub>CSE</sub> (mg/L)	3.61	5.18	5.27	4.49	5.18	6.10	4.97	
Log P	4.32	4.33	4.34	4.40	4.40	4.39	4.36	
S <sub>GSE</sub> (mg/L)	1.35	1.32	1.29	1.12	1.12	1.15	1.23	
	Space cut-off = 6.5 (Å)							
SFE (kcal/mol)	-19.00	-19.63	-19.07	-19.02	-18.93	-19.44	-19.18	
P x 10 <sup>-16</sup> (atm)	0.017	0.019	0.015	0.019	0.021	0.029	0.020	
S <sub>CSE</sub> (mg/L)	2.38	7.69	2.27	2.74	2.53	8.45	4.34	
Log P	4.33	4.46	4.39	4.34	4.41	4.49	4.40	
S <sub>GSE</sub> (mg/L)	1.32	0.98	1.15	1.29	1.10	0.91	1.13	
	Space cut-off = 7.0 (Å)							
SFE (kcal/mol)	-17.74	-17.82	-17.81	-17.71	-17.68	-17.63	-17.73	
P x 10 <sup>-16</sup> (atm)	0.025	0.025	0.023	0.034	0.038	0.043	0.032	
S <sub>CSE</sub> (mg/L)	0.42	0.48	0.43	0.53	0.56	0.59	0.50	
Log P	4.48	4.52	4.51	4.53	4.55	4.57	4.53	
S <sub>GSE</sub> (mg/L)	0.93	0.85	0.87	0.83	0.79	0.76	0.84	
	Space cut-off = 8.0 (Å)							
SFE (kcal/mol)	-19.81	-19.64	-19.67	-19.76	-18.97	-18.93	-19.46	
P x 10 <sup>-16</sup> (atm)	0.024	0.017	0.017	0.030	0.032	0.022	0.021	
S <sub>CSE</sub> (mg/L)	12.86	7.00	7.19	14.85	2.42	2.65	7.83	
Log P	4.42	4.42	4.44	4.47	4.40	4.43	4.43	
S <sub>GSE</sub> (mg/L)	1.07	1.07	1.02	1.00	1.12	1.04	1.05	

**Table A. 3:** Solvation free energy (SFE), vapor pressure (p), octanol-water partition coefficient (Log P) and aqueous solubility ( $S_{CSE}$  and  $S_{GSE}$ ) at 25 °C for D3 (Molecular weight. = 413.26 g).

Calculated properties	$\epsilon = 78.4$						Average values	Experimental solubility* (mg/L)
	NSPA							
	92	272	362	482	642	1082		
Space cut-off = 3.0 (Å)								
SFE (kcal/mol)	-11.50	-11.53	-11.54	-11.42	-11.40	-11.35	-11.46	1.0
$p \times 10^{-15}$ (atm)	2.42	2.31	2.26	2.91	3.05	3.42	2.73	
$S_{CSE}$ (mg/L)	0.01	0.01	0.01	0.01	0.01	0.01	0.01	
Log P	6.40	6.48	6.46	6.47	6.50	6.50	6.47	
$S_{GSE}$ (mg/L)	0.03	0.03	0.03	0.03	0.02	0.02	0.03	
Space cut-off = 3.5 (Å)								
SFE (kcal/mol)	-15.20	-15.23	-15.24	-15.15	-15.11	-15.07	-15.17	1.0
$p \times 10^{-15}$ (atm)	0.38	0.38	0.38	0.48	0.50	0.53	0.44	
$S_{CSE}$ (mg/L)	0.90	0.94	0.96	1.06	1.02	1.02	0.98	
Log P	6.15	6.21	6.22	6.23	6.25	6.23	6.22	
$S_{GSE}$ (mg/L)	0.06	0.05	0.05	0.05	0.04	0.05	0.05	
Space cut-off = 4.5 (Å)								
SFE (kcal/mol)	-15.76	-15.85	-15.86	-15.75	-15.72	-15.64	-15.76	1.0
$p \times 10^{-15}$ (atm)	0.064	0.051	0.051	0.057	0.073	0.092	0.066	
$S_{CSE}$ (mg/L)	0.39	0.36	0.37	0.41	0.42	0.46	0.40	
Log P	5.89	5.96	5.96	5.98	5.98	5.98	5.96	
$S_{GSE}$ (mg/L)	0.10	0.09	0.09	0.08	0.08	0.08	0.09	
Space cut-off = 5.5 (Å)								
SFE (kcal/mol)	-15.66	-15.73	-15.74	-14.80	-15.58	-14.75	-15.38	1.0
$p \times 10^{-15}$ (atm)	0.036	0.032	0.031	0.035	0.045	0.044	0.037	
$S_{CSE}$ (mg/L)	0.19	0.19	0.19	0.04	0.20	0.05	0.14	
Log P	5.77	5.81	5.83	5.84	5.83	5.88	5.83	
$S_{GSE}$ (mg/L)	0.13	0.12	0.12	0.11	0.12	0.10	0.12	
Space cut-off = 6.5 (Å)								
SFE (kcal/mol)	-16.03	-16.08	-16.08	-15.98	-15.94	-15.90	-16.00	1.0
$p \times 10^{-15}$ (atm)	0.033	0.031	0.031	0.041	0.044	0.051	0.038	
$S_{CSE}$ (mg/L)	0.31	0.32	0.32	0.37	0.37	0.39	0.35	
Log P	5.81	5.86	5.86	5.87	5.88	5.90	5.86	
$S_{GSE}$ (mg/L)	0.12	0.11	0.11	0.11	0.10	0.10	0.11	
Space cut-off = 7.0 (Å)								
SFE (kcal/mol)	-16.07	-16.13	-16.18	-16.02	-16.04	-15.95	-16.07	1.0
$p \times 10^{-15}$ (atm)	0.033	0.030	0.028	0.041	0.040	0.050	0.037	
$S_{CSE}$ (mg/L)	0.34	0.34	0.35	0.39	0.40	0.42	0.37	
Log P	5.81	5.85	5.85	5.87	5.87	5.90	5.86	
$S_{GSE}$ (mg/L)	0.12	0.11	0.11	0.11	0.11	0.10	0.11	
Space cut-off = 8.0 (Å)								
SFE (kcal/mol)	-16.07	-16.12	-16.11	-16.01	-15.96	-15.89	-16.03	1.0
$p \times 10^{-15}$ (atm)	0.037	0.031	0.030	0.041	0.048	0.048	0.039	
$S_{CSE}$ (mg/L)	0.39	0.35	0.33	0.39	0.42	0.37	0.38	
Log P	5.82	5.85	5.86	5.87	5.89	5.88	5.86	
$S_{GSE}$ (mg/L)	0.12	0.11	0.11	0.11	0.10	0.10	0.11	



**Table A. 4:** Solvation free energy (SFE), vapor pressure (p), octanol-water partition coefficient (Log P) and aqueous solubility ( $S_{CSE}$  and  $S_{GSE}$ ) 25 °C for D4 (Molecular weight. = 423.50 g).

Calculated properties	$\epsilon = 78.4$						Average values	Experimental solubility* (mg/L)
	NSPA							
	92	272	362	482	642	1082		
	Space cut-off = 3.0 (Å)							
SFE (kcal/mol)	-14.57	-14.49	-14.50	-14.40	-14.47	-14.32	-14.46	
$p \times 10^{-16}$ (atm)	3.19	3.12	3.05	3.75	4.02	4.31	3.57	
$S_{CSE}$ (mg/L)	0.26	0.23	0.23	0.24	0.29	0.24	0.25	
Log P	5.90	5.95	5.97	5.96	5.96	6.01	5.96	
$S_{GSE}$ (mg/L)	0.04	0.04	0.04	0.04	0.04	0.03	0.04	
	Space cut-off = 3.5 (Å)							0.20
SFE (kcal/mol)	-16.12	-16.19	-16.17	-16.10	-16.07	-16.02	-16.11	
$p \times 10^{-16}$ (atm)	0.28	0.26	0.26	0.31	0.31	0.36	0.30	
$S_{CSE}$ (mg/L)	0.32	0.34	0.33	0.35	0.33	0.35	0.34	
Log P	5.58	5.61	5.62	5.61	5.62	5.66	5.62	
$S_{GSE}$ (mg/L)	0.09	0.08	0.08	0.08	0.08	0.08	0.08	
	Space cut-off = 4.5 (Å)							
SFE (kcal/mol)	-19.27	-19.31	-19.33	-19.23	-19.24	-19.20	-19.26	
$p \times 10^{-16}$ (atm)	0.024	0.022	0.021	0.029	0.027	0.030	0.025	
$S_{CSE}$ (mg/L)	5.74	5.48	5.54	6.32	6.13	6.28	5.92	
Log P	5.20	5.23	5.25	5.26	5.24	5.27	5.24	
$S_{GSE}$ (mg/L)	0.22	0.20	0.19	0.19	0.20	0.18	0.20	
	Space cut-off = 5.5 (Å)							
SFE (kcal/mol)	-19.15	-19.21	-19.22	-19.12	-19.08	-19.02	-19.13	
$p \times 10^{-16}$ (atm)	0.014	0.013	0.011	0.015	0.016	0.020	0.015	
$S_{CSE}$ (mg/L)	2.69	2.42	2.42	2.82	2.75	3.14	2.71	
Log P	5.11	5.14	5.15	5.17	5.15	5.19	5.15	
$S_{GSE}$ (mg/L)	0.27	0.25	0.24	0.23	0.24	0.22	0.24	
	Space cut-off = 6.5 (Å)							
SFE (kcal/mol)	-19.22	-19.29	-19.31	-19.20	-19.16	-19.12	-19.22	
$p \times 10^{-16}$ (atm)	0.014	0.012	0.012	0.016	0.017	0.020	0.015	
$S_{CSE}$ (mg/L)	3.03	2.97	3.02	3.46	3.31	3.63	3.24	
Log P	5.10	5.13	5.15	5.15	5.15	5.18	5.14	
$S_{GSE}$ (mg/L)	0.27	0.26	0.24	0.24	0.24	0.23	0.25	
	Space cut-off = 7.0 (Å)							
SFE (kcal/mol)	-19.25	-19.30	-19.32	-19.22	-19.17	-19.14	-19.23	
$p \times 10^{-16}$ (atm)	0.014	0.012	0.012	0.016	0.017	0.019	0.015	
$S_{CSE}$ (mg/L)	3.12	2.97	2.99	3.40	3.37	3.66	3.25	
Log P	5.10	5.14	5.15	5.14	5.15	5.18	5.14	
$S_{GSE}$ (mg/L)	0.27	0.25	0.24	0.25	0.24	0.23	0.25	
	Space cut-off = 8.0 (Å)							
SFE (kcal/mol)	-19.26	-19.31	-19.33	-19.18	-19.18	-19.13	-19.23	
$p \times 10^{-16}$ (atm)	0.013	0.011	0.012	0.017	0.017	0.019	0.015	
$S_{CSE}$ (mg/L)	3.10	3.02	3.05	3.42	3.42	3.60	3.27	
Log P	5.09	5.12	5.15	5.12	5.14	5.18	5.13	
$S_{GSE}$ (mg/L)	0.28	0.26	0.24	0.26	0.25	0.23	0.25	

**Table A. 5:** Absolute energies of the optimized D1, D2, D3 and D4 molecules in gas and aqueous phases.

Cut-off (Å)	$E_{\text{gas}}$ (kcal/mol)	COSMO Energies ( $\epsilon = 78.4$ ) (kcal/mol)					
		Number of surface segment per atom (NSPA)					
		92	272	362	482	642	1082
D1							
3.0	-1028828.46	-1028842.40	-1028842.23	-1028842.02	-1028841.96	-1028840.56	-1028840.35
3.5	-1028850.49	-1028864.68	-1028865.86	-1028865.86	-1028865.73	-1028865.73	-1028865.69
4.5	-1028856.63	-1028873.04	-1028873.12	-1028873.08	-1028872.98	-1028872.98	-1028872.91
5.5	-1028861.15	-1028875.74	-1028875.78	-1028875.80	-1028875.68	-1028875.64	-1028875.60
6.5	-1028860.59	-1028877.45	-1028877.50	-1028877.50	-1028877.39	-1028877.36	-1028877.32
7.0	-1028860.71	-1028877.46	-1028877.49	-1028877.53	-1028877.42	-1028877.38	-1028877.34
8.0	-1028860.70	-1028877.48	-1028877.51	-1028877.52	-1028877.40	-1028877.39	-1028877.35
D2							
3.0	-868781.63	-868796.58	-868796.60	-868796.62	-868796.47	-868796.46	-868796.40
3.5	-868799.77	-868818.51	-868818.55	-868818.56	-868818.46	-868818.43	-868818.37
4.5	-868807.04	-868824.39	-868824.44	-868824.46	-868824.34	-868824.30	-868824.25
5.5	-868807.26	-868826.55	-868826.75	-868826.76	-868826.53	-868826.56	-868826.56
6.5	-868809.34	-868828.34	-868828.97	-868828.41	-868828.36	-868828.27	-868828.78
7.0	-868811.31	-868829.05	-868829.13	-868829.12	-868829.02	-868828.99	-868828.94
8.0	-868809.33	-868829.14	-868828.97	-868829.00	-868829.09	-868828.30	-868828.26
D3							
3.0	-1317248.32	-1317259.82	-1317259.85	-1317259.86	-1317259.74	-1317259.72	-1317259.67
3.5	-1317275.91	-1317291.11	-1317291.14	-1317291.15	-1317291.06	-1317291.02	-1317290.98
4.5	-1317284.03	-1317299.79	-1317299.88	-1317299.89	-1317299.78	-1317299.75	-1317299.67
5.5	-1317286.73	-1317302.39	-1317302.46	-1317302.47	-1317301.53	-1317302.31	-1317301.48
6.5	-1317288.18	-1317304.21	-1317304.26	-1317304.26	-1317304.16	-1317304.12	-1317304.08
7.0	-1317288.13	-1317304.20	-1317304.26	-1317304.31	-1317304.15	-1317304.17	-1317304.08
8.0	-1317288.16	-1317304.23	-1317304.28	-1317304.27	-1317304.17	-1317304.12	-1317304.05
D4							
3.0	-1157203.91	-1157218.48	-1157218.40	-1157218.41	-1157218.31	-1157218.38	-1157218.23
3.5	-1157227.24	-1157243.36	-1157243.43	-1157243.41	-1157243.34	-1157243.31	-1157243.26
4.5	-1157231.91	-1157251.18	-1157251.22	-1157251.24	-1157251.14	-1157251.15	-1157251.11
5.5	-1157235.05	-1157254.20	-1157254.26	-1157254.27	-1157254.17	-1157254.13	-1157254.07
6.5	-1157236.63	-1157255.85	-1157255.92	-1157255.94	-1157255.83	-1157255.79	-1157255.75
7.0	-1157236.63	-1157255.88	-1157255.93	-1157255.95	-1157255.85	-1157255.80	-1157255.77
8.0	-1157236.62	-1157255.88	-1157255.93	-1157255.95	-1157255.80	-1157255.80	-1157255.75

**Table A. 6:** Reactivity indices for D1.

Reactivity Parameters	Gas phase	COSMO ( $\epsilon = 78.4$ )					
		Number of segment per atom (NSPA)					
		92	272	362	482	642	1082
Space cut-off = 3.0 (Å)							
HOMO (eV)	-4.93	-4.87	-4.87	-4.90	-4.86	-4.86	-4.89
LUMO (eV)	-3.37	-3.56	-3.56	-3.58	-3.55	-3.56	-3.57
$E_g$ (eV)	1.56	1.31	1.31	1.32	1.31	1.30	1.32
$\eta$ (eV)	0.78	0.66	0.66	0.66	0.66	0.65	0.66
$\sigma$ (eV <sup>-1</sup> )	1.28	1.52	1.52	1.52	1.52	1.54	1.52
$\chi$ (eV)	4.15	4.22	4.22	4.24	4.21	4.21	4.23
$\mu$ (eV)	-4.15	-4.22	-4.22	-4.24	-4.21	-4.21	-4.23
$\omega$ (eV)	11.04	13.49	13.49	13.62	13.43	13.63	13.56
Space cut-off = 3.5 (Å)							
HOMO (eV)	-5.23	-5.12	-5.12	-5.13	-5.13	-5.13	-5.11
LUMO (eV)	-3.72	-3.80	-3.80	-3.80	-3.80	-3.80	-3.79
$E_g$ (eV)	1.31	1.32	1.32	1.33	1.33	1.33	1.32
$\eta$ (eV)	0.66	0.66	0.66	0.67	0.67	0.67	0.66
$\sigma$ (eV <sup>-1</sup> )	1.52	1.52	1.52	1.49	1.49	1.49	1.52
$\chi$ (eV)	4.58	4.46	4.46	4.47	4.47	4.47	4.45
$\mu$ (eV)	-4.58	-4.46	-4.46	-4.47	-4.47	-4.47	-4.45
$\omega$ (eV)	15.89	15.07	15.07	14.91	14.91	14.91	15.00
Space cut-off = 4.5 (Å)							
HOMO (eV)	-5.30	-5.21	-5.21	-5.22	-5.22	-5.21	-5.20
LUMO (eV)	-3.75	-3.89	-3.89	-3.90	-3.90	-3.90	-3.90
$E_g$ (eV)	1.55	1.32	1.32	1.32	1.32	1.31	1.30
$\eta$ (eV)	0.78	0.66	0.66	0.66	0.66	0.66	0.65
$\sigma$ (eV <sup>-1</sup> )	1.28	1.52	1.52	1.52	1.52	1.52	1.54
$\chi$ (eV)	4.53	4.55	4.55	4.56	4.56	4.56	4.55
$\mu$ (eV)	-4.53	-4.55	-4.55	-4.56	-4.56	-4.56	-4.55
$\omega$ (eV)	13.15	15.68	15.68	15.75	15.75	15.75	15.93
Space cut-off = 5.5 (Å)							
HOMO (eV)	-5.31	-5.23	-5.23	-5.24	-5.24	-5.24	-5.24
LUMO (eV)	-3.77	-3.91	-3.91	-3.91	-3.91	-3.91	-3.91
$E_g$ (eV)	1.54	1.32	1.32	1.33	1.33	1.33	1.33
$\eta$ (eV)	0.77	0.66	0.66	0.67	0.67	0.67	0.67
$\sigma$ (eV <sup>-1</sup> )	1.30	1.52	1.52	1.49	1.49	1.49	1.49
$\chi$ (eV)	4.54	4.57	4.57	4.58	4.58	4.58	4.58
$\mu$ (eV)	-4.54	-4.57	-4.57	-4.58	-4.58	-4.58	-4.58
$\omega$ (eV)	13.38	15.82	15.82	15.65	15.65	15.65	15.65
Space cut-off = 6.5 (Å)							
HOMO (eV)	-5.32	-5.23	-5.23	-5.23	-5.23	-5.23	-5.22
LUMO (eV)	-3.78	-3.92	-3.92	-3.92	-3.92	-3.92	-3.91
$E_g$ (eV)	1.54	1.31	1.31	1.31	1.31	1.31	1.31
$\eta$ (eV)	0.77	0.66	0.66	0.66	0.66	0.66	0.66
$\sigma$ (eV <sup>-1</sup> )	1.30	1.52	1.52	1.52	1.52	1.52	1.52
$\chi$ (eV)	4.55	4.58	4.58	4.58	4.58	4.58	4.57
$\mu$ (eV)	-4.55	-4.58	-4.58	-4.58	-4.58	-4.58	-4.57
$\omega$ (eV)	13.44	15.89	15.89	15.89	15.89	15.89	15.82
Space cut-off = 7.0 (Å)							
HOMO (eV)	-5.32	-5.23	-5.23	-5.22	-5.23	-5.22	-5.23
LUMO (eV)	-3.77	-3.92	-3.92	-3.92	-3.91	-3.91	-3.92
$E_g$ (eV)	1.55	1.31	1.31	1.30	1.32	1.31	1.31
$\eta$ (eV)	0.78	0.66	0.66	0.66	0.66	0.66	0.66
$\sigma$ (eV <sup>-1</sup> )	1.28	1.52	1.52	1.52	1.52	1.52	1.52

$\chi$ (eV)	4.55	4.58	4.58	4.58	4.57	4.57	4.58
$\mu$ (eV)	-4.55	-4.58	-4.58	-4.58	-4.57	-4.57	-4.58
$\omega$ (eV)	13.27	15.89	15.89	15.89	15.82	15.82	15.89
Space cut-off = 8.0 (Å)							
HOMO (eV)	-5.32	-5.22	-5.23	-5.23	-5.23	-5.22	-5.23
LUMO (eV)	-3.77	-3.91	-3.92	-3.91	-3.92	-3.91	-3.91
$E_g$ (eV)	1.55	1.31	1.31	1.32	1.31	1.31	1.32
$\eta$ (eV)	0.78	0.66	0.66	0.66	0.66	0.66	0.66
$\sigma$ (eV <sup>-1</sup> )	1.28	1.52	1.52	1.52	1.52	1.52	1.52
$\chi$ (eV)	4.55	4.57	4.58	4.57	4.58	4.57	4.57
$\mu$ (eV)	-4.55	-4.57	-4.58	-4.57	-4.58	-4.57	-4.57
$\omega$ (eV)	13.27	15.82	15.89	15.82	15.89	15.82	15.82

**Table A. 7:** Reactivity indices for D2.

Reactivity Parameters	Gas phase	COSMO ( $\epsilon = 78.4$ )					
		Number of segment per atom (NSPA)					
		92	272	362	482	642	1082
Space cut-off = 3.0 (Å)							
HOMO (eV)	-5.15	-5.03	-5.03	-5.03	-5.03	-5.03	-5.03
LUMO (eV)	-3.60	-3.69	-3.69	-3.69	-3.69	-3.69	-3.69
$E_g$ (eV)	1.55	1.34	1.34	1.34	1.34	1.34	1.34
$\eta$ (eV)	0.78	0.67	0.67	0.67	0.67	0.67	0.67
$\sigma$ (eV <sup>-1</sup> )	1.28	1.49	1.49	1.49	1.49	1.49	1.49
$\chi$ (eV)	4.38	4.36	4.36	4.36	4.36	4.36	4.36
$\mu$ (eV)	-4.38	-4.36	-4.36	-4.36	-4.36	-4.36	-4.36
$\omega$ (eV)	12.30	14.19	14.19	14.19	14.19	14.19	14.19
Space cut-off = 3.5 (Å)							
HOMO (eV)	-5.36	-5.21	-5.21	-5.21	-5.21	-5.21	-5.21
LUMO (eV)	-3.79	-3.88	-3.88	-3.88	-3.88	-3.88	-3.88
$E_g$ (eV)	1.57	1.33	1.33	1.33	1.33	1.33	1.33
$\eta$ (eV)	0.79	0.67	0.67	0.67	0.67	0.67	0.67
$\sigma$ (eV <sup>-1</sup> )	1.27	1.49	1.49	1.49	1.49	1.49	1.49
$\chi$ (eV)	4.58	4.55	4.55	4.55	4.55	4.55	4.55
$\mu$ (eV)	-4.58	-4.55	-4.55	-4.55	-4.55	-4.55	-4.55
$\omega$ (eV)	13.28	15.45	15.45	15.45	15.45	15.45	15.45
Space cut-off = 4.5 (Å)							
HOMO (eV)	-5.50	-5.28	-5.28	-5.28	-5.28	-5.28	-5.28
LUMO (eV)	-3.90	-3.97	-3.97	-3.97	-3.97	-3.97	-3.97
$E_g$ (eV)	1.60	1.31	1.31	1.31	1.31	1.31	1.31
$\eta$ (eV)	0.80	0.66	0.66	0.66	0.66	0.66	0.66
$\sigma$ (eV <sup>-1</sup> )	1.25	1.52	1.52	1.52	1.52	1.52	1.52
$\chi$ (eV)	4.70	4.63	4.63	4.63	4.63	4.63	4.63
$\mu$ (eV)	-4.70	-4.63	-4.63	-4.63	-4.63	-4.63	-4.63
$\omega$ (eV)	13.80	16.24	16.24	16.24	16.24	16.24	16.24
Space cut-off = 5.5 (Å)							
HOMO (eV)	-5.51	-5.28	-5.28	-5.28	-5.28	-5.28	-5.28
LUMO (eV)	-3.93	-3.99	-3.98	-3.98	-3.99	-3.98	-3.98
$E_g$ (eV)	1.58	1.29	1.30	1.30	1.29	1.30	1.30
$\eta$ (eV)	0.79	0.65	0.65	0.65	0.65	0.65	0.65
$\sigma$ (eV <sup>-1</sup> )	1.27	1.54	1.54	1.54	1.54	1.54	1.54
$\chi$ (eV)	4.72	4.64	4.63	4.63	4.64	4.63	4.63
$\mu$ (eV)	-4.72	-4.64	-4.63	-4.63	-4.64	-4.63	-4.63

$\omega$ (eV)	14.10	16.56	16.49	16.49	16.56	16.49	16.49
Space cut-off = 6.5 (Å)							
HOMO (eV)	-5.50	-5.28	-5.29	-5.28	-5.29	-5.28	-5.29
LUMO (eV)	-3.93	-3.99	-3.98	-3.99	-3.99	-3.99	-3.98
$E_g$ (eV)	1.57	1.29	1.31	1.29	1.30	1.29	1.31
$\eta$ (eV)	0.79	0.65	0.66	0.65	0.65	0.65	0.66
$\sigma$ (eV <sup>-1</sup> )	1.27	1.54	1.51	1.54	1.54	1.54	1.51
$\chi$ (eV)	4.72	4.64	4.64	4.64	4.64	4.64	4.64
$\mu$ (eV)	-4.72	-4.64	-4.64	-4.64	-4.64	-4.64	-4.64
$\omega$ (eV)	14.10	16.56	16.31	16.56	16.56	16.56	16.31
Space cut-off = 7.0 (Å)							
HOMO (eV)	-5.51	-5.28	-5.28	-5.28	-5.28	-5.28	-5.28
LUMO (eV)	-3.92	-3.98	-3.98	-3.98	-3.98	-3.98	-3.98
$E_g$ (eV)	1.59	1.30	1.30	1.30	1.30	1.30	1.30
$\eta$ (eV)	0.80	0.65	0.65	0.65	0.65	0.65	0.65
$\sigma$ (eV <sup>-1</sup> )	1.25	1.54	1.54	1.54	1.54	1.54	1.54
$\chi$ (eV)	4.72	4.63	4.63	4.63	4.63	4.63	4.63
$\mu$ (eV)	-4.72	-4.63	-4.63	-4.63	-4.63	-4.63	-4.63
$\omega$ (eV)	13.92	16.49	16.49	16.49	16.49	16.49	16.49
Space cut-off = 8.0 (Å)							
HOMO (eV)	-5.50	-5.29	-5.29	-5.28	-5.30	-5.29	-5.29
LUMO (eV)	-3.93	-3.98	-3.98	-3.98	-3.98	-3.99	-3.99
$E_g$ (eV)	1.57	1.31	1.31	1.30	1.32	1.30	1.30
$\eta$ (eV)	0.79	0.66	0.66	0.65	0.66	0.65	0.65
$\sigma$ (eV <sup>-1</sup> )	1.27	1.51	1.51	1.54	1.51	1.54	1.54
$\chi$ (eV)	4.72	4.64	4.64	4.63	4.64	4.64	4.64
$\mu$ (eV)	-4.72	-4.64	-4.64	-4.63	-4.64	-4.64	-4.64
$\omega$ (eV)	14.10	16.31	16.31	16.49	16.45	16.56	16.56

**Table A. 8:** Reactivity indices for D3.

Reactivity Parameters	Gas phase	COSMO ( $\epsilon = 78.4$ )					
		Number of segment per atom (NSPA)					
		92	272	362	482	642	1082
Space cut-off = 3.0 (Å)							
HOMO (eV)	-4.83	-4.81	-4.81	-4.81	-4.81	-4.81	-4.81
LUMO (eV)	-3.33	-3.53	-3.53	-3.53	-3.53	-3.53	-3.53
$E_g$ (eV)	1.50	1.28	1.28	1.28	1.28	1.28	1.28
$\eta$ (eV)	0.75	0.64	0.64	0.64	0.64	0.64	0.64
$\sigma$ (eV <sup>-1</sup> )	1.33	1.56	1.56	1.56	1.56	1.56	1.56
$\chi$ (eV)	4.08	4.17	4.17	4.17	4.17	4.17	4.17
$\mu$ (eV)	-4.08	-4.17	-4.17	-4.17	-4.17	-4.17	-4.17
$\omega$ (eV)	11.10	13.59	13.59	13.59	13.59	13.59	13.59
Space cut-off = 3.5 (Å)							
HOMO (eV)	-5.11	-5.07	-5.07	-5.07	-5.07	-5.07	-5.07
LUMO (eV)	-3.58	-3.77	-3.77	-3.77	-3.77	-3.77	-3.77
$E_g$ (eV)	1.53	1.30	1.30	1.30	1.30	1.30	1.30
$\eta$ (eV)	0.77	0.65	0.65	0.65	0.65	0.65	0.65
$\sigma$ (eV <sup>-1</sup> )	1.30	1.54	1.54	1.54	1.54	1.54	1.54
$\chi$ (eV)	4.35	4.42	4.42	4.42	4.42	4.42	4.42
$\mu$ (eV)	-4.35	-4.42	-4.42	-4.42	-4.42	-4.42	-4.42
$\omega$ (eV)	12.29	15.03	15.03	15.03	15.03	15.03	15.03

Space cut-off = 4.5 (Å)							
HOMO (eV)	-5.25	-5.17	-5.17	-5.17	-5.17	-5.17	-5.17
LUMO (eV)	-3.69	-3.87	-3.87	-3.88	-3.88	-3.88	-3.87
E <sub>g</sub> (eV)	1.56	1.30	1.30	1.29	1.29	1.29	1.30
η (eV)	0.78	0.65	0.65	0.65	0.65	0.65	0.65
σ (eV <sup>-1</sup> )	1.28	1.54	1.54	1.54	1.54	1.54	1.54
χ (eV)	4.47	4.52	4.52	4.53	4.53	4.53	4.52
μ (eV)	-4.47	-4.52	-4.52	-4.53	-4.53	-4.53	-4.52
ω (eV)	12.81	15.72	15.72	15.79	15.79	15.79	15.72
Space cut-off = 5.5 (Å)							
HOMO (eV)	-5.25	-5.17	-5.17	-5.17	-5.18	-5.17	-5.18
LUMO (eV)	-3.69	-3.88	-3.88	-3.88	-3.88	-3.88	-3.88
E <sub>g</sub> (eV)	1.56	1.29	1.29	1.29	1.30	1.29	1.30
η (eV)	0.78	0.65	0.65	0.65	0.65	0.65	0.65
σ (eV <sup>-1</sup> )	1.28	1.54	1.54	1.54	1.54	1.54	1.54
χ (eV)	4.47	4.53	4.53	4.53	4.53	4.53	4.53
μ (eV)	-4.47	-4.53	-4.53	-4.53	-4.53	-4.53	-4.53
ω (eV)	12.81	15.79	15.79	15.79	15.78	15.79	15.78
Space cut-off = 6.5 (Å)							
HOMO (eV)	-5.30	-5.18	-5.18	-5.18	-5.18	-5.18	-5.18
LUMO (eV)	-3.67	-3.88	-3.88	-3.89	-3.89	-3.89	-3.89
E <sub>g</sub> (eV)	1.63	1.30	1.30	1.29	1.29	1.29	1.29
η (eV)	0.82	0.65	0.65	0.65	0.65	0.65	0.65
σ (eV <sup>-1</sup> )	1.22	1.54	1.54	1.54	1.54	1.54	1.54
χ (eV)	4.49	4.53	4.53	4.54	4.54	4.54	4.54
μ (eV)	-4.49	-4.53	-4.53	-4.54	-4.54	-4.54	-4.54
ω (eV)	12.29	15.78	15.78	15.86	15.86	15.86	15.86
Space cut-off = 7.0 (Å)							
HOMO (eV)	-5.27	-5.18	-5.18	-5.18	-5.18	-5.19	-5.18
LUMO (eV)	-3.69	-3.88	-3.89	-3.89	-3.89	-3.89	-3.89
E <sub>g</sub> (eV)	1.58	1.30	1.29	1.29	1.29	1.30	1.29
η (eV)	0.79	0.65	0.65	0.65	0.65	0.65	0.65
σ (eV <sup>-1</sup> )	1.27	1.54	1.54	1.54	1.54	1.54	1.54
χ (eV)	4.48	4.53	4.54	4.54	4.54	4.54	4.54
μ (eV)	-4.48	-4.53	-4.54	-4.54	-4.54	-4.54	-4.54
ω (eV)	12.70	15.78	15.86	15.86	15.86	15.86	15.86
Space cut-off = 8.0 (Å)							
HOMO (eV)	-5.29	-5.18	-5.18	-5.18	-5.18	-5.18	-5.17
LUMO (eV)	-3.67	-3.88	-3.88	-3.88	-3.88	-3.88	-3.88
E <sub>g</sub> (eV)	1.62	1.30	1.30	1.30	1.30	1.30	1.30
η (eV)	0.81	0.65	0.65	0.65	0.65	0.65	0.65
σ (eV <sup>-1</sup> )	1.23	1.54	1.54	1.54	1.54	1.54	1.54
χ (eV)	4.48	4.53	4.53	4.53	4.53	4.53	4.53
μ (eV)	-4.48	-4.53	-4.53	-4.53	-4.53	-4.53	-4.53
ω (eV)	12.39	15.78	15.78	15.78	15.78	15.78	15.78

**Table A. 9:** Reactivity indices for D4.

Reactivity Parameters	Gas phase	COSMO ( $\epsilon = 78.4$ )					
		Number of segment per atom (NSPA)					
		92	272	362	482	642	1082
Space cut-off = 3.0 (Å)							
HOMO (eV)	-5.09	-5.03	-5.02	-5.02	-5.02	-5.03	-5.02
LUMO (eV)	-3.58	-3.68	-3.69	-3.69	-3.69	-3.68	-3.69
$E_g$ (eV)	1.51	1.35	1.33	1.33	1.33	1.35	1.33
$\eta$ (eV)	0.76	0.68	0.67	0.67	0.67	0.68	0.67
$\sigma$ (eV <sup>-1</sup> )	1.32	1.47	1.49	1.49	1.49	1.47	1.49
$\chi$ (eV)	4.34	4.36	4.36	4.36	4.36	4.36	4.36
$\mu$ (eV)	-4.34	-4.36	-4.36	-4.36	-4.36	-4.36	-4.36
$\omega$ (eV)	12.39	13.98	14.19	14.19	14.19	13.98	14.19
Space cut-off = 3.5 (Å)							
HOMO (eV)	-5.31	-5.21	-5.21	-5.21	-5.21	-5.21	-5.21
LUMO (eV)	-3.82	-3.88	-3.88	-3.88	-3.88	-3.87	-3.88
$E_g$ (eV)	1.49	1.33	1.33	1.33	1.33	1.34	1.33
$\eta$ (eV)	0.75	0.67	0.67	0.67	0.67	0.67	0.67
$\sigma$ (eV <sup>-1</sup> )	1.33	1.49	1.49	1.49	1.49	1.49	1.49
$\chi$ (eV)	4.57	4.55	4.55	4.55	4.55	4.54	4.55
$\mu$ (eV)	-4.57	-4.55	-4.55	-4.55	-4.55	-4.54	-4.55
$\omega$ (eV)	13.92	15.45	15.45	15.45	15.45	15.38	15.45
Space cut-off = 4.5 (Å)							
HOMO (eV)	-5.43	-5.30	-5.30	-5.30	-5.30	-5.30	-5.30
LUMO (eV)	-3.97	-3.97	-3.97	-3.97	-3.97	-3.97	-3.97
$E_g$ (eV)	1.46	1.33	1.33	1.33	1.33	1.33	1.33
$\eta$ (eV)	0.73	0.67	0.67	0.67	0.67	0.67	0.67
$\sigma$ (eV <sup>-1</sup> )	1.37	1.49	1.49	1.49	1.49	1.49	1.49
$\chi$ (eV)	4.70	4.64	4.64	4.64	4.64	4.64	4.64
$\mu$ (eV)	-4.70	-4.64	-4.64	-4.64	-4.64	-4.64	-4.64
$\omega$ (eV)	15.13	16.07	16.07	16.07	16.07	16.07	16.07
Space cut-off = 5.5 (Å)							
HOMO (eV)	-5.48	-5.31	-5.31	-5.31	-5.31	-5.31	-5.31
LUMO (eV)	-3.93	-3.97	-3.97	-3.98	-3.98	-3.98	-3.98
$E_g$ (eV)	1.55	1.34	1.34	1.33	1.33	1.33	1.33
$\eta$ (eV)	0.78	0.67	0.67	0.67	0.67	0.67	0.67
$\sigma$ (eV <sup>-1</sup> )	1.28	1.49	1.49	1.49	1.49	1.49	1.49
$\chi$ (eV)	4.71	4.64	4.64	4.65	4.65	4.65	4.65
$\mu$ (eV)	-4.71	-4.64	-4.64	-4.65	-4.65	-4.65	-4.65
$\omega$ (eV)	14.22	16.07	16.07	16.14	16.14	16.14	16.14
Space cut-off = 6.5 (Å)							
HOMO (eV)	-5.48	-5.31	-5.31	-5.31	-5.31	-5.31	-5.31
LUMO (eV)	-3.93	-3.98	-3.98	-3.98	-3.98	-3.98	-3.98
$E_g$ (eV)	1.55	1.33	1.33	1.33	1.33	1.33	1.33
$\eta$ (eV)	0.78	0.67	0.67	0.67	0.67	0.67	0.67
$\sigma$ (eV <sup>-1</sup> )	1.28	1.49	1.49	1.49	1.49	1.49	1.49
$\chi$ (eV)	4.71	4.65	4.65	4.65	4.65	4.65	4.65
$\mu$ (eV)	-4.71	-4.65	-4.65	-4.65	-4.65	-4.65	-4.65
$\omega$ (eV)	14.22	16.14	16.14	16.14	16.14	16.14	16.14
Space cut-off = 7.0 (Å)							
HOMO (eV)	-5.48	-5.31	-5.31	-5.31	-5.31	-5.31	-5.31
LUMO (eV)	-3.93	-3.98	-3.98	-3.98	-3.98	-3.98	-3.98
$E_g$ (eV)	1.55	1.33	1.33	1.33	1.33	1.33	1.33

$\eta$ (eV)	0.78	0.67	0.67	0.67	0.67	0.67	0.67
$\sigma$ (eV <sup>-1</sup> )	1.28	1.49	1.49	1.49	1.49	1.49	1.49
$\chi$ (eV)	4.71	4.65	4.65	4.65	4.65	4.65	4.65
$\mu$ (eV)	-4.71	-4.65	-4.65	-4.65	-4.65	-4.65	-4.65
$\omega$ (eV)	14.22	16.14	16.14	16.14	16.14	16.14	16.14
Space cut-off = 8.0 (Å)							
HOMO (eV)	-5.48	-5.31	-5.31	-5.31	-5.31	-5.31	-5.31
LUMO (eV)	-3.93	-3.98	-3.98	-3.98	-3.98	-3.98	-3.98
$E_g$ (eV)	1.55	1.33	1.33	1.33	1.33	1.33	1.33
$\eta$ (eV)	0.78	0.67	0.67	0.67	0.67	0.67	0.67
$\sigma$ (eV <sup>-1</sup> )	1.28	1.49	1.49	1.49	1.49	1.49	1.49
$\chi$ (eV)	4.71	4.65	4.65	4.65	4.65	4.65	4.65
$\mu$ (eV)	-4.71	-4.65	-4.65	-4.65	-4.65	-4.65	-4.65
$\omega$ (eV)	14.22	16.14	16.14	16.14	16.14	16.14	16.14

**Table A. 10:** Solvation free energy (SFE), vapor pressure (p), octanol-water partition coefficient (Log P) and aqueous solubility ( $S_{CSE}$  and  $S_{GSE}$ ) at 25 °C for B1 (Molecular weight. = 314 g/mol).

Calculated properties	Solvent radius						Log $S_{Expt}$ (mol/L)
	0.5	0.8	1.1	1.3	1.6	1.9	
Space cut-off = 3.5 (Å)							
SFE (kcal/mol)	-11.22	-10.93	-10.57	-10.38	-10.13	-9.90	-6.02
$p \times 10^{-14}$ (atm)	0.17	0.35	0.78	1.36	1.88	2.54	
$S_{CSE}$ (mg/L)	0.37	0.47	0.57	0.72	0.65	0.60	
Log $S_{CSE}$ (mol/L)	-5.93	-5.82	-5.74	-5.64	-5.68	-5.72	
Log P	5.04	5.15	5.25	5.42	5.66	5.81	
$S_{GSE}$ (kcal/mol)	0.38	0.29	0.23	0.16	0.09	0.06	
Log $S_{GSE}$ (mol/L)	-5.92	-6.03	-6.14	-6.29	-6.54	-6.72	
Space cut-off = 4.5 (Å)							
SFE (kcal/mol)	-12.29	-11.97	-11.66	-11.40	-11.15	-10.89	-6.02
$p \times 10^{-14}$ (atm)	0.031	0.062	0.16	0.31	0.38	0.56	
$S_{CSE}$ (mg/L)	0.41	0.48	0.74	0.92	0.74	0.70	
Log $S_{CSE}$ (mol/L)	-5.88	-5.82	-5.63	-5.53	-5.63	-5.65	
Log P	4.79	4.90	5.01	5.16	5.40	5.55	
$S_{GSE}$ (kcal/mol)	0.67	0.52	0.40	0.29	0.16	0.12	
Log $S_{GSE}$ (mol/L)	-5.67	-5.78	-5.89	-6.03	-6.29	-6.42	
Space cut-off = 5.5 (Å)							
SFE (kcal/mol)	-13.02	-12.65	-12.59	-12.38	-12.12	-11.90	-6.02
$p \times 10^{-14}$ (atm)	0.020	0.052	0.12	0.21	0.28	0.41	
$S_{CSE}$ (mg/L)	0.91	1.27	2.65	3.26	2.80	2.83	
Log $S_{CSE}$ (mol/L)	-5.54	-5.39	-5.07	-4.98	-5.05	-5.05	
Log P	4.77	4.91	4.90	5.11	5.38	5.48	
$S_{GSE}$ (kcal/mol)	0.70	0.51	0.52	0.32	0.17	0.14	
Log $S_{GSE}$ (mol/L)	-5.65	-5.79	-5.78	-5.99	-6.27	-6.35	
Space cut-off = 6.5 (Å)							
SFE (kcal/mol)	-13.46	-13.15	-12.61	-12.54	-12.25	-12.00	-6.02
$p \times 10^{-14}$ (atm)	0.018	0.042	0.094	0.18	0.23	0.35	
$S_{CSE}$ (mg/L)	1.73	2.39	2.15	3.66	2.86	2.86	
Log $S_{CSE}$ (mol/L)	-5.26	-5.12	-5.16	-4.93	-5.04	-5.04	
Log P	4.70	4.80	4.90	5.03	5.32	5.45	
$S_{GSE}$ (kcal/mol)	0.83	0.66	0.52	0.39	0.20	0.15	
Log $S_{GSE}$ (mol/L)	-5.58	-5.68	-5.78	-5.91	-6.20	-6.32	
Space cut-off = 7.0 (Å)							



SFE (kcal/mol)	-12.95	-12.63	-12.29	-12.08	-11.81	-11.57
$p \times 10^{-14}$ (atm)	0.020	0.041	0.099	0.17	0.24	0.32
$S_{CSE}$ (mg/L)	0.81	0.97	1.32	1.59	1.42	1.26
Log $S_{CSE}$ (mol/L)	-5.59	-5.51	-5.38	-5.30	-5.34	-5.40
Log P	4.71	4.82	4.88	5.05	5.30	5.43
$S_{GSE}$ (kcal/mol)	0.81	0.63	0.55	0.37	0.21	0.15
Log $S_{GSE}$ (mol/L)	-5.59	-5.70	-5.76	-5.93	-6.17	-6.32
Space cut-off = 8.0 (Å)						
SFE (kcal/mol)	-12.95	-12.63	-12.28	-12.09	-11.81	-11.58
$p \times 10^{-14}$ (atm)	0.020	0.034	0.099	0.17	0.25	0.33
$S_{CSE}$ (mg/L)	0.81	0.80	1.30	1.62	1.48	1.33
Log $S_{CSE}$ (mol/L)	-5.59	-5.59	-5.38	-5.29	-5.33	-5.37
Log P	4.71	4.80	4.86	5.05	5.31	5.43
$S_{GSE}$ (kcal/mol)	0.81	0.66	0.57	0.37	0.20	0.15

**Table A. 11:** Solvation free energy (SFE), vapor pressure (p), octanol-water partition coefficient (Log P) and aqueous solubility ( $S_{CSE}$  and  $S_{GSE}$ ) at 25 °C for B2 (Molecular weight. = 330 g/mol).

Calculated properties	Solvent radius						Log $S_{Expt}$ (mol/L)
	0.5	0.8	1.1	1.3	1.6	1.9	
Space cut-off = 3.5 (Å)							-5.92
SFE (kcal/mol)	-17.75	-17.28	-16.87	-16.61	-16.25	-15.95	
$p \times 10^{-14}$ (atm)	0.024	0.088	0.33	0.75	1.53	2.48	
$S_{CSE}$ (mg/L)	34.04	56.42	105.85	155.05	172.19	168.15	
Log $S_{CSE}$ (mol/L)	-3.99	-3.77	-3.49	-3.33	-3.28	-3.29	
Log P	4.01	4.20	4.31	4.51	4.81	4.94	
$S_{GSE}$ (kcal/mol)	1.54	1.00	0.77	0.49	0.24	0.18	
Log $S_{GSE}$ (mol/L)	-5.33	-5.52	-5.63	-5.83	-6.14	-6.26	
Space cut-off = 4.5 (Å)							-5.92
SFE (kcal/mol)	-19.00	-18.40	-18.00	-17.68	-17.28	-16.99	
$p \times 10^{-14}$ (atm)	0.0034	0.010	0.043	0.11	0.23	0.44	
$S_{CSE}$ (mg/L)	39.83	42.52	93.03	138.60	147.46	172.84	
Log $S_{CSE}$ (mol/L)	-3.92	-3.89	-3.55	-3.38	-3.35	-3.28	
Log P	3.74	3.88	4.00	4.17	4.50	4.59	
$S_{GSE}$ (kcal/mol)	2.87	2.08	1.58	1.07	0.50	0.41	
Log $S_{GSE}$ (mol/L)	-5.06	-5.20	-5.32	-5.49	-5.82	-5.91	
Space cut-off = 5.5 (Å)							-5.92
SFE (kcal/mol)	-18.95	-18.44	-17.96	-17.58	-17.27	-16.95	
$p \times 10^{-14}$ (atm)	0.0017	0.0051	0.025	0.056	0.12	0.23	
$S_{CSE}$ (mg/L)	18.30	23.20	50.55	59.59	75.65	84.45	
Log $S_{CSE}$ (mol/L)	-4.26	-4.15	-3.81	-3.74	-3.64	-3.59	
Log P	3.66	3.79	3.93	4.06	4.40	4.53	
$S_{GSE}$ (kcal/mol)	3.45	2.56	1.86	1.38	0.63	0.47	
Log $S_{GSE}$ (mol/L)	-4.98	-5.11	-5.25	-5.38	-5.72	-5.85	
Space cut-off = 6.5 (Å)							-5.92
SFE (kcal/mol)	-19.46	-18.82	-18.46	-18.14	-17.77	-17.44	
$p \times 10^{-14}$ (atm)	0.0018	0.0057	0.023	0.056	0.12	0.24	
$S_{CSE}$ (mg/L)	45.86	49.27	108.22	153.47	176.03	201.62	
Log $S_{CSE}$ (mol/L)	-3.86	-3.83	-3.48	-3.33	-3.27	-3.21	
Log P	3.63	3.77	3.90	4.07	4.36	4.50	
$S_{GSE}$ (kcal/mol)	3.70	2.68	1.99	1.34	0.69	0.50	
Log $S_{GSE}$ (mol/L)	-4.95	-5.09	-5.22	-5.39	-5.68	-5.82	
Space cut-off = 7.0 (Å)							-5.92
SFE (kcal/mol)	-16.86	-16.39	-15.84	-15.55	-15.21	-14.88	

$p \times 10^{-14}$ (atm)	0.0017	0.0054	0.024	0.058	0.11	0.22
$S_{CSE}$ (mg/L)	0.54	0.77	1.35	2.00	2.14	2.45
Log $S_{CSE}$ (mol/L)	-5.79	-5.63	-5.39	-5.22	-5.19	-5.13
Log P	3.68	3.78	3.91	4.11	4.36	4.49
$S_{GSE}$ (kcal/mol)	3.30	2.62	1.94	1.23	0.69	0.51
Log $S_{GSE}$ (mol/L)	-5.00	-5.10	-5.23	-5.43	-5.68	-5.81
Space cut-off = 8.0 (Å)						
SFE (kcal/mol)	-16.91	-16.44	-15.92	-15.60	-15.24	-14.92
$p \times 10^{-14}$ (atm)	0.0017	0.0054	0.022	0.053	0.12	0.22
$S_{CSE}$ (mg/L)	0.58	0.84	1.42	1.99	2.45	2.62
Log $S_{CSE}$ (mol/L)	-5.76	-5.59	-5.37	-5.22	-5.13	-5.10
Log P	3.65	3.78	3.88	4.06	4.34	4.49
$S_{GSE}$ (kcal/mol)	3.54	2.62	2.08	1.38	0.72	0.51
Log $S_{GSE}$ (mol/L)	-4.97	-5.10	-5.20	-5.38	-5.66	-5.81

**Table A. 12:** Solvation free energy (SFE), vapor pressure (p), octanol-water partition coefficient (Log P) and aqueous solubility ( $S_{CSE}$  and  $S_{GSE}$ ) at 25 °C for B3 (Molecular weight. = 344 g/mol).

Calculated properties	Solvent radius						Log $S_{Expt.}$ (mol/L)
	0.5	0.8	1.1	1.3	1.6	1.9	
Space cut-off = 3.5 (Å)							-5.46
SFE (kcal/mol)	-17.37	-16.67	-16.28	-15.68	-15.43	-15.09	
$p \times 10^{-14}$ (atm)	0.024	0.12	0.29	0.81	1.72	3.50	
$S_{CSE}$ (mg/L)	18.67	28.62	35.79	36.28	50.51	57.87	
Log $S_{CSE}$ (mol/L)	-4.27	-4.08	-3.98	-3.98	-3.83	-3.77	
Log P	4.90	4.97	5.19	5.32	5.45	5.54	
$S_{GSE}$ (mg/L)	0.61	0.52	0.31	0.23	0.17	0.14	
Log $S_{GSE}$ (mol/L)	-5.75	-5.82	-6.05	-6.17	-6.31	-6.39	
Space cut-off = 4.5 (Å)							
SFE (kcal/mol)	-18.30	-17.56	-17.15	-16.88	-16.34	-15.99	
$p \times 10^{-14}$ (atm)	0.0029	0.012	0.038	0.099	0.25	0.57	
$S_{CSE}$ (mg/L)	10.86	12.87	20.39	33.66	34.15	43.10	
Log $S_{CSE}$ (mol/L)	-4.50	-4.43	-4.23	-4.01	-4.00	-3.90	
Log P	4.62	4.60	4.83	4.90	5.13	5.20	
$S_{GSE}$ (mg/L)	1.17	1.22	0.72	0.61	0.36	0.31	
Log $S_{GSE}$ (mol/L)	-5.47	-5.45	-5.68	-5.75	-5.98	-6.05	
Space cut-off = 5.5 (Å)							
SFE (kcal/mol)	-18.82	-18.08	-17.67	-17.38	-16.82	-16.43	
$p \times 10^{-14}$ (atm)	0.0015	0.0073	0.019	0.052	0.14	0.31	
$S_{CSE}$ (mg/L)	13.52	18.84	24.54	41.15	43.02	49.29	
Log $S_{CSE}$ (mol/L)	-4.41	-4.26	-4.15	-3.92	-3.90	-3.84	
Log P	4.50	4.54	4.74	4.83	5.05	5.11	
$S_{GSE}$ (mg/L)	1.54	1.40	0.88	0.72	0.43	0.38	
Log $S_{GSE}$ (mol/L)	-5.35	-5.39	-5.59	-5.68	-5.90	-5.96	
Space cut-off = 6.5 (Å)							
SFE (kcal/mol)	-16.22	-15.55	-15.13	-14.83	-14.27	-13.88	
$p \times 10^{-14}$ (atm)	0.0014	0.0061	0.018	0.044	0.12	0.31	
$S_{CSE}$ (mg/L)	0.16	0.22	0.32	0.47	0.50	0.66	
Log $S_{CSE}$ (mol/L)	-6.33	-6.19	-6.03	-5.86	-5.84	-5.72	
Log P	4.50	4.50	4.71	4.80	5.02	5.07	
$S_{GSE}$ (mg/L)	1.54	1.54	0.95	0.77	0.46	0.41	
Log $S_{GSE}$ (mol/L)	-5.35	-5.35	-5.56	-5.65	-5.87	-5.92	
Space cut-off = 7.0 (Å)							
SFE (kcal/mol)	-16.23	-15.56	-15.14	-14.83	-14.28	-13.89	

$p \times 10^{-14}$ (atm)	0.0014	0.0061	0.018	0.044	0.12	0.30
$S_{CSE}$ (mg/L)	0.16	0.22	0.32	0.47	0.51	0.65
Log $S_{CSE}$ (mol/L)	-6.33	-6.19	-6.03	-5.86	-5.83	-5.72
Log P	4.50	4.49	4.70	4.81	5.01	5.07
$S_{GSE}$ (mg/L)	1.54	1.57	0.97	0.75	0.47	0.41
Log $S_{GSE}$ (mol/L)	-5.35	-5.34	-5.55	-5.66	-5.86	-5.92
Space cut-off = 8.0 (Å)						
SFE (kcal/mol)	-16.23	-15.55	-15.14	-14.84	-14.28	-13.89
$p \times 10^{-14}$ (atm)	0.0014	0.0059	0.018	0.043	0.12	0.30
$S_{CSE}$ (mg/L)	0.16	0.21	0.32	0.47	0.51	0.65
Log $S_{CSE}$ (mol/L)	-6.33	-6.21	-6.03	-5.86	-5.83	-5.72
Log P	4.50	4.50	4.70	4.81	5.01	5.07
$S_{GSE}$ (mg/L)	1.54	1.54	0.97	0.75	0.47	0.41
Log $S_{GSE}$ (mol/L)	-5.35	-5.35	-5.55	-5.66	-5.86	-5.92

**Table A. 13:** Solvation free energy (SFE), vapor pressure (p), octanol-water partition coefficient (Log P) and aqueous solubility ( $S_{CSE}$  and  $S_{GSE}$ ) 25 °C for B4 (Molecular weight. = 359 g/mol).

Calculated properties	Solvent radius						Log $S_{Expt.}$ (mol/L)
	0.5	0.8	1.1	1.3	1.6	1.9	
Space cut-off = 3.5 (Å)							-5.78
SFE (kcal/mol)	-14.40	-14.10	-13.43	-13.25	-12.91	-12.62	
$p \times 10^{-14}$ (atm)	0.11	0.28	1.01	1.53	2.31	2.91	
$S_{CSE}$ (mg/L)	0.59	0.91	1.06	1.18	1.00	0.77	
Log $S_{CSE}$	-5.78	-5.60	-5.53	-5.48	-5.56	-5.67	
Log P	5.11	5.31	5.46	5.52	5.80	5.98	
$S_{GSE}$ (mg/L)	0.56	0.35	0.25	0.22	0.11	0.08	
Log $S_{GSE}$	-5.81	-6.01	-6.16	-6.21	-6.51	-6.65	
Space cut-off = 4.5 (Å)							-5.78
SFE (kcal/mol)	-15.44	-15.14	-14.65	-14.17	-13.83	-13.79	
$p \times 10^{-14}$ (atm)	0.028	0.065	0.19	0.52	0.65	0.70	
$S_{CSE}$ (mg/L)	0.87	1.22	1.56	1.90	1.34	1.34	
Log $S_{CSE}$	-5.62	-5.47	-5.36	-5.28	-5.43	-5.43	
Log P	4.93	5.06	5.13	5.32	5.64	5.70	
$S_{GSE}$ (mg/L)	0.84	0.62	0.53	0.34	0.16	0.14	
Log $S_{GSE}$	-5.63	-5.76	-5.83	-6.02	-6.35	-6.41	
Space cut-off = 5.5 (Å)							-5.78
SFE (kcal/mol)	-15.89	-15.36	-14.87	-14.72	-14.42	-14.13	
$p \times 10^{-14}$ (atm)	0.016	0.047	0.14	0.23	0.33	0.44	
$S_{CSE}$ (mg/L)	1.07	1.28	1.67	2.12	1.83	1.50	
Log $S_{CSE}$	-5.53	-5.45	-5.33	-5.23	-5.29	-5.38	
Log P	4.85	4.98	5.06	5.21	5.45	5.61	
$S_{GSE}$ (mg/L)	1.01	0.75	0.62	0.44	0.25	0.18	
Log $S_{GSE}$	-5.55	-5.68	-5.76	-5.91	-6.16	-6.30	
Space cut-off = 6.5 (Å)							-5.78
SFE (kcal/mol)	-15.90	-15.43	-14.92	-14.74	-14.36	-14.08	
$p \times 10^{-14}$ (atm)	0.012	0.035	0.11	0.18	0.28	0.43	
$S_{CSE}$ (mg/L)	0.81	1.07	1.42	1.72	1.41	1.35	
Log $S_{CSE}$	-5.65	-5.53	-5.40	-5.32	-5.41	-5.42	
Log P	4.76	4.96	5.00	5.21	5.47	5.60	
$S_{GSE}$ (mg/L)	1.24	0.79	0.72	0.44	0.24	0.18	
Log $S_{GSE}$	-5.46	-5.66	-5.70	-5.91	-6.17	-6.30	
Space cut-off = 7.0 (Å)							-5.78
SFE (kcal/mol)	-15.92	-15.45	-14.93	-14.76	-14.36	-14.10	
$p \times 10^{-14}$ (atm)	0.012	0.035	0.11	0.18	0.31	0.41	

$S_{CSE}$ (mg/L)	0.84	1.11	1.45	1.78	1.56	1.33
Log $S_{CSE}$	-5.63	-5.51	-5.39	-5.30	-5.36	-5.43
Log P	4.76	4.95	5.01	5.23	5.45	5.58
$S_{GSE}$ (mg/L)	1.24	0.80	0.70	0.42	0.25	0.19
Log $S_{GSE}$	-5.46	-5.65	-5.71	-5.93	-6.16	-6.28
Space cut-off = 8.0 (Å)						
SFE (kcal/mol)	-15.90	-15.42	-14.93	-14.72	-14.37	-14.09
$\rho \times 10^{-14}$ (atm)	0.012	0.038	0.10	0.18	0.31	0.38
$S_{CSE}$ (mg/L)	0.81	1.14	1.32	1.66	1.59	1.21
Log $S_{CSE}$	-5.65	-5.50	-5.43	-5.33	-5.35	-5.47
Log P	4.75	4.97	4.99	5.16	5.46	5.57
$S_{GSE}$ (mg/L)	1.27	0.77	0.73	0.50	0.25	0.19
Log $S_{GSE}$	-5.45	-5.67	-5.69	-5.86	-6.16	-6.28

**Table A. 14:** Solubility related properties of the studied substituents.

Substituents	$\chi$ (eV)	$\Phi$ (eV)	$\mu$ (Debye)	$\Delta G_{sol}$ (kcal/mol)	$\tau$ [46]	
					<i>meta</i>	<i>para</i>
CN	4.66	-4.66	1.17	-1.07	0.56	0.66
NO <sub>2</sub>	5.98	-5.98	0.23	-0.89	0.71	0.78
NH <sub>2</sub>	5.89	-5.89	1.75	-4.47	-0.16	-0.66
NHCH <sub>3</sub>	5.00	-5.00	1.97	-4.48	-	-0.84
N(CH <sub>3</sub> ) <sub>2</sub>	4.56	-4.56	1.68	-3.83	-0.15	-0.83

$\chi$  = Electronegativity,  $\Phi$  = Chemical potential,  $\mu$  = Dipole moment,  $\Delta G_{sol}$  = Solvation free energy in water and  $\tau$  = Hammett constant

**Table A. 15:** Calculated band structures for the studied catalysts.

Photocatalysts	Cut-off (Å)	CBE (eV)	VBE (eV)	$E_g$ (eV)	Expt. $E_g$ (eV)
Si (primitive)	4.5	-4.24	-5.04	0.8	1.1*
CdSe (primitive)	3.5	-3.24	-4.82	1.6	1.7*
CdS (002)	5.8	-3.49	-5.85	2.4	2.4*
TiO <sub>2</sub> (rutile 110)	5.5	-5.02	-7.80	2.8	3.0**
ZnO (001)	2.6	-0.99	-4.20	3.2	3.2*
ZnS (110)	3.3	-1.63	-5.29	3.6	3.6*

CBE = Conduction band edge, VBE = Valence band edge and  $E_g$  = Band gap

\* K. Mondal and A. Sharma. Photocatalytic oxidation of pollutant dyes in wastewater by TiO<sub>2</sub> and ZnO nano-materials - a mini-review. *Nanoscience & Technology for Mankind, The Academy of Sciences India (NASI)*, Allahabad, India (2014) 36-72.

\*\*X. Li, J. Yu, J. Low, Y. Fang, J. Xiao, X. Chen. Engineering heterogeneous semiconductors for solar water splitting. *Journal of Material Chemistry A* 3 (2015) 2485-2534.

**Table A. 16:** Vapor pressure ( $p$ ), SFE ( $\Delta G_{sol}$ ), aqueous solubility ( $S_{aq}$ ) and the Gibb's free energies ( $G_{gas}$ ) obtained for DY119 and its studied derivatives at 25 °C.

Dye No.	R1	R2	R3	R4	R5	Mwt. (g/mol)	pE-11 (atm)	$\Delta G_{sol}$ (kcal/mol)	$S_{aq}$ (mg/L)	$G_{gas}$ (kcal/mol)
DY 119	H	NO <sub>2</sub>	H	CH <sub>3</sub>	C <sub>2</sub> H <sub>5</sub>	327.30	1.92	-11.38	57.33	-37.07
EWS and EDS substitution										
E30	NO <sub>2</sub>	NO <sub>2</sub>	H	NH <sub>2</sub>	C <sub>2</sub> H <sub>5</sub>	373.28	3.19E-05	-17.07	16.24	-35.68
E31	NO <sub>2</sub>	NO <sub>2</sub>	H	NHCH <sub>3</sub>	C <sub>2</sub> H <sub>5</sub>	387.31	2.91E-05	-16.83	10.25	-36.60
E32	NO <sub>2</sub>	NO <sub>2</sub>	H	N(CH <sub>3</sub> ) <sub>2</sub>	C <sub>2</sub> H <sub>5</sub>	401.34	1.16E-04	-17.26	87.41	-37.69
E33	NO <sub>2</sub>	NO <sub>2</sub>	H	CH <sub>3</sub>	NH <sub>2</sub>	359.26	5.06E-03	-15.96	380.00	-35.58
E34	NO <sub>2</sub>	NO <sub>2</sub>	H	CH <sub>3</sub>	NHCH <sub>3</sub>	373.28	3.19E-03	-15.28	78.99	-37.26
E35	NO <sub>2</sub>	NO <sub>2</sub>	H	CH <sub>3</sub>	N(CH <sub>3</sub> ) <sub>2</sub>	387.31	9.87E-03	-14.50	67.82	-36.83
E36	CN	NO <sub>2</sub>	H	NH <sub>2</sub>	C <sub>2</sub> H <sub>5</sub>	353.30	5.18E-05	-17.66	67.55	-33.73
E37	CN	NO <sub>2</sub>	H	NHCH <sub>3</sub>	C <sub>2</sub> H <sub>5</sub>	367.32	3.93E-05	-17.17	23.29	-35.66
E38	CN	NO <sub>2</sub>	H	N(CH <sub>3</sub> ) <sub>2</sub>	C <sub>2</sub> H <sub>5</sub>	381.35	2.21E-04	-17.76	368.30	-35.97
E39	CN	NO <sub>2</sub>	H	CH <sub>3</sub>	NH <sub>2</sub>	339.27	5.18E-03	-16.38	746.52	-32.60
E40	CN	NO <sub>2</sub>	H	CH <sub>3</sub>	NHCH <sub>3</sub>	353.30	3.58E-03	-15.51	123.71	-34.68
E41	CN	NO <sub>2</sub>	H	CH <sub>3</sub>	N(CH <sub>3</sub> ) <sub>2</sub>	367.32	1.19E-02	-14.89	149.44	-36.14
E42	NO <sub>2</sub>	NO <sub>2</sub>	H	NH <sub>2</sub>	CH <sub>3</sub>	359.26	3.58E-05	-17.72	52.59	-34.47
E43	NO <sub>2</sub>	NO <sub>2</sub>	H	NHCH <sub>3</sub>	CH <sub>3</sub>	373.28	3.75E-05	-17.15	21.85	-35.61
E44	NO <sub>2</sub>	NO <sub>2</sub>	H	N(CH <sub>3</sub> ) <sub>2</sub>	CH <sub>3</sub>	387.31	7.15E-05	-17.20	47.00	-34.95
E45	NO <sub>2</sub>	NO <sub>2</sub>	H	C <sub>2</sub> H <sub>5</sub>	NH <sub>2</sub>	373.28	4.11E-05	-15.40	124.62	-36.92
E46	NO <sub>2</sub>	NO <sub>2</sub>	H	C <sub>2</sub> H <sub>5</sub>	NHCH <sub>3</sub>	387.31	2.66E-03	-14.83	31.88	-37.63
E47	NO <sub>2</sub>	NO <sub>2</sub>	H	C <sub>2</sub> H <sub>5</sub>	N(CH <sub>3</sub> ) <sub>2</sub>	401.34	8.40E-03	-13.96	24.03	-37.45
E48	CN	NO <sub>2</sub>	H	NH <sub>2</sub>	CH <sub>3</sub>	339.27	4.51E-05	-17.77	68.04	-32.98
E49	CN	NO <sub>2</sub>	H	NHCH <sub>3</sub>	CH <sub>3</sub>	353.30	5.06E-05	-17.73	74.30	-34.90
E50	CN	NO <sub>2</sub>	H	N(CH <sub>3</sub> ) <sub>2</sub>	CH <sub>3</sub>	367.32	3.50E-05	-18.07	94.92	-35.50
E51	CN	NO <sub>2</sub>	H	C <sub>2</sub> H <sub>5</sub>	NH <sub>2</sub>	353.30	5.18E-03	-15.92	357.42	-34.83
E52	CN	NO <sub>2</sub>	H	C <sub>2</sub> H <sub>5</sub>	NHCH <sub>3</sub>	367.32	2.85E-03	-15.42	87.76	-36.92
E53	CN	NO <sub>2</sub>	H	C <sub>2</sub> H <sub>5</sub>	N(CH <sub>3</sub> ) <sub>2</sub>	381.35	1.08E-02	-14.08	36.02	-34.95
E54	NO <sub>2</sub>	NO <sub>2</sub>	H	NH <sub>2</sub>	NH <sub>2</sub>	360.25	3.05E-06	-19.61	109.31	-34.39
E55	NO <sub>2</sub>	NO <sub>2</sub>	H	NH <sub>2</sub>	NHCH <sub>3</sub>	374.27	4.41E-07	-18.97	5.57	-33.76
E56	NO <sub>2</sub>	NO <sub>2</sub>	H	NH <sub>2</sub>	N(CH <sub>3</sub> ) <sub>2</sub>	388.30	9.21E-07	-18.15	3.02	-35.85
E57	NO <sub>2</sub>	NO <sub>2</sub>	H	NHCH <sub>3</sub>	NH <sub>2</sub>	374.27	2.54E-06	-19.37	62.97	-35.15
E58	NO <sub>2</sub>	NO <sub>2</sub>	H	NHCH <sub>3</sub>	NHCH <sub>3</sub>	388.30	7.66E-07	-18.55	4.94	-35.75
E59	NO <sub>2</sub>	NO <sub>2</sub>	H	NHCH <sub>3</sub>	N(CH <sub>3</sub> ) <sub>2</sub>	402.33	1.24E-06	-18.23	4.83	-38.52
E60	NO <sub>2</sub>	NO <sub>2</sub>	H	N(CH <sub>3</sub> ) <sub>2</sub>	NH <sub>2</sub>	388.30	5.68E-06	-19.27	123.53	-36.67
E61	NO <sub>2</sub>	NO <sub>2</sub>	H	N(CH <sub>3</sub> ) <sub>2</sub>	NHCH <sub>3</sub>	402.33	1.01E-06	-19.01	14.67	-37.73
E62	NO <sub>2</sub>	NO <sub>2</sub>	H	N(CH <sub>3</sub> ) <sub>2</sub>	N(CH <sub>3</sub> ) <sub>2</sub>	416.35	2.48E-05	-17.56	32.18	-38.61
E63	CN	NO <sub>2</sub>	H	NH <sub>2</sub>	NH <sub>2</sub>	340.26	3.93E-06	-20.00	257.02	-32.20
E64	CN	NO <sub>2</sub>	H	NH <sub>2</sub>	NHCH <sub>3</sub>	354.28	7.66E-07	-19.20	13.51	-34.51
E65	CN	NO <sub>2</sub>	H	NH <sub>2</sub>	N(CH <sub>3</sub> ) <sub>2</sub>	368.31	8.40E-07	-18.94	9.93	-34.42
E66	CN	NO <sub>2</sub>	H	NHCH <sub>3</sub>	NH <sub>2</sub>	354.28	2.37E-06	-19.96	150.71	-35.84
E67	CN	NO <sub>2</sub>	H	NHCH <sub>3</sub>	NHCH <sub>3</sub>	368.31	9.65E-07	-19.33	22.02	-35.91
E68	CN	NO <sub>2</sub>	H	NHCH <sub>3</sub>	N(CH <sub>3</sub> ) <sub>2</sub>	382.34	1.72E-06	-18.66	13.11	-37.24
E69	CN	NO <sub>2</sub>	H	N(CH <sub>3</sub> ) <sub>2</sub>	NH <sub>2</sub>	368.31	7.15E-06	-19.34	166.03	-34.21
E70	CN	NO <sub>2</sub>	H	N(CH <sub>3</sub> ) <sub>2</sub>	NHCH <sub>3</sub>	382.34	1.19E-06	-19.50	37.48	-36.26
E71	CN	NO <sub>2</sub>	H	N(CH <sub>3</sub> ) <sub>2</sub>	N(CH <sub>3</sub> ) <sub>2</sub>	396.36	3.34E-06	-19.28	75.42	-37.65
E72	H	NO <sub>2</sub>	NO <sub>2</sub>	NH <sub>2</sub>	C <sub>2</sub> H <sub>5</sub>	373.28	1.40E-02	-14.36	73.19	-35.55
E73	H	NO <sub>2</sub>	NO <sub>2</sub>	NHCH <sub>3</sub>	C <sub>2</sub> H <sub>5</sub>	387.31	7.20E-03	-14.20	29.81	-36.85
E74	H	NO <sub>2</sub>	NO <sub>2</sub>	N(CH <sub>3</sub> ) <sub>2</sub>	C <sub>2</sub> H <sub>5</sub>	401.34	2.50E-04	-15.76	14.96	-35.00
E75	H	NO <sub>2</sub>	NO <sub>2</sub>	CH <sub>3</sub>	NH <sub>2</sub>	359.26	5.10E-02	-15.09	880.66	-33.62
E76	H	NO <sub>2</sub>	NO <sub>2</sub>	CH <sub>3</sub>	NHCH <sub>3</sub>	373.28	2.60E-02	-14.47	163.68	-35.49
E77	H	NO <sub>2</sub>	NO <sub>2</sub>	CH <sub>3</sub>	N(CH <sub>3</sub> ) <sub>2</sub>	387.31	8.80E-02	-13.42	97.55	-35.88
E78	H	NO <sub>2</sub>	CN	NH <sub>2</sub>	C <sub>2</sub> H <sub>5</sub>	353.30	3.27E-02	-14.21	125.52	-34.21

E79	H	NO <sub>2</sub>	CN	NHCH <sub>3</sub>	C <sub>2</sub> H <sub>5</sub>	367.32	5.18E-02	-13.74	93.50	-34.55
E80	H	NO <sub>2</sub>	CN	N(CH <sub>3</sub> ) <sub>2</sub>	C <sub>2</sub> H <sub>5</sub>	381.35	1.97E-03	-15.44	65.20	-35.99
E81	H	NO <sub>2</sub>	CN	CH <sub>3</sub>	NH <sub>2</sub>	339.27	5.06E-02	-15.33	1238.10	-31.55
E82	H	NO <sub>2</sub>	CN	CH <sub>3</sub>	NHCH <sub>3</sub>	353.30	2.26E-02	-15.27	520.40	-33.62
E83	H	NO <sub>2</sub>	CN	CH <sub>3</sub>	N(CH <sub>3</sub> ) <sub>2</sub>	367.32	7.66E-02	-13.84	163.75	-35.49
E84	H	NO <sub>2</sub>	NO <sub>2</sub>	NH <sub>2</sub>	CH <sub>3</sub>	359.26	1.70E-02	-14.90	212.96	-33.33
E85	H	NO <sub>2</sub>	NO <sub>2</sub>	NHCH <sub>3</sub>	CH <sub>3</sub>	373.28	8.20E-02	-15.11	152.18	-34.19
E86	H	NO <sub>2</sub>	NO <sub>2</sub>	N(CH <sub>3</sub> ) <sub>2</sub>	CH <sub>3</sub>	387.31	3.60E-03	-15.15	74.17	-35.60
E87	H	NO <sub>2</sub>	NO <sub>2</sub>	C <sub>2</sub> H <sub>5</sub>	NH <sub>2</sub>	373.28	4.50E-02	-14.53	313.51	-34.98
E88	H	NO <sub>2</sub>	NO <sub>2</sub>	C <sub>2</sub> H <sub>5</sub>	NHCH <sub>3</sub>	387.31	1.90E-02	-14.25	85.59	-37.23
E89	H	NO <sub>2</sub>	NO <sub>2</sub>	C <sub>2</sub> H <sub>5</sub>	N(CH <sub>3</sub> ) <sub>2</sub>	401.34	5.30E-02	-13.00	29.95	-36.82
E90	H	NO <sub>2</sub>	CN	NH <sub>2</sub>	CH <sub>3</sub>	339.27	5.06E-02	-14.84	540.91	-32.36
E91	H	NO <sub>2</sub>	CN	NHCH <sub>3</sub>	CH <sub>3</sub>	353.30	8.40E-03	-14.19	311.92	-35.10
E92	H	NO <sub>2</sub>	CN	N(CH <sub>3</sub> ) <sub>2</sub>	CH <sub>3</sub>	367.32	4.02E-03	-15.66	185.93	-34.89
E93	H	NO <sub>2</sub>	CN	C <sub>2</sub> H <sub>5</sub>	NH <sub>2</sub>	353.30	1.88E-02	-15.48	617.16	-32.97
E94	H	NO <sub>2</sub>	CN	C <sub>2</sub> H <sub>5</sub>	NHCH <sub>3</sub>	367.32	1.60E-02	-14.86	191.63	-34.50
E95	H	NO <sub>2</sub>	CN	C <sub>2</sub> H <sub>5</sub>	N(CH <sub>3</sub> ) <sub>2</sub>	381.35	6.09E-02	-13.77	119.98	-37.36
E96	H	NO <sub>2</sub>	NO <sub>2</sub>	NH <sub>2</sub>	NH <sub>2</sub>	360.25	2.20E-03	-16.80	684.42	-33.56
E97	H	NO <sub>2</sub>	NO <sub>2</sub>	NH <sub>2</sub>	NHCH <sub>3</sub>	374.27	3.80E-04	-16.51	75.25	-34.93
E98	H	NO <sub>2</sub>	NO <sub>2</sub>	NH <sub>2</sub>	N(CH <sub>3</sub> ) <sub>2</sub>	388.30	8.00E-04	-15.60	35.34	-37.19
E99	H	NO <sub>2</sub>	NO <sub>2</sub>	NHCH <sub>3</sub>	NH <sub>2</sub>	374.27	1.40E-03	-16.66	357.19	-35.08
E100	H	NO <sub>2</sub>	NO <sub>2</sub>	NHCH <sub>3</sub>	NHCH <sub>3</sub>	388.30	2.50E-04	-16.34	38.54	-36.43
E101	H	NO <sub>2</sub>	NO <sub>2</sub>	NHCH <sub>3</sub>	N(CH <sub>3</sub> ) <sub>2</sub>	402.33	2.10E-04	-15.98	18.26	-36.24
E102	H	NO <sub>2</sub>	NO <sub>2</sub>	N(CH <sub>3</sub> ) <sub>2</sub>	NH <sub>2</sub>	388.30	2.90E-04	-17.20	191.11	-35.55
E103	H	NO <sub>2</sub>	NO <sub>2</sub>	N(CH <sub>3</sub> ) <sub>2</sub>	NHCH <sub>3</sub>	402.33	1.10E-04	-16.78	36.95	-36.58
E104	H	NO <sub>2</sub>	NO <sub>2</sub>	N(CH <sub>3</sub> ) <sub>2</sub>	N(CH <sub>3</sub> ) <sub>2</sub>	416.35	3.3.E-05	-17.55	42.12	-36.60
E105	H	NO <sub>2</sub>	CN	NH <sub>2</sub>	NH <sub>2</sub>	340.26	4.31E-03	-16.65	982.61	-31.84
E106	H	NO <sub>2</sub>	CN	NH <sub>2</sub>	NHCH <sub>3</sub>	354.28	8.40E-04	-16.22	96.49	-33.36
E107	H	NO <sub>2</sub>	CN	NH <sub>2</sub>	N(CH <sub>3</sub> ) <sub>2</sub>	368.31	9.87E-04	-15.81	58.96	-35.72
E108	H	NO <sub>2</sub>	CN	NHCH <sub>3</sub>	NH <sub>2</sub>	354.28	6.67E-03	-16.17	704.04	-32.99
E109	H	NO <sub>2</sub>	CN	NHCH <sub>3</sub>	NHCH <sub>3</sub>	368.31	2.91E-03	-15.75	157.23	-33.60
E110	H	NO <sub>2</sub>	CN	NHCH <sub>3</sub>	N(CH <sub>3</sub> ) <sub>2</sub>	382.34	4.21E-03	-15.43	137.41	-37.23
E111	H	NO <sub>2</sub>	CN	N(CH <sub>3</sub> ) <sub>2</sub>	NH <sub>2</sub>	368.31	3.50E-04	-17.79	592.71	-34.64
E112	H	NO <sub>2</sub>	CN	N(CH <sub>3</sub> ) <sub>2</sub>	NHCH <sub>3</sub>	382.34	1.60E-04	-17.41	148.10	-36.18
E113	H	NO <sub>2</sub>	CN	N(CH <sub>3</sub> ) <sub>2</sub>	N(CH <sub>3</sub> ) <sub>2</sub>	396.36	5.95E-04	-16.30	87.48	-36.67

**Table A. 17:** Screening charges,  $q$  and dipole moment,  $\mu$  of DY119 and its studied derivatives at 25 °C.

Dye No.	R1	R2	R3	R4	R5	Screening charge, $q$	$\mu$ (Debye)
DY 119	H	NO <sub>2</sub>	H	CH <sub>3</sub>	C <sub>2</sub> H <sub>5</sub>	-0.00119	6.80
EWS and EDS substitution							
E30	NO <sub>2</sub>	NO <sub>2</sub>	H	NH <sub>2</sub>	C <sub>2</sub> H <sub>5</sub>	-0.00084	1.72
E31	NO <sub>2</sub>	NO <sub>2</sub>	H	NHCH <sub>3</sub>	C <sub>2</sub> H <sub>5</sub>	-0.00087	2.45
E32	NO <sub>2</sub>	NO <sub>2</sub>	H	N(CH <sub>3</sub> ) <sub>2</sub>	C <sub>2</sub> H <sub>5</sub>	-0.00089	2.81
E33	NO <sub>2</sub>	NO <sub>2</sub>	H	CH <sub>3</sub>	NH <sub>2</sub>	-0.00076	1.71
E34	NO <sub>2</sub>	NO <sub>2</sub>	H	CH <sub>3</sub>	NHCH <sub>3</sub>	-0.00078	1.73
E35	NO <sub>2</sub>	NO <sub>2</sub>	H	CH <sub>3</sub>	N(CH <sub>3</sub> ) <sub>2</sub>	-0.00091	0.80
E36	CN	NO <sub>2</sub>	H	NH <sub>2</sub>	C <sub>2</sub> H <sub>5</sub>	-0.00095	1.64
E37	CN	NO <sub>2</sub>	H	NHCH <sub>3</sub>	C <sub>2</sub> H <sub>5</sub>	-0.00098	2.67
E38	CN	NO <sub>2</sub>	H	N(CH <sub>3</sub> ) <sub>2</sub>	C <sub>2</sub> H <sub>5</sub>	-0.00101	3.68
E39	CN	NO <sub>2</sub>	H	CH <sub>3</sub>	NH <sub>2</sub>	-0.00086	1.72
E40	CN	NO <sub>2</sub>	H	CH <sub>3</sub>	NHCH <sub>3</sub>	-0.00090	1.75
E41	CN	NO <sub>2</sub>	H	CH <sub>3</sub>	N(CH <sub>3</sub> ) <sub>2</sub>	-0.00101	0.48
E42	NO <sub>2</sub>	NO <sub>2</sub>	H	NH <sub>2</sub>	CH <sub>3</sub>	-0.00076	1.78
E43	NO <sub>2</sub>	NO <sub>2</sub>	H	NHCH <sub>3</sub>	CH <sub>3</sub>	-0.00081	2.73

E44	NO <sub>2</sub>	NO <sub>2</sub>	H	N(CH <sub>3</sub> ) <sub>2</sub>	CH <sub>3</sub>	-0.00082	3.98
E45	NO <sub>2</sub>	NO <sub>2</sub>	H	C <sub>2</sub> H <sub>5</sub>	NH <sub>2</sub>	-0.00080	1.60
E46	NO <sub>2</sub>	NO <sub>2</sub>	H	C <sub>2</sub> H <sub>5</sub>	NHCH <sub>3</sub>	-0.00084	1.65
E47	NO <sub>2</sub>	NO <sub>2</sub>	H	C <sub>2</sub> H <sub>5</sub>	N(CH <sub>3</sub> ) <sub>2</sub>	-0.00096	1.01
E48	CN	NO <sub>2</sub>	H	NH <sub>2</sub>	CH <sub>3</sub>	-0.00090	2.00
E49	CN	NO <sub>2</sub>	H	NHCH <sub>3</sub>	CH <sub>3</sub>	-0.00091	2.94
E50	CN	NO <sub>2</sub>	H	N(CH <sub>3</sub> ) <sub>2</sub>	CH <sub>3</sub>	-0.00093	5.05
E51	CN	NO <sub>2</sub>	H	C <sub>2</sub> H <sub>5</sub>	NH <sub>2</sub>	-0.00091	1.88
E52	CN	NO <sub>2</sub>	H	C <sub>2</sub> H <sub>5</sub>	NHCH <sub>3</sub>	-0.00093	1.90
E53	CN	NO <sub>2</sub>	H	C <sub>2</sub> H <sub>5</sub>	N(CH <sub>3</sub> ) <sub>2</sub>	-0.00106	0.70
E54	NO <sub>2</sub>	NO <sub>2</sub>	H	NH <sub>2</sub>	NH <sub>2</sub>	-0.00078	2.34
E55	NO <sub>2</sub>	NO <sub>2</sub>	H	NH <sub>2</sub>	NHCH <sub>3</sub>	-0.00083	2.11
E56	NO <sub>2</sub>	NO <sub>2</sub>	H	NH <sub>2</sub>	N(CH <sub>3</sub> ) <sub>2</sub>	-0.00088	1.11
E57	NO <sub>2</sub>	NO <sub>2</sub>	H	NHCH <sub>3</sub>	NH <sub>2</sub>	-0.00081	1.16
E58	NO <sub>2</sub>	NO <sub>2</sub>	H	NHCH <sub>3</sub>	NHCH <sub>3</sub>	-0.00084	3.09
E59	NO <sub>2</sub>	NO <sub>2</sub>	H	NHCH <sub>3</sub>	N(CH <sub>3</sub> ) <sub>2</sub>	-0.00090	2.08
E60	NO <sub>2</sub>	NO <sub>2</sub>	H	N(CH <sub>3</sub> ) <sub>2</sub>	NH <sub>2</sub>	-0.00084	4.75
E61	NO <sub>2</sub>	NO <sub>2</sub>	H	N(CH <sub>3</sub> ) <sub>2</sub>	NHCH <sub>3</sub>	-0.00085	4.96
E62	NO <sub>2</sub>	NO <sub>2</sub>	H	N(CH <sub>3</sub> ) <sub>2</sub>	N(CH <sub>3</sub> ) <sub>2</sub>	-0.00100	3.12
E63	CN	NO <sub>2</sub>	H	NH <sub>2</sub>	NH <sub>2</sub>	-0.00091	2.76
E64	CN	NO <sub>2</sub>	H	NH <sub>2</sub>	NHCH <sub>3</sub>	-0.00094	2.63
E65	CN	NO <sub>2</sub>	H	NH <sub>2</sub>	N(CH <sub>3</sub> ) <sub>2</sub>	-0.00099	1.39
E66	CN	NO <sub>2</sub>	H	NHCH <sub>3</sub>	NH <sub>2</sub>	-0.00092	3.69
E67	CN	NO <sub>2</sub>	H	NHCH <sub>3</sub>	NHCH <sub>3</sub>	-0.00094	3.62
E68	CN	NO <sub>2</sub>	H	NHCH <sub>3</sub>	N(CH <sub>3</sub> ) <sub>2</sub>	-0.00101	2.78
E69	CN	NO <sub>2</sub>	H	N(CH <sub>3</sub> ) <sub>2</sub>	NH <sub>2</sub>	-0.00094	4.61
E70	CN	NO <sub>2</sub>	H	N(CH <sub>3</sub> ) <sub>2</sub>	NHCH <sub>3</sub>	-0.00097	5.34
E71	CN	NO <sub>2</sub>	H	N(CH <sub>3</sub> ) <sub>2</sub>	N(CH <sub>3</sub> ) <sub>2</sub>	-0.00110	4.72
E72	H	NO <sub>2</sub>	NO <sub>2</sub>	NH <sub>2</sub>	C <sub>2</sub> H <sub>5</sub>	-0.00102	8.12
E73	H	NO <sub>2</sub>	NO <sub>2</sub>	NHCH <sub>3</sub>	C <sub>2</sub> H <sub>5</sub>	-0.00108	8.36
E74	H	NO <sub>2</sub>	NO <sub>2</sub>	N(CH <sub>3</sub> ) <sub>2</sub>	C <sub>2</sub> H <sub>5</sub>	-0.00108	8.18
E75	H	NO <sub>2</sub>	NO <sub>2</sub>	CH <sub>3</sub>	NH <sub>2</sub>	-0.00093	8.13
E76	H	NO <sub>2</sub>	NO <sub>2</sub>	CH <sub>3</sub>	NHCH <sub>3</sub>	-0.00097	8.45
E77	H	NO <sub>2</sub>	NO <sub>2</sub>	CH <sub>3</sub>	N(CH <sub>3</sub> ) <sub>2</sub>	-0.00110	6.72
E78	H	NO <sub>2</sub>	CN	NH <sub>2</sub>	C <sub>2</sub> H <sub>5</sub>	-0.00110	8.47
E79	H	NO <sub>2</sub>	CN	NHCH <sub>3</sub>	C <sub>2</sub> H <sub>5</sub>	-0.00116	8.57
E80	H	NO <sub>2</sub>	CN	N(CH <sub>3</sub> ) <sub>2</sub>	C <sub>2</sub> H <sub>5</sub>	-0.00113	8.23
E81	H	NO <sub>2</sub>	CN	CH <sub>3</sub>	NH <sub>2</sub>	-0.00101	8.08
E82	H	NO <sub>2</sub>	CN	CH <sub>3</sub>	NHCH <sub>3</sub>	-0.00099	8.49
E83	H	NO <sub>2</sub>	CN	CH <sub>3</sub>	N(CH <sub>3</sub> ) <sub>2</sub>	-0.00113	7.23
E84	H	NO <sub>2</sub>	NO <sub>2</sub>	NH <sub>2</sub>	CH <sub>3</sub>	-0.00097	8.35
E85	H	NO <sub>2</sub>	NO <sub>2</sub>	NHCH <sub>3</sub>	CH <sub>3</sub>	-0.00099	8.63
E86	H	NO <sub>2</sub>	NO <sub>2</sub>	N(CH <sub>3</sub> ) <sub>2</sub>	CH <sub>3</sub>	-0.00096	8.31
E87	H	NO <sub>2</sub>	NO <sub>2</sub>	C <sub>2</sub> H <sub>5</sub>	NH <sub>2</sub>	-0.00101	8.14
E88	H	NO <sub>2</sub>	NO <sub>2</sub>	C <sub>2</sub> H <sub>5</sub>	NHCH <sub>3</sub>	-0.00105	8.48
E89	H	NO <sub>2</sub>	NO <sub>2</sub>	C <sub>2</sub> H <sub>5</sub>	N(CH <sub>3</sub> ) <sub>2</sub>	-0.00116	6.92
E90	H	NO <sub>2</sub>	CN	NH <sub>2</sub>	CH <sub>3</sub>	-0.00101	8.62
E91	H	NO <sub>2</sub>	CN	NHCH <sub>3</sub>	CH <sub>3</sub>	-0.00109	8.81
E92	H	NO <sub>2</sub>	CN	N(CH <sub>3</sub> ) <sub>2</sub>	CH <sub>3</sub>	-0.00104	8.54
E93	H	NO <sub>2</sub>	CN	C <sub>2</sub> H <sub>5</sub>	NH <sub>2</sub>	-0.00104	8.05
E94	H	NO <sub>2</sub>	CN	C <sub>2</sub> H <sub>5</sub>	NHCH <sub>3</sub>	-0.00108	8.52
E95	H	NO <sub>2</sub>	CN	C <sub>2</sub> H <sub>5</sub>	N(CH <sub>3</sub> ) <sub>2</sub>	-0.00122	6.86
E96	H	NO <sub>2</sub>	NO <sub>2</sub>	NH <sub>2</sub>	NH <sub>2</sub>	-0.00097	8.28
E97	H	NO <sub>2</sub>	NO <sub>2</sub>	NH <sub>2</sub>	NHCH <sub>3</sub>	-0.00098	8.80
E98	H	NO <sub>2</sub>	NO <sub>2</sub>	NH <sub>2</sub>	N(CH <sub>3</sub> ) <sub>2</sub>	-0.00104	7.99
E99	H	NO <sub>2</sub>	NO <sub>2</sub>	NHCH <sub>3</sub>	NH <sub>2</sub>	-0.00100	8.69
E100	H	NO <sub>2</sub>	NO <sub>2</sub>	NHCH <sub>3</sub>	NHCH <sub>3</sub>	-0.00103	9.05
E101	H	NO <sub>2</sub>	NO <sub>2</sub>	NHCH <sub>3</sub>	N(CH <sub>3</sub> ) <sub>2</sub>	-0.00111	8.21

E102	H	NO <sub>2</sub>	NO <sub>2</sub>	N(CH <sub>3</sub> ) <sub>2</sub>	NH <sub>2</sub>	-0.00103	8.35
E103	H	NO <sub>2</sub>	NO <sub>2</sub>	N(CH <sub>3</sub> ) <sub>2</sub>	NHCH <sub>3</sub>	-0.00106	8.45
E104	H	NO <sub>2</sub>	NO <sub>2</sub>	N(CH <sub>3</sub> ) <sub>2</sub>	N(CH <sub>3</sub> ) <sub>2</sub>	-0.00118	7.20
E105	H	NO <sub>2</sub>	CN	NH <sub>2</sub>	NH <sub>2</sub>	-0.00104	8.63
E106	H	NO <sub>2</sub>	CN	NH <sub>2</sub>	NHCH <sub>3</sub>	-0.00107	9.15
E107	H	NO <sub>2</sub>	CN	NH <sub>2</sub>	N(CH <sub>3</sub> ) <sub>2</sub>	-0.00113	8.52
E108	H	NO <sub>2</sub>	CN	NHCH <sub>3</sub>	NH <sub>2</sub>	-0.000109	8.87
E109	H	NO <sub>2</sub>	CN	NHCH <sub>3</sub>	NHCH <sub>3</sub>	-0.00114	9.27
E110	H	NO <sub>2</sub>	CN	NHCH <sub>3</sub>	N(CH <sub>3</sub> ) <sub>2</sub>	-0.00118	8.58
E111	H	NO <sub>2</sub>	CN	N(CH <sub>3</sub> ) <sub>2</sub>	NH <sub>2</sub>	-0.00107	8.74
E112	H	NO <sub>2</sub>	CN	N(CH <sub>3</sub> ) <sub>2</sub>	NHCH <sub>3</sub>	-0.00110	8.66
E113	H	NO <sub>2</sub>	CN	N(CH <sub>3</sub> ) <sub>2</sub>	N(CH <sub>3</sub> ) <sub>2</sub>	-0.00122	7.44

**Table A. 18a:** Calculated HOMO and LUMO energies (i.e.  $E_{\text{HOMO}}$  and  $E_{\text{LUMO}}$ ), HOMO-LUMO energy gap ( $E_g$ ) and hardness ( $\eta$ ) values for DY119 and its studied derivatives.

Dye No.	R1	R2	R3	R4	R5	$E_{\text{HOMO}}$ (eV)		$E_{\text{LUMO}}$ (eV)		$E_g$ (eV)		$\eta$ (eV)	
						Gas	Water	Gas	Water	Gas	Water	Gas	Water
DY 119	H	NO <sub>2</sub>	H	CH <sub>3</sub>	C <sub>2</sub> H <sub>5</sub>	-6.25	-6.03	-4.37	-4.22	1.88	1.81	0.94	0.91
EWS and EDS Substitution													
E30	NO <sub>2</sub>	NO <sub>2</sub>	H	NH <sub>2</sub>	C <sub>2</sub> H <sub>5</sub>	-6.48	-6.11	-4.76	-4.38	1.72	1.73	0.86	0.87
E31	NO <sub>2</sub>	NO <sub>2</sub>	H	NHCH <sub>3</sub>	C <sub>2</sub> H <sub>5</sub>	-6.27	-5.95	-4.67	-4.34	1.60	1.61	0.80	0.81
E32	NO <sub>2</sub>	NO <sub>2</sub>	H	N(CH <sub>3</sub> ) <sub>2</sub>	C <sub>2</sub> H <sub>5</sub>	-6.12	-5.30	-4.61	-4.34	1.51	0.96	0.76	0.48
E33	NO <sub>2</sub>	NO <sub>2</sub>	H	CH <sub>3</sub>	NH <sub>2</sub>	-6.60	-6.25	-4.92	-4.52	1.68	1.73	0.84	0.87
E34	NO <sub>2</sub>	NO <sub>2</sub>	H	CH <sub>3</sub>	NHCH <sub>3</sub>	-6.41	-6.14	-4.88	-4.51	1.53	1.63	0.77	0.82
E35	NO <sub>2</sub>	NO <sub>2</sub>	H	CH <sub>3</sub>	N(CH <sub>3</sub> ) <sub>2</sub>	-5.91	-5.61	-4.79	-4.47	1.12	1.14	0.56	0.57
E36	CN	NO <sub>2</sub>	H	NH <sub>2</sub>	C <sub>2</sub> H <sub>5</sub>	-6.44	-6.09	-4.69	-4.31	1.75	1.78	0.88	0.89
E37	CN	NO <sub>2</sub>	H	NHCH <sub>3</sub>	C <sub>2</sub> H <sub>5</sub>	-6.21	-5.93	-4.59	-4.26	1.62	1.67	0.81	0.84
E38	CN	NO <sub>2</sub>	H	N(CH <sub>3</sub> ) <sub>2</sub>	C <sub>2</sub> H <sub>5</sub>	-6.07	-5.77	-4.50	-4.25	1.57	1.52	0.79	0.76
E39	CN	NO <sub>2</sub>	H	CH <sub>3</sub>	NH <sub>2</sub>	-6.56	-6.22	-4.84	-4.44	1.72	1.78	0.86	0.89
E40	CN	NO <sub>2</sub>	H	CH <sub>3</sub>	NHCH <sub>3</sub>	-6.35	-6.12	-4.80	-4.43	1.55	1.69	0.78	0.85
E41	CN	NO <sub>2</sub>	H	CH <sub>3</sub>	N(CH <sub>3</sub> ) <sub>2</sub>	-5.86	-5.59	-4.70	-4.39	1.16	1.20	0.58	0.60
E42	NO <sub>2</sub>	NO <sub>2</sub>	H	NH <sub>2</sub>	CH <sub>3</sub>	-6.53	-6.12	-4.80	-4.38	1.73	1.74	0.87	0.87
E43	NO <sub>2</sub>	NO <sub>2</sub>	H	NHCH <sub>3</sub>	CH <sub>3</sub>	-6.29	-5.96	-4.70	-4.34	1.59	1.62	0.80	0.81
E44	NO <sub>2</sub>	NO <sub>2</sub>	H	N(CH <sub>3</sub> ) <sub>2</sub>	CH <sub>3</sub>	-6.12	-5.81	-4.58	-4.29	1.54	1.52	0.77	0.76
E45	NO <sub>2</sub>	NO <sub>2</sub>	H	C <sub>2</sub> H <sub>5</sub>	NH <sub>2</sub>	-6.58	-6.25	-4.90	-4.53	1.68	1.72	0.84	0.86
E46	NO <sub>2</sub>	NO <sub>2</sub>	H	C <sub>2</sub> H <sub>5</sub>	NHCH <sub>3</sub>	-6.40	-6.14	-4.87	-4.52	1.53	1.62	0.77	0.81
E47	NO <sub>2</sub>	NO <sub>2</sub>	H	C <sub>2</sub> H <sub>5</sub>	N(CH <sub>3</sub> ) <sub>2</sub>	-5.90	-5.60	-4.77	-4.47	1.13	1.13	0.57	0.57
E48	CN	NO <sub>2</sub>	H	NH <sub>2</sub>	CH <sub>3</sub>	-6.47	-6.07	-4.71	-4.31	1.76	1.76	0.88	0.88
E49	CN	NO <sub>2</sub>	H	NHCH <sub>3</sub>	CH <sub>3</sub>	-6.24	-5.94	-4.62	-4.27	1.62	1.67	0.81	0.84
E50	CN	NO <sub>2</sub>	H	N(CH <sub>3</sub> ) <sub>2</sub>	CH <sub>3</sub>	-6.05	-5.78	-4.45	-4.19	1.60	1.59	0.80	0.80
E51	CN	NO <sub>2</sub>	H	C <sub>2</sub> H <sub>5</sub>	NH <sub>2</sub>	-6.54	-6.23	-4.82	-4.44	1.72	1.79	0.86	0.90
E52	CN	NO <sub>2</sub>	H	C <sub>2</sub> H <sub>5</sub>	NHCH <sub>3</sub>	-6.34	-6.11	-4.79	-4.43	1.55	1.68	0.78	0.84
E53	CN	NO <sub>2</sub>	H	C <sub>2</sub> H <sub>5</sub>	N(CH <sub>3</sub> ) <sub>2</sub>	-5.85	-5.57	-4.68	-4.40	1.17	1.17	0.59	0.59
E54	NO <sub>2</sub>	NO <sub>2</sub>	H	NH <sub>2</sub>	NH <sub>2</sub>	-6.34	-5.94	-4.85	-4.40	1.49	1.54	0.75	0.77
E55	NO <sub>2</sub>	NO <sub>2</sub>	H	NH <sub>2</sub>	NHCH <sub>3</sub>	-6.22	-5.92	-4.83	-4.41	1.39	1.51	0.70	0.76
E56	NO <sub>2</sub>	NO <sub>2</sub>	H	NH <sub>2</sub>	N(CH <sub>3</sub> ) <sub>2</sub>	-5.85	-5.54	-4.75	-4.38	1.10	1.16	0.55	0.58
E57	NO <sub>2</sub>	NO <sub>2</sub>	H	NHCH <sub>3</sub>	NH <sub>2</sub>	-6.16	-5.82	-4.74	-4.36	1.42	1.46	0.71	0.73
E58	NO <sub>2</sub>	NO <sub>2</sub>	H	NHCH <sub>3</sub>	NHCH <sub>3</sub>	-6.08	-5.82	-4.72	-4.36	1.36	1.46	0.68	0.73
E59	NO <sub>2</sub>	NO <sub>2</sub>	H	NHCH <sub>3</sub>	N(CH <sub>3</sub> ) <sub>2</sub>	-5.74	-5.52	-4.65	-4.34	1.09	1.18	0.55	0.59
E60	NO <sub>2</sub>	NO <sub>2</sub>	H	N(CH <sub>3</sub> ) <sub>2</sub>	NH <sub>2</sub>	-6.10	-5.75	-4.64	-4.33	1.46	1.42	0.73	0.71
E61	NO <sub>2</sub>	NO <sub>2</sub>	H	N(CH <sub>3</sub> ) <sub>2</sub>	NHCH <sub>3</sub>	-5.96	-5.72	-4.57	-4.28	1.39	1.44	0.70	0.72
E62	NO <sub>2</sub>	NO <sub>2</sub>	H	N(CH <sub>3</sub> ) <sub>2</sub>	N(CH <sub>3</sub> ) <sub>2</sub>	-5.73	-5.51	-4.56	-4.31	1.17	1.20	0.59	0.60
E63	CN	NO <sub>2</sub>	H	NH <sub>2</sub>	NH <sub>2</sub>	-6.29	-5.93	-4.76	-4.34	1.53	1.59	0.77	0.80
E64	CN	NO <sub>2</sub>	H	NH <sub>2</sub>	NHCH <sub>3</sub>	-6.19	-5.88	-4.74	-4.33	1.45	1.55	0.73	0.78
E65	CN	NO <sub>2</sub>	H	NH <sub>2</sub>	N(CH <sub>3</sub> ) <sub>2</sub>	-5.79	-5.51	-4.66	-4.30	1.13	1.21	0.57	0.61



E66	CN	NO <sub>2</sub>	H	NHCH <sub>3</sub>	NH <sub>2</sub>	-6.11	-5.80	-4.66	-4.28	1.45	1.52	0.73	0.76
E67	CN	NO <sub>2</sub>	H	NHCH <sub>3</sub>	NHCH <sub>3</sub>	-6.05	-5.79	-4.64	-4.29	1.41	1.50	0.71	0.75
E68	CN	NO <sub>2</sub>	H	NHCH <sub>3</sub>	N(CH <sub>3</sub> ) <sub>2</sub>	-5.70	-5.49	-4.57	-4.26	1.13	1.23	0.57	0.62
E69	CN	NO <sub>2</sub>	H	N(CH <sub>3</sub> ) <sub>2</sub>	NH <sub>2</sub>	-6.06	-5.72	-4.58	-4.26	1.48	1.46	0.74	0.73
E70	CN	NO <sub>2</sub>	H	N(CH <sub>3</sub> ) <sub>2</sub>	NHCH <sub>3</sub>	-5.92	-5.69	-4.50	-4.21	1.42	1.48	0.71	0.74
E71	CN	NO <sub>2</sub>	H	N(CH <sub>3</sub> ) <sub>2</sub>	N(CH <sub>3</sub> ) <sub>2</sub>	-5.67	-5.51	-4.45	-4.23	1.22	1.28	0.61	0.64
E72	H	NO <sub>2</sub>	NO <sub>2</sub>	NH <sub>2</sub>	C <sub>2</sub> H <sub>5</sub>	-6.23	-6.10	-4.56	-4.33	1.67	1.77	0.84	0.89
E73	H	NO <sub>2</sub>	NO <sub>2</sub>	NHCH <sub>3</sub>	C <sub>2</sub> H <sub>5</sub>	-5.98	-5.94	-4.48	-4.30	1.50	1.64	0.75	0.82
E74	H	NO <sub>2</sub>	NO <sub>2</sub>	N(CH <sub>3</sub> ) <sub>2</sub>	C <sub>2</sub> H <sub>5</sub>	-5.82	-5.76	-4.38	-4.21	1.44	1.55	0.72	0.78
E75	H	NO <sub>2</sub>	NO <sub>2</sub>	CH <sub>3</sub>	NH <sub>2</sub>	-6.40	-6.24	-4.68	-4.44	1.72	1.80	0.86	0.90
E76	H	NO <sub>2</sub>	NO <sub>2</sub>	CH <sub>3</sub>	NHCH <sub>3</sub>	-6.22	-6.13	-4.65	-4.44	1.57	1.69	0.79	0.85
E77	H	NO <sub>2</sub>	NO <sub>2</sub>	CH <sub>3</sub>	N(CH <sub>3</sub> ) <sub>2</sub>	-5.75	-5.58	-4.56	-4.40	1.19	1.18	0.60	0.59
E78	H	NO <sub>2</sub>	CN	NH <sub>2</sub>	C <sub>2</sub> H <sub>5</sub>	-6.15	-6.04	-4.55	-4.30	1.60	1.74	0.80	0.87
E79	H	NO <sub>2</sub>	CN	NHCH <sub>3</sub>	C <sub>2</sub> H <sub>5</sub>	-5.90	-5.90	-4.48	-4.26	1.42	1.64	0.71	0.82
E80	H	NO <sub>2</sub>	CN	N(CH <sub>3</sub> ) <sub>2</sub>	C <sub>2</sub> H <sub>5</sub>	-5.81	-5.74	-4.39	-4.21	1.42	1.53	0.71	0.77
E81	H	NO <sub>2</sub>	CN	CH <sub>3</sub>	NH <sub>2</sub>	-6.42	-6.22	-4.71	-4.43	1.71	1.79	0.86	0.90
E82	H	NO <sub>2</sub>	CN	CH <sub>3</sub>	NHCH <sub>3</sub>	-6.22	-6.11	-4.68	-4.41	1.54	1.70	0.77	0.85
E83	H	NO <sub>2</sub>	CN	CH <sub>3</sub>	N(CH <sub>3</sub> ) <sub>2</sub>	-5.72	-5.57	-4.52	-4.35	1.20	1.22	0.60	0.61
E84	H	NO <sub>2</sub>	NO <sub>2</sub>	NH <sub>2</sub>	CH <sub>3</sub>	-6.26	-6.09	-4.57	-4.33	1.69	1.76	0.85	0.88
E85	H	NO <sub>2</sub>	NO <sub>2</sub>	NHCH <sub>3</sub>	CH <sub>3</sub>	-6.01	-5.95	-4.48	-4.29	1.53	1.66	0.77	0.83
E86	H	NO <sub>2</sub>	NO <sub>2</sub>	N(CH <sub>3</sub> ) <sub>2</sub>	CH <sub>3</sub>	-5.86	-5.77	-4.44	-4.26	1.42	1.51	0.71	0.76
E87	H	NO <sub>2</sub>	NO <sub>2</sub>	C <sub>2</sub> H <sub>5</sub>	NH <sub>2</sub>	-6.39	-6.24	-4.67	-4.44	1.72	1.80	0.86	0.90
E88	H	NO <sub>2</sub>	NO <sub>2</sub>	C <sub>2</sub> H <sub>5</sub>	NHCH <sub>3</sub>	-6.21	-6.12	-4.64	-4.43	1.57	1.69	0.79	0.85
E89	H	NO <sub>2</sub>	NO <sub>2</sub>	C <sub>2</sub> H <sub>5</sub>	N(CH <sub>3</sub> ) <sub>2</sub>	-5.72	-5.58	-4.53	-4.40	1.19	1.18	0.60	0.59
E90	H	NO <sub>2</sub>	CN	NH <sub>2</sub>	CH <sub>3</sub>	-6.16	-6.05	-4.58	-4.31	1.58	1.74	0.79	0.87
E91	H	NO <sub>2</sub>	CN	NHCH <sub>3</sub>	CH <sub>3</sub>	-5.93	-5.91	-4.49	-4.27	1.44	1.64	0.72	0.82
E92	H	NO <sub>2</sub>	CN	N(CH <sub>3</sub> ) <sub>2</sub>	CH <sub>3</sub>	-5.83	-5.75	-4.42	-4.22	1.41	1.53	0.71	0.77
E93	H	NO <sub>2</sub>	CN	C <sub>2</sub> H <sub>5</sub>	NH <sub>2</sub>	-6.39	-6.21	-4.69	-4.44	1.70	1.77	0.85	0.89
E94	H	NO <sub>2</sub>	CN	C <sub>2</sub> H <sub>5</sub>	NHCH <sub>3</sub>	-6.23	-6.12	-4.66	-4.43	1.57	1.69	0.79	0.85
E95	H	NO <sub>2</sub>	CN	C <sub>2</sub> H <sub>5</sub>	N(CH <sub>3</sub> ) <sub>2</sub>	-5.69	-5.56	-4.55	-4.38	1.14	1.18	0.57	0.59
E96	H	NO <sub>2</sub>	NO <sub>2</sub>	NH <sub>2</sub>	NH <sub>2</sub>	-6.09	-5.91	-4.63	-4.37	1.46	1.54	0.73	0.77
E97	H	NO <sub>2</sub>	NO <sub>2</sub>	NH <sub>2</sub>	NHCH <sub>3</sub>	-6.04	-5.92	-4.62	-4.37	1.42	1.55	0.71	0.78
E98	H	NO <sub>2</sub>	NO <sub>2</sub>	NH <sub>2</sub>	N(CH <sub>3</sub> ) <sub>2</sub>	-5.66	-5.50	-4.54	-4.34	1.12	1.16	0.56	0.58
E99	H	NO <sub>2</sub>	NO <sub>2</sub>	NHCH <sub>3</sub>	NH <sub>2</sub>	-5.92	-5.81	-4.53	-4.31	1.39	1.50	0.70	0.75
E100	H	NO <sub>2</sub>	NO <sub>2</sub>	NHCH <sub>3</sub>	NHCH <sub>3</sub>	-5.83	-5.82	-4.51	-4.32	1.32	1.50	0.66	0.75
E101	H	NO <sub>2</sub>	NO <sub>2</sub>	NHCH <sub>3</sub>	N(CH <sub>3</sub> ) <sub>2</sub>	-5.58	-5.50	-4.45	-4.29	1.13	1.21	0.57	0.61
E102	H	NO <sub>2</sub>	NO <sub>2</sub>	N(CH <sub>3</sub> ) <sub>2</sub>	NH <sub>2</sub>	-5.83	-5.70	-4.47	-4.28	1.36	1.42	0.68	0.71
E103	H	NO <sub>2</sub>	NO <sub>2</sub>	N(CH <sub>3</sub> ) <sub>2</sub>	NHCH <sub>3</sub>	-5.76	-5.72	-4.46	-4.29	1.30	1.43	0.65	0.72
E104	H	NO <sub>2</sub>	NO <sub>2</sub>	N(CH <sub>3</sub> ) <sub>2</sub>	N(CH <sub>3</sub> ) <sub>2</sub>	-5.54	-5.50	-4.32	-4.21	1.22	1.29	0.61	0.65
E105	H	NO <sub>2</sub>	CN	NH <sub>2</sub>	NH <sub>2</sub>	-6.03	-5.90	-4.61	-4.32	1.42	1.58	0.71	0.79
E106	H	NO <sub>2</sub>	CN	NH <sub>2</sub>	NHCH <sub>3</sub>	-5.95	-5.88	-4.60	-4.33	1.35	1.55	0.68	0.78
E107	H	NO <sub>2</sub>	CN	NH <sub>2</sub>	N(CH <sub>3</sub> ) <sub>2</sub>	-5.63	-5.50	-4.53	-4.30	1.10	1.20	0.55	0.60
E108	H	NO <sub>2</sub>	CN	NHCH <sub>3</sub>	NH <sub>2</sub>	-5.85	-5.53	-4.62	-4.35	1.23	1.18	0.62	0.59
E109	H	NO <sub>2</sub>	CN	NHCH <sub>3</sub>	NHCH <sub>3</sub>	-5.80	-5.77	-4.52	-4.29	1.28	1.48	0.64	0.74
E110	H	NO <sub>2</sub>	CN	NHCH <sub>3</sub>	N(CH <sub>3</sub> ) <sub>2</sub>	-5.56	-5.49	-4.44	-4.25	1.12	1.24	0.56	0.62
E111	H	NO <sub>2</sub>	CN	N(CH <sub>3</sub> ) <sub>2</sub>	NH <sub>2</sub>	-5.76	-5.68	-4.37	-4.24	1.39	1.44	0.70	0.72
E112	H	NO <sub>2</sub>	CN	N(CH <sub>3</sub> ) <sub>2</sub>	NHCH <sub>3</sub>	-5.73	-5.69	-4.44	-4.24	1.29	1.45	0.65	0.73
E113	H	NO <sub>2</sub>	CN	N(CH <sub>3</sub> ) <sub>2</sub>	N(CH <sub>3</sub> ) <sub>2</sub>	-5.55	-5.49	-4.35	-4.21	1.20	1.28	0.60	0.64

**Table A.18b:** Softness,  $\sigma$ , electronegativity,  $\chi$ , chemical potential,  $\Phi$ , and electrophilicity index,  $\omega$ , values for DY 119 and its studied derivatives.

Dye No.	R1	R2	R3	R4	R5	$\sigma$ (eV <sup>-1</sup> )		$\chi$ (eV)		$\Phi$ (eV)		$\omega$ (eV)	
						Gas	Water	Gas	Water	Gas	Water	Gas	Water
DY 119	H	NO <sub>2</sub>	H	CH <sub>3</sub>	C <sub>2</sub> H <sub>5</sub>	1.06	1.10	5.31	5.13	-5.31	-5.13	15.00	14.46
EWS and EDS Substitution													
E30	NO <sub>2</sub>	NO <sub>2</sub>	H	NH <sub>2</sub>	C <sub>2</sub> H <sub>5</sub>	1.16	1.16	5.62	5.25	-5.62	-5.25	18.36	15.90
E31	NO <sub>2</sub>	NO <sub>2</sub>	H	NHCH <sub>3</sub>	C <sub>2</sub> H <sub>5</sub>	1.25	1.24	5.47	5.15	-5.47	-5.15	18.70	16.44
E32	NO <sub>2</sub>	NO <sub>2</sub>	H	N(CH <sub>3</sub> ) <sub>2</sub>	C <sub>2</sub> H <sub>5</sub>	1.32	2.08	5.37	4.82	-5.37	-4.82	19.06	24.20
E33	NO <sub>2</sub>	NO <sub>2</sub>	H	CH <sub>3</sub>	NH <sub>2</sub>	1.19	1.16	5.76	5.39	-5.76	-5.39	19.75	16.76
E34	NO <sub>2</sub>	NO <sub>2</sub>	H	CH <sub>3</sub>	NHCH <sub>3</sub>	1.31	1.23	5.65	5.33	-5.65	-5.33	20.83	17.40
E35	NO <sub>2</sub>	NO <sub>2</sub>	H	CH <sub>3</sub>	N(CH <sub>3</sub> ) <sub>2</sub>	1.79	1.75	5.35	5.04	-5.35	-5.04	25.56	22.28
E36	CN	NO <sub>2</sub>	H	NH <sub>2</sub>	C <sub>2</sub> H <sub>5</sub>	1.14	1.12	5.57	5.20	-5.57	-5.20	17.70	15.19
E37	CN	NO <sub>2</sub>	H	NHCH <sub>3</sub>	C <sub>2</sub> H <sub>5</sub>	1.23	1.20	5.40	5.10	-5.40	-5.10	18.00	15.54
E38	CN	NO <sub>2</sub>	H	N(CH <sub>3</sub> ) <sub>2</sub>	C <sub>2</sub> H <sub>5</sub>	1.27	1.32	5.29	5.01	-5.29	-5.01	17.79	16.51
E39	CN	NO <sub>2</sub>	H	CH <sub>3</sub>	NH <sub>2</sub>	1.16	1.12	5.70	5.33	-5.70	-5.33	18.89	15.96
E40	CN	NO <sub>2</sub>	H	CH <sub>3</sub>	NHCH <sub>3</sub>	1.29	1.18	5.58	5.28	-5.58	-5.28	20.05	16.46
E41	CN	NO <sub>2</sub>	H	CH <sub>3</sub>	N(CH <sub>3</sub> ) <sub>2</sub>	1.72	1.67	5.28	4.99	-5.28	-4.99	24.03	20.75
E42	NO <sub>2</sub>	NO <sub>2</sub>	H	NH <sub>2</sub>	CH <sub>3</sub>	1.16	1.15	5.67	5.25	-5.67	-5.25	18.55	15.84
E43	NO <sub>2</sub>	NO <sub>2</sub>	H	NHCH <sub>3</sub>	CH <sub>3</sub>	1.26	1.23	5.50	5.15	-5.50	-5.15	18.99	16.37
E44	NO <sub>2</sub>	NO <sub>2</sub>	H	N(CH <sub>3</sub> ) <sub>2</sub>	CH <sub>3</sub>	1.30	1.32	5.35	5.05	-5.35	-5.05	18.59	16.78
E45	NO <sub>2</sub>	NO <sub>2</sub>	H	C <sub>2</sub> H <sub>5</sub>	NH <sub>2</sub>	1.19	1.16	5.74	5.39	-5.74	-5.39	19.61	16.89
E46	NO <sub>2</sub>	NO <sub>2</sub>	H	C <sub>2</sub> H <sub>5</sub>	NHCH <sub>3</sub>	1.31	1.23	5.64	5.33	-5.64	-5.33	20.75	17.54
E47	NO <sub>2</sub>	NO <sub>2</sub>	H	C <sub>2</sub> H <sub>5</sub>	N(CH <sub>3</sub> ) <sub>2</sub>	1.77	1.77	5.34	5.04	-5.34	-5.04	25.19	22.43
E48	CN	NO <sub>2</sub>	H	NH <sub>2</sub>	CH <sub>3</sub>	1.14	1.14	5.59	5.19	-5.59	-5.19	17.75	15.30
E49	CN	NO <sub>2</sub>	H	NHCH <sub>3</sub>	CH <sub>3</sub>	1.23	1.20	5.43	5.11	-5.43	-5.11	18.20	15.61
E50	CN	NO <sub>2</sub>	H	N(CH <sub>3</sub> ) <sub>2</sub>	CH <sub>3</sub>	1.25	1.26	5.25	4.99	-5.25	-4.99	17.23	15.63
E51	CN	NO <sub>2</sub>	H	C <sub>2</sub> H <sub>5</sub>	NH <sub>2</sub>	1.16	1.12	5.68	5.34	-5.68	-5.34	18.76	15.90
E52	CN	NO <sub>2</sub>	H	C <sub>2</sub> H <sub>5</sub>	NHCH <sub>3</sub>	1.29	1.19	5.57	5.27	-5.57	-5.27	19.98	16.53
E53	CN	NO <sub>2</sub>	H	C <sub>2</sub> H <sub>5</sub>	N(CH <sub>3</sub> ) <sub>2</sub>	1.71	1.71	5.27	4.99	-5.27	-4.99	23.69	21.24
E54	NO <sub>2</sub>	NO <sub>2</sub>	H	NH <sub>2</sub>	NH <sub>2</sub>	1.34	1.30	5.60	5.17	-5.60	-5.17	21.01	17.36
E55	NO <sub>2</sub>	NO <sub>2</sub>	H	NH <sub>2</sub>	NHCH <sub>3</sub>	1.44	1.32	5.53	5.16	-5.53	-5.16	21.96	17.67
E56	NO <sub>2</sub>	NO <sub>2</sub>	H	NH <sub>2</sub>	N(CH <sub>3</sub> ) <sub>2</sub>	1.82	1.72	5.30	4.96	-5.30	-4.96	25.54	21.21
E57	NO <sub>2</sub>	NO <sub>2</sub>	H	NHCH <sub>3</sub>	NH <sub>2</sub>	1.41	1.37	5.45	5.09	-5.45	-5.09	20.92	17.75
E58	NO <sub>2</sub>	NO <sub>2</sub>	H	NHCH <sub>3</sub>	NHCH <sub>3</sub>	1.47	1.37	5.40	5.09	-5.40	-5.09	21.44	17.75
E59	NO <sub>2</sub>	NO <sub>2</sub>	H	NHCH <sub>3</sub>	N(CH <sub>3</sub> ) <sub>2</sub>	1.83	1.69	5.20	4.93	-5.20	-4.93	24.76	20.60
E60	NO <sub>2</sub>	NO <sub>2</sub>	H	N(CH <sub>3</sub> ) <sub>2</sub>	NH <sub>2</sub>	1.37	1.41	5.37	5.04	-5.37	-5.04	19.75	17.89
E61	NO <sub>2</sub>	NO <sub>2</sub>	H	N(CH <sub>3</sub> ) <sub>2</sub>	NHCH <sub>3</sub>	1.44	1.39	5.27	5.00	-5.27	-5.00	19.94	17.36
E62	NO <sub>2</sub>	NO <sub>2</sub>	H	N(CH <sub>3</sub> ) <sub>2</sub>	N(CH <sub>3</sub> ) <sub>2</sub>	1.71	1.67	5.15	4.91	-5.15	-4.91	22.62	20.09
E63	CN	NO <sub>2</sub>	H	NH <sub>2</sub>	NH <sub>2</sub>	1.31	1.26	5.53	5.14	-5.53	-5.14	19.95	16.58
E64	CN	NO <sub>2</sub>	H	NH <sub>2</sub>	NHCH <sub>3</sub>	1.38	1.29	5.47	5.11	-5.47	-5.11	20.60	16.81
E65	CN	NO <sub>2</sub>	H	NH <sub>2</sub>	N(CH <sub>3</sub> ) <sub>2</sub>	1.77	1.65	5.23	4.91	-5.23	-4.91	24.16	19.88
E66	CN	NO <sub>2</sub>	H	NHCH <sub>3</sub>	NH <sub>2</sub>	1.38	1.32	5.39	5.04	-5.39	-5.04	20.00	16.71
E67	CN	NO <sub>2</sub>	H	NHCH <sub>3</sub>	NHCH <sub>3</sub>	1.42	1.33	5.35	5.04	-5.35	-5.04	20.26	16.93
E68	CN	NO <sub>2</sub>	H	NHCH <sub>3</sub>	N(CH <sub>3</sub> ) <sub>2</sub>	1.77	1.63	5.14	4.88	-5.14	-4.88	23.33	19.32
E69	CN	NO <sub>2</sub>	H	N(CH <sub>3</sub> ) <sub>2</sub>	NH <sub>2</sub>	1.35	1.37	5.32	4.99	-5.32	-4.99	19.12	17.05
E70	CN	NO <sub>2</sub>	H	N(CH <sub>3</sub> ) <sub>2</sub>	NHCH <sub>3</sub>	1.41	1.35	5.21	4.95	-5.21	-4.95	19.12	16.56
E71	CN	NO <sub>2</sub>	H	N(CH <sub>3</sub> ) <sub>2</sub>	N(CH <sub>3</sub> ) <sub>2</sub>	1.64	1.56	5.06	4.87	-5.06	-4.87	20.99	18.53
E72	H	NO <sub>2</sub>	NO <sub>2</sub>	NH <sub>2</sub>	C <sub>2</sub> H <sub>5</sub>	1.20	1.13	5.40	5.22	-5.40	-5.22	17.43	15.37
E73	H	NO <sub>2</sub>	NO <sub>2</sub>	NHCH <sub>3</sub>	C <sub>2</sub> H <sub>5</sub>	1.33	1.22	5.23	5.12	-5.23	-5.12	18.24	15.98
E74	H	NO <sub>2</sub>	NO <sub>2</sub>	N(CH <sub>3</sub> ) <sub>2</sub>	C <sub>2</sub> H <sub>5</sub>	1.39	1.29	5.10	4.99	-5.10	-4.99	18.06	16.03
E75	H	NO <sub>2</sub>	NO <sub>2</sub>	CH <sub>3</sub>	NH <sub>2</sub>	1.16	1.11	5.54	5.34	-5.54	-5.34	17.84	15.84
E76	H	NO <sub>2</sub>	NO <sub>2</sub>	CH <sub>3</sub>	NHCH <sub>3</sub>	1.27	1.18	5.44	5.29	-5.44	-5.29	18.81	16.53
E77	H	NO <sub>2</sub>	NO <sub>2</sub>	CH <sub>3</sub>	N(CH <sub>3</sub> ) <sub>2</sub>	1.68	1.69	5.16	4.99	-5.16	-4.99	22.33	21.10

E78	H	NO <sub>2</sub>	CN	NH <sub>2</sub>	C <sub>2</sub> H <sub>5</sub>	1.25	1.14	5.35	5.17	-5.35	-5.17	17.89	15.36
E79	H	NO <sub>2</sub>	CN	NHCH <sub>3</sub>	C <sub>2</sub> H <sub>5</sub>	1.41	1.22	5.19	5.08	-5.19	-5.08	18.97	15.74
E80	H	NO <sub>2</sub>	CN	N(CH <sub>3</sub> ) <sub>2</sub>	C <sub>2</sub> H <sub>5</sub>	1.41	1.31	5.10	4.98	-5.10	-4.98	18.32	16.18
E81	H	NO <sub>2</sub>	CN	CH <sub>3</sub>	NH <sub>2</sub>	1.17	1.12	5.57	5.33	-5.57	-5.33	18.11	15.84
E82	H	NO <sub>2</sub>	CN	CH <sub>3</sub>	NHCH <sub>3</sub>	1.30	1.18	5.45	5.26	-5.45	-5.26	19.29	16.28
E83	H	NO <sub>2</sub>	CN	CH <sub>3</sub>	N(CH <sub>3</sub> ) <sub>2</sub>	1.67	1.64	5.12	4.96	-5.12	-4.96	21.85	20.17
E84	H	NO <sub>2</sub>	NO <sub>2</sub>	NH <sub>2</sub>	CH <sub>3</sub>	1.18	1.14	5.42	5.21	-5.42	-5.21	17.35	15.42
E85	H	NO <sub>2</sub>	NO <sub>2</sub>	NHCH <sub>3</sub>	CH <sub>3</sub>	1.31	1.20	5.25	5.12	-5.25	-5.12	17.98	15.79
E86	H	NO <sub>2</sub>	NO <sub>2</sub>	N(CH <sub>3</sub> ) <sub>2</sub>	CH <sub>3</sub>	1.41	1.32	5.15	5.02	-5.15	-5.02	18.68	16.66
E87	H	NO <sub>2</sub>	NO <sub>2</sub>	C <sub>2</sub> H <sub>5</sub>	NH <sub>2</sub>	1.16	1.11	5.53	5.34	-5.53	-5.34	17.78	15.84
E88	H	NO <sub>2</sub>	NO <sub>2</sub>	C <sub>2</sub> H <sub>5</sub>	NHCH <sub>3</sub>	1.27	1.18	5.43	5.28	-5.43	-5.28	18.75	16.46
E89	H	NO <sub>2</sub>	NO <sub>2</sub>	C <sub>2</sub> H <sub>5</sub>	N(CH <sub>3</sub> ) <sub>2</sub>	1.68	1.69	5.13	4.99	-5.13	-4.99	22.07	21.10
E90	H	NO <sub>2</sub>	CN	NH <sub>2</sub>	CH <sub>3</sub>	1.27	1.15	5.37	5.18	-5.37	-5.18	18.25	15.42
E91	H	NO <sub>2</sub>	CN	NHCH <sub>3</sub>	CH <sub>3</sub>	1.39	1.22	5.21	5.09	-5.21	-5.09	18.85	15.80
E92	H	NO <sub>2</sub>	CN	N(CH <sub>3</sub> ) <sub>2</sub>	CH <sub>3</sub>	1.42	1.31	5.13	4.99	-5.13	-4.99	18.63	16.24
E93	H	NO <sub>2</sub>	CN	C <sub>2</sub> H <sub>5</sub>	NH <sub>2</sub>	1.18	1.13	5.54	5.33	-5.54	-5.33	18.05	16.02
E94	H	NO <sub>2</sub>	CN	C <sub>2</sub> H <sub>5</sub>	NHCH <sub>3</sub>	1.27	1.18	5.45	5.28	-5.45	-5.28	18.88	16.46
E95	H	NO <sub>2</sub>	CN	C <sub>2</sub> H <sub>5</sub>	N(CH <sub>3</sub> ) <sub>2</sub>	1.75	1.69	5.12	4.97	-5.12	-4.97	23.00	20.93
E96	H	NO <sub>2</sub>	NO <sub>2</sub>	NH <sub>2</sub>	NH <sub>2</sub>	1.37	1.30	5.36	5.14	-5.36	-5.14	19.68	17.16
E97	H	NO <sub>2</sub>	NO <sub>2</sub>	NH <sub>2</sub>	NHCH <sub>3</sub>	1.41	1.29	5.33	5.15	-5.33	-5.15	20.01	17.08
E98	H	NO <sub>2</sub>	NO <sub>2</sub>	NH <sub>2</sub>	N(CH <sub>3</sub> ) <sub>2</sub>	1.79	1.72	5.10	4.92	-5.10	-4.92	23.22	20.87
E99	H	NO <sub>2</sub>	NO <sub>2</sub>	NHCH <sub>3</sub>	NH <sub>2</sub>	1.44	1.33	5.23	5.06	-5.23	-5.06	19.64	17.07
E100	H	NO <sub>2</sub>	NO <sub>2</sub>	NHCH <sub>3</sub>	NHCH <sub>3</sub>	1.52	1.33	5.17	5.07	-5.17	-5.07	20.25	17.14
E101	H	NO <sub>2</sub>	NO <sub>2</sub>	NHCH <sub>3</sub>	N(CH <sub>3</sub> ) <sub>2</sub>	1.77	1.65	5.02	4.90	-5.02	-4.90	22.26	19.80
E102	H	NO <sub>2</sub>	NO <sub>2</sub>	N(CH <sub>3</sub> ) <sub>2</sub>	NH <sub>2</sub>	1.47	1.41	5.15	4.99	-5.15	-4.99	19.50	17.54
E103	H	NO <sub>2</sub>	NO <sub>2</sub>	N(CH <sub>3</sub> ) <sub>2</sub>	NHCH <sub>3</sub>	1.54	1.40	5.11	5.01	-5.11	-5.01	20.09	17.52
E104	H	NO <sub>2</sub>	NO <sub>2</sub>	N(CH <sub>3</sub> ) <sub>2</sub>	N(CH <sub>3</sub> ) <sub>2</sub>	1.64	1.55	4.93	4.86	-4.93	-4.86	19.92	18.27
E105	H	NO <sub>2</sub>	CN	NH <sub>2</sub>	NH <sub>2</sub>	1.41	1.27	5.32	5.11	-5.32	-5.11	19.93	16.53
E106	H	NO <sub>2</sub>	CN	NH <sub>2</sub>	NHCH <sub>3</sub>	1.48	1.29	5.28	5.11	-5.28	-5.11	20.61	16.81
E107	H	NO <sub>2</sub>	CN	NH <sub>2</sub>	N(CH <sub>3</sub> ) <sub>2</sub>	1.82	1.67	5.08	4.90	-5.08	-4.90	23.46	20.01
E108	H	NO <sub>2</sub>	CN	NHCH <sub>3</sub>	NH <sub>2</sub>	1.63	1.69	5.24	4.94	-5.24	-4.94	22.28	20.68
E109	H	NO <sub>2</sub>	CN	NHCH <sub>3</sub>	NHCH <sub>3</sub>	1.56	1.35	5.16	5.03	-5.16	-5.03	20.80	17.10
E110	H	NO <sub>2</sub>	CN	NHCH <sub>3</sub>	N(CH <sub>3</sub> ) <sub>2</sub>	1.79	1.61	5.00	4.87	-5.00	-4.87	22.32	19.13
E111	H	NO <sub>2</sub>	CN	N(CH <sub>3</sub> ) <sub>2</sub>	NH <sub>2</sub>	1.44	1.39	5.07	4.96	-5.07	-4.96	18.46	17.08
E112	H	NO <sub>2</sub>	CN	N(CH <sub>3</sub> ) <sub>2</sub>	NHCH <sub>3</sub>	1.55	1.38	5.09	4.97	-5.09	-4.97	20.04	17.00
E113	H	NO <sub>2</sub>	CN	N(CH <sub>3</sub> ) <sub>2</sub>	N(CH <sub>3</sub> ) <sub>2</sub>	1.67	1.56	4.95	4.85	-4.95	-4.85	20.42	18.38

**Table A. 19:** Radical attack Fukui functions,  $f^0$  for the most active sites in DY 119 and its studied derivatives.

Dye No.	R1	R2	R3	R4	R5	$f^0$			
						C4	N7	N8	C9
DY 119	H	NO <sub>2</sub>	H	CH <sub>3</sub>	C <sub>2</sub> H <sub>5</sub>	0.021	0.022	0.038	0.045
EWS and EDS Substitution									
E30	NO <sub>2</sub>	NO <sub>2</sub>	H	NH <sub>2</sub>	C <sub>2</sub> H <sub>5</sub>	0.021	0.010	0.035	0.030
E31	NO <sub>2</sub>	NO <sub>2</sub>	H	NHCH <sub>3</sub>	C <sub>2</sub> H <sub>5</sub>	0.021	0.005	0.029	0.025
E32	NO <sub>2</sub>	NO <sub>2</sub>	H	N(CH <sub>3</sub> ) <sub>2</sub>	C <sub>2</sub> H <sub>5</sub>	0.020	0.004	0.031	0.024
E33	NO <sub>2</sub>	NO <sub>2</sub>	H	CH <sub>3</sub>	NH <sub>2</sub>	0.018	0.011	0.041	0.025
E34	NO <sub>2</sub>	NO <sub>2</sub>	H	CH <sub>3</sub>	NHCH <sub>3</sub>	0.018	0.008	0.041	0.022
E35	NO <sub>2</sub>	NO <sub>2</sub>	H	CH <sub>3</sub>	N(CH <sub>3</sub> ) <sub>2</sub>	0.018	0.004	0.039	0.018
E36	CN	NO <sub>2</sub>	H	NH <sub>2</sub>	C <sub>2</sub> H <sub>5</sub>	0.020	0.012	0.034	0.032
E37	CN	NO <sub>2</sub>	H	NHCH <sub>3</sub>	C <sub>2</sub> H <sub>5</sub>	0.019	0.007	0.030	0.026
E38	CN	NO <sub>2</sub>	H	N(CH <sub>3</sub> ) <sub>2</sub>	C <sub>2</sub> H <sub>5</sub>	0.019	0.006	0.031	0.025
E39	CN	NO <sub>2</sub>	H	CH <sub>3</sub>	NH <sub>2</sub>	0.017	0.014	0.041	0.028
E40	CN	NO <sub>2</sub>	H	CH <sub>3</sub>	NHCH <sub>3</sub>	0.017	0.010	0.040	0.023
E41	CN	NO <sub>2</sub>	H	CH <sub>3</sub>	N(CH <sub>3</sub> ) <sub>2</sub>	0.016	0.005	0.040	0.018
E42	NO <sub>2</sub>	NO <sub>2</sub>	H	NH <sub>2</sub>	CH <sub>3</sub>	0.021	0.010	0.037	0.031
E43	NO <sub>2</sub>	NO <sub>2</sub>	H	NHCH <sub>3</sub>	CH <sub>3</sub>	0.021	0.005	0.030	0.025
E44	NO <sub>2</sub>	NO <sub>2</sub>	H	N(CH <sub>3</sub> ) <sub>2</sub>	CH <sub>3</sub>	0.021	0.004	0.031	0.024

E45	NO <sub>2</sub>	NO <sub>2</sub>	H	C <sub>2</sub> H <sub>5</sub>	NH <sub>2</sub>	0.018	0.011	0.041	0.024
E46	NO <sub>2</sub>	NO <sub>2</sub>	H	C <sub>2</sub> H <sub>5</sub>	NHCH <sub>3</sub>	0.018	0.008	0.041	0.022
E47	NO <sub>2</sub>	NO <sub>2</sub>	H	C <sub>2</sub> H <sub>5</sub>	N(CH <sub>3</sub> ) <sub>2</sub>	0.019	0.003	0.039	0.018
E48	CN	NO <sub>2</sub>	H	NH <sub>2</sub>	CH <sub>3</sub>	0.020	0.013	0.035	0.033
E49	CN	NO <sub>2</sub>	H	NHCH <sub>3</sub>	CH <sub>3</sub>	0.019	0.007	0.030	0.026
E50	CN	NO <sub>2</sub>	H	N(CH <sub>3</sub> ) <sub>2</sub>	CH <sub>3</sub>	0.020	0.006	0.031	0.024
E51	CN	NO <sub>2</sub>	H	C <sub>2</sub> H <sub>5</sub>	NH <sub>2</sub>	0.017	0.014	0.041	0.028
E52	CN	NO <sub>2</sub>	H	C <sub>2</sub> H <sub>5</sub>	NHCH <sub>3</sub>	0.017	0.010	0.040	0.023
E53	CN	NO <sub>2</sub>	H	C <sub>2</sub> H <sub>5</sub>	N(CH <sub>3</sub> ) <sub>2</sub>	0.016	0.005	0.040	0.018
E54	NO <sub>2</sub>	NO <sub>2</sub>	H	NH <sub>2</sub>	NH <sub>2</sub>	0.018	0.005	0.037	0.021
E55	NO <sub>2</sub>	NO <sub>2</sub>	H	NH <sub>2</sub>	NHCH <sub>3</sub>	0.019	0.004	0.036	0.021
E56	NO <sub>2</sub>	NO <sub>2</sub>	H	NH <sub>2</sub>	N(CH <sub>3</sub> ) <sub>2</sub>	0.021	0.001	0.036	0.025
E57	NO <sub>2</sub>	NO <sub>2</sub>	H	NHCH <sub>3</sub>	NH <sub>2</sub>	0.019	0.003	0.032	0.021
E58	NO <sub>2</sub>	NO <sub>2</sub>	H	NHCH <sub>3</sub>	NHCH <sub>3</sub>	0.020	0.002	0.031	0.021
E59	NO <sub>2</sub>	NO <sub>2</sub>	H	NHCH <sub>3</sub>	N(CH <sub>3</sub> ) <sub>2</sub>	0.022	-0.000	0.031	0.026
E60	NO <sub>2</sub>	NO <sub>2</sub>	H	N(CH <sub>3</sub> ) <sub>2</sub>	NH <sub>2</sub>	0.019	0.003	0.033	0.020
E61	NO <sub>2</sub>	NO <sub>2</sub>	H	N(CH <sub>3</sub> ) <sub>2</sub>	NHCH <sub>3</sub>	0.021	0.001	0.030	0.019
E62	NO <sub>2</sub>	NO <sub>2</sub>	H	N(CH <sub>3</sub> ) <sub>2</sub>	N(CH <sub>3</sub> ) <sub>2</sub>	0.021	0.000	0.032	0.022
E63	CN	NO <sub>2</sub>	H	NH <sub>2</sub>	NH <sub>2</sub>	0.017	0.007	0.038	0.021
E64	CN	NO <sub>2</sub>	H	NH <sub>2</sub>	NHCH <sub>3</sub>	0.017	0.006	0.036	0.021
E65	CN	NO <sub>2</sub>	H	NH <sub>2</sub>	N(CH <sub>3</sub> ) <sub>2</sub>	0.019	0.003	0.036	0.024
E66	CN	NO <sub>2</sub>	H	NHCH <sub>3</sub>	NH <sub>2</sub>	0.017	0.005	0.032	0.021
E67	CN	NO <sub>2</sub>	H	NHCH <sub>3</sub>	NHCH <sub>3</sub>	0.018	0.004	0.032	0.021
E68	CN	NO <sub>2</sub>	H	NHCH <sub>3</sub>	N(CH <sub>3</sub> ) <sub>2</sub>	0.020	0.001	0.032	0.024
E69	CN	NO <sub>2</sub>	H	N(CH <sub>3</sub> ) <sub>2</sub>	NH <sub>2</sub>	0.017	0.005	0.033	0.021
E70	CN	NO <sub>2</sub>	H	N(CH <sub>3</sub> ) <sub>2</sub>	NHCH <sub>3</sub>	0.019	0.003	0.030	0.020
E71	CN	NO <sub>2</sub>	H	N(CH <sub>3</sub> ) <sub>2</sub>	N(CH <sub>3</sub> ) <sub>2</sub>	0.019	0.001	0.031	0.021
E72	H	NO <sub>2</sub>	NO <sub>2</sub>	NH <sub>2</sub>	C <sub>2</sub> H <sub>5</sub>	0.020	0.008	0.022	0.024
E73	H	NO <sub>2</sub>	NO <sub>2</sub>	NHCH <sub>3</sub>	C <sub>2</sub> H <sub>5</sub>	0.019	0.004	0.016	0.020
E74	H	NO <sub>2</sub>	NO <sub>2</sub>	N(CH <sub>3</sub> ) <sub>2</sub>	C <sub>2</sub> H <sub>5</sub>	0.020	0.003	0.018	0.018
E75	H	NO <sub>2</sub>	NO <sub>2</sub>	CH <sub>3</sub>	NH <sub>2</sub>	0.018	0.011	0.034	0.025
E76	H	NO <sub>2</sub>	NO <sub>2</sub>	CH <sub>3</sub>	NHCH <sub>3</sub>	0.018	0.008	0.033	0.021
E77	H	NO <sub>2</sub>	NO <sub>2</sub>	CH <sub>3</sub>	N(CH <sub>3</sub> ) <sub>2</sub>	0.018	0.003	0.031	0.016
E78	H	NO <sub>2</sub>	CN	NH <sub>2</sub>	C <sub>2</sub> H <sub>5</sub>	0.020	0.007	0.029	0.025
E79	H	NO <sub>2</sub>	CN	NHCH <sub>3</sub>	C <sub>2</sub> H <sub>5</sub>	0.021	0.003	0.023	0.022
E80	H	NO <sub>2</sub>	CN	N(CH <sub>3</sub> ) <sub>2</sub>	C <sub>2</sub> H <sub>5</sub>	0.019	0.003	0.022	0.021
E81	H	NO <sub>2</sub>	CN	CH <sub>3</sub>	NH <sub>2</sub>	0.018	0.012	0.039	0.027
E82	H	NO <sub>2</sub>	CN	CH <sub>3</sub>	NHCH <sub>3</sub>	0.018	0.009	0.037	0.023
E83	H	NO <sub>2</sub>	CN	CH <sub>3</sub>	N(CH <sub>3</sub> ) <sub>2</sub>	0.016	0.004	0.035	0.018
E84	H	NO <sub>2</sub>	NO <sub>2</sub>	NH <sub>2</sub>	CH <sub>3</sub>	0.019	0.008	0.023	0.024
E85	H	NO <sub>2</sub>	NO <sub>2</sub>	NHCH <sub>3</sub>	CH <sub>3</sub>	0.019	0.003	0.016	0.019
E86	H	NO <sub>2</sub>	NO <sub>2</sub>	N(CH <sub>3</sub> ) <sub>2</sub>	CH <sub>3</sub>	0.020	0.002	0.017	0.019
E87	H	NO <sub>2</sub>	NO <sub>2</sub>	C <sub>2</sub> H <sub>5</sub>	NH <sub>2</sub>	0.018	0.010	0.033	0.024
E88	H	NO <sub>2</sub>	NO <sub>2</sub>	C <sub>2</sub> H <sub>5</sub>	NHCH <sub>3</sub>	0.018	0.007	0.032	0.021
E89	H	NO <sub>2</sub>	NO <sub>2</sub>	C <sub>2</sub> H <sub>5</sub>	N(CH <sub>3</sub> ) <sub>2</sub>	0.019	0.002	0.028	0.015
E90	H	NO <sub>2</sub>	CN	NH <sub>2</sub>	CH <sub>3</sub>	0.021	0.007	0.029	0.025
E91	H	NO <sub>2</sub>	CN	NHCH <sub>3</sub>	CH <sub>3</sub>	0.020	0.004	0.024	0.022
E92	H	NO <sub>2</sub>	CN	N(CH <sub>3</sub> ) <sub>2</sub>	CH <sub>3</sub>	0.019	0.003	0.022	0.021
E93	H	NO <sub>2</sub>	CN	C <sub>2</sub> H <sub>5</sub>	NH <sub>2</sub>	0.018	0.012	0.039	0.026
E94	H	NO <sub>2</sub>	CN	C <sub>2</sub> H <sub>5</sub>	NHCH <sub>3</sub>	0.018	0.009	0.037	0.024
E95	H	NO <sub>2</sub>	CN	C <sub>2</sub> H <sub>5</sub>	N(CH <sub>3</sub> ) <sub>2</sub>	0.018	0.004	0.036	0.019
E96	H	NO <sub>2</sub>	NO <sub>2</sub>	NH <sub>2</sub>	NH <sub>2</sub>	0.018	0.004	0.024	0.017
E97	H	NO <sub>2</sub>	NO <sub>2</sub>	NH <sub>2</sub>	NHCH <sub>3</sub>	0.019	0.003	0.024	0.018
E98	H	NO <sub>2</sub>	NO <sub>2</sub>	NH <sub>2</sub>	N(CH <sub>3</sub> ) <sub>2</sub>	0.020	0.001	0.022	0.021
E99	H	NO <sub>2</sub>	NO <sub>2</sub>	NHCH <sub>3</sub>	NH <sub>2</sub>	0.019	0.002	0.019	0.017
E100	H	NO <sub>2</sub>	NO <sub>2</sub>	NHCH <sub>3</sub>	NHCH <sub>3</sub>	0.019	0.001	0.017	0.016
E101	H	NO <sub>2</sub>	NO <sub>2</sub>	NHCH <sub>3</sub>	N(CH <sub>3</sub> ) <sub>2</sub>	0.020	0.000	0.018	0.020
E102	H	NO <sub>2</sub>	NO <sub>2</sub>	N(CH <sub>3</sub> ) <sub>2</sub>	NH <sub>2</sub>	0.019	0.002	0.020	0.017

E103	H	NO <sub>2</sub>	NO <sub>2</sub>	N(CH <sub>3</sub> ) <sub>2</sub>	NHCH <sub>3</sub>	0.020	0.001	0.020	0.017
E104	H	NO <sub>2</sub>	NO <sub>2</sub>	N(CH <sub>3</sub> ) <sub>2</sub>	N(CH <sub>3</sub> ) <sub>2</sub>	0.020	-0.001	0.018	0.017
E105	H	NO <sub>2</sub>	CN	NH <sub>2</sub>	NH <sub>2</sub>	0.019	0.004	0.030	0.020
E106	H	NO <sub>2</sub>	CN	NH <sub>2</sub>	NHCH <sub>3</sub>	0.019	0.003	0.029	0.020
E107	H	NO <sub>2</sub>	CN	NH <sub>2</sub>	N(CH <sub>3</sub> ) <sub>2</sub>	0.021	0.001	0.028	0.024
E108	H	NO <sub>2</sub>	CN	NHCH <sub>3</sub>	NH <sub>2</sub>	0.014	0.004	0.007	0.008
E109	H	NO <sub>2</sub>	CN	NHCH <sub>3</sub>	NHCH <sub>3</sub>	0.020	0.002	0.025	0.020
E110	H	NO <sub>2</sub>	CN	NHCH <sub>3</sub>	N(CH <sub>3</sub> ) <sub>2</sub>	0.021	0.000	0.024	0.023
E111	H	NO <sub>2</sub>	CN	N(CH <sub>3</sub> ) <sub>2</sub>	NH <sub>2</sub>	0.019	0.002	0.023	0.017
E112	H	NO <sub>2</sub>	CN	N(CH <sub>3</sub> ) <sub>2</sub>	NHCH <sub>3</sub>	0.018	0.001	0.023	0.019
E113	H	NO <sub>2</sub>	CN	N(CH <sub>3</sub> ) <sub>2</sub>	N(CH <sub>3</sub> ) <sub>2</sub>	0.019	0.000	0.025	0.020

**Table A. 20:** Calculated energy gaps between the frontier molecular orbitals (i.e. HOMO and LUMO) of the studied dyes and the band edges (CBE and VBE) of the catalysts.

Dye No.	$\alpha_{Si}$ (eV)	$\beta_{Si}$ (eV)	$\alpha_{CdSe}$ (eV)	$\beta_{CdSe}$ (eV)	$\alpha_{CdS}$ (eV)	$\beta_{CdS}$ (eV)	$\alpha_{TiO_2}$ (eV)	$\beta_{TiO_2}$ (eV)	$\alpha_{ZnO}$ (eV)	$\beta_{ZnO}$ (eV)	$\alpha_{ZnS}$ (eV)	$\beta_{ZnS}$ (eV)
DY 119	0.67	2.01	0.45	3.01	1.48	2.76	3.43	1.23	-0.17	5.26	0.90	4.62
EWS and EDS Substitution												
E30	0.28	2.24	0.06	3.24	1.09	2.99	3.04	1.46	-0.56	5.49	0.53	4.85
E31	0.37	2.03	0.15	3.03	1.18	2.78	3.13	1.25	-0.47	5.28	0.62	4.64
E32	0.43	1.88	0.21	2.88	1.24	2.63	3.19	1.10	-0.41	5.13	0.68	4.49
E33	0.12	2.36	-0.10	3.36	0.93	3.11	2.88	1.58	-0.72	5.61	0.37	4.97
E34	0.16	2.17	-0.06	3.17	0.97	2.92	2.92	1.39	-0.68	5.42	0.41	4.78
E35	0.25	1.67	0.03	2.67	1.06	2.42	3.01	0.89	-0.59	4.92	0.50	4.28
E36	0.35	2.20	0.13	3.20	1.16	2.95	3.11	1.42	-0.49	5.45	0.60	4.81
E37	0.45	1.97	0.23	2.97	1.26	2.72	3.21	1.19	-0.39	5.22	0.70	4.58
E38	0.54	1.83	0.32	2.83	1.35	2.58	3.30	1.05	-0.30	5.08	0.79	4.44
E39	0.20	2.32	-0.02	3.32	1.01	3.07	2.96	1.54	-0.64	5.57	0.45	4.93
E40	0.24	2.11	0.02	3.11	1.05	2.86	3.00	1.33	-0.60	5.36	0.49	4.72
E41	0.34	1.62	0.12	2.62	1.15	2.37	3.10	0.84	-0.50	4.87	0.59	4.23
E42	0.24	2.29	0.02	3.29	1.05	3.04	3.00	1.51	-0.60	5.54	0.49	4.90
E43	0.34	2.05	0.12	3.05	1.15	2.80	3.10	1.27	-0.50	5.30	0.59	4.66
E44	0.46	1.88	0.24	2.88	1.27	2.63	3.22	1.10	-0.38	5.13	0.71	4.49
E45	0.14	2.34	-0.08	3.34	0.95	3.09	2.90	1.56	-0.70	5.59	0.39	4.95
E46	0.17	2.16	-0.05	3.16	0.98	2.91	2.93	1.38	-0.67	5.41	0.42	4.77
E47	0.27	1.66	0.05	2.66	1.08	2.41	3.03	0.88	-0.57	4.91	0.52	4.27
E48	0.33	2.23	0.11	3.23	1.14	2.98	3.09	1.45	-0.51	5.48	0.58	4.84
E49	0.42	2.00	0.20	3.00	1.23	2.75	3.18	1.22	-0.42	5.25	0.67	4.61
E50	0.59	1.81	0.37	2.81	1.40	2.56	3.35	1.03	-0.25	5.06	0.84	4.42
E51	0.22	2.30	0.00	3.30	1.03	3.05	2.98	1.52	-0.62	5.55	0.47	4.91
E52	0.25	2.10	0.03	3.10	1.06	2.85	3.01	1.32	-0.59	5.35	0.50	4.71
E53	0.36	1.61	0.14	2.61	1.17	2.36	3.12	0.83	-0.48	4.86	0.61	4.22
E54	0.19	2.10	-0.03	3.10	1.00	2.85	2.95	1.32	-0.65	5.35	0.44	4.71
E55	0.21	1.98	-0.01	2.98	1.02	2.73	2.97	1.20	-0.63	5.23	0.46	4.59
E56	0.29	1.61	0.07	2.61	1.10	2.36	3.05	0.83	-0.55	4.86	0.54	4.22
E57	0.30	1.92	0.08	2.92	1.11	2.67	3.06	1.14	-0.54	5.17	0.55	4.53
E58	0.32	1.84	0.10	2.84	1.13	2.59	3.08	1.06	-0.52	5.09	0.57	4.45
E59	0.39	1.50	0.17	2.50	1.20	2.25	3.15	0.72	-0.45	4.75	0.64	4.11
E60	0.40	1.86	0.18	2.86	1.21	2.61	3.16	1.08	-0.44	5.11	0.65	4.47
E61	0.47	1.72	0.25	2.72	1.28	2.47	3.23	0.94	-0.37	4.97	0.72	4.33
E62	0.48	1.49	0.26	2.49	1.29	2.24	3.24	0.71	-0.36	4.74	0.73	4.10
E63	0.28	2.05	0.06	3.05	1.09	2.80	3.04	1.27	-0.56	5.30	0.53	4.66
E64	0.30	1.95	0.08	2.95	1.11	2.70	3.06	1.17	-0.54	5.20	0.55	4.56
E65	0.38	1.55	0.16	2.55	1.19	2.30	3.14	0.77	-0.46	4.80	0.63	4.16
E66	0.38	1.87	0.16	2.87	1.19	2.62	3.14	1.09	-0.46	5.12	0.63	4.48
E67	0.40	1.81	0.18	2.81	1.21	2.56	3.16	1.03	-0.44	5.06	0.65	4.42

E68	0.47	1.46	0.25	2.46	1.28	2.21	3.23	0.68	-0.37	4.71	0.72	4.07
E69	0.46	1.82	0.24	2.82	1.27	2.57	3.22	1.04	-0.38	5.07	0.71	4.43
E70	0.54	1.68	0.32	2.68	1.35	2.43	3.30	0.90	-0.30	4.93	0.79	4.29
E71	0.59	1.43	0.37	2.43	1.40	2.18	3.35	0.65	-0.25	4.68	0.84	4.04
E72	0.48	1.99	0.26	2.99	1.29	2.74	3.24	1.21	-0.36	5.24	0.73	4.60
E73	0.56	1.74	0.34	2.74	1.37	2.49	3.32	0.96	-0.28	4.99	0.81	4.35
E74	0.66	1.58	0.44	2.58	1.47	2.33	3.42	0.80	-0.18	4.83	0.91	4.19
E75	0.36	2.16	0.14	3.16	1.17	2.91	3.12	1.38	-0.48	5.41	0.61	4.77
E76	0.39	1.98	0.17	2.98	1.20	2.73	3.15	1.20	-0.45	5.23	0.64	4.59
E77	0.48	1.51	0.26	2.51	1.29	2.26	3.24	0.73	-0.36	4.76	0.73	4.12
E78	0.49	1.91	0.27	2.91	1.30	2.66	3.25	1.13	-0.35	5.16	0.74	4.52
E79	0.56	1.66	0.34	2.66	1.37	2.41	3.32	0.88	-0.28	4.91	0.81	4.27
E80	0.65	1.57	0.43	2.57	1.46	2.32	3.41	0.79	-0.19	4.82	0.90	4.18
E81	0.33	2.18	0.11	3.18	1.14	2.93	3.09	1.40	-0.51	5.43	0.58	4.79
E82	0.36	1.98	0.14	2.98	1.17	2.73	3.12	1.20	-0.48	5.23	0.61	4.59
E83	0.52	1.48	0.30	2.48	1.33	2.23	3.28	0.70	-0.32	4.73	0.77	4.09
E84	0.47	2.02	0.25	3.02	1.28	2.77	3.23	1.24	-0.37	5.27	0.72	4.63
E85	0.56	1.77	0.34	2.77	1.37	2.52	3.32	0.99	-0.28	5.02	0.81	4.38
E86	0.60	1.62	0.38	2.62	1.41	2.37	3.36	0.84	-0.24	4.87	0.85	4.23
E87	0.37	2.15	0.15	3.15	1.18	2.90	3.13	1.37	-0.47	5.40	0.62	4.76
E88	0.40	1.97	0.18	2.97	1.21	2.72	3.16	1.19	-0.44	5.22	0.65	4.58
E89	0.51	1.48	0.29	2.48	1.32	2.23	3.27	0.70	-0.33	4.73	0.76	4.09
E90	0.46	1.92	0.24	2.92	1.27	2.67	3.22	1.14	-0.38	5.17	0.71	4.53
E91	0.55	1.69	0.33	2.69	1.36	2.44	3.31	0.91	-0.29	4.94	0.80	4.30
E92	0.62	1.59	0.40	2.59	1.43	2.34	3.38	0.81	-0.22	4.84	0.87	4.20
E93	0.35	2.15	0.13	3.15	1.16	2.90	3.11	1.37	-0.49	5.40	0.60	4.76
E94	0.38	1.99	0.16	2.99	1.19	2.74	3.14	1.21	-0.46	5.24	0.63	4.60
E95	0.49	1.45	0.27	2.45	1.30	2.20	3.25	0.67	-0.35	4.70	0.74	4.06
E96	0.41	1.85	0.19	2.85	1.22	2.60	3.17	1.07	-0.43	5.10	0.66	4.46
E97	0.42	1.80	0.20	2.80	1.23	2.55	3.18	1.02	-0.42	5.05	0.67	4.41
E98	0.50	1.42	0.28	2.42	1.31	2.17	3.26	0.64	-0.34	4.67	0.75	4.03
E99	0.51	1.68	0.29	2.68	1.32	2.43	3.27	0.90	-0.33	4.93	0.76	4.29
E100	0.53	1.59	0.31	2.59	1.34	2.34	3.29	0.81	-0.31	4.84	0.78	4.20
E101	0.59	1.34	0.37	2.34	1.40	2.09	3.35	0.56	-0.25	4.59	0.84	3.95
E102	0.57	1.59	0.35	2.59	1.38	2.34	3.33	0.81	-0.27	4.84	0.82	4.20
E103	0.58	1.52	0.36	2.52	1.39	2.27	3.34	0.74	-0.26	4.77	0.83	4.13
E104	0.72	1.30	0.50	2.30	1.53	2.05	3.48	0.52	-0.12	4.55	0.97	3.91
E105	0.43	1.79	0.21	2.79	1.24	2.54	3.19	1.01	-0.41	5.04	0.68	4.40
E106	0.44	1.71	0.22	2.71	1.25	2.46	3.20	0.93	-0.40	4.96	0.69	4.32
E107	0.51	1.39	0.29	2.39	1.32	2.14	3.27	0.61	-0.33	4.64	0.76	4.00
E108	0.42	1.61	0.20	2.61	1.23	2.36	3.18	0.83	-0.42	4.86	0.67	4.22
E109	0.52	1.56	0.30	2.56	1.33	2.31	3.28	0.78	-0.32	4.81	0.77	4.17
E110	0.60	1.32	0.38	2.32	1.41	2.07	3.36	0.54	-0.24	4.57	0.85	3.93
E111	0.67	1.52	0.45	2.52	1.48	2.27	3.43	0.74	-0.17	4.77	0.92	4.13
E112	0.60	1.49	0.38	2.49	1.41	2.24	3.36	0.71	-0.24	4.74	0.85	4.10
E113	0.69	1.31	0.47	2.31	1.50	2.06	3.45	0.53	-0.15	4.56	0.94	3.92

**Table A. 21:** Softness ( $\sigma$ ), electronegativity ( $\chi$ ), chemical potential ( $\Phi$ ) and electrophilicity ( $\omega$ ) of DR 73 and its studied derivatives.

Dyes	R <sub>3</sub>	R <sub>4</sub>	R <sub>5</sub>	R <sub>6</sub>	R <sub>7</sub>	$\sigma$ (eV <sup>-1</sup> )		$\chi$ (eV)		$\Phi$ (eV)		$\omega$ (eV)	
						Gas	Water	Gas	Water	Gas	Water	Gas	Water
DR 73	H	H	H	CN	H	1.22	1.49	4.98	4.77	-4.98	-4.77	15.12	16.98
X <sup>-</sup> Substitution													
F1	NO <sub>2</sub>	H	H	CN	H	1.25	1.49	5.20	4.94	-5.20	-4.94	16.90	18.21
F2	CN	H	H	CN	H	1.32	1.52	5.21	4.93	-5.21	-4.93	17.86	18.41
F3	H	H	H	CN	CN	1.20	1.43	5.20	4.86	-5.20	-4.86	16.29	16.87
F4	NO <sub>2</sub>	H	H	CN	CN	1.22	1.43	5.42	5.04	-5.42	-5.04	17.91	18.14
F5	CN	H	H	CN	CN	1.32	1.45	5.41	5.03	-5.41	-5.03	19.26	18.33
X <sup>+</sup> Substitution													
F6	H	NH <sub>2</sub>	H	CN	H	1.25	1.45	4.85	4.66	-4.85	-4.66	14.70	15.74
F7	H	NHCH <sub>3</sub>	H	CN	H	1.33	1.52	4.72	4.57	-4.72	-4.57	14.85	15.82
F8	H	N(CH <sub>3</sub> ) <sub>2</sub>	H	CN	H	1.30	1.49	4.65	4.54	-4.65	-4.54	14.04	15.38
F9	H	H	NH <sub>2</sub>	CN	H	1.33	1.79	5.01	4.70	-5.01	-4.70	16.73	19.72
F10	H	H	NHCH <sub>3</sub>	CN	H	1.49	1.96	4.90	4.64	-4.90	-4.64	17.92	21.11
F11	H	H	N(CH <sub>3</sub> ) <sub>2</sub>	CN	H	1.45	1.92	4.83	4.59	-4.83	-4.59	16.91	20.26
F12	H	NH <sub>2</sub>	H	CN	CN	1.25	1.45	5.00	4.68	-5.00	-4.68	15.63	15.87
F13	H	NHCH <sub>3</sub>	H	CN	CN	1.32	1.52	4.93	4.64	-4.93	-4.64	15.99	16.31
F14	H	N(CH <sub>3</sub> ) <sub>2</sub>	H	CN	CN	1.25	1.49	4.85	4.60	-4.85	-4.60	14.70	15.79
F15	H	H	NH <sub>2</sub>	CN	CN	1.28	1.64	5.20	4.78	-5.20	-4.78	17.33	18.73
F16	H	H	NHCH <sub>3</sub>	CN	CN	1.45	1.96	5.13	4.69	-5.13	-4.69	19.07	21.56
F17	H	H	N(CH <sub>3</sub> ) <sub>2</sub>	CN	CN	1.43	1.92	5.07	4.67	-5.07	-4.67	18.36	20.97
X <sup>-</sup> versus X <sup>+</sup> Substitution													
F18	NO <sub>2</sub>	NH <sub>2</sub>	H	CN	H	1.30	1.45	5.05	4.84	-5.05	-4.84	16.56	16.98
F19	NO <sub>2</sub>	NHCH <sub>3</sub>	H	CN	H	1.37	1.47	4.93	4.78	-4.93	-4.78	16.65	16.80
F20	NO <sub>2</sub>	N(CH <sub>3</sub> ) <sub>2</sub>	H	CN	H	1.35	1.52	4.86	4.68	-4.86	-4.68	15.96	16.59
F21	NO <sub>2</sub>	H	NH <sub>2</sub>	CN	H	1.43	1.89	5.18	4.84	-5.18	-4.84	19.17	22.10
F22	NO <sub>2</sub>	H	NHCH <sub>3</sub>	CN	H	1.61	2.08	5.00	4.75	-5.00	-4.75	20.16	23.50
F23	NO <sub>2</sub>	H	N(CH <sub>3</sub> ) <sub>2</sub>	CN	H	1.56	2.04	5.02	4.74	-5.02	-4.74	19.69	22.93
F24	NO <sub>2</sub>	NH <sub>2</sub>	H	CN	CN	1.27	1.43	5.27	4.90	-5.27	-4.90	17.58	17.15
F25	NO <sub>2</sub>	NHCH <sub>3</sub>	H	CN	CN	1.35	1.52	5.13	4.83	-5.13	-4.83	17.78	17.67
F26	NO <sub>2</sub>	N(CH <sub>3</sub> ) <sub>2</sub>	H	CN	CN	1.35	1.49	5.01	4.74	-5.01	-4.74	16.96	16.77
F27	NO <sub>2</sub>	H	NH <sub>2</sub>	CN	CN	1.35	1.82	5.42	4.94	-5.42	-4.94	19.85	22.19
F28	NO <sub>2</sub>	H	NHCH <sub>3</sub>	CN	CN	1.49	2.08	5.31	4.86	-5.31	-4.86	21.04	24.60
F29	NO <sub>2</sub>	H	N(CH <sub>3</sub> ) <sub>2</sub>	CN	CN	1.52	2.04	5.24	4.81	-5.24	-4.81	20.80	23.61
F30	CN	NH <sub>2</sub>	H	CN	H	1.30	1.41	5.04	4.83	-5.04	-4.83	16.49	16.43
F31	CN	NHCH <sub>3</sub>	H	CN	H	1.37	1.45	4.94	4.77	-4.94	-4.77	16.71	16.49
F32	CN	N(CH <sub>3</sub> ) <sub>2</sub>	H	CN	H	1.37	1.52	4.85	4.66	-4.85	-4.66	16.11	16.45
F33	CN	H	NH <sub>2</sub>	CN	H	1.45	1.85	5.21	4.84	-5.21	-4.84	19.67	21.69
F34	CN	H	NHCH <sub>3</sub>	CN	H	1.61	2.08	5.11	4.76	-5.11	-4.76	21.06	23.60
F35	CN	H	N(CH <sub>3</sub> ) <sub>2</sub>	CN	H	1.56	2.00	5.03	4.74	-5.03	-4.74	19.77	22.47
F36	CN	NH <sub>2</sub>	H	CN	CN	1.28	1.41	5.24	4.89	-5.24	-4.89	17.60	16.84
F37	CN	NHCH <sub>3</sub>	H	CN	CN	1.35	1.47	5.14	4.81	-5.14	-4.81	17.85	17.01
F38	CN	N(CH <sub>3</sub> ) <sub>2</sub>	H	CN	CN	1.39	1.54	5.02	4.72	-5.02	-4.72	17.50	17.13
F39	CN	H	NH <sub>2</sub>	CN	CN	1.37	1.82	5.43	4.93	-5.43	-4.93	20.20	22.10
F40	CN	H	NHCH <sub>3</sub>	CN	CN	1.56	2.08	5.35	4.86	-5.35	-4.86	22.36	24.60
F41	CN	H	N(CH <sub>3</sub> ) <sub>2</sub>	CN	CN	1.52	2.00	5.28	4.79	-5.28	-4.79	21.12	22.94

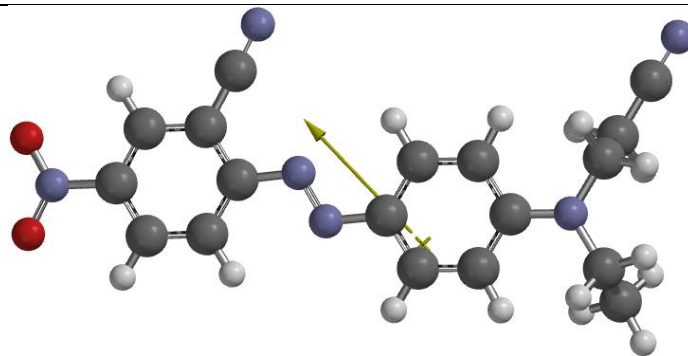


**Figure A. 1:** Equilibrium geometry of DR73 dye (obtained at B3LYP/6-31G\* level of theory) showing the direction of dipole moment vectors.

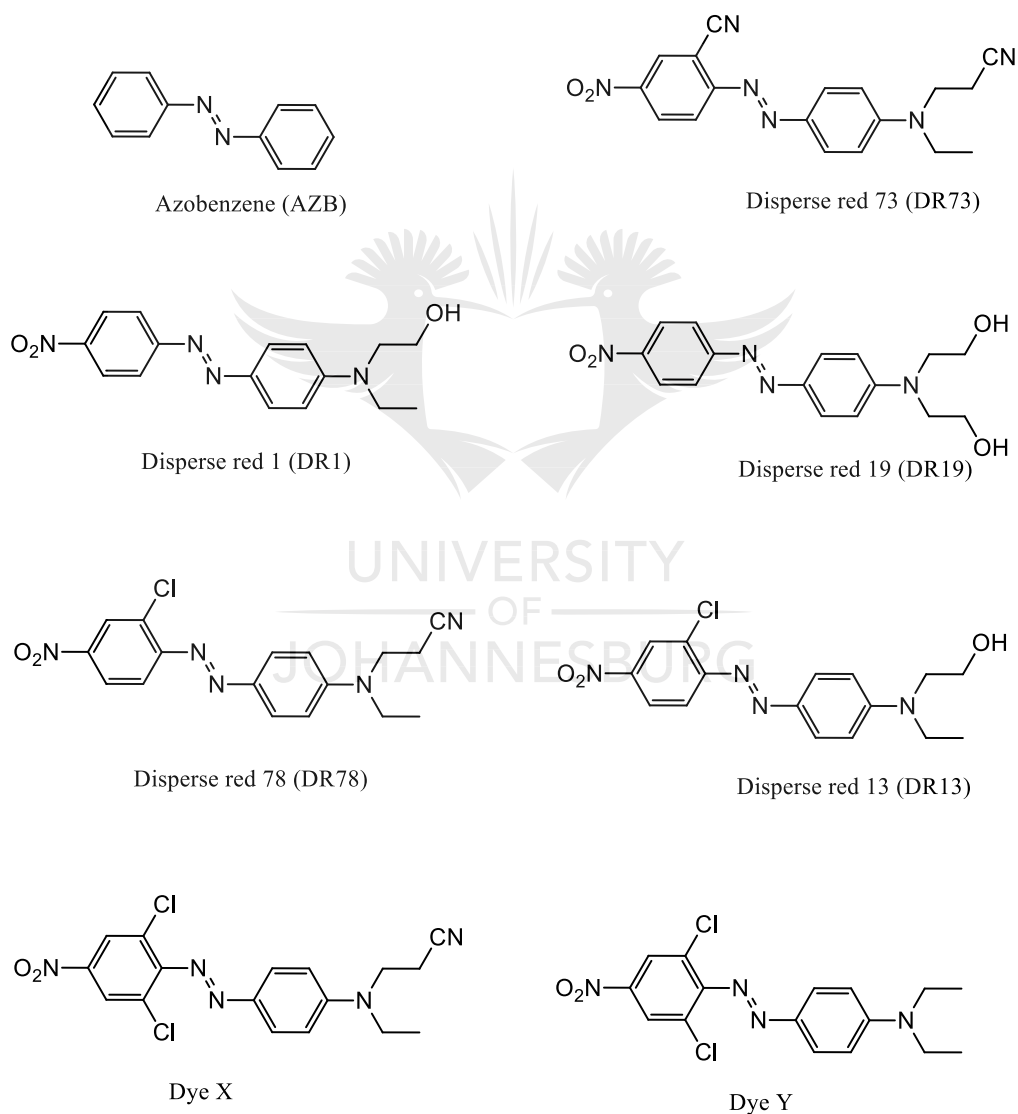


**Figure A. 2:** Molecular structures of the test azo disperse dyes.



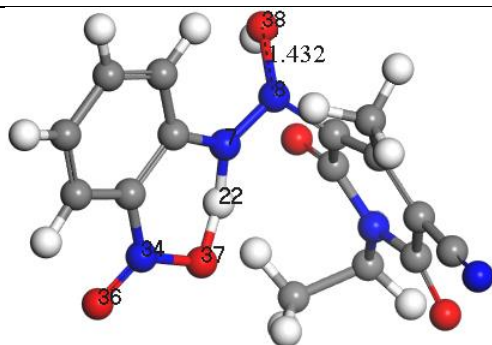


**Figure A. 3:** Geometry of the cyclic transition state structure,  $TS_{2N}$ .

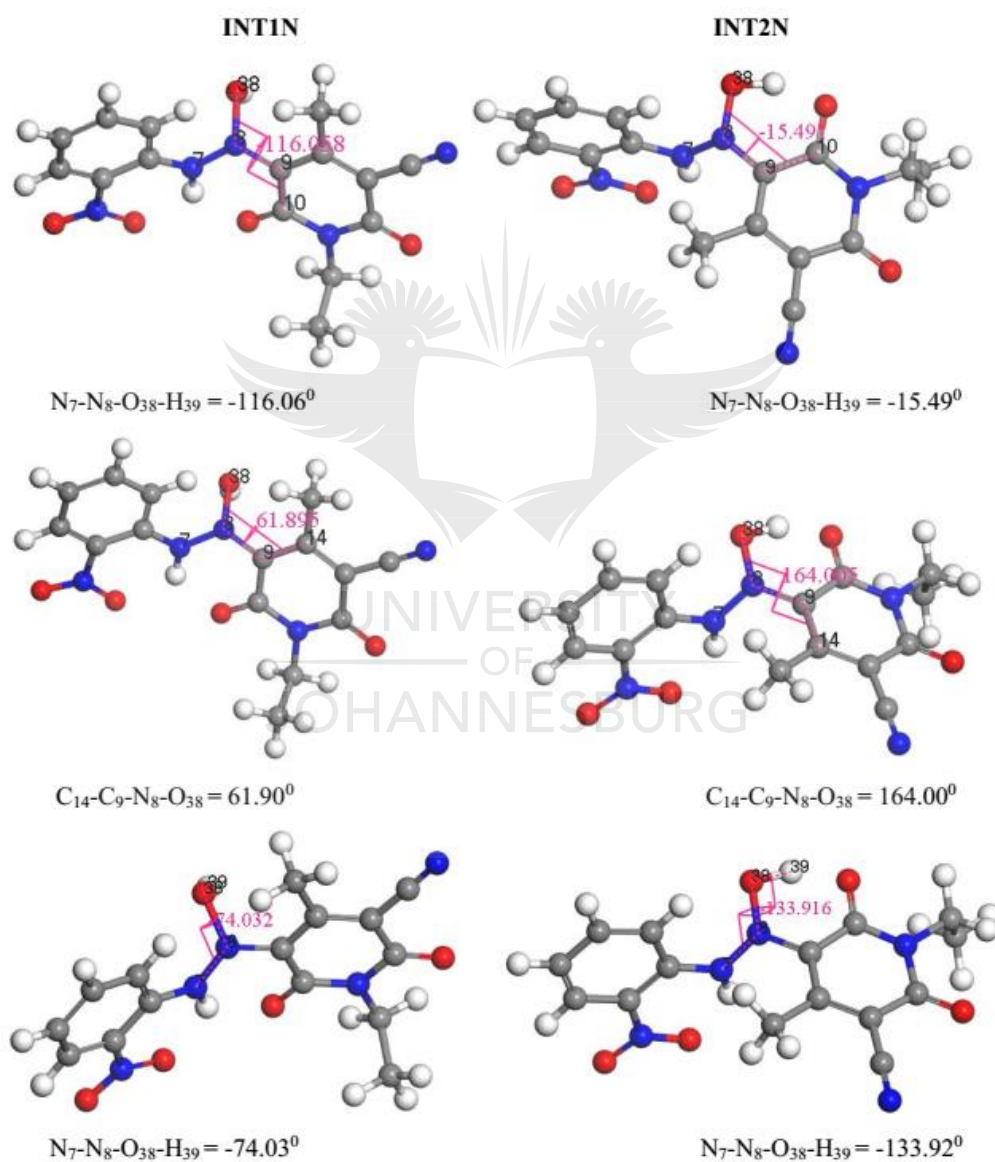


**Figure A. 4:** Comparison of selected dihedral angles between  $INT_{1N}$  and  $INT_{2N}$ . The differences between the angles are as a result of structural differences of the intermediates.

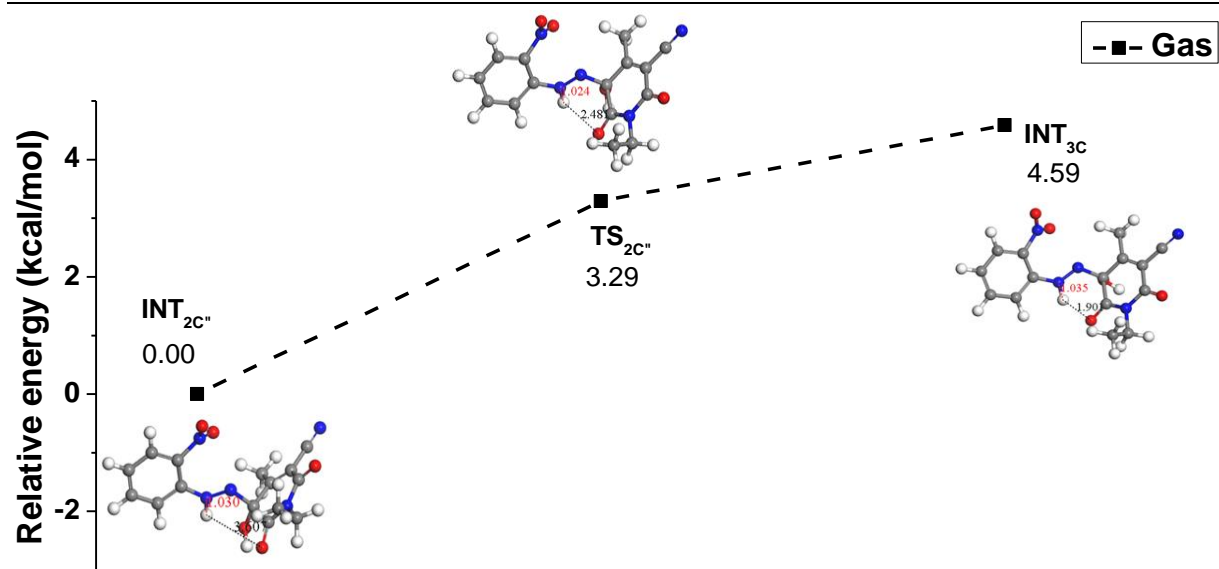


**Figure A. 5:** Potential energy profile for isolated proton transfer reaction of the radical addition product,  $\text{INT}_{2\text{C}^*}$  in the gas phase.

